
Studies on metal-poor stars and chemical enrichment of the Galaxy

A thesis
submitted for the degree of
Doctor of Philosophy
in
The Department of Physics,
Pondicherry University,
Puducherry - 605 014, India



by
Shejeelammal J
Indian Institute of Astrophysics,
Bangalore - 560 034, India



June 2022

Studies on metal-poor stars and chemical enrichment of the Galaxy

Shejeelammal J.

Indian Institute of Astrophysics



Indian Institute of Astrophysics

Bangalore - 560 034, India

Title of the thesis : **Studies on metal-poor stars
and chemical enrichment of the
Galaxy**

Name of the author : **Shejeelammal J.**

Address : Indian Institute of Astrophysics
II Block, Koramangala
Bangalore - 560 034, India

Email : shejeelammal.j@iiap.res.in

Name of the supervisor : **Prof. Aruna Goswami**

Address : Indian Institute of Astrophysics
II Block, Koramangala
Bangalore - 560 034, India

Email : aruna@iiap.res.in

Declaration of Authorship

I hereby declare that the matter contained in this thesis is the result of the investigations carried out by me at the Indian Institute of Astrophysics, Bangalore, under the supervision of Prof. Aruna Goswami. This work has not been submitted for the award of any other degree, diploma, associateship, fellowship, etc. of any other university or institute.

Signed:

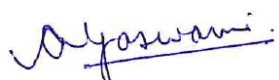


Date: 09/06/2022

Certificate

This is to certify that the thesis entitled '**Studies on metal-poor stars and chemical enrichment of the Galaxy**' submitted to the Pondicherry University by Ms. Shejeelammal J. for the award of the degree of Doctor of Philosophy, is based on the results of the investigations carried out by her under my supervision and guidance, at the Indian Institute of Astrophysics. This thesis has not been submitted for the award of any other degree, diploma, associateship, fellowship, etc. of any other university or institute.

Signed:



Date: 09/06/2022

List of Publications

Refereed Journals

1. *Chemical analysis of CH stars - III. Atmospheric parameters and elemental abundances,*
Meenakshi Purandardas, Aruna Goswami, Partha Pratim Goswami, **J. Shejeelammal**, Thomas Masseron, 2019, MNRAS, Vol. 486, page: 3266 -3289.
2. *Characterizing the companion AGBs using surface chemical composition of barium stars,*
J. Shejeelammal, Aruna Goswami, Partha Pratim Goswami, Rajeev Singh Rathour, Thomas Masseron, 2020, MNRAS, Vol. 492, page: 3708 - 3727.
3. *HCT/HESP study of two carbon stars from the LAMOST survey,*
J. Shejeelammal, Aruna Goswami, Jianrong Shi, 2021, MNRAS, Vol. 502, Page: 1008 - 1025.
4. *Probing the nucleosynthetic contribution of low-metallicity, low-mass star companions of CEMP stars,*
J. Shejeelammal, Aruna Goswami, 2021, APJ, Vol. 921, Page: 77 - 105.
5. *Spectroscopic study of three carbon stars from the Hamburg/ESO Survey:On confirming the low-mass nature of their companions,*
J. Shejeelammal, Aruna Goswami, Alain Jorissen, 2021, under preparation.

Conference proceedings

1. *Probing the Galactic s-process nucleosynthesis using metal-deficient barium stars,*
J. Shejeelammal, Aruna Goswami, 2019, BSRSL, Vol. 88, page: 215 - 223.

2. *[Rb/Zr] ratio in Ba stars as a diagnostic of the companion AGB stellar mass,*

J. Shejeelammal, Aruna Goswami, 2020, JApA, Vol. 41, article ID 37 (8 pages).

Conference participation

1. Oral presentation titled “Probing the Galactic s-process nucleosynthesis using metal-deficient barium stars” in the international conference *The 2nd Belgo-Indian Network for Astronomy & astrophysics (BINA) workshop* held at Royal Observatory of Belgium, Brussels, during 09 - 12 October, 2018
2. Oral presentation titled “Chemical and kinematic analysis of metal-deficient barium stars” in the conference *Astronomical Society of India meeting 2019 (ASI:2019)* held at Christ university, Bangalore, India, during 18 - 22 February, 2019.
3. Oral presentation titled “[Rb/Zr] ratio in Ba stars as a diagnostics of the companion AGB star nucleosynthesis” in the international conference *150 years of the periodic table: “Chemical elements in the universe: origin and evolution”* held at Indian Institute of Astrophysics, Bangalore, India, during 16 - 19 December, 2019.
4. Poster presentation titled “On the determination of mass of the now-extinct AGB companion of a binary system; clues from Rb and Zr nucleosynthesis” in the IIA In-House Science Meeting, held at Indian Institute of Astrophysics, Bangalore, India, during 17 - 18 June, 2021.

Acknowledgements

I express my humble gratitude before The Almighty, without whose blessings, it would not have been possible to bring this venture to a successful completion.

My heartfelt thanks to my supervising guide, Dr. Aruna Goswami, for her invaluable guidance, suggestions, and encouragement given during the whole phase of my work.

I thank the Directors, Prof. Annapurni Subramaniam, Prof. P. Sreekumar, and the Deans, Prof. B. E. Reddy and Prof. G. C. Anupama, of the Indian Institute of Astrophysics, for providing me with all the facilities during my research work. I would like to thank the BGS, all the administrative and library staff of IIA for their help. I thank all the people of the Data Center for assisting me with all my computer and internet related problems.

I would like to thank all the staff of IIA and Bhaskara for their support and help. I also thank the people at IAO and CREST, Pramod, Venkatesh, Kiran, Anaswar, and Rakesh, who have helped and supported me with their assistance during the nights there. I thank all the people at VBO Kavalur for their help and assistance during my observations there. A special thanks to Selvakumar Sir for teaching me the basics of data reduction.

I am very thankful to Dr. Drisya K, who has helped me a lot in all stages of my work. Thank you, Drisyechi. I have disturbed you a lot. A special thanks to my best friend, Meenu, for being an important person in my life. Thank you so much for comforting me during each power-down phase of mine. It was your friendship that helped me a lot to overcome most of my personal struggles. Thank you, Susmiyechi, for your help. I would like to thank my beloved junior, Partha, for his help, support, and brotherly affection.

A special thanks to my friends, Alikka, Bismi, Remya chechi, Varun, Pramod ettan, Venki ettan, Dhanu ettan, Prashobh ettan, Vivek ettan, Vishnu unni, Ananthu, Jay, Devu, Ajin ettan, Vineeth ettan, Kshama, Joice ettan, Binu chettan, Bharath, Athira, Rehma, Prajwel, Arun ettan, Dhanush, Lechu, Megha, Avrajith, Anirban Bhowmick, Vishnu Madhu, Priya, Pavana, Deepthi, and Fazlu. I thank all my friends for their love, help and encouragement without which it would have been difficult to complete this work.

I would like to thank my doctoral committee members, Prof. Gajendra Pandey (IIA) and Prof. Suraj Kumar Sinha (PU) for their suggestions and help.

I take this opportunity to place my sincere thanks and gratitude towards my beloved parents for letting me choose my way and for their love, support, and prayers. *Atha and Amma*, the faith and love you have in me helped me to reach here. Thanks for being my friends rather than parents. Your sacrifices and prayers have been the fuel for my journey. Thank you so much for having faith in your daughters even when the odds were stacked against you. I can't thank you enough for whatever you have done for me. Thank you, my dearest, super cool sister Shajila, for filling me with positive energy when I was down. It will not be an exaggeration if I say you are the best sister in the world. Thank you so much for your unconditional and selfless love, my dearest *kochumon*. I thank my grandma for her love, prayers, and affection. Thanks for comforting me with your words and prayers during my hard times.

I thank all my teachers from nursery till now for their support, help, encouragement, love, blessings, and faith. It is your blessings that have brought every success in my life. A special thanks to my first teacher, Achaamma, who led me to the world of letters. Your blessing is one of the main reasons for all my achievements. Thank you, Shali Kumar Sir, for your encouragement, support, and guidance in my life.

Special thanks to those people who said "no" to me whenever I had turning points in my life. This "no" ignited a fire in me which gave me the energy to pursue my career further and further ahead. This acknowledgement would be incomplete if I do not thank them

Once again, I thank each and every person in my life.

Data usage

The present study is based on the data acquired through various ground based telescopes. I would like to thank all the instrument teams for making the data available in the public domain.

High-resolution spectra of several objects are obtained through the observations with 2m Himalayan Chandra Telescope (HCT) operated at the Indian Astronomical Observatory, Hanle. Hanle Echelle SPectrograph (HESP) attached to HCT is used for the data acquisition. We thank the staff of IAO, Hanle and CREST, Hosakote, that made these observations possible. The facilities at IAO and CREST are operated by the Indian Institute of Astrophysics, Bangalore.

The Mercator telescope is also used for observations of a few stars. A part of this work is based on observations obtained with the HERMES spectrograph, supported by the Fund for Scientific Research of Flanders (FWO), the Research Council of K.U.Leuven, the Fonds National de la Recherche Scientifique (F.R.S.-FNRS), Belgium, the Royal Observatory of Belgium, the Observatoire de Genéve, Switzerland and the Thüringer Landessternwarte Tautenburg, Germany.

This study made use of archival data from the European Southern Observatory (ESO). The observations were made using the VLT/UVES and ESO/FEROS. I thank the ESO team for the data.

This research is based [in part] on data collected at Subaru Telescope (archival data), which is operated by the National Astronomical Observatory of Japan. We are honored and grateful for the opportunity of observing the Universe from Maunakea, which has the cultural, historical and natural significance in Hawaii.

This work made use of the SIMBAD astronomical database, operated at CDS, Strasbourg, France, and the NASA ADS, USA. This work has made use of data from the European Space Agency (ESA) mission Gaia (<https://www.cosmos.esa.int/gaia>), processed by the Gaia Data Processing and Analysis Consortium (DPAC, <https://www.cosmos.esa.int/web/gaia/dpac/consortium>).

*Dedicated to my beloved
parents*

*Es
sister*

“The nitrogen in our DNA, the calcium in our teeth, the iron in our blood, the carbon in our apple pies were made in the interiors of collapsing stars. We are made of star stuff.”

-Carl Sagan

Abstract

The low- and intermediate-mass stars are the major inhabitants of our Galaxy. They play an important role in the chemical evolution of the Galaxy. These stars have enriched the ISM with the products of various nucleosynthesis processes. They pass through the Asymptotic Giant Branch (AGB) phase during their evolution, and it is during this phase that the richest nucleosynthesis occurs. AGB stars are the predominant sites for s-process nucleosynthesis and major producers of ^{12}C , ^{13}C , ^{14}N , F, Na, Mg, etc. in the Galaxy. So, understanding the nucleosynthesis and evolution of AGB stars is of primary importance. Studies on the Galactic chemical evolution remain incomplete without considering the yields from AGB stars. However, the theoretical uncertainties associated with the AGB nucleosynthesis and observational constraints of the AGB stars make their direct studies difficult. In this regard, the AGB binary system, where these stars have transferred their products of AGB nucleosynthesis to the now observed secondary through binary mass-transfer, could be of help. These extrinsic stars in the binary system, such as Ba stars, CH stars along with their more metal-poor counterparts, Carbon-Enhanced Metal-Poor (CEMP) stars, could be used as a tool to investigate the AGB nucleosynthesis.

The abundance data available for metal-poor stars has been used extensively to constrain the Galactic chemical evolution. However, the sparse data available for the heavy element abundances in the lower metallicity underscores the need for a detailed study of a larger sample. A major motivation of our work is to understand the diverse abundance pattern observed for the heavy elements in the metal-poor stars that still remains poorly understood. We have attempted to understand the s-process nucleosynthesis, as well as the physical properties of the companion stars, through a detailed analysis of observed elemental abundances of a selected sample of metal-poor stars. The main objective of the thesis is to understand the role of metal-poor stars in

the chemical enrichment of the Galaxy and to provide observational constraints to the AGB nucleosynthesis theories from an analysis of a sample of extrinsic metal-poor stars at different metallicity. The problem is addressed through a spectroscopic analysis of three sets of metal-poor stellar samples: i) a comparatively metal-rich Ba stars sample; ii) a moderately metal-poor CH stars sample; and iii) a very metal-poor CEMP-s and CEMP-r/s stars sample.

The procedures we have adopted to address the problem and the results obtained from each set of stellar samples investigated are briefly outlined here:

- **Stellar sample:** As a first step towards our goal, we have performed an extensive literature survey of potential metal-poor stars including, Ba, CH, and CEMP stars. We have selected a sample of metal-poor star candidates from various sources in the literature and from the catalogue of carbon stars identified from the HES, HK and LAMOST surveys. The objects selected are then subjected to high-resolution spectroscopic analysis by obtaining their spectra from various observing facilities. The detailed chemical abundance analysis is performed using the recent version of the radiative transfer code MOOG that assumes Local Thermodynamic Equilibrium (LTE) conditions and using model atmospheres selected from the Kurucz grid of model atmospheres (Chapter 2).
- We present the first time abundance analysis of the objects BD–19 132, BD–19 290, HD 30443, LAMOSTJ091608.81+230734.6, HE 1304–2111, HE 1354–2257, BD+19 3109 and HD 179832. Even though the abundances of Fe and C derived from the medium-resolution spectra are available in the literature for the stars HE 0457–1805, HE 0920–0506, and HE 1327–2116, we present the first time high-resolution abundance analysis for these objects. The abundances of a few light elements derived from high-resolution IR spectra for the object LAMOSTJ151003.74+305407.3 are available in the literature, but we present the first time detailed abundance analysis for this object based on high-resolution optical spectra.

- Our sample contains 23 stars covering a metallicity [Fe/H] range of -2.86 to $+0.23$. The program stars are found to belong to the main-sequence and giant phase of stellar-evolution. Our analysis shows that they are enhanced in neutron-capture elements and are likely binaries, pointing to their surface chemical composition being influenced by pollution from the companions. The abundances of several elements C, N , O, Na, Al, α -elements, Fe-peak elements and several neutron-capture elements such as Rb, Sr, Y, Zr, Ba, La, Ce, Pr, Nd, Sm, and Eu are determined. The carbon isotopic ratio, $^{12}\text{C}/^{13}\text{C}$, an important mixing indicator, is also measured whenever possible.
- We have investigated the mass of companion AGB stars using several diagnostics, such as C, N, O, Na, and Mg abundances, [hs/ls] ratio, and [Rb/Zr] ratio. Rb plays a unique role as a diagnostic of the neutron density at the s-process site. In the low neutron density branch, Rb is the only element available to the stellar spectroscopists as a neutron densitometer. However, the important neutron density dependent abundance ratio, [Rb/Zr], is not explored much in the literature to determine the mass of the AGBs. We have explored this ratio for our stellar sample, to investigate the characteristics of their companion AGB stars.
- **Analysis of Ba star sample:** In order to understand the chemical and kinematic properties of the program stars, as a first step, a detailed chemical and kinematic analysis of a sample of ten Ba star candidates based on high-resolution spectra obtained from HCT/HESP, VLT/UVES, and ESO-MPG/FEROS is carried out. The stellar sample covers the metallicity range $-0.55 \leq [\text{Fe}/\text{H}] \leq +0.23$, temperature range $4550 - 6350$ K, $\log g$ range $2.20 - 4.28$, and micro-turbulent velocity range $0.63 - 1.59$ km s $^{-1}$. We have derived the neutron-density dependent [Rb/Zr] ratios to investigate the neutron source in the former companion AGB stars. The detection of the Rb I line at 7800.259 Å in the spectra of four program stars allowed us to determine the [Rb/Zr] ratio for these objects. The negative values obtained for this ratio in these stars indicate the operation

of $^{13}\text{C}(\alpha, \text{n})^{16}\text{O}$ reaction. As this reaction occurs in the low-mass AGB stars, we confirm that the former companions of these stars are low-mass AGB stars with $M \leq 3 M_{\odot}$. A comparison of the observed abundances with the predictions from FRUITY models, also confirms low-mass for the former companion AGB stars. The lack of Na and Mg enhancement, combined with the positive [hs/ls] ratio values, rules out $^{22}\text{Ne}(\alpha, \text{n})^{25}\text{Mg}$ as the neutron-source and corroborate the low-mass AGB companions for the Ba stars. The kinematic analysis shows that Ba stars are members of the Galactic disk (Chapter 3).

The main results of this study are published in the papers Shejelammal and Goswami (2019); Shejelammal et al. (2020); Shejelammal and Goswami (2020).

- **Analysis of CH, CEMP-s and CEMP-r/s star sample:** After completing the analysis of the sample of Ba stars, we have extended our analysis to the low-metallicity regime to understand the role of low-metallicity stars in the Galactic chemical enrichment and have performed a detailed spectroscopic analysis of a selected sample of CH and CEMP stars. The metallicity ranges of CH stars (3 objects) and CEMP stars (10 objects) are $-0.89 \leq [\text{Fe}/\text{H}] \leq -0.75$ and $-2.86 \leq [\text{Fe}/\text{H}] \leq -1.57$ respectively. The stellar sample has a temperature in the range of 4005 - 5380 K, $\log g$ in the range of 0.61 - 2.65, and micro-turbulent velocity in the range of 0.63 - 3.45 km s⁻¹. The high-resolution spectra of these objects were obtained using HCT/HESP, Mercator/HERMES, and SUBARU/HDS. Our analysis based on different diagnostics confirms the low-mass companions of the program stars. The possible origin(s) of the CEMP-r/s stars in our sample are also investigated by carefully analyzing their observed abundance pattern. The continuity in CEMP-s and CEMP-r/s stars in terms of various abundance ratios with respect to metallicity indicates that the astrophysical site responsible for the origin of these two classes of stars may be the same. Our analysis confirms that a modified s-process, namely the intermediate neutron-capture process, the i-process, is responsible for the observed abundance patterns in CEMP-r/s stars. The abundance patterns of the CEMP-r/s stars in our sample are well reproduced by the model predictions of the i-process in low-mass, low-metallicity

AGB stars. The parametric model-based analysis using the FRUITY models performed for the CH and CEMP-s stars also confirms low-mass for the former AGB companions. Kinematic analysis shows that CH stars belong to the Galactic disk and the majority of CEMP stars are members of the Galactic halo (Chapter 4).

The main results of this study are published in the papers Purandaras et al. (2019); Shejeelammal et al. (2021); Shejeelammal and Goswami (2021).

Contents

Abstract	i
List of Figures	xi
List of Tables	xix
Abbreviations	xxi
1 Introduction	1
1.1 Introduction	1
1.2 Origin of elements in the universe	3
1.2.1 Primordial nucleosynthesis	3
1.2.2 Stellar nucleosynthesis: Fusion	4
1.2.3 Neutron-capture nucleosynthesis	8
1.3 Contribution of AGB stars to the Galactic chemical enrichment . .	12
1.4 Metal-poor stars	16
1.4.1 Nomenclature	16
1.4.2 Metal-poor stars: Fossil records of the Universe	17
1.4.3 Sub-classification of metal-poor stars	19
1.5 Scope of the thesis	24
1.6 Outline of the thesis	26
2 Spectroscopic methodology: Sample selection, observation/data acquisition and data analysis	29
2.1 Introduction	29
2.2 Sample selection	30
2.2.1 Hamburg/ESO Survey (HES)	30
2.2.2 LAMOST Survey	32
2.2.3 Criteria for sample selection	34
2.3 Observations and data acquisition	36
2.3.1 Himalayan Chandra Telescope (HCT)	39
2.3.2 Very Large Telescope (VLT)	41

2.3.3	MPG/ESO 2.2 meter Telescope	42
2.3.4	Mercator Telescope	42
2.3.5	Subaru Telescope	43
2.4	Data reduction	44
2.4.1	Radial velocity	45
2.5	Basic ingredients of stellar spectroscopy	46
2.5.1	Stellar atmosphere	46
2.5.2	Atomic excitation and ionization: Boltzmann and Saha equations	51
2.5.3	Equivalent width	54
2.6	Data analysis	54
2.6.1	Modelling the stellar atmosphere	55
2.6.2	Line list	57
2.6.3	MOOG	58
2.6.4	Determination of stellar atmospheric parameters	58
2.6.5	Abundance analysis	62
2.6.6	Calculation of abundance uncertainties	65
2.7	Kinematic analysis	66
3	Analysis of Ba stars	71
3.1	Introduction	71
3.2	Object selection, data acquisition and data reduction	73
3.3	Stellar atmospheric parameters and radial velocity estimation	75
3.4	Abundance analysis and discussion	79
3.4.1	Light elements: C, N, O, carbon isotopic ratio $^{12}\text{C}/^{13}\text{C}$, odd-Z elements Na, Al, α -, and Fe-peak elements	82
3.4.2	Heavy elements	89
3.4.3	Abundance uncertainties	101
3.4.4	s-process content of the program stars	102
3.5	Binary status of the program stars	105
3.6	Diagnostics to understand the nature of companion AGB stars	106
3.6.1	The [hs/ls] ratio as an indicator of neutron source	106
3.6.2	Rb as a probe of the neutron density at the s-process site	109
3.6.3	Na and Mg abundances	111
3.7	Comparison with the AGB stars	115
3.7.1	Comparison of the observed abundances with literature values of AGB stars	115
3.7.2	Comparison with the FRUITY models and a parametric model-based analysis	118
3.8	Kinematic analysis	123
3.9	Discussion on individual stars	123
3.10	Conclusions	126
3.11	Appendix A	127

4 Analysis of CH and CEMP stars	145
4.1 Introduction	145
4.2 Stellar sample: selection, observation/data acquisition and data reduction	149
4.3 Stellar atmospheric parameters and radial velocity	152
4.4 Abundance determination and discussion	158
4.4.1 Light elements: C, N, O, $^{12}\text{C}/^{13}\text{C}$, Na, α -, and Fe-peak elements	158
4.4.2 Heavy elements	163
4.4.3 Abundance uncertainties	174
4.5 Classification of the program stars	175
4.6 Binary status of the program stars	181
4.7 Abundance profile analysis and interpretations	185
4.7.1 Carbon, nitrogen, oxygen abundances	185
4.7.2 The [hs/ls] ratio	191
4.7.3 Na, Mg and heavy elements	197
4.7.4 The [Rb/Zr] ratio	200
4.8 Origin of CEMP-r/s stars: clues from the abundance pattern	202
4.9 Parametric model-based analysis	206
4.9.1 CEMP-r/s stars	206
4.9.2 CH and CEMP-s stars: parametric model-based analysis using FRUITY models	209
4.10 Kinematic Analysis	209
4.11 Discussion on individual stars	212
4.12 Conclusions	215
4.13 Appendix B	216
5 Conclusions and future work	229
5.1 Future work	240
Bibliography	245

List of Figures

1.1	Evolution of $1 M_{\odot}$ (lower panel) and $5 M_{\odot}$ (upper panel) stars on the H-R diagram. Image source: <i>M. Pettini: Structure and Evolution of Stars - Lecture 13.</i>	6
1.2	Schematic representation of the structure of an AGB star. Image source: Karakas (2010).	8
1.3	Different evolutionary stages of low-, intermediate-, and high-mass stars. Image Credit: https://www.britannica.com/science/star-astronomy/Star-formation-and-evolution	9
1.4	The s-process peaks for the solar system abundance. Image source: Karakas (2010)	13
2.1	Metallicity Distribution Function (MDF) of the HES from Christlieb (2003) (upper panel) and Frebel <i>et al.</i> (2006) (lower panel).	33
2.2	Metallicity Distribution Function (MDF) of the LAMOST DR3 by Li <i>et al.</i> (2018b).	35
2.3	Location of the selected stellar sample in color - magnitude diagram. Blue open squares are Ba stars from literature (Allen and Barbuy 2006; Yang <i>et al.</i> 2016; de Castro <i>et al.</i> 2016). Red circles are CH stars from literature (Karinkuzhi and Goswami 2014, 2015; Goswami <i>et al.</i> 2016). Green starred triangles are CEMP stars from literature (Masseron <i>et al.</i> 2010 and references therein). Our stellar sample is represented by black filled triangles.	37
2.4	Sketch of the mean temperature as function of height above the convective layer in the sun. The photosphere is characterised by a negative temperature gradient. Image credit: http://www-star.st-and.ac.uk/~protect/unhbox\voidb@x\protect\penalty\OM\{}pw31/education.html	49
2.5	Definition of equivalent width in the case of an absorption line. Image credit: https://www.open.edu/openlearn/science-maths-technology/overview-active-galaxies/content-section-8.4	55
2.6	The iron abundances derived from Fe I lines as functions of excitation potential, equivalent width, and wavelength. The yellow dotted line is the mean Fe I abundance and the green line represent the trend of the Fe I abundance.	61
2.7	The iterative process employed to determine the abundance in spectrum synthesis method	64

2.8	Schematic representation of the components of spatial velocity in a right-handed cylindrical coordinate system. $(R, \theta, z) \sim$ (Galactocentric distance, azimuthal coordinate, height above/below the Galactic plane).	68
3.1	Sample spectra of the program stars in the wavelength region 5840 to 5863 Å	74
3.2	Iron abundances of the program stars derived from individual Fe I and Fe II lines as function of excitation potential (lower panel), and equivalent width (upper panel). The dotted lines correspond to the derived and adopted Fe abundance for each star. Solid circles correspond to Fe I and solid triangles correspond to Fe II lines.	76
3.3	Location of the program stars on the H-R diagram (Girardi <i>et al.</i> 2000). Evolutionary tracks (from bottom to top) for (i) 0.6, 0.7, 0.8 and 0.9 M_{\odot} for $z = 0.004$ (upper panel), (ii) 1.0, 1.1, 2.2 and 2.5 M_{\odot} for $z = 0.008$ (lower panel).	80
3.4	Location of the program stars on the H-R diagram (Girardi <i>et al.</i> 2000). Evolutionary tracks (from bottom to top) for (i) 0.9, 1.0, 1.2, 1.7, 1.8, 2.0, 2.2, and 2.5 M_{\odot} for $z = 0.019$ (upper panel), (ii) 2.2, 2.5 and 3.0 M_{\odot} for $z = 0.030$ (lower panel).	81
3.5	Synthesis of [O I] line around 6300 Å (upper panel) and O I triplet around 7770 Å (lower panel, LTE abundance estimates). Dotted and solid lines represent synthesized and the observed spectra. Short-dashed and long-dashed lines represent the synthetic spectra corresponding to $\Delta[\text{O}/\text{Fe}] = -0.3$ and $+0.3$ respectively.	84
3.6	Synthesis of C ₂ band around 5165 Å. Dotted and solid lines represent synthesized and the observed spectra. Short-dashed and long-dashed lines represent the synthetic spectra corresponding to $\Delta[\text{C}/\text{Fe}] = -0.3$ and $+0.3$ respectively	85
3.7	Observed [C+N+O/Fe] ratios of the program stars as function of surface gravity, log g. HD 32712 (starred triangle), HD 36650 (filled triangle), HD 94518 (filled circle), HD 207585 (six-sided cross), HD 211173 (nine-sided star), and HD 219116 (filled square).	88
3.8	Observed [X/Fe] ratios of the light elements (Tables 3.5 - 3.7) for the program stars with respect to metallicity [Fe/H]. Red open circles represent normal giants from literature (Luck and Heiter 2007). Green four-sided stars represent Ba stars from literature (Allen and Barbuy 2006; de Castro <i>et al.</i> 2016; Yang <i>et al.</i> 2016; Karinkuzhi <i>et al.</i> 2018a,b). HD 24035 (filled hexagon), HD 32712 (starred triangle), HD 36650 (filled triangle), HD 94518 (filled circle), HD 147609 (five-sided star), HD 154276 (open hexagon), HD 179832 (open triangle), HD 207585 (six-sided cross), HD 211173 (nine-sided star), and HD 219116 (filled square).	90
3.9	Spectral synthesis of Rb I line around 7800 Å. Dotted and solid lines represent synthesized and the observed spectra. Short-dashed and long-dashed lines represent the synthetic spectra corresponding to $\Delta[\text{Rb}/\text{Fe}] = -0.3$ and $+0.3$ respectively	91
3.10	Synthesis of Zr I line at 6134.585 Å. Dotted and solid lines represent synthesized and the observed spectra. Short-dashed and long-dashed lines represent the synthetic spectra corresponding to $\Delta[\text{Zr}/\text{Fe}] = -0.3$ and $+0.3$ respectively	93

3.11 Synthesis of Ba II line at 5853.668 Å. Dotted and solid lines represent synthesized and the observed spectra. Short-dashed and long-dashed lines represent the synthetic spectra corresponding to $\Delta[\text{Ba}/\text{Fe}] = -0.3$ and $+0.3$ respectively	94
3.12 Observed [X/Fe] ratios of the neutron-capture elements (Tables 3.5 - 3.7) for the program stars with respect to metallicity [Fe/H]. Symbols have the same meaning as in Figure 3.8	102
3.13 Observed [s/Fe] ratios of the program stars with respect to metallicity [Fe/H]. Red open circles represent normal giants from literature (Luck and Heiter 2007). Green crosses, blue four-sided stars, cyan filled pentagons, red eight-sided crosses represent strong Ba giants, weak Ba giants, Ba dwarfs, Ba subgiants respectively from literature (de Castro <i>et al.</i> 2016; Yang <i>et al.</i> 2016; Allen and Barbuy 2006). Magenta six-sided stars represent the stars rejected as Ba stars by de Castro <i>et al.</i> (2016). HD 24035 (filled hexagon), HD 32712 (starred triangle), HD 36650 (filled triangle), HD 94518 (filled circle), HD 147609 (five-sided star), HD 154276 (open hexagon), HD 179832 (open triangle), HD 207585 (six-sided cross), HD 211173 (nine-sided star), and HD 219116 (filled square).	104
3.14 The A(C) - [Fe/H] diagram for known/likely binary and single stars. The binary and single stars are separated by the dashed line at $A(\text{C}) = 7.10$. The long-dash dot line corresponds to $[\text{C}/\text{Fe}] = 0$. Green and magenta open hexagons represent binary and single CEMP stars, respectively from literature (Yoon <i>et al.</i> 2016). Black open squares represent the binary CH stars from literature (Purandardas <i>et al.</i> 2019; Karinkuzhi and Goswami 2014, 2015; Luck 2017). Binary Ba stars from literature (Karinkuzhi <i>et al.</i> 2018a) are represented by cyan open pentagons. The prefixes B- and S- in the figure imply binary and single stars, respectively. The blue squares represent the confirmed binary program stars, and the red squares represent the program stars with unknown binary status.	107
3.15 The observed abundances [Rb/Fe] vs [Zr/Fe]. HD 32712 (starred triangle), HD 36650 (filled triangle), HD 179832 (open triangle), and HD 211173 (nine-sided star). The shaded region corresponds to the observed range of Zr and Rb in intermediate-mass AGB stars in the Galaxy and the Magellanic Clouds (van Raai <i>et al.</i> 2012). The four program stars occupy the region of low-mass AGB stars.	112
3.16 The observed abundances [Na/Fe] and [Mg/Fe]. Red open circles represent the normal filed giants from literature (Luck and Heiter 2007). Blue squares are the disk dwarfs from literature (Reddy <i>et al.</i> 2003; Bensby <i>et al.</i> 2005; Reddy <i>et al.</i> 2006). HD 24035 (filled hexagon), HD 32712 (starred triangle), HD 36650 (filled triangle), HD 94518 (filled circle), HD 147609 (five-sided star), HD 179832 (open triangle), HD 207585 (six-sided cross), HD 211173 (nine-sided star), and HD 219116 (filled square).	116

3.17 Comparison of abundance ratios of neutron-capture elements observed in the program stars and the low-mass AGB stars with respect to metallicity [Fe/H]. Red crosses represent the AGB stars from literature (Smith and Lambert 1985, 1986b, 1990; Abia and Wallerstein 1998). HD 24035 (filled hexagon), HD 32712 (starred triangle), HD 36650 (filled triangle), HD 94518 (filled circle), HD 147609 (five-sided star), HD 179832 (open triangle), HD 207585 (six-sided cross), HD 211173 (nine-sided star), and HD 219116 (filled square).	117
3.18 Comparison of the predicted and observed values of [hs/ls] ratios. The black circles with error bars represent the observed [hs/ls] ratio in the program stars. The curves correspond to the predicted [hs/ls] ratios for AGB stars of different masses in the range $1.3 - 6 M_{\odot}$ from the FRUITY models.	120
3.19 The solid curves are the best fit for the parametric model function obtained from the comparison of the observed abundances in the Ba stars and predicted abundances from the FRUITY models by minimizing the χ^2 . The observed abundances in the program stars are indicated by the points with error bars.	122
4.1 Sample spectra of the program stars in the wavelength region 5160 to 5190 Å.	153
4.2 Iron abundances of the program stars derived from individual Fe I and Fe II lines as function of excitation potential (lower panel), and equivalent width (upper panel). The dotted lines correspond to the derived and adopted Fe abundance for each star. Solid circles correspond to Fe I, and solid triangles correspond to Fe II lines.	154
4.3 The evolutionary tracks (Girardi <i>et al.</i> 2000) for $1.0, 1.1$, and $1.3 M_{\odot}$ for $z = 0.004$ (upper panel), and for $0.6, 0.8, 1.0, 1.4$, and $1.8 M_{\odot}$ for $z = 0.0004$ (lower panel) are shown from bottom to top.	156
4.4 Synthesis of C ₂ band around 5165 Å (lower panel) and 5635 Å (upper panel). Dotted and solid lines represent synthesized and observed spectra respectively. short-dashed and long-dashed lines represent the synthetic spectra for $\Delta [C/Fe] = -0.3$ and $+0.3$ respectively.	160
4.5 Spectral synthesis of CN band around 8005 Å. Dotted and solid lines represent synthesized and observed spectra respectively. short-dashed and long-dashed lines are the synthetic spectra for $^{12}C/^{13}C \simeq 90$ and 4 respectively.	161

4.6	Observed [X/Fe] ratios of the light elements in the program stars with respect to metallicity [Fe/H]. Red open circles represent normal giants from literature (Honda <i>et al.</i> 2004; Venn <i>et al.</i> 2004; Aoki <i>et al.</i> 2005, 2007; Reddy <i>et al.</i> 2006; Luck and Heiter 2007; Hansen <i>et al.</i> 2016a; Yoon <i>et al.</i> 2016). Magenta open squares and blue starred triangles are CEMP-s and CEMP-r/s stars respectively from literature (Masseron <i>et al.</i> 2010; Purandardas <i>et al.</i> 2019; Karinkuzhi <i>et al.</i> 2021; Purandardas and Goswami 2021). Cyan crosses and green open triangles are CH (Vanture 1992; Karinkuzhi and Goswami 2014, 2015; Goswami <i>et al.</i> 2016) and Ba stars (Allen and Barbuy 2006; de Castro <i>et al.</i> 2016; Yang <i>et al.</i> 2016; Karinkuzhi <i>et al.</i> 2018a; Shejelammal <i>et al.</i> 2020) respectively from literature. BD-19 132 (filled square), BD-19 290 (open hexagon), HD 30443 (open pentagon), HE 0457-1805 (filled triangle), LAMOSTJ091608.81+230734.6 (five-sided cross), HE 0920-0506 (nine-sided cross), HE 1157-0518 (starred triangle), HE 1304-2111 (four-sided star), HE 1327-2116 (nine-sided star), HE 1354-2257 (filled circle), LAMOSTJ151003.74+305407.3 (open square), BD+19 3109 (filled pentagon), and HD 202851 (six-sided star).	164
4.7	Observed [X/Fe] ratios of the light elements in the program stars with respect to metallicity [Fe/H]. Symbols have the same meaning as in Figure 4.6.	165
4.8	Synthesis of Sr I line at 4607.327 Å. Dotted and solid lines represent synthesized and observed spectra respectively. short-dashed and long-dashed lines represent the synthetic spectra for $\Delta[\text{Sr}/\text{Fe}] = -0.3$ and $+0.3$ respectively.	167
4.9	Synthesis of Ba II 5853.668 Å (lower panel) and 6141.713 Å (upper panel) lines. Dotted and solid lines represent synthesized and observed spectra respectively. short-dashed and long-dashed lines represent the synthetic spectra for $\Delta[\text{Ba}/\text{Fe}] = -0.3$ and $+0.3$ respectively.	169
4.10	Synthesis of Eu II 6645.064 Å line. Dotted and solid lines represent synthesized and observed spectra respectively. short-dashed and long-dashed lines represent the synthetic spectra for $\Delta[\text{Eu}/\text{Fe}] = -0.3$ and $+0.3$ respectively.	171
4.11	Observed [X/Fe] ratios of the heavy elements in the program stars with respect to metallicity [Fe/H]. Symbols have same meaning as in Figure 4.6	173
4.12	Observed [C/Fe] ratios as a function of $\log(L/L_\odot)$. Red filled hexagons represent CEMP stars from literature (Aoki <i>et al.</i> 2007 and references therein, Goswami <i>et al.</i> 2016; Purandardas <i>et al.</i> 2019; Karinkuzhi <i>et al.</i> 2021; Goswami <i>et al.</i> 2021). Blue crosses represent carbon-normal metal-poor stars from literature (Aoki <i>et al.</i> 2005, 2007; Cayrel <i>et al.</i> 2004; Honda <i>et al.</i> 2004). BD-19 132 (filled square), BD-19 290 (open hexagon), HD 30443 (open pentagon), HE 0457-1805 (filled triangle), LAMOSTJ091608.81+230734.6 (five-sided cross), HE 0920-0506 (nine-sided cross), HE 1157-0518 (starred triangle), HE 1304-2111 (four-sided star), HE 1327-2116 (nine-sided star), HE 1354-2257 (filled circle), LAMOSTJ151003.74+305407.3 (open square), BD+19 3109 (filled pentagon), and HD 202851 (six-sided star). The threshold [C/Fe] is shown by the dashed line. A representative error bar is shown at the top right corner.	180

- 4.13 Observed [Ba/Fe] (upper panel) and [La/Fe] (lower panel) as functions of observed [Eu/Fe] for CEMP and r stars. Magenta squares, blue starred triangles, and red five-sided stars represent CEMP-s, CEMP-r/s, and r (including both CEMP-r and rI/rII stars) stars, respectively from literature (Masseron *et al.* 2010; Karinkuzhi *et al.* 2021; Purandardas *et al.* 2019; Goswami *et al.* 2021). BD–19 132 (filled square), BD–19 290 (open hexagon), HD 30443 (open pentagon), HE 0457–1805 (filled triangle), LAMOSTJ091608.81+230734.6 (five-sided cross), HE 0920–0506 (nine-sided cross), HE 1157–0518 (starred triangle), HE 1304–2111 (four-sided star), HE 1327–2116 (nine-sided star), HE 1354–2257 (filled circle), LAMOSTJ151003.74+305407.3 (open square), BD+19 3109 (filled pentagon), and HD 202851 (six-sided star). Region (i) and (ii) are the CEMP-s, and (iii) is CEMP-r/s star region as given by Goswami *et al.* (2021). The dashed line is the least-square fit to the observed abundances in r-stars. A representative error bar is shown at the top left corner of each panel. 182
- 4.14 Distribution of A(C) as a function of [Fe/H] for known (and likely) binary and single stars. The binary and single stars are separated by the dashed line at $A(C) = 7.10$. The long-dash dot line corresponds to $[C/Fe] = 0$. Green and magenta open hexagons represent binary and single CEMP stars, respectively from literature (Yoon *et al.* 2016). Black open squares represent the binary CH stars from literature (Purandardas *et al.* 2019; Karinkuzhi and Goswami 2014, 2015; Luck 2017). Binary Ba stars from literature (Karinkuzhi *et al.* 2018a) are represented by cyan open pentagons. The prefixes B- and S- in the figure imply binary and single stars, respectively. The blue squares represent the confirmed binary program stars, and the red squares represent the program stars with unknown binary status. 186
- 4.15 The A(C) - [Fe/H] diagram. Green open hexagons represent CEMP-s and CEMP-r/s stars, and magenta open hexagons represent CEMP-no stars from literature (Yoon *et al.* 2016). Cyan open pentagons are the CH stars from literature (Purandardas *et al.* 2019; Karinkuzhi and Goswami 2014, 2015; Luck 2017). Yellow crosses are the Ba stars from literature (Karinkuzhi *et al.* 2018a; Sheejelammal *et al.* 2020). All red, blue, and black symbols, respectively represent CEMP-r/s, CEMP-s, and CH stars of our sample. BD–19 132 (filled square), BD–19 290 (open hexagon), HD 30443 (open pentagon), HE 0457–1805 (filled triangle), LAMOSTJ091608.81+230734.6 (five-sided cross), HE 0920–0506 (nine-sided cross), HE 1157–0518 (starred triangle), HE 1304–2111 (four-sided star), HE 1327–2116 (nine-sided star), HE 1354–2257 (filled circle), LAMOSTJ151003.74+305407.3 (open square), BD+19 3109 (filled pentagon), and HD 202851 (six-sided star). The low- and high-carbon bands at $A(C) = 6.28$ and 7.96 noted by Yoon *et al.* (2016) is shown as dashed lines. The solid line corresponds to $[C/Fe] = 0.70$, and long-dash dot line to $[C/Fe] = 0$ 189

4.21 The observed [Rb/Fe] and [Zr/Fe] in the program stars. BD–19 132 (filled square), BD–19 290 (open hexagon), HD 30443 (open pentagon), HE 0457–1805 (filled triangle), LAMOSTJ091608.81+230734.6 (five-sided cross), HE 0920–0506 (nine-sided cross), LAMOSTJ151003.74+305407.3 (open square), BD+19 3109 (filled pentagon), and HD 202851 (six-sided star). The observed ranges of [Rb/Fe] and [Zr/Fe] in intermediate-mass AGB stars of the Galaxy and the Magellanic Clouds (van Raai <i>et al.</i> 2012) are shown as shaded region.	201
4.22 The observed [hs/Fe] - [ls/Fe] (upper panel) and [Eu/Fe] - [hs/Fe] (lower panel) in CEMP-s (blue circles) and CEMP-r/s (red circles) stars from literature (Goswami <i>et al.</i> 2021, references therein).	205
4.23 Parametric model fits for CEMP-r/s stars. The best fit for the parametric model function is represented by the solid curves. The observed abundances are indicated by the points with error bars.	208
4.24 The parametric model fits for CH (upper panel) and CEMP-s stars (lower panel). The best fit for the parametric model function is represented by the solid curves. The observed abundances are indicated by the points with error bars.	210

List of Tables

1.1	Nomenclature of metal-poor stars	17
1.2	Classification of metal-poor stars	19
2.1	Photometric temperature estimates (in Kelvin) of the stellar sample	38
2.2	Details of the spectra	39
3.1	Basic data about the program stars	75
3.2	Derived atmospheric parameters for the program stars.	77
3.3	Comparison of estimated stellar parameters with literature values .	78
3.4	Estimates of log g and Mass using parallax method	79
3.5	Elemental abundances in HD 24035, HD 32712, and HD 36650 . . .	97
3.6	Elemental abundances in HD 94518, HD 147609, and HD 154276 . .	98
3.7	Elemental abundances in HD 179832, HD 207585, HD 211173, and HD 219116	99
3.8	Comparison of the heavy elemental abundances of program stars with literature values.	100
3.9	Differential Abundance ($\Delta \log \epsilon$) of different element species with the variations in stellar atmospheric parameters for HD 211173 (columns 2 - 9).	101
3.10	Estimates of [ls/Fe], [hs/Fe], [s/Fe], [hs/ls], [Rb/Sr], [Rb/Zr], C/O .	103
3.11	Radial velocity data of the program stars	106
3.12	The best fit mass, dilution factor and reduced chi-square values. .	122
3.13	Spatial velocity and probability estimates for the program stars .	123
4.1	Primary information of the program stars.	151
4.2	Derived atmospheric parameters and radial velocity of the program stars.	155
4.3	Mass and log g estimated from the parallax method	157
4.4	Estimates of [ls/Fe], [hs/Fe], [s/Fe], [hs/ls], [Rb/Zr]	170
4.5	Elemental abundances in BD-19 132, BD-19 290, and HD 30443 .	172
4.6	Elemental abundances in HE 0457-1805, LAMOSTJ091608.81+230734.6, and HE 0920-0506	174
4.7	Elemental abundances in HE 1157-0518, HE 1304-2111, and HE 1327-2116175	
4.8	Elemental abundances in HE 1354-2257, LAMOSTJ151003.74+305407.3, BD+19 3109, and HD 202851	176

4.9 Comparison of the elemental abundances of our program stars with the literature values.	177
4.10 Change in the abundances ($\Delta \log \epsilon$) of different elemental species with the variations in stellar atmospheric parameters for the representative star HD 202851 (columns 2 - 5). The rms uncertainty, computed from the random error (σ_{ran}) and the differential abundances given in second to fifth columns, is given in sixth column. Total uncertainty in [X/Fe] of each elemental species is given in seventh column.	178
4.11 The [C/Fe], [Ba/Eu] and [La/Eu] ratios in the program stars	183
4.12 Radial velocity data of the program stars	184
4.13 Estimates of spatial velocity and probabilities for the membership to the Galactic population of the program stars	211
5.1 Program stars with important results	240

Abbreviations

NASA	National Aeronautics and Space Administration
VLT	Very Large Telescope
ESO	European Southern Observatory
HCT	Himalayan Chandra Telescope
HESP	Hanle Echelle SPectrograph
IAO	Indian Astronomical Observatory
FEROS	Fiber-fed Extended Range Optical Spectrograph
UVES	Ultraviolet and Visible Echelle Spectrograph
HERMES	High-efficiency and high-Resolution Mercator Echelle Spectrograph
HDS	High Dispersion Spectrograph
LAMOST	Large sky Area Multi-Object fiber Spectroscopic Telescope
AGB	Asymptotic Giant Branch
LM AGB	Low-Mass Asymptotic Giant Branch
IM AGB	Intermediate-Mass Asymptotic Giant Branch
ISM	Inter-Stellar Medium
TDU	Third Dredge-Up
TP	Thermal Pulse
IP	Inter Pulse
CCD	Charge Coupled Device
R_⊕	Solar Radius
M_⊕	Solar Mass
L_⊕	Solar Luminosity

Chapter 1

Introduction

1.1 Introduction

In astronomy, all the elements heavier than hydrogen and helium are called as ‘metals’. The primordial ISM contained only H, He, and Li, and all other metals were formed in the stellar interiors through various nucleosynthesis processes. Supernova explosions as well as the ejecta from the stars dispersed the metals into the ISM. The very first stars were formed from the metal-free, pristine gas clouds. These hypothetical short-lived massive stars (10 to several hundreds of solar mass), known as population III stars, first introduced the metals to the ISM through SN explosions. The next generation of stars, population II stars, were formed from this enriched ISM that contains metals. Thus, the successive enrichment of the gas clouds by several nucleosynthesis sites and processes throughout cosmic time has resulted in an increased metallic content of the ISM, and stars with varying metallicity have been formed. The low abundance of metals in a star,

hence, indicates that it is formed relatively early. Therefore, metallicity is taken as a proxy for the age of the Universe.

Until the twentieth century, it was long believed that all the stars had similar chemical compositions as the sun. In the middle of the twentieth-century, unusually weak metallic lines of Ca and Fe, about 1/20th of the solar values, were observed in the stellar spectra of a dwarf star (Chamberlain and Aller 1951). Subsequent research on such metal-weak stars over the last half-century has revealed that each star has its own distinctive abundance pattern; different stars may have different metallicity, indicating different evolutionary stages that the Galaxy has gone through. The scatter observed in the abundances of the stars of the same metallicity (age) has suggested that the ISM from which they were formed was not mixed well and in-homogeneous (Argast *et al.* 2000). However, the little scatter found for the light elements ($Z < 30$) in a sample of stars studied by Cayrel *et al.* (2004) discarded the claim of an unmixed ISM. This indicates different astrophysical origins for the elements. Depending on the time and environment, the relative contribution from each astronomical source vary.

The origin as well as the evolution of elements, especially the neutron-capture elements, in the Galaxy is poorly known. Besides the firm constraints on the stellar astrophysics, elemental abundances in the Galaxy is remarkably a powerful tool to understand the formation and chemical evolution history of the Universe. So, stellar astrophysicists started to look at the chemical abundances of different components of the Galaxy. The pivotal works of several authors in the late twentieth century, for instance Sneden *et al.* (1981); Ryan *et al.* (1991); Edvardsson *et al.* (1993); McWilliam *et al.* (1995a,b), on detailed abundance patterns of the disk and halo stars of the Galaxy, have provided better insight into the chemical history of the Galaxy. For the past three decades, studies on the chemical composition of the stars in the disk and halo of the Milky Way have considerably contributed to our understanding of the chemical evolution of the Galaxy (Goswami and Prantzos

2000). The chemical evolution of the Universe is explored through the interpretations of the observational data available for the chemical composition of stars with the help of Galactic Chemical Evolution (GCE) models (Goswami and Prantzos 2000; Matteucci 2016; Kobayashi *et al.* 2020). The GCE models provide a strong theoretical probe to investigate the complex astrophysical processes that govern the chemical evolution of the Galaxy. The GCE models deal with the study of element formation and the evolution of abundances of chemical elements in stars with different metallicities, at different times.

Hence, the Galactic chemical enrichment process is a complex problem and needs special attention. In order to address this problem, the basic step is to understand the nucleosynthesis processes that synthesize chemical elements and enrich the Universe.

1.2 Origin of elements in the universe

The history of the chemical composition and evolution of the Galaxy, except for the lightest elements, is related to the nucleosynthesis that occurred in many generations of stars. The various mechanisms of element formation in the Universe will be discussed in this section.

1.2.1 Primordial nucleosynthesis

The very first elements in the Universe were formed in the first three minutes after the Big Bang (Fields *et al.* 2014; Maoz 2016). The Big Bang nucleosynthesis (BBN) is responsible for synthesizing various light element isotopes such as ^1H , ^2H , ^3H , ^3He , ^4He , and traces of ^7Li (Steigman 2007; Iocco *et al.* 2009; Pospelov

and Pradler 2010). BBN was originally proposed by Alpher *et al.* (1948). Once the Universe cooled enough ($\sim 10^9$ K), after a minute of the big bang, stable neutrons and protons were formed, which marked the beginning of BBN (Maoz 2016; Dodelson and Schmidt 2021). The protons and neutrons were combined to form deuterium and then into other light elements up to ${}^7\text{Li}$. The elements Be and B are formed by the cosmic ray spallation; ie, by the interaction of cosmic rays with the ISM (Meneguzzi *et al.* 1971; Vangioni-Flam and Cassé 1999). All the elements beyond this are produced in the stellar interiors.

1.2.2 Stellar nucleosynthesis: Fusion

Once a protostar is formed from a collapsing gas cloud of interstellar medium, as a result of its gravitational collapse, the core temperature increases. When the temperature of the core is high enough, hydrogen fusion to form He sets in, either through the proton - proton fusion (PP chains) or the CNO cycle, depending on the stellar mass and density. The PP chain occurs in solar mass stars at core temperature $\sim 4 \times 10^6$ K, whereas the CNO cycle operates in stars of mass $> 1.3 M_{\odot}$ when the core temperature reaches $\sim 15 \times 10^6$ K. This stage of stellar evolution is known as main sequence (MS). The radiation pressure balances the gravity (hydrostatic equilibrium) and the gravitational collapse stops. In the case of massive stars, due to their higher gravity, larger pressure gradient is required to maintain them in hydrostatic equilibrium. This results in increased core temperature and luminosity, and the fuel burns faster. Hence, the life time of massive stars is smaller compared to low-mass stars. The stars spend longest time on MS.

Once the hydrogen in the core is exhausted, the star again collapses under its gravity and it enters the giant phase. The major nuclear reaction is the hydrogen burning in a shell surrounding the core. While the He core keeps contracting under the gravity, more and more He is added to the core as a result of the hydrogen

burning. The outer layers of the star expands, cools and becomes convective. As a result, the star moves towards lower temperature on H-R diagram (Figure 1.1). This phase is known as the sub-giant phase. As the convective envelope deepens, the products of the stellar nucleosynthesis is brought to the surface by a process called First Dredge-Up (FDU). FDU alters the surface composition of the star. Then the star ascends the giant branch known as Red Giant Branch (RGB). The core continues to contract until the temperature reaches $\sim 10^8$ K. At this temperature, He in the core is ignited and carbon is formed through triple alpha reaction. In the case of low-mass stars, the He ignition takes place under degenerate condition which leads to an explosive burning known as core He flash. In massive stars, He burns in a quiescent manner under non-degenerate condition. This terminates the RGB phase. The maximum mass limit for the degenerate core He burning is $2.25 M_{\odot}$ at $z = 0.02$ (Karakas 2010). This mass limit separates low- and intermediate-mass stars.

When the luminosity of the star decreases, the star contracts and the core temperature increases. It settles to a stage where He burning occurs in a convective core, and hydrogen burning in a shell. This stage is known as Horizontal Branch (HB). This phase is also known as He main sequence.

After the core He exhaustion, low- and intermediate-mass stars ($0.8 - 8 M_{\odot}$) ascends the giant branch for the second time, which is known as Asymptotic Giant Branch (AGB). The schematic diagram of the structure of an AGB star is shown in Figure 1.2. AGB stars have an inert C-O core, a He-shell, an intershell region, a H-shell, and a convective envelope. Due to the structural re-adjustment of the nuclear burning to a He-shell, the star expands and the H-shell extinguishes. This results in an inward movement of the convective envelope up to the region of hydrogen burning and mixes the products of nucleosynthesis to the surface. This is called the Second Dredge-Up (SDU). The SDU alters the surface abundances of ${}^4\text{He}$ and ${}^{14}\text{N}$. This phase of stellar evolution is known as Early-AGB (E-AGB) stage. After

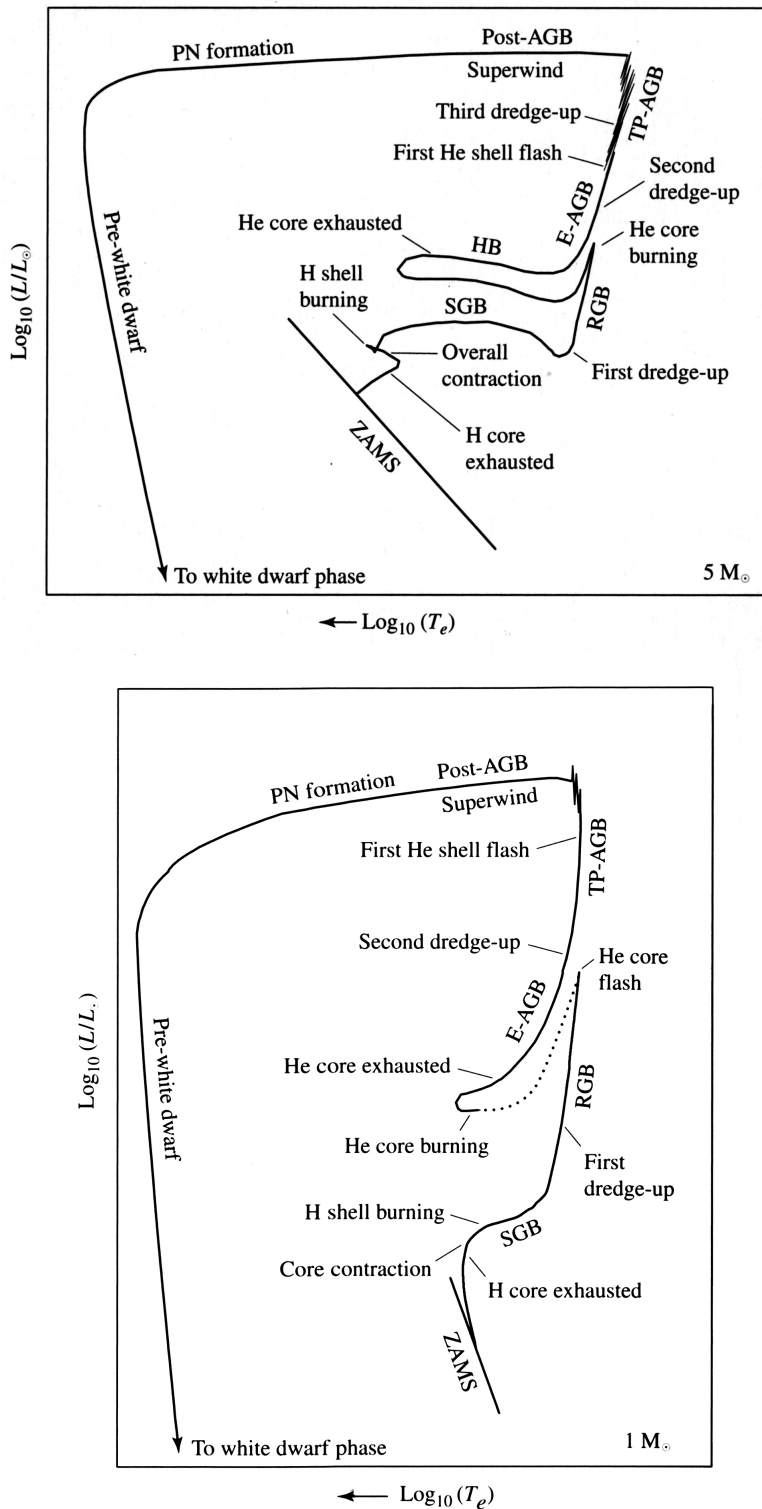


FIGURE 1.1: Evolution of $1 M_{\odot}$ (lower panel) and $5 M_{\odot}$ (upper panel) stars on the H-R diagram. Image source: *M. Pettini: Structure and Evolution of Stars - Lecture 13*.

the SDU, the star contracts, and H-shell burning is sustained. This restricts the He-shell to be thin. The H-shell burning builds up He and it burns explosively in the He-shell (He-shell flash). This marks the beginning of Thermally Pulsing AGB (TP-AGB) phase. The He-shell burning is known as thermal pulse (TP) and H-shell burning is known as interpulse (IP). The TP lasts for a few hundred years and IP lasts for $\sim 10^4$ years. During the TP, He-shell flash produces luminosity up to $\sim 10^8 L_\odot$, which causes the expansion of the outer layers of the star, and extinguishes the H-shell. The energy produced during the TP creates a convective region in the He-shell which is called a He-intershell (IS) region. This flash driven convection homogenizes the abundance in the IS region. Once the flash dies down, the convective envelope moves inward to the region which was previously mixed by the preceding flash-driven convection and mixes carbon and other products of He burning to the surface. This is known as Third Dredge-Up (TDU). The star then contracts and the H-shell is re-ignited and the process repeats. So, series of TP-TDP-IP alters the surface abundance of AGB stars significantly. The final surface composition depends on the metallicity and initial mass of the AGB star. This TDU can convert a star to a carbon star ($C/O > 1$). However, extra-mixing processes on the AGB such as Hot-Bottom Burning (HBB, in inter-mediate mass AGB stars) and Cool-Bottom Processing (CBP, in low-mass AGB stars) prevents a star from becoming a carbon star. These extra-mixing are operated when the base of the convective envelope dips into the top of H-burning shell. The Ne - Na, Mg - Al cycle etc. operates during the HBB depending on the temperature. These mixing processes also alter the surface abundances of Li, N, F, Na, Mg, Al etc. Strong expansion and contraction of the envelope of the AGB star causes the substantial mass-loss in the form of planetary nebula, and enrich the ISM with various nucleosynthesis products.. Mass-loss terminates the TP-AGB phase.

The low- and intermediate-mass stars do not attain the temperature sufficient to ignite the central carbon burning and end their life as C-O white dwarfs. However, massive stars ($> 11 M_\odot$), undergo central carbon, neon, oxygen and silicon

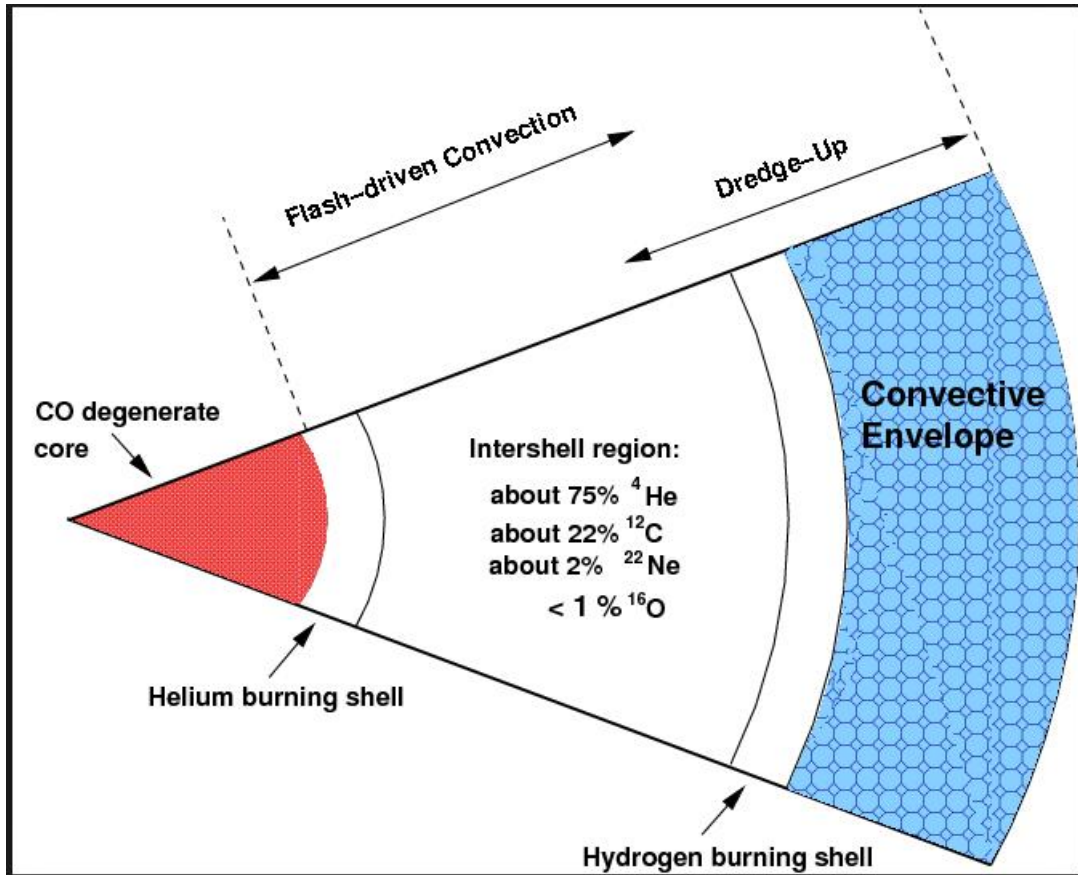


FIGURE 1.2: Schematic representation of the structure of an AGB star. Image source: Karakas (2010).

burning. At the end of these different burning stages, they attain an Fe core, and explode as core collapse supernova. Different evolutionary stages of low-, intermediate-, and high-mass stars are shown in Figure 1.3.

1.2.3 Neutron-capture nucleosynthesis

Elements beyond Fe can not be produced through charged particle interactions such as α and proton capture reactions due to the higher electrostatic repulsion. All the elements beyond Fe are produced through neutron capture reactions of abundant Fe-peak elements. Depending on the neutron flux available for the

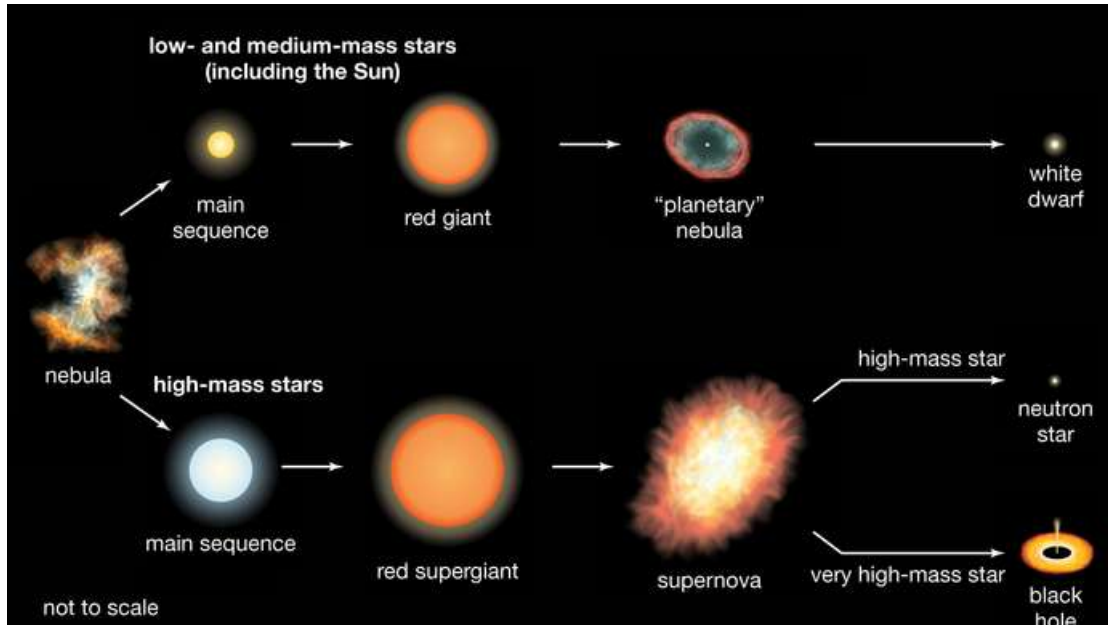


FIGURE 1.3: Different evolutionary stages of low-, intermediate-, and high-mass stars. Image Credit: <https://www.britannica.com/science/star-astronomy/Star-formation-and-evolution>

seed nuclei, it is classified as slow-neutron capture process (s-process) and rapid-neutron-capture process (r-process).

1.2.3.1 The rapid-neutron capture process

In r-process, neutron capture occurs much faster than the β -decay of the unstable isotope and occurs in 0.01 - 100 sec. It requires high neutron flux of the order of $N_n \approx 10^{22-25}$ neutrons cm^{-3} and produces isotopes up to neutron drip line which then decay to stable neutron-rich isotopes when the neutron flux stops. Because of the extreme conditions required, it is hypothesized to occur during core-collapse SNe (Qian 2000; Argast *et al.* 2004; Arcones and Thielemann 2013), fallback SNe (Fryer *et al.* 2006), neutron star mergers (Tanvir *et al.* 2013; Rosswog *et al.* 2014; Abbott *et al.* 2017; Drout *et al.* 2017; Lippuner *et al.* 2017; Shappee *et al.* 2017) or neutron star - black hole mergers (Surman *et al.* 2008). It mainly produces

elements in the range $70 \leq A \leq 209$. Examples of r-process elements are Eu, Hf, Th etc.

1.2.3.2 The slow-neutron-capture process: AGB nucleosynthesis

As the name suggests, s-process is slow compared to the β -decay of unstable isotopes, i.e, the neutron-capture occurs on a larger timescale than the β -decay timescale ($\tau_n \gg \tau_\beta$). Hence, the unstable isotope will undergo β -decay before proceeding to another n-capture. As a result, s-process produces isotopes along the valley of β -stability. It occurs at relatively low neutron densities. Low- and intermediate-mass AGB stars are the predominant sites for s-process nucleosynthesis (Busso *et al.* 1999; Karakas *et al.* 2006; Herwig 2005; Karakas and Lattanzio 2014). Sr, Y, Zr, Ba, La, Pb etc. are a few examples of s-process elements. The neutron source, neutron density, and final abundance pattern depends on the metallicity and initial stellar mass. The two important neutron sources in AGB stars are $^{13}\text{C}(\alpha, \text{n})^{16}\text{O}$ and $^{22}\text{Ne}(\alpha, \text{n})^{25}\text{Mg}$.

The main neutron source in low-mass (LM) AGB stars ($M \leq 3 M_\odot$) is $^{13}\text{C}(\alpha, \text{n})^{16}\text{O}$. There must be enough ^{13}C present in the intershell region for the s-process to take place effectively. However, the amount ^{13}C left in this region from the CN cycle is not sufficient to run the s-process. So, the operation of this neutron source demands the occurrence of proton capture as well as α capture reactions. However, intershell region is devoid of protons. So, additional protons have to be mixed to this region. During each TDU, the penetration of the H-rich convective envelope to the intershell region results in the partial mixing of protons and a Partial Mixing Zone (PMZ) forms. The proton capture of abundant ^{12}C in the intershell region lead to the formation of ^{13}C in a tiny region (^{13}C pocket) in the top layers of the intershell region through $^{12}\text{C}(\text{p},\gamma)^{13}\text{N}(\beta^+\nu)^{13}\text{C}$ (Busso *et al.* 1999; Goriely and Mowlavi 2000; Karakas 2010; Karakas and Lattanzio 2014; Bisterzo *et al.* 2017;

Kobayashi *et al.* 2020). The $^{13}\text{C}(\alpha, \text{n})^{16}\text{O}$ reaction occurs under the radiative conditions (Straniero *et al.* 1995) at temperatures $\geq 90 \times 10^6$ K. Then neutrons are produced in the ^{13}C pocket, and the s-process takes place here during the IP. Then, the products of s-process are mixed over the intershell region during the next TP and brought to the surface by TDU (Straniero *et al.* 1995; Karakas and Lattanzio 2014). This neutron source operates at a timescale of 10^3 - 10^4 years and produces neutron densities of the order of $\sim 10^8$ neutrons cm^{-3} (Karakas 2010; Karakas and Lattanzio 2014; Frebel 2018).

The major neutron source in intermediate-mass (IM) AGB stars ($M \geq 4 M_\odot$) is $^{22}\text{Ne}(\alpha, \text{n})^{25}\text{Mg}$. Unlike the $^{13}\text{C}(\alpha, \text{n})^{16}\text{O}$, this neutron source is direct, i.e., successive α capture and β -decay of the ^{14}N in the intershell region produces ^{22}Ne through $^{14}\text{N}(\alpha, \gamma)^{18}\text{F}(\beta^+ \nu)^{18}\text{O}(\alpha, \gamma)^{22}\text{Ne}$ (Busso *et al.* 1999; Karakas 2010; Karakas *et al.* 2012; Karakas and Lattanzio 2014). This reaction occurs under convective conditions during TP at temperatures $\geq 300 \times 10^6$ K, at timescales of ~ 10 years and produces relatively higher neutron densities of the order of $\sim 10^{13}$ neutrons cm^{-3} (Busso *et al.* 1999; Karakas and Lattanzio 2014). Since relatively high temperature is required for the operation of this neutron source, it may be marginally activated during the last few TPs in LM AGB stars.

Among the two neutron sources, $^{13}\text{C}(\alpha, \text{n})^{16}\text{O}$ source has the higher neutron exposure (τ , time averaged neutron flux in mbarn^{-1}) due to the larger timescale. The s-process pattern has three distinct components that are characterized by three different neutron exposures, namely, weak component, main component and strong component. The weak component requires $\tau \sim 0.06 \text{ mbarn}^{-1}$ and produces elements from Fe to Sr ($A \leq 90$). It occurs in the He and C burning shells of the massive stars ($M > 12 M_\odot$). This produces s-process abundance pattern similar to the IM AGB stars (Heil *et al.* 2008b; Pignatari *et al.* 2010). Fast rotating, low-metallicity stars are also found to produce the weak component (Frischknecht *et al.* 2016; Choplin *et al.* 2018; Limongi and Chieffi 2018). The neutron source

for the weak component is $^{22}\text{Ne}(\alpha, \text{n})^{25}\text{Mg}$. The main component is produced in LM AGB stars, and results in the production of elements from Sr to Pb ($90 \leq A \leq 204$) where $\tau \sim 0.3 \text{ mbarn}^{-1}$ (Busso *et al.* 1999, 2001; Herwig 2005). The strong component is responsible for the production of Pb when $\tau \sim 7.0 \text{ mbarn}^{-1}$ and it occurs in very low-metallicity, low-mass AGB stars (Busso *et al.* 1999; Karakas and Lattanzio 2014).

The s-process abundance pattern is characterized by three s-process peaks: first peak at $Z = 38 - 40$ (Sr, Y, Zr; light s-process elements - ls), second peak at $Z = 56 - 60$ (Ba - Nd; heavy s-process elements - hs) and third peak at $Z = 82$ (Pb). These nuclei have magic number of neutrons (50, 82 and 126, Pb has magic number of protons as well with $Z = 82$) and act as bottlenecks during the s-process. Hence, this results in the piling up of these nuclei and give rise to the observed peaks. The s-process peaks for solar system abundance are shown in Figure 1.4. In LM AGB stars, second peak elements are produced in excess over the first peak, and vice-versa in IM AGB stars.

1.3 Contribution of AGB stars to the Galactic chemical enrichment

The stellar population in our Galaxy is dominated by stars in the mass range $0.8 - 10 M_{\odot}$ (Karakas and Lattanzio 2014). The stars with masses in the range $0.8 - 2.25 M_{\odot}$ are called as low-mass stars, and those with masses in the range $2.25 - 10 M_{\odot}$ are generally called as intermediate-mass stars (Karakas and Lattanzio 2014). These stars are the sites of various nucleosynthesis and important participants of chemical evolution of the Universe (Travaglio *et al.* 2001, 2004; Romano *et al.* 2010; Kobayashi *et al.* 2011, 2020). As they evolve through different stages of stellar evolution, they enriched the ISM through stellar outflows or

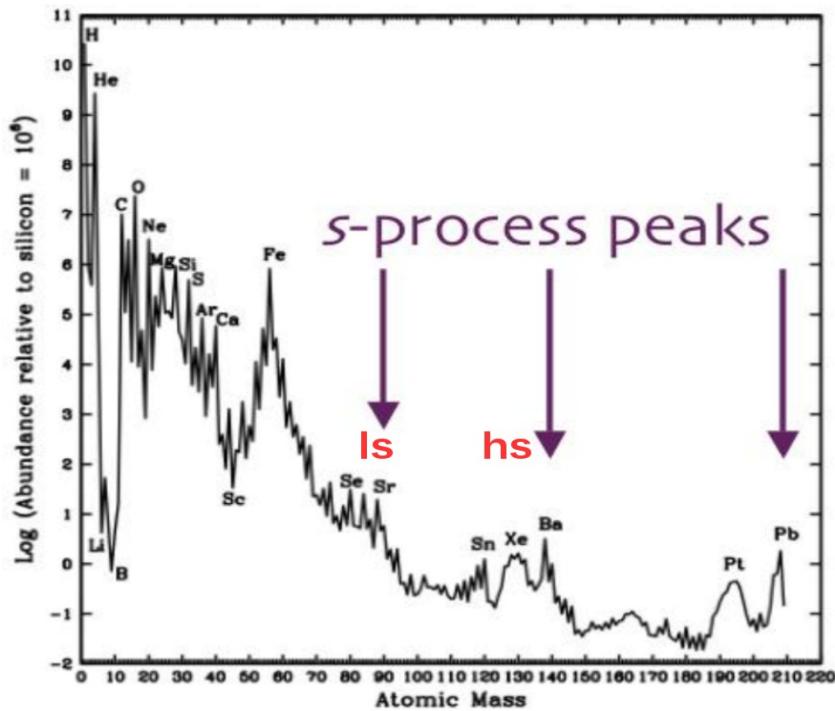


FIGURE 1.4: The s-process peaks for the solar system abundance. Image source: Karakas (2010)

winds. The pollution from these low- and intermediate- mass stars account for about 90% of the ISM dust, and the rest comes from massive stars (Sloan *et al.* 2008). The rich nucleosynthesis occurs during the AGB phase that produces a diverse range of elements, which are subsequently ejected to the ISM. All the low- and intermediate-mass stars pass through the AGB phase. Since the AGB stars we observe today were formed in the past, their presence carry information about the galactic history, which makes them tracers of stellar population (Habing and Whitelock 2004). Until recently, it was believed that the core-collapse and Type 1a SNe had contributed the elements to the Universe and the contribution from AGB stars were ignored (Timmes *et al.* 1995; Gibson 1997; Kobayashi *et al.* 2006). The last decade has witnessed several studies that revealed the importance of AGB stars in the chemical evolution of the galaxies without which the picture of origin and evolution of elements in the Galaxy would be incomplete. So, the knowledge about the AGB evolution as well as nucleosynthesis is vital to understand the contribution of low- and intermediate-mass stars to the chemical evolution of the

Galaxy.

AGB stars are important polluters of the ISM and predominant sites for the slow neutron-capture nucleosynthesis, and major contributors of elements heavier than iron; up to half of all the heavy elements are produced through s-process (Busso *et al.* 1999). There are certain isotopes like ^{86}Sr , ^{96}Mo , ^{104}Pd , ^{116}Sn etc., which are known to be produced exclusively through s-process. It has been estimated that a third of the total carbon content in the Galaxy is produced in AGB stars, which is about the same amount as produced in CCSNe and Wolf-Rayet stars (Dray *et al.* 2003; Kobayashi *et al.* 2011). Besides these, the intermediate-mass AGB stars are the major producers of ^{13}C and ^{14}N in the Galaxy (Henry *et al.* 2000; Kobayashi *et al.* 2011; Merle *et al.* 2016). AGB stars contribute considerably to the Galactic fluorine (Renda *et al.* 2004; Kobayashi *et al.* 2011), sodium (Mowlavi 1999a; Goriely and Mowlavi 2000), Mg (Fenner *et al.* 2004) and neutron rich isotopes of neon and oxygen (Kobayashi *et al.* 2011). Understanding the nucleosynthesis and evolution of Asymptotic Giant Branch (AGB) stars are of primary importance as they are the major factories of some key elements in the Universe (Busso *et al.* 1999; Herwig 2005).

Even though, AGB stars are important probes for the chemical evolution studies of the Galaxy, there are still many unknowns about their evolution and nucleosynthesis. There are a number of uncertainties related to the modelling of AGB stars. The physics of mixing is poorly understood and the associated roles of convection, rotation, overshooting, thermohaline mixing, magnetic field must be constrained properly (Karakas and Lattanzio 2014; Abate *et al.* 2015b). Despite the various mechanisms suggested for the proton diffusion (convective overshoot (Herwig 2000; Cristallo *et al.* 2009, 2011), gravity waves (Denissenkov and Tout 2003), rotation (Herwig *et al.* 2003; Piersanti *et al.* 2013)), the exact mechanism is not yet clearly understood. The extent and the exact shape of the ^{13}C pocket in the intershell region also remains unknown. Other uncertainties include the

unknown mass-loss rate, unknown reaction rates of the two major neutron sources, unknown neutron-capture cross-sections of several key isotopes etc. (Izzard *et al.* 2007; Marigo and Aringer 2009; Bisterzo *et al.* 2015; Karakas and Lugaro 2016; Buntain *et al.* 2017; Cescutti *et al.* 2018). These theoretical uncertainties hinder a better understanding of the contribution of these stars to the Galactic chemical enrichment. This demands a need for detailed chemical composition studies for an extended sample of AGB stars. However, there are certain challenges associated with the observations of AGB stars. The spectra of the AGB stars are complicated as it is overwhelmed with the molecular contributions arising due to their low photospheric temperature (\sim 3000 - 4000 K, see eg. Jeffery 2010). This makes the derivation of exact elemental abundance difficult. Another challenge is that, due to the short duration of the AGB phase (1% of the total stellar lifetime), they are relatively rare compared to other evolutionary stages (Abate *et al.* 2015b). So, to overcome these observational limits, we have to search for the signatures of the AGB nucleosynthesis outside them. In this regard, the extrinsic stars in a binary system (with AGB companion), which are known to have received products of AGB phase of evolution via binary mass transfer mechanisms, form vital tools to trace the AGB nucleosynthesis. The AGB nucleosynthesis is accessible observationally in these metal-poor extrinsic stars. The important classes of such extrinsic stars are barium, CH, CEMP-s, and CEMP-r/s stars. The analysis of generally hotter spectra of these stars is relatively accurate. A discussion on these stars is given in the next section.

1.4 Metal-poor stars

1.4.1 Nomenclature

The quantity of a chemical element in a star is expressed in terms of absolute abundance. It is defined relative to hydrogen in logarithmic scale and is given by,

$$\log \epsilon(A) = \log_{10}\left(\frac{N_A}{N_H}\right) + 12$$

where N_A and N_H stand for the number of atoms of any element A and hydrogen, respectively. Here, 12 is the absolute abundance of hydrogen. In the absolute abundance scale, by definition, hydrogen abundance is set to 12 (Piersanti *et al.* 2007).

In astronomy, usually, the abundance of an element with respect to another is defined relative to their abundance ratios in sun. For the elements A and B, the abundance ratio can be expressed mathematically as;

$$[A/B]_\star = \log_{10}\left(\frac{N_A}{N_B}\right)_\star - \log_{10}\left(\frac{N_A}{N_B}\right)_\odot$$

where N_A and N_B are number of atoms of A and B respectively.

The metallic content of a star is represented by the term ‘metallicity’, which has traditionally been represented by the iron content of the star, [Fe/H]. Because of the ample number of Fe lines found in the solar spectra, Fe is taken as a proxy for metals. By definition, solar metallicity $[Fe/H] = 0$. The stars with lower Fe content than the sun are known as metal-poor stars, and those with higher Fe content than the sun are metal-rich stars. Table 1.1 shows the metallicity-based nomenclature of the metal-poor stars. To date, stars with metallicities $[Fe/H]$ ranging from $+0.7$ to -7.3 have been discovered (Keller *et al.* 2014; Ness and Freeman 2016). The lowest predicted observable metallicity in the Galaxy is ~ -8.0 (Frebel *et al.* 2009).

TABLE 1.1: Nomenclature of metal-poor stars

Description	Definition	abbreviation
Population III stars	Postulated first stars, formed from metal-free gas	Pop III
Population II stars	Old (halo) stars formed from low-metallicity gas	Pop II
Population I stars	Young (disk) metal-rich stars	Pop I
Super-metal-rich stars	$[Fe/H] > 0$	MR
Solar	$[Fe/H] = 0$	None
Metal-poor	$[Fe/H] < -1$	MP
Very metal-poor	$[Fe/H] < -2$	VMP
Extremely metal-poor	$[Fe/H] < -3$	EMP
Ultra metal-poor	$[Fe/H] < -4$	UMP
Hyper metal-poor	$[Fe/H] < -5$	HMP
Mega metal-poor	$[Fe/H] < -6$	MMP
Septa metal-poor	$[Fe/H] < -7$	SMP
Octa metal-poor	$[Fe/H] < -8$	OMP
Giga metal-poor	$[Fe/H] < -9$	GMP
Ridiculously metal-poor	$[Fe/H] < -10$	RMP

Note: Adopted from Frebel (2018)

1.4.2 Metal-poor stars: Fossil records of the Universe

The chemical evolution of the Universe is a long-term process that started from the element enrichment by the exploding first stars that hardly contains any metals and progressing till now to the formation of the stars that contains 2 - 4 % metals (Frebel 2018). As the Universe started with a very low-metallicity, i.e., mostly with H, He and a trace of other heavy elements, low-metallicity of stars also indicate ‘old age’ for the stars. These ancient, undisturbed stars are the window to the early Galaxy. They are the local equivalents of high red-shift universe that enable us to look back in time, up to the era of the very first stars that set in motion the chemical evolution that continues even now. They are of greatest importance for stellar archaeology. The stars in the Galaxy can tell us the chemical history of the 13 billion year old Universe.

Metal-poor stars are long-lived, low-mass Pop II objects formed from the ejecta of Pop III stars. They are mostly in their Main-Sequence and giant phase of stellar evolution. They are powerful tool to investigate the chemical and dynamical evolution of the Galaxy as their least-evolved atmospheres preserve the true chemical imprints of the nucleosynthesis process operated at the earlier time. They help us to reconstruct the chemical evolution of the elements; the earliest stages of Galactic chemical evolution are probed by the most metal-poor stars. Thus, the metal-poor stars, the fossil records of the Universe, form unique treasures to the nuclear astrophysicists by providing the insight about the nucleosynthesis history that cannot be studied with nuclear physics experiments. The systematic research in the stellar observations complemented with the nuclear physics experiments and the theoretical investigations would lead to the complete understanding of the cosmic origin and evolution of elements. Among several contemporary issues of interest, metal-poor stars can provide insight into;

- i) the nature of first stars (Pop III) in the universe
- ii) predictions of element production by supernovae
- iii) early nucleosynthesis and early Galactic chemical evolution
- iv) astrophysical sites for the production of neutron-capture elements
- v) the primordial Li abundance

For the wealth of information they could provide on the chemical evolution of the Galaxy, they have been extensively exploited in literature in past few decades. Considerable efforts have been invested to identify them by means of several surveys such as HK survey (Beers *et al.* 1985, 1992, 2007; Beers 1999), Hamburg/ESO Survey (HES; Christlieb *et al.* 2001a,b; Christlieb 2003; Christlieb *et al.* 2008), Sloan Digital Sky Survey (SDSS; York *et al.* 2000), Sloan Extension for Galactic Understanding and Exploration (SEGUE; Yanny *et al.* 2009), LAMOST (Large Sky Area Multi-Object Fiber Spectroscopic Telescope) survey (Cui *et al.* 2012; Deng *et al.* 2012; Zhao *et al.* 2012) etc.

TABLE 1.2: Classification of metal-poor stars

Signature	Definition	abbreviation
Main r-process	$0.3 \leq [\text{Eu}/\text{Fe}] \leq +1.0$ and $[\text{Ba}/\text{Eu}] < 0.0$	r-I
	$[\text{Eu}/\text{Fe}] > +1.0$ and $[\text{Ba}/\text{Eu}] < 0.0$	r-II
Limited r-process	$[\text{Eu}/\text{Fe}] < 0.3$, $[\text{Sr}/\text{Ba}] > 0.5$ and $[\text{Sr}/\text{Eu}] > 0.0$	r _{lim}
s-process	$[\text{Ba}/\text{Fe}] > +1.0$, $[\text{Ba}/\text{Eu}] > +0.5$, $[\text{Ba}/\text{Pb}] > -1.5$	s
r- and s-processes	$0.0 < [\text{Ba}/\text{Eu}] < +0.5$ and $-1.0 < [\text{Ba}/\text{Pb}] < -0.5$	r+s
i-process	$0.0 < [\text{La}/\text{Eu}] < 0.6$ and $[\text{Hf}/\text{Ir}] \sim 1.0$	i
Neutron-capture normal	$[\text{Ba}/\text{Fe}] < 0.0$	No
Carbon enhancement	$[\text{C}/\text{Fe}] \begin{cases} \geq +0.7; & \text{if } \log(L/L_\odot) \leq 2.3 \\ \geq +3.0 - \log(L/L_\odot); & \text{if } \log(L/L_\odot) > 2.3 \end{cases}$	CEMP
α -enhancement	$[\text{Mg}, \text{Si}, \text{Ca}, \text{Ti}/\text{Fe}] \sim +0.4$	α -enhanced

Note: Adopted from Frebel (2018)

1.4.3 Sub-classification of metal-poor stars

With the advent of high-resolution spectroscopy, analysis of metal-poor stars have shown that they show diverse abundance patterns, especially enhanced abundance of neutron-capture elements (both r-process and s-process). Some stars are enhanced in r-process elements, some in s-process elements and some in both.

A classification of metal-poor stars based on the level of enhancement of different elements is given in Table 1.2. Here, we will discuss in detail the different classes of metal-poor stars, along with the relatively metal-rich Ba stars that are relevant to this study.

1.4.3.1 Ba stars

Barium (Ba II) stars belong to a family of peculiar G and K spectral type which were first identified by Bidelman and Keenan (1951). They are mostly in their

main sequence and giant phase of stellar evolution, with a surface temperature of 4000 - 6500 K. Their envelope exhibits overabundance of elements heavier than iron, and usually $\text{C}/\text{O} < 1$ (Barbuy *et al.* 1992; Allen and Barbuy 2006; Drake and Pereira 2008; Pereira and Drake 2009). They exhibit abnormally strong lines of Ba II 4554 Å, Sr II 4077 Å, as well as enhanced CH, CN, and C_2 molecular bands. They also show enhanced abundances of other neutron-capture elements. Analysis of Luck and Bond (1991) shows that, in metal-deficient Ba stars, C_2 molecular bands are not strong as compared to the classical Ba stars. They are low radial-velocity ($|\text{V}_r| < 100 \text{ km s}^{-1}$) objects and generally members of Galactic disk.

Most of the barium stars are found to be in binaries (McClure *et al.* 1980; McClure 1983, 1984; McClure and Woodsworth 1990; Jorissen *et al.* 1998; Udry *et al.* 1998a,b) with radial velocity variability. Nucleosynthesis theories do not support occurrence of heavy element nucleosynthesis during the stellar evolutionary phases to which these stars belong. A generally accepted scenario that explains the observed high abundances of neutron-capture elements is a binary picture. These stars are believed to have received, via binary mass transfer mechanisms, the products of the companion stars produced during their AGB phase of evolution, and the companions have become white dwarfs (WD). The presence of WDs in such binary systems is confirmed by the X-ray, UV and IR observations (Boehm-Vitense 1980; Schindler *et al.* 1982; Jorissen *et al.* 1996; Böhm-Vitense *et al.* 2000; Frankowski and Jorissen 2006; Gratton *et al.* 2021).

1.4.3.2 CH stars

CH stars are metal-poor ($-2 \leq [\text{Fe}/\text{H}] \leq -0.2$) giants, identified by Keenan (1942), with similar spectroscopic characteristics as Ba stars. They are characterized by the strong CH and C_2 molecular bands, $\text{C}/\text{O} > 1$, and strong features due to the

neutron-capture elements. The surface temperature of these objects ranges from 4000 to 4750 K. They are high radial-velocity ($|V_r| > 100 \text{ km s}^{-1}$) objects and members of the Galactic halo. Later, Bond (1974) have identified a new class of peculiar G type sub-giant stars with weak metallic lines and enhanced features due to CH and s-process elements. These stars are known as sub-giant CH stars. They are moderately metal-deficient ($-0.8 \leq [\text{Fe}/\text{H}] \leq -0.1$). They have high radial velocities ($|V_r| > 100 \text{ km s}^{-1}$) and members of Galactic thick disk. Most of the CH stars (here after CH stars refers to giant, sub-giant, and dwarf CH stars) are also found to be radial velocity variables (McClure and Woodsworth 1990; Jorissen *et al.* 2016b), which confirmed the pollution from an AGB companion through binary mass transfer. The spectral characteristics of CH stars resemble quite closely with C-R stars which are warmer than CH stars and generally belong to disk population (Goswami 2005 and references therein). Hence, CH stars can be easily mistaken as C-R stars and vice-versa. In a search for CH stars at high Galactic latitude by Goswami (2005), CH stars are distinguished from C-R stars using Ca spectral features around 4226 Å. This Ca I line is marginally noticed in CH stars, whereas in C-R stars it is as deep as the ^{12}CN band head at 4215 Å. The CN 4215 Å band in CH stars is weaker than that in C-R stars. Like CH stars, the C-R stars also exhibit strong swan C_2 bands around 4700 and 4395 Å, however, unlike the CH stars, they show near-solar abundances of s-process elements (Dominy 1984; Goswami 2005; Giridhar 2010). While CH stars are Galactic halo objects, C-R stars are found to be disk objects, in general. Detailed discussions on C-R stars can be found in Dominy (1984), Goswami (2005), Goswami (2005), Goswami *et al.* (2007), and Goswami *et al.* (2010) identified a large number of CH stars (that constitute about 30 -35% of the sample) from low- and medium-resolution spectroscopic observations of about 500 field stars and pre-select carbon stars at high Galactic latitude using HCT/HFOSC.

1.4.3.3 Carbon Enhanced Metal-Poor (CEMP) stars

Among the metal-poor stars, about 25 to 30% are known to be rich in carbon (Beers and Christlieb 2005; Frebel *et al.* 2006; Lucatello *et al.* 2006). These stars are called the Carbon-Enhanced Metal-Poor (CEMP) stars. CEMP stars are more metal-poor counterparts of CH stars ($[\text{Fe}/\text{H}] < -1$; Lucatello *et al.* 2005; Abate *et al.* 2016) which has been traditionally defined as the stars with $[\text{C}/\text{Fe}] > 1$ (Beers and Christlieb 2005). However, the definition of CEMP stars is being revised and $[\text{C}/\text{Fe}] \geq 0.70$ (Aoki *et al.* 2007; Carollo *et al.* 2012; Lee *et al.* 2013; Norris *et al.* 2013b; Skúladóttir *et al.* 2015) and $[\text{C}/\text{Fe}] > 0.90$ (Jonsell *et al.* 2006; Masseron *et al.* 2010) are also used. It has been identified that a significant fraction ($\sim 20\%$) of Very Metal-Poor ($[\text{Fe}/\text{H}] < -2$) stars in the Galaxy are CEMP stars (Rossi *et al.* 1999; Christlieb 2003; Lucatello *et al.* 2006; Carollo *et al.* 2012). The fraction of carbon-enhanced stars increases with decreasing metallicity; $\sim 40\%$ for $[\text{Fe}/\text{H}] < -3$ and $\sim 75\%$ for $[\text{Fe}/\text{H}] < -4$ (Aoki *et al.* 2013; Lee *et al.* 2013; Yong *et al.* 2013; Placco *et al.* 2014; Frebel and Norris 2015).

Based on the level of relative enrichment of neutron-capture elements, CEMP stars are classified into different sub-classes:

CEMP-s stars: These stars show enhanced abundances of s-process elements. The CEMP-s stars are considered as the metal-poor analog of Ba and CH stars, and the binary mass transfer from an evolved low-mass AGB companion is the most accepted scenario for their abundance peculiarity (Herwig 2005). The long-term radial velocity monitoring studies have shown that most of the CEMP-s stars are binaries (Lucatello *et al.* 2005; Starkenburg *et al.* 2014; Jorissen *et al.* 2016b; Hansen *et al.* 2016c), supporting the pollution from companion AGB stars.

CEMP-r stars: They show enhancement of r-process elements. Analysis of

Hansen *et al.* (2011) and Hansen *et al.* (2015) have shown that the abundance peculiarity of CEMP-r stars are not resulted from a binary mass transfer, instead due to the enrichment of their birth cloud with r-process elements from other external sources. Suggested sources that might have polluted the ISM with r-elements, from which the CEMP-r/s stars are believed to have formed, are core-collapse SNe (Qian 2000; Argast *et al.* 2004; Arcones and Thielemann 2013), fallback SNe (Fryer *et al.* 2006), neutron star mergers (Tanvir *et al.* 2013; Rosswog *et al.* 2014; Shappee *et al.* 2017; Drout *et al.* 2017; Lippuner *et al.* 2017) or neutron star - black hole mergers (Surman *et al.* 2008). The exact mechanism of their origin is not yet clear. Only a very few CEMP-r stars have been identified so far and more such stars have to be discovered and studied in detail to unravel their origin.

CEMP-r/s stars: They show simultaneous enhancement of both s- and r-process elements. A number of scenarios have been proposed for their origin (Jonsell *et al.* 2006 and references therein). Since most of the CEMP-r/s stars are also found to be binaries just like CEMP-s stars (Lucatello *et al.* 2005; Starkenburg *et al.* 2014; Jorissen *et al.* 2016b; Hansen *et al.* 2016c), binary mass transfer from the AGB companion is thought to be the reason for their origin as well, however, the presence of r-process component posed a challenge (Jonsell *et al.* 2006; Herwig *et al.* 2011; Abate *et al.* 2016). The i-process, intermediate neutron-capture process, with neutron density between s- and r- process can produce both s- and r- process elements at a single stellar site (Cowan and Rose 1977). Many studies in literature have successfully used model yields of i-process in low-metallicity, low-mass AGB stars to account for the observed abundance patterns in CEMP-r/s stars (Hampel *et al.* 2016, 2019; Goswami *et al.* 2021). Although there are several suggestions for the i-process sites, such as, super-massive AGB stars (Doherty *et al.* 2015; Jones *et al.* 2016), low-mass, low-metallicity stars (Campbell and Lattanzio 2008; Campbell *et al.* 2010; Cruz *et al.* 2013; Cristallo *et al.* 2016), Rapidly Accreting White Dwarfs (Herwig *et al.* 2014; Denissenkov *et al.* 2017) etc., the exact astrophysical site for the i-process is still debated (Koch *et al.* 2019). Several studies have shown

that the most probable site for the i-process is low-mass, low-metallicity AGB stars (Hampel *et al.* 2016; Goswami *et al.* 2021; Karinkuzhi *et al.* 2021; Purandardas and Goswami 2021). A comprehensive review of the formation scenarios and the production sites of CEMP-r/s stars is provided in Goswami *et al.* (2021).

CEMP-no stars: These stars, with a high abundance of carbon, do not show any enhanced abundance of neutron-capture elements. The origin of CEMP-no stars is also not clearly understood. They are believed to be formed from the pre-enriched ISM (Cooke and Madau 2014; Frebel and Norris 2015; Norris *et al.* 2013a). The suggested progenitors of these stars are faint SNe (Umeda and Nomoto 2005; Nomoto *et al.* 2013; Tominaga *et al.* 2014), spinstars (Meynet *et al.* 2010; Chiappini 2013), and metal-free massive stars (Heger and Woosley 2010). A recent study by Arentsen *et al.* (2019a) has shown that the binary mass-transfer from extremely metal-poor AGB companions could also be the possible progenitors of CEMP-no stars. Lot more studies need to be conducted to understand the origin and evolution of this class of peculiar stars.

1.5 Scope of the thesis

Studies on the chemical composition of metal-poor stars available in the literature are widely exploited to understand the chemical and dynamical evolution of our Galaxy. Light element abundances are available for as many as thousands of stars. However, the heavy element abundances of metal-poor stars are scarce in literature. Detailed abundance studies available for CEMP and CH stars are still limited by numbers, resolution, and wavelength regions. Several authors have discussed the need for considerably more abundance data for the lower metallicity regime (Masseron *et al.* 2010; Yong *et al.* 2013; Cristallo *et al.* 2016; Yoon *et al.*

2016; Frebel 2018). In an attempt by Cristallo *et al.* (2016) to constrain the low-mass AGB nucleosynthesis using CH stars, the scope of enhancing such studies based on a larger abundance data was highlighted. The diverse abundance ratios of neutron-capture elements observed in these stars underscore the necessity for significantly larger samples to be studied in detail. We propose to enhance this study by making a comprehensive analysis of the observed stellar abundance peculiarities. We have derived necessary clues about the evolutionary nature of these objects, as well as the production of heavy-elements via neutron-capture process operating at low-metallicity.

The thesis aims at understanding the role of metal-poor stars in the Galactic chemical enrichment and to provide tighter observational constraints from observed elemental abundances. In particular, we aim to study the contribution of low-mass stars ($0.8 - 3.0 M_{\odot}$) that undergo AGB nucleosynthesis. A detailed chemical composition analysis of stars in binary systems with now invisible white dwarf companions provide such an opportunity to understand AGB nucleosynthesis. The problem is addressed through detailed spectroscopic analysis of three sets of metal-poor stellar samples: i) a Ba stars sample, comparatively more metal-rich than CH and CEMP stars; ii) a moderately metal-poor CH stars sample; and iii) a very metal-poor CEMP-r/s and CEMP-s stars sample. The objects are selected from different catalogs of metal-poor stars identified from several large sky survey programs. High-resolution optical spectra of these objects were obtained using various observing facilities and a detailed spectroscopic analysis is performed to understand their role in the chemical enrichment of the Galaxy.

1.6 Outline of the thesis

Chapter 1: Introduction

This chapter contains a discussion of various nucleosynthesis processes and sites that contributed different elements to the Universe. A description of the AGB stars and their contribution to the chemical enrichment of the Galaxy is also provided. This chapter also includes a brief overview of metal-poor stars, as well as a discussion of their significance to Galactic chemical evolution. A detailed discussion of the different sub-classes of metal-poor stars along with their possible formation scenarios in the context of the thesis is also given. This chapter also provides a brief discussion on the scope of the thesis.

Chapter 2: Spectroscopic methodology: Sample selection, observation/- data acquisition and data analysis

This chapter describes the methods of object selection, data acquisition, data reduction and data analysis. A discussion on the stellar sample investigated in this thesis and the criteria adopted for sample selection is provided in this chapter. Details of various observing facilities used to acquire the spectra of the stellar sample are discussed here. A discussion of basic terminologies, equations, and assumptions that are used in our analysis is also given in this chapter. The data reduction and data analysis procedures, along with the codes and software used, are discussed here. A discussion on the atmospheric models, atomic and molecular line data used is also provided in this chapter. This chapter also contains, a discussion on the calculation of abundance uncertainties and the procedure adopted for the kinematic analysis of stellar sample.

Chapter 3: Analysis of Ba stars

This chapter deals with the analysis of the comparatively metal-rich stars among the sample, the Ba stars. The results of a detailed spectroscopic and kinematic analysis of 10 barium stars are presented. Several diagnostics, such as C, N, O, Na,

and Mg abundances, [hs/ls] ratio and [Rb/Zr] ratio, used to understand the nature of companion AGB stars are discussed. A comparison of the observed abundances with their counterparts observed in AGB stars is also presented. The observed abundances are also compared with the predictions from AGB nucleosynthesis models (FRUITY models). A discussion and interpretation of these results in the context of Galactic chemical enrichment history are presented in this chapter.

Chapter 4: Analysis of CH and CEMP stars

In this chapter, we have extended our analysis to the low-metallicity regime to understand the implications of low-metallicity stars on the Galactic chemical enrichment. We performed a detailed spectroscopic analysis of a selected sample of 13 CH/CEMP-s/CEMP-r/s stars. The results of the kinematic analysis and the binary status of the program stars are also discussed. The diagnostics discussed in chapter 2 are extended to these objects in order to understand the nature of their companions. A discussion on the possible origin of the CEMP-r/s stars in our sample is presented based on a comprehensive analysis of a sample of CEMP stars. Results obtained from a parametric model-based analysis considering i-process model yields for CEMP-r/s stars and yields from FRUITY models for CH and CEMP-s stars are also provided.

Chapter 5: Conclusions and future works

The key results of each chapter, as well as the conclusions of the thesis, are summarized in this chapter. Future plans following the thesis submission and future prospects of the thesis are also discussed.

Chapter 2

Spectroscopic methodology: Sample selection, observation/data acquisition and data analysis

2.1 Introduction

The light coming from the celestial bodies are the important source of most of what we know about them. This light coming from various celestial sources are analyzed through various methods to draw conclusions regarding the nature of the source. These include, spectroscopy, photometry, polarimetry etc. The most powerful among these to study the stars is spectroscopy. It is the study of the spectrum of light produced as the result of its interaction with matter. Stellar spectroscopic studies began with the discovery of spectral lines in the solar spectra by Joseph Fraunhofer in 19th century. It can be used to infer various properties of

stars such as, mass, temperature, velocities, distance, chemical compositions etc. Spectroscopy is done at different wavelengths across the electromagnetic spectrum depending on the properties to be studied, and this study deals with optical spectroscopy. This chapter discuss the methods of sample selection, observation, data processing, and analysis.

2.2 Sample selection

As a first step towards our goal, we have performed an extensive literature survey of potential metal-poor star candidates including Ba, CH, and CEMP stars. We have selected a sample of metal-poor star candidates from various sources in the literature (Lü 1991; Bartkevicius 1996; Goswami 2005; Frebel *et al.* 2006; Goswami *et al.* 2010; Beers *et al.* 2017), Catalogues of carbon stars identified from the Hamburg/ESO Survey (HES) (Christlieb *et al.* 2001a; Christlieb 2003; Christlieb *et al.* 2008), and from the LAMOST DR2 (Ji *et al.* 2016). A discussion on HES and LAMOST survey, and the criteria employed to select the targets for the high-resolution follow-up is given in this section.

2.2.1 Hamburg/ESO Survey (HES)

The Hamburg/ESO Survey (HES) is an objective-prism survey with ESO 1 m-Schmidt telescope, originally designed for bright quasar ($12.5 \leq B \leq 17.5$) searches (Wisotzki *et al.* 1996; Reimers *et al.* 1996; Wisotzki *et al.* 2000). The HES survey covers the galactic latitudes $|b| > 30^\circ$, and the declination range $-78^\circ < \delta < +25^\circ$, resulting in an effective area of 6400 deg^2 of the southern extragalactic sky (Wisotzki *et al.* 2000; Christlieb *et al.* 2001b). The wavelength coverage of the HES spectra is $3200 - 5300 \text{ \AA}$ with a spectral resolution of $\Delta\lambda \sim 10 \text{ \AA}$ at Ca II K

line ($R \sim 400$, Christlieb *et al.* 2008). Even though it is conceived for finding the quasars, resolution of the HES spectra enabled to exploit the stellar content of the survey. Among the total ~ 10 million digitized HES spectra, the stellar database consist of ~ 4 million spectra with $S/N > 5$ at Ca II K (Christlieb *et al.* 2001a,b; Frebel *et al.* 2006). Later, the stellar contents of the HES was explored by several authors in search of carbon stars (Christlieb *et al.* 2001a; Goswami 2005; Goswami *et al.* 2010), metal-poor stars (Christlieb 2003; Christlieb *et al.* 2008; Frebel *et al.* 2006; Beers *et al.* 2017), white dwarfs (Christlieb *et al.* 2001b), Horizontal Branch stars (Christlieb *et al.* 2005) etc. The spectral resolution and high S/N ratio of the HES spectra is well-suited for the identification of carbon stars and metal-poor stars without the need for follow-up spectroscopy (Christlieb *et al.* 2001a, 2008). From the HES stellar content, Christlieb *et al.* (2001a) identified 403 faint high-latitude carbon (FHLC) carbon stars based on the strength of C₂ bands around 4737 and 5165 Å, and CN bands around 3883 and 4215 Å. Follow-up medium resolution spectroscopic observations of these FHLC sample by Goswami (2005) and Goswami *et al.* (2010) have shown that $\sim 35\%$ of them are CH stars.

At the HES spectral resolution, it is possible to detect the Ca II K 3934 Å line, an indicator of [Fe/H], even in very low metallicity stars. The strength of this Ca II line combined with the B-V color information obtained from the spectra allow to effectively identify the metal-poor star candidates. The color information helps to avoid any bias against cool metal-poor giants as Ca II line is strong in cool giants even if they are metal-poor (Christlieb 2003; Christlieb *et al.* 2008). According to Christlieb *et al.* (2001b), the color range relevant to select the metal-poor stars is $-0.6 < B-V < 2.0$. About 6133 giants and 2194 turn-off stars in the range $0.5 < B-V < 1.2$ have been identified as candidate metal-poor stars from the HES spectra (Christlieb *et al.* 2008). The medium-resolution (~ 2 Å) follow-up observations carried out for 3200 candidates have shown that ~ 200 stars have $[Fe/H] < -3.0$, which outnumbers the number of extremely metal-poor stars identified in all previous surveys. About, 1785 stars among these are expected

to show enhanced abundance of carbon (characterized by the strong CH G band in the HES spectra) with $[C/Fe] > 1$ (Christlieb *et al.* 2008). A sample of 1777 bright ($9 < B < 14$) metal-poor star candidates ($0.3 < B-V < 1.2$) from HES is presented by Frebel *et al.* (2006) from the moderate-resolution ($\sim 2 \text{ \AA}$) follow-up studies.

The Metallicity Distribution Function (MDF) of HES from Christlieb (2003) and Frebel *et al.* (2006) is shown in Figure 2.1. As noted from this figure, HES is a rich source of metal-poor stars and it provides the opportunity to enhance the number of VMP and EMP stars. Several studies have shown that the probability of finding CEMP stars is higher at lower metallicity (e.g Norris *et al.* 1997; Rossi *et al.* 1999, Section 1.4.3.3). The HES sample contains many CEMP stars, as demonstrated by recent follow-up observations (e.g Aoki *et al.* 2006; Goswami *et al.* 2006; Cohen *et al.* 2006; Barklem *et al.* 2005; Goswami *et al.* 2021).

2.2.2 LAMOST Survey

Large sky Area Multi-Object Fiber Spectroscopic Telescope (LAMOST also known as Guo Shou Jing Telescope) is a large-aperture (effective aperture $\sim 3.6 - 4.9 \text{ m}$) and a wide-FOV (5°) reflecting telescope designed for astronomical spectroscopic surveys (Cui *et al.* 2012; Zhao *et al.* 2012). The first phase of the survey is the LAMOST low-resolution spectroscopic survey (LAMOST-LRS) between 2011 - 2017. LAMOST-LRS spectra covers the wavelength range $3700 - 9000 \text{ \AA}$ with a spectral resolution of $R \sim 1800$ (Zhao *et al.* 2012). This survey targeted the objects in the magnitude range $9 \leq r \leq 17.5$, and galactic longitude range $90^\circ \leq l \leq 220^\circ$ (Deng *et al.* 2012). One of the important advantages of the LAMOST survey is that the apparent magnitudes are in the range suitable for the high-resolution follow-up observations with 4 - 10 m class telescopes (Li *et al.* 2018a). The LAMOST-LRS has two main parts: i) the LAMOST Experiment for Galactic

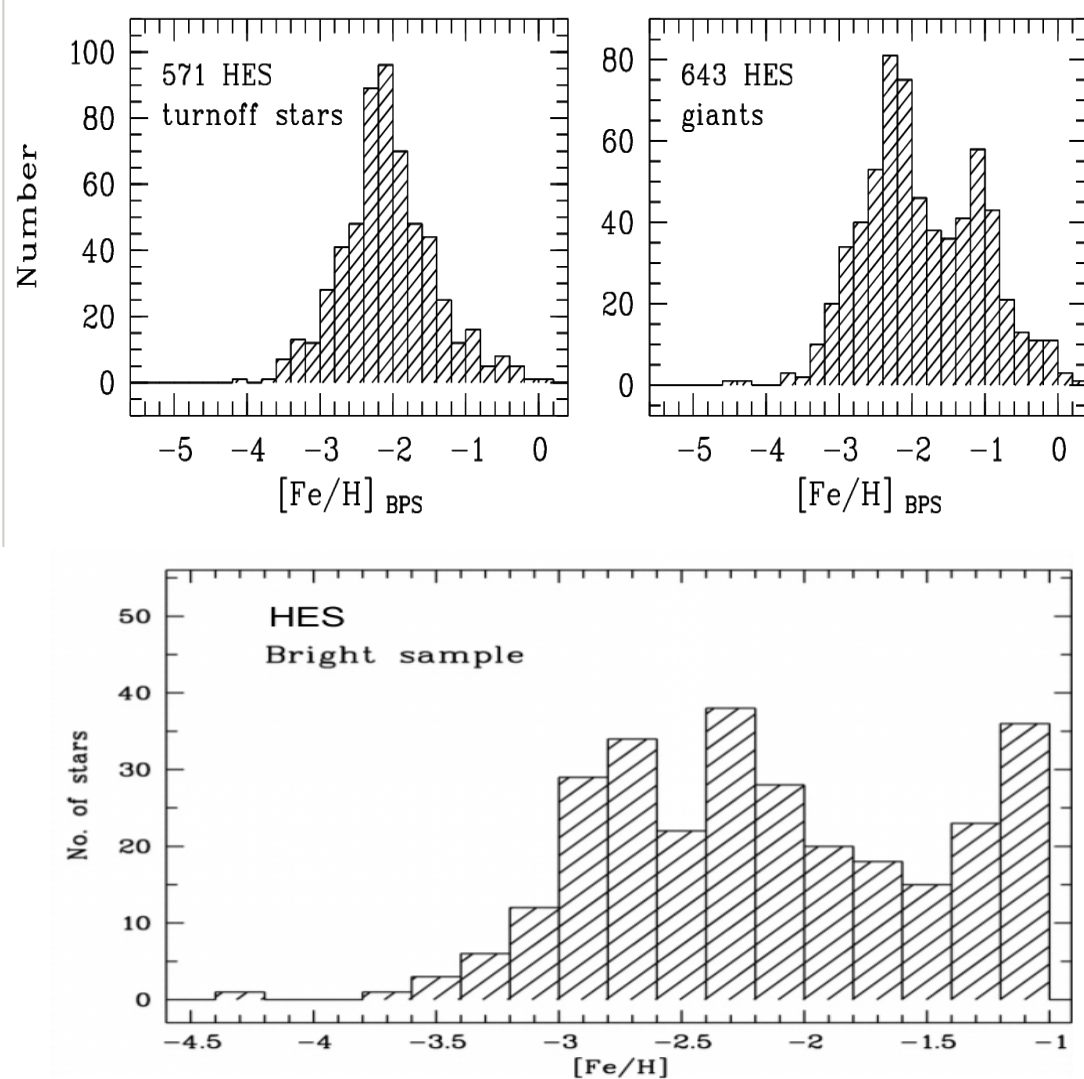


FIGURE 2.1: Metallicity Distribution Function (MDF) of the HES from Christlieb (2003) (upper panel) and Frebel *et al.* (2006) (lower panel).

Understanding and Exploration (LEGUE) survey that focused to study the stars and the Milky Way (MW), and ii) the LAMOST Extra Galactic Survey (LEGAS) focused mainly on galaxies and quasars (Deng *et al.* 2012; Yan *et al.* 2022). The LEGUE survey is a larger, deeper, and denser spectroscopic survey of the MW that surveyed large samples of stars in the disk and halo of the Galaxy. The majority of the stars observed in this survey belong to the F, G, and K spectral types on either main-sequence or giant phase (Liu *et al.* 2015; Yan *et al.* 2022), and constitutes the largest set of stellar spectral database (~ 10 million) in the

northern sky (Yan *et al.* 2022) till date.

The spectral resolution and the wavelength coverage of the LAMOST spectra allowed for the reliable estimation of the atmospheric parameters of the stars (e.g Figure 4 of Li *et al.* 2018a), and resulted in the identification of many metal-poor stars and carbon stars. From the LAMOST pilot survey (first phase of LEGUE survey between 2011 - 2012, Deng *et al.* 2012; Zhao *et al.* 2012; Luo *et al.* 2012), 183 carbon stars were identified by Si *et al.* (2015), among which 69 stars are identified to be CH stars. Ji *et al.* (2016) have identified 894 carbon stars from 4 million stellar spectra in the LAMOST DR2. Among these carbon stars, 339 stars ($\sim 38\%$) are identified to be CH stars from the spectral features such as CH G band, CN band, Ca II, Ba II, and H_{α} lines (Ji *et al.* 2016). Li *et al.* (2018b) presented a catalogue of 10,008 VMP stars ($-4.5 \leq [\text{Fe}/\text{H}] \leq -2$, $4000 \leq T_{\text{eff}} \leq 7000$ K) identified from the LAMOST DR3, the largest catalogue of VMP stars ever. The MDF of these sample of stars (adopted from Li *et al.* 2018a) is shown in Figure 2.2. Majority of the stars in this sample belongs to the metallicity range -3 to -2 . Among these 10,008 stars, they have identified 636 CEMP star candidates. A catalogue of 2651 carbon stars identified from LAMOST DR4 is presented by Li *et al.* (2018b), based on a series of spectral features. Among these carbon stars, 864 stars are identified to be CH stars. Besides these carbon stars, they have identified 17 CEMP turn-off star candidates, an extremely rare class of stars.

2.2.3 Criteria for sample selection

- Ba star candidates are selected from the catalogue of Ba stars by Lü (1991) and from the catalogue of CH and related stars by Bartkevicius (1996). A few CH star candidates are also selected from the catalogue of Bartkevicius (1996).

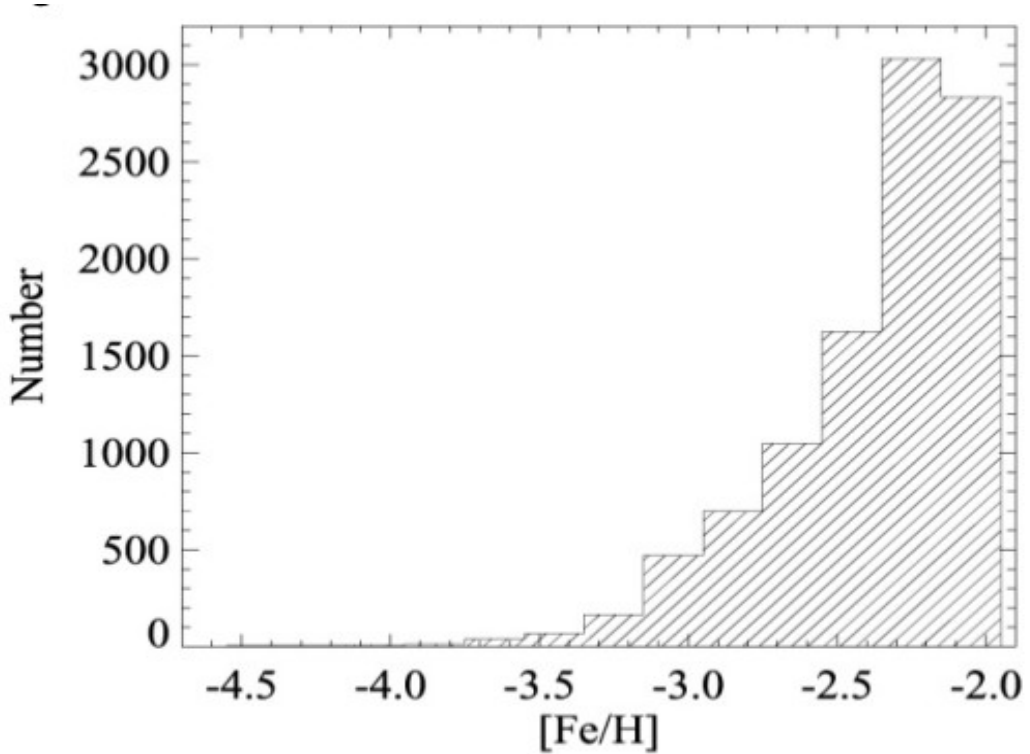


FIGURE 2.2: Metallicity Distribution Function (MDF) of the LAMOST DR3 by Li *et al.* (2018b).

- We have also selected a few stars from the list of stars that are identified to be CH stars from medium-resolution spectroscopic follow-up of carbon star candidates from the HES (Christlieb *et al.* 2001a; Goswami 2005; Goswami *et al.* 2010) based on the spectral features such as CH, C₂, CN bands, Ca II K, and Ca I 4227 Å lines.
- The CH stars identified from the LAMOST survey based on the spectral features such as CH G, C₂, CN bands, Ca I, Ba II, and H _{α} lines (Ji *et al.* 2016) are also included in our sample.
- The CEMP-s and CEMP-r/s stars generally have metallicity in the range -3 to -1 as shown by several studies (eg. Yoon *et al.* 2016 and references therein). As seen from Figure 2.1, HES contains plenty of stars in this metallicity range. Since we are interested in CEMP-s and CEMP-r/s stars among the CEMP stars, we have selected the metal-poor candidates with -1

$\leq [\text{Fe}/\text{H}] \leq -3$ identified from HES through medium-resolution spectroscopy by Frebel *et al.* (2006); Christlieb *et al.* (2008); Beers *et al.* (2017).

- The typical surface temperatures of the Ba, CH, and CEMP stars occupy a range 4000 - 6500 K (See Section 1.4.3). Hence, we have considered stars with photometric temperatures in this range (Table 2.1). Procedure adopted for the calculation of photometric temperature is discussed in Section 2.6.4.
- The locations of the sample of stars considered for this study are shown in the color - magnitude ((B-V) v/s M_V) diagram (Figure 2.3). The color of the star is an indicator of its temperature. A color-magnitude diagram is a scatter graph that shows the relation between the absolute magnitude and color (temperature) of the astronomical objects. The (B-V) color in the range -0.6 to 2.0 is relevant to select the metal-poor stars (Christlieb *et al.* 2001b). In Figure 2.3, all the stars in our sample fall within this range, except for three objects - BD-19 132, HD 30443, and LAMOSTJ151003.74+305407.3. However, these three objects are found to be CH stars based on their spectral features from low-resolution spectra by Alksnis *et al.* (2001), Yamashita (1975), and Ji *et al.* (2016) respectively. Hence, we have included these objects in our sample.

The objects thus short-listed are then subjected to the high-resolution follow-up studies using various telescopes.

2.3 Observations and data acquisition

High-quality, high-resolution spectrum is crucial for detailed chemical abundance analysis of a star. In this section, we discuss the facilities used to acquire the

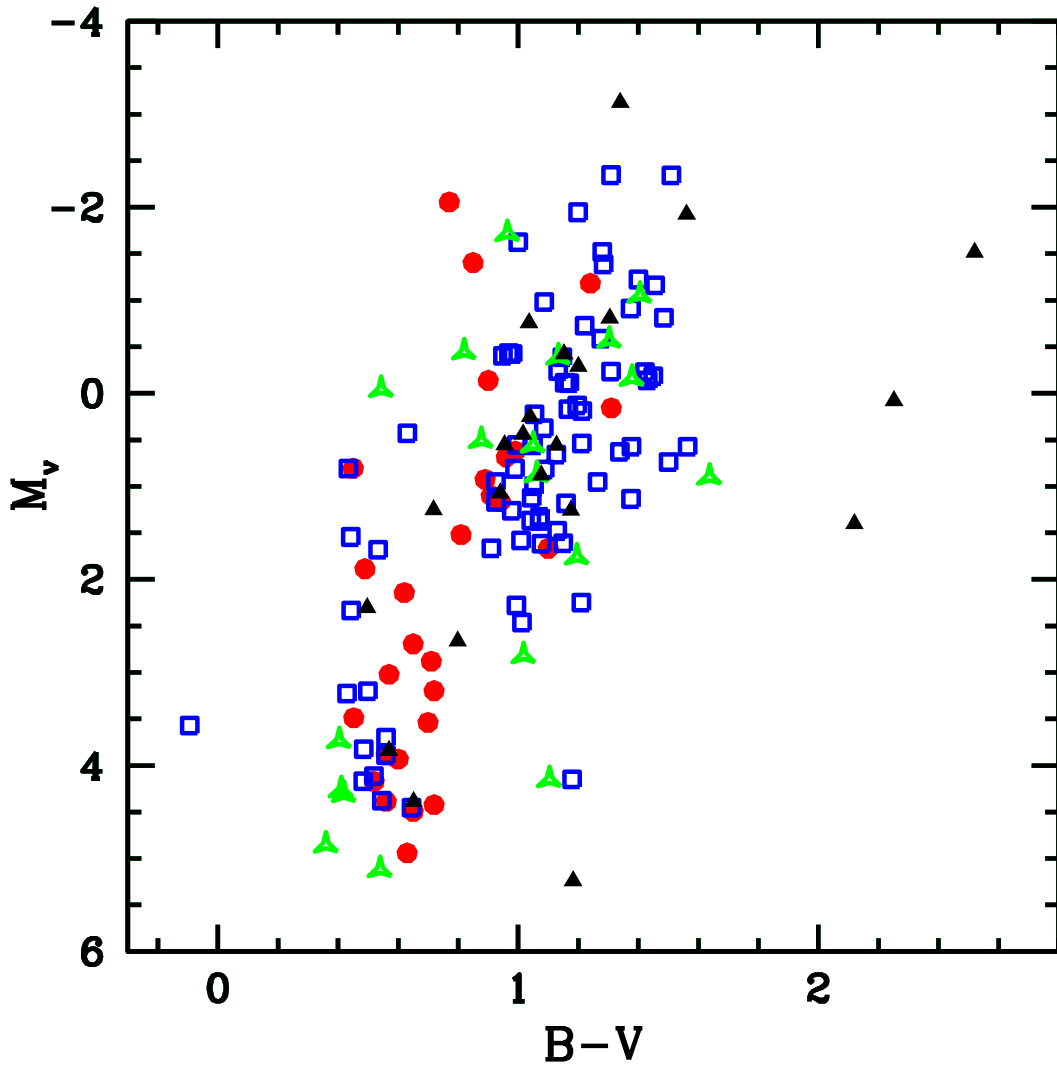


FIGURE 2.3: Location of the selected stellar sample in color - magnitude diagram. Blue open squares are Ba stars from literature (Allen and Barbuy 2006; Yang *et al.* 2016; de Castro *et al.* 2016). Red circles are CH stars from literature (Karinkuzhi and Goswami 2014, 2015; Goswami *et al.* 2016). Green starred triangles are CEMP stars from literature (Masseron *et al.* 2010 and references therein). Our stellar sample is represented by black filled triangles.

TABLE 2.1: Photometric temperature estimates (in Kelvin) of the stellar sample

Star name	T_{eff} (J-K)	T_{eff} (-0.50) (J-H)	T_{eff} (-0.05) (J-H)	T_{eff} (+0.05) (J-H)
		Ba stars		
HD 24035	4684.12	4755.15	4716.20	4705.18
HD 32712	4484.39	4569.26	4534.17	4524.18
HD 36650	4768.20	4814.32	4774.10	4762.07
HD 94518	5780.58	5953.08	5884.96	5866.22
HD 147609	6310.38	6100.99	6702.52	6677.25
HD 154276	5846.47	5990.51	5977.11	5974.15
HD 179832	4740.76	4887.54	4845.72	4915.93
HD 207585	5922.54	5940.32	5884.96	5866.22
HD 211173	4862.67	4959.03	4915.63	4903.43
HD 219116	4862.67	5046.19	5000.83	4988.11
		CH/CEMP stars		
	T_{eff}	T_{eff} (-2.0)	T_{eff} (-1.5)	T_{eff} (-1.0)
BD-19 132	3858.67	4090.30	4110.91	4114.65
BD-19 290	4296.16	4465.88	4488.12	4490.23
HE 0457-1805	4405.01	4809.19	4832.93	4833.31
LAMOSTJ091608.81+230734.6	4731.70	4821.40	4845.19	4845.50
HE 0920-0506	5515.12	5630.71	5658.03	5653.32
HE 1157-0518	4921.67	4870.92	4894.92	4894.97
HE 1304-2111	4096.60	4352.54	4374.29	4376.92
HE 1327-2116	4774.36	4956.04	4980.42	4979.98
HE 1354-2257	4540.34	4797.06	4820.74	4821.18
LAMOSTJ151003.74+305407.3	4307.90	4518.05	4540.51	4542.38
BD+19 3109	4291.48	4323.63	4345.25	4348.01
HD 202851	4586.99	4725.66	4749.03	4749.85

Note: The numbers in the parentheses below T_{eff} indicate the metallicity values at which the temperatures are calculated.

TABLE 2.2: Details of the spectra

Instrument	wavelength coverage (Å)	Resolution ($\lambda/\delta\lambda$)
HCT/HESP	3530 - 9970	30,000 & 60,000
Mercator/HERMES	3800 - 9000	86,000
VLT/UVES	3290 - 6650	48,000
ESO-MPG/FEROS	3520 - 9200	48,000
SUBARU/HDS	4100 - 6850	50,000

high-resolution spectra of the stellar sample. The details of the spectra used in this study are listed in Table 2.2.

2.3.1 Himalayan Chandra Telescope (HCT)

The Himalayan Chandra Telescope (HCT) is 2.01m IR-Optical telescope at Indian Astronomical Observatory (IAO), Mt.Saraswati, Hanle, operated by Indian Institute of Astrophysics, Bangalore (https://www.iiap.res.in/?q=telescope_iao). The observatory is located at an altitude of 4500 m above mean sea level. The latitude and longitude are $32^{\circ}46'46''$ N and $78^{\circ}57'51''$ E respectively. The low temperature, low humidity, low dust, and the high altitude enable to achieve good seeing (slightly less than 1 arcsec) at this site. The telescope has a modified Ritchey-Chrétien design with f/1.75 primary and f/9 Cassegrain focus and an alt-azimuth mounting. The telescope has three instruments at the Cassegrain focal plane; Hanle Faint Object Spectrograph Camera (HFOSC), TIFR Near Infrared Spectrograph (TIRSPEC) and Hanle Echelle SPectrograph (HESP). The instruments are mounted on an instrument mount cube with four side ports and

one on-axis port such that switching between instruments could be achieved easily in the same observing night. The telescope as well as the instruments are remotely operated using a dedicated satellite communication link from the Centre for Research & Education in Science & Technology (CREST), Indian Institute of Astrophysics, Hosakote.

2.3.1.1 Hanle Echelle SPecrograph (HESP)

The Hanle Echelle Spectroraph is a high-resolution dual fiber-fed echelle spectrograph with White pupil optical layout, attached to the 2m HCT (https://www.iiap.res.in/?q=hanle_echelle_spectrograph). It operates at two distinct resolutions $R \sim 30,000$ and 60,000. The spectra are recorded on a 4K x 4K CCD detector. The higher resolution (60,000) is achieved by using an image slicer. The instrument covers the wavelength region 3500 - 10000 Å without any gap in the wavelength coverage, in a single instrument set up. The instrument is equipped with four sub-systems:

Cassegrain unit: Directs light from the telescope to the spectrograph and the autoguider system, and it is attached to one of the side ports of the telescope.

Spectrograph unit: It comprises of an off-axis paraboloidal collimator mirror of 1.85m focal length, an echelle grating, two thick prisms that act as a cross-disperse system and an f/2.7 camera. The whole set-up is mounted on an optical table in a thermally controlled room in the ground floor of the telescope building.

Calibration unit: Consist of ThAr and ThArNe calibration lamps, filters, and the halogen lamp for flat fielding.

CCD detector system: 4K x 4K CCD detector with pixel size of 15 micron kept inside the spectrograph room.

2.3.2 Very Large Telescope (VLT)

The Very Large Telescope (VLT) is one of the world's most advanced telescope facility, operated by European Southern Observatory (ESO) at Cerro Paranal observatory, Chile, located at an altitude of 2635 m from sea level (<https://www.eso.org/public/teles-instr/paranal-observatory/vlt/>). The latitude and longitude are $24^{\circ}37'38''S$ and $70^{\circ}24'15''W$ respectively. It consists of four Unit telescopes (UT) with 8.2m main mirrors along with four movable 1.8m Auxiliary Telescopes (AT). The ATs are installed in the system to make it available while the UTs are used for other projects. The UTs have Ritchey-Chrétien design with Cassegrain-Nasmyth focus. The UTs can be used individually, and with the entire telescope system working together forms ESO Very Large Telescope Interferometer. VLT operates at visible and IR region, and each individual UTs can detect objects four billion times fainter than that can be seen with naked eyes. The UTs are equipped with instruments that allow observation from near-UV to mid-IR wavelengths. The four UTs are named as Antu (Sun), Kueyen (Moon), Melipal (Southern Cross) and Yepun (Evening Star).

2.3.2.1 Ultraviolet and Visual Echelle Spectrograph (UVES)

The Ultraviolet and Visual Echelle Spectrograph (UVES) is the high-resolution optical spectrograph of the VLT located at the NasmythB focus of UT2 (Kueyen). It is a cross-dispersed echelle spectrograph and designed to operate in the wavelength range 3000 - 11000 Å. For this, the light beam is split into two arms (uv - blue & visible - red) within the instrument. The two arms can be operated separately, or in parallel with the help of a dichroic beam splitter. The spectral resolution for 1 arcsec slit is $R \sim 40,000$. The maximum resolution that can be attained, using a narrow slit, is $R \sim 110,000$ in the red and $R \sim 80,000$ in the blue (<https://www.eso.org/public/teles-instr/paranal-observatory/vlt/vlt-instr/uves/>).

2.3.3 MPG/ESO 2.2 meter Telescope

The MPG/ESO 2.2 meter Telescope is an optical-NIR telescope operated by ESO at La Silla Observatory, Chile, originally constructed by the Max Planck Institute for Astronomy (Heidelberg, Germany). The observatory is located at an altitude of 2375 m above sea level. The telescope has Ritchey-Chrétien design with equatorial mounting. This telescope hosts three science instruments currently - Wide Field Imager (WFI) to image the celestial objects, the Gamma-Ray Burst Optical/Near-Infrared Detector (GROND) to chase the gamma-ray bursts, and Fiber-fed Extended Range Optical Spectrograph (FEROS) to study stars (<https://www.eso.org/sci/facilities/lasilla/telescopes/national/2p2.html>).

2.3.3.1 Fiber-fed Extended Range Optical Spectrograph (FEROS)

The Fiber-fed Extended Range Optical Spectrograph (FEROS) is a fiber-fed echelle spectrograph mounted on the Cassegrain focus of the MPG/ESO 2.2 meter Telescope (<https://www.eso.org/sci/facilities/lasilla/instruments/feros.html>). It was originally installed on the ESO 1.52-metre telescope. It operates at a resolution of $R \sim 48,000$, and covers the wavelength region 3500 - 9200 Å.

2.3.4 Mercator Telescope

The Mercator telescope is a semi-robotic 1.2m telescope at the Roque de los Muchachos Observatory on La Palma, Canary Islands, Spain, operated by Institute of Astronomy of the KU Leuven, Belgium (<http://www.mercator.iac.es/>). The observatory is located at an altitude of 2333 m above sea level. It is an f/12 telescope with alt-azimuth mounting. This telescope was built by the Institute of

Astronomy of the KU Leuven in collaboration with Geneva Observatory, and is a twin telescope of the Swiss Euler telescope at the La Silla Observatory, Chile.

2.3.4.1 High-Efficiency and high-Resolution Mercator Echelle Spectrograph (HERMES)

The High-Efficiency and high-Resolution Mercator Echelle Spectrograph (HERMES) is a fiber-fed echelle spectrograph of Mercator telescope (Raskin *et al.* 2011). It was built at Institute of Astronomy of the KU Leuven in collaboration with the Université Libre de Bruxelles, the Royal Observatory of Belgium, the Geneva Observatory (Switzerland), and the Tautenburg Observatory (Germany). HERMES covers a wavelength range 3770 - 9000 Å at a resolution of R~86,000 in 55 spectral orders on a 2k x 4.5k CCD detector.

2.3.5 Subaru Telescope

The Subaru telescope is the 8.2m optical-IR telescope, operated by the National Astronomical Observatory of Japan (NAOJ), at the summit of Maunakea, Hawaii, USA (<https://subarutelescope.org/en/about/>). The observatory is situated at an altitude of 4139 m above sea level at latitude and longitude 19°49'32"N and 155°28'34"W respectively. The telescope has Ritchey-Chrétien design with alt-azimuth mounting and f/1.83 focus. Subaru is the only 8-m class telescope which is capable of mounting an instrument at the prime focus. The main instruments that the telescope hosts are Hyper Suprime-Cam (HSC), High Dispersion Spectrograph (HDS), Infrared Camera and Spectrograph (IRCS) and Adaptive Optics (AO) System, Multi-Object Infrared Camera and Spectrograph (MOIRCS), Cooled Mid-Infrared Camera and Spectrometer (COMICS), and Faint Object Camera And Spectrograph (FOCAS).

2.3.5.1 High Dispersion Spectrograph (HDS)

The High Dispersion Spectrograph (HDS) is an echelle spectrograph at Nasmyth focus of the Subaru telescope (Noguchi *et al.* 2002). It covers, in multiple exposures, the entire wavelength region 3000 - 10000 Å; a single exposure covers 1500 - 2500 Å. The spectrograph operates at different resolutions up to $R \sim 160,000$ depending on the slit width used. Two 4K x 2K CCDs of pixel size 13.5 micron are used as the detectors.

2.4 Data reduction

The raw two dimensional data from the CCD detector is processed into one dimensional data for further analysis using Image Reduction and Analysis Facility (IRAF)* software. The data recorded by the CCD is affected by the atmosphere, telescope and spectrograph optics, and CCD sensitivity. Such effects can be reduced by obtaining additional image frames along with the target. This additional frames include bias, flat, and dark frames. All the image frames are first trimmed to get an area that contain only useful data. The bias frames taken with a zero exposure, in order to correct for the zero of the detector, are median combined to a master bias using ZERO COMBINE task and then subtracted from all other image frames using CCDPROC task. Dark frames are taken with shutter closed, so that no light enters the CCD, for long exposure that are similar to the target exposure time. These frames are used to remove the thermal noise generated in the CCD as a result of long exposures. Since most of the CCDs are equipped with cooling system, the dark current is negligible. The light sensitivity of each pixel of the CCD is different, hence, the image frames have to be corrected for

*IRAF is distributed by the National Optical Astronomical Observatories (NOAO), which is operated by the Association for Universities for Research in Astronomy, Inc., under contract to the National Science Foundation

it. This is known as flat correction. A number of flat frames are taken by the illumination with a constant light source that does not have any spectral line, such as halogen lamp, and then median combined to a master flat using the task FLATCOMBINE. It is then normalized using either APNORM or RESPONSE task. The image frames are then corrected by dividing them with the normalized flat using the task CCDPROC. Then the spectra are extracted using the APALL task, which now contain counts vs pixels. The pixels are converted to wavelengths by using Th-Ar arc spectrum. The spectral lines in the extracted arc spectrum are identified with the help of identification charts using ECIDENTIFY task. Then the object frames are wavelength calibrated using these arc frames as reference frames using REFSPEC task. The wavelength calibrated images are then dispersion corrected using DISPCOR task. The spectra are continuum fitted using CONTINU task. The data reduction pipeline developed by A. Surya, which is publicly available (<https://www.iiap.res.in/hesp/>), is used for the reduction of HESP data.

2.4.1 Radial velocity

Radial velocity of the program stars are calculated using a set of clean unblended lines in the spectra using Doppler equation

$$V_r = \frac{(\lambda_{obs} - \lambda_{lab})}{\lambda_{lab}} * c$$

where c is the velocity of light in vacuum. Then, the obtained radial velocity is corrected for heliocentric motion using the task RVCORRECT in the IRAF package. The continuum fitted spectra are then radial velocity corrected using DISPCOR task in the IRAF for further analysis.

2.5 Basic ingredients of stellar spectroscopy

Stellar spectroscopy is a tool that connects the astrophysicists to the stellar atmosphere. Various properties of stars are encrypted in the light we observe from stars. We study the stellar spectra to infer various characteristics of the stars. This section deals with the description of basic ingredients to decode the information about stars from their emitted radiation that we record, ie, the spectra.

2.5.1 Stellar atmosphere

Stellar atmosphere, in simple terms, is the outer layers of the star that emit light. It is the outer region of the star through which the photons pass before escaping into the ISM. It can be considered as the transition region from opaque stellar interior to the ISM. In stellar astronomy, the stellar atmosphere usually refers to the stellar photosphere which is the only visible region to the outside world. As the spectral lines are formed in this region, it is of significant importance for the spectroscopic studies. Stellar atmosphere can be used as a probe to derive the properties of the star, through the spectra. There are certain empirical parameters or physical variables, such as effective temperature, surface gravity, micro-turbulence, metallicity, opacity, magnitude, luminosity etc., that characterize the stellar atmosphere.

2.5.1.1 Absolute Bolometric Magnitude (M_{bol})

Magnitudes are used to quantify the brightness of an astronomical object. Absolute magnitude is the measure of intrinsic brightness of a celestial object. Absolute bolometric magnitude, which is the total luminosity expressed in magnitude units,

takes into account the energy radiated at all wavelengths of electromagnetic spectrum. Detectors are designed in such a way that they are sensitive to only a certain wavelength region. So, in order to get bolometric magnitude from any other magnitude, some corrections have to be applied. The correction added to the photo-visual magnitude is called Bolometric Correction (BC). The correction for very hot and cool stars are larger compared to the sun because they emit radiations more in UV and IR respectively than visible region, which are inaccessible from earth. The bolometric magnitude is given by;

$$M_{bol} = M_V + BC = V + 5 + 5\log(\pi) - A_v + BC$$

where M_V is the absolute visual magnitude, π is the parallax in arcsecond, V is the apparent visual magnitude, and A_v is the interstellar extinction.

2.5.1.2 Luminosity (L)

Luminosity is the total amount of energy radiated from the surface per unit time of an astronomical object. Its unit is erg/s and is often expressed in terms of solar luminosity. Absolute magnitude is used to quantify the luminosity. Luminosity of a star is related to its absolute bolometric magnitude through the relation,

$$M_{bol\odot} - M_{bol\star} = 2.5\log_{10}(L\star/L\odot)$$

where \star and \odot refer to the stellar and the solar values respectively.

2.5.1.3 Effective temperature (T_{eff})

The effective temperature of a star is the temperature of a black body that would emit the same amount of electromagnetic power per unit area, flux, as the star.

The effective temperature is related to the luminosity and flux through Stefan-Boltzmann law as,

$$\sigma T_{\text{eff}}^4 = \frac{L}{4\pi R^2} = \int F_\nu d\nu$$

where R and L are the stellar radius and luminosity respectively, $\sigma = 5.67 \times 10^{-5}$ erg cm $^{-2}$ s $^{-1}$ K $^{-4}$ is the Stefan-Boltzmann constant and T_{eff} is the effective temperature. The temperature of the stellar photosphere decreases as we move away from the core (Figure 2.4). Effective temperature can be derived using spectroscopic as well as photometric methods

2.5.1.4 Surface gravity ($\log g$)

Surface gravity of a star is the acceleration due to gravity experienced by a hypothetical test particle of negligible mass on the stellar surface, which is defined as

$$g = g_\odot \frac{M}{R^2}$$

where, g_\odot is the surface gravity of the sun ($\sim 2.738 \times 10^4$ cm s $^{-2}$), and M and R are the stellar mass and radius in solar units. In astrophysics, the surface gravity is expressed in logarithmic units as $\log g$. It is a measure of the compactness of a star; the higher the surface gravity, the more compact the object is, and it results in more collisions of the atomic species, hence leading to the broadening of the spectral lines. The surface gravity of a star decreases as it evolves off the main sequence to the giant stage, due to the increase in the radius. The surface gravity is also related to the gas pressure and the electron pressure of the stellar atmosphere as $P_g \propto g^{2/3}$ and $P_e \propto g^{1/3}$ respectively. The $\log g$ can be estimated from the spectroscopic and photometric methods

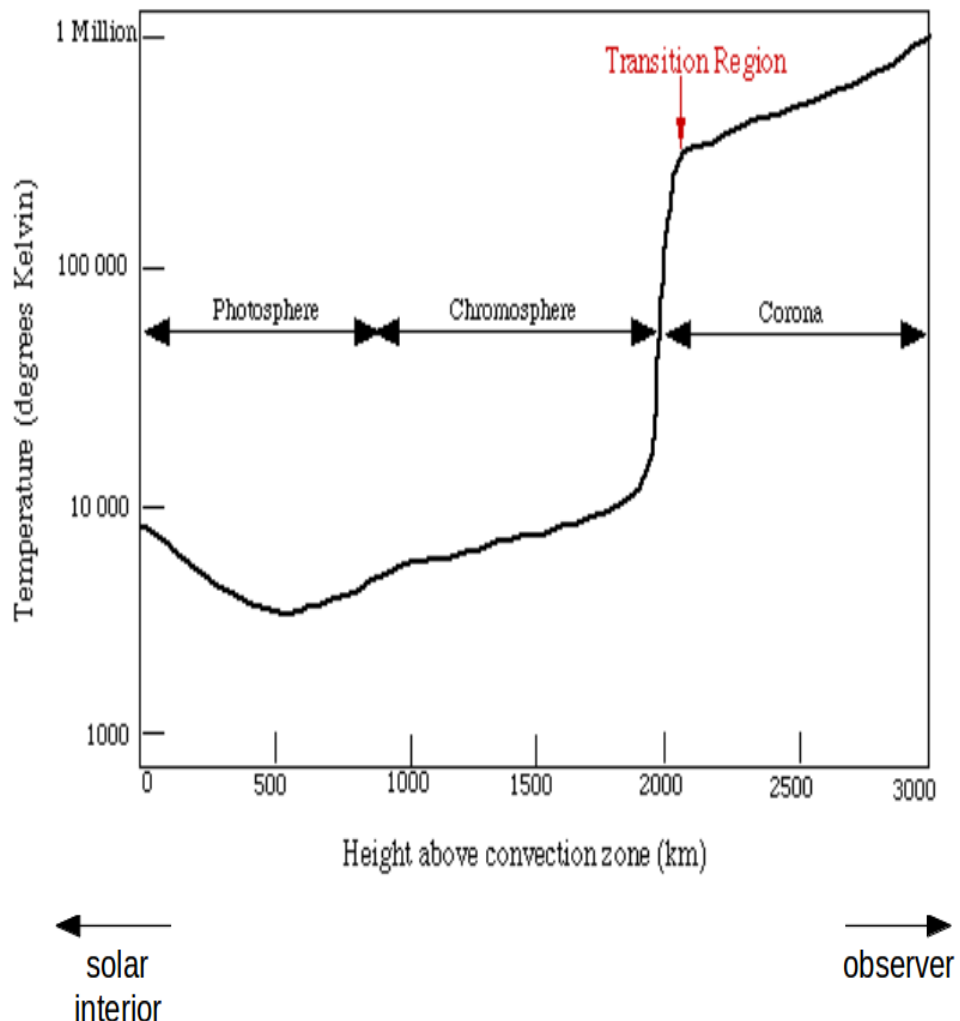


FIGURE 2.4: Sketch of the mean temperature as function of height above the convective layer in the sun. The photosphere is characterised by a negative temperature gradient. Image credit: <http://www-star.st-and.ac.uk/~pw31/education.html>

2.5.1.5 Micro-turbulent velocity (ζ)

Micro-turbulent velocity arises due to the small-scale (of the order of mean free path of the photons) non-thermal motion of the particles in the spectral line forming regions. This contributes to the extra broadening of the spectral lines without the chemical abundance being affected. This fact is advocated in determining the micro-turbulent velocity. It has negligible effect on the weak lines as they are

Gaussian and can be important for strong lines. It is expressed in cm s^{-1} .

2.5.1.6 Metallicity ([Fe/H])

In astronomy, the metallicity is the abundance of all elements heavier than He. Usually, Fe is taken as the representative of metals as there will be enough number of lines in the stellar spectra.

2.5.1.7 Opacity and optical depth

When a light beam of intensity I_λ passes through a gas, its intensity will be reduced as a result of absorption and scattering. The change in the intensity can be expressed mathematically as,

$$dI_\lambda = -\kappa_\lambda \rho I_\lambda ds$$

where ds is the distance travelled, ρ is the density of the gas, and κ_λ is the absorption coefficient or the opacity. Opacity has the unit $\text{cm}^2 \text{ g}^{-1}$, and is defined as the cross-section for absorbing photons of wavelength λ per unit mass of stellar material. It is a measure of the interaction between radiation and matter. The intensity of the radiation at any distance, s , from stellar interior to the surface can be obtained by integrating the above equation from $s=0$ (stellar interior) to $s=s$ (surface)

$$I_\lambda = I_{\lambda,0} \exp \left(- \int_0^s \kappa_\lambda \rho ds \right)$$

where $I_{\lambda,0}$ is the intensity at wavelength λ in the absence of any absorption or scattering. The optical depth is;

$$\tau_{\lambda} = \int_0^s \kappa_{\lambda} \rho ds$$

Re-writing the intensity equation in terms of optical depth;

$$I_{\lambda} = I_{\lambda,0} \exp(-\tau_{\lambda})$$

The intensity of light decreases exponentially. The medium with $\tau_{\lambda} \gg 1$ is called optically thick and with $\tau_{\lambda} \ll 1$ is called optically thin. At the stellar surface $\tau_{\lambda} = 0$, and the stellar interior beyond $\tau_{\lambda} \sim 1$ is opaque to us. The mean free path of the photons is defined as;

$$l = \frac{1}{\kappa_{\lambda} \rho} = \frac{1}{\sigma_{\lambda} n}$$

where σ is the interaction cross-section and n is the number density of the particle. $\kappa_{\lambda} \rho$ (and $\sigma_{\lambda} n$) is the fraction of photons scattered off the beam for unit distance travelled. So, in terms of the mean free path, optical depth can be defined as the number of mean free paths taken by the photon to travel from the stellar interior to the surface.

2.5.2 Atomic excitation and ionization: Boltzmann and Saha equations

The spectral lines are formed as result of the transition between different energy levels of atoms. So the strength or the intensity of a spectral line depends on

the number of atoms in the initial energy level of the transition. So, it is important to know the relative population in the excited and ionized state of atoms of different elements. The excitations can be collisional and radiative. At thermodynamic equilibrium, the excitations and de-excitations are balanced and the relative population of atoms/ions in each energy level is given by the Boltzmann equation;

$$\frac{n_b}{n_a} = \frac{g_b e^{-E_b/kT}}{g_a e^{-E_a/kT}} = \frac{g_b}{g_a} e^{\frac{-(E_b-E_a)}{kT}}$$

where $n_{a,b}$: number density of atoms in the energy states a, b

$E_{a,b}$: energy of the states a, b

k : Boltzmann constant

T : temperature of the gas

$g_{a,b}$: statistical weight of the states a, b

So, the relative population of atoms in various excitation states of a particular ionization state is a function of the temperature. If we know the relative population of atoms in a star, derived from the spectral features, it is possible to determine its temperature.

At high enough temperatures, the higher frequency of the thermal collisions will ionize the atoms. The ionization and recombination will be balanced at equilibrium. Under thermodynamic equilibrium, the relative population of atoms in different ionization state is given by the Saha's ionization equation;

$$\frac{n_{i+1}}{n_i} = \frac{2Z_{i+1}}{n_e Z_i} \left(\frac{2\pi m_e k T}{h^2} \right)^{3/2} e^{-\frac{\chi_i}{kT}}$$

where n_i : number density of atoms in the i^{th} stage of ionization

n_{i+1} : number density of atoms in the $(i + 1)^{th}$ stage of ionization

Z : partition function, the weighted sum of the different ways that an atom or ion distribute its electron among the energy levels

$$Z = \sum_{j=1}^{\infty} g_j e^{-\left(\frac{E_j - E_1}{kT}\right)}$$

m_e : mass of electron

T : ionization temperature

h : Planck's constant

χ_i : energy required to ionize the atom from i^{th} stage to $(i + 1)^{th}$ stage

For the ideal gas condition, in terms of electron pressure, P_e ,

$$n_e = \frac{P_e}{kT}$$

Saha's equation becomes,

$$\frac{n_{i+1}}{n_i} P_e = \frac{2Z_{i+1}}{Z_i} \left(\frac{2\pi m_e}{h^2} \right)^{3/2} (kT)^{5/2} e^{-\frac{\chi_i}{kT}}$$

In logarithmic form, the above equation can be re-written as;

$$\log_{10} \frac{n_{i+1}}{n_i} = -0.1761 - \log_{10} P_e + \log_{10} \frac{Z_{i+1}}{Z_i} + 2.5 \log_{10} T - \frac{5040}{T} \chi_i$$

ie, fraction of atoms in the ionized state depends on P_e , which is $\propto g^{1/3}$, hence this equation can be used to find the surface gravity of the star.

2.5.3 Equivalent width

Equivalent width is a measure of the strength of spectral lines. It is defined as the width of a rectangle of height equal to the continuum level of spectral line and area same as the area enclosed by the spectral line. It is demonstrated in Figure 2.5. In terms of flux, equivalent width, W_λ can be expressed as;

$$W_\lambda = \int_{\lambda_1}^{\lambda_2} \left(\frac{F_{\lambda_c} - F_\lambda}{F_{\lambda_c}} \right) d\lambda$$

where, F_{λ_c} and F_λ are the flux at continuum and at the particular wavelength λ respectively. The quantity $\frac{F_{\lambda_c} - F_\lambda}{F_{\lambda_c}}$ is defined as the depth of the spectral line. Higher the equivalent width, stronger will be the spectral lines.

Since the area of the spectral line is related to the number of atoms participated in that particular transition, the measured equivalent widths of spectral lines can be used to derive the abundances of elements. This is achieved through Curve of Growth (CoG) method. CoG is an empirical relation between W_λ and the abundances of elements. For the weaker lines, $W_\lambda \propto$ abundance and for stronger lines, $W_\lambda \propto \sqrt{\text{abundance}}$. So, weaker lines give more accurate abundances.

2.6 Data analysis

This section describes the basic inputs and methods adopted for the detailed analysis of the reduced, wavelength calibrated stellar spectra.

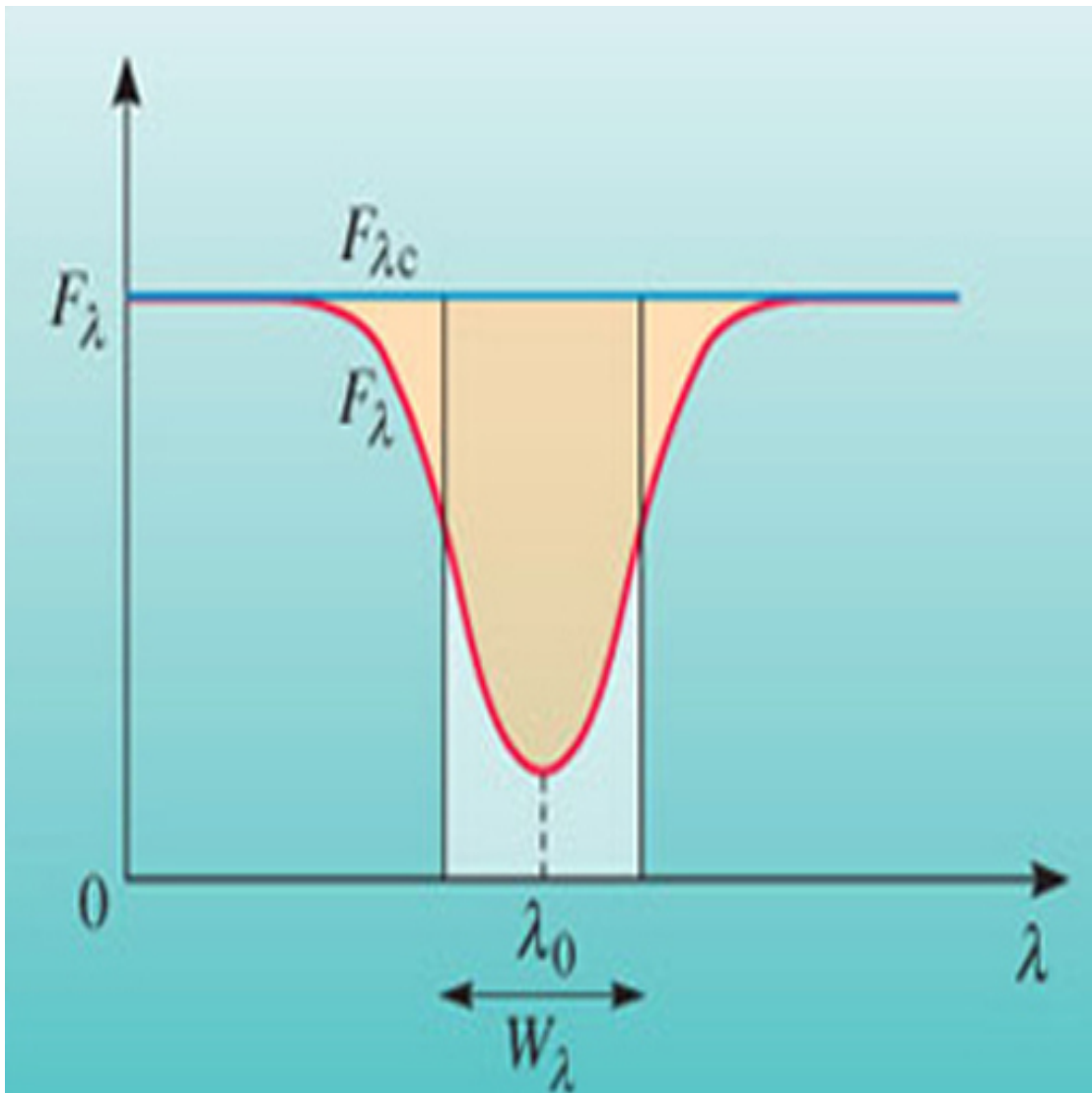


FIGURE 2.5: Definition of equivalent width in the case of an absorption line.
Image credit: <https://www.open.edu/openlearn/science-maths-technology/overview-active-galaxies/content-section-8.4>

2.6.1 Modelling the stellar atmosphere

The model atmosphere is a mathematical model of stellar photosphere that helps to interpret the observations. In order to study the properties of the star, the observed spectra are to be compared with the computed one. To generate such

spectra, we have to have a self-consistent and adequate model describing the physical conditions (temperature, pressure etc.) of stellar atmosphere. The model atmosphere is the analytic link between the physical properties of the star and the observed spectra. The following assumptions are made in constructing a model atmosphere:

- Plane parallel: Even though the stars are spherical in shape, the thickness of the stellar photosphere is very small compared to the stellar radius ($\Delta R/R \ll 1$). Hence, the assumption of plane parallel atmosphere holds well. This assumption simplifies the model, as the physical variables are functions of only one spatial coordinate (depth), and g is constant throughout the surface.
- Homogeneous: Granules, spots, magnetic field etc. are ignored such that the atmosphere is homogeneous.
- Hydrostatic equilibrium: The photosphere is not undergoing large scale accelerations, ie, pressure balances the gravity.

$$\frac{dP}{dr} = -\rho g$$

$$\frac{dP}{d\tau} = \frac{g}{\kappa}$$

$$d\tau = -\kappa \rho dr$$

where ρ is the density, g is surface gravity, P is the pressure, κ is the opacity, and τ is the optical depth.

- Steady state: The properties do not change with time. Rotation, pulsation, expanding envelopes, winds, shocks, magnetic fields, etc. are neglected.
- Radiative equilibrium (flux constancy): The energy coming from the core is entirely transported by the atmosphere, such that the flux is constant at any depth. ie, flux, $F = \sigma T_{\text{eff}}^4 = \text{constant}$

- Local Thermodynamic Equilibrium (LTE): The temperature is not uniform at different parts of stellar atmosphere. So, it is difficult to attain a global thermodynamic equilibrium. However, the thermodynamic equilibrium can be assumed in a small region of unit optical depth and is called the Local Thermodynamic Equilibrium (LTE). At LTE, photosphere can be represented by one temperature and optical depth.

2.6.1.1 Model atmosphere

1D model atmosphere is generated by the ATLAS9 code of R.L.Kurucz (Kurucz 1993), which is coded in FORTRAN language. It is a large table which describes the temperature, pressure, and many other physical properties of stellar atmosphere as a function of optical depth for an assumed chemical composition. The model atmosphere contains seventy-two rows representing each layer of the atmosphere.

2.6.2 Line list

Each line in the spectra is the result of atomic/molecular transitions in the star. Each spectral line is associated with certain specific parameters such as wavelength, excitation potential, transition energy levels, oscillator strength (probability of a particular transition) etc. A line list is the compilation of these information of each spectral line. Since all the information we derive about the stellar atmosphere is based on the measurement of these spectral lines, a proper line list is a crucial part of the spectral analysis. Hence, utmost care should be given in building a line list. All the lines have to be chosen carefully and the line parameters have to be precise and accurate. In this study

the latest available line parameters are adopted from Kurucz data base (<https://lweb.cfa.harvard.edu/amp/ampdata/kurucz23/sekur.html>).

2.6.3 MOOG

MOOG is an astronomical software package developed by Christopher Sneden in 1973 for his PhD thesis, and is subsequently maintained by him. **MOOG is a FORTRAN code which can be used to determine** the chemical composition of a star through spectral synthesis as well as spectral line analysis techniques, based on the assumption of LTE. It generates an emergent spectrum by solving the radiative transfer equation, with a model atmosphere and a line list. The detailed description of the code is available in Sneden (1973). The MOOG coding is done in different subroutines which are called using various master programs called *driver*. The parameter file is an essential to run the MOOG. This file instructs MOOG on which driver routine to use, how to analyze the data, and how to display the result. The name of the driver routine to be used appears on the first line of the parameter file.

2.6.4 Determination of stellar atmospheric parameters

The stellar atmospheric parameters; the effective temperature T_{eff} , the surface gravity $\log g$, micro-turbulent velocity ζ , and the metallicity [Fe/H], are of fundamental astrophysical importance. They are the pre-requisites to any detailed chemical abundance analysis.

We have estimated the photometric temperature of the program stars using the color - temperature calibration equations of Alonso *et al.* (1994, 1996) for dwarfs,

and Alonso *et al.* (1999, 2001) for giants. We made use of the 2MASS J, H, K magnitudes taken from the SIMBAD (Cutri *et al.* 2003) for this calculation. The photometric temperature estimates had been used as an initial guess for deriving the spectroscopic effective temperature of each object.

To determine the spectroscopic stellar atmospheric parameters, we have used clean and unblended lines of Fe I and Fe II. The lines are selected such that they have excitation potentials ranging from 0.0 to 6.0 eV, and equivalent widths ranging from 18 to 180 mÅ. In certain cases, we have considered lines with equivalent width < 18 mÅ as the lines in the most metal-poor stars are too few and weak. The IRAF software is used for the equivalent width measurement. A pseudo continuum (at 1) is fitted to the observed spectrum using the spline function. The equivalent width is measured for each spectral line by fitting a Gaussian profile. An initial model atmosphere was selected from the Kurucz grid of model atmosphere with no convective overshooting (<http://kurucz.harvard.edu/grids.html>), using the photometric temperature estimate and the guess of log g value for giants/dwarfs. A final model atmosphere was adopted by the iterative method from the initially selected one, using the radiative transfer code MOOG (Sneden 1973, version 2013) based on the assumptions of Local Thermodynamic Equilibrium (LTE).

The effective temperature is determined by the method of excitation balance, forcing the slope of the abundances from Fe I lines versus excitation potentials of the measured lines to be zero. The micro-turbulent velocity at a fixed effective temperature is determined by employing equivalent width balance, ie, by demanding that there will be no dependence of the derived Fe I abundance on the reduced equivalent width of the corresponding lines. The spectral lines of different strengths are affected differently by micro-turbulent velocity; weak lines (equivalent width < 70 mÅ) are least sensitive to ζ , whereas moderate/strong lines are heavily affected (Mucciarelli 2011). Micro-turbulent velocity is fixed at a value which gives zero slope for the plot of equivalent width versus abundances of Fe I lines. This is

demonstrated in Figure 2.6. Good Fe II lines are not enough in number to remove any correlation of the abundances derived from them with the excitation potentials and the reduced equivalent width. But, we need the consistent abundances from both Fe I and Fe II lines to fix the metallicity of the star. So, we try to match the abundances derived from the Fe II lines with that from the Fe I lines which we have obtained with the help of excitation balance and equivalent width balance. In F, G, K type stars, the singly ionized species are sensitive to the pressure and thereby the surface gravity of the star, whereas the neutral species are almost independent of the surface gravity. So, the surface gravity value is changed such that the mean abundance derived from the Fe II lines matches with that from the Fe I lines. Thus, the surface gravity, $\log g$, value is determined by means of ionization balance, that is by forcing the Fe I and Fe II lines to produce the same abundance at the selected effective temperature and micro-turbulent velocity. The final model atmosphere is adopted from the initial one through an iterative process until the three conditions, excitation balance, equivalent width balance, and ionization balance, are satisfied simultaneously. Once this is achieved, [Fe/H] is estimated from the derived iron abundance.

2.6.4.1 Derivation of $\log g$ from parallax

The $\log g$ value is also calculated from the parallax using the relation

$$\log\left(\frac{g}{g_\odot}\right) = \log\left(\frac{M}{M_\odot}\right) + 4\log\left(\frac{T_{\text{eff}}}{T_{\text{eff}\odot}}\right) + 0.4(M_{\text{bol}} - M_{\text{bol}\odot})$$

Using the definition in section 2.5.1.2, re-writing in terms of luminosity;

$$\log\left(\frac{g}{g_\odot}\right) = \log\left(\frac{M}{M_\odot}\right) + 4\log\left(\frac{T_{\text{eff}}}{T_{\text{eff}\odot}}\right) - \log\left(\frac{L}{L_\odot}\right)$$

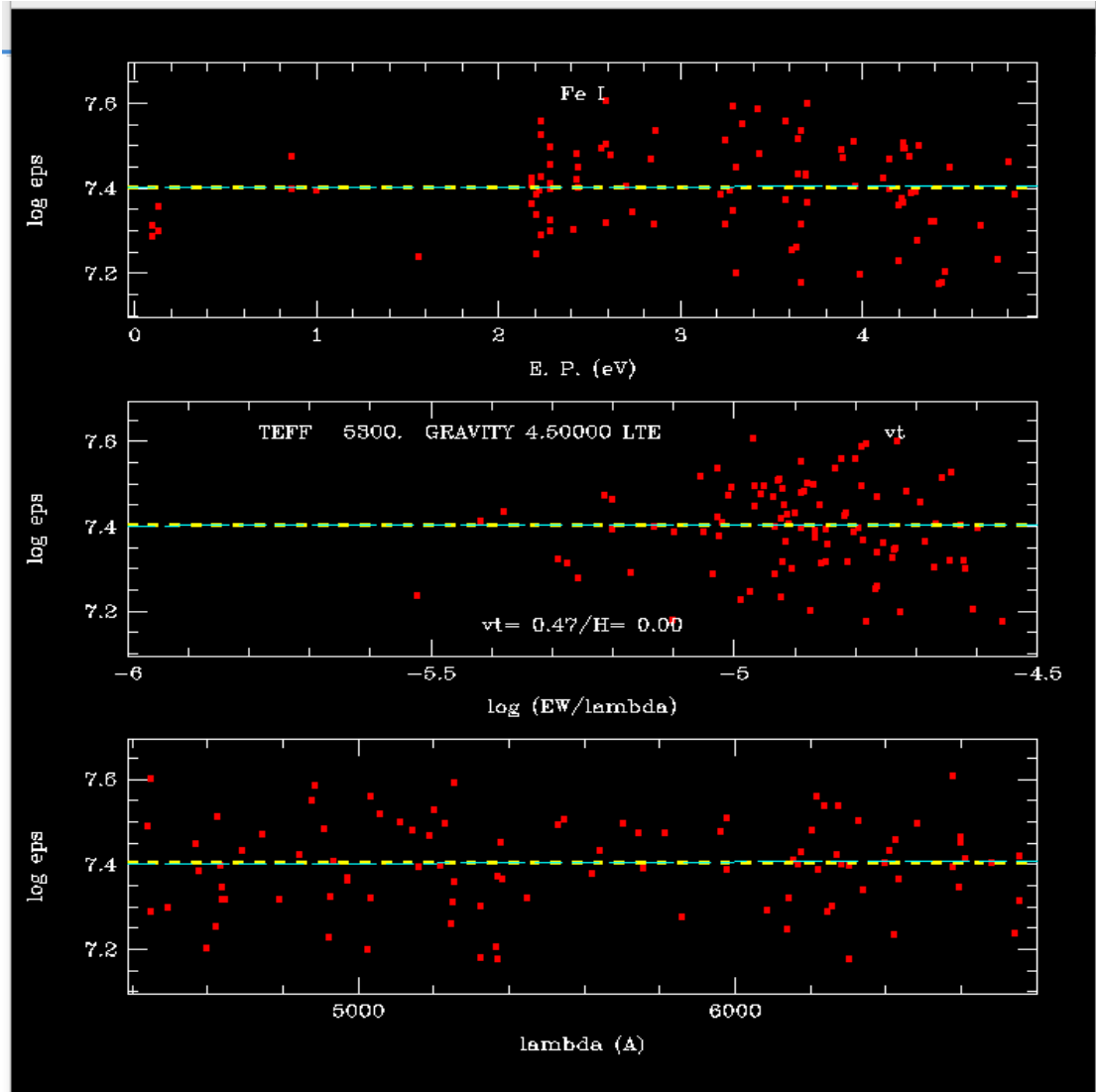


FIGURE 2.6: The iron abundances derived from Fe I lines as functions of excitation potential, equivalent width, and wavelength. The yellow dotted line is the mean Fe I abundance and the green line represent the trend of the Fe I abundance.

Using the definition in section 2.5.1.1,

$$\log\left(\frac{g}{g_{\odot}}\right) = \log\left(\frac{M}{M_{\odot}}\right) + 4\log\left(\frac{T_{\text{eff}}}{T_{\text{eff}\odot}}\right) - 0.4(M_{\text{bol}\odot} - V - 5 - 5\log(\pi) + A_v - BC)$$

where,

$$\log\left(\frac{L}{L_{\odot}}\right) = 0.4(M_{\text{bol}\odot} - V - 5 - 5\log(\pi) + A_v - BC)$$

where M is the stellar mass, which is determined from their location on the Hertzsprung - Russell (H - R) diagram ($\log(L/L_\odot)$ - $\log(T_{\text{eff}})$) using the stellar evolutionary tracks of Girardi *et al.* (2000). For the determination of mass, we have used the spectroscopic temperature estimate, T_{eff} , and the luminosity, $\log(L/L_\odot)$. The visual magnitudes V are taken from the SIMBAD astronomical database and the parallaxes, π , from the Gaia DR2 (<https://gea.esac.esa.int/archive/>). The bolometric correction, BC, is calculated using the empirical calibration equations of Alonso *et al.* (1995) for dwarfs, and Alonso *et al.* (1999) for giants. The interstellar extinction, A_v , is calculated using the calibration equations given in Chen *et al.* (1998). We have adopted the solar values $\log g_\odot = 4.44$, $T_{\text{eff}\odot} = 5770$ K, and $M_{\text{bol}\odot} = 4.74$ mag.

2.6.5 Abundance analysis

One of the most important ventures of stellar spectroscopy is to determine the chemical abundances with great accuracy as they are related to the chemical history of the Universe. The determination of abundances in the stellar atmosphere is indirect, and based on the intensity of the spectral lines. It is based on the comparison of the observed quantities with computed ones. This strongly depends on the assumptions made for generating the model atmosphere and for the line formation mechanisms. The line list and the model atmosphere are the pre-requisite for the chemical abundance analysis. All the abundances are found relative to the respective solar values. The solar abundances are adopted from Asplund *et al.* (2009). Even though the abundance estimation is performed under the assumption of LTE, we have applied the non-LTE (NLTE) corrections whenever available. The abundances of elements are derived by two methods, using the MOOG software:

- (1) **Fine Analysis Method:** For fine analysis method, the driver ABFIND in MOOG is used. Here, the measured equivalent width of a given unblended line

is compared with the equivalent width calculated using the line list and adopted model atmosphere. The line list contains the following line information, wavelength (in Å) of the spectral lines, element ID (atomic number with ionization state, for eg. 26.00 for Fe I and 26.10 for Fe II), excitation potential (in eV), log gf, and measured equivalent widths (in mÅ). This method force-fits the theoretically calculated equivalent width to the observed equivalent width. The equivalent width of each spectral line is computed as a function of the abundance of the respective atom. The elemental abundance is varied through an iterative process until the computed equivalent width matches with the measured equivalent width within a prefixed limit (say within 0.05 - 0.1 mÅ). The abundance thus obtained is taken as the final abundance of that element. The absorption lines of neutral and ionized atoms with equivalent widths of 18 - 180 mÅ are used for the abundance determination as they are on the linear portion of the Curve of Growth (CoG) as discussed in Section 2.5.3. Absorption lines corresponding to different elements are identified by comparing closely the spectra of program stars with the Doppler corrected spectrum of the star Arcturus. The equivalent width of the spectral lines are measured using various tasks in the IRAF

(2) **Spectral Synthesis Method:** For the spectrum synthesis method, the driver SYNTH of MOOG is used. This method requires an extensive line list containing the line parameters such as wavelength, ionization state, excitation potential, log gf etc. of all the possible atomic and molecular transitions in the wavelength region of interest. In this method, the observed spectral line profile is compared with the theoretically computed one. The theoretical spectrum for a particular species is computed, based on the model atmosphere, the line parameters in the line list, stellar rotational velocity, limb darkening coefficient, and the FWHM of the spectral line. The elemental abundance is varied until the computed theoretical line profile matches with the observed line profile. The abundance corresponding to this is taken as the final abundance of that particular species under consideration. The line broadening mechanisms such as natural broadening, collisional broadening,

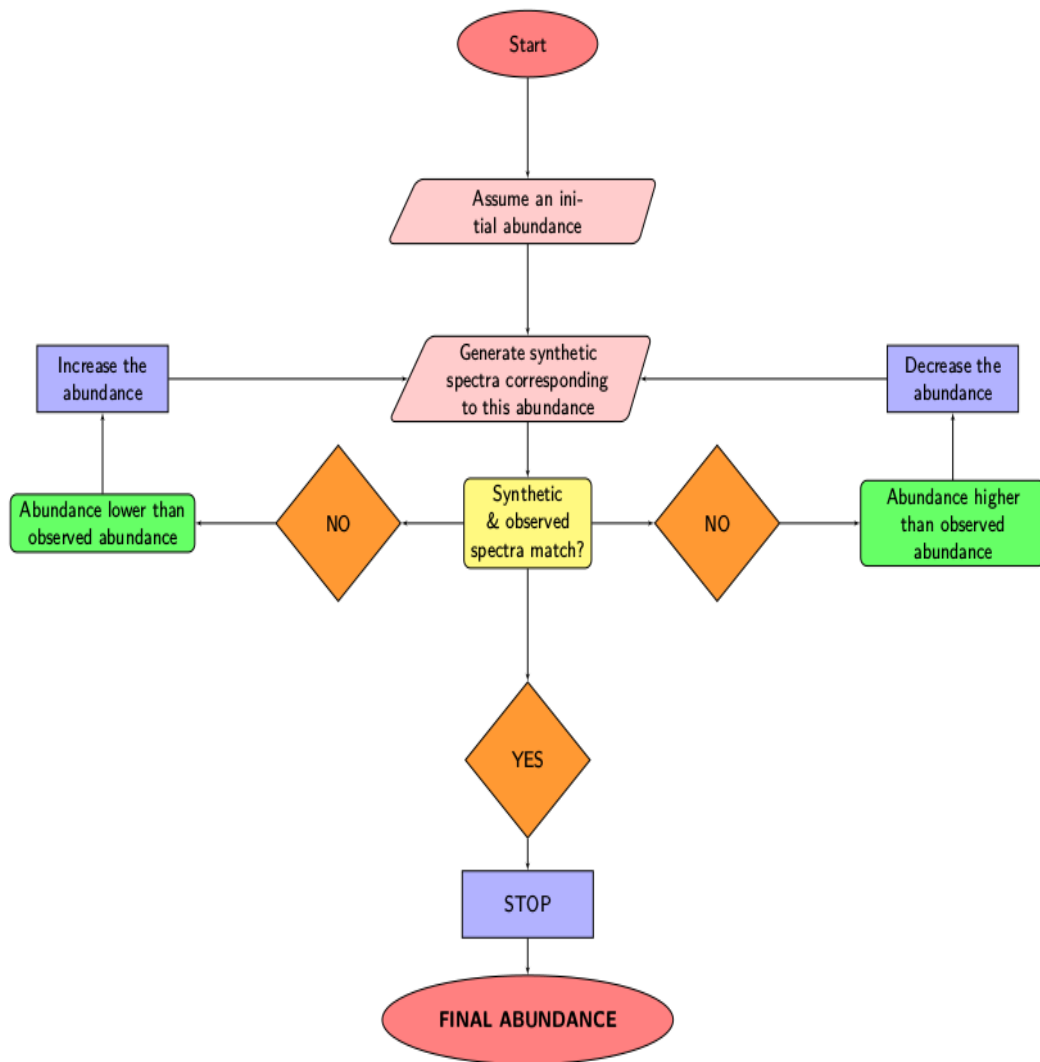


FIGURE 2.7: The iterative process employed to determine the abundance in spectrum synthesis method

and Doppler broadening are taken into consideration for generating the theoretical line profile. This method can be used to confirm the abundances obtained with the fine analysis method. We have used the method of spectrum synthesis for elements that show hyperfine splitting, for weak lines, and for molecular bands to derive the abundance. The spectral synthesis method is shown as a flow chart in Figure 2.7.

2.6.5.1 Hyperfine splitting (HFS) and chemical abundances

The interactions between the electron cloud and nucleus of an atom, molecule, or ion with non-zero spin causes small shifts in their otherwise degenerate energy levels, and results in the splitting of energy levels. This is known as hyperfine splitting, and it arises due to the interaction between the spin angular momentum of the nucleus and the total angular momentum of the electron cloud. As a result of the transition between these hyperfine energy levels, the spectral lines appear to be broader, which in turn lead to an inaccurate estimation of elemental abundances and wrong conclusions. So, for the elements with odd number of nucleons, their hyperfine components should be taken into consideration for an exact estimation of elemental abundances. In our analysis, we have considered the hyperfine components and their contributions to the abundances for the elements Sc, V, Mn, Co, Cu, Rb, Ba, La, and Eu.

2.6.6 Calculation of abundance uncertainties

The uncertainties in the elemental abundances has two main components: random error and systematic error. Random error arises from the uncertainties in the line parameters such as measured equivalent width, line blending, and oscillator strength. Since the random error varies inversely as the square-root of the number of lines, we can reduce this error by using maximum possible number of lines. Systematic error is due to the uncertainties in the adopted stellar atmospheric parameters. The uncertainties in the stellar atmospheric parameters may depend on the method and codes used to derive them, quality and resolution of the spectra etc. For example, in the case of low-resolution spectra, the typical uncertainties in $\log g$ obtained from most pipelines are about 0.2 dex or larger (Xiang *et al.* 2017 and references therein). Depending on the method used, whether the equivalent

width method or the spectral line fitting technique (Section 2.6.5), various aspects such as continuum normalization may differ. This may also be a possible source of uncertainty in the atmospheric parameters.

The total uncertainty in the elemental abundance $\log \epsilon$ is calculated as;

$$\sigma_{\log \epsilon}^2 = \sigma_{ran}^2 + \left(\frac{\partial \log \epsilon}{\partial T}\right)^2 \sigma_{T_{eff}}^2 + \left(\frac{\partial \log \epsilon}{\partial \log g}\right)^2 \sigma_{\log g}^2 + \left(\frac{\partial \log \epsilon}{\partial \zeta}\right)^2 \sigma_{\zeta}^2 + \left(\frac{\partial \log \epsilon}{\partial [Fe/H]}\right)^2 \sigma_{[Fe/H]}^2$$

where $\sigma_{ran} = \frac{\sigma_s}{\sqrt{N}}$. σ_s is the standard deviation of the abundances derived from the N number of lines of the particular species. The σ' s are the typical uncertainties in the stellar atmospheric parameters, which are $(\sigma_{T_{eff}}, \sigma_{\log g}, \sigma_{\zeta}, \sigma_{[Fe/H]}) \sim (\pm 100 \text{ K}, \pm 0.2 \text{ dex}, \pm 0.2 \text{ km s}^{-1}, \pm 0.1 \text{ dex})$. The abundance uncertainties arising from the error of each stellar atmospheric parameters is estimated by varying one parameter at a time by an amount equal to their corresponding uncertainty, by keeping other parameters the same and computing the changes in the abundances. In order to simplify the calculation, we made the assumption that the uncertainties due to different parameters are independent, following de Castro *et al.* (2016), Karinkuzhi *et al.* (2018a), Cseh *et al.* (2018). However, since most of the stellar atmospheric parameters are correlated, our estimates are to be taken as upper limits. The procedure has been applied to the abundances estimated from the equivalent width measurement as well as the spectral synthesis calculation. Finally, the uncertainty in $[X/Fe]$ is calculated as,

$$\sigma_{[X/Fe]}^2 = \sigma_X^2 + \sigma_{Fe}^2$$

2.7 Kinematic analysis

It is equally as important as the chemical composition of a star to understand its kinematics and the Galactic population to which it belongs. This help us to

understand the spatial distribution of the stars and the galaxy formation better. The spatial velocity of a star in the solar neighborhood is measured with respect to the Local Standard of Rest (LSR). LSR is a point in space that is moving on a perfectly circular orbit around the Galactic center at the Sun's Galactocentric distance (~ 8 kpc). The components of the spatial velocity are U_{LSR} , V_{LSR} , and W_{LSR} ; measured positive along the axes pointing towards the Galactic center, the direction of Galactic rotation, and the Galactic North Pole respectively (Johnson and Soderblom 1987). A right-handed coordinate system is used so that both the coordinates and velocities have the same direction, and it is shown in Figure 2.8. Space velocity of the program stars are calculated following the procedures in Bensby *et al.* (2003).

Components of the spatial velocity of the star with respect to LSR:

$$(U, V, W)_{\text{LSR}} = (U, V, W)_o + (U, V, W)_{\odot} \text{ km/s.}$$

where, $(U, V, W)_o$ is the stellar motion with respect to sun, $(U, V, W)_{\odot}$ is the solar motion with respect to LSR, and its value is $(11.1, 12.2, 7.3)$ km s^{-1} (Schönrich *et al.* 2010) and

$$\begin{bmatrix} U_o \\ V_o \\ W_o \end{bmatrix} = B \cdot \begin{bmatrix} V_r \\ k \cdot \mu_{\alpha} / \pi \\ k \cdot \mu_{\delta} / \pi \end{bmatrix}$$

where, $B=TA$, T is the transformation matrix connecting the Galactic coordinate system and equatorial coordinate system, and A is a coordinate matrix defined below

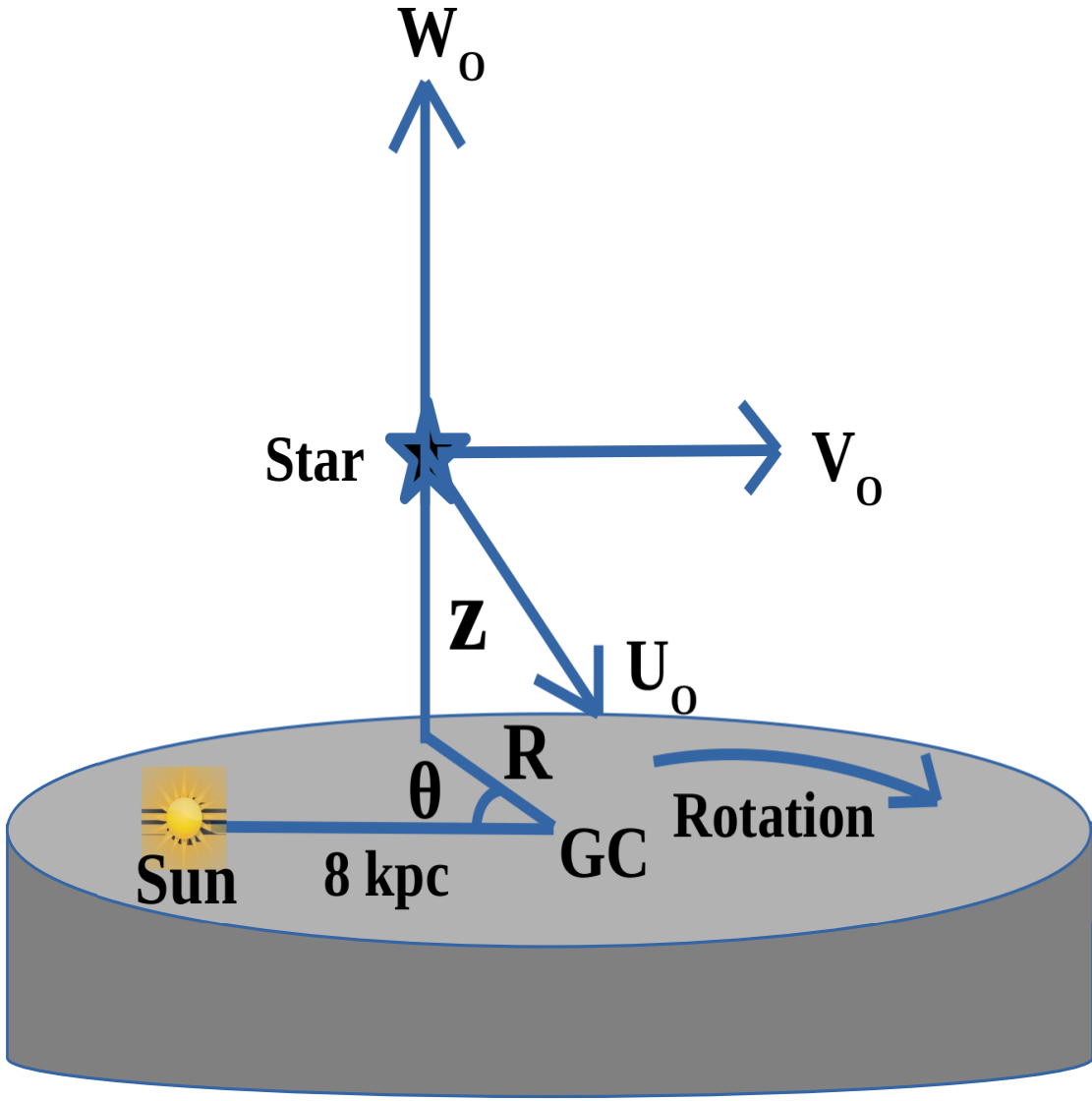


FIGURE 2.8: Schematic representation of the components of spatial velocity in a right-handed cylindrical coordinate system. $(R, \theta, z) \sim (\text{Galactocentric distance}, \text{azimuthal coordinate}, \text{height above/below the Galactic plane})$.

$$T = \begin{bmatrix} -0.06699 & -0.87276 & -0.48354 \\ +0.49273 & -0.45035 & +0.74458 \\ -0.86760 & -0.18837 & 0.46020 \end{bmatrix}; A = \begin{bmatrix} \text{Cos}\alpha.\text{Cos}\delta & -\text{Sin}\alpha & -\text{Cos}\alpha.\text{Sin}\delta \\ \text{Sin}\alpha.\text{Cos}\delta & \text{Cos}\alpha & -\text{Sin}\alpha.\text{Sin}\delta \\ \text{Sin}\delta & 0 & \text{Cos}\delta \end{bmatrix}$$

where α is the right ascension (RA), δ the declination (DEC), V_r the radial velocity in km s^{-1} , $k=4.74057 \text{ km s}^{-1}$ equivalent of 1 AU in one year, μ_α and μ_δ respectively the proper motions in RA and DEC in arcsec/year, and π the parallax

in arcsec. The proper motion and parallax values are taken from the Gaia DR2 (Gaia Collaboration *et al.* 2018, <https://gea.esac.esa.int/archive/>). The spectroscopic radial velocity estimates have been used in this calculation.

The total spatial velocity of the star is calculated as:

$$V_{\text{spa}}^2 = U_{\text{LSR}}^2 + V_{\text{LSR}}^2 + W_{\text{LSR}}^2$$

Errors in the respective velocity components are calculated as follows:

$$\begin{bmatrix} \sigma_U^2 \\ \sigma_V^2 \\ \sigma_W^2 \end{bmatrix} = C \cdot \begin{bmatrix} \sigma_{V_r}^2 \\ (k/\pi)^2[\sigma_{\mu_\alpha}^2 + (\mu_\alpha \sigma_\pi / \pi)^2] \\ (k/\pi)^2[\sigma_{\mu_\delta}^2 + (\mu_\delta \sigma_\pi / \pi)^2] \end{bmatrix} + \frac{2\mu_\alpha \mu_\delta k^2 \sigma_\pi^2}{\pi^4} \cdot \begin{bmatrix} b_{12}.b_{13} \\ b_{22}.b_{23} \\ b_{32}.b_{33} \end{bmatrix}$$

where $C_{ij} = b_{ij}^2$, and σ'_s the errors in respective quantities.

The probability that a star belongs to the Galactic thin/thick disk or halo population is calculated following the procedure described in Mishenina *et al.* (2004), Bensby *et al.* (2003, 2004), and Reddy *et al.* (2006), with assumption that the space velocities follow a Gaussian distribution.

$$P_{\text{thin}} = \frac{f_1 \cdot p_1}{P}, P_{\text{thick}} = \frac{f_2 \cdot p_2}{P}, P_{\text{halo}} = \frac{f_3 \cdot p_3}{P}$$

$$P = \sum f_i \cdot p_i$$

$$p_i = K_i \cdot \exp \left[\frac{-U_{\text{LSR}}^2}{2 \cdot \sigma_{U_i}^2} - \frac{(V_{\text{LSR}} - V_{\text{ad}})^2}{2 \cdot \sigma_{V_i}^2} - \frac{W_{\text{LSR}}^2}{2 \cdot \sigma_{W_i}^2} \right]$$

$$K_i = \frac{1}{(2 \cdot \pi)^{(3/2)} \cdot \sigma_{U_i} \cdot \sigma_{V_i} \cdot \sigma_{W_i}}$$

$$i = 1, 2, 3$$

where σ'_s are the dispersion in velocities, V_{ad} the mean galactic rotation velocity for each stellar population relative to LSR, and f the fractional population. These values are taken from Reddy *et al.* (2006).

Chapter 3

Analysis of Ba stars^{*}

3.1 Introduction

Barium stars (Ba II) are peculiar G and K type giant or dwarf stars in a binary system, whose envelope bear the products of AGB nucleosynthesis that is transferred from the companion (now invisible white dwarf) in a past mass-transfer event. Their envelope show enhanced abundance of s-process elements (and carbon). Ba stars are the largest stellar sample among the chemically peculiar stars which amounts around 800 - 20,000 ($V \leq 10$) in the Galaxy (Han *et al.* 1995; de Castro *et al.* 2016). The spectra of Ba stars are generally less contaminated by the molecular contributions, and hence it is easier for analysis compared to cool AGB stars. So, Ba stars are one of the important targets for constraining the AGB nucleosynthesis.

A number of studies in the past have been dedicated to model AGB nucleosynthesis

^{*}Results of this chapter are published in Shejelammal and Goswami (2019); Shejelammal *et al.* (2020); Shejelammal and Goswami (2020)

based on the chemical abundances of Ba stars (Busso *et al.* 2001; Liang *et al.* 2003; Smiljanic *et al.* 2007; Husti *et al.* 2009). Detailed studies on barium stars include Allen and Barbuy (2006), Smiljanic *et al.* (2007), de Castro *et al.* (2016), Yang *et al.* (2016), and many others. However, these studies have not included abundances of several heavy elements such as Rb for all the stars and also for C, N, and O. In this work, we have undertaken to carry out a detailed spectroscopic analysis for a sample of ten barium star candidates and derived whenever possible the abundances of C, N, O, and the neutron density dependent [Rb/Zr] abundance ratio to investigate the neutron source in the former companion AGB stars. There are two important neutron sources for the s-process in the He intershell of AGB stars: $^{13}\text{C}(\alpha, n)^{16}\text{O}$ reaction during the radiative interpulse period and $^{22}\text{Ne}(\alpha, n)^{25}\text{Mg}$ reaction during the convective thermal pulses. $^{13}\text{C}(\alpha, n)^{16}\text{O}$ reaction is the dominant neutron source in low-mass AGB stars with initial mass $\leq 3 \text{ M}_\odot$. The temperature $T \geq 90 \times 10^6 \text{ K}$ required for the operation of this reaction provides a neutron density $N_n \sim 10^8 \text{ cm}^{-3}$ in a timescale of $\geq 10^3$ years (Straniero *et al.* 1995; Gallino *et al.* 1998; Goriely and Mowlavi 2000; Busso *et al.* 2001). A temperature $300 \times 10^6 \text{ K}$, required for the activation of ^{22}Ne source is achieved during the TPs in intermediate-mass AGB stars (initial mass $\geq 4 \text{ M}_\odot$). It produces a neutron density $N_n \sim 10^{13} \text{ cm}^{-3}$ in a timescale of ~ 10 years. The temperature required for the ^{22}Ne source is reached in low-mass stars during the last few TPs providing $N_n \sim 10^{10} - 10^{11} \text{ cm}^{-3}$ (Iben 1975; Busso *et al.* 2001). The Rb is produced only when the $N_n > 5 \times 10^8 \text{ cm}^{-3}$, otherwise Sr, Y, Zr etc. are produced. Hence, the [Rb/Zr] ratio can be used as an indicator of mass of AGB stars.

In this chapter, the results of the detailed spectroscopic analysis and the origin of the abundance peculiarity of our first stellar sample, Ba stars, are discussed. In Section 3.2, we describe the source of the spectra used in this study. Section 3.3 describes estimated atmospheric parameters and radial velocities. A discussion on the stellar mass is also provided in the same section. A comparison of our results with the literature values is presented in section 3.3. In section 3.4, we have

discussed the abundance estimation. Same section provides a discussion on abundance uncertainties. Binary status of the program stars are discussed in section 3.5. A discussion on several diagnostics to understand the nature of companion AGB stars is given in section 3.6. A comparison of the observed abundances of the program stars with AGB stars is provided in section 3.7. This section also provides a comparison of the observational data with the FRUITY models of Cristallo *et al.* (2009, 2011, 2015) and a parametric model based analysis. Results of the kinematic analysis is given in section 3.8. A discussion on the individual stars is given in section 3.9. Conclusions are drawn in section 3.10.

3.2 Object selection, data acquisition and data reduction

The objects analyzed in this study are taken from the CH star catalogue of Bartkevicius (1996). Six of them are also listed in the barium star catalogue of Lü (1991). The spectra of these objects were acquired from three different sources. For HD 219116, HD 154276, and HD 147609, the high-resolution spectra ($\lambda/\delta\lambda \sim 60,000$) were obtained in October 2015, May 2017, and June 2017 using HCT/HESP. For all these objects, we had acquired three frames; each frame was taken with 2400 seconds exposure time. The three frames were added to enhance the S/N ratio, and the co-added spectrum was used for further analysis. Data is reduced using the HESP data reduction pipeline and IRAF software. For HD 24035 and HD 207585, high-resolution spectra ($\lambda/\delta\lambda \sim 48,000$) were obtained with the VLT/UVES. A high-resolution spectrum of HD 219116 is also obtained from VLT/UVES. For HD 32712, HD 36650, HD 94518, HD 211173, and HD 179832, high-resolution spectra ($\lambda/\delta\lambda \sim 48,000$) were obtained with the FEROS of the 1.52 m telescope of ESO at La Silla, Chile. Basic data about the

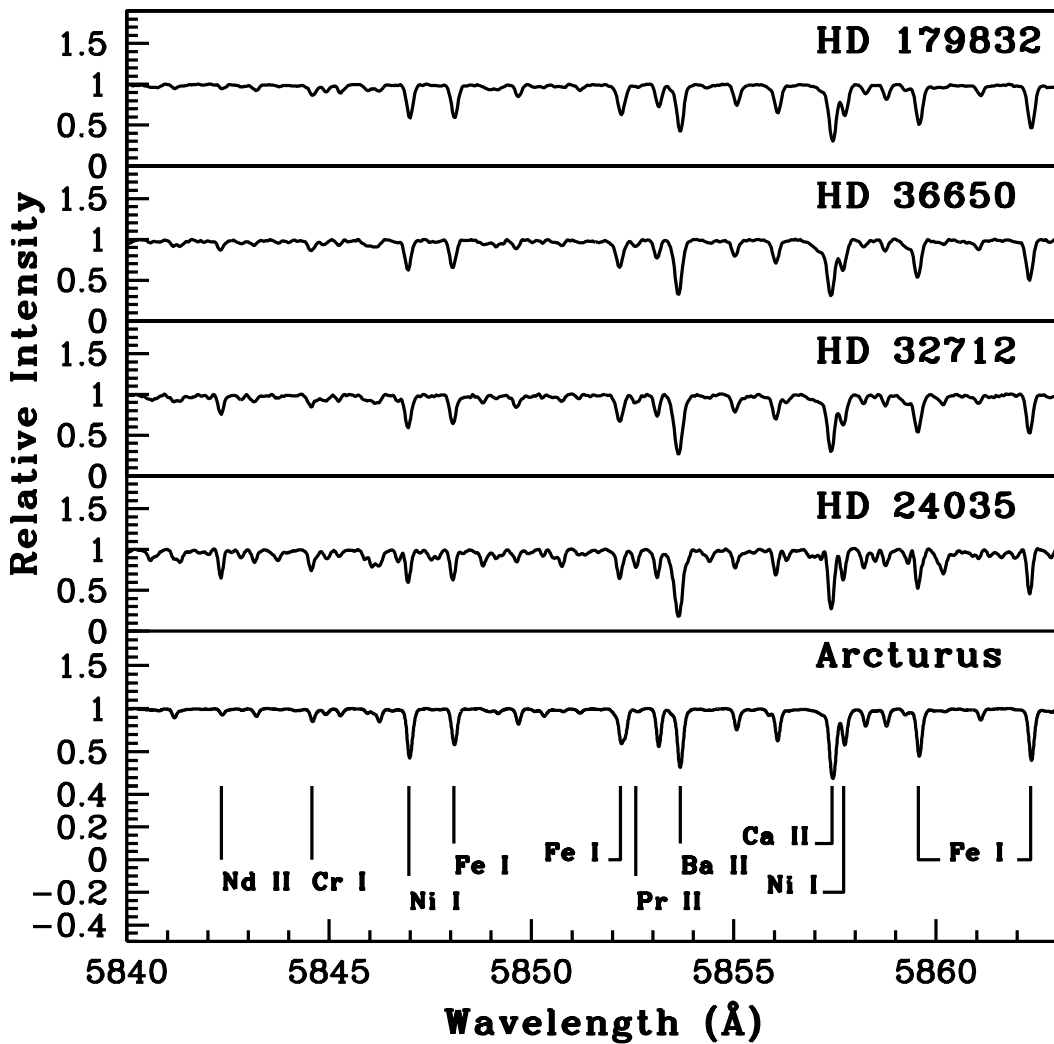


FIGURE 3.1: Sample spectra of the program stars in the wavelength region 5840 to 5863 Å

program stars, as well as the source of the spectra, are given in Table 3.1. A few sample spectra are shown in Figure 3.1.

TABLE 3.1: Basic data about the program stars

Star	RA(2000)	Dec.(2000)	B	V	J	H	K	Exposure (seconds)	Date of obs.	Source of spectrum	S/N (5500 Å)
HD 24035	03 43 42.53	-72 36 32.80	9.74	8.51	6.567	6.043	5.919	900	05/04/2002	UVES	110.35
HD 32712	05 01 34.91	-58 31 15.05	9.71	8.55	6.634	6.054	5.912	1200	11/11/1999	FEROS	86.20
HD 36650	05 27 42.92	-68 04 27.16	9.91	8.79	6.812	6.297	6.190	1200	10/11/1999	FEROS	79.67
HD 94518	10 54 12.20	-31 09 34.58	8.95	8.36	7.182	6.891	6.824	900	02/01/2000	FEROS	154.39
HD 147609	16 21 51.99	+27 22 27.19	9.69	9.18	8.211	8.035	7.948	2400(3)	01/06/2017	HESP	67.21
HD 154276	17 03 49.15	+17 11 21.08	9.80	9.13	7.911	7.624	7.549	2400(3)	06/05/2017	HESP	74.78
HD 179832	19 16 30.00	-49 13 13.01	9.46	8.44	6.660	6.163	6.031	600	14/07/2000	FEROS	161.26
HD 207585	21 50 34.71	-24 11 11.68	10.50	9.78	8.633	8.341	8.301	240	24/04/2002	UVES	110.59
HD 211173	22 15 57.01	-31 51 38.52	9.43	8.49	6.810	6.332	6.218	600	14/07/2000	FEROS	92.57
HD 219116	23 13 30.24	-17 22 08.71	10.29	9.25	7.602	7.137	7.012	240	19/05/2002	UVES	184.64
								2400(3)	30/10/2015	HESP	62.94

Note: The numbers in the parenthesis with exposures indicate the number of frames taken

3.3 Stellar atmospheric parameters and radial velocity estimation

Stellar atmospheric parameters are derived from Fe I and Fe II lines with excitation potentials ranging from 0.0 to 6.0 eV, and equivalent width ranging from 20 to 180 mÅ. The detailed procedure is given in section 2.6.4. The estimated abundances from Fe I and Fe II lines as function of excitation potential and equivalent widths are shown in Figure 3.2.

Radial velocities of the program stars are calculated using a set of clean and unblended lines of several elements. In Table 3.2, we present the derived atmospheric parameters and radial velocities of the program stars, along with their uncertainties. Discussion on uncertainties is given in detail in Section 2.6.6.

A comparison of our results with the literature values whenever available is given in Table 3.3. In most of the cases, our estimates of stellar atmospheric parameters match closely with the literature values. However, we note a difference in T_{eff} of ~ 400 K in the case of HD 147609 and HD 207585. The object HD 219116 shows a

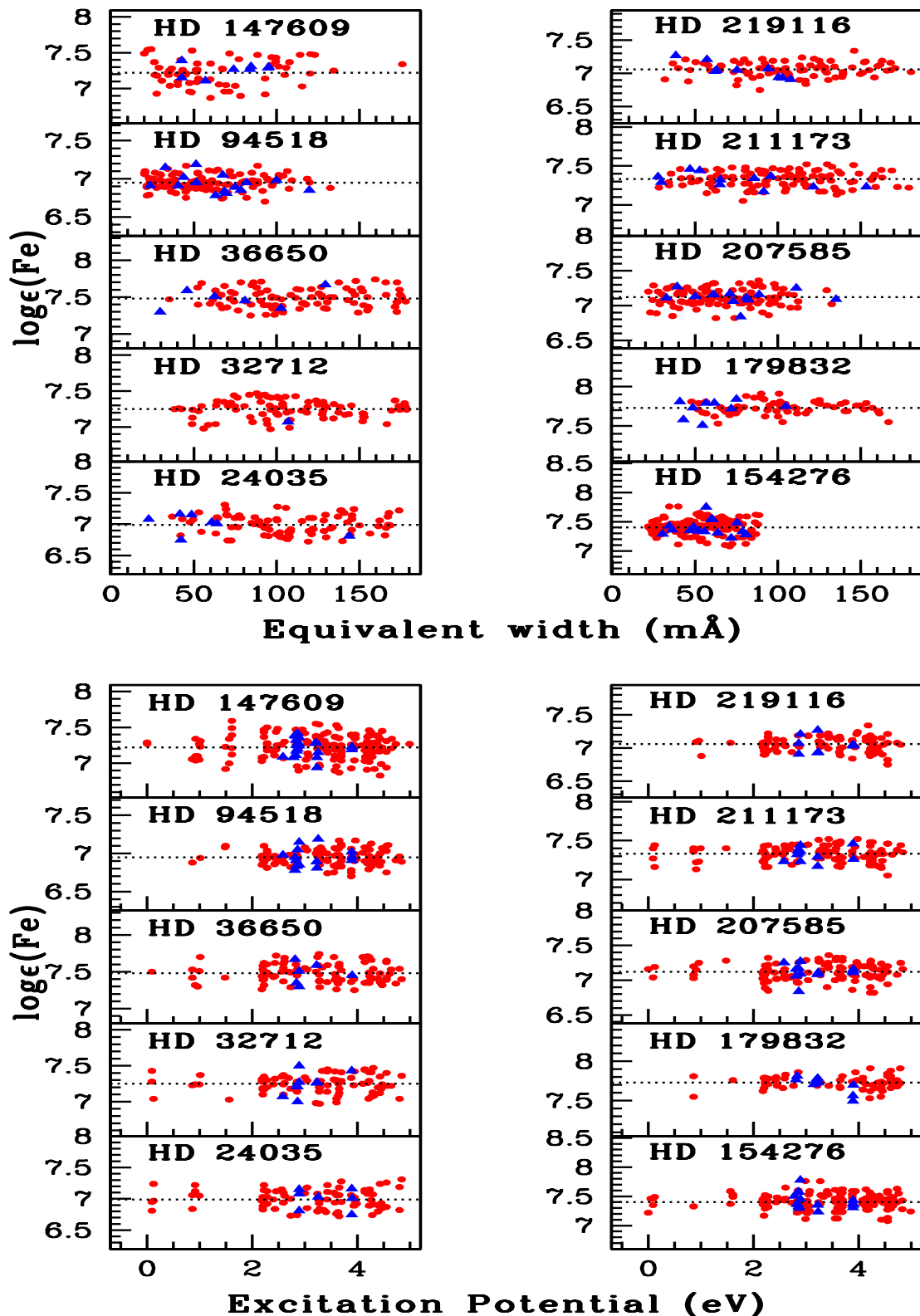


FIGURE 3.2: Iron abundances of the program stars derived from individual Fe I and Fe II lines as function of excitation potential (lower panel), and equivalent width (upper panel). The dotted lines correspond to the derived and adopted Fe abundance for each star. Solid circles correspond to Fe I and solid triangles correspond to Fe II lines.

TABLE 3.2: Derived atmospheric parameters for the program stars.

Star	T_{eff}	$\log g$	ζ	[Fe I/H]	[Fe II/H]	V_r
	(K)	cgs	(km s $^{-1}$)			(km s $^{-1}$)
	± 100	± 0.2	± 0.2			
HD 24035	4750	2.20	1.58	-0.51 ± 0.19	-0.50 ± 0.16	-1.56 ± 0.25
HD 32712	4550	2.53	1.24	-0.25 ± 0.12	-0.25 ± 0.12	$+10.37 \pm 0.02$
HD 36650	4880	2.40	1.30	-0.02 ± 0.12	-0.02 ± 0.14	$+36.40 \pm 0.19$
HD 94518	5700	3.86	1.30	-0.55 ± 0.10	-0.55 ± 0.12	$+92.20 \pm 0.43$
HD 147609	6350	3.50	1.55	-0.28 ± 0.16	-0.28 ± 0.12	-18.17 ± 1.47
HD 154276	5820	4.28	0.63	-0.09 ± 0.13	-0.10 ± 0.14	-64.17 ± 1.42
HD 179832	4780	2.70	0.99	$+0.23 \pm 0.04$	$+0.22 \pm 0.06$	$+6.73 \pm 0.03$
HD 207585	5800	3.80	1.00	-0.38 ± 0.12	-0.38 ± 0.11	-65.97 ± 0.07
HD 211173	4900	2.60	1.15	-0.17 ± 0.10	-0.17 ± 0.09	-27.84 ± 0.25
HD 219116	5050	2.50	1.59	-0.45 ± 0.11	-0.44 ± 0.11	-40.90 ± 0.25

difference of ~ 1 dex in $\log g$ from the literature. In the case of the stars HD 94518 and HD 207585, a difference of ~ 1 km s $^{-1}$ in ζ is recorded. These differences may be due to the difference in choices of line parameters, codes used, and the method of abundance analysis.

TABLE 3.3: Comparison of estimated stellar parameters with literature values

Star	T_{eff}	$\log g$	ζ	[Fe I/H]	[Fe II/H]	Ref.	Star	T_{eff}	$\log g$	ζ	[Fe I/H]	[Fe II/H]	Ref.
	(K)		(km s ⁻¹)					(K)		(km s ⁻¹)			
HD 24035	4750	2.20	1.58	-0.51	-0.50	1	HD 154276	5820	4.28	0.63	-0.09	-0.10	1
	4700	2.50	1.30	-0.23	-0.28	2		5722	4.28	0.93	-0.29	-	5
	4500	2.00	-	-0.14	-	3		5731	4.35	1.28	-0.30	-	11
HD 32712	4550	2.53	1.24	-0.25	-0.25	1	HD 179832	4780	2.70	0.99	+0.23	+0.22	1
	4600	2.10	1.30	-0.24	-0.25	2		5800	3.80	1.00	-0.38	-0.38	1
HD 36650	4880	2.40	1.30	-0.02	-0.02	1	HD 207585	5800	4.00	-	-0.20	-	3
	4800	2.30	1.50	-0.28	-0.28	2		5400	3.30	1.80	-0.57	-	12
HD 94518	5700	3.86	1.30	-0.55	-0.55	1	HD 211173	5400	3.50	1.50	-0.50	-	13
	5859	4.20	4.15	-0.56	-	4		4900	2.60	1.15	-0.17	-0.17	1
	5859	4.15	1.20	-0.49	-0.50	5		4800	2.50	-	-0.12	-	3
	5709	3.86	2.23	-0.84	-	6		5050	2.50	1.59	-0.45	-0.44	1
HD 147609	6350	3.50	1.55	-0.28	-0.28	1	HD 219116	4900	2.30	1.60	-0.61	-0.62	2
	6411	3.90	1.26	-0.23	-	7		4800	1.80	-	-0.34	-	3
	5960	3.30	1.50	-0.45	+0.08	8		5300	3.50	2.00	-0.30	-	14
	6270	3.50	1.20	-	-	9		5300	3.50	-	-0.34	-	15
	6300	3.61	1.20	-	-	10							

References: 1. Our work, 2. de Castro *et al.* (2016), 3. Masseron *et al.* (2010), 4. Battistini and Bensby (2015), 5. Bensby *et al.* (2014), 6. Axer *et al.* (1994), 7. Escorza *et al.* (2019) 8. Allen and Barbuy (2006), 9. North *et al.* (1994), 10. Thévenin and Idiart (1999), 11. Ramírez *et al.* (2013), 12. Luck and Bond (1991), 13. Smith and Lambert (1986a), 14. Smith *et al.* (1993), 15. Cenarro *et al.* (2007)

TABLE 3.4: Estimates of $\log g$ and Mass using parallax method

Star name	Parallax (mas)	M_{bol}	$\log(L/L_\odot)$	Mass(M_\odot)	$\log g$ (cgs)	$\log g$ (spectroscopic) (cgs)
HD 24035	4.612 ± 0.101	1.401 ± 0.05	1.339 ± 0.02	0.70 ± 0.21	2.61 ± 0.02	2.20
HD 32712	2.621 ± 0.026	0.081 ± 0.022	1.868 ± 0.01	1.80 ± 0.26	2.41 ± 0.005	2.53
HD 36650	2.655 ± 0.027	0.474 ± 0.023	1.710 ± 0.01	2.20 ± 0.26	2.78 ± 0.01	2.40
HD 94518	13.774 ± 0.05	3.872 ± 0.01	0.351 ± 0.003	0.85 ± 0.06	4.00 ± 0.005	3.86
HD 147609	4.301 ± 0.107	1.955 ± 0.055	1.118 ± 0.02	1.70 ± 0.05	3.71 ± 0.02	3.50
HD 154276	11.554 ± 0.025	4.339 ± 0.005	0.164 ± 0.002	1.00 ± 0.05	4.29 ± 0.002	4.28
HD 179832	2.914 ± 0.052	0.216 ± 0.041	1.814 ± 0.02	2.5 ± 0.28	2.70 ± 0.02	2.70
HD 207585	5.3146 ± 0.407	3.313 ± 0.165	0.575 ± 0.065	1.05 ± 0.05	3.90 ± 0.045	3.80
HD 211173	3.387 ± 0.066	0.839 ± 0.042	1.564 ± 0.02	2.20 ± 0.24	2.93 ± 0.02	2.60
HD 219116	1.584 ± 0.044	0.002 ± 0.06	1.901 ± 0.02	2.35 ± 0.17	2.68 ± 0.015	2.50

We have also calculated the $\log g$ values from the parallax method as described in Section 2.6.4.1. The masses of the program stars are determined from their location on the Hertzsprung-Russell diagram using the spectroscopic temperature estimate, T_{eff} , and the luminosity, $\log(L/L_\odot)$. The H-R diagram is generated using the stellar evolutionary tracks of Girardi *et al.* (2000).

We have used $z = 0.004$ tracks for HD 24035 and HD 94518; $z = 0.008$ for HD 207585 and HD 219116; $z = 0.019$ for HD 32712, HD 36650, HD 147609, HD 154276, and HD 211173, and $z = 0.030$ for HD 179832. The evolutionary tracks for the program stars are shown in Figures 3.3 and 3.4. The mass and $\log g$ estimates are presented in Table 3.4.

3.4 Abundance analysis and discussion

In this section, we discuss the details of abundance determination of various elements and the observed abundances.

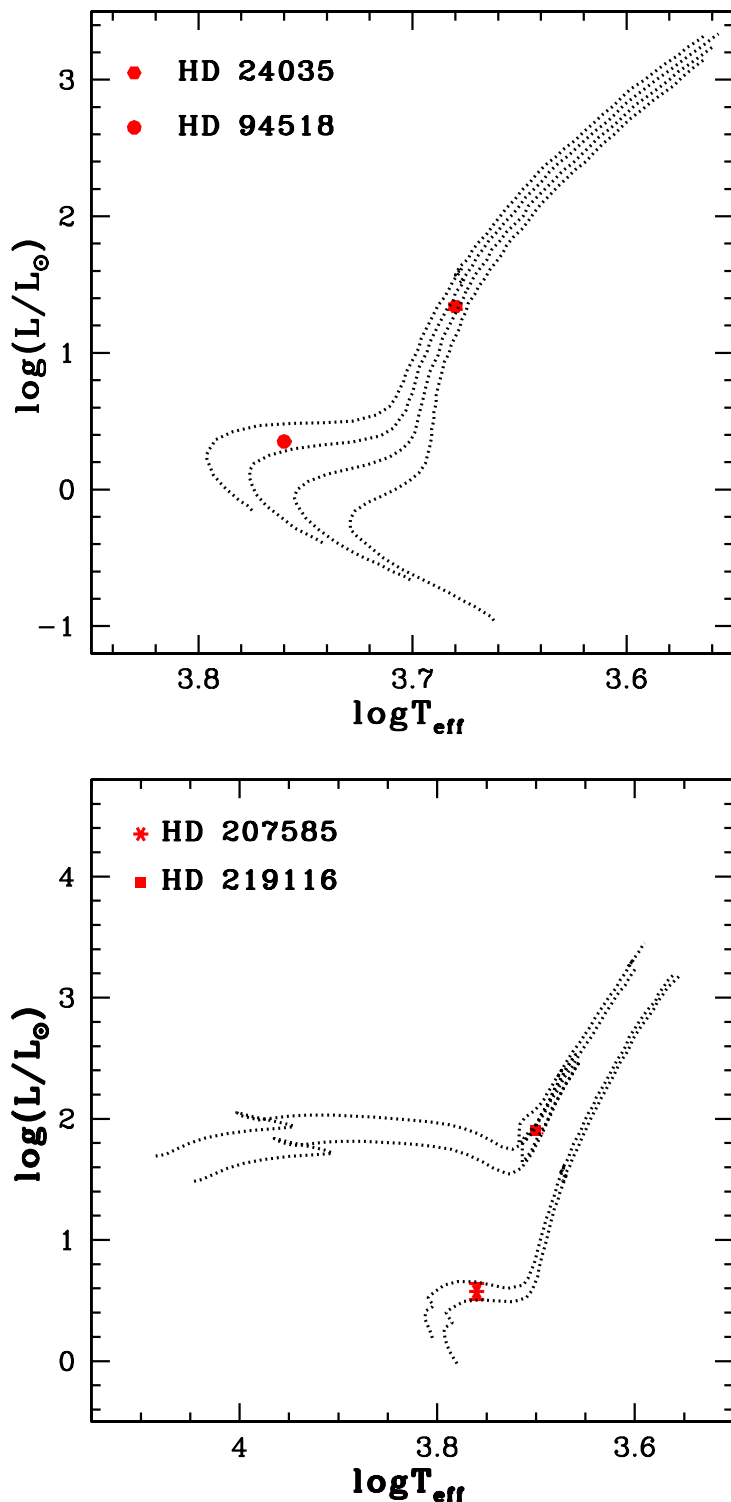


FIGURE 3.3: Location of the program stars on the H-R diagram (Girardi *et al.* 2000). Evolutionary tracks (from bottom to top) for (i) 0.6, 0.7, 0.8 and 0.9 M_\odot for $z = 0.004$ (upper panel), (ii) 1.0, 1.1, 2.2 and 2.5 M_\odot for $z = 0.008$ (lower panel).

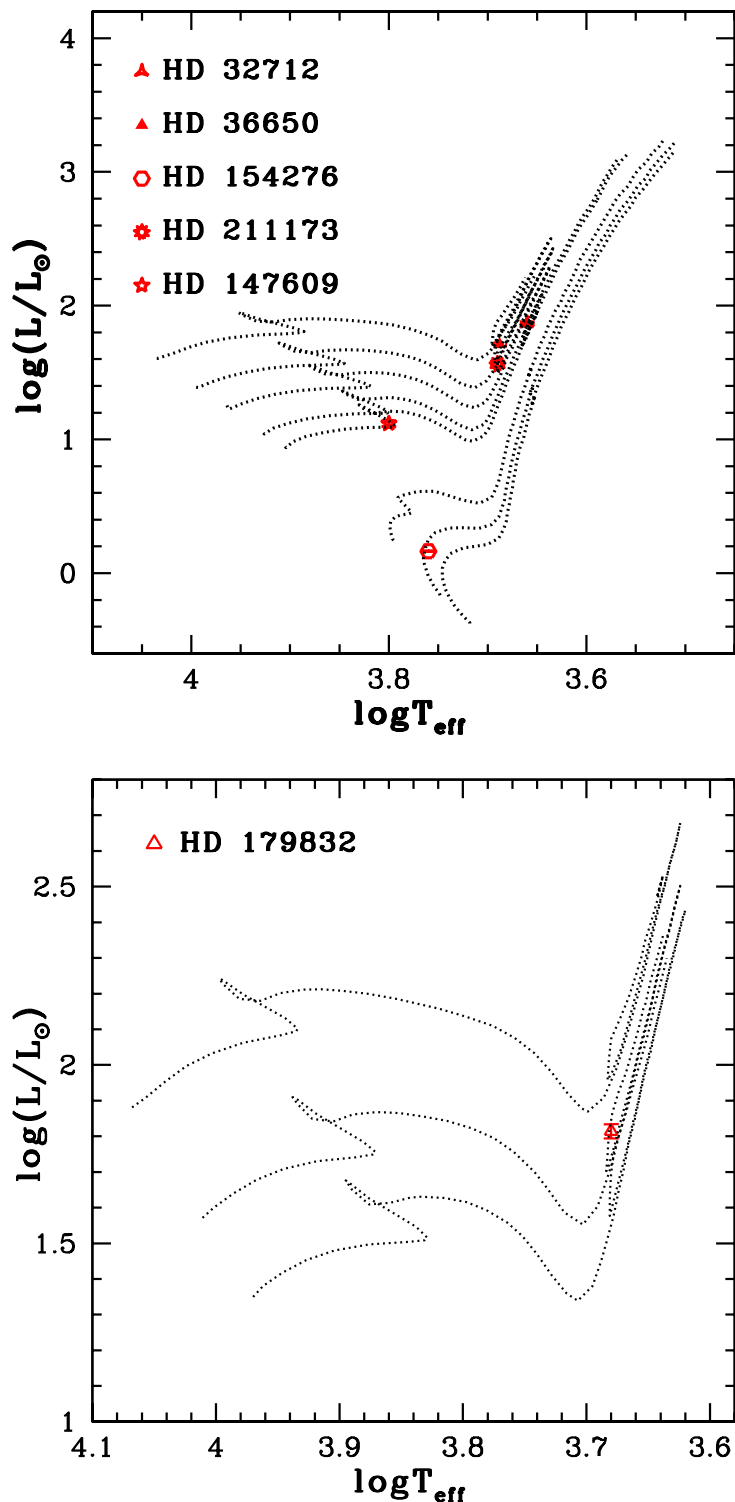


FIGURE 3.4: Location of the program stars on the H-R diagram (Girardi *et al.* 2000). Evolutionary tracks (from bottom to top) for (i) 0.9, 1.0, 1.2, 1.7, 1.8, 2.0, 2.2, and 2.5 M_\odot for $z = 0.019$ (upper panel), (ii) 2.2, 2.5 and 3.0 M_\odot for $z = 0.030$ (lower panel).

3.4.1 Light elements: C, N, O, carbon isotopic ratio $^{12}\text{C}/^{13}\text{C}$, odd-Z elements Na, Al, α -, and Fe-peak elements

The [O I] line at 6300.304 Å is used to derive the oxygen abundances whenever possible; otherwise, the resonance O I triplet lines around 7770 Å are used. The O I triplet lines are known to be affected by the NLTE effects (Eriksson and Toft 1979; Johnson *et al.* 1974; Baschek *et al.* 1977; Kiselman 1993; Amarsi *et al.* 2016). Corrections are made to the LTE abundance obtained from these lines following Bensby *et al.* (2004) and Afşar *et al.* (2012). The [O I] line at 6363.776 Å is found to be blended and not usable for abundance determination in any of the stars. This line is generally affected by the contributions from CN feature (Lambert 1978), and Ca I line around 6362 Å (Mitchell and Mohler 1965; Allende Prieto *et al.* 2001; Bensby *et al.* 2004). In Sun, this Ca I line contributes ~ 1.1 mÅ to the equivalent width of the [O I] 6363.776 Å line (Bensby *et al.* 2004).

We could use [O I] 6300.304 Å line for O abundance determination. Although the [O I] 6300.304 Å line is known to be affected by a Ni I feature at 6300.335 Å (Lambert 1978), the Ni I contamination is smaller on this [O I] 6300.304 Å line compared to the CN contamination on the [O I] 6363.776 Å line (Allende Prieto *et al.* 2001 and references therein). Also, the spectra of the program stars are not contaminated by the telluric absorption features in this region. The Sc II 6300.7 Å line is well displaced from this [O I] line and not blended. The Ni I 6300.335 Å line is taken into consideration while estimating the oxygen abundance using [O I] 6300.304 Å line. The average value of the Ni abundances derived from a number of lines of Ni I (10 - 27 lines) is adopted to derive the oxygen abundance from [O I] 6300.304 Å line.

The spectrum synthesis fits of O I triplet lines for a few program stars are shown in Figure 3.5. All three lines of the O I triplet gave the same abundance values, except for HD 147609. In the case of HD 147609, the lines at 7771 and 7774 Å

gave the same abundance, and the line at 7775 Å gave an abundance that is 0.15 dex lower. In this case, we have taken the average of the three values as the final oxygen abundance.

We have estimated the oxygen abundance in all the program stars except HD 24035. The derived abundance of oxygen is in the range $-0.47 \leq [\text{O}/\text{Fe}] \leq 0.97$. Oxygen is under abundant in HD 36650 and HD 211173 with $[\text{O}/\text{Fe}]$ values -0.47 and -0.26 respectively. HD 32712 and HD 179832 show near-solar values (Tables 3.5 - 3.7). Purandardas *et al.* (2019) found $[\text{O}/\text{Fe}] \sim -0.33$ for a barium star in their sample, somewhat closer to our lower limit. A mild overabundance is found in the stars HD 154276 and HD 219116 with $[\text{O}/\text{Fe}]$ values 0.32 and 0.21 respectively. In the other three stars, we found an $[\text{O}/\text{Fe}] > 0.6$, with HD 207585 showing the largest enhancement of oxygen $[\text{O}/\text{Fe}] \sim 0.97$. The first dredge-up (FDU) is not expected to alter the oxygen abundance.

For six objects, the carbon abundances are derived using the spectral synthesis calculation of C₂ band at 5165 Å, as illustrated in Figure 3.6. The G-band of CH at 4300 Å is used for two stars as the C₂ band at 5165 Å is not usable for the abundance determination. In the objects for which we could estimate the carbon abundance using both C₂ and CH bands, we find that the CH band returns a lower value for carbon by about 0.2 to 0.3 dex. We could determine the carbon abundance in all the objects except for HD 154276 and HD 179832. Carbon is found to be under abundant in most of the stars analyzed here. The $[\text{C}/\text{Fe}]$ value ranges from -0.28 to 0.61 . The stars HD 24035, HD 147609, and HD 207585 show a mild overabundance of carbon with values 0.41, 0.38, and 0.61 respectively, whereas it is near-solar in HD 32712 and HD 219116. HD 36650, HD 94518, and HD 211173 show mild under abundance with $[\text{C}/\text{Fe}]$ values, -0.22 , -0.28 , and -0.23 respectively (Tables 3.5 - 3.7). These values are consistent with those generally noticed in barium stars (Barbuy *et al.* 1992; North *et al.* 1994).

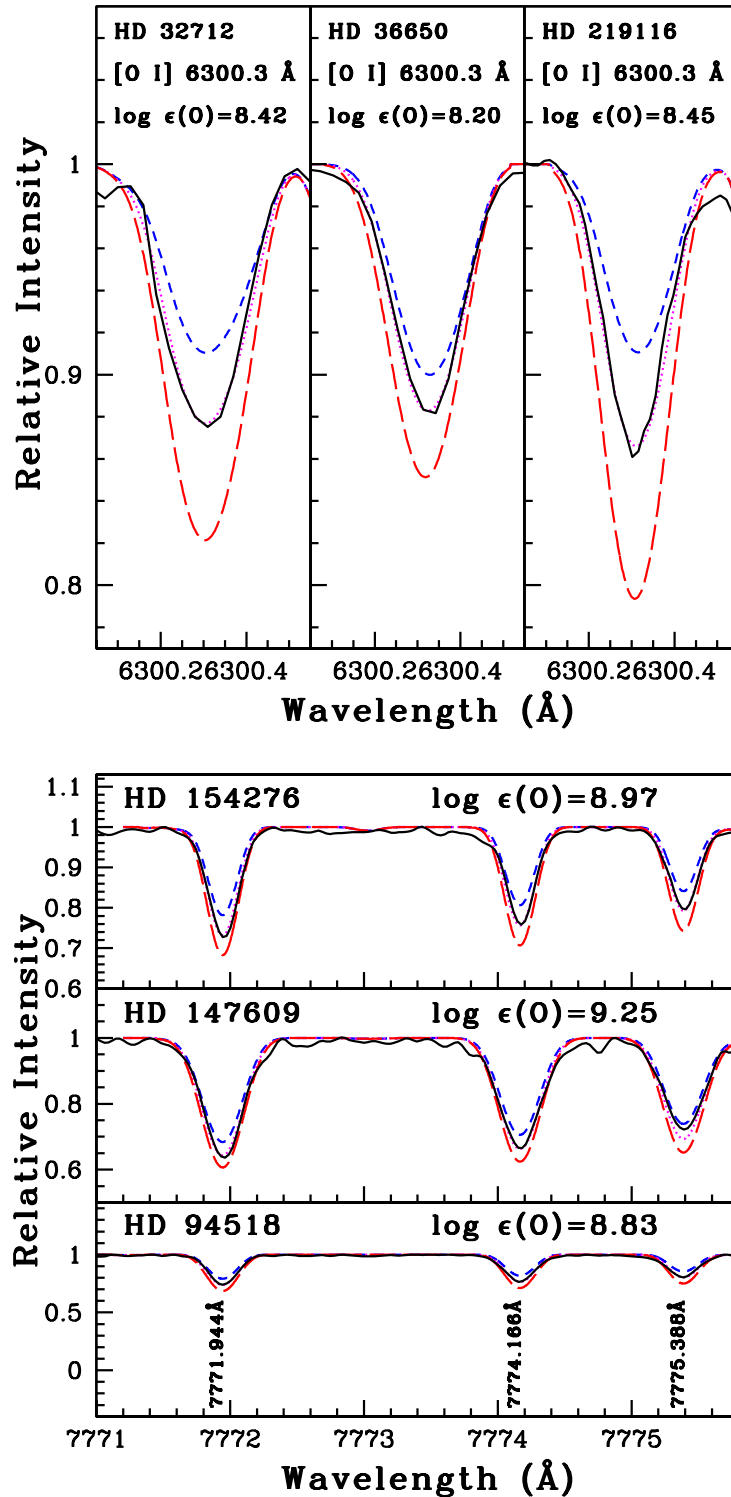


FIGURE 3.5: Synthesis of [O I] line around 6300 Å (upper panel) and O I triplet around 7770 Å (lower panel, LTE abundance estimates). Dotted and solid lines represent synthesized and the observed spectra. Short-dashed and long-dashed lines represent the synthetic spectra corresponding to $\Delta[\text{O}/\text{Fe}] = -0.3$ and $+0.3$ respectively.

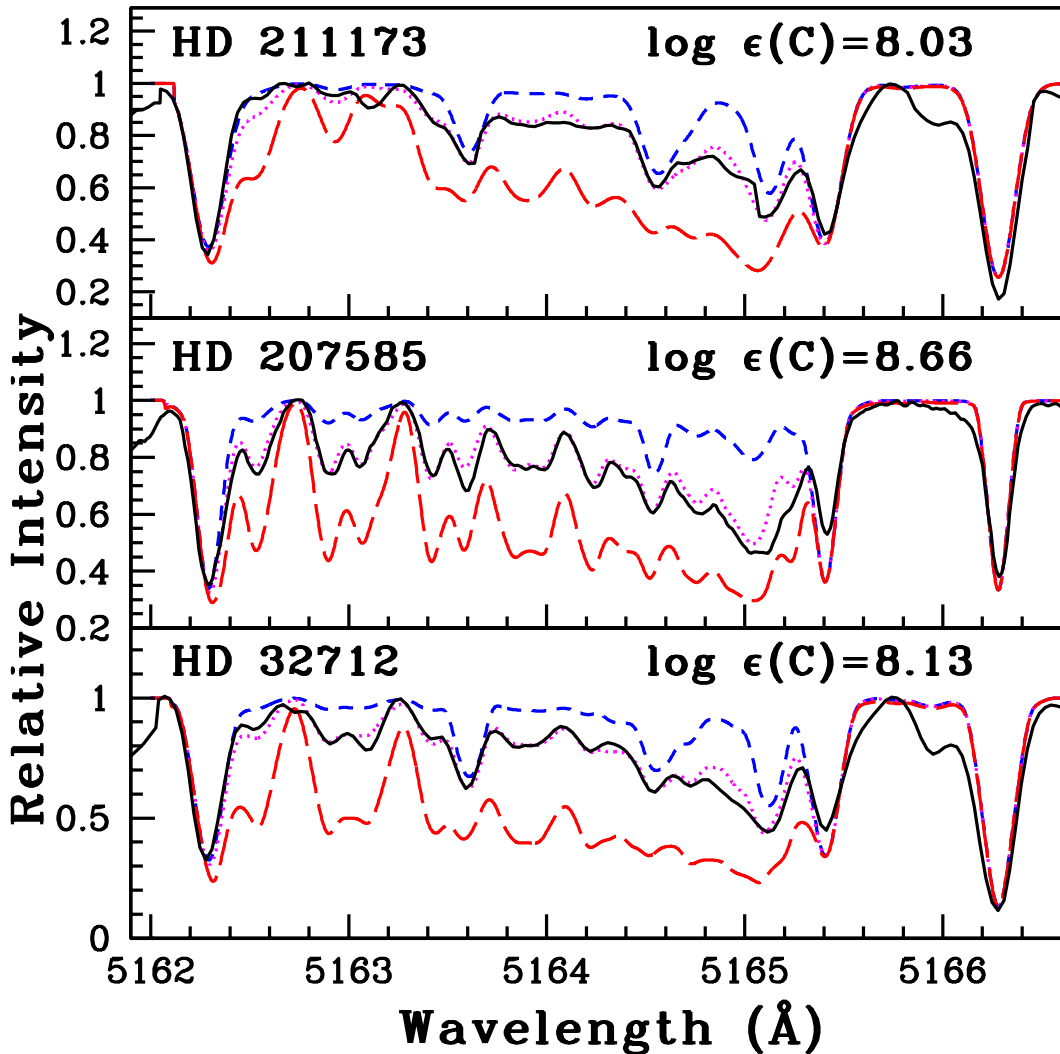


FIGURE 3.6: Synthesis of C₂ band around 5165 Å. Dotted and solid lines represent synthesized and the observed spectra. Short-dashed and long-dashed lines represent the synthetic spectra corresponding to Δ [C/Fe] = −0.3 and +0.3 respectively

With the estimated carbon abundance, we have derived the abundances of nitrogen using the spectrum synthesis calculation of ¹²CN lines at 8000 Å region in HD 32712, HD 36650, HD 94518 and HD 211173. For other objects, where this region is not usable or unavailable, ¹²CN band at 4215 Å is used. The molecular lines for ¹²CN and C₂ are taken from Brooke *et al.* (2013), Sneden *et al.* (2014), Ram *et al.* (2014).

The nitrogen abundance is estimated in seven of the program stars. Estimated

[N/Fe] values range from 0.47 to 1.41 dex with HD 24035 and HD 94518 showing [N/Fe] > 1.0 dex (Tables 3.5 - 3.7). Such higher values of nitrogen have already been noted in some barium stars by several authors (Smith 1984; Luck and Lambert 1985; Barbuy *et al.* 1992; Allen and Barbuy 2006; Smiljanic *et al.* 2006; Merle *et al.* 2016; Karinkuzhi *et al.* 2018a). Nitrogen enhancement with [N/Fe] > 1 is possible if the star is previously enriched by the pollution from a massive AGB companion experiencing Hot-Bottom Burning (HBB). In super-massive AGB stars, nitrogen can be substantially produced at the base of the convective envelope when the temperature of the envelope exceeds $\sim 10^8$ K (Doherty *et al.* 2014). The final C, N, and O abundances are determined by an iterative process. Using the first estimate of oxygen abundance, the abundance of carbon is estimated from the C₂/CH molecular bands. The abundance of nitrogen is then determined using these derived abundance estimates of O and C. Once the nitrogen abundance is obtained, the oxygen and carbon abundances are re-determined using this nitrogen abundance. This iteration process is continued until a convergence is reached.

We could derive the carbon isotopic ratio, ¹²C/¹³C, using the spectral synthesis calculation of the ¹²CN lines at 8003.292, 8003.553, 8003.910 Å, and ¹³CN features at 8004.554, 8004.728, 8004.781 Å, for four stars, HD 32712, HD 36650, HD 211173, and HD 219116. The values for this ratio are 20.0, 7.34, 20.0, and 7.34, respectively (Tables 3.5 - 3.7). Values in the range 7 - 20 (Barbuy *et al.* 1992; Smith *et al.* 1993; Smith 1984; Harris *et al.* 1985; Karinkuzhi *et al.* 2018a), and 13 - 33 (Tomkin and Lambert 1979; Sneden *et al.* 1981) are found in the literature for barium stars.

The lower level of carbon enrichment and the low ¹²C/¹³C ratio, along with the larger overabundance of nitrogen, indicate that the matter has undergone CN processing and the products have been brought to the surface by the FDU. From their locations on the H-R diagram, the four stars for which we could estimate the ¹²C/¹³C ratio (HD 32712, HD 36650, HD 94518, HD 211173, and HD 219116) are on the ascent of the first giant branch (FGB). These stars underwent the

FDU at the beginning of FGB. It has been noted that less evolved barium stars show higher carbon abundance as they have not reached the FDU (Barbuy *et al.* 1992; Allen and Barbuy 2006). Among our program stars, HD 207585 shows the maximum enhancement of carbon, which is on the sub-giant branch. However, the star HD 94518 shows the least enrichment among the program stars despite being less evolved one, a sub-giant barium star. According to Vanture (1992), if the accreted material is mixed into the hydrogen burning region of the star, either during the main sequence or the first ascent of the giant branch, certain nucleosynthesis can happen, thereby reducing the carbon abundance. Smiljanic *et al.* (2006) attribute the rotational mixing to the reduction in the surface carbon abundance. Even though the star has not reached the stage of dredge-up, the difference in the mean molecular weight of the accreted material and the inherent stellar materials in the interiors can induce thermohaline mixing, and this could also reduce the surface carbon abundance by an order of magnitude compared to the unaltered case (Stancliffe *et al.* 2007).

We have calculated the [C+N+O/Fe] ratios of the program stars, for which we could estimate the abundances of C, N, and O. This ratio can provide clues to the origin of heavy element enrichment in the stars. The values obtained for [C+N+O/Fe] for HD 32712, HD 36650, HD 94518, HD 207585, HD 211173, and HD 219116 are 0.05, -0.15 , 0.67, 0.87, -0.10 , and 0.20, respectively. For Ba giants, a value in the range $0.06 \leq [\text{C}+\text{N}+\text{O}/\text{Fe}] \leq 0.24$ is noted by Barbuy *et al.* (1992). Allen and Barbuy (2006) obtained values in the range of 0.01 - 0.73 for their sample of Ba stars that includes dwarfs as well as giants, with the least evolved star showing the largest value. The estimated [C+N+O/Fe] ratios of the program stars as a function of $\log g$ is shown in Figure 3.7. The four stars, HD 32712, HD 36650, HD 94518, HD 211173, and HD 219116, are on the FGB (Figures 3.3 - 3.4), and might have undergone the FDU. In giants, after the FDU, [N/Fe] can reach a value ~ 0.55 (Allen and Barbuy 2006). We have noted similar values ([N/Fe] ~ 0.5 , Tables 3.5 - 3.7) in these four giants, indicating the operation of

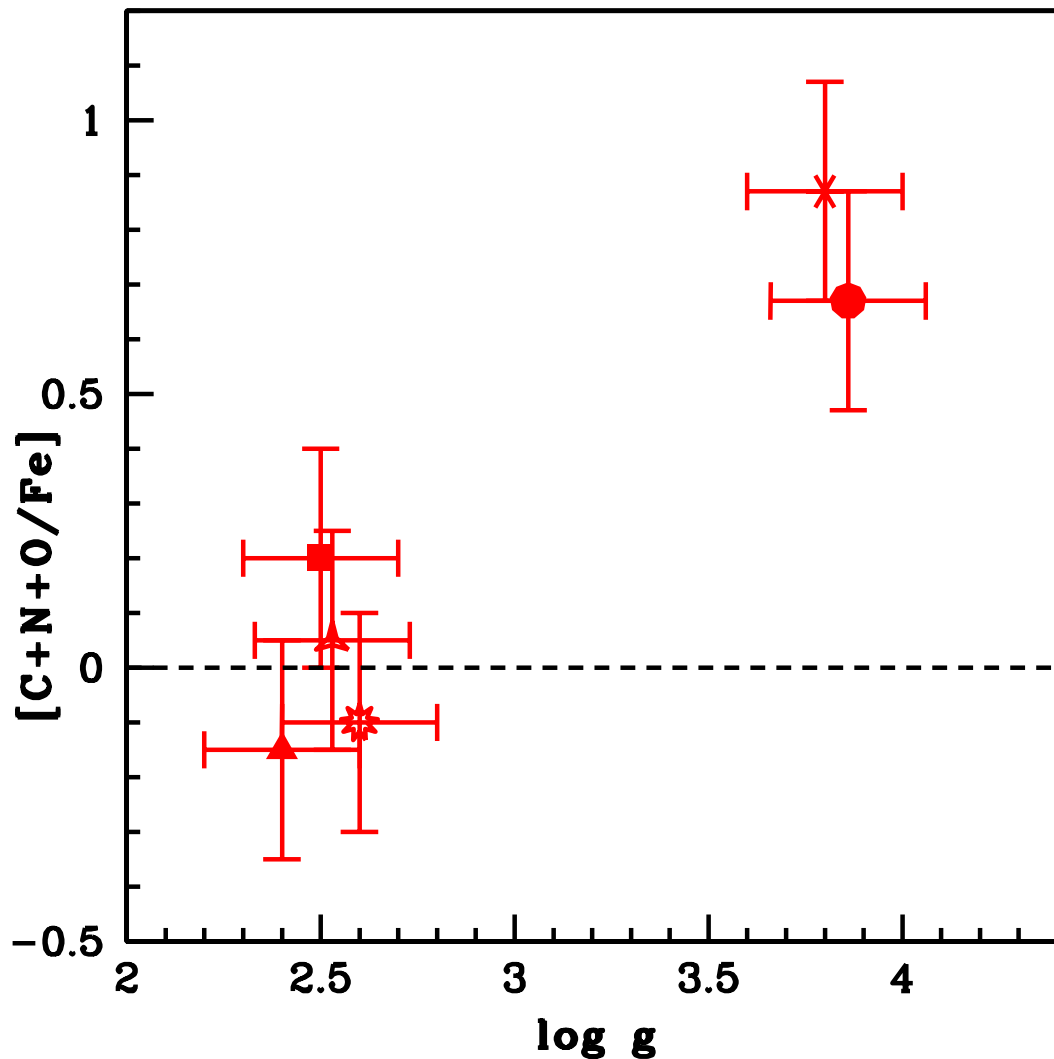


FIGURE 3.7: Observed $[C+N+O/Fe]$ ratios of the program stars as function of surface gravity, $\log g$. HD 32712 (starred triangle), HD 36650 (filled triangle), HD 94518 (filled circle), HD 207585 (six-sided cross), HD 211173 (nine-sided star), and HD 219116 (filled square).

FDU. However, these stars, except for HD 219116, do not show any $[C+N+O/Fe]$ excess (values are close to zero). The stars HD 94518 (0.67) and HD 207585 (0.87) show the highest values for $[C+N+O/Fe]$ ratio. Less evolved Ba stars are expected to show $[C+N+O/Fe]$ excess due to their enhanced N abundance (Allen and Barbuy 2006). As discussed previously, these two are the least evolved (Figure 3.7), and show higher N abundances ($[N/Fe] > 0.7$, Tables 3.5 - 3.7). This may be responsible for their $[C+N+O/Fe]$ excess.

We have estimated the C/O ratios of the program stars except for HD 24035, HD 154276, and HD 179832. The estimated C/O < 1, as normally seen in barium stars (Table 3.10).

The estimated Na abundances in the range $0.05 \leq [\text{Na}/\text{Fe}] \leq 0.42$ are similar to what is normally seen for the disk stars, normal field giants, and some barium stars (Antipova *et al.* 2004; de Castro *et al.* 2016; Karinkuzhi *et al.* 2018a). The derived abundance of aluminium in HD 154276 and HD 211173 returns near-solar values $[\text{Al}/\text{Fe}] \sim -0.12$ and -0.11 respectively. Yang *et al.* (2016) found a range $-0.22 \leq [\text{Al}/\text{Fe}] \leq 0.56$, Allen and Barbuy (2006) $-0.1 \leq [\text{Al}/\text{Fe}] \leq 0.1$, and de Castro *et al.* (2016) $-0.07 \leq [\text{Al}/\text{Fe}] \leq 0.43$ for their sample of barium stars. The estimated abundances of Mg are in the range $-0.10 \leq [\text{Mg}/\text{Fe}] \leq 0.34$. The estimated abundances for other elements, from Si to Zn, are found to be well within the range normally seen for the disk stars (Tables 3.5 - 3.7). The hyperfine components of Sc and Mn are taken from Prochaska and McWilliam (2000), V, Co and Cu from Prochaska *et al.* (2000).

A comparison of the light element abundances observed in our program stars with their counterparts in normal stars and other Ba stars in literature is shown in Figure 3.8. The observed abundances of our program stars are found to match closely with the abundances of other Ba and normal stars from literature.

3.4.2 Heavy elements

3.4.2.1 The light s-process elements: Rb, Sr, Y, Zr

The abundance of Rb is derived using the spectral synthesis calculation of Rb I resonance line at 7800.259 Å in the stars HD 32712, HD 36650, HD 179832 and

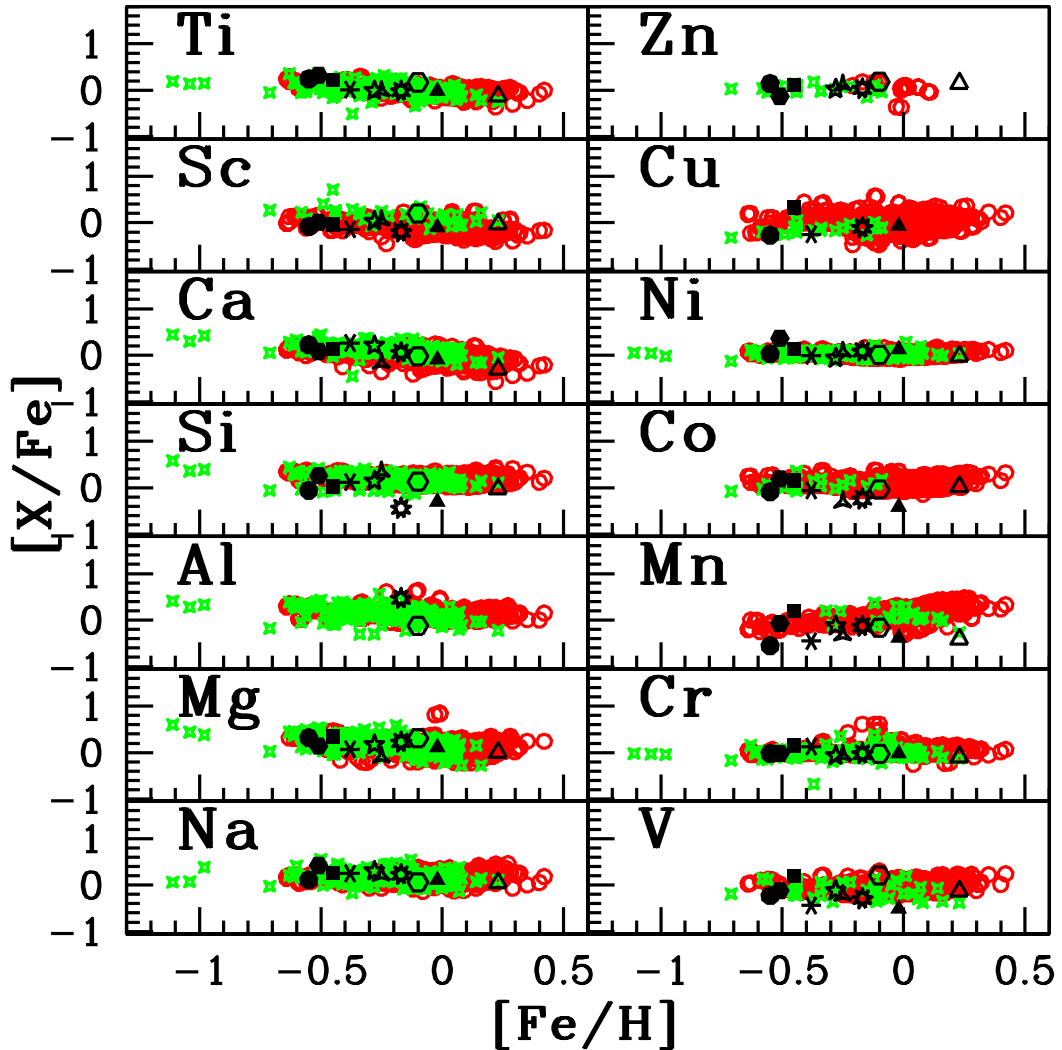


FIGURE 3.8: Observed $[X/\text{Fe}]$ ratios of the light elements (Tables 3.5 - 3.7) for the program stars with respect to metallicity $[\text{Fe}/\text{H}]$. Red open circles represent normal giants from literature (Luck and Heiter 2007). Green four-sided stars represent Ba stars from literature (Allen and Barbay 2006; de Castro *et al.* 2016; Yang *et al.* 2016; Karinkuzhi *et al.* 2018a,b). HD 24035 (filled hexagon), HD 32712 (starred triangle), HD 36650 (filled triangle), HD 94518 (filled circle), HD 147609 (five-sided star), HD 154276 (open hexagon), HD 179832 (open triangle), HD 207585 (six-sided cross), HD 211173 (nine-sided star), and HD 219116 (filled square).

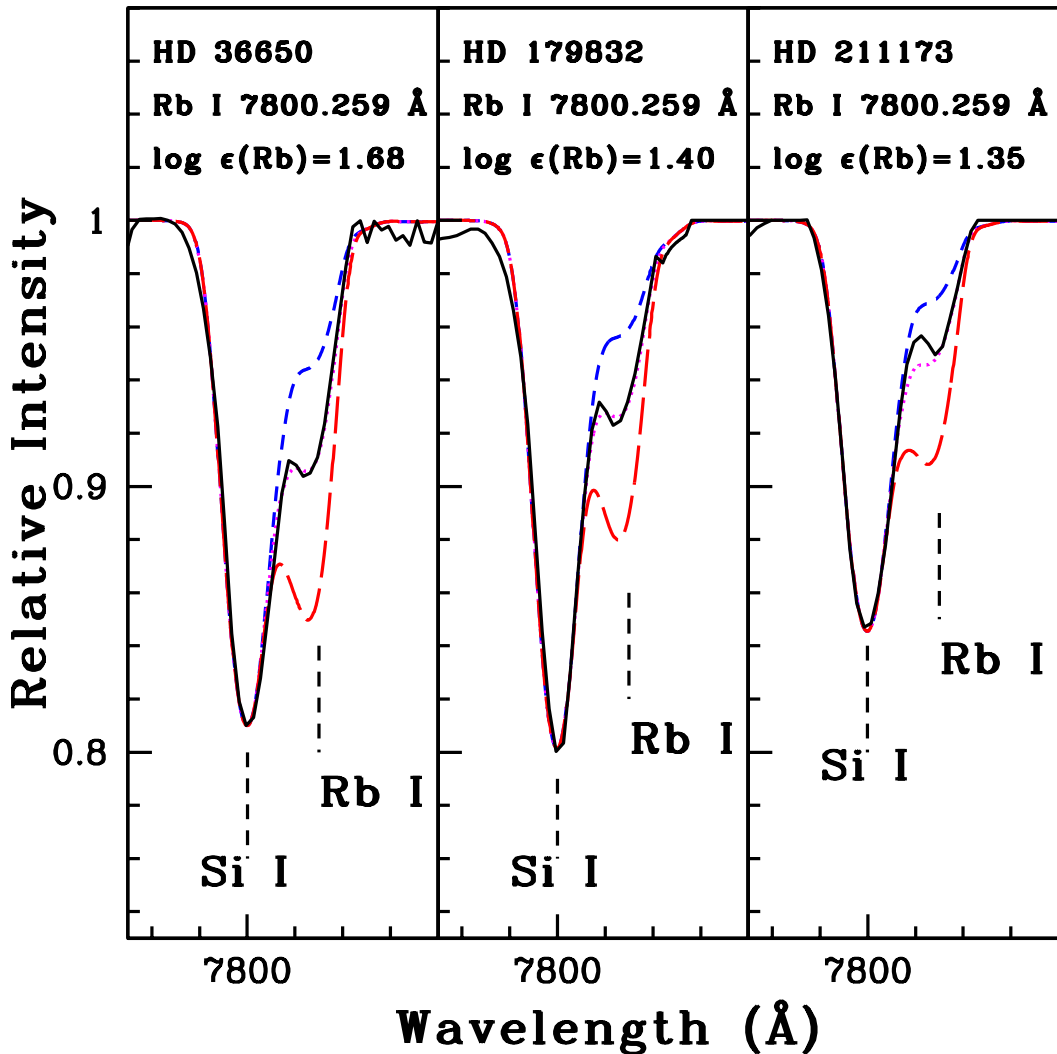


FIGURE 3.9: Spectral synthesis of Rb I line around 7800 Å. Dotted and solid lines represent synthesized and the observed spectra. Short-dashed and long-dashed lines represent the synthetic spectra corresponding to $\Delta[\text{Rb}/\text{Fe}] = -0.3$ and $+0.3$ respectively

HD 211173. We could not detect the Rb I lines in the warmer program stars. The NLTE effect on the abundance derived from this line is negligible ($|\Delta_{NLTE}| < 0.05$) for the temperatures and surface gravities of our program stars (Takeda 2021). The Rb I resonance line at 7947.597 Å is very weak and could not be used for abundance estimation. The hyperfine components of Rb are taken from Lambert and Luck (1976). The spectrum synthesis fits of Rb for a few program stars are shown in Figure 3.9. Rubidium is found to be under abundant in all the four program stars with $[\text{Rb}/\text{Fe}]$ ranging from -1.35 to -0.82 (Tables 3.5 - 3.7).

Strontium abundances are derived from the spectral synthesis calculation of Sr I line at 4607.327 Å whenever possible. The NLTE correction to the abundance derived from this line is adopted from Bergemann *et al.* (2012). HD 154276 shows a mild under abundance with value $[\text{Sr}/\text{Fe}] \sim -0.22$, while HD 32712 and HD 179832 show near-solar values. Other stars show enrichment with values $[\text{Sr}/\text{Fe}] \geq 0.66$ (Tables 3.5 - 3.7).

The abundance of Y is derived from the spectral synthesis calculation of Y I line at 6435.004 Å in all the program stars except for HD 94518, HD 147609, HD 154276, and HD 179832, where no useful Y I line were detected. While the spectral synthesis of Y II line at 5289.815 Å is used in HD 94518, the equivalent width measurement of several lines of Y II is used in other stars. We could not find any useful Y II lines in HD 24035 for the abundance determination. The abundances estimated from Y I lines range from 0.38 to 1.61, and that from Y II lines 0.07 to 1.37 (Tables 3.5 - 3.7).

The spectral synthesis of Zr I line at 6134.585 Å is used in all the stars except HD 94518, HD 147609, and HD 154276, where this line was not detected. We could detect useful Zr II lines in all the program stars except HD 36650 and HD 219116. In HD 24035, the equivalent width measurement of Zr II lines at 4317.321 and 5112.297 Å are used. Spectral synthesis calculation of Zr II line at 4208.977 Å is used in HD 94518, HD 147609 and HD 154276, line at 5112.297 Å is used in HD 32712, HD 179832, HD 207585 and HD 211173. The measurement using Zr I lines gives the value $0.38 \leq [\text{Zr I}/\text{Fe}] \leq 1.29$ and Zr II lines return $-0.08 \leq [\text{Zr II}/\text{Fe}] \leq 1.89$ (Tables 3.5 - 3.7). The spectrum synthesis of Zr for a few program stars are shown in Figure 3.10.

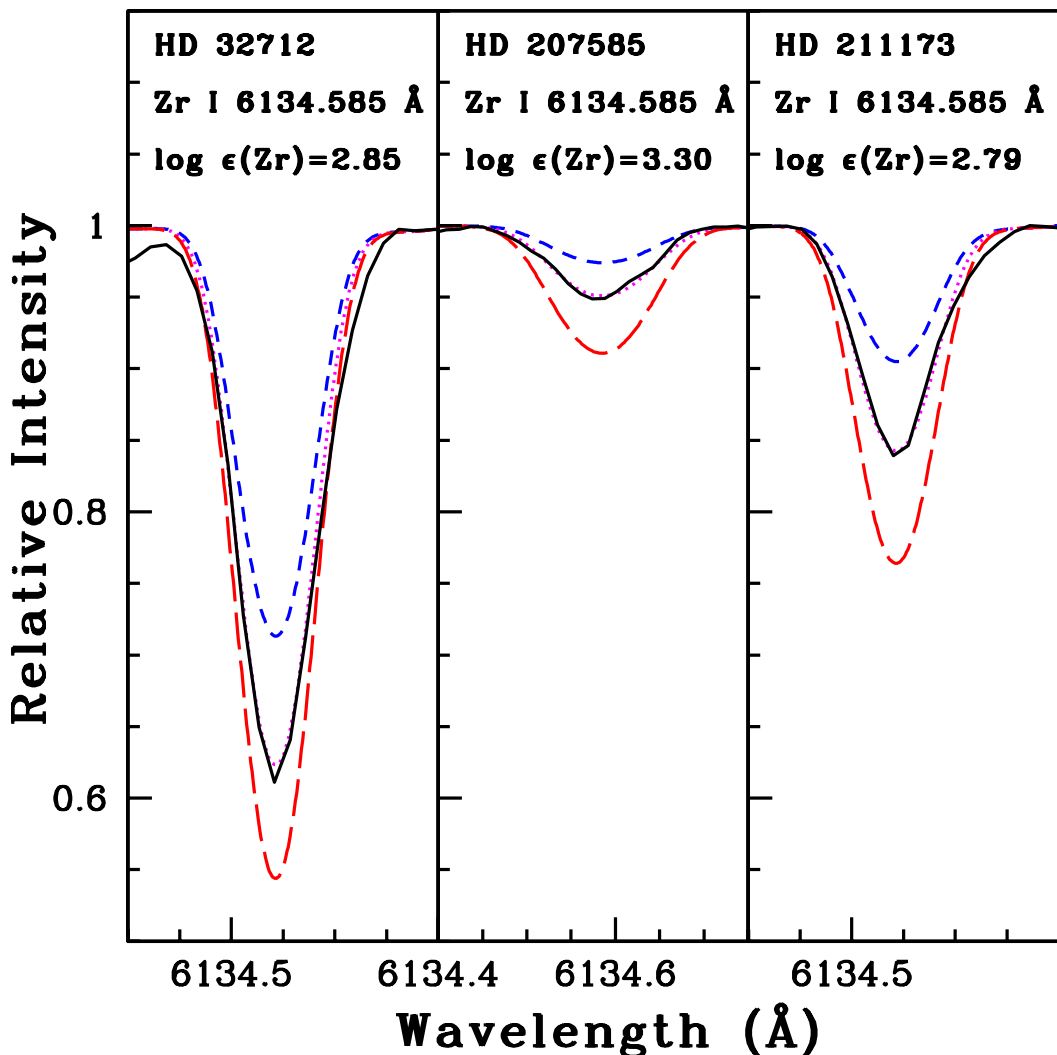


FIGURE 3.10: Synthesis of Zr I line at 6134.585 Å. Dotted and solid lines represent synthesized and the observed spectra. Short-dashed and long-dashed lines represent the synthetic spectra corresponding to $\Delta[\text{Zr}/\text{Fe}] = -0.3$ and $+0.3$ respectively

3.4.2.2 The heavy s-process elements: Ba, La, Ce, Pr, Nd

The abundance of Ba is derived from the spectral synthesis calculation. Ba II lines at 5853.668, 6141.713, and 6496.897 Å are used in HD 154276, whereas in all other stars, we have used the line at 5853.668 Å. The hyperfine components of Ba are taken from McWilliam (1998). The spectrum synthesis fits for Ba for a few program stars are shown in Figure 3.11. Ba shows slight overabundance in

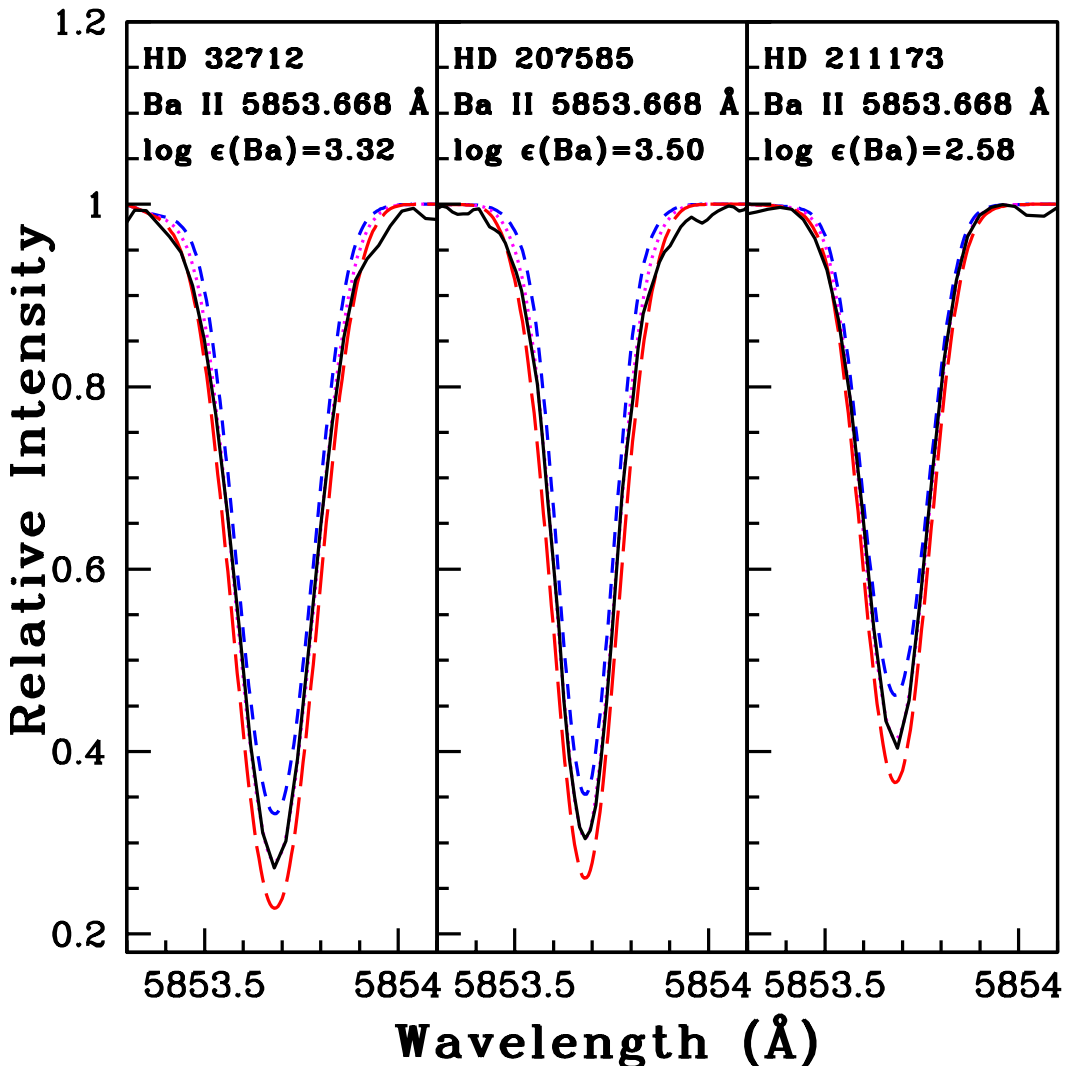


FIGURE 3.11: Synthesis of Ba II line at 5853.668 Å. Dotted and solid lines represent synthesized and the observed spectra. Short-dashed and long-dashed lines represent the synthetic spectra corresponding to $\Delta[\text{Ba}/\text{Fe}] = -0.3$ and $+0.3$ respectively

HD 154276 with $[\text{Ba}/\text{Fe}] \sim 0.22$, whereas HD 179832 and HD 211173 show moderate enhancement with values 0.41 and 0.57 respectively. All other program stars show the overabundance of Ba in the range 0.79 to 1.71 (Tables 3.5 - 3.7).

Lanthanum abundance is obtained from the spectral synthesis analysis of La II line at 4322.503 Å in HD 147609. For all other stars, spectral synthesis analysis of La II line at 4921.776 Å is used. The hyperfine components of La are taken from Jonsell *et al.* (2006). The estimated La abundances are in the range $0.20 \leq$

$[\text{La}/\text{Fe}] \leq 1.70$. HD 154276 shows a mild enhancement of La with $[\text{La}/\text{Fe}] \sim 0.20$. All other program stars are enhanced in La with $[\text{La}/\text{Fe}]$ ranging from 0.52 to 1.70 (Tables 3.5 - 3.7).

The abundance of Ce is obtained from the equivalent width measurement of several Ce II lines. The star HD 154276 show near-solar abundance for Ce with $[\text{Ce}/\text{Fe}] \sim 0.18$, whereas all other stars are over abundant in Ce with $[\text{Ce}/\text{Fe}] > 0.7$ (Tables 3.5 - 3.7). The abundance of Pr is derived from the equivalent width measurement of Pr II lines, whenever possible. We could not estimate Pr abundance in HD 94518 and HD 154276 as there were no useful lines detected. While HD 179832 is mildly enhanced in Pr with $[\text{Pr}/\text{Fe}] \sim 0.23$, other stars show the enrichment in the range 0.85 to 1.98 (Tables 3.5 - 3.7). Abundance of Nd is estimated from the spectral synthesis calculation of Nd II lines at 4177.320 and 4706.543 Å in HD 154276. In all other stars, we have used the equivalent width measurement of several Nd II lines. A near-solar value is obtained for the Nd abundance in the star HD 179832 with $[\text{Nd}/\text{Fe}] \sim 0.04$, whereas a moderate enhancement is found in HD 154276 with $[\text{Nd}/\text{Fe}] \sim 0.40$. All other objects show an enrichment in Nd with $[\text{Nd}/\text{Fe}] > 0.70$ (Tables 3.5 - 3.7).

3.4.2.3 The r-process elements: Sm, Eu

Samarium abundance is derived by the spectral synthesis of Sm II line at 4467.341 Å in HD 154276. The equivalent width measurement of several Sm II lines is used to obtain the Sm abundance in the rest of the program stars. All the good Sm lines are found in the bluer wavelength region of the spectra. The maximum number of Sm II lines used is eight, in HD 207585. The estimated Sm abundances give a near-solar value for HD 154276 with $[\text{Sm}/\text{Fe}] \sim 0.07$, while all other stars are enriched in Sm with values ranging from 0.78 to 2.04 (Tables 3.5 - 3.7).

The Eu abundance is derived from the spectral synthesis of Eu II line at 4129.725 Å in HD 94518, HD 147609, and HD 207585. In all other stars except HD 154276, spectral synthesis calculation of Eu II line at 6645.064 Å is used. In HD 154276, no useful lines for abundance analysis is detected. The hyperfine components are taken from Worley *et al.* (2013). The estimated Eu abundance covers the range $0.00 \leq [\text{Eu}/\text{Fe}] \leq 0.49$ (Tables 3.5 - 3.7). The r-process element Eu is not expected to show enhancement in Ba stars according to their formation scenario.

The abundance estimates are given in Tables 3.5 through 3.7 and the lines used for the the abundance estimation are presented in Tables A1 and A2 (Section 3.11).

A comparison of the heavy element abundances with the literature values, whenever available, is presented in Table 3.8. In most of the cases, our estimates agree, within error bars, with the literature values. However, in a few cases, our estimates show deviation from those available in literature. For instance, in the case of HD 24035, we got a [La II/Fe] value that is 1.07 dex lower than the estimate of de Castro *et al.* (2016). In HD 32712, our estimates of [Ce II, Nd II/Fe] are ~ 0.50 dex higher than those of de Castro *et al.* (2016) (Table 3.8). These differences between our estimated abundances with those by other authors may be due to the difference in stellar atmospheric parameters (Table 3.3).

The observed abundance ratios of the heavy elements in the program stars are compared with those in normal stars and other Ba stars from literature. This comparison is shown in Figure 3.12. The observed abundance ratios when compared with their counterparts in other barium stars from the literature, the light as well as the heavy element Eu, are found to follow the Galactic trend (Figure 3.8 and 3.12).

TABLE 3.5: Elemental abundances in HD 24035, HD 32712, and HD 36650

	Z	HD 24035				HD 32712				HD 36650	
		solar log ϵ^*	log ϵ	[X/H]	[X/Fe]	log ϵ	[X/H]	[X/Fe]	log ϵ	[X/H]	[X/Fe]
C	6	8.43	8.33(syn)	-0.10	0.41	8.13(syn)	-0.3	-0.05	8.19(syn)	-0.24	-0.22
$^{12}\text{C}/^{13}\text{C}$	-	-	-	-	-	-	-	20.0	-	-	7.34
N	7	7.83	8.73(syn)	0.90	1.41	8.10(syn)	0.27	0.52	8.38(syn)	0.55	0.57
O	8	8.69	-	-	-	8.42(syn)	-0.27	-0.02	8.20(syn)	-0.49	-0.47
Na I	11	6.24	6.15±0.17(4)	-0.09	0.42	6.20±0.13(4)	-0.04	0.21	6.33±0.08(4)	0.09	0.11
Mg I	12	7.60	7.23(1)	-0.37	0.14	7.25±0.20(2)	-0.35	-0.10	7.69±0.04(2)	0.09	0.11
Si I	14	7.51	7.26±0.04(2)	-0.25	0.14	7.60±0.19(3)	0.09	0.34	7.28±0.10(3)	-0.23	-0.21
Ca I	20	6.34	5.91±0.13(10)	0.43	0.08	5.92±0.09(11)	-0.42	-0.17	6.23±0.12(16)	-0.11	-0.09
Sc II	21	3.15	2.65(syn)	-0.50	0.01	2.95(syn)	-0.20	0.05	3.08(syn)	-0.12	-0.10
Ti I	22	4.95	4.76±0.11(19)	-0.19	0.32	4.68±0.11(27)	-0.27	-0.02	4.92±0.09(24)	-0.03	-0.01
Ti II	22	4.95	4.68±0.03(2)	-0.27	0.24	4.75±0.11(5)	-0.20	0.05	4.97±0.14(7)	0.02	0.04
V I	23	3.93	3.30(syn)	-0.63	-0.12	3.46(syn)	-0.47	-0.22	3.92(syn)	-0.53	-0.51
Cr I	24	5.64	5.11±0.06(6)	-0.53	-0.02	5.33±0.17(7)	-0.31	-0.06	5.60±0.15(9)	-0.04	-0.02
Cr II	24	5.64	-	-	-	5.72±0.17(4)	0.08	0.33	5.54±0.08(3)	-0.10	-0.08
Mn I	25	5.43	4.85(syn)	-0.58	-0.07	4.86(syn)	-0.57	-0.32	5.08(syn)	-0.40	-0.38
Fe I	26	7.50	6.99±0.19(87)	-0.51	-	7.25±0.12(84)	-0.25	-	7.48±0.12(92)	-0.02	-
Fe II	26	7.50	7.00±0.16(7)	-0.50	-	7.25±0.15(9)	-0.25	-	7.48±0.14(6)	-0.02	-
Co I	27	4.99	4.67(syn)	-0.32	0.19	4.43(syn)	-0.56	-0.31	4.86(syn)	-0.43	-0.41
Ni I	28	6.22	6.07±0.14(13)	-0.15	0.36	6.04±0.18(11)	-0.18	0.07	6.33±0.10(11)	0.11	0.13
Cu I	29	4.19	-	-	-	-	-	-	4.57(syn)	-0.09	-0.07
Zn I	30	4.56	3.92(1)	-0.64	-0.13	4.42(1)	-0.14	0.11	-	-	-
Rb I	37	2.52	-	-	-	1.14(syn)	-1.38	-1.13	1.68(syn)	-0.84	-0.82
Sr I	38	2.87	-	-	-	2.65(syn)	-0.22	0.03	3.78(syn)	0.64	0.66
Y I	39	2.21	3.31(syn)	1.1	1.61	2.52(syn)	0.31	0.56	2.70(syn)	0.49	0.51
Y II	39	2.21	-	-	-	3.00±0.15(6)	0.79	1.04	2.89±0.13(10)	0.68	0.70
Zr I	40	2.58	3.28(syn)	0.7	1.21	2.85(syn)	0.27	0.52	3.07(syn)	0.49	0.51
Zr II	40	2.58	3.96±0.07(2)	1.38	1.89	3.15(syn)	0.57	0.82	-	-	-
Ba II	56	2.18	3.38(syn)	1.20	1.71	3.32(syn)	1.14	1.39	2.95(syn)	0.77	0.79
La II	57	1.10	2.22(syn)	1.12	1.63	2.10(syn)	1.00	1.25	1.81(syn)	0.60	0.62
Ce II	58	1.58	2.77±0.12(9)	1.19	1.70	3.01±0.11(11)	1.43	1.68	2.55±0.13(11)	0.97	0.99
Pr II	59	0.72	2.19±0.18(6)	1.47	1.98	2.14±0.18(6)	1.42	1.67	1.55±0.13(3)	0.83	0.85
Nd II	60	1.42	2.32±0.17(15)	0.90	1.41	2.93±0.18(11)	1.51	1.76	2.34±0.16(15)	0.92	0.94
Sm II	62	0.96	2.48±0.13(4)	1.52	2.03	2.42±0.17(6)	1.46	1.71	1.93±0.12(6)	0.97	0.99
Eu II	63	0.52	0.50(syn)	-0.02	0.49	0.61(syn)	0.09	0.34	0.59(syn)	0.07	0.09

Note: * Asplund *et al.* (2009), The number of lines used to determine abundance is indicated in parentheses.

TABLE 3.6: Elemental abundances in HD 94518, HD 147609, and HD 154276

	Z	HD 94518			HD 147609			HD 154276		
		solar log ϵ^*	log ϵ	[X/H]	[X/Fe]	log ϵ	[X/H]	[X/Fe]	log ϵ	[X/H]
C	6	8.43	7.60(syn)	-0.83	-0.28	8.53(syn)	0.10	0.38	-	-
N	7	7.83	8.63(syn)	0.80	1.35	-	-	-	-	-
O	8	8.69	8.79(syn)	0.10	0.65	9.05(syn)	0.36	0.64	8.91(syn)	0.22
Na I	11	6.24	5.88±0.06(4)	-0.44	0.11	6.26±0.19(2)	0.02	0.30	6.20±0.05(3)	-0.04
Mg I	12	7.60	7.37±0.12(4)	-0.23	0.32	7.49±0.08(4)	-0.11	0.17	7.81±0.06(3)	0.21
Al I	13	6.45	-	-	-	-	-	6.23±0.08(2)	-0.22	-0.12
Si I	14	7.51	6.90±0.20(4)	-0.61	-0.06	7.37±0.05(4)	-0.14	0.14	7.54±0.05(5)	0.03
Ca I	20	6.34	6.01±0.13(18)	-0.33	0.22	6.04±0.21(21)	-0.30	0.21	6.22±0.20(27)	-0.12
Sc II	21	3.15	2.72(syn)	-0.63	-0.08	2.90(syn)	-0.25	0.03	3.25(syn)	0.10
Ti I	22	4.95	4.64±0.13(12)	-0.31	0.24	4.66±0.06(10)	-0.29	-0.01	5.02±0.17(27)	0.07
Ti II	22	4.95	4.81±0.14(13)	-0.14	0.41	4.67±0.16(8)	-0.28	0.00	5.06±0.21(18)	0.11
V I	23	3.93	3.15(syn)	-0.78	-0.23	3.53(syn)	-0.40	-0.12	3.90(syn)	-0.03
Cr I	24	5.64	5.07±0.14(15)	-0.57	-0.02	5.29±0.15(9)	-0.35	-0.07	5.51±0.20(11)	-0.13
Cr II	24	5.64	5.06±0.19(4)	-0.58	-0.03	5.29±0.11(3)	-0.35	-0.07	5.53±0.07(5)	-0.11
Mn I	25	5.43	4.61(syn)	-1.1	-0.55	5.03(syn)	-0.40	-0.12	5.17±0.15(6)	-0.26
Fe I	26	7.50	6.95±0.10(110)	-0.55	-	7.22±0.16(151)	-0.28	-	7.41±0.13(150)	-0.09
Fe II	26	7.50	6.95±0.12(15)	-0.55	-	7.22±0.12(20)	-0.28	-	7.40±0.14(15)	-0.10
Co I	27	4.99	4.52(syn)	-0.64	-0.09	-	-	-	4.85±0.10(2)	-0.14
Ni I	28	6.22	5.70±0.15(26)	-0.52	0.03	5.88±0.11(14)	-0.34	-0.06	6.13±0.15(19)	-0.09
Cu I	29	4.19	3.67(syn)	-0.82	-0.27	-	-	-	-	-
Zn I	30	4.56	4.15±0.10(2)	-0.41	0.14	4.30 ±0.07(2)	-0.26	0.02	4.64±0.00(2)	0.08
Sr I	38	2.87	3.59(syn)	0.63	1.18	4.10(syn)	1.23	1.51	2.55(syn)	-0.32
Y II	39	2.21	2.16(syn)	-0.05	0.50	3.00±0.14(9)	0.79	1.07	2.18±0.19(4)	-0.03
Zr II	40	2.58	2.32(syn)	-0.26	0.29	3.30(syn)	0.72	1.00	2.40(syn)	-0.18
Ba II	56	2.18	2.58(syn)	0.35	0.90	3.30(syn)	1.12	1.40	2.30(syn)	0.12
La II	57	1.10	2.12(syn)	0.08	0.58	2.09(syn)	0.99	1.27	1.20(syn)	0.10
Ce II	58	1.58	1.94±0.09(9)	0.36	0.91	2.56±0.11(8)	0.98	1.26	1.66±0.03(2)	0.08
Pr II	59	0.72	-	-	-	1.79(1)	1.07	1.35	-	-
Nd II	60	1.42	1.92±0.20(9)	0.50	1.05	2.21±0.17(8)	0.79	1.07	1.72±0.12(syn)(2)	0.30
Sm II	62	0.96	1.80±0.08(4)	0.84	1.39	1.97±0.19(4)	1.01	1.29	0.93(syn)	-0.03
Eu II	63	0.52	0.12(syn)	-0.40	0.15	0.37(syn)	-0.15	0.13	-	-

Note: * Asplund *et al.* (2009), The number of lines used for abundance determination are given

within the parentheses.

TABLE 3.7: Elemental abundances in HD 179832, HD 207585, HD 211173, and HD 219116

	Z	HD 179832			HD 207585			HD 211173			HD 219116			
		solar log ϵ^*	log ϵ	[X/H]	[X/Fe]	log ϵ	[X/H]	[X/Fe]	log ϵ	[X/H]	[X/Fe]	log ϵ	[X/H]	[X/Fe]
C	6	8.43	—	—	—	8.66(syn)	0.23	0.61	8.03(syn)	-0.40	-0.23	8.03(syn)	-0.43	0.02
¹² C/ ¹³ C	—	—	—	—	—	—	—	—	—	20.0	—	—	—	7.34
N	7	7.83	—	—	—	8.20(syn)	0.37	0.75	8.20(syn)	0.37	0.54	7.85(syn)	0.02	0.47
O I	8	8.69	8.93(syn)	0.24	0.01	9.28(syn)	0.59	0.97	8.26(syn)	-0.43	-0.26	8.45(syn)	-0.24	0.21
Na I	11	6.24	6.52±0.13(2)	0.28	0.05	6.11±0.11(4)	-0.13	0.25	6.30±0.14(4)	0.06	0.23	6.05±0.16(4)	-0.19	0.26
Mg I	12	7.60	7.83±0.02(2)	0.23	0.00	7.29±0.12(3)	-0.31	0.07	7.66±0.08(2)	0.06	0.23	7.47±0.02(3)	-0.11	0.34
Al I	13	6.45	—	—	—	—	—	—	6.17±0.07(2)	-0.28	-0.11	—	—	—
Si I	14	7.51	7.71±0.08(4)	0.20	-0.03	7.25±0.02(2)	-0.26	0.12	6.97±0.11(2)	-0.54	-0.37	7.08±0.20(2)	-0.43	0.02
Ca I	20	6.34	6.27±0.06(9)	-0.07	-0.30	6.22±0.17(11)	-0.12	0.26	6.23±0.17(15)	-0.11	0.06	6.02±0.14(16)	-0.34	0.13
Sc II	21	3.15	3.35(syn)	0.20	-0.03	2.63(syn)	-0.52	-0.14	2.79(syn)	-0.36	-0.19	2.66(syn)	-0.49	-0.04
Ti I	22	4.95	5.06±0.07(4)	0.11	-0.12	4.58±0.15(7)	-0.37	0.01	4.77±0.11(27)	-0.18	-0.01	4.73±0.09(21)	-0.22	0.23
Ti II	22	4.95	5.39±0.08(4)	0.44	0.21	4.82±0.12(9)	-0.13	0.25	4.76±0.16(9)	-0.19	-0.02	4.65±0.15(6)	-0.3	0.15
V I	23	3.93	4.03(syn)	0.10	-0.13	3.11(syn)	-0.82	-0.44	3.47(syn)	-0.46	-0.29	3.67(syn)	-0.26	0.19
Cr I	24	5.64	5.78±0.12(2)	0.14	-0.09	5.39±0.15(11)	-0.25	0.13	5.45±0.16(11)	-0.19	-0.02	5.34±0.16(9)	-0.3	0.15
Cr II	24	5.64	5.71±0.02(2)	0.07	-0.16	5.38±0.15(4)	-0.26	0.12	5.24±0.16(4)	-0.4	-0.23	5.20±0.09(2)	-0.44	0.01
Mn I	25	5.43	5.25±0.09(3)	-0.18	-0.41	4.60(syn)	-0.83	-0.45	5.13(syn)	-0.30	-0.13	4.78(syn)	-0.65	0.2
Fe I	26	7.50	7.73±0.01(68)	0.23	-	7.12±0.12(107)	-0.38	-	7.33±0.10(109)	-0.17	-	7.05±0.11(92)	-0.45	-
Fe II	26	7.50	7.72±0.04(9)	0.22	-	7.12±0.11(12)	-0.38	-	7.33±0.09(11)	-0.17	-	7.06±0.12(9)	-0.44	-
Co I	27	4.99	5.24±0.08(6)	0.25	0.02	4.55(syn)	-0.44	-0.06	4.58(syn)	-0.41	-0.24	4.69±0.10(7)	-0.3	0.15
Ni I	28	6.22	6.43±0.07(10)	0.21	-0.02	5.83±0.14(16)	-0.39	-0.01	6.14±0.17(27)	-0.08	0.09	5.91±0.12(11)	-0.31	0.14
Cu I	29	4.19	—	—	—	4.36(syn)	-0.63	-0.25	3.92(syn)	-0.27	-0.10	4.09(syn)	-0.12	0.33
Zn I	30	4.56	4.94±0.11(2)	0.38	0.15	—	—	—	4.43±0.02(2)	-0.13	0.04	4.04(1)	-0.56	0.11
Rb I	37	2.52	1.40(syn)	-1.12	-1.35	—	—	—	1.35(syn)	-1.17	-1.00	—	—	—
Sr I	38	2.87	3.12(syn)	0.25	0.02	—	—	—	3.40(syn)	0.53	0.70	3.13(syn)	0.26	0.71
Y I	39	2.21	—	—	—	2.77(syn)	0.56	0.94	2.42(syn)	0.21	0.38	2.49(syn)	0.28	0.73
Y II	39	2.21	2.55±0.05(5)	0.34	0.11	3.20±0.08(9)	0.99	1.37	2.69±0.07(8)	0.48	0.65	2.51±0.09(3)	0.30	0.75
Zr I	40	2.58	4.10(syn)	1.52	1.29	3.30(syn)	0.72	1.10	2.79(syn)	0.21	0.38	2.79(syn)	0.21	0.66
Zr II	40	2.58	4.25(syn)	1.67	1.44	3.74(syn)	0.82	1.20	2.80(syn)	0.22	0.39	—	—	—
Ba II	56	2.18	2.82(syn)	0.64	0.41	3.50(syn)	1.22	1.60	2.58(syn)	0.40	0.57	2.90(syn)	0.77	1.22
La II	57	1.10	1.85(syn)	0.75	0.52	2.47(syn)	1.32	1.70	1.88(syn)	0.78	0.95	2.00(syn)	0.9	1.35
Ce II	58	1.58	2.55±0.11(2)	0.97	0.74	2.92±0.16(14)	1.34	1.72	2.15±0.10(11)	0.57	0.74	2.70±0.20(10)	1.12	1.57
Pr II	59	0.72	1.18±0.05(2)	0.46	0.23	1.93±0.11(3)	1.21	1.59	1.93±0.11(2)	1.21	1.59	1.54±0.18(3)	0.82	1.27
Nd II	60	1.42	1.69±0.04(2)	0.27	0.04	2.66±0.10(19)	1.24	1.62	1.98±0.17(14)	0.56	0.73	2.10±0.12(10)	0.68	1.13
Sm II	62	0.96	1.97±0.04(5)	1.01	0.78	2.62±0.17(8)	1.66	2.04	1.66±0.07(4)	0.70	0.87	2.09±0.18(7)	1.13	1.58
Eu II	63	0.52	0.75(syn)	0.23	0.00	0.42(syn)	-0.10	0.28	0.48(syn)	-0.04	0.13	0.50(syn)	-0.02	0.43

Note: * Asplund *et al.* (2009), The number of lines used to determine abundance is indicated in parentheses.

TABLE 3.8: Comparison of the heavy elemental abundances of program stars with literature values.

Star name	[Fe I/H] (±0.17)	[Fe II/H] (±0.18)	[Fe/H] (±0.17)	[Rb I/Fe] (±0.20)	[Sr/Fe] (±0.32)	[Y I/Fe] (±0.24)	[Y II/Fe] (±0.24)	[Zr I/Fe] (±0.26)	[Zr II/Fe] (±0.23)	[Ba II/Fe] (±0.24)	[La II/Fe] (±0.21)	[Ce II/Fe] (±0.25)	[Pr II/Fe] (±0.21)	[Nd II/Fe] (±0.21)	[Sm II/Fe] (±0.21)	[Eu II/Fe] (±0.20)	Ref
HD 24035	-0.51	-0.50	-0.51	-	-	1.61	-	1.21	1.89	1.71	1.63	1.70	1.98	1.41	2.03	0.19	1
	-0.23	-0.28	-0.26	-	-	1.35	-	1.20	-	-	2.70	1.58	-	1.58	-	-	2
	-	-	-0.14	-	-	-	-	-	-	1.07	1.01	1.63	-	-	-	0.32	3
HD 32712	-0.25	-0.25	-0.25	-1.13	0.03	0.56	1.04	0.52	0.82	1.39	1.25	1.68	1.67	1.76	1.71	0.04	1
	-0.24	-0.25	-0.25	-	-	0.74	-	0.56	-	-	1.53	1.16	-	1.19	-	-	2
HD 36650	-0.02	-0.02	-0.02	-0.82	0.66	0.51	0.70	0.51	-	0.79	0.62	0.99	0.85	0.94	0.99	-0.21	1
	-0.28	-0.28	-0.28	-	-	0.55	-	0.46	-	-	0.83	0.68	-	0.57	-	-	2
HD 94518	-0.55	-0.55	-0.55	-	1.18	-	0.50	-	0.29	0.90	0.58	0.91	-	1.05	1.39	-0.17	1
	-0.49	-0.50	-0.50	-	0.55	-	-	-	-	0.77	-	-	-	-	-	-	4
HD 147609	-0.28	-0.28	-0.28	-	1.51	-	1.07	-	1.00	1.40	1.27	1.26	1.35	1.07	1.29	0.13	1
	-0.45	+0.08	-0.45	-	1.32	-	1.57	0.89	1.56	1.57	1.63	1.64	1.22	1.32	1.09	0.74	5
	-	-	-	-	-	0.96	-	0.80	-	-	-	-	-	0.98	-	-	6
HD 154276	-0.09	-0.10	-0.10	-	-0.22	-	0.07	-	-0.08	0.22	0.20	0.18	-	0.40	0.07	-	1
	-	-	-0.29	-	-	-0.07	-	-	-	-0.03	-	-	-	-	-	-	4
HD 179832	+0.23	+0.23	+0.22	-1.35	0.02	-	0.11	1.29	1.44	0.41	0.52	0.74	0.23	0.04	0.78	0.00	1
HD 207585	-0.38	-0.38	-0.38	-	-	0.94	1.37	1.10	1.20	1.60	1.70	1.72	1.59	1.62	2.04	-0.02	1
	-	-	-0.50	-	-	-	-	-	-	1.23	1.37	1.41	-	-	-	0.58	3
	-	-	-0.57	-	-	1.29	-	1.50	-	-	1.60	0.84	0.61	0.93	1.05	-	7
HD 211173	-0.17	-0.17	-0.17	-1.00	0.70	0.38	0.65	0.38	0.39	0.57	0.95	0.74	1.59	0.73	0.87	-0.17	1
	-	-	-0.12	-	-	-	-	-	-	0.35	0.29	0.73	-	-	-	0.15	3
HD 219116	-0.45	-0.44	-0.45	-	0.71	0.73	0.75	0.66	-	1.22	1.35	1.57	1.27	1.13	1.58	0.13	1
	-0.61	-0.62	-0.62	-	-	0.59	-	0.65	-	-	1.21	1.07	-	-	-	-	2
	-	-	-0.34	-	-	-	-	-	-	0.77	0.56	0.80	-	-	-	0.17	3
	-	-	-0.30	-	-	-	-	-	-	0.90	-	-	-	1.43	-	-	8

References: 1. Our work, 2. de Castro *et al.* (2016), 3. Masseron *et al.* (2010), 4. Bensby *et al.* (2014), 5. Allen and Barbuy (2006), 6. North *et al.* (1994), 7. Luck and Bond (1991), 8. Smith *et al.* (1993)

3.4.3 Abundance uncertainties

The uncertainties in the elemental abundances are calculated for the representative star, HD 211173, in our sample as explained in section 2.6.6. The estimated differential abundances, $\Delta \log \epsilon$, for the variations in each stellar atmospheric parameters are given in Table 3.9.

TABLE 3.9: Differential Abundance ($\Delta \log \epsilon$) of different element species with the variations in stellar atmospheric parameters for HD 211173 (columns 2 - 9).

Element	ΔT_{eff} (+100 K)	ΔT_{eff} (-100 K)	$\Delta \log g$ (+0.2 dex)	$\Delta \log g$ (-0.2 dex)	$\Delta \zeta$ (+0.2 km s ⁻¹)	$\Delta \zeta$ (-0.2 km s ⁻¹)	$\Delta [\text{Fe}/\text{H}]$ (+0.1 dex)	$\Delta [\text{Fe}/\text{H}]$ (-0.1 dex)	$(\sum \sigma_i^2)^{1/2}$ (+Δ)	$(\sum \sigma_i^2)^{1/2}$ (-Δ)	$\sigma_{[\text{X}/\text{Fe}]}$ (+Δ)	$\sigma_{[\text{X}/\text{Fe}]}$ (-Δ)
C	0.00	0.00	+0.03	-0.03	-0.03	+0.03	+0.01	-0.01	0.04	0.04	0.19	0.18
N	+0.10	-0.10	0.00	0.00	+0.02	-0.02	+0.05	-0.05	0.11	0.11	0.21	0.21
O	-0.19	+0.19	+0.06	-0.06	0.00	0.00	0.00	0.00	0.20	0.20	0.27	0.26
Na I	+0.07	-0.08	-0.02	+0.02	-0.05	+0.05	0.00	+0.01	0.09	0.10	0.21	0.21
Mg I	+0.06	-0.05	0.00	+0.01	-0.06	+0.07	0.00	+0.01	0.08	0.09	0.21	0.20
Al I	+0.06	-0.07	0.00	0.00	-0.02	+0.02	0.00	0.00	0.06	0.07	0.20	0.19
Si I	-0.03	+0.03	+0.04	-0.04	-0.03	+0.03	+0.01	-0.01	0.06	0.06	0.20	0.20
Ca I	+0.10	-0.11	-0.04	+0.03	-0.10	+0.09	0.00	0.00	0.15	0.15	0.24	0.23
Sc II	-0.02	+0.02	+0.09	-0.09	-0.09	+0.08	+0.02	-0.03	0.13	0.13	0.22	0.21
Ti I	+0.14	-0.15	-0.01	+0.01	-0.08	+0.08	0.00	0.00	0.16	0.17	0.24	0.24
Ti II	-0.02	0.00	+0.07	-0.08	-0.10	+0.09	+0.02	-0.03	0.13	0.12	0.23	0.22
V I	+0.16	-0.17	-0.01	0.00	-0.07	+0.07	-0.01	+0.01	0.18	0.18	0.25	0.25
Cr I	+0.13	-0.13	-0.02	+0.02	-0.13	+0.12	0.00	0.00	0.18	0.18	0.26	0.25
Cr II	-0.08	+0.07	+0.10	-0.09	-0.08	+0.09	+0.01	-0.02	0.15	0.15	0.25	0.24
Mn I	+0.09	-0.10	-0.02	+0.01	-0.16	+0.14	-0.01	0.00	0.18	0.17	0.26	0.24
Fe I	+0.07	-0.07	0.00	-0.01	-0.13	+0.12	+0.10	-0.10	0.18	0.17	—	—
Fe II	-0.09	+0.07	+0.10	-0.10	-0.10	+0.09	+0.10	-0.10	0.20	0.18	—	—
Co I	+0.07	-0.07	+0.02	-0.03	-0.06	+0.06	+0.01	-0.02	0.09	0.10	0.20	0.20
Ni I	+0.04	-0.03	+0.02	-0.02	-0.10	+0.10	+0.01	-0.01	0.11	0.11	0.21	0.20
Cu I	+0.09	-0.09	-0.01	0.00	-0.15	+0.12	+0.03	-0.02	0.18	0.15	0.25	0.23
Zn I	-0.05	+0.06	+0.07	-0.06	-0.08	+0.09	+0.02	-0.01	0.12	0.12	0.22	0.21
Rb I	+0.10	-0.10	0.00	0.00	-0.03	+0.03	0.00	0.00	0.10	0.10	0.21	0.20
Sr I	+0.15	-0.16	-0.03	+0.02	-0.22	+0.22	0.00	+0.01	0.27	0.27	0.32	0.32
Y I	+0.16	-0.17	-0.01	0.00	-0.02	+0.03	0.00	+0.01	0.16	0.17	0.24	0.24
Y II	-0.01	0.00	+0.08	-0.08	-0.14	+0.14	+0.02	-0.03	0.16	0.16	0.24	0.24
Zr I	+0.17	-0.19	-0.01	0.00	-0.03	+0.03	-0.01	0.00	0.17	0.19	0.25	0.26
Zr II	-0.03	+0.01	+0.09	-0.09	-0.09	+0.11	+0.02	-0.03	0.13	0.15	0.22	0.23
Ba II	+0.02	-0.03	+0.05	-0.06	-0.19	+0.15	+0.03	-0.04	0.20	0.17	0.27	0.24
La II	+0.01	0.00	+0.09	-0.09	-0.06	+0.07	+0.03	-0.03	0.11	0.12	0.21	0.21
Ce II	+0.01	-0.01	+0.09	-0.08	-0.11	+0.15	+0.04	-0.03	0.15	0.17	0.23	0.25
Pr II	+0.01	-0.02	+0.08	-0.09	-0.03	+0.03	+0.03	-0.04	0.09	0.10	0.22	0.21
Nd II	+0.01	-0.02	+0.08	-0.09	-0.09	+0.09	+0.03	-0.04	0.12	0.11	0.22	0.21
Sm II	+0.02	-0.02	+0.09	-0.08	-0.05	+0.07	+0.04	-0.03	0.11	0.11	0.21	0.21
Eu II	-0.02	+0.01	+0.09	-0.09	-0.03	+0.04	+0.03	-0.03	0.10	0.10	0.21	0.20

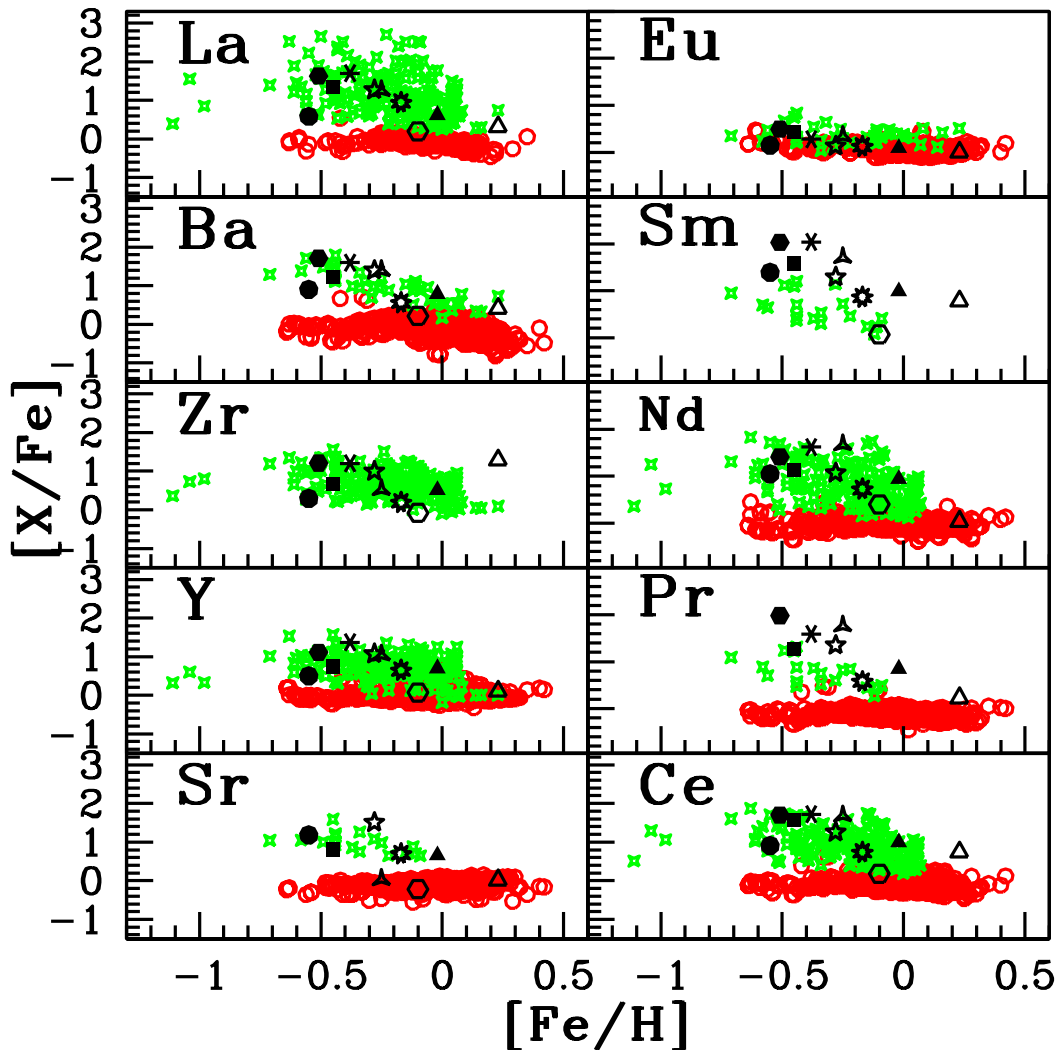


FIGURE 3.12: Observed $[X/\text{Fe}]$ ratios of the neutron-capture elements (Tables 3.5 - 3.7) for the program stars with respect to metallicity $[\text{Fe}/\text{H}]$. Symbols have the same meaning as in Figure 3.8

3.4.4 s-process content of the program stars

We have calculated the $[\text{hs}/\text{Fe}]$, $[\text{ls}/\text{Fe}]$, and $[\text{hs}/\text{ls}]$ ratios of the program stars, where ls refers to the light s-process elements (Sr, Y, and Zr) and hs to the heavy s-process elements (Ba, La, Ce, and Nd). In order to find the s-process content in the stars, we have estimated the mean abundance ratio $[\text{s}/\text{Fe}]$ of the s-process elements (Sr, Y, Zr, Ba, La, Ce, Nd), for our stars. The estimated values of these

TABLE 3.10: Estimates of [ls/Fe], [hs/Fe], [s/Fe], [hs/ls], [Rb/Sr], [Rb/Zr], C/O

Star name	[Fe/H]	[ls/Fe]	[hs/Fe]	[s/Fe]	[hs/ls]	[Rb/Sr]	[Rb/Zr]	C/O
HD 24035	-0.51	1.41	1.61	1.55	0.20	–	–	–
HD 32712	-0.25	0.37	1.52	1.03	1.15	-1.06	-1.65	0.51
HD 36650	-0.02	0.56	0.84	0.72	0.28	-1.48	-1.33	0.56
HD 94518	-0.55	0.67	0.86	0.77	0.19	–	–	0.06
HD 147609	-0.28	1.19	1.25	1.23	0.06	–	–	0.27
HD 154276	-0.10	-0.08	0.25	0.11	0.33	–	–	–
HD 179832	+0.23	0.47	0.66	0.45	0.19	-1.37	-2.64	–
HD 207585	-0.38	1.02	1.66	1.45	0.64	–	–	0.24
HD 211173	-0.17	0.49	0.75	0.64	0.26	-1.70	-1.38	0.59
HD 219116	-0.45	0.70	1.32	1.05	0.62	–	–	0.95

ratios are provided in Table 3.10. The star HD 154276 shows the least value for [s/Fe] ratio. A comparison of [s/Fe] ratio observed in our program stars with that in Ba stars and normal giants from literature is shown in Figure 3.13. The stars which are rejected as Ba stars from the analysis of de Castro *et al.* (2016) are also shown for a comparison. The [s/Fe] value of HD 154276 falls among these rejected stars. Most of these rejected Ba stars are listed as marginal Ba stars by MacConnell *et al.* (1972). There is no clear mention in the literature on how high should be the [s/Fe] value for a star to be considered as a Ba star. According to de Castro *et al.* (2016), this value is +0.25, while Sneden *et al.* (1981) found a value +0.21, Pilachowski (1977) found +0.50 and Rojas *et al.* (2013) found a value > 0.34 . If we stick on to the values of these authors, the star HD 154276 with [s/Fe] ~ 0.11 , can not be consider as a Ba star. However, according to Yang *et al.* (2016), [Ba/Fe] should be at least 0.17 for the star even to be a mild Ba star. Following this, HD 154276 can be considered as a mild Ba star with [Ba/Fe] ~ 0.22 .

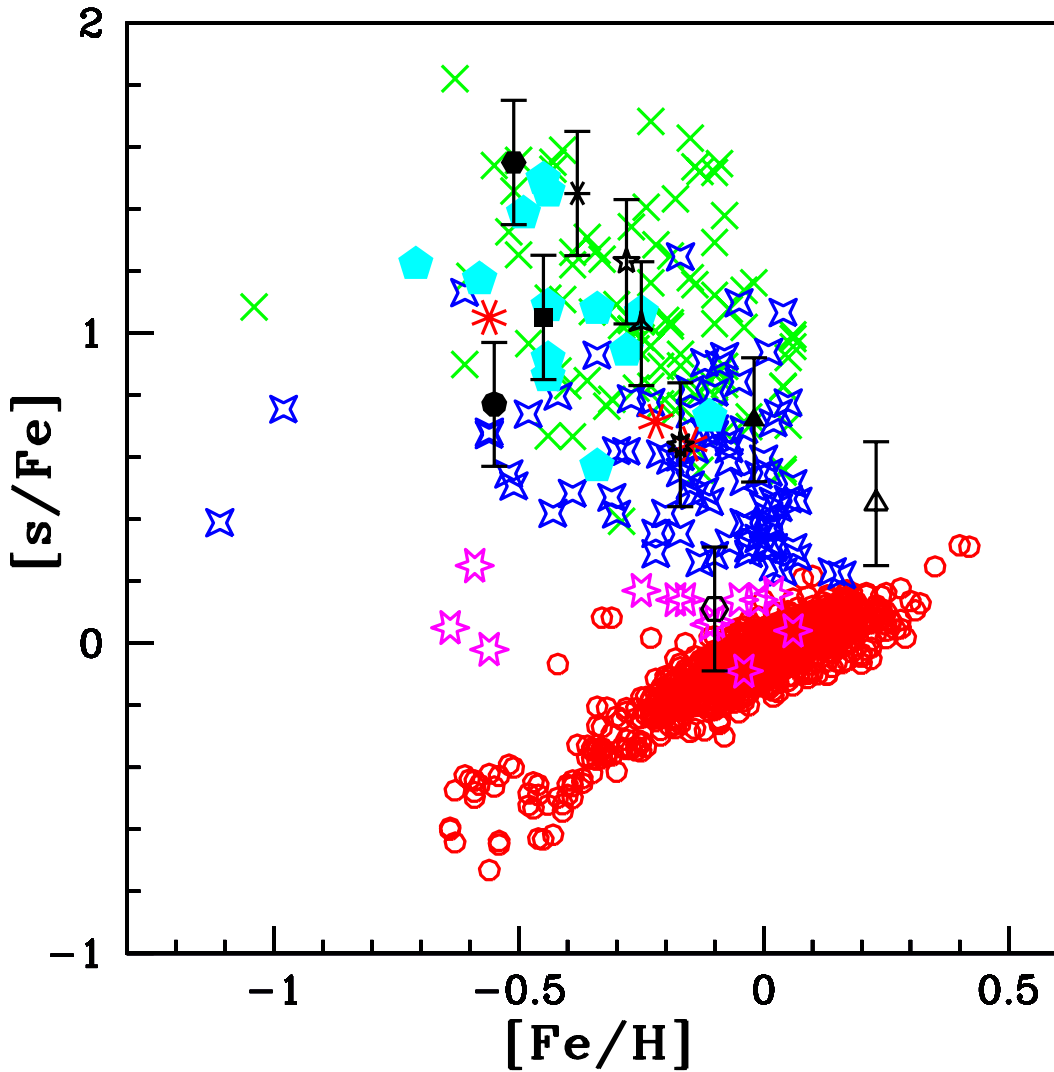


FIGURE 3.13: Observed $[s/\text{Fe}]$ ratios of the program stars with respect to metallicity $[\text{Fe}/\text{H}]$. Red open circles represent normal giants from literature (Luck and Heiter 2007). Green crosses, blue four-sided stars, cyan filled pentagons, red eight-sided crosses represent strong Ba giants, weak Ba giants, Ba dwarfs, Ba sub-giants respectively from literature (de Castro *et al.* 2016; Yang *et al.* 2016; Allen and Barbuy 2006). Magenta six-sided stars represent the stars rejected as Ba stars by de Castro *et al.* (2016). HD 24035 (filled hexagon), HD 32712 (starred triangle), HD 36650 (filled triangle), HD 94518 (filled circle), HD 147609 (five-sided star), HD 154276 (open hexagon), HD 179832 (open triangle), HD 207585 (six-sided cross), HD 211173 (nine-sided star), and HD 219116 (filled square).

3.5 Binary status of the program stars

For a precise identification of the source of carbon and heavy-element enrichment in peculiar stars, it is very crucial to know their binary status. A number of investigations dedicated to identify the binarity of the peculiar stars have been carried out to date. The precise radial velocity monitoring studies have shown that most of the Ba stars (McClure *et al.* 1980; McClure 1983, 1984; McClure and Woodsworth 1990; Jorissen *et al.* 1998; Udry *et al.* 1998a,b) are in binary systems.

A comparison of the estimated radial velocity of the program stars with that available in the Gaia (Gaia Collaboration *et al.* 2018) is given in Table 3.11. Three objects in our sample, HD 24035, HD 147609, and HD 207585 are confirmed binaries with orbital periods of 377.83 ± 0.35 days (Udry *et al.* 1998a), 672 ± 2 days (Escorza *et al.* 2019), and 1146 ± 1.5 days (Escorza *et al.* 2019) respectively. Our estimated radial velocity (-1.56 km s^{-1}) for HD 24035 is slightly higher than the range of radial velocities found in literature (-2.14 to -19.81 km s^{-1}) for this object. However, for HD 207585 (-65.9 km s^{-1}) and HD 147609 (-18.17 km s^{-1}), our estimates fall well within the range of velocities available in literature, i.e., (-52.2 to -74.1 km s^{-1}) and (-19.2 to -11.9 km s^{-1}) respectively. Radial velocity studies are not available for other program stars. The estimated radial velocity for the stars HD 36650, HD 154276, and HD 219116 differ from the literature values (Table 3.11), indicating that these stars are likely binaries.

Analysis of Yoon *et al.* (2016) have shown that, in the absolute carbon abundance $A(C)$ - $[\text{Fe}/\text{H}]$ diagram, the majority of binary stars lie above $A(C) \sim 7.1$. So this diagram could be used as a tool to understand the binary nature of carbon stars when the radial velocity studies are not available. We have extended this method to the higher-metallicity regime to check the binarity of the Ba stars. The distribution of absolute carbon abundance with metallicity for different classes of chemically peculiar stars are shown in Figure 3.14. In this figure, all the program

TABLE 3.11: Radial velocity data of the program stars

Star	V_r	V_r	period (days)
	(km s $^{-1}$) (our estimate)	(km s $^{-1}$) (Gaia)	
HD 24035	-1.56 ± 0.25	-12.51 ± 0.13	377.83 ± 0.35
HD 32712	$+10.37 \pm 0.02$	$+11.27 \pm 0.16$	-
HD 36650	$+36.40 \pm 0.19$	$+31.52 \pm 0.47$	RV variation
HD 94518	$+92.20 \pm 0.43$	92.69 ± 0.015	-
HD 147609	-18.17 ± 1.47	-17.11 ± 0.82	672 ± 2
HD 154276	-64.17 ± 1.42	-55.94 ± 0.17	RV variation
HD 179832	$+6.73 \pm 0.03$	$+7.64 \pm 0.13$	-
HD 207585	-65.97 ± 0.07	-60.10 ± 1.20	1146 ± 1.5
HD 211173	-27.84 ± 0.25	-28.19 ± 0.63	-
HD 219116	-40.90 ± 0.25	-11.00 ± 7.30	RV variation

stars lie in the region occupied by binary stars, indicating that our program stars are likely binaries.

3.6 Diagnostics to understand the nature of companion AGB stars

In this section, we try to understand the nature of the companions for our sample of Ba stars based on various abundance profile analysis.

3.6.1 The [hs/ls] ratio as an indicator of neutron source

The [hs/ls] ratio is a useful indicator of neutron source in the former AGB star. As the metallicity decreases, the neutron exposure increases. As a result, lighter

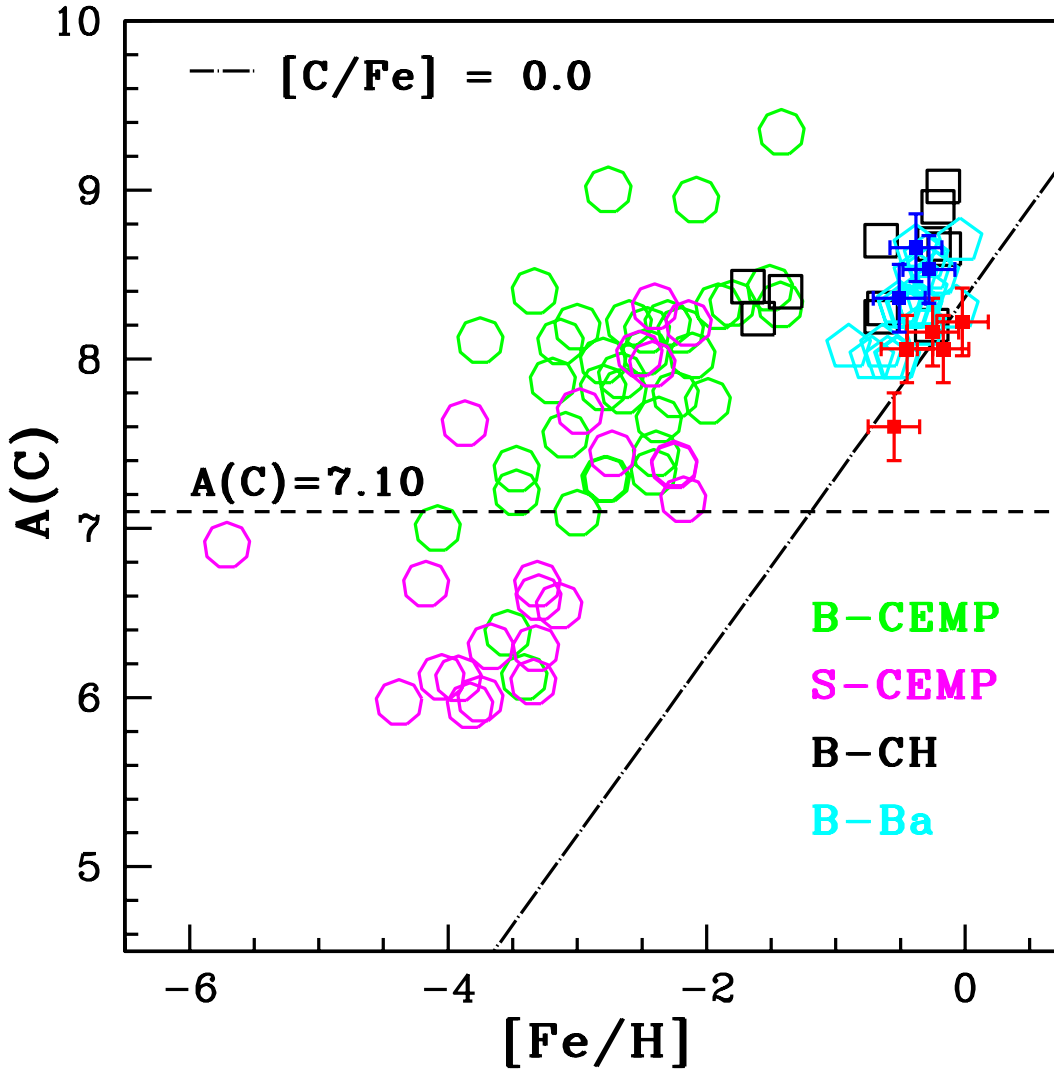


FIGURE 3.14: The $A(C)$ - $[\text{Fe}/\text{H}]$ diagram for known/likely binary and single stars. The binary and single stars are separated by the dashed line at $A(C) = 7.10$. The long-dash dot line corresponds to $[\text{C}/\text{Fe}] = 0$. Green and magenta open hexagons represent binary and single CEMP stars, respectively from literature (Yoon *et al.* 2016). Black open squares represent the binary CH stars from literature (Purandardas *et al.* 2019; Karinkuzhi and Goswami 2014, 2015; Luck 2017). Binary Ba stars from literature (Karinkuzhi *et al.* 2018a) are represented by cyan open pentagons. The prefixes B- and S- in the figure imply binary and single stars, respectively. The blue squares represent the confirmed binary program stars, and the red squares represent the program stars with unknown binary status.

s-process elements are bypassed in favour of heavy elements. Hence, [hs/ls] ratio increases with decreasing metallicity. The models of Busso *et al.* (2001) have shown the behaviour of this ratio with metallicity for AGB stars of mass 1.5 and $3.0 M_{\odot}$ for different ^{13}C pocket efficiencies. According to these models, the maximum value of [hs/ls] is ~ 1.2 which is at metallicities ~ -1.0 and ~ -0.8 for the 3 and $1.5 M_{\odot}$ models respectively for the standard ^{13}C pocket efficiency. In their models, Goriely and Mowlavi (2000), have shown the run of [hs/ls] ratio with metallicity for different thermal pulses for AGB stars in the mass range of 1.5 - 3 M_{\odot} . The maximum value of [hs/ls] ~ 0.6 occurs at metallicity ~ -0.5 . It was noted that, in all these models, the [hs/ls] ratio does not follow a linear anti-correlation with metallicity, rather exhibits a loop like behaviour. The ratio increases with decreasing metallicity up to a particular value of [Fe/H] and then starts to drop. Our [hs/ls] ratio has a maximum value of ~ 1.15 which occurs at a metallicity of ~ -0.25 . The anti-correlation of [hs/ls] suggests the operation of $^{13}\text{C}(\alpha, n)^{16}\text{O}$ neutron source, since $^{13}\text{C}(\alpha, n)^{16}\text{O}$ is found to be anti-correlated with metallicity (Clayton 1988; Wallerstein *et al.* 1997).

At metallicities higher than solar, a negative value is expected for this ratio and at lower metallicities, a positive value is expected for low-mass AGB stars where $^{13}\text{C}(\alpha, n)^{16}\text{O}$ is the neutron source (Busso *et al.* 2001; Goriely and Mowlavi 2000). However, it is possible that AGB stars with masses in the range 5 - $8 M_{\odot}$ can also exhibit low [hs/ls] ratios considering the $^{22}\text{Ne}(\alpha, n)^{25}\text{Mg}$ neutron source (Karakas and Lattanzio 2014). The models of Karakas and Lattanzio (2014) predicted that the ls elements are predominantly produced over the hs elements for AGB stars of mass 5 and $6 M_{\odot}$. The [hs/ls] ratio is correlated to the neutron exposure. The $^{22}\text{Ne}(\alpha, n)^{25}\text{Mg}$ source has smaller neutron exposure compared to the $^{13}\text{C}(\alpha, n)^{16}\text{O}$ source. Hence, in the stars where $^{22}\text{Ne}(\alpha, n)^{25}\text{Mg}$ operates, we expect a lower [hs/ls] ratio. The lower neutron exposure of the neutrons produced from the ^{22}Ne source together with the predictions of low [hs/ls] ratio in massive AGB star models have been taken as the evidence of operation of $^{22}\text{Ne}(\alpha, n)^{25}\text{Mg}$ in massive

AGB stars. As seen from the Table 3.10, all the program stars show positive values for [hs/ls] ratio. This indicates low-mass AGB companions for the program stars.

3.6.2 Rb as a probe of the neutron density at the s-process site

In addition to the [hs/ls] ratio, the abundance of rubidium can also provide clues to the mass of the companion AGB stars. The AGB star models predict higher Rb abundances for massive AGB stars where the neutron source is $^{22}\text{Ne}(\alpha,\text{n})^{25}\text{Mg}$ reaction (Abia *et al.* 2001; van Raai *et al.* 2012). In the s-process nucleosynthesis path, the branching points at the unstable nuclei ^{85}Kr and ^{86}Rb controls the Rb production. The amount of Rb produced along this s-process path is determined by the probability of these unstable nuclei to capture the neutron before β -decaying, which in turn depends on the neutron density at the s-process site (Beer and Macklin 1989; Tomkin and Lambert 1983; Lambert *et al.* 1995).

The production of ^{87}Rb from ^{85}Kr and ^{86}Rb is possible only at higher neutron densities $N_n > 5 \times 10^8 \text{ n/cm}^3$; Sr, Y, Zr etc. are produced otherwise (Beer 1991; Lugaro and Chieffi 2011). The ^{87}Rb isotope has a magic number of neutrons, and hence it is fairly stable against neutron capture. Furthermore, the neutron capture cross-section of ^{87}Rb is very small ($\sigma \sim 15.7 \text{ mbarn}$ at 30 KeV) compared to that of ^{85}Rb ($\sigma \sim 234 \text{ mbarn}$) (Heil *et al.* 2008a). Hence, once the nucleus ^{87}Rb is produced, it will be accumulated. Therefore, the isotopic ratio $^{87}\text{Rb}/^{85}\text{Rb}$ could be a direct indicator of the neutron density at the s-process site, and thus helps to infer the mass of the AGB star. But, it is impossible to distinguish the lines due to these two isotopes of Rb in the stellar spectra (Lambert and Luck 1976; García-Hernández *et al.* 2006), as the isotopic shift between the two isotopes is very small (of the order of 1 mÅ). However, the abundance of Rb relative to other elements in this region of the s-process path, such as Sr, Y, and Zr, can be used to estimate

the average neutron density of the s-process. Detailed nucleosynthesis models for the stars with masses between $5 - 9 M_{\odot}$ at solar metallicity predict $[Rb/(Sr,Zr)] > 0$ (Karakas *et al.* 2012). A positive value of $[Rb/Sr]$ or $[Rb/Zr]$ ratio indicates a high neutron density, whereas a negative value indicates a low neutron density. This fact has been used as an evidence to conclude that $^{13}C(\alpha, n)^{16}O$ reaction act as the neutron source in M, MS and S stars (Lambert *et al.* 1995). The same fact was used to conclude that the C stars are low-mass AGB stars with $M < 3 M_{\odot}$ (Abia *et al.* 2001). The observed $[Rb/Zr]$ ratios in the AGB stars, both in our Galaxy and the Magellanic Clouds, show a value < 0 for low-mass AGB stars and a value > 0 for intermediate-mass ($4 - 6 M_{\odot}$) AGB stars (Plez *et al.* 1993; Lambert *et al.* 1995; Abia *et al.* 2001; García-Hernández *et al.* 2006, 2007, 2009; van Raai *et al.* 2012).

M stars are late type O-rich giants ($C/O \sim 0.5$) characterized by the presence of strong TiO molecular band in their spectra (Merrill 1922; Smith and Lambert 1988; Karakas and Lattanzio 2014). They do not show any enhancement of s-process elements, despite some of them showing the Tc I line in their spectra (Merrill 1952; Keenan 1954; Smith and Lambert 1985, 1988). These stars may belong to the earliest phase of TP-AGB that not yet experienced the TDU (Smith and Lambert 1988). They show abundances similar to those observed in G and K giants with deep convective envelope and have undergone FDU (Smith and Lambert 1990). S stars are late type giants whose spectra are characterized by strong ZrO molecular band (Merrill 1922; Smith and Lambert 1986b; Van Eck and Jorissen 1999). MS stars are also late type giants, intermediate between M and S type, having a weaker ZrO band than the S stars (Smith and Lambert 1986b). MS and S stars are characterized by the enhanced abundances of carbon and s-process elements in their atmosphere (Merrill 1922; Smith and Lambert 1985, 1986b; Van Eck *et al.* 2017). The MS and S stars with Tc I line in their spectra (intrinsic MS and S stars) are AGB stars (TP-AGB) where s-process operates in the He-shell (Smith and Lambert 1985, 1986b, 1990; Lambert *et al.* 1995; Van Eck *et al.* 2017).

The MS and S stars without Tc I in their spectra (extrinsic MS and S stars) are results of pollution from binary AGB companion (Smith and Lambert 1985, 1986b, 1990; Jorissen and Mayor 1988; Jorissen *et al.* 1993; Van Eck and Jorissen 1999; Van Eck *et al.* 2000; Van Eck and Jorissen 2000; Van Eck *et al.* 2017). The MS and S stars show a higher abundance of N than the M giants (Smith and Lambert 1990). The S stars show C/O ratio close to unity (Karakas and Lattanzio 2014; Van Eck *et al.* 2017), attributing to the TDU episodes. The sequence M-MS-S-C is based on the increasing order of C/O ratio with the transition from C/O < 1 to C/O > 1 (Smith and Lambert 1986b; Karakas and Lattanzio 2014). The Ba giants are known to be the warmer counterparts of extrinsic S stars (Jorissen and Mayor 1988; Smith and Lambert 1988).

The estimated [Rb/Zr] and [Rb/Sr] ratios (Table 3.10) give negative values for our stars, for which we could estimate these ratios. The observed [Rb/Fe] and [Zr/Fe] ratios are shown in Figure 3.15. The observed ranges of Rb and Zr in intermediate-mass AGB stars (shaded region) in the Galaxy and the Magellanic Clouds are also shown for a comparison. It is clear that the abundances of Rb and Zr observed in the program stars are consistent with the range normally observed in the low-mass AGB stars.

3.6.3 Na and Mg abundances

Here, we will discuss the astrophysical origin and possible sources of overabundances of Na and Mg. The light elements Na and Mg are significantly produced in TP-AGB stars. When the temperature reaches $\sim 15 \times 10^6$ K, secondary Na is produced in the H-burning shell during the interpulse stage from ^{22}Ne produced in the previous hot pulses via $^{22}\text{Ne}(\text{p}, \gamma)^{23}\text{Na}$ (Ne - Na chain). If the temperature exceeds 35×10^6 K, the burning of the abundant ^{20}Ne also contributes to ^{23}Na . However, at temperatures $T > 60 \times 10^6$ K, the ^{23}Na depletes through $^{23}\text{Na}(\text{p}, \gamma)^{24}\text{Mg}$ and/or

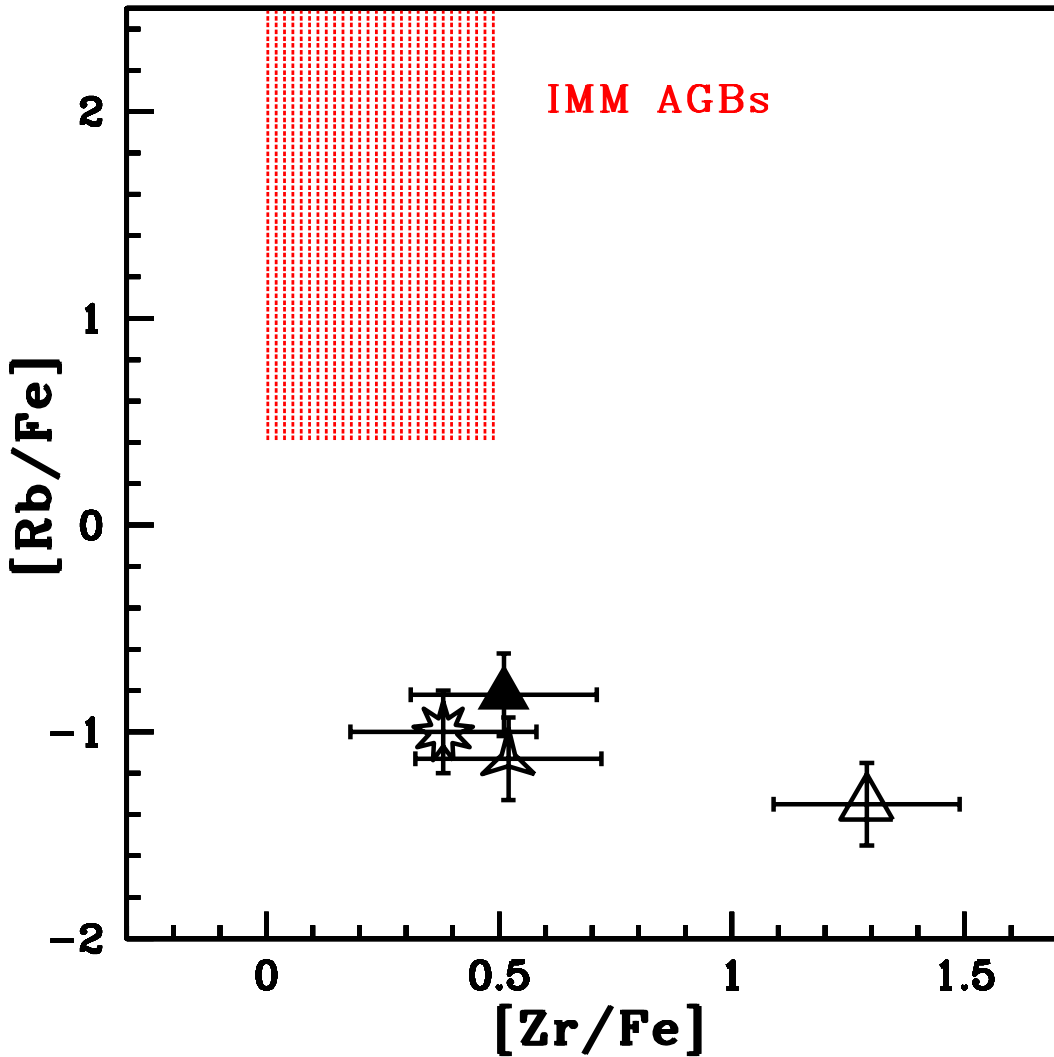


FIGURE 3.15: The observed abundances $[{\rm Rb/Fe}]$ vs $[{\rm Zr/Fe}]$. HD 32712 (starred triangle), HD 36650 (filled triangle), HD 179832 (open triangle), and HD 211173 (nine-sided star). The shaded region corresponds to the observed range of Zr and Rb in intermediate-mass AGB stars in the Galaxy and the Magellanic Clouds (van Raai *et al.* 2012). The four program stars occupy the region of low-mass AGB stars.

$^{23}\text{Na}(\text{p}, \alpha)^{20}\text{Ne}$ (Arnould and Mowlavi 1995; Mowlavi 1999b; Goriely and Mowlavi 2000; Karakas *et al.* 2006). The isotope ^{24}Mg is produced during the interpulse from the ^{23}Na as mentioned above. However, the competing reaction $^{23}\text{Na}(\text{p}, \alpha)^{20}\text{Ne}$ is faster than the one producing ^{24}Mg (El Eid and Champagne 1995; Il- iadis *et al.* 2001; Izzard *et al.* 2007). When the temperature of the TP reaches $\sim 300 \times 10^6$ K, other isotopes of Mg are produced during the TP via $^{22}\text{Ne}(\alpha, \text{n})^{25}\text{Mg}$ and $^{22}\text{Ne}(\alpha, \gamma)^{26}\text{Mg}$ reactions (Karakas and Lattanzio 2003; Karakas *et al.* 2006; Kaeppeler *et al.* 1994). But, if the temperature reaches 70×10^6 K, ^{24}Mg , and then ^{25}Mg are depleted into ^{27}Al (Denissenkov and Weiss 1996; Arnould *et al.* 1999). However, such high temperatures are attained only in the case of massive AGB stars ($3 - 8 M_{\odot}$) in their Hot-Bottom Burning regions, and it is impossible for the low-mass AGB stars to sustain these reactions (Boothroyd and Sackmann 1992; Gratton *et al.* 2000).

Since the mass of the intershell material dredged-up to the surface is very small compared to the envelope mass, the secondary Na produced (produced from the ^{22}Ne dredged-up to the surface) has negligible impact on the total Na surface abundance (Bisterzo *et al.* 2011). If the ^{23}Na produced is primary, ie, produced through a chain of TP/TDU/IP events from the ^{12}C and ^{22}Ne (produced during the TP) dredged-up to the surface from the He-burning shell of the AGB stars, a larger amount of it would be expected (Mowlavi 1999b; Gallino *et al.* 2006). The primary ^{12}C produced by the 3α -reaction are brought to the surface from the intershell region by the TDU. Then, during the following interpulse, this ^{12}C is transformed into ^{14}N through the CNO cycle by the H-burning shell, and accumulated in the top layers of the intershell-region. This ^{14}N is converted to ^{22}Ne during the early phase of next thermal instability via $^{14}\text{N}(\alpha, \gamma)^{18}\text{F}(\beta^+ \nu)^{18}\text{O}(\alpha, \gamma)^{22}\text{Ne}$ (Mowlavi 1999b; Gallino *et al.* 2006). This ^{22}Ne results in the primary production of the ^{23}Na via the n-capture reaction: $^{22}\text{Ne}(\text{n}, \gamma)^{23}\text{Ne}(\beta^- \nu)^{23}\text{Na}$, and isotopes of Mg through the n-capture reaction: $^{23}\text{Na}(\text{n}, \gamma)^{24}\text{Na}(\beta^- \nu)^{24}\text{Mg}$, and α -capture reactions: $^{22}\text{Ne}(\alpha, \text{n})^{25}\text{Mg}$ and $^{22}\text{Ne}(\alpha, \gamma)^{26}\text{Mg}$ (Gallino *et al.* 2006). These reactions are significant

at low-metallicities due to the large amount of ^{22}Ne produced, and have negligible effect at metallicities $[\text{Fe}/\text{H}] \geq -1$ (Gallino *et al.* 2006; Bisterzo *et al.* 2011). So at metallicities characteristics of Ba stars, the Na and Mg are not primary.

However, Na enrichment can be expected in stars prior to the AGB phase. El Eid and Champagne (1995) and Antipova *et al.* (2004) related this overabundance of Na to the nucleosynthesis associated with the evolutionary stage of the star. According to them, Na is synthesized in the convective H-burning core of the main sequence stars through the Ne - Na chain. Later, these products are mixed to the surface during the FDU. As a result, it is possible to observe sodium enrichment in giants rather than in dwarfs. An anti-correlation between $[\text{Na}/\text{Fe}]$ and $\log g$ was reported by Boyarchuk *et al.* (2001) and de Castro *et al.* (2016). We observed a similar trend in our sample. According to Denisenkov and Ivanov (1987), a star with a minimum mass of $1.5 M_{\odot}$ will be able to raise the Na abundance through the Ne - Na chain even in the main sequence itself. Even though the Na-enriched material can be synthesized in AGB, and subsequently transferred to the barium stars, there may be a non-negligible contribution to the Na enrichment from the barium star itself.

A comparison of the observed Na and Mg abundances in the program stars with those in the field giants and disk dwarfs is shown in Figure 3.16. Na and Mg enhancement is expected if the s-process pattern results from the massive AGB stars, as mentioned above. We could not find any such enhancement in our sample when compared with the disk stars and normal giants. This discards the possibility of the neutron source $^{22}\text{Ne}(\alpha,\text{n})^{25}\text{Mg}$ as well as a massive AGB companion for the program stars. The observed Na and Mg abundances also confirm the low-mass former AGB companions of the program stars.

The studies of the disk dwarfs and field giants of the Galaxy have shown that they do not show any trend in $[\text{Na}/\text{Fe}]$ ratio with metallicity (Edvardsson *et al.* 1993;

Reddy *et al.* 2003, 2006; Mishenina *et al.* 2006; Luck and Heiter 2007). Since Na, Mg, and Al are produced in the carbon burning stages of massive stars, SNe II are the likely sources of these elements in the Galactic disk (Burbidge *et al.* 1957; Woosley and Weaver 1995; Wallerstein *et al.* 1997). Owing to this common origin, all the stars in the disk are expected to show similar abundances. This fact is clearly seen from Figures 3.8 and 3.16.

3.7 Comparison with the AGB stars

The analysis based on different diagnostics and abundance profiles discussed in the previous section confirmed the low-mass nature of the former AGB companions of the program stars. Now, to corroborate this results, we have performed a comparison of the estimated abundances of the program stars with the observed abundances as well as the model yields of AGB stars.

3.7.1 Comparison of the observed abundances with literature values of AGB stars

The observed abundance ratios for eight neutron-capture elements are compared with their counterparts in the low-mass AGB stars from literature, which are found to be associated with the $^{13}\text{C}(\alpha, \text{n})^{16}\text{O}$ neutron source. This comparison is shown in Figure 3.17. The observed abundances of the Ba stars are in agreement with those of the low-mass AGB stars. The scatter observed in the ratios may be a consequence of different dilution factors during the mass transfer, as well as the orbital parameters, metallicity, and initial mass as discussed in de Castro *et al.* (2016).

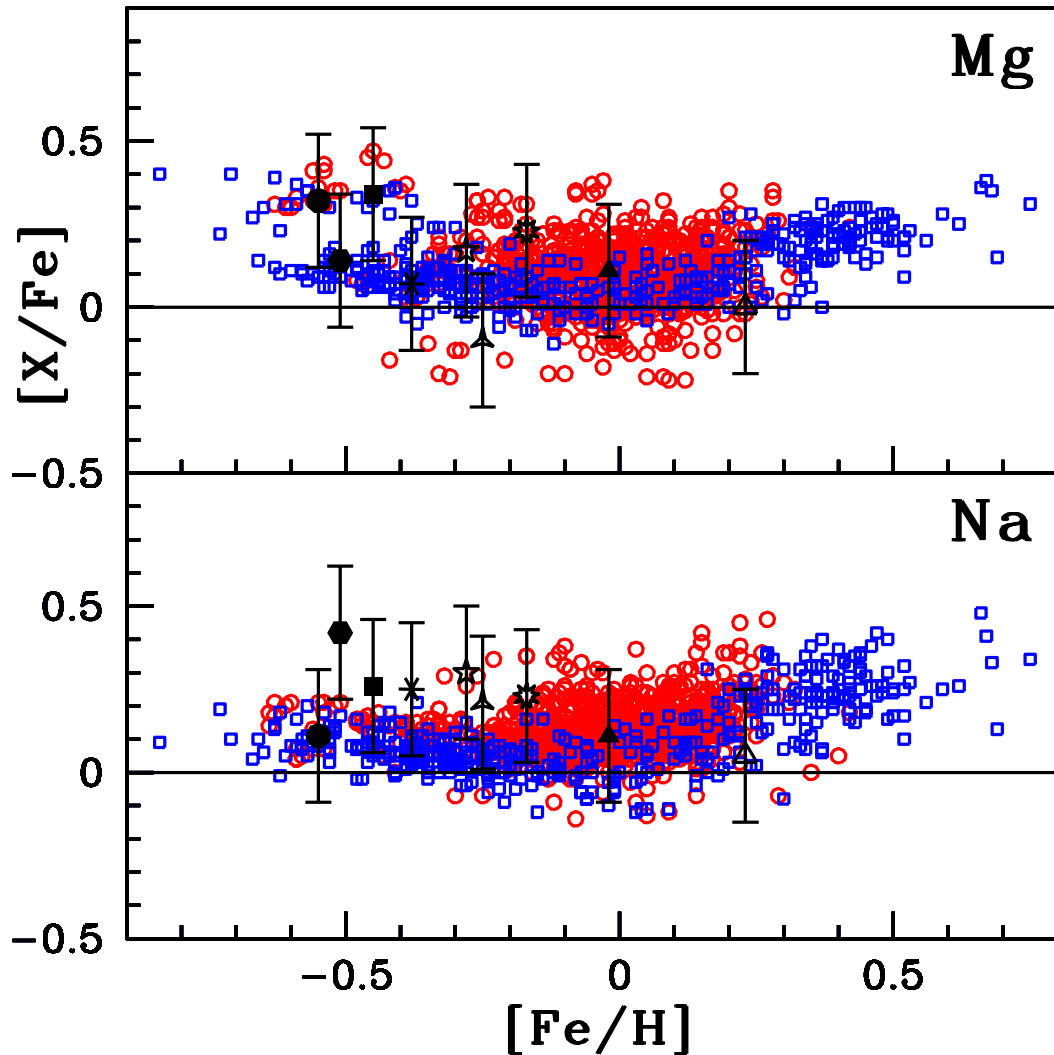


FIGURE 3.16: The observed abundances $[\text{Na}/\text{Fe}]$ and $[\text{Mg}/\text{Fe}]$. Red open circles represent the normal field giants from literature (Luck and Heiter 2007). Blue squares are the disk dwarfs from literature (Reddy *et al.* 2003; Bensby *et al.* 2005; Reddy *et al.* 2006). HD 24035 (filled hexagon), HD 32712 (starred triangle), HD 36650 (filled triangle), HD 94518 (filled circle), HD 147609 (five-sided star), HD 179832 (open triangle), HD 207585 (six-sided cross), HD 211173 (nine-sided star), and HD 219116 (filled square).

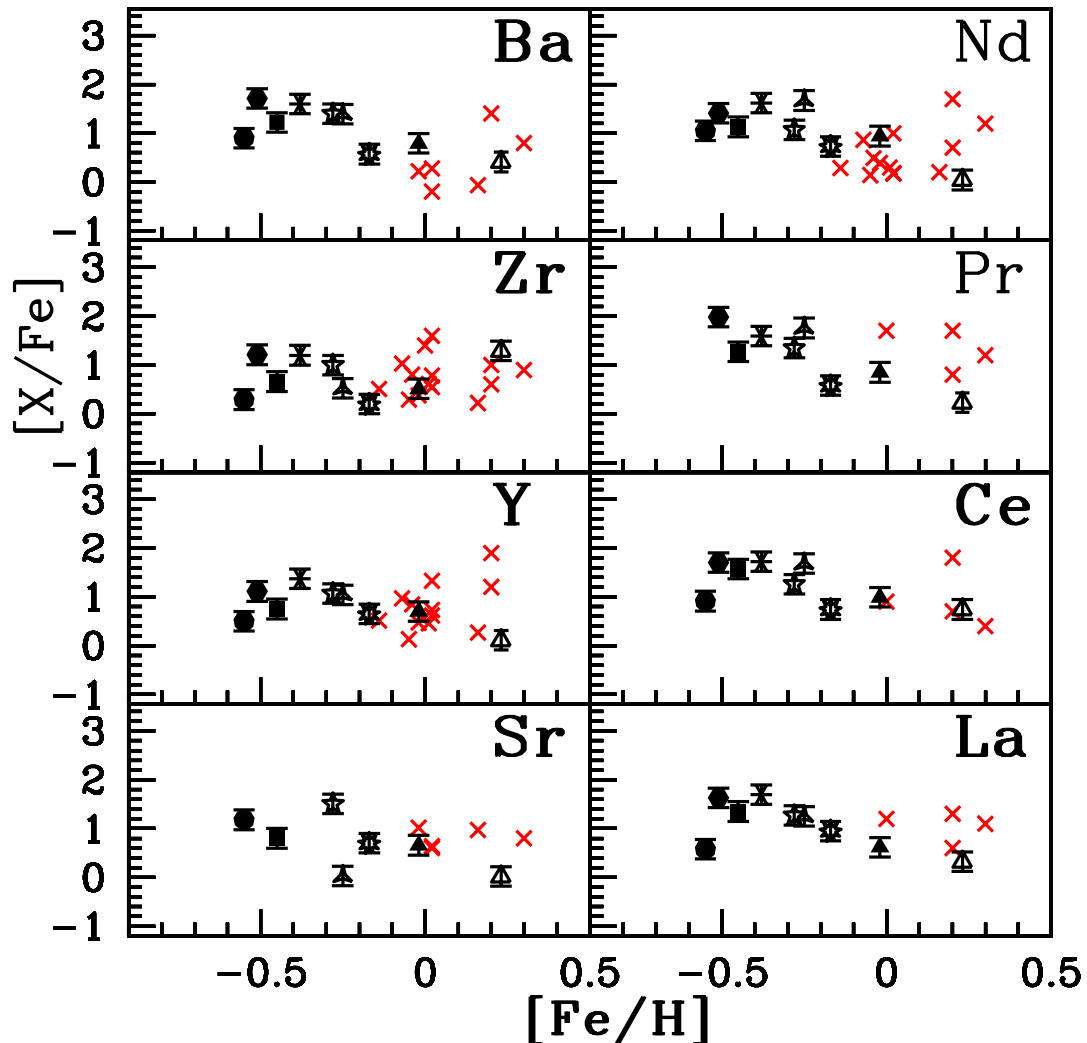


FIGURE 3.17: Comparison of abundance ratios of neutron-capture elements observed in the program stars and the low-mass AGB stars with respect to metallicity $[\text{Fe}/\text{H}]$. Red crosses represent the AGB stars from literature (Smith and Lambert 1985, 1986b, 1990; Abia and Wallerstein 1998). HD 24035 (filled hexagon), HD 32712 (starred triangle), HD 36650 (filled triangle), HD 94518 (filled circle), HD 147609 (five-sided star), HD 179832 (open triangle), HD 207585 (six-sided cross), HD 211173 (nine-sided star), and HD 219116 (filled square).

3.7.2 Comparison with the FRUITY models and a parametric model-based analysis

A publicly available (<http://fruity.oa-teramo.inaf.it/>, Web sites of the Teramo Observatory (INAF)) data set for the s-process in AGB stars is the FRANEC Repository of Updated Isotopic Tables & Yields (FRUITY) models (Cristallo *et al.* 2009, 2011, 2015). These models cover the range of metallicity from $z = 0.000020$ to $z = 0.020$ for the mass range $1.3 - 6.0 M_{\odot}$. The computations comprise of the evolutionary models starting from the pre-main sequence to the tip of AGB phase through the core He-flash. During the core H-burning, no core overshoot has been considered, a semi-convection is assumed during the core He-burning. The only mixing considered in this model is arising from the convection, additional mixing phenomena such as rotation is not considered here. The calculations are based on a full nuclear network, considering all the stable and relevant unstable isotopes from hydrogen to bismuth. This includes 700 isotopes and about 1000 nuclear processes such as charged particle reactions, neutron captures, and β -decays (Straniero *et al.* 2006; Görres *et al.* 2000; Jaeger *et al.* 2001; Abbondanno *et al.* 2004; Patronis *et al.* 2004; Heil *et al.* 2008c). The details of the input physics and the computational algorithms are provided in Straniero *et al.* (2006). In this model, ^{13}C pocket is formed through time-dependent overshoot mechanisms, which is controlled by a free overshoot parameter (β) in the exponentially declining convective velocity function. This parameter is set in such a way that the neutrons released are enough to maximize the production of s-process elements. For the low-mass AGB star models (initial mass $< 4 M_{\odot}$), neutrons are released by the $^{13}\text{C}(\alpha, n)^{16}\text{O}$ reaction during the interpulse phase in radiative conditions, when temperatures within the pockets reaches $T \sim 1.0 \times 10^8$ K, with typical densities of $10^6 - 10^7$ neutrons cm^{-3} . However, in the case of the metal-rich models ($z = 0.0138$, $z = 0.006$, and $z = 0.003$), ^{13}C is only partially burned during the interpulse; surviving part is ingested in the convective zone generated by the subsequent thermal pulse (TP), and then burned at $T \sim 1.5 \times 10^8$ K, producing a neutron density of 10^{11} neutrons

cm^{-3} . For larger z , $^{22}\text{Ne}(\alpha, n)^{25}\text{Mg}$ neutron source is marginally activated during the TPs; but for low z , it becomes an important source when most of the ^{22}Ne is primary (Cristallo *et al.* 2009, 2011). For the intermediate-mass AGB star models, the s-process distributions are dominated by the $^{22}\text{Ne}(\alpha, n)^{25}\text{Mg}$ neutron source, which is efficiently activated during TPs. The contribution from the $^{13}\text{C}(\alpha, n)^{16}\text{O}$ reaction is strongly reduced in the massive stars. This is due to the lower extent of the ^{13}C pocket in them. It is shown that the extent of ^{13}C pocket decreases with increasing core mass of the AGB star, due to the shrinking and compression of He-intershell (Cristallo *et al.* 2009). These massive models experience Hot-Bottom Burning and Hot-TDUs at lower metallicities (Cristallo *et al.* 2015).

We have compared our observational data with the FRUITY model. The model predictions are unable to reproduce the [hs/ls] ratios characterizing the surface composition of the stars. A comparison of the observed [hs/ls] ratios with metallicity shows a large spread (Figure 3.18), somewhat similar to the comparison between the model and observational data as shown in Cristallo *et al.* (2011) (Figure 12 of theirs).

The observed discrepancy may be explained by considering the different ^{13}C pocket efficiencies in the AGB models. In the FRUITY models, a standard ^{13}C pocket is being considered. However, if a variation in the amount of ^{13}C pocket would give a better match with the observed spread, is yet to be examined. The absence of stellar rotation in the current FRUITY models may also be a cause of the observed discrepancy. The rotation induced mixing alters the extent of the ^{13}C pocket (Langer *et al.* 1999), which in turn affects the s-process abundance pattern. However, a study conducted by Cseh *et al.* (2018) using the rotating star models available for the metallicity range of Ba stars (Piersanti *et al.* 2013) could not reproduce the observed abundance ratios of stars studied by de Castro *et al.* (2016).

We have performed a parametric model-based analysis in order to find the mass of

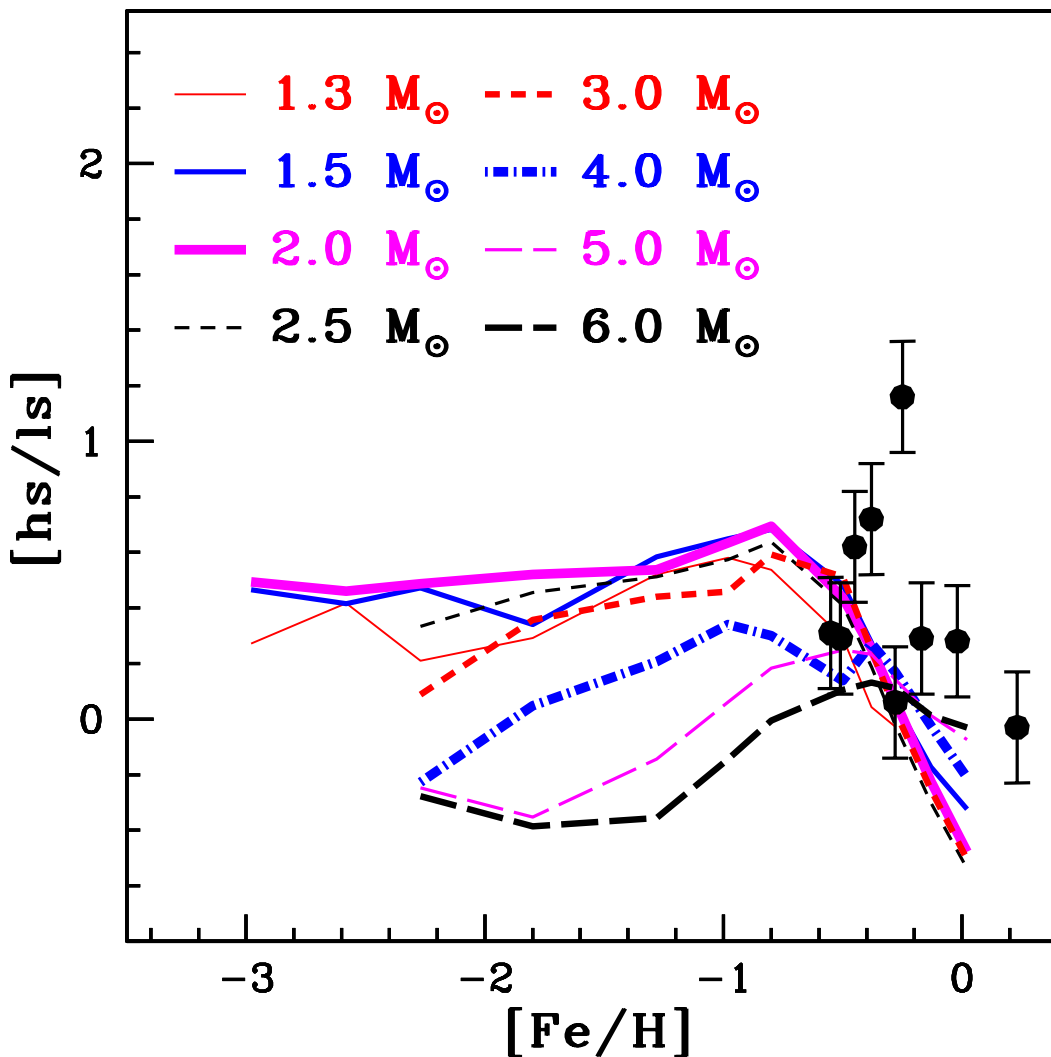


FIGURE 3.18: Comparison of the predicted and observed values of [hs/ls] ratios. The black circles with error bars represent the observed [hs/ls] ratio in the program stars. The curves correspond to the predicted [hs/ls] ratios for AGB stars of different masses in the range $1.3 - 6 M_{\odot}$ from the FRUITY models.

the companion AGB stars of our program stars. The observed abundance in the atmosphere of the Ba stars might not be the actual signature of the progenitor AGB stars. The accreted s-rich material may undergo mixing and dilution in the envelope of these secondary Ba stars. So, the dilution experienced by the accreted material after the mass transfer should be incorporated in the analysis. The diluted theoretical abundance on the surface of Ba stars;

$$[\text{X}/\text{Fe}] = \log(10^{[\text{X}/\text{Fe}]^{\text{ini}}} \cdot f + 10^{[\text{X}/\text{Fe}]^{\text{AGB}}} \cdot 10^{-d})$$

where d is the dilution factor, $f = 1 - 10^{-d}$, and $[\text{X}/\text{Fe}]^{\text{AGB}}$ is the abundance of element X in the AGB star (Husti *et al.* 2009). The solar values have been taken as the initial composition. The dilution factor, d , is defined as $M_{\star}^{\text{env}}/M_{\text{AGB}}^{\text{transf}} = 10^d$, where M_{\star}^{env} is the mass of the envelope of the observed star after the mass transfer, $M_{\text{AGB}}^{\text{transf}}$ is the mass transferred from the AGB. Both the AGB and Ba stars are assumed to be formed from the same cloud of interstellar medium. The dilution factor, d , is a free parameter that can be varied between 0 to 1. The case $d = 0$ means that no mixing has happened on the surface of the Ba stars, and the observed abundance is the actual nucleosynthesis products of the companion AGB star. The mass of the AGB stars responsible for the observed abundances of the Ba stars are derived by comparing the observed abundance with the predicted abundance from the FRUITY model for the heavy elements (Sr, Y, Zr, Ba, La, Ce, Pr, Nd, Sm, and Eu) using the above parametric model function. The dilution factor is varied by minimizing the χ^2_{min} between the observed and predicted abundances.

$$\chi^2 = \sum \frac{([\text{X}/\text{Fe}]_{\text{obs}} - [\text{X}/\text{Fe}]_{\text{mod}})^2}{\sigma_{\text{obs}}^2}$$

where $[\text{X}/\text{Fe}]_{\text{obs}}$, $[\text{X}/\text{Fe}]_{\text{mod}}$ are the observed abundance and model prediction, and σ_{obs}^2 is the uncertainty on $[\text{X}/\text{Fe}]_{\text{obs}}$. The best fit masses and corresponding dilution factors, along with the χ^2 values are given in Table 3.12. The goodness of fit of the parametric model function is determined by the uncertainty in the observed abundance. The best fits obtained are shown in Figure 3.19. All the Ba stars are found to have low-mass AGB companions with $M \leq 3 M_{\odot}$. Among our stars, HD 147609 is found to have a companion of $3 M_{\odot}$ by Husti *et al.* (2009), whereas our estimate is $2.5 M_{\odot}$.

TABLE 3.12: The best fit mass, dilution factor and reduced chi-square values.

Star name/ mass (M/M_\odot)	HD 24035	HD 32712	HD 36650	HD 94518	HD 147609	HD 179832	HD 207585	HD 211173	HD 219116
1.5	d	-	-	-	0.22	-	0.21	-	-
	χ^2	-	-	-	9.91	-	51.39	-	0.04
2.0	d	-	0.001	-	0.52	-	0.65	-	1.40
	χ^2	-	16.14	-	10.14	-	48.04	-	0.36
2.5	d	0.07	0.08	0.10	0.62	0.08	0.82	0.07	1.55
	χ^2	1.92	17.64	8.15	10.31	1.39	48.06	4.28	0.46
3.0	d	-	-	0.04	0.27	-	0.75	-	0.10
	χ^2	-	-	8.08	9.92	-	48.01	-	1.66
									1.33

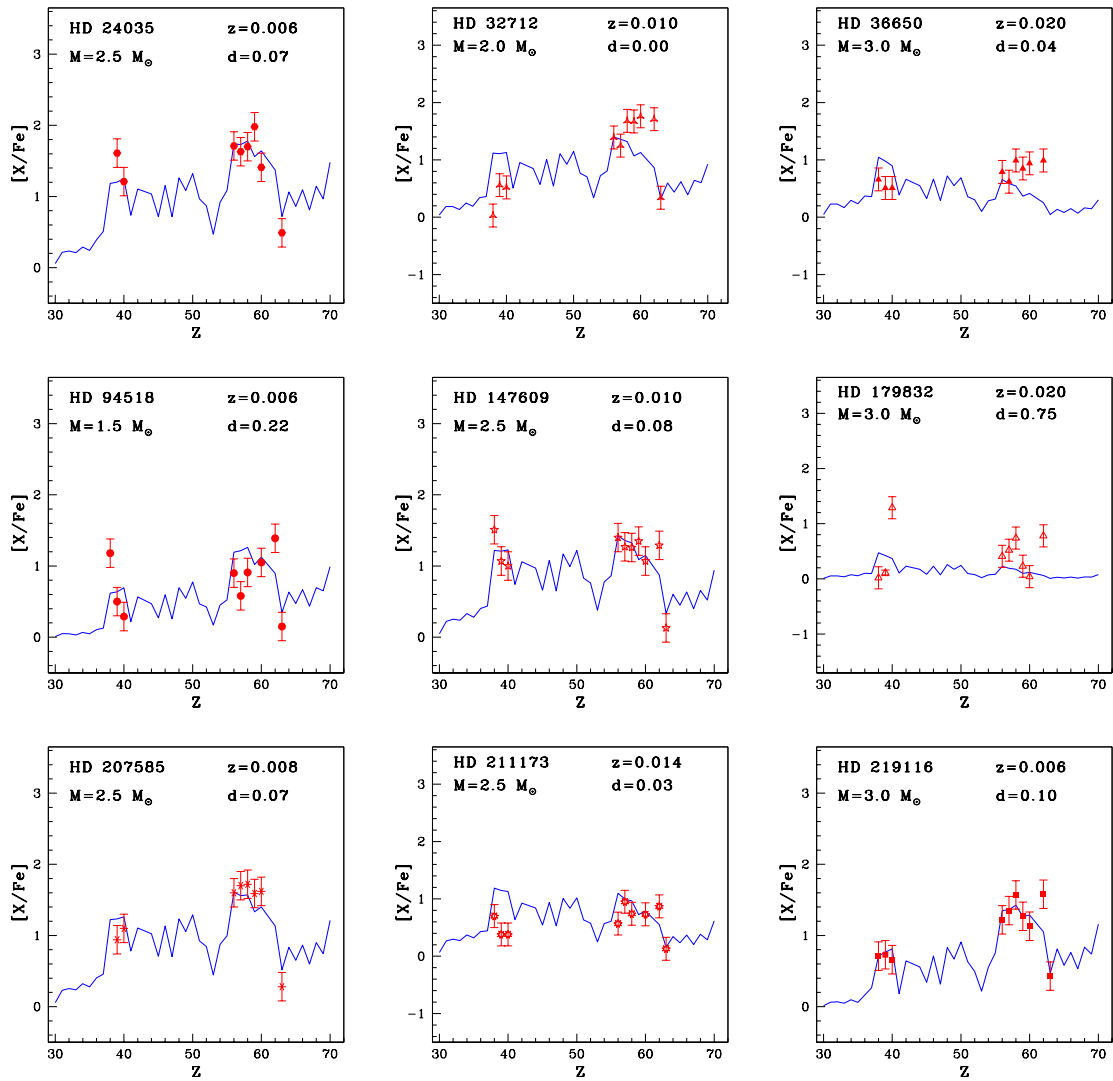
FIGURE 3.19: The solid curves are the best fit for the parametric model function obtained from the comparison of the observed abundances in the Ba stars and predicted abundances from the FRUITY models by minimizing the χ^2 . The observed abundances in the program stars are indicated by the points with error bars.

TABLE 3.13: Spatial velocity and probability estimates for the program stars

Star name	U_{LSR} (km s $^{-1}$)	V_{LSR} (km s $^{-1}$)	W_{LSR} (km s $^{-1}$)	V_{spa} (km s $^{-1}$)	P_{thin}	P_{thick}	P_{halo}	Population
HD 24035	-11.18 ± 0.52	27.32 ± 0.38	-16.35 ± 0.58	33.74 ± 0.15	0.99	0.01	0.00	Thin disk
HD 32712	76.78 ± 0.66	-11.17 ± 0.16	17.13 ± 0.17	79.46 ± 0.65	0.97	0.03	0.00	Thin disk
HD 36650	21.44 ± 0.13	-18.64 ± 0.17	-10.09 ± 0.13	30.15 ± 0.06	0.99	0.01	0.00	Thin disk
HD 94518	46.24 ± 0.11	-119.85 ± 0.43	-62.49 ± 0.44	142.85 ± 0.52	0.00	0.95	0.05	Thick disk
HD 147609	19.45 ± 0.87	-15.64 ± 0.90	-4.11 ± 1.03	25.30 ± 0.06	0.99	0.01	0.00	Thin disk
HD 154276	1.75 ± 0.96	-116.16 ± 0.76	22.48 ± 0.76	118.33 ± 0.58	0.07	0.92	0.01	Thick disk
HD 179832	9.21 ± 0.15	-5.80 ± 0.32	-4.98 ± 0.21	11.97 ± 0.41	0.99	0.01	0.00	Thin disk
HD 182274	35.72 ± 0.05	17.56 ± 0.05	-2.76 ± 0.03	39.90 ± 0.06	0.99	0.01	0.00	Thin disk
HD 207585	-27.10 ± 0.32	-41.91 ± 2.68	44.05 ± 1.04	66.57 ± 1.13	0.72	0.28	0.00	Thin disk
HD 211173	-48.53 ± 0.88	27.71 ± 0.42	4.79 ± 0.54	56.09 ± 0.51	0.99	0.01	0.00	Thin disk
HD 219116	-46.22 ± 1.31	-17.18 ± 0.49	25.18 ± 0.59	55.37 ± 0.98	0.97	0.03	0.00	Thin disk

3.8 Kinematic analysis

The methodology followed for kinematic analysis is discussed in detail in section 2.7. The results of the kinematic analysis for the stellar sample is presented in this section. The estimates of the total spatial velocity and components of spatial velocity, along with the probability estimates are given in Table 3.13. All the stars are found to be members of the Galactic disk.

3.9 Discussion on individual stars

HD 24035, HD 32712, HD 36650, HD 207585, HD 211173, and HD 219116:

These objects are listed in the CH star catalogue of Bartkevicius (1996) as well as in the barium star catalogue of Lü (1991). While Smith *et al.* (1993) classified

HD 219116 as a CH sub-giant, MacConnell *et al.* (1972) and Mennessier *et al.* (1997) suggested these objects to be giant barium stars. Based on our temperature and luminosity estimates, their locations on the H-R diagram correspond to the giant phase of evolution, except for HD 207585 which is found to be a strong Ba sub-giant. Earlier studies on these objects include abundance analysis by Masseron *et al.* (2010) and de Castro *et al.* (2016). We have estimated the abundances of all the important s-process elements and Eu in these objects except Sr in HD 24035. Based on our abundance analysis, we find these objects to satisfy the criteria for s-process enriched stars by Beers and Christlieb (2005) with $[\text{Ba}/\text{Fe}] > 1$ and $[\text{Ba}/\text{Eu}] > 0.50$. Following Yang *et al.* (2016), they can also be included in the strong Ba giant category, while HD 211173 is a mild Ba giant. They show the characteristics of Ba stars with an estimated $\text{C}/\text{O} \sim 0.95$, 0.51, 0.56, 0.24, and 0.59 for HD 219116, HD 32712, HD 36650, HD 207585, and HD 211173, respectively. HD 24035 shows the largest enhancement of Ba among our program stars with $[\text{Ba}/\text{Fe}] \sim 1.71$ and the largest mean s-process abundance with $[\text{s}/\text{Fe}] \sim 1.55$. A comparison with the FRUITY models shows that the former AGB companions of HD 24035, HD 32712, HD 36650, HD 207585, HD 211173, and HD 219116 are low-mass objects with masses 2.5 M_\odot , 2.0 M_\odot , 3.0 M_\odot , 2.5 M_\odot , 2.5 M_\odot , and 3.0 M_\odot , respectively. From kinematic analysis, we find these objects to belong to the thin disk population with probability ≥ 0.97 . The estimated spatial velocities $< 85 \text{ km s}^{-1}$ also satisfy the criterion of Chen *et al.* (2004) for stars to be the thin disk objects. From radial velocity monitoring, HD 24035 and HD 207585 are confirmed to be binaries with orbital periods of 377.83 ± 0.35 days (Udry *et al.* 1998a) and 1146 ± 1.5 days (Escorza *et al.* 2019) respectively.

HD 94518: This object belongs to the CH star catalogue of Bartkevicius (1996). Our abundance analysis places this object in the strong Ba star category with $\text{C}/\text{O} \sim 0.06$. The abundance pattern observed in this star resembles with that of a 1.5 M_\odot AGB star. The position of this star on the H-R diagram shows this object

to be a sub-giant star. Kinematic analysis shows this object to belong to the thick disk population with a probability ~ 0.95 .

HD 147609: This object is listed in the CH star catalogue of Bartkevicius (1996). This star is a strong Ba dwarf with a C/O ~ 0.27 . Comparison of the observed abundance in HD 147609 with the FRUITY model shows a close resemblance to that seen in the $2.5 M_{\odot}$ AGB star. Kinematic analysis has shown that this object belongs to the thin disk population with the characteristic spatial velocity of the thin disk objects. The radial velocity monitoring study by Escorza *et al.* (2019) has confirmed this object to be a binary with an orbital period of 672 ± 2 days.

HD 154276: This star is listed in the CH star catalogue of Bartkevicius (1996). Our analysis has shown that this star is a dwarf. Our analysis based on mean s-process abundance, [s/Fe], revealed that this object cannot be considered as a Ba star.

HD 179832: This object belongs to the CH star catalogue of Bartkevicius (1996). We have presented a first-time detailed abundance analysis for this object. Our analysis has shown that this object is a mild Ba giant. The abundance trend observed in this star suggests that the former companion AGB star's mass is $3 M_{\odot}$. From kinematic analysis, HD 179832 is found to be a thin disk object with a probability of 0.99. The spatial velocity is estimated to be 11.97 km s^{-1} , as expected for the thin disk stars (Chen *et al.* 2004).

3.10 Conclusions

Results from high-resolution spectroscopic analysis of ten objects are presented. All the objects are listed in the CH star catalogue of Bartkevicius (1996). Six of them are also listed in the barium star catalog of Lü (1991). Except for one object, HD 154276, all other objects are shown to be bona fide barium stars from our analysis. Although it satisfies the criteria of Yang *et al.* (2016) to be a mild barium star, our detailed abundance analysis shows this object to be a normal star. An analysis based on the mean s-process abundance clearly shows that this particular star lies among the stars rejected as barium stars by de Castro *et al.* (2016).

Although some of the objects analyzed here are common to the sample analyzed by different authors, abundances of important heavy elements such as Rb, and C, N, and O are not found in the literature. New results for these elements are presented in this work.

We have presented the first time abundance results for HD 179832 and shown it to be a mild barium giant. Kinematic analysis has shown it to be a thin disk object. A parametric model-based analysis has shown the object's former companion AGB star's mass to be about $3 M_{\odot}$.

The sample of stars analyzed here covers a metallicity range from -0.55 to $+0.23$, and a kinematic analysis has shown that all of them belong to the Galactic disk, as expected for barium stars.

The estimated masses of the barium stars are consistent with that observed for other barium stars (Allen and Barbuy 2006; Liang *et al.* 2003; Antipova *et al.* 2004; de Castro *et al.* 2016). The abundance estimates are consistent with the operation of the $^{13}\text{C}(\alpha, \text{n})^{16}\text{O}$ source in the former low-mass AGB companion.

We did not find any enhancement of Mg in our sample, which discards the source of neutron as the $^{22}\text{Ne}(\alpha, n)^{25}\text{Mg}$ reaction. An enhancement of Mg abundances when compared with their counterparts in disk stars and normal giants would have indicated the operation of $^{22}\text{Ne}(\alpha, n)^{25}\text{Mg}$.

The detection of the Rb I line at 7800.259 Å in the spectra of HD 32712, HD 36650, HD 179832, and HD 211173 allowed us to determine the [Rb/Zr] ratio. This ratio gives an indication of the neutron source at the s-process site and in turn provides clues to the mass of the star. We have obtained negative values for this ratio in all four stars. The negative values obtained for these stars indicate the operation of $^{13}\text{C}(\alpha, n)^{16}\text{O}$ reaction. As this reaction occurs in the low-mass AGB stars, we confirm that the former companions of these stars are low-mass AGB stars with $M \leq 3 M_{\odot}$.

The distribution of abundance patterns and [hs/ls] ratios indicate low-mass companions for the objects for which [Rb/Zr] could not be estimated. A comparison of observed abundances with the predictions from the FRUITY models, and with those observed in low-mass AGB stars from literature confirms low-mass for the former companion AGB stars.

3.11 Appendix A

Atomic lines and line information used to derive the elemental abundances are listed in Tables A1 and A2.

Table A1 : Equivalent widths (in mÅ) of Fe lines used for deriving atmospheric parameters

Wavelength(Å)	El	E_{low} (eV)	log gf	HD 24035	HD 32712	HD 36650	HD 94518	HD 147609	HD 154276	HD 179832	HD 207585	HD 211173	HD 219116	Ref
4132.9	Fe I	2.85	-1.01	-	-	-	88.70(6.94)	-	-	-	83.40(6.96)	132.2(7.31)	-	1
4139.927		0.99	-3.629	-	-	-	-	-	-	-	-	-	-	1
4147.669		1.485	-2.104	-	-	-	-	-	-	-	-	-	-	1
4153.9		3.4	-0.32	129.9(6.79)	-	-	-	-	-	-	90.80(6.90)	-	-	1
4154.499		2.832	-0.688	-	-	-	-	-	-	-	-	-	-	2
4184.891		2.831	-0.860	-	-	-	-	-	-	-	-	-	-	1
4187.039		2.449	-0.548	-	-	-	132.4(6.88)	-	-	-	132.60(7.02)	-	-	1
4202.029		1.485	-0.708	-	-	-	-	-	-	-	-	-	-	1
4203.569		1.011	-3.869	-	-	-	-	34.6(7.23)	-	-	-	-	-	2
4210.343		2.482	-0.87	-	-	-	-	120.4(7.48)	-	-	-	-	-	1
4213.648		2.845	-1.29	-	-	-	-	68.5(6.96)	-	-	-	-	-	1
4216.18		0	-3.36	-	-	-	-	-	-	-	106.4(7.16)	-	-	1
4217.546		3.43	-0.51	-	-	-	-	99.6(7.43)	-	-	-	-	-	1
4222.213		2.449	-0.967	-	-	-	-	104.9(7.19)	-	-	-	-	-	1
4224.171		3.368	-0.41	-	-	-	-	101.2(7.31)	-	-	-	-	-	1
4238.81		3.397	-0.28	-	-	-	-	105.7(7.29)	-	-	-	-	-	1
4239.362		3.642	-1.52	-	-	-	-	34.7(7.19)	-	-	-	-	-	1
4240.371		3.547	-1.34	-	-	-	-	51.4(7.26)	-	-	-	-	-	1
4250.119		2.469	-0.405	-	-	-	-	134.5(7.25)	-	-	-	-	-	1
4250.787		1.557	-0.71	-	-	-	-	175.9(7.34)	-	-	-	-	-	1
4276.675		3.882	-1.21	-	-	-	-	27.5(6.93)	-	-	-	-	-	1
4282.403		2.176	-0.81	-	-	-	-	115.4(7.03)	-	-	-	-	-	1
4327.096		3.547	-0.96	-	-	-	-	-	88.57(7.61)	-	-	-	-	1
4343.697		3.047	-1.88	-	-	-	-	-	62.40(7.53)	-	-	-	-	1
4347.233		0	-5.503	-	-	-	-	-	26.68(7.22)	-	-	-	-	1
4348.937		2.99	-2.130	-	-	-	-	-	39.82(7.11)	-	-	-	-	1
4360.804		3.642	-1.87	-	-	-	-	-	39.52(7.46)	-	-	-	-	1
4352.735		2.223	-1.26	-	-	-	-	114.2(7.47)	-	-	-	-	-	1
4365.896		2.99	-2.21	-	-	-	-	-	42.47(7.26)	-	-	-	-	1
4369.772		3.047	-0.73	-	-	-	-	93.0(7.14)	-	-	-	-	-	1
4373.561		3.018	-1.826	-	-	-	-	40.2(7.05)	53.86(7.21)	-	-	-	-	3
4376.773		3.017	-2.336	-	-	-	-	-	42.79(7.42)	-	-	-	-	2
4377.791		3.274	-2.31	-	-	-	-	-	32.49(7.37)	-	-	-	-	1
4387.891		3.071	-1.47	-	-	-	-	67.1(7.28)	66.95(7.25)	-	-	-	-	1
4388.407		3.603	-0.59	-	-	-	-	71.3(6.96)	80.63(7.12)	-	-	-	-	1
4389.245		0.052	-4.583	-	-	-	-	-	65.79(7.46)	-	-	-	-	1
4392.58		3.882	-2	-	-	-	-	-	31.02(7.59)	-	-	-	-	1
4422.568		2.845	-1.11	-	143.5(7.18)	-	88.50(6.97)	-	-	-	-	-	-	1
4423.841		3.654	-1.61	-	-	-	-	-	42.89(7.29)	-	-	-	-	1
4430.614		2.223	-1.659	-	-	-	-	97.0(7.44)	-	-	-	-	-	1
4432.568		3.573	-1.6	-	-	-	-	30.6(7.11)	44.03(7.23)	-	-	-	-	1
4433.218		3.654	-0.7	-	-	-	-	60.0(6.87)	-	-	-	-	-	1
4436.921		3.047	-2.11	-	-	-	-	36.5(7.28)	-	-	-	-	-	1
4438.345		3.882	-1.63	-	-	-	29.60(7.06)	-	-	-	-	-	-	1
4442.831		2.176	-2.792	-	-	-	-	-	55.74(7.43)	-	-	-	-	1
4445.471		0.087	-5.38	95.02(6.81)	111.4(7.43)	-	-	-	31.41(7.35)	-	-	92.30(7.40)	-	1
4446.833		3.687	-1.33	-	-	-	-	35.5(7.04)	63.89(7.56)	-	56.40(7.28)	-	-	1
4447.13		2.198	-2.59	-	-	-	-	-	53.12(7.17)	-	-	-	-	1
4447.717		2.223	-1.342	-	-	-	-	107.7(7.37)	-	-	-	-	-	1
4454.381		2.832	-1.250	-	-	-	-	-	84.05(7.22)	-	-	-	-	1
4456.326		3.047	-2.17	-	-	-	-	-	45.08(7.34)	-	-	-	-	1
4461.653		0.073	-3.210	-	-	-	-	-	-	-	-	-	-	1
4466.551		2.832	-0.590	-	-	-	118.5(7.00)	123.0(7.47)	-	-	107.7(6.97)	172.3(7.23)	-	1
4466.551		2.832	-0.590	-	-	-	118.5(7.00)	123.0(7.47)	-	-	107.7(6.97)	172.3(7.23)	-	1
4481.609		3.686	-1.42	-	-	-	-	-	47.42(7.23)	-	-	-	-	1
4482.739		3.654	-1.35	-	-	-	-	52.0(7.35)	-	-	-	-	-	1

The abundance obtained from each line is given in parenthesis.

Table A1 : continues....

Wavelength(Å)	El	E_{low} (eV)	log gf	HD 24035	HD 32712	HD 36650	HD 94518	HD 147609	HD 154276	HD 179832	HD 207585	HD 211173	HD 219116	Ref
4484.22		3.603	-0.720	106.5(6.76)	107.7(6.99)	137.6(7.70)	70.30(6.82)	-	83.77(7.31)	-	76.70(7.15)	104.4(7.17)	-	1
4485.676		3.686	-1.02	-	-	-	-	-	69.49(7.38)	-	-	-	-	1
4489.739		0.121	-3.966	161.5(6.97)	166.6(7.04)	-	-	-	86.26(7.49)	-	83.80(7.19)	138.4(7.16)	-	1
4490.084		3.017	-1.58	-	-	-	-	48.5(6.95)	-	-	-	-	-	1
4502.591		3.573	-2.35	-	-	-	-	-	22.06(7.40)	-	-	-	-	1
4517.524		3.071	-1.84	-	-	-	-	40.2(7.10)	66.19(7.59)	-	-	-	-	1
4531.15		1.49	-2.15	-	-	-	106.4(7.10)	-	-	-	-	-	-	1
4531.626		3.211	-2.511	-	-	-	-	24.1(7.55)	-	-	-	-	-	2
4547.847		3.546	-0.780	-	124.9(7.31)	-	67.60(6.75)	69.4(7.05)	78.87(7.23)	-	-	109.2(7.26)	-	1
4566.514		3.301	-2.250	-	74.60(7.29)	-	21.60(6.91)	-	-	-	-	67.70(7.36)	-	1
4574.215		3.211	-2.5	-	-	-	-	-	-	-	58.40(7.27)	-	-	1
4587.128		3.573	-1.78	-	-	-	-	26.4(7.19)	46.48(7.46)	-	-	-	-	1
4595.358		3.301	-1.72	-	-	-	52.30(7.08)	-	60.15(7.51)	-	-	-	-	1
4596.06		3.603	-1.64	-	-	-	-	48.9(7.53)	-	-	-	-	-	1
4596.415		3.654	-2.32	-	-	-	-	-	24.29(7.50)	-	-	-	-	1
4602.001		1.608	-3.154	-	-	-	-	45.3(7.21)	65.00(7.49)	-	-	-	-	1
4602.941		1.485	-1.95	-	-	-	-	93.1(6.92)	-	-	-	-	-	3
4619.288		3.603	-1.120	-	94.40(7.04)	98.70(7.26)	60.90(6.98)	-	71.18(7.44)	-	-	93.00(7.25)	-	1
4625.045		3.241	-1.34	102.0(6.80)	-	-	-	-	-	-	-	-	-	1
4630.12		2.278	-2.600	-	-	-	54.60(7.01)	-	-	-	61.90(7.32)	-	-	1
4632.911		1.608	-2.913	-	-	-	-	71.6(7.49)	-	-	-	-	-	1
4635.846		2.845	-2.42	72.55(6.74)	84.10(7.14)	90.40(7.45)	32.40(6.89)	-	45.52(7.39)	-	35.40(7.05)	80.90(7.35)	-	1
4637.503		3.283	-1.39	99.86(6.84)	96.20(6.97)	-	57.30(6.85)	-	75.18(7.52)	-	64.30(7.14)	100.20(7.34)	104.2(7.19)	1
4643.464		3.654	-1.29	94.65(7.06)	91.50(7.18)	-	51.90(6.98)	-	-	-	56.50(7.19)	81.70(7.16)	-	1
4647.434		2.949	-1.31	-	-	-	-	88.4(7.47)	79.76(7.25)	-	-	-	-	1
4657.585		2.845	-1.9	-	-	-	-	-	25.12(7.34)	-	-	-	-	1
4661.97		2.99	-2.46	-	-	-	-	-	37.41(7.36)	-	-	-	-	1
4678.846		3.603	-0.66	-	-	-	-	-	86.78(7.29)	-	-	-	-	1
4679.218		4.558	-1.115	-	-	-	-	-	37.84(7.45)	-	-	-	-	2
4683.56		2.832	-2.53	-	-	-	-	-	43.43(7.42)	-	-	-	-	1
4690.138		3.686	-1.64	72.70(6.95)	80.50(7.29)	-	31.10(6.90)	-	45.28(7.43)	-	39.50(7.17)	-	-	1
4704.948		3.686	-1.57	-	-	-	-	35.1(7.25)	57.54(7.62)	-	-	-	-	1
4705.457		3.547	-2.31	-	-	-	-	-	25.13(7.41)	-	-	-	-	1
4707.488		2.845	-2.34	-	-	-	-	-	56.59(7.60)	-	-	-	-	1
4721.001		2.99	-2.801	-	-	-	-	-	39.90(7.76)	-	-	-	-	2
4728.546		3.654	-1.28	-	-	-	-	-	68.00(7.56)	-	-	-	-	2
4733.591		1.484	-2.71	-	-	146.7(7.42)	85.00(7.08)	-	65.91(6.92)	-	86.00(7.28)	138.0(7.40)	-	3
4735.843		4.076	-1.22	-	-	-	-	35.5(7.25)	48.31(7.39)	-	-	-	-	1
4736.772		3.211	-0.74	-	-	154.8(7.50)	94.40(7.00)	99.5(7.38)	-	-	-	-	-	1
4741.529		2.831	-2.000	-	-	114.2(7.60)	51.30(6.87)	52.1(7.26)	61.88(7.38)	-	-	101.7(7.45)	-	1
4745.8		3.654	-1.27	-	-	-	-	-	64.59(7.46)	-	-	-	-	2
4749.948		4.559	-1.34	-	-	-	-	-	24.04(7.34)	-	-	-	-	1
4768.319		3.686	-1.109	-	-	-	64.50(7.12)	52.8(7.14)	-	-	-	-	-	2
4772.804		1.557	-2.897	-	-	-	-	-	81.22(7.59)	-	-	-	-	2
4786.807		3.017	-1.59	-	-	-	-	-	72.73(7.42)	-	-	-	-	1
4787.827		2.998	-2.770	64.40(7.09)	72.20(7.34)	74.50(7.55)	20.20(7.08)	-	-	-	24.90(7.29)	65.50(7.44)	-	1
4788.751		3.236	-1.810	-	-	-	48.70(6.96)	40.2(7.20)	55.72(7.40)	-	56.90(7.27)	-	-	1
4789.651		3.546	-0.91	119.8(7.10)	-	-	67.00(6.84)	-	72.34(7.12)	-	68.50(7.00)	110.8(7.36)	-	3
4791.247		3.274	-2.51	-	-	-	-	22.0(7.54)	-	-	-	-	-	1
4798.265		4.186	-1.55	-	-	-	-	-	26.27(7.27)	-	-	-	-	1
4798.732		1.608	-4.25	-	-	-	-	-	27.32(7.53)	-	-	-	-	1
4799.406		3.64	-2.23	-	-	-	-	20.0(7.49)	25.68(7.43)	-	-	-	-	1
4800.649		4.143	-1.26	-	-	-	-	27.8(7.18)	54.31(7.62)	-	-	-	-	1
4802.88		3.642	-1.514	-	-	-	-	-	50.78(7.34)	-	-	-	-	2
4834.506		2.424	-3.410	-	-	-	-	-	-	-	-	-	-	1

The abundance obtained from each line is given in parenthesis.

Table A1 : continues....

Wavelength(Å)	El	E_{low} (eV)	log gf	HD 24035	HD 32712	HD 36650	HD 94518	HD 147609	HD 154276	HD 179832	HD 207585	HD 211173	HD 219116	Ref
4842.788		4.104	-1.56	-	-	78.30(7.70)	22.80(7.01)	-	33.28(7.39)	-	27.70(7.20)	-	-	1
4843.143		3.397	-1.84	-	-	-	-	-	56.01(7.59)	-	-	-	-	1
4844.014		3.547	-2.03	-	-	-	-	-	38.20(7.46)	-	-	-	-	1
4845.655		3.267	-2.687	-	-	-	-	-	34.36(7.76)	-	-	-	-	2
4871.318		2.865	-0.410	-	-	-	-	-	-	-	-	-	-	1
4875.871		3.332	-2.02	-	89.40(7.43)	90.20(7.56)	36.80(7.05)	-	47.74(7.49)	-	-	80.30(7.44)	-	1
4882.143		3.417	-1.64	91.20(6.99)	100.4(7.42)	-	44.10(6.92)	-	61.14(7.53)	-	54.20(7.25)	90.80(7.44)	90.70(7.22)	1
4885.43		3.882	-1.095	-	-	-	-	-	61.13(7.40)	-	-	-	-	2
4886.332		4.154	-0.685	-	-	-	-	-	51.6(7.09)	63.71(7.27)	-	-	-	2
4890.755		2.876	-0.43	-	-	-	-	-	120.2(7.21)	-	-	-	-	1
4892.859		4.218	-1.29	-	-	-	-	-	28.9(7.29)	40.71(7.39)	-	-	-	1
4896.439		3.884	-2.05	-	-	-	-	-	27.54(7.52)	-	-	-	-	1
4903.31		2.881	-1.080	-	-	-	-	-	96.3(7.33)	-	-	-	-	1
4907.732		3.43	-1.840	86.80(7.11)	92.70(7.45)	94.20(7.59)	33.60(6.97)	-	-	-	43.00(7.19)	79.80(7.36)	77.10(7.15)	1
4908.031		4.217	-1.396	70.29(7.14)	70.70(7.29)	90.70(7.71)	-	-	-	-	23.00(6.90)	60.70(7.22)	-	2
4909.383		3.929	-1.327	-	-	-	-	-	34.5(7.20)	-	-	-	-	2
4917.229		4.191	-1.180	74.70(7.10)	-	-	38.60(7.08)	-	-	-	40.60(7.20)	-	-	1
4924.77		2.278	-2.220	122.2(6.92)	-	-	71.50(7.04)	67.3(7.27)	-	-	72.70(7.22)	-	121.9(7.22)	1
4927.418		3.573	-1.99	-	-	-	-	26.1(7.37)	-	-	-	-	-	1
4930.315		3.959	-1.350	-	-	-	45.30(7.17)	26.1(7.37)	-	-	45.30(7.26)	-	-	1
4938.174		3.943	-1.018	-	-	-	-	51.6(7.23)	-	-	-	-	-	2
4938.814		2.876	-1.077	-	-	-	-	78.2(6.90)	-	-	-	-	-	2
4939.687		0.859	-3.340	162.2(7.06)	169.4(7.23)	166.2(7.53)	-	65.2(7.06)	-	166.9(7.55)	78.50(7.03)	149.0(7.40)	-	1
4946.387		3.368	-1.17	-	-	-	-	77.2(7.41)	-	-	-	-	-	1
4950.104		3.417	-1.670	-	-	-	-	43.2(7.26)	-	-	-	-	-	1
4967.89		4.191	-0.622	100.0(7.08)	99.20(7.26)	99.90(7.36)	54.80(6.87)	59.8(7.13)	-	-	59.40(7.07)	93.50(7.32)	84.90(6.93)	2
4969.917		4.216	-0.71	-	100.6(7.41)	100.1(7.49)	51.00(6.90)	47.4(7.08)	-	-	53.20(7.04)	92.50(7.43)	81.90(6.99)	1
4973.102		3.96	-0.95	-	-	-	-	60.1(7.35)	-	-	-	-	-	1
4985.253		3.93	-0.560	108.5(6.89)	115.1(7.23)	117.7(7.40)	70.80(6.92)	-	-	-	69.00(6.99)	113.1(7.42)	104.9(7.01)	2
4994.129		0.914	-3.080	-	-	-	-	75.0(7.04)	-	-	-	-	-	1
5001.863		3.882	0.01	-	-	-	92.90(6.70)	-	-	-	94.50(6.86)	-	-	1
5002.792		3.397	-1.58	-	-	-	-	44.8(7.19)	-	-	-	-	-	1
5005.712		3.884	-0.142	-	-	-	81.80(6.75)	-	-	-	-	-	116.9(6.84)	2
5006.119		2.833	-0.61	-	-	-	119.9(6.95)	-	-	-	112.0(6.97)	179.2(7.22)	168.2(7.05)	2
5014.942		3.943	-0.25	-	-	-	-	79.8(7.04)	-	-	-	-	-	1
5022.236		3.984	-0.530	108.5(6.92)	-	-	70.70(6.93)	-	-	-	78.80(7.23)	117.4(7.52)	114.6(7.24)	1
5028.126		3.573	-1.474	-	95.80(7.30)	95.20(7.39)	52.50(7.07)	-	-	-	57.50(7.29)	90.20(7.40)	-	2
5031.915		4.372	-1.67	-	-	-	-	-	-	-	41.70(7.34)	-	-	1
5044.211		2.851	-2.15	-	103.9(7.28)	108.4(7.53)	47.20(6.92)	-	-	-	-	-	97.00(7.19)	1
5049.819		2.278	-1.420	-	-	-	109.2(6.98)	100.9(7.22)	-	-	109.6(7.15)	-	168.2(7.16)	1
5051.635		0.915	-2.795	-	-	-	-	100.7(7.34)	-	-	81.10(6.74)	-	-	1
5054.642		3.64	-2.140	-	-	72.54(7.57)	20.20(7.06)	-	-	70.4097.68)	-	63.40(7.46)	50.40(7.17)	1
5074.748		4.22	-0.2	-	-	-	-	87.9(7.39)	-	-	-	-	-	1
5079.223		2.2	-2.067	-	141.3(7.17)	152.0(7.58)	80.60(6.97)	-	-	-	81.30(7.14)	136.5(7.43)	128.5(7.04)	1
5083.338		0.958	-2.958	-	-	172.7(7.30)	-	81.8(7.10)	-	-	98.80(7.25)	159.2(7.23)	160.4(7.11)	1
5090.767		4.256	-0.400	-	-	-	-	68.0(7.21)	-	118.6(7.70)	-	-	-	1
5096.998		4.283	-0.196	-	-	-	-	71.1(7.09)	-	-	-	-	-	2
5109.652		4.302	-0.98	-	87.90(7.47)	87.80(7.54)	-	-	-	-	-	-	-	1
5110.413		0	-3.76	-	-	-	-	94.8(7.29)	-	-	-	-	-	1
5123.72		1.011	-3.068	-	-	-	-	84.5(7.31)	-	-	-	-	-	1
5126.193		4.256	-1.08	-	-	-	-	42.6(7.39)	-	-	-	-	-	1
5127.359		0.915	-3.307	174.0(7.22)	-	154.8(7.32)	-	-	-	-	83.40(7.15)	135.6(7.13)	145.0(7.09)	1
5133.681		4.178	0.14	-	-	-	101.3(7.05)	-	-	-	-	-	146.1(7.34)	1
5141.739		2.424	-2.150	-	-	-	63.60(6.86)	56.9(7.11)	-	138.2(7.78)	-	-	113.9(7.04)	1
5150.839		0.99	-3.07	-	-	-	-	83.9(7.27)	-	-	-	-	-	1

The abundance obtained from each line is given in parenthesis.

Table A1 : continues....

Wavelength(Å)	El	E_{low} (eV)	log gf	HD 24035	HD 32712	HD 36650	HD 94518	HD 147609	HD 154276	HD 179832	HD 207585	HD 211173	HD 219116	Ref
5151.911		1.011	-3.32	-	171.5(7.37)	172.7(7.70)	78.40(6.94)	-	-	-	-	-	-	1
5159.058		4.283	-0.82	70.43(6.74)	-	-	43.40(6.90)	42.6(7.15)	-	-	51.20(7.16)	-	82.30(7.15)	1
5162.273		4.178	0.02	-	-	-	-	95.3(7.30)	-	-	-	-	-	1
5166.282		0	-4.195	-	-	-	-	74.1(7.27)	-	-	-	-	-	1
5171.6		1.485	-1.790	-	-	-	-	117.9(7.23)	-	-	-	-	-	1
5187.915		4.143	-1.26	77.31(7.14)	83.50(7.45)	87.90(7.63)	29.70(6.90)	22.5(7.03)	-	-	34.40(7.07)	-	65.90(7.11)	1
5192.344		2.998	-0.421	-	-	-	-	-	-	-	-	-	-	2
5194.941		1.557	-2.090	-	-	-	-	92.3(7.00)	-	-	-	-	170.9(7.08)	1
5195.472		4.22	0.08	119.5(6.89)	-	128.7(7.35)	-	80.6(7.02)	-	-	73.90(6.82)	117.3(7.23)	-	2
5198.711		2.222	-2.135	145.5(7.14)	-	150.9(7.62)	74.70(6.90)	66.2(7.09)	-	152.2(7.71)	76.50(7.10)	-	128.3(7.09)	1
5215.179		3.266	-0.933	132.4(6.93)	137.4(7.20)	142.9(7.46)	85.60(6.98)	-	-	157.2(7.73)	83.60(7.07)	131.7(7.38)	-	1
5216.274		1.608	-2.15	-	-	-	-	93.0(7.12)	-	-	-	-	-	1
5217.389		3.211	-1.097	-	-	-	-	78.7(7.27)	-	142.1(7.69)	-	-	-	1
5226.862		3.038	-0.667	156.4(6.85)	-	-	-	-	-	-	-	-	163.0(7.19)	2
5228.376		4.221	-1.29	-	-	86.00(7.70)	-	37.2(7.46)	44.14(7.47)	-	-	-	-	1
5229.845		3.283	-1.136	-	-	-	-	81.6(7.37)	-	-	-	-	-	2
5232.939		2.94	-0.640	-	-	-	-	-	-	-	-	-	-	1
5242.491		3.634	-0.840	103.8(6.79)	106.9(7.08)	113.8(7.34)	63.20(6.86)	67.3(7.08)	75.91(7.23)	-	70.00(7.13)	104.0(7.26)	100.6(6.94)	1
5243.776		4.256	-1.15	-	-	-	-	33.3(7.27)	-	-	-	-	-	1
5247.05		0.087	-4.946	133.7(6.95)	138.5(7.28)	134.4(7.50)	-	-	58.50(7.46)	-	45.70(7.04)	116.0(7.27)	-	1
5250.209		0.121	-4.938	146.7(7.24)	-	-	-	-	-	-	-	122.6(7.44)	-	1
5250.646		2.198	-2.050	-	-	-	-	-	-	-	-	-	-	1
5253.462		3.283	-1.670	92.50(6.82)	99.90(7.19)	103.3(7.38)	53.50(6.99)	-	-	-	54.20(7.11)	92.30(7.27)	93.00(7.08)	1
5263.305		3.265	-0.970	-	-	159.6(7.74)	83.90(6.97)	82.7(7.21)	-	-	90.70(7.27)	-	132.0(7.19)	1
5266.555		2.998	-0.490	-	-	-	-	126.1(7.42)	-	-	-	-	-	1
5269.537		0.859	-1.321	-	-	-	-	168.6(7.06)	-	-	-	-	-	1
5281.79		3.038	-1.020	167.9(7.18)	173.8(7.29)	174.6(7.53)	103.8(7.04)	94.1(7.31)	-	-	100.0(7.11)	162.6(7.45)	153.0(7.18)	1
5283.621		3.241	-0.630	-	-	-	-	104.7(7.33)	-	-	-	-	-	1
5285.118		4.434	-1.640	-	-	-	-	-	-	54.40(7.67)	-	-	-	1
5288.52		3.69	-1.510	-	-	-	-	28.0(7.18)	47.22(7.44)	-	-	-	-	4
5307.36		1.608	-2.987	-	-	-	-	66.9(7.39)	76.32(7.50)	147.5(7.76)	-	-	-	1
5321.11		4.42	-1.190	54.50(6.88)	-	70.00(7.36)	-	-	-	65.30(7.74)	-	57.10(7.15)	-	4
5322.04		2.28	-2.840	-	106.10(7.20)	111.5(7.49)	39.00(6.81)	23.2(7.18)	49.70(7.50)	104.5(7.78)	36.40(6.85)	91.40(7.16)	89.20(6.96)	4
5324.178		3.211	-0.240	-	-	-	-	127.6(7.37)	-	-	-	-	-	1
5329.99		4.076	-1.300	-	-	-	-	-	45.33(7.37)	-	-	-	-	1
5332.9		1.557	-2.940	-	-	-	-	-	75.14(7.37)	-	-	-	-	1
5339.93		3.27	-0.680	150.0(6.98)	152.4(7.14)	155.2(7.37)	97.70(6.97)	85.6(6.98)	-	-	97.90(7.12)	144.1(7.29)	139.4(7.02)	4
5341.024		1.608	-2.06	-	-	-	-	118.6(7.59)	-	-	-	-	-	1
5349.738		4.386	-1.300	-	-	-	-	-	-	-	35.98(7.43)	-	-	1
5364.858		4.445	0.22	121.9(6.93)	127.5(7.18)	130.2(7.34)	85.70(6.89)	80.6(6.99)	-	-	89.40(7.07)	119.9(7.24)	113.1(6.90)	4
5365.399		3.573	-1.44	92.84(6.94)	105.2(7.42)	-	50.00(6.97)	52.1(6.90)	-	-	60.90(7.32)	97.00(7.47)	92.20(7.15)	2
5367.479		4.415	0.35	128.6(6.89)	134.3(7.12)	-	91.50(6.84)	96.9(7.17)	-	-	95.00(7.02)	125.1(7.17)	-	1
5369.961		4.37	0.35	-	-	-	97.20(6.91)	-	-	-	98.10(7.04)	127.9(7.17)	129.5(7.01)	1
5373.698		4.437	-0.860	63.20(6.85)	75.40(7.24)	-	41.30(7.07)	36.1(7.22)	49.60(7.39)	86.50(7.72)	42.40(7.16)	72.90(7.33)	65.00(7.05)	4
5379.574		3.694	-1.480	100.5(7.28)	96.80(7.41)	-	36.20(6.83)	33.3(7.10)	50.31(7.32)	101.5(7.81)	42.70(7.05)	82.30(7.28)	-	1
5383.369		4.312	0.5	145.4(6.91)	152.0(7.08)	-	107.5(6.87)	-	-	-	112.3(7.06)	145.1(7.19)	138.8(6.95)	1
5387.488		4.142	-2.140	-	-	-	-	-	-	-	-	-	-	1
5389.479		4.415	-0.410	-	-	-	-	59.3(7.17)	-	102.9(7.55)	-	-	-	1
5391.459		4.154	-0.812	-	-	-	-	-	67.99(7.47)	-	-	-	-	2
5393.17		3.24	-0.720	145.5(7.08)	-	165.9(7.70)	92.30(7.05)	-	-	-	97.90(7.31)	145.8(7.51)	134.3(7.10)	4
5397.127		0.914	-1.993	-	-	-	-	129.6(7.10)	-	-	-	-	-	1
5398.277		4.445	-0.670	-	-	-	-	-	61.59(7.43)	92.30(7.68)	-	-	-	1
5400.502		4.371	-0.160	-	-	-	-	84.1(7.38)	-	-	-	-	-	1
5405.774		0.99	-1.844	-	-	-	-	-	-	-	-	-	-	1
5415.192		4.386	0.5	-	-	-	-	105.5(7.17)	-	-	-	-	-	1

The abundance obtained from each line is given in parenthesis.

Table A1 : continues....

Wavelength(Å)	El	E_{low} (eV)	log gf	HD 24035	HD 32712	HD 36650	HD 94518	HD 147609	HD 154276	HD 179832	HD 207585	HD 211173	HD 219116	Ref
5424.07	4.32	0.58	-	-	-	-	-	116.2(7.29)	-	-	-	-	-	4
5434.523	1.011	-2.122	-	-	-	-	-	-	-	-	-	-	-	1
5436.588	2.279	-3.390	-	-	-	-	-	-	28.69(7.32)	-	-	-	-	1
5441.34	4.31	-1.580	-	-	-	-	-	-	21.82(7.42)	56.70(7.66)	-	-	-	4
5445.042	4.39	-0.020	107.7(6.80)	118.3(7.20)	124.7(7.41)	69.50(6.96)	84.2(7.25)	-	-	83.80(7.15)	115.4(7.33)	107.1(6.94)	1	
5466.39	4.371	-0.630	-	-	-	-	-	55.5(7.28)	-	103.7(7.77)	-	-	-	1
5472.709	4.209	-1.550	-	-	-	-	-	-	31.49(7.57)	-	-	-	-	1
5473.901	4.154	-0.76	-	-	-	-	-	48.8(7.09)	-	-	-	-	-	1
5487.745	4.32	-0.352	-	-	-	-	-	54.3(6.92)	-	-	-	-	-	1
5501.464	0.958	-2.950	-	-	-	-	-	83.1(7.07)	-	-	-	-	-	1
5506.78	0.99	-2.800	-	-	-	-	-	88.2(7.05)	-	-	-	-	-	4
5522.45	4.21	-1.400	-	-	-	-	-	-	32.81(7.44)	63.90(7.53)	-	-	-	4
5525.544	4.231	-1.33	69.58(7.15)	-	74.30(7.33)	29.90(7.05)	-	43.21(7.49)	-	36.80(7.28)	65.80(7.35)	58.00(7.12)	1	
5532.75	3.57	-2.000	-	-	-	-	-	-	-	-	-	-	-	4
5543.147	3.694	-1.570	-	-	-	-	-	-	-	-	-	-	-	1
5543.936	4.217	-1.14	78.36(7.10)	-	-	35.50(6.97)	34.0(7.23)	48.12(7.40)	-	44.30(7.24)	80.50(7.48)	73.50(7.19)	1	
5546.506	4.371	-1.31	-	-	-	-	-	21.9(7.26)	-	-	-	-	-	1
5554.894	4.549	-0.440	-	-	-	59.00(7.11)	59.3(7.31)	76.79(7.59)	-	-	42.30(6.94)	-	-	1
5557.983	4.473	-1.28	-	-	-	-	-	27.5(7.45)	-	-	-	-	-	1
5560.212	4.435	-1.19	69.36(7.24)	68.10(7.35)	71.70(7.48)	25.70(7.00)	-	28.1(7.34)	40.36(7.46)	-	33.10(7.24)	63.20(7.38)	55.50(7.12)	1
5562.706	4.435	-0.58	-	-	-	-	-	32.9(6.83)	-	-	-	-	-	2
5563.6	4.191	-0.99	-	-	-	-	-	50.3(7.37)	-	-	-	-	-	1
5567.39	2.61	-2.560	-	-	-	-	-	25.8(7.30)	52.82(7.65)	-	-	-	-	4
5569.62	3.42	-0.490	-	153.0(7.14)	155.7(7.36)	100.8(7.00)	-	-	-	102.2(7.17)	145.9(7.30)	139.4(6.99)	4	
5576.09	3.43	-0.851	138.6(7.22)	128.0(7.23)	-	66.90(6.74)	72.6(7.15)	-	140.6(7.69)	88.40(7.36)	129.9(7.52)	125.0(7.19)	1	
5586.756	3.368	-0.210	165.5(6.82)	-	-	-	-	-	-	129.6(7.22)	-	166.0(7.04)	1	
5615.644	3.332	-0.140	-	-	-	-	-	-	-	-	-	-	-	1
5617.19	3.252	-2.88	-	54.60(7.29)	63.00(7.59)	-	-	-	-	-	47.10(7.35)	-	-	1
5618.631	4.209	-1.380	-	63.10(7.04)	-	23.00(6.79)	-	37.86(7.39)	-	-	62.60(7.18)	-	-	1
5624.022	4.386	-1.48	-	-	-	-	-	20.1(7.39)	-	-	-	-	-	1
5624.542	3.417	-0.9	-	-	-	-	-	79.0(7.17)	-	-	-	-	-	1
5633.946	4.991	-0.270	-	-	-	-	-	46.5(7.27)	50.62(7.24)	-	-	-	-	1
5636.696	3.64	-2.61	-	42.60(7.25)	-	-	-	-	-	-	34.30(7.25)	-	-	1
5638.26	4.22	-0.720	-	-	-	-	-	-	65.13(7.51)	-	-	-	-	4
5641.436	4.256	-1.180	-	-	-	-	-	-	-	-	-	-	-	1
5653.865	4.386	-1.640	-	-	-	-	-	-	25.81(7.51)	-	-	-	-	1
5662.516	4.178	-0.573	-	-	-	-	-	48.5(6.91)	-	-	-	-	-	2
5679.02	4.65	-0.770	-	-	-	-	-	31.9(7.34)	-	75.30(7.68)	-	-	-	4
5679.025	4.652	-0.920	-	-	-	-	-	-	45.14(7.49)	-	-	-	-	1
5686.53	4.55	-0.450	-	-	-	-	-	-	-	-	-	-	-	4
5701.544	2.559	-2.216	129.5(7.15)	128.1(7.35)	127.5(7.50)	58.80(6.90)	-	-	-	63.00(7.12)	111.6(7.32)	113.1(7.12)	1	
5717.833	4.284	-1.130	-	-	-	-	-	-	48.0(7.46)	-	-	-	-	1
5731.76	4.26	-1.150	-	76.30(7.41)	84.90(7.66)	34.10(7.13)	34.6(7.43)	45.35(7.52)	-	-	72.30(7.48)	-	-	4
5741.848	4.256	-1.73	43.00(7.08)	-	52.50(7.40)	-	-	-	-	57.90(7.20)	42.40(7.25)	36.60(7.15)	1	
5752.032	4.549	-0.864	-	-	-	-	-	30.3(7.16)	41.59(7.27)	-	-	-	-	2
5753.12	4.26	-0.760	90.40(6.98)	85.50(7.07)	-	45.10(6.83)	49.6(7.18)	-	-	-	82.90(7.18)	82.50(7.01)	1	
5775.08	4.22	-1.203	-	-	-	-	-	27.7(7.25)	47.04(7.52)	90.00(7.91)	-	-	64.70(7.08)	2
5793.913	4.22	-1.700	-	-	-	-	-	-	24.21(7.36)	61.80(7.62)	-	-	-	1
5806.73	4.61	-0.900	-	-	-	-	-	-	39.80(7.46)	80.90(7.88)	-	-	-	4
5809.22	3.88	-1.690	-	-	81.60(7.44)	21.70(6.78)	23.5(7.40)	35.56(7.47)	-	31.20(7.08)	72.70(7.36)	65.50(7.12)	4	
5816.373	4.549	-0.680	-	-	-	-	-	-	63.59(7.56)	-	-	-	-	1
5852.22	4.55	-1.180	-	-	68.50(7.65)	20.50(7.10)	-	29.33(7.43)	-	21.80(7.20)	-	44.20(7.21)	4	
5855.091	4.607	-1.760	-	-	35.10(7.47)	-	-	-	47.90(7.81)	-	-	-	-	1
5856.088	4.294	-1.64	49.45(7.07)	49.10(7.13)	59.80(7.41)	-	-	23.56(7.35)	-	-	51.20(7.30)	39.80(7.08)	1	
5859.586	4.549	-0.386	105.6(7.26)	101.9(7.40)	99.10(7.39)	45.20(6.75)	43.1(6.94)	57.23(7.13)	-	50.90(6.94)	79.00(7.05)	75.10(6.82)	2	

The abundance obtained from each line is given in parenthesis.

Table A1 : continues....

Wavelength(Å)	EI	E_{low} (eV)	log gf	HD 24035	HD 32712	HD 36650	HD 94518	HD 147609	HD 154276	HD 179832	HD 207585	HD 211173	HD 219116	Ref
5862.357		4.549	-0.051	-	-	-	-	-	70.94(7.08)	-	62.60(6.82)	-	89.10(6.75)	2
5883.813		3.959	-1.360	76.60(6.95)	-	-	38.60(6.99)	-	-	95.00(7.76)	42.80(7.17)	-	79.70(7.21)	1
5916.249		2.453	-2.994	-	-	-	-	-	45.43(7.48)	99.30(7.69)	-	-	-	1
5927.786		4.65	-1.090	-	-	-	-	-	31.50(7.34)	-	-	-	-	1
5930.173		4.652	-0.230	-	-	-	-	60.9(7.21)	73.96(7.40)	113.2(7.72)	-	-	-	1
5934.65		3.93	-1.020	-	-	-	-	47.7(7.26)	-	105.1(7.75)	-	-	-	4
5949.346		4.608	-1.248	-	-	-	-	-	24.98(7.29)	-	-	-	-	2
5956.692		0.859	-4.605	107.6(6.84)	-	115.5(7.42)	27.50(6.88)	-	38.63(7.33)	122.2(7.81)	30.90(7.08)	104.3(7.36)	-	1
5975.35		4.835	-0.883	68.71(7.31)	64.10(7.36)	65.50(7.42)	21.50(6.89)	-	-	-	30.00(7.16)	59.50(7.35)	-	2
5976.777		3.943	-1.31	84.89(7.02)	94.60(7.42)	65.50(7.40)	37.60(6.90)	34.5(7.35)	52.75(7.59)	-	41.50(7.06)	80.00(7.27)	73.40(7.02)	2
5984.814		4.733	-0.343	-	-	84.20(7.25)	-	49.1(7.27)	-	-	-	-	-	2
5987.066		4.795	-0.556	-	-	-	-	-	55.43(7.55)	-	-	-	-	2
6003.01		3.881	-1.120	100.3(7.06)	103.6(7.33)	101.4(7.36)	51.60(6.95)	53.1(7.26)	68.97(7.53)	109.8(7.74)	58.20(7.19)	92.90(7.31)	92.40(7.10)	1
6007.96		4.652	-0.978	-	-	-	-	-	40.95(7.45)	-	-	-	-	2
6008.556		3.884	-1.291	-	-	-	-	50.0(7.39)	-	-	-	-	-	2
6024.049		4.548	-0.120	101.8(6.87)	108.5(7.22)	116.3(7.42)	73.60(7.03)	-	-	-	79.30(7.12)	113.0(7.46)	104.7(7.08)	1
6024.06		4.55	-0.060	-	-	-	-	-	87.92(7.45)	-	-	-	-	4
6027.05		4.076	-1.210	-	-	-	-	-	53.43(7.44)	97.50(7.79)	-	-	-	1
6055.992		4.733	-0.460	-	-	-	-	-	-	-	-	-	-	1
6056.01		4.73	-0.400	-	-	-	-	-	58.98(7.40)	93.80(7.70)	-	-	-	4
6065.482		2.608	-1.530	-	-	-	-	-	-	-	-	-	-	1
6078.491		4.795	-0.424	-	-	-	-	-	-	-	-	-	-	2
6078.999		4.652	-1.120	-	-	-	-	-	-	100.8(7.91)	-	-	-	1
6082.71		2.222	-3.573	75.2(6.96)	90.40(7.35)	84.50(7.40)	-	-	24.27(7.29)	68.30(7.68)	-	71.70(7.26)	59.30(7.04)	1
6096.66		3.98	-1.780	-	-	-	-	-	-	-	-	-	-	4
6120.246		0.915	-5.95	36.93(7.12)	49.20(7.24)	-	-	-	-	-	-	28.20(7.22)	-	1
6127.906		4.143	-1.550	-	-	-	-	-	32.29(7.34)	-	-	-	-	2
6136.61		2.45	-1.400	-	-	-	-	-	-	-	-	-	158.4(6.94)	4
6136.994		2.198	-2.95	107.0(6.88)	108.2(7.10)	-	-	-	-	40.40(6.96)	-	95.70(7.01)	1	
6137.694		2.588	-1.403	166.1(6.94)	178.5(7.24)	171.5(7.37)	98.90(6.96)	87.8(7.07)	-	-	96.60(7.07)	168.9(7.44)	155.2(7.05)	1
6151.62		2.18	-3.290	94.00(6.97)	103.5(7.31)	93.50(7.26)	30.60(6.97)	-	40.25(7.36)	1002.(7.62)	28.70(7.02)	84.90(7.23)	79.20(7.04)	4
6157.725		4.076	-1.260	-	-	-	-	-	51.13(7.43)	-	-	-	-	4
6165.36		4.14	-1.470	64.00(7.11)	74.30(7.44)	67.10(7.35)	26.60(7.08)	-	32.29(7.34)	76.50(7.71)	24.40(7.08)	60.20(7.29)	56.10(7.16)	4
6173.34		2.22	-2.880	-	118.8(7.28)	121.1(7.50)	44.00(6.88)	-	56.99(7.40)	124.3(7.79)	48.20(7.08)	103.1(7.27)	100.0(7.05)	4
6180.204		2.727	-2.780	86.40(7.00)	-	97.00(7.49)	29.70(6.98)	-	40.16(7.39)	-	29.20(7.06)	88.50(7.45)	-	1
6187.989		3.94	-1.570	-	-	-	-	-	85.80(7.86)	-	-	-	-	1
6191.56		2.43	-1.420	-	-	-	-	-	-	-	-	-	-	4
6200.314		2.608	-2.437	115.4(7.05)	119.2(7.35)	127.0(7.64)	46.70(6.87)	-	61.89(7.46)	125.2(7.83)	48.70(7.02)	107.1(7.39)	98.90(7.03)	1
6213.429		2.222	-2.660	139.2(7.22)	130.0(7.28)	132.4(7.50)	57.10(6.92)	-	70.91(7.52)	134.0(7.74)	64.20(7.21)	116.1(7.33)	114.1(7.07)	1
6219.279		2.198	-2.433	142.8(7.03)	145.2(7.30)	147.3(7.53)	68.70(6.92)	-	78.79(7.46)	153.4(7.79)	69.20(7.07)	129.6(7.36)	121.7(6.96)	1
6229.225		2.845	-2.970	-	-	-	-	-	27.71(7.38)	8.60(7.86)	-	-	-	1
6230.72		2.56	-1.280	-	-	-	-	104.5(7.26)	-	-	-	-	-	4
6232.639		3.653	-1.271	-	-	120.9(7.61)	56.60(6.96)	-	67.64(7.36)	116.9(7.66)	58.70(7.11)	107.0(7.47)	94.50(7.00)	2
6240.646		2.222	-3.380	95.60(6.91)	100.9(7.17)	100.4(7.32)	-	-	37.31(7.42)	-	26.70(6.89)	85.80(7.16)	76.00(6.90)	1
6246.318		3.603	-0.960	128.4(7.06)	128.9(7.30)	130.6(7.43)	77.80(7.06)	72.4(7.22)	-	-	83.60(7.32)	124.3(7.45)	119.7(7.12)	1
6252.554		2.404	-1.687	167.5(6.99)	174.5(7.24)	172.6(7.43)	-	87.6(7.16)	-	-	94.60(7.11)	156.6(7.32)	149.8(6.99)	1
6254.258		2.279	-2.48	-	-	-	-	71.2(7.50)	-	-	-	-	-	1
6256.361		2.453	-2.62	-	-	-	-	51.1(7.44)	-	-	-	-	-	1
6265.131		2.176	-2.550	-	-	-	61.30(6.85)	48.9(7.08)	74.59(7.45)	-	66.40(7.09)	126.3(7.37)	123.5(7.08)	1
6270.223		2.858	-2.71	-	-	-	25.60(6.94)	-	37.33(7.37)	-	35.80(7.26)	-	-	1
6280.617		0.859	-4.39	-	-	-	-	-	-	-	48.50(7.20)	-	-	1
6290.965		4.733	-0.874	-	-	-	-	-	60.95(7.63)	-	-	-	-	2
6297.8		2.222	-2.74	-	-	-	62.40(7.10)	-	64.27(7.43)	-	-	113.0(7.33)	106.6(6.99)	1
6301.5		3.654	-0.672	119.1(6.72)	128.3(7.30)	-	-	-	-	-	79.20(7.04)	125.6(7.30)	116.7(6.89)	2
6302.494		3.686	-1.131	-	-	-	-	-	69.65(7.36)	-	-	-	-	2

The abundance obtained from each line is given in parenthesis.

Table A1 : continues....

Wavelength(Å)	El	E_{low} (eV)	log gf	HD 24035	HD 32712	HD 36650	HD 94518	HD 147609	HD 154276	HD 179832	HD 207585	HD 211173	HD 219116	Ref
6315.809		4.076	-1.710	-	-	-	-	-	-	70.90(7.64)	-	-	-	2
6318.018		2.453	-2.33	137.1(7.12)	-	147.8(7.72)	-	-	-	-	-	-	-	2
6322.69		2.588	-2.426	121.9(7.10)	123.9(7.37)	125.5(7.55)	49.40(6.89)	-	62.74(7.43)	125.9(7.78)	51.00(7.04)	108.5(7.35)	102.3(7.04)	2
6335.328		2.198	-2.230	144.4(6.83)	152.1(7.19)	152.5(7.39)	-	-	83.95(7.36)	161.4(7.66)	76.80(7.03)	134.3(7.22)	130.5(6.90)	1
6336.823		3.686	-1.05	-	-	-	71.70(7.10)	-	786.68(7.62)	-	6.70(7.32)	-	-	1
6344.148		2.433	-2.923	-	-	-	-	-	47.41(7.40)	-	-	-	-	1
6380.74		4.19	-1.320	-	-	-	-	-	40.69(7.42)	-	-	-	-	4
6380.746		4.186	-1.400	-	-	-	-	-	-	-	-	-	-	1
6393.602		2.432	-1.620	-	-	178.0(7.44)	98.50(6.97)	-	-	-	103.3(7.24)	163.1(7.35)	161.9(7.13)	1
6408.016		3.686	-1.048	-	-	127.3(7.52)	64.70(6.94)	-	-	-	63.70(7.02)	105.1(7.21)	105.9(7.01)	2
6411.647		3.653	-0.820	140.7(7.18)	-	145.5(7.58)	88.50(7.17)	-	-	149.6(7.76)	88.70(7.31)	132.7(7.49)	126.1(7.13)	1
6416.933		4.796	-0.885	-	48.90(7.04)	-	23.50(6.96)	-	-	-	33.20(7.25)	94.50(7.38)	47.00(7.05)	2
6419.95		4.73	-0.090	-	-	97.60(7.34)	53.50(6.91)	-	68.17(7.10)	105.9(7.68)	57.80(7.08)	-	89.00(7.08)	4
6421.349		2.278	-2.027	176.2(7.12)	-	174.3(7.60)	86.30(6.96)	82.8(7.28)	-	-	87.10(7.13)	-	152.3(7.17)	1
6430.85		2.18	-2.010	168.6(6.98)	178.0(7.28)	173.1(7.44)	-	-	-	-	87.90(7.03)	157.4(7.35)	151.3(7.01)	4
6469.192		4.835	-0.77	-	-	-	-	-	42.59(7.43)	-	-	-	-	1
6475.626		2.559	-2.940	-	-	-	-	-	43.77(7.45)	-	-	-	-	1
6481.87		2.278	-2.984	-	-	-	39.60(6.93)	-	51.87(7.41)	-	37.20(6.98)	105.4(7.44)	95.60(7.09)	1
6494.98		2.404	-1.273	-	-	-	-	-	-	-	-	-	-	1
6495.741		4.835	-0.94	-	-	-	-	-	29.25(7.28)	-	-	-	-	1
6533.93		4.558	-1.460	-	-	-	-	-	-	-	-	-	-	1
6546.239		2.758	-1.650	-	-	-	-	-	-	160.6(7.69)	-	-	-	1
6569.209		4.733	-0.420	-	-	-	-	-	-	101.4(7.76)	-	-	-	1
6574.227		0.99	-5.04	89.39(7.05)	96.40(7.24)	97.20(7.51)	-	-	-	-	-	83.60(7.40)	-	1
6575.019		2.588	-2.820	92.90(6.94)	-	112.1(7.61)	34.50(6.97)	-	-	-	39.30(7.16)	87.90(7.25)	-	1
6592.91		2.72	-1.470	139.8(6.73)	152.6(7.18)	149.3(7.29)	79.20(6.82)	-	-	-	82.90(7.04)	135.1(7.19)	135.0(6.94)	4
6593.871		2.432	-2.422	121.1(6.84)	134.7(7.32)	142.3(7.62)	60.70(6.94)	-	-	140.9(7.80)	58.40(7.02)	121.2(7.37)	115.9(7.05)	1
6597.557		4.759	-1.070	53.00(7.19)	-	64.30(7.54)	-	-	-	66.30(7.72)	-	55.70(7.44)	-	1
6608.024		2.278	-4.030	47.60(7.03)	63.40(7.30)	61.40(7.46)	-	-	-	70.30(7.71)	-	47.90(7.29)	-	1
6609.11		2.559	-3.227	-	-	-	-	-	-	111.7(7.66)	-	-	-	1
6627.54		4.548	-1.680	-	-	52.20(7.63)	-	-	-	56.50(7.81)	-	41.00(7.46)	-	1
6646.931		2.609	-3.99	-	40.90(7.26)	54.60(7.69)	-	-	-	-	-	35.50(7.40)	-	1
6677.989		2.692	-1.470	-	177.3(7.33)	175.7(7.50)	95.10(6.98)	-	-	-	-	158.7(7.39)	-	1
6725.356		4.103	-2.17	-	38.30(7.25)	-	-	-	-	-	-	34.00(7.29)	-	1
6733.151		4.638	-1.580	-	-	-	-	-	-	51.80(7.71)	-	-	-	1
6739.521		1.557	-4.950	-	58.70(7.03)	-	-	-	-	-	-	-	-	1
6750.15		2.424	-2.621	-	-	-	52.70(6.96)	-	-	129.9(7.76)	-	114.8(7.40)	-	1
6752.707		4.64	-1.2	-	52.7(7.22)	66.50(7.53)	-	-	-	-	-	52.50(7.32)	-	1
6810.26		4.61	-1.200	-	-	-	-	-	-	75.70(7.75)	-	-	-	4
6843.648		4.548	-0.930	-	-	-	-	-	-	91.70(7.84)	-	-	-	1
6858.145		4.607	-1.060	-	-	-	-	-	-	74.50(7.66)	-	-	-	1
7071.854		4.607	-1.700	-	-	-	-	-	-	52.30(7.79)	-	-	-	1
7219.678		4.076	-1.690	-	-	-	-	-	-	79.50(7.74)	-	-	-	1
4233.172	Fe II	2.583	-2.000	-	106.9(7.07)	-	99.90(6.98)	123.6(7.09)	-	-	111.1(7.25)	121.5(7.23)	-	1
4369.411		2.778	-3.67	-	-	-	-	46.5(7.08)	-	-	-	-	-	1
4416.83		2.778	-2.6	-	-	-	-	-	75.43(7.48)	-	-	-	-	1
4489.183		2.828	-2.97	-	-	-	-	90.3(7.38)	-	-	-	-	-	1
4491.405		2.855	-2.700	-	73.80(7.21)	-	67.50(7.05)	93.0(7.20)	63.71(7.31)	-	71.20(7.17)	85.70(7.34)	94.20(7.07)	1
4508.288		2.855	-2.210	-	84.70(7.00)	-	78.30(6.85)	-	80.78(7.28)	-	77.40(6.84)	-	107.8(6.91)	1
4515.339		2.84	-2.480	-	83.70(7.22)	102.6(7.35)	68.30(6.83)	101.5(7.17)	-	-	-	95.90(7.37)	-	1
4520.224		2.81	-2.600	-	-	-	63.10(6.78)	105.8(7.39)	-	-	73.10(7.06)	-	-	1
4541.524		2.856	-3.05	-	-	-	-	87.8(7.42)	59.95(7.55)	-	-	-	-	1
4576.34		2.844	-3.04	-	-	-	-	82.0(7.25)	60.50(7.54)	-	-	-	-	1
4582.835		2.844	-3.1	-	-	-	-	-	52.11(7.34)	-	-	-	-	1
4620.521		2.828	-3.280	-	-	-	40.50(6.91)	66.1(7.11)	46.88(7.35)	75.10(7.84)	-	65.30(7.32)	-	1

The abundance obtained from each line is given in parenthesis.

Table A1 : continues....

Wavelength(Å)	El	E_{low} (eV)	log gf	HD 24035	HD 32712	HD 36650	HD 94518	HD 147609	HD 154276	HD 179832	HD 207585	HD 211173	HD 219116	Ref
4629.339		2.807	-2.280	-	-	129.4(7.67)	81.80(6.95)	-	-	-	88.70(7.16)	-	-	1
4731.453		2.891	-3.360	-	-	-	-	72.1(7.36)	-	-	-	-	-	1
4923.927		2.891	-1.320	143.8(6.81)	143.6(7.27)	-	119.8(6.85)	170.8(7.27)	-	-	135.20(7.09)	153.5(7.23)	-	1
4993.35		2.81	-3.670	-	-	-	-	-	-	71.70(7.79)	-	-	-	2
5120.352		2.828	-4.214	-	-	-	-	31.1(7.32)	-	-	-	-	-	2
5197.56		3.23	-2.250	-	82.90(7.27)	-	69.50(6.81)	97.6(6.94)	71.90(7.22)	-	81.00(7.11)	-	100.4(6.94)	4
5234.62		3.22	-2.240	-	84.70(7.26)	-	74.90(6.89)	-	78.75(7.33)	104.8(7.75)	82.20(7.08)	91.40(7.17)	102.8(6.93)	4
5256.938		2.891	-4.25	-	-	-	-	24.0(7.24)	-	-	-	-	-	2
5264.812		3.23	-3.19	-	-	-	-	53.9(7.08)	-	-	-	-	-	1
5284.1		2.89	-3.010	-	-	-	-	-	-	-	-	-	-	4
5325.56		3.22	-3.170	-	-	-	-	-	-	-	-	-	-	4
5414.05		3.22	-3.620	-	-	45.80(7.59)	-	33.9(7.28)	-	40.80(7.81)	-	29.50(7.29)	38.30(7.27)	4
5425.257		3.199	-3.360	-	-	-	-	57.0(7.28)	-	56.60(7.79)	-	-	-	4
5534.83		3.25	-2.770	60.80(7.03)	-	-	51.20(7.19)	70.0(7.15)	-	-	-	-	-	4
5991.37		3.15	-3.560	-	-	-	-	-	-	48.60(7.73)	-	-	-	4
6147.741		3.889	-2.721	-	-	-	-	57.2(7.23)	-	-	-	-	-	2
6149.25		3.89	-2.720	-	-	-	-	-	30.37(7.29)	42.90(7.48)	-	-	-	4
6238.392		3.889	-2.63	-	-	-	-	59.8(7.19)	36.14(7.36)	-	-	-	-	2
6247.55		3.89	-2.340	42.10(6.75)	48.00(7.43)	-	-	-	49.14(7.41)	54.50(7.51)	-	-	62.00(7.03)	4
6369.462		2.891	-4.253	22.61(7.08)	23.10(7.50)	29.60(7.30)	43.80(7.02)	-	-	-	-	27.70(7.36)	-	2
6416.919		3.891	-2.470	41.50(7.16)	-	-	23.70(6.91)	-	-	-	32.80(7.11)	47.00(7.46)	-	2
6432.68		2.891	-3.708	48.50(7.15)	-	62.40(7.51)	32.70(7.15)	-	34.40(7.43)	-	39.20(7.27)	52.90(7.44)	57.20(7.21)	2
6456.383		3.903	-2.075	63.90(7.01)	-	80.80(7.45)	51.40(6.95)	-	55.64(7.33)	71.80(7.72)	61.20(7.16)	65.10(7.26)	75.40(7.05)	1
6516.08		2.891	-3.45	-	-	-	-	-	56.71(7.75)	-	-	-	-	1

The abundance obtained from each line is given in parenthesis.

References: 1. Fuhr *et al.* (1988), 2. Kurucz (1988), 3. Bridges and Kornblith (1974), 4. Lambert *et al.* (1996)

Table A2 : Equivalent widths (in mÅ) of lines used for deriving elemental abundances

Wavelength(Å)	El	E_{low} (eV)	log gf	HD 24035	HD 32712	HD 36650	HD 94518	HD 147609	HD 154276	HD 179832	HD 207585	HD 211173	HD 219116	Ref
5682.633	Na I	2.102	-0.700	126.7(6.29)	133.5(6.31)	126.0(6.44)	63.50(5.86)	66.2(6.13)	83.46(6.23)	132.2(6.55)	79.00(6.17)	121.5(6.43)	104.5(6.13)	1
5688.205		2.1	-0.450	137.1(6.21)	151.3(6.31)	130.1(6.26)	85.20(5.94)	98.2(6.39)	-	145.1(6.50)	98.00(6.22)	136.2(6.41)	126.8(6.24)	1
6154.226		2.102	-1.560	49.40(5.91)	66.90(6.04)	67.70(6.30)	20.50(5.90)	-	27.36(6.13)	-	22.20(6.00)	60.10(6.21)	37.90(5.92)	1
6160.747		2.104	-1.260	88.30(6.20)	92.70(6.16)	87.50(6.31)	29.20(5.81)	-	47.85(6.22)	-	38.00(6.03)	74.80(6.15)	57.20(5.93)	1
4571.096	Mg I	0	-5.691	-	-	-	-	-	108.9(7.88)	-	-	-	-	2
4702.991		4.346	-0.666	-	179.6(7.10)	-	179.6(7.27)	156.2(7.56)	-	-	149.0(7.16)	-	177.3(7.48)	3
4730.029		4.346	-2.523	-	-	85.10(7.71)	45.50(7.46)	32.3(7.48)	60.20(7.80)	87.10(7.81)	-	76.80(7.60)	-	3
5528.405		4.346	-0.620	-	-	-	175.6(7.26)	153.3(7.53)	-	-	168.7(7.34)	-	170.8(7.44)	3
5711.088		4.346	-1.833	111.1(7.23)	118.5(7.39)	125.7(7.66)	88.80(7.48)	68.1(7.38)	101.4(7.76)	130.4(7.84)	78.10(7.39)	125.1(7.72)	114.6(7.48)	3
6696.023	Al I	3.143	-1.347	-	-	-	-	-	36.21(6.29)	-	-	53.50(6.12)	-	4
6698.673		3.143	-1.647	-	-	-	-	-	18.39(6.17)	-	-	36.40(6.22)	-	4
4782.991	Si I	4.95	-2.47	-	-	-	-	-	-	26.90(7.55)	-	-	-	1
5645.613		4.93	-2.14	-	-	-	-	20.5(7.37)	30.77(7.52)	-	-	-	-	5
5665.555		4.92	-2.04	-	-	-	-	26.7(7.41)	35.58(7.51)	-	-	-	-	5
5690.425		4.929	-1.870	56.60(7.23)	65.10(7.66)	57.70(7.39)	30.80(7.14)	29.2(7.30)	43.50(7.50)	-	33.10(7.23)	-	53.60(7.24)	5
5793.073		4.93	-2.06	-	-	-	-	-	39.57(7.62)	61.90(7.89)	-	-	-	5
5948.541		5.083	-1.23	86.85(7.29)	95.40(7.76)	-	59.10(7.17)	63.9(7.41)	74.91(7.54)	-	61.60(7.26)	-	-	5
6131.852		5.616	-1.140	-	47.60(7.39)	47.80(7.23)	-	-	-	-	-	29.80(6.89)	35.20(6.92)	1
6145.016		5.616	-0.820	-	-	-	25.30(6.61)	-	-	-	-	-	-	6
6155.134		5.619	-0.400	-	-	-	-	-	-	-	-	-	-	6
6237.319		5.613	-0.530	-	-	81.40(7.22)	44.90(6.70)	-	-	-	-	68.50(7.04)	-	6
6414.98		5.87	-1.1	-	-	-	-	-	51.30(7.75)	-	-	-	-	1
6555.463		5.98	-1	-	-	-	-	-	45.30(7.64)	-	-	-	-	1
4098.528	Ca I	2.526	-0.540	-	-	-	86.70(6.10)	-	-	-	95.90(6.37)	-	-	4
4283.011		1.886	-0.224	-	-	-	124.4(5.90)	-	-	-	147.3(6.29)	177.1(6.26)	-	4
4318.652		1.899	-0.208	-	-	156.70(6.10)	-	105.4(6.02)	116.3(5.91)	-	-	146.9(5.95)	149.8(5.95)	4
4425.437		1.879	-0.385	154.0(5.88)	-	152.3(6.17)	111.9(5.88)	113.0(6.33)	-	-	122.7(6.18)	152.7(6.16)	152.2(6.12)	4
4435.679		1.89	-0.52	-	-	-	120.0(6.13)	-	123.6(6.27)	-	-	-	-	4
4455.887		1.899	-0.510	-	178.7(6.13)	-	119.2(6.12)	-	137.6(6.43)	-	123.8(6.33)	173.9(6.51)	-	4
4456.616		1.899	-1.66	-	-	-	58.40(6.14)	51.6(6.32)	68.56(6.53)	-	72.90(6.57)	-	93.00(6.26)	4
4526.928		2.709	-0.43	-	-	-	-	51.6(5.78)	77.36(6.10)	-	-	-	-	4
4578.55		2.521	-0.56	-	-	114.0(6.29)	-	61.7(5.94)	71.03(5.99)	103.9(6.12)	-	-	-	4
4585.865		2.526	-0.16	-	-	-	-	98.6(6.28)	132.1(6.45)	-	-	-	-	4
5260.387		2.521	-1.900	57.60(6.15)	56.90(6.00)	61.00(6.38)	-	-	26.90(6.38)	-	-	48.60(6.18)	41.10(6.12)	4
5261.704		2.521	-0.730	-	-	-	78.30(6.13)	-	-	-	75.70(6.21)	121.3(6.54)	-	4
5349.465		2.709	-1.178	-	-	-	-	-	-	-	-	-	-	7
5512.98		2.932	-0.290	-	109.2(5.92)	110.6(6.22)	67.70(5.87)	52.0(5.82)	76.65(6.13)	108.8(6.24)	-	101.1(6.12)	94.60(5.92)	4
5581.965		2.523	-1.833	-	-	117.8(6.31)	-	68.9(6.20)	85.75(6.39)	124.9(6.50)	75.70(6.18)	115.7(6.37)	108.5(6.15)	4
5588.749		2.525	0.21	-	-	-	-	121.1(6.29)	133.6(6.10)	124.5(6.49)	-	-	-	4
5590.114		2.521	-0.710	109.6(5.91)	112.2(5.89)	113.9(6.22)	75.80(6.07)	64.7(6.11)	86.73(6.40)	-	68.80(6.03)	106.5(6.18)	104.0(6.06)	4
5594.462		2.523	-0.050	-	-	-	-	-	130.4(6.31)	-	114.6(6.03)	-	-	4
5857.451		2.932	0.23	129.6(5.78)	137.0(5.81)	133.5(6.07)	101.2(5.90)	104.1(6.28)	114.8(6.15)	-	-	140.2(6.17)	132.2(6.04)	4
6102.723		1.879	-0.890	141.5(5.81)	153.5(5.88)	146.2(6.12)	102.4(6.12)	89.0(6.19)	-	-	96.80(6.16)	-	137.7(6.08)	4
6122.217		1.886	-2.303	-	-	-	-	-	158.6(6.42)	-	-	-	-	4
6161.297		1.523	-1.02	-	-	-	-	33.7(5.84)	53.72(6.05)	-	-	-	-	4
6162.173		1.899	0.1	-	-	-	156.3(5.81)	142.1(6.20)	175.5(6.04)	-	-	-	-	4
6166.439		2.521	-0.900	103.1(5.91)	105.9(5.88)	100.5(6.06)	-	36.1(5.76)	62.24(6.10)	-	-	-	85.00(5.84)	4
6169.042		2.523	-0.55	126.8(5.99)	126.1(5.90)	127.9(6.24)	-	57.9(5.82)	82.07(6.14)	-	-	115.9(6.13)	102.4(5.82)	4
6169.563		2.523	-0.27	129.6(5.78)	137.7(5.81)	139.2(6.19)	87.30(5.83)	73.9(5.84)	144.6(5.90)	-	-	-	118.4(5.84)	4
6439.075		2.525	0.47	-	-	-	-	129.3(6.13)	-	-	-	-	-	4
6449.808		2.523	-0.550	-	-	140.1(6.40)	85.30(6.05)	-	-	131.7(6.31)	-	122.7(6.21)	-	4
6455.598		2.523	-1.350	-	-	-	38.50(5.95)	-	50.95(6.31)	163.0(6.06)	-	89.80(6.38)	75.70(6.11)	4
6471.662		2.525	-0.590	132.6(6.09)	124.5(5.87)	129.6(6.25)	74.90(5.90)	60.4(5.90)	84.48(6.21)	128.8(6.29)	-	-	113.1(6.02)	4
6493.781		2.521	0.14	163.0(5.81)	-	-	-	101.4(5.94)	115.5(5.92)	-	-	-	-	4
6499.65		2.523	-0.590	-	133.3(6.00)	127.7(6.22)	-	55.9(5.80)	79.67(6.11)	-	79.60(6.05)	108.1(5.98)	101.6(5.81)	4

The abundance obtained from each line is given in parenthesis.

Table A2 : continues....

Wavelength(Å)	El	E_{low} (eV)	log gf	HD 24035	HD 32712	HD 36650	HD 94518	HD 147609	HD 154276	HD 179832	HD 207585	HD 211173	HD 219116	Ref
6572.779		0	-4.290	-	-	113.4(6.46)	-	-	-	-	-	96.10(6.31)	76.80(6.13)	4
6717.692		2.709	-0.61	-	-	-	82.30(6.22)	-	101.9(6.64)	-	-	-	-	7
7148.15		2.709	0.208	-	-	-	-	-	-	-	-	-	-	7
4374.457	Sc II	0.618	-0.44	159.5(3.08)	139.0(3.14)	144.7(3.29)	102.8(2.97)	-	-	-	99.40(3.01)	131.7(3.16)	-	8
4400.389		0.606	-0.51	-	-	-	81.00(2.48)	-	-	-	-	-	-	4
4431.352		0.605	-1.880	-	-	-	32.50(2.70)	-	-	-	37.80(2.87)	76.70(3.20)	-	4
5031.021		1.357	-0.260	-	-	-	68.10(2.58)	-	-	-	-	112.3(3.23)	-	8
5239.813		1.455	-0.770	-	-	-	-	-	-	-	-	-	-	4
5526.79		1.768	0.13	131.7(3.07)	119.8(3.31)	120.7(3.23)	74.90(2.71)	-	-	-	85.60(3.03)	103.6(3.02)	-	4
6245.637		1.507	-0.980	83.70(2.83)	72.50(3.00)	75.30(2.99)	33.50(2.62)	-	-	75.30(3.38)	37.80(2.75)	68.90(2.97)	70.80(2.69)	4
6300.698		1.507	-1.84	-	-	23.00(2.80)	-	-	-	-	-	-	-	4
6309.92		1.497	-1.57	-	39.40(2.94)	50.00(3.08)	-	-	-	-	-	33.40(2.82)	37.40(2.68)	4
6604.6		1.357	-1.48	-	79.60(3.42)	33.60(2.95)	-	-	-	36.20(3.04)	65.30(3.19)	-	-	8
4417.273	Ti I	1.887	-0.02	-	-	-	-	-	38.97(4.97)	-	-	-	-	8
4449.143		1.887	0.5	-	-	-	-	-	51.60(4.76)	-	-	-	-	8
4453.312		1.43	-0.051	-	-	-	-	35.2(4.76)	59.89(5.10)	-	-	-	-	8
4453.71		1.873	-0.01	91.28(4.81)	98.50(4.94)	83.50(4.94)	31.90(4.62)	-	36.52(4.88)	100.3(5.48)	35.20(4.68)	-	-	8
4465.805		1.739	-0.163	-	-	-	-	-	36.98(4.91)	-	-	-	-	8
4471.237		1.734	-0.103	-	-	-	-	-	42.09(4.97)	-	-	-	-	1
4480.588		1.739	-0.847	-	-	-	-	-	32.45(5.49)	-	-	-	-	1
4512.734		0.836	-0.480	118.1(4.61)	123.3(4.67)	-	57.00(4.62)	39.3(4.74)	65.66(5.11)	-	50.30(4.59)	101.5(4.77)	-	8
4518.022		0.826	-0.325	-	-	-	-	41.2(4.61)	69.63(5.05)	-	-	-	-	8
4527.304		0.813	-0.47	-	-	-	-	-	76.86(5.37)	-	-	-	-	8
4533.239		0.848	0.476	-	-	158.0(4.88)	92.70(4.55)	-	-	-	-	145.3(4.74)	-	8
4534.776		0.836	0.28	-	-	-	-	72.8(4.63)	92.29(5.00)	-	-	-	-	8
4548.763		0.826	-0.354	-	-	-	-	36.7(4.55)	68.71(5.05)	-	-	-	-	8
4555.485		0.848	-0.488	-	-	-	-	-	-	-	-	-	-	8
4617.269		1.749	0.389	-	112.5(4.66)	-	51.10(4.51)	37.5(4.64)	61.36(4.98)	-	47.20(4.52)	95.40(4.78)	-	8
4656.468		0	-1.345	130.2(4.62)	132.3(4.58)	124.1(4.95)	54.20(4.56)	30.8(4.68)	67.18(5.16)	-	-	112.9(4.85)	-	8
4681.909		0.048	-1.071	-	-	-	-	-	75.03(5.16)	-	-	-	-	8
4742.789		2.236	0.21	-	-	-	-	-	28.69(4.79)	-	-	-	-	8
4758.118		2.249	0.425	-	-	-	-	-	20.0(4.64)	39.33(4.85)	-	-	-	8
4759.272		2.255	0.514	88.70(4.62)	96.40(4.74)	86.80(4.87)	-	24.3(4.67)	47.72(4.96)	-	-	74.20(4.66)	-	8
4778.255		2.24	-0.220	-	58.80(4.56)	-	-	-	-	-	-	36.50(4.54)	-	8
4805.415		2.345	0.15	-	-	-	-	-	29.84(4.98)	-	-	-	-	8
4820.41		1.503	-0.441	-	-	-	40.60(4.85)	-	41.85(5.05)	-	-	-	-	8
4840.874		0.899	-0.509	-	117.8(4.50)	122.0(5.08)	51.90(4.55)	-	57.94(4.94)	-	-	-	97.50(4.61)	8
4870.126		2.249	0.34	-	-	-	-	-	48.41(5.14)	-	-	-	-	4
4926.147		0.818	-2.17	49.54(4.77)	53.40(4.55)	45.30(4.94)	-	-	-	-	-	33.90(4.76)	23.30(4.73)	8
4937.73		0.813	-2.23	49.50(4.82)	54.60(4.62)	37.60(4.85)	-	-	-	44.60(4.86)	-	35.30(4.83)	-	1
4999.5		0.83	0.31	-	-	-	104.0(4.86)	-	-	-	-	-	-	8
5009.646		0.021	-2.259	-	-	86.60(4.81)	-	-	-	-	-	72.40(4.63)	71.90(4.76)	8
5024.842		0.818	-0.602	129.2(4.75)	139.6(4.87)	-	56.50(4.65)	-	-	-	49.70(4.63)	-	103.3(4.68)	8
5039.96		0.02	-1.13	149.6(4.65)	159.4(4.70)	146.6(5.06)	62.90(4.53)	-	-	-	47.40(4.30)	124.1(4.75)	-	8
5064.653		0.048	-0.991	-	-	139.5(4.75)	71.90(4.58)	-	-	142.8(4.93)	64.50(4.55)	133.9(4.80)	-	8
5087.06		1.429	-0.78	-	-	86.50(5.07)	-	-	-	82.00(4.98)	-	76.30(4.96)	-	8
5210.386		0.047	-0.884	167.2(4.69)	179.9(4.70)	163.3(5.08)	86.80(4.87)	52.3(4.62)	85.54(5.14)	-	74.00(4.71)	144.3(4.89)	141.0(4.79)	8
5282.38		1.052	-1.300	-	-	-	-	-	-	-	-	-	-	8
5426.237		0.021	-3.006	-	-	-	-	-	-	-	-	-	-	8
5460.499		0.05	-2.880	70.80(4.79)	84.60(4.72)	64.80(4.95)	-	-	-	-	57.80(4.92)	44.30(4.91)	9	
5471.197		1.443	-1.440	62.50(4.97)	57.90(4.65)	45.70(4.91)	-	-	-	-	35.60(4.75)	23.80(4.68)	8	
5512.524		1.46	-0.35	-	-	-	-	-	85.54(5.14)	-	-	-	-	4
5716.457		2.297	-0.77	-	35.60(4.65)	28.30(4.90)	-	-	-	-	21.50(4.76)	-	8	
5739.982		2.236	-0.67	-	45.90(4.66)	-	-	-	-	-	-	27.20(4.86)	8	
5766.33		3.294	0.254	30.02(4.93)	24.20(4.63)	22.20(4.88)	-	-	-	-	23.00(4.91)	-	1	

The abundance obtained from each line is given in parenthesis.

Table A2 : continues....

Wavelength(Å)	El	E_{low} (eV)	log gf	HD 24035	HD 32712	HD 36650	HD 94518	HD 147609	HD 154276	HD 179832	HD 207585	HD 211173	HD 219116	Ref
5866.451		1.067	-0.84	-	-	-	-	-	45.24(5.03)	-	-	-	-	8
5918.535		1.07	-1.460	69.90(4.60)	-	-	-	-	-	-	-	46.30(4.49)	38.50(4.53)	8
5922.11		1.046	-1.466	77.50(4.70)	81.60(4.54)	70.40(4.83)	-	-	-	-	-	64.20(4.80)	56.70(4.82)	8
5937.811		1.067	-1.89	58.26(4.84)	62.90(4.64)	45.20(4.85)	-	-	-	-	-	34.00(4.68)	21.90(4.62)	8
5941.751		1.05	-1.510	78.30(4.76)	76.20(4.48)	-	-	-	-	-	-	60.20(4.77)	44.60(4.67)	8
5965.828		1.879	-0.409	-	93.50(4.83)	71.20(4.80)	-	-	-	-	-	71.70(4.91)	54.90(4.69)	8
5978.543		1.873	-0.496	-	84.60(4.73)	75.30(4.95)	-	-	-	-	-	57.40(4.70)	55.10(4.77)	8
6064.629		1.046	-1.944	-	67.60(4.74)	53.00(5.00)	-	-	-	-	-	42.90(4.87)	26.80(4.76)	8
6091.174		2.268	-0.423	-	67.80(4.83)	53.90(4.97)	-	-	-	-	-	42.00(4.79)	32.10(4.73)	8
6126.216		1.067	-0.84	-	-	-	-	-	21.42(5.02)	-	-	-	-	8
6303.757		1.443	-1.566	49.63(4.83)	53.40(4.62)	39.70(4.86)	-	-	-	-	-	-	24.40(4.77)	8
6556.062		1.46	-1.074	79.80(4.81)	89.80(4.77)	-	-	-	-	-	-	55.00(4.69)	46.20(4.69)	8
6599.133		0.9	-2.085	70.36(4.95)	74.10(4.73)	59.50(5.01)	-	-	-	-	-	40.00(4.74)	32.80(4.82)	8
6743.124		0.899	-1.630	-	-	-	-	-	-	-	-	-	-	8
4161.535	Ti II	1.084	-2.360	-	-	-	77.20(4.98)	-	-	-	-	70.20(4.87)	-	-
4337.915		1.08	-1.13	-	-	-	-	-	-	-	-	-	-	8
4394.051		1.221	-1.59	-	-	-	-	-	88.07(5.26)	-	-	-	-	8
4395.85		1.243	-2.17	-	-	-	-	-	65.74(5.27)	-	-	-	-	8
4399.772		1.27	-1.27	-	-	-	-	-	-	-	-	-	-	8
4417.719		1.165	-1.430	-	-	-	108.9(5.03)	-	-	-	-	-	-	8
4418.33		1.237	-2.460	-	-	-	70.60(4.74)	-	-	-	-	72.80(4.87)	-	8
4421.938		2.061	-1.77	-	-	-	-	56.8(4.81)	-	-	-	-	-	8
4443.794		1.08	-0.700	-	-	180.0(4.88)	-	142.3(4.76)	133.8(4.97)	-	136.3(4.75)	177.2(4.88)	-	8
4464.45		1.161	-2.08	-	-	-	-	83.0(4.86)	-	-	-	-	-	8
4468.52		1.13	-0.6	-	-	-	137.9(4.60)	-	133.4(4.90)	-	136.0(4.70)	-	-	8
4470.857		1.164	-2.280	-	-	-	67.80(4.87)	65.0(4.66)	67.68(5.34)	-	-	-	-	8
4493.51		1.08	-2.73	-	-	-	-	33.6(4.44)	33.61(4.78)	-	-	-	-	8
4501.273		1.116	-0.75	-	-	-	-	-	-	-	-	-	-	8
4533.969		1.237	-0.77	-	-	-	-	-	131.6(5.14)	-	-	-	-	8
4563.761		1.22	-0.960	-	-	-	120.2(4.78)	-	130.2(5.28)	-	-	-	-	8
4568.314		1.22	-2.650	-	69.40(4.81)	-	-	-	32.25(4.80)	78.30(5.42)	-	67.60(4.83)	-	8
4571.96		1.571	-0.53	-	146.2(4.81)	154.4(4.92)	123.1(4.73)	-	140.8(5.29)	-	-	142.1(4.83)	-	8
4583.409		1.164	-2.720	-	-	-	-	-	33.15(4.83)	-	-	-	-	7
4589.959		1.237	-1.79	-	-	-	-	-	-	-	-	-	-	8
4636.32		1.164	-2.855	-	-	66.30(4.82)	-	-	-	-	-	55.80(4.68)	67.00(4.63)	8
4657.21		1.24	-2.32	-	-	-	53.20(4.60)	-	-	101.9(5.57)	-	-	-	8
4708.665		1.236	-2.210	-	82.80(4.70)	-	-	-	53.28(4.91)	-	56.50(4.62)	71.80(4.49)	-	8
4764.526		1.236	-2.770	-	54.80(4.59)	-	-	-	34.44(4.98)	-	-	48.90(4.51)	76.80(4.81)	8
4779.985		2.048	-1.37	97.06(4.70)	-	98.50(5.11)	67.00(4.78)	72.2(4.67)	67.49(5.22)	-	69.10(4.89)	86.60(4.96)	97.50(4.77)	8
4798.521		1.08	-2.43	-	-	-	-	-	43.59(4.71)	-	-	-	82.40(4.40)	8
4805.085		2.061	-1.100	-	-	-	87.60(5.02)	-	-	-	-	-	-	8
4865.612		1.116	-2.61	-	-	91.30(5.07)	-	-	-	-	-	76.20(4.84)	80.60(4.57)	8
5185.9		1.89	-1.35	-	93.90(4.85)	97.80(4.82)	-	-	-	99.50(5.36)	-	89.80(4.78)	-	8
5226.543		1.566	-1.300	-	-	131.1(5.14)	91.20(4.77)	-	-	-	88.10(4.77)	-	-	8
5336.771		1.58	-1.700	109.4(4.66)	-	-	74.60(4.77)	-	76.28(5.27)	-	76.80(4.89)	-	107.4(4.70)	8
5381.015		1.566	-2.08	-	-	-	60.00(4.79)	64.2(4.73)	59.91(5.21)	-	66.30(4.99)	-	-	8
5418.751		1.581	-1.999	-	-	-	-	50.8(4.42)	52.70(4.95)	-	-	-	-	8
4379.23	V I	0.301	0.58	179.6(4.06)	-	-	93.90(4.00)	-	-	-	92.40(4.15)	-	-	8
4406.63		0.3	-0.19	-	-	-	69.60(4.14)	-	-	-	68.10(4.26)	-	-	8
4831.646		0.017	-1.38	91.65(3.74)	100.1(3.71)	84.30(3.94)	-	-	-	-	-	69.70(3.73)	59.60(3.68)	8
4851.482		0	-1.139	-	-	-	-	-	-	-	39.00(4.13)	-	-	8
4864.731		0.017	-0.96	-	-	108.3(4.09)	-	-	-	-	37.00(3.92)	94.50(3.93)	87.10(3.79)	8
5703.575		1.05	-0.211	99.80(3.89)	111.0(3.98)	85.80(3.91)	-	-	-	-	-	76.80(3.84)	62.40(3.67)	8
5727.048		1.08	-0.012	-	-	-	-	-	-	116.1(4.47)	-	-	-	8
5727.652		1.051	-0.870	59.50(3.83)	69.20(3.75)	53.20(3.96)	-	-	-	66.20(4.12)	-	40.90(3.79)	-	8

The abundance obtained from each line is given in parenthesis.

Table A2 : continues....

Wavelength(Å)	El	E_{low} (eV)	log gf	HD 24035	HD 32712	HD 36650	HD 94518	HD 147609	HD 154276	HD 179832	HD 207585	HD 211173	HD 219116	Ref	
5737.059		1.063	-0.740	64.90(3.81)	74.80(3.75)	60.50(3.98)	-	-	-	-	-	46.10(3.78)	29.30(3.64)	8	
6039.722		1.064	-0.65	-	-	57.10(3.80)	-	-	-	-	-	44.30(3.63)	31.10(3.57)	8	
6081.441		1.051	-0.579	66.96(3.63)	-	-	-	-	-	-	-	44.40(3.54)	38.30(3.61)	8	
6119.523		1.063	-0.320	101.9(3.99)	93.60(3.65)	84.40(3.94)	-	-	-	-	-	71.50(3.81)	49.90(3.56)	8	
6216.354		0.275	-1.29	105.7(3.97)	114.6(3.91)	-	-	-	-	-	-	82.90(4.00)	62.40(3.80)	8	
6243.105		0.3	-0.980	102.4(3.63)	-	97.40(3.83)	-	-	-	-	-	84.80(3.75)	75.00(3.72)	8	
6251.827		0.286	-1.340	-	107.9(3.83)	89.00(4.02)	-	-	-	-	-	69.90(3.80)	50.00(3.67)	8	
6274.649		0.267	-1.67	86.43(4.00)	82.50(3.64)	62.30(3.88)	-	-	-	-	-	48.90(3.73)	31.40(3.65)	8	
6292.825		0.287	-1.47	-	-	73.50(3.88)	-	-	-	-	-	60.00(3.75)	46.00(3.73)	8	
6531.415		1.218	-0.840	43.60(3.70)	51.40(3.56)	41.00(3.87)	-	-	-	-	-	27.90(3.65)	-	8	
4274.8	Cr I	0	-0.23	-	-	-	-	149.5(5.38)	-	-	-	-	-	-	8
4289.72		0	-0.36	-	-	-	-	-	164.8(5.04)	-	-	-	-	-	8
4351.05		0.97	-1.45	-	-	-	-	-	75.77(5.74)	-	66.80(5.36)	-	-	-	8
4545.945		0.941	-1.370	-	-	-	-	-	-	-	-	-	-	-	8
4600.748		1.004	-1.260	-	-	-	63.90(4.93)	54.6(5.16)	74.17(5.50)	-	-	126.2(5.53)	-	8	
4616.12		0.982	-1.190	-	-	133.5(5.47)	70.90(5.02)	66.6(5.31)	81.85(5.59)	-	-	116.6(5.23)	-	8	
4626.173		0.968	-1.320	-	-	-	61.70(4.90)	47.7(5.05)	73.93(5.50)	-	67.40(5.20)	-	-	-	8
4652.157		1.004	-1.030	-	170.7(5.34)	161.9(5.79)	77.70(5.05)	74.3(5.34)	88.85(5.60)	167.1(5.80)	91.30(5.54)	144.1(5.59)	-	8	
4737.347		3.087	-0.099	-	-	91.20(5.79)	39.80(5.23)	-	41.48(5.41)	-	-	81.50(5.65)	-	8	
4829.372		2.544	-0.810	-	-	-	33.00(5.27)	-	-	-	37.10(5.45)	-	-	-	8
4870.801		3.079	0.05	-	102.6(5.57)	91.40(5.61)	50.10(5.29)	-	-	-	59.60(5.60)	-	89.30(5.55)	8	
5206.04		0.94	0.02	-	-	-	139.4(4.95)	135.8(5.53)	163.0(5.34)	-	-	-	-	-	8
5247.565		0.961	-1.640	128.3(5.11)	131.3(5.12)	124.4(5.42)	53.80(4.97)	39.1(5.16)	69.88(5.62)	-	59.70(5.23)	110.4(5.28)	-	-	8
5296.691		0.982	-1.400	-	161.3(5.40)	145.4(5.64)	67.10(5.06)	-	-	-	73.00(5.35)	133.8(5.56)	125.6(5.31)	8	
5298.277		0.983	-1.15	-	-	-	-	-	-	-	-	-	151.3(5.55)	-	8
5300.744		0.982	-2.120	101.8(5.05)	110.0(5.13)	102.5(5.40)	27.10(4.87)	-	-	-	-	94.30(5.38)	86.50(5.20)	8	
5312.871		3.45	-0.562	28.97(5.12)	-	-	-	-	-	-	-	27.60(5.24)	22.00(5.19)	8	
5345.801		1.003	-0.980	167.4(5.19)	-	175.5(5.70)	88.50(5.16)	82.0(5.39)	85.08(5.56)	-	101.3(5.60)	164.7(5.62)	160.9(5.55)	8	
5348.312		1.003	-1.290	146.0(5.13)	159.6(5.27)	-	73.80(5.13)	61.0(5.25)	88.17(5.73)	156.5(5.76)	74.00(5.28)	138.1(5.53)	126.5(5.23)	8	
5409.772		1.03	-0.720	174.1(5.04)	-	-	103.7(5.23)	-	-	-	104.7(5.42)	-	163.1(5.33)	8	
5787.965		3.323	-0.083	-	86.10(5.50)	78.00(5.59)	20.20(4.94)	-	-	-	28.20(5.22)	63.00(5.35)	53.00(5.17)	8	
4588.19	Cr II	4.072	-0.63	-	78.60(5.61)	89.60(5.60)	55.40(4.92)	92.5(5.42)	64.04(5.49)	71.90(5.62)	-	66.80(5.13)	-	8	
4592.04		4.073	-1.220	-	57.60(5.64)	-	35.80(5.02)	59.5(5.24)	41.61(5.46)	57.60(5.80)	-	49.40(5.25)	-	8	
4634.07		4.072	-1.240	-	-	-	48.00(5.34)	-	47.46(5.65)	-	48.90(5.37)	-	-	-	8
4812.337		3.864	-1.800	-	-	-	-	39.4(5.22)	29.06(5.49)	-	-	68.80(5.46)	-	8	
4848.25		3.864	-1.140	-	-	-	-	-	53.80(5.53)	-	-	30.70(5.11)	-	8	
5305.853		3.827	-2.357	-	-	26.20(5.45)	-	-	-	-	23.90(5.59)	-	-	7	
5308.404		4.072	-1.81	-	45.90(5.97)	41.70(5.57)	-	-	-	-	25.50(5.32)	-	37.80(5.26)	8	
5334.869		4.073	-1.562	-	43.30(5.65)	-	21.70(4.98)	-	-	-	31.80(5.23)	-	43.50(5.13)	7	
4034.483	Mn I	0	-0.811	-	-	-	159.8(4.76)	-	-	-	-	-	-	-	8
4041.355		2.114	0.285	-	-	-	-	-	-	-	-	-	-	-	8
4451.586		2.888	0.278	143.2(5.38)	147.1(5.40)	-	71.70(4.85)	-	-	141.1(5.73)	-	119.6(5.38)	-	8	
4453.012		2.941	-0.49	-	-	-	-	-	-	-	-	-	66.90(4.84)	-	8
4455.31		3.072	-0.246	-	-	-	-	-	-	-	-	-	79.30(5.02)	7	
4470.144		2.941	-0.444	-	-	75.70(4.97)	21.60(4.42)	-	-	-	3.80(4.96)	-	-	8	
4709.712		2.889	-0.34	107.0(5.20)	-	93.00(5.20)	36.60(4.63)	-	-	-	-	-	83.40(4.96)	8	
4739.087		2.941	-0.490	103.6(5.31)	111.0(5.57)	85.80(5.21)	24.80(4.54)	-	-	-	59.40(5.27)	88.90(5.43)	-	8	
4761.53		2.953	-0.138	-	114.2(5.29)	-	33.30(4.41)	-	-	118.1(5.81)	45.90(4.79)	103.9(5.45)	-	8	
4765.846		2.941	-0.080	-	-	-	44.30(4.59)	-	-	116.0(5.70)	53.20(4.90)	-	-	8	
4766.418		2.919	0.1	-	129.8(5.30)	-	61.90(4.79)	-	-	-	66.30(5.02)	127.0(5.64)	-	8	
4783.427		2.298	0.042	-	-	-	-	-	-	-	100.8(5.29)	162.2(5.51)	-	8	
5394.677		0	-3.503	-	-	-	27.00(4.63)	-	-	-	31.40(4.86)	-	-	8	
5399.499		3.853	-0.287	71.68(5.42)	67.80(5.36)	54.50(5.28)	-	-	-	-	53.60(5.32)	-	7		
5420.355		2.142	-1.462	-	-	-	26.00(4.72)	-	-	-	-	-	-	8	
5516.774		2.178	-1.847	-	-	-	-	-	-	-	87.40(5.67)	60.00(5.09)	8		

The abundance obtained from each line is given in parenthesis.

Table A2 : continues....

Wavelength(Å)	El	E_{low} (eV)	log gf	HD 24035	HD 32712	HD 36650	HD 94518	HD 147609	HD 154276	HD 179832	HD 207585	HD 211173	HD 219116	Ref
5537.76		2.187	-2.017	-	-	-	-	-	-	-	-	81.20(5.69)	-	7
6013.513		3.072	-0.251	129.5(5.51)	138.8(5.73)	-	27.80(4.45)	-	-	-	44.70(4.93)	116.7(5.72)	90.20(5.05)	8
6021.819		3.075	0.034	142.9(5.46)	136.7(5.41)	-	45.90(4.58)	-	-	-	58.10(4.95)	118.9(5.47)	100.2(4.97)	8
4121.311	Co I	0.922	-0.320	-	-	-	110.4(4.72)	-	-	-	104.6(4.82)	155.0(4.65)	-	10
4693.165		3.232	-0.545	-	65.40(5.20)	-	-	-	-	-	-	41.20(4.82)	36.00(4.73)	7
4749.66		3.053	-0.321	-	-	-	-	28.95(4.92)	-	-	-	-	-	7
4771.08		3.133	-0.504	69.61(4.96)	-	-	-	-	-	-	-	-	-	7
4781.43		1.882	-2.15	64.78(4.98)	64.80(5.09)	38.10(4.76)	-	-	-	54.10(5.20)	-	40.30(4.84)	-	10
4792.846		3.252	-0.067	73.00(4.73)	-	60.90(4.74)	-	-	25.95(4.77)	68.60(5.15)	22.20(4.59)	54.80(4.67)	49.80(4.52)	7
4813.467		3.216	0.05	76.60(4.65)	78.60(4.91)	79.30(5.02)	25.40(4.44)	-	-	81.90(5.36)	25.00(4.51)	70.50(4.91)	65.30(4.66)	7
4867.872		3.117	0.226	-	-	-	40.60(4.53)	-	-	-	53.30(4.94)	-	-	7
5331.452		1.785	-1.960	80.70(4.92)	90.50(5.31)	-	-	-	-	-	-	64.00(4.99)	55.20(4.80)	10
5342.695		4.021	0.609	-	-	54.40(4.68)	20.60(4.44)	-	-	-	20.20(4.49)	49.10(4.62)	-	7
5352.045		3.577	0.06	-	-	52.50(4.76)	-	-	-	-	-	43.80(4.62)	-	10
5483.344		1.71	-1.490	-	-	-	25.50(4.45)	-	-	-	27.90(4.62)	-	-	10
5530.774		1.711	-2.06	88.40(5.05)	90.50(5.27)	69.60(4.99)	-	-	-	-	-	58.10(4.84)	51.70(4.74)	10
5590.72		2.042	-1.87	-	-	-	-	-	-	70.40(5.42)	-	49.60(4.87)	-	10
6116.996		1.785	-2.49	38.66(4.63)	-	36.00(4.83)	-	-	-	-	-	27.50(4.68)	-	10
6454.99		3.632	-0.233	51.34(4.82)	47.70(4.87)	46.80(4.94)	-	-	-	48.60(5.13)	-	-	-	10
6632.433		2.28	-2.000	-	53.40(5.04)	42.00(5.00)	-	-	-	46.10(5.19)	-	30.30(4.81)	25.30(4.77)	10
4470.472	Ni I	3.399	-0.310	-	-	-	59.00(5.98)	51.8(5.72)	69.99(6.11)	106.2(6.49)	-	-	-	7
4686.207		3.597	-0.64	-	-	90.00(6.34)	41.70(5.72)	-	-	-	40.40(5.77)	82.20(6.25)	75.00(5.86)	7
4703.803		3.658	-0.735	88.44(6.14)	-	-	33.20(5.68)	-	-	-	46.10(6.05)	75.20(6.22)	77.60(6.07)	7
4714.408		3.38	0.23	-	-	-	92.30(5.75)	88.8(5.95)	106.0(6.12)	-	-	130.0(6.13)	-	10
4731.793		3.833	-0.85	-	-	-	20.20(5.63)	-	-	-	-	55.80(6.03)	61.00(6.03)	10
4732.46		4.106	-0.55	-	-	-	25.40(5.73)	27.4(6.05)	34.30(6.08)	-	-	-	-	10
4752.415		3.658	-0.7	80.22(5.91)	-	80.90(6.22)	35.80(5.70)	-	-	-	33.40(5.72)	73.20(6.12)	76.40(6.00)	10
4756.51		3.48	-0.340	-	88.90(5.81)	-	59.90(5.72)	-	-	-	58.70(5.80)	93.90(6.10)	90.80(5.77)	7
4814.59		3.597	-1.68	41.19(6.01)	28.90(5.85)	-	-	-	-	44.00(6.36)	-	38.10(6.18)	-	7
4821.13		4.153	-0.85	45.46(5.91)	52.20(6.21)	56.10(6.33)	-	-	30.46(6.33)	-	-	51.50(6.28)	-	10
4852.56		3.542	-1.07	-	-	-	24.00(5.67)	-	-	76.50(6.61)	26.90(5.81)	66.30(6.18)	-	10
4855.406		3.542	0	-	-	-	63.80(5.52)	-	-	-	62.50(5.60)	-	-	1
4857.39		3.74	-1.199	-	-	-	-	-	-	-	-	-	-	7
4937.341		3.606	-0.390	112.2(6.23)	98.80(6.20)	103.1(6.37)	52.90(5.72)	47.6(5.88)	66.03(6.24)	100.3(6.59)	62.80(6.06)	94.80(6.28)	-	1
4953.2		3.74	-0.67	90.49(6.17)	-	87.30(6.41)	34.90(5.72)	24.0(5.68)	43.64(6.01)	-	39.30(5.89)	79.00(6.31)	-	7
4980.166		3.606	-0.110	-	-	-	77.30(5.99)	72.1(5.92)	87.71(6.19)	-	-	130.3(6.67)	-	10
5035.357		3.635	0.29	-	-	-	72.90(5.51)	75.2(5.80)	84.47(5.95)	121.3(6.31)	74.30(5.66)	-	-	10
5081.107		3.847	0.3	-	-	-	72.20(5.67)	70.0(5.85)	78.81(6.00)	107.2(6.27)	68.60(5.71)	105.1(6.05)	-	10
5082.35		3.657	-0.54	-	-	-	41.60(5.66)	42.9(5.97)	52.81(6.11)	-	-	87.80(6.30)	-	10
5084.089		3.678	0.03	-	97.00(5.81)	-	64.70(5.63)	58.4(5.73)	76.57(6.09)	106.5(6.35)	71.70(5.90)	96.10(5.95)	-	1
5099.927		3.678	-0.100	-	109.4(6.18)	-	60.90(5.67)	57.7(5.84)	70.97(6.10)	102.7(6.40)	-	99.10(6.14)	97.40(5.85)	1
5102.96		1.676	-2.62	-	-	-	27.50(5.45)	-	38.60(5.93)	-	-	87.80(6.05)	-	10
5115.389		3.834	-0.11	-	-	-	51.80(5.62)	-	-	-	51.20(5.70)	-	-	10
5146.48		3.706	0.12	-	-	-	57.10(5.39)	-	-	-	67.40(5.73)	-	-	11
5259.47		3.74	-1.502	-	-	45.00(6.24)	-	-	-	-	-	28.30(5.91)	-	7
6007.306		1.676	-3.330	-	-	-	-	-	-	-	-	-	-	10
6086.28		4.266	-0.53	71.05(6.17)	-	60.70(6.16)	23.80(5.78)	21.6(6.00)	31.76(6.11)	64.60(6.50)	31.10(6.03)	55.70(6.13)	-	10
6111.066		4.088	-0.870	55.10(5.90)	56.00(6.12)	-	-	-	25.77(6.13)	57.80(6.45)	-	-	-	1
6128.963		1.676	-3.330	-	-	-	-	-	-	-	-	45.90(5.95)	-	10
6175.36		4.089	-0.530	72.30(5.97)	66.30(6.09)	75.60(6.27)	24.10(5.62)	-	-	-	29.10(5.81)	62.90(6.08)	52.00(5.74)	10
6176.807		4.088	-0.260	83.90(6.20)	-	84.30(6.46)	35.10(5.88)	37.9(5.94)	52.23(6.16)	-	-	76.00(6.38)	70.50(6.09)	7
6177.236		1.826	-3.5	54.30(5.85)	54.70(5.96)	-	-	-	-	-	-	38.30(5.87)	32.60(5.79)	10
6186.71		4.106	-0.777	-	45.70(5.91)	-	-	-	22.33(6.14)	-	-	42.70(5.90)	-	10
6204.6		4.088	-1.130	-	48.50(6.29)	51.30(6.35)	-	-	-	-	-	35.20(6.06)	31.30(5.94)	10
6327.593		1.676	-3.150	106.2(6.23)	-	100.0(6.46)	-	-	-	-	24.80(5.94)	79.10(6.17)	-	10

The abundance obtained from each line is given in parenthesis.

Table A2 : continues....

Wavelength(Å)	El	E_{low} (eV)	log gf	HD 24035	HD 32712	HD 36650	HD 94518	HD 147609	HD 154276	HD 179832	HD 207585	HD 211173	HD 219116	Ref
6314.622		1.935	-1.770	-	-	-	-	-	-	-	-	-	-	10
6378.247		4.154	-0.89	-	-	-	-	-	-	-	-	43.50(6.07)	37.80(5.90)	7
6643.629		1.676	-2.300	153.8(6.20)	-	-	64.60(5.87)	48.1(5.98)	83.94(6.60)	-	-	-	-	1
6767.768		1.826	-2.170	-	-	-	-	-	-	-	-	-	-	10
6772.313		3.657	-0.980	-	-	-	-	-	-	-	-	-	-	10
5105.537	Cu I	1.389	-1.516	-	-	-	62.70(3.80)	-	-	-	83.10(4.49)	143.7(4.77)	116.3(3.99)	12
5782.127		1.642	-1.72	-	-	-	34.80(3.54)	-	-	-	59.00(4.23)	141.5(5.07)	109.4(4.19)	12
4722.15	Zn I	4.029	-0.370	-	-	-	60.80(4.22)	65.7(4.35)	65.35(4.65)	92.80(5.18)	-	81.20(4.42)	-	13
4810.53		4.08	-0.170	79.0(3.92)	79.80(4.42)	-	63.00(4.08)	68.5(4.25)	72.22(4.64)	79.90(4.70)	-	21.40(4.45)	84.20(4.04)	13
4607.327	Sr I	0	-0.570	-	109.6(3.64)	97.10(3.78)	50.60(3.59)	-	-	72.30(3.17)	-	92.00(3.83)	74.60(3.22)	14
5630.134	Y I	1.336	0.211	-	21.70(2.36)	-	-	-	-	-	-	-	-	15
6435.004		0.066	-0.82	102.5(3.48)	73.00(2.66)	47.50(2.77)	-	-	-	-	-	31.40(2.52)	27.50(2.66)	15
4854.863	Y II	0.992	-0.380	-	-	112.5(2.94)	54.90(2.04)	-	-	83.80(2.71)	92.90(3.18)	97.30(2.75)	-	15
4883.684		1.084	0.07	-	-	128.0(2.90)	73.30(2.19)	119.5(3.12)	50.74(2.10)	-	115.8(3.22)	108.4(2.65)	-	15
5087.416		1.084	-0.170	-	114.1(2.80)	118.3(2.89)	60.00(2.04)	104.8(2.97)	41.43(2.01)	84.80(2.58)	103.7(3.23)	99.70(2.64)	-	15
5119.112		0.992	-1.360	-	86.20(3.19)	82.60(3.06)	-	56.5(2.92)	-	40.80(2.39)	-	61.80(2.67)	73.50(7.56)	15
5200.406		0.992	-1.360	-	113.7(3.06)	106.1(2.87)	53.50(2.16)	-	-	-	90.40(3.25)	93.30(2.74)	101.3(2.41)	15
5205.724		1.033	-0.34	-	-	103.7(2.62)	63.60(2.24)	113.6(3.28)	43.10(2.17)	-	90.40(3.06)	-	-	15
5289.815		1.033	-1.85	-	57.10(2.96)	55.20(2.90)	-	27.9(2.85)	-	24.90(2.49)	37.60(3.12)	38.60(2.62)	-	15
5402.774		1.839	-0.510	-	67.20(2.87)	70.00(2.85)	22.90(2.15)	-	-	-	60.60(3.21)	55.80(2.62)	-	16
5544.611		1.738	-1.090	-	59.30(3.12)	49.10(2.81)	-	37.8(2.93)	-	26.10(2.58)	48.60(3.34)	44.40(2.79)	47.00(2.56)	15
5546.009		1.748	-1.11	-	-	-	-	41.5(3.02)	-	-	-	-	-	15
5662.925		1.944	0.16	-	-	102.2(3.07)	52.40(2.33)	84.6(2.87)	40.63(2.45)	-	-	-	-	16
6613.733		1.748	-1.1	-	-	-	-	45.7(3.06)	-	-	45.40(3.21)	-	-	15
4739.48	Zr I	0.651	0.23	104.9(3.60)	-	69.80(3.10)	-	-	-	-	44.20(3.78)	62.50(3.05)	-	17
4772.323		0.623	0.044	83.20(3.22)	77.60(2.94)	64.20(3.12)	-	-	-	-	27.60(3.49)	51.90(3.92)	38.30(2.78)	17
4805.889		0.687	-0.420	64.90(3.35)	51.40(2.82)	34.90(3.03)	-	-	-	-	-	22.70(2.77)	-	17
6134.585		0	-1.280	82.90(3.46)	73.20(2.98)	42.70(3.04)	-	-	-	-	-	33.10(2.92)	20.00(2.87)	17
4208.99	Zr II	0.71	-0.46	-	-	-	56.50(2.47)	-	-	-	-	-	-	17
4210.631		1.665	-0.800	-	-	-	-	-	-	-	-	-	-	18
4317.321		0.713	-1.38	123.5(4.00)	-	-	31.00(2.66)	-	-	-	68.30(3.86)	-	-	17
4414.539		1.24	-1.171	-	-	-	-	-	-	78.80(4.25)	-	-	-	16
5112.297		1.665	-0.59	114.8(3.91)	-	-	-	-	-	-	59.80(3.61)	51.50(2.89)	-	17
4130.65	Ba II	2.72	0.56	-	-	104.8(3.39)	66.30(2.72)	-	-	-	107.3(3.59)	-	-	4
5853.668		0.604	-1.020	-	-	154.7(3.10)	88.10(2.51)	-	-	116.9(2.97)	137.8(3.40)	-	169.2(2.97)	4
6141.713		0.703	-0.076	-	-	-	152.2(2.52)	-	-	176.1(2.82)	-	-	-	4
6496.897		0.604	-0.377	-	-	-	138.2(2.56)	-	-	162.8(2.85)	-	-	-	4
4123.23	La II	0.32	0.12	-	-	93.70(1.85)	70.10(1.85)	-	-	-	92.00(2.56)	-	-	19
4238.38		0.4	-0.058	158.4(2.73)	-	-	69.00(2.04)	-	-	-	-	-	-	19
4322.51		0.17	-1.05	113.6(2.67)	-	-	-	-	-	-	-	-	-	14
4662.498		0	-1.240	-	82.90(2.21)	68.10(1.83)	-	-	-	54.60(2.40)	-	80.60(1.88)	20	
4748.726		0.926	-0.860	-	56.60(2.21)	39.60(1.78)	-	-	-	23.40(1.65)	43.80(2.59)	34.60(1.74)	55.80(1.95)	20
4921.776		0.244	-0.680	148.5(2.85)	-	-	54.60(1.92)	-	-	-	-	-	110.7(2.30)	14
5303.528		0.321	-1.43	-	73.30(2.37)	48.00(1.80)	-	-	-	41.90(2.43)	-	57.90(1.82)	20	
5936.21		0.173	-2.06	93.25(2.74)	64.50(2.48)	-	-	-	-	-	-	-	34.20(1.78)	20
6320.376		0.172	-1.940	-	-	-	-	-	-	-	-	43.10((2.04))	-	20
6390.477		0.321	-1.450	110.7(2.61)	85.70(2.51)	51.40(1.80)	-	-	-	41.10(2.34)	-	66.60(1.93)	21	
4073.47	Ce II	0.48	0.32	-	-	-	-	-	-	-	68.40(2.74)	-	-	21
4117.29		0.74	-0.45	-	-	-	-	-	-	38.50(2.72)	-	-	-	21
4257.12		0.46	-1.116	76.78(2.85)	62.20(2.88)	52.60(2.66)	-	-	-	31.60(2.88)	35.60(2.30)	-	21	
4336.244		0.704	-0.564	-	-	62.30(2.65)	-	-	-	-	40.80(2.16)	-	-	21
4349.789		0.701	-0.107	-	95.40(3.17)	-	22.60(1.76)	-	-	-	62.00(3.09)	53.90(2.08)	-	16
4364.653		0.495	-0.201	-	-	-	31.60(1.91)	-	-	-	62.70(3.00)	57.70(2.05)	-	21
4407.273		0.701	-0.741	80.30(2.82)	68.80(2.97)	-	-	-	-	-	-	-	77.70(2.95)	21
4418.78		0.863	0.177	111.4(2.93)	-	80.30(2.64)	33.10(1.94)	60.1(2.59)	-	-	-	58.10(2.11)	102.2(2.87)	21

The abundance obtained from each line is given in parenthesis.

Table A2 : continues....

Wavelength(Å)	El	E_{low} (eV)	log gf	HD 24035	HD 32712	HD 36650	HD 94518	HD 147609	HD 154276	HD 179832	HD 207585	HD 211173	HD 219116	Ref
4427.916		0.535	-0.460	-	84.10(2.95)	68.30(2.51)	22.20(1.94)	36.1(2.38)	-	-	46.50(2.73)	50.30(2.12)	77.20(2.44)	21
4483.893		0.864	0.01	-	-	-	28.60(1.97)	-	-	-	62.00(3.11)	-	84.00(2.53)	21
4486.900		0.295	-0.474	99.17(2.55)	9.10(3.08)	80.20(2.59)	35.70(2.08)	-	-	-	65.10(3.12)	64.00(2.28)	94.50(2.64)	21
4508.079		0.621	-1.238	62.40(2.74)	-	-	-	-	-	-	24.00(2.90)	-	62.60(2.94)	21
4560.28		0.91	0	-	-	-	24.00(1.89)	53.5(2.62)	-	-	-	-	-	21
4562.359		0.477	0.081	-	106.5(2.90)	90.80(2.55)	46.20(2.00)	69.2(2.53)	19.21(1.63)	75.40(2.64)	-	74.00(2.24)	-	21
4628.161		0.516	0.008	-	-	95.20(2.77)	43.00(2.01)	69.7(2.64)	17.67(1.68)	-	-	-	119.2(2.82)	21
4725.069		0.521	-1.204	67.90(2.68)	60.40(2.88)	-	-	-	-	-	32.40(3.00)	-	46.00(2.41)	21
4747.167		0.32	-1.246	-	-	51.60(2.52)	-	20.2(2.56)	-	-	29.80(2.76)	-	-	21
4773.941		0.924	-0.498	-	-	47.00(2.35)	-	22.9(2.43)	-	-	34.20(2.74)	28.60(1.98)	-	21
4873.999		1.107	-0.892	60.50(2.89)	57.30(3.21)	-	-	-	-	-	-	-	-	21
5187.458		1.211	-0.104	87.10(2.81)	78.10(3.07)	56.10(2.48)	-	-	-	-	48.50(3.02)	40.20(2.19)	64.10(2.43)	21
5274.229		1.044	-0.323	-	-	-	-	-	-	39.50(2.44)	-	-	-	8
5330.556		0.869	-0.760	72.90(2.70)	67.80(2.98)	40.60(2.36)	-	27.8(2.73)	-	-	39.50(3.05)	29.40(2.17)	-	21
5556.941		1.813	-0.405	-	-	-	-	-	-	-	-	-	-	21
5613.694		1.42	-0.999	-	-	-	-	-	-	-	-	-	-	21
6034.205		1.458	-1.019	-	30.60(3.04)	-	-	-	-	-	-	-	32.00(2.91)	21
5188.217	Pr II	0.922	-1.145	39.10(2.32)	30.10(2.39)	-	-	-	-	-	-	-	-	21
5219.045		0.795	-0.24	74.12(1.98)	58.70(2.00)	30.60(1.41)	-	-	-	-	20.50(1.82)	20.40(1.19)	-	22
5259.728		0.633	-0.682	80.30(2.36)	55.80(2.16)	30.30(1.65)	-	-	-	27.60(1.09)	-	-	-	22
5292.619		0.648	-0.300	89.00(2.19)	75.70(2.31)	-	-	19.6(1.79)	-	-	31.40(2.04)	-	57.50(1.70)	22
5322.772		0.482	-0.315	103.3(2.33)	-	51.90(1.58)	-	-	-	-	33.00(1.93)	26.20(1.06)	60.10(1.57)	21
6165.891		0.923	-0.205	71.60(1.95)	53.60(1.92)	-	-	-	-	-	-	-	31.80(1.35)	21
6278.676		1.196	-0.63	-	26.80(2.08)	-	-	-	-	-	-	-	-	22
4061.08	Nd II	0.471	0.55	120.6(2.24)	-	109.4(2.58)	61.30(1.93)	-	-	-	81.80(2.71)	90.00(2.27)	114.3(2.31)	23
4069.27		0.06	-0.4	-	-	87.60(2.46)	-	-	-	-	63.10(2.70)	-	-	21
4446.384		0.204	-0.590	87.50(2.06)	102.2(3.00)	79.60(2.42)	30.20(1.80)	44.9(2.24)	-	-	57.20(2.75)	64.70(2.14)	-	23
4451.563		0.38	-0.040	-	-	-	-	-	-	-	-	-	-	23
4475.555		0.063	-1.980	-	-	-	-	-	-	-	-	-	-	23
4516.346		0.32	-0.950	-	-	-	-	-	-	-	-	-	-	21
4556.133		0.064	-1.610	-	-	-	-	-	-	-	-	-	-	21
4645.76		0.559	-0.750	84.10(2.48)	-	-	-	-	-	-	37.70(2.56)	-	55.80(2.00)	21
4703.572		0.38	-1.07	-	-	55.30(2.30)	-	-	-	-	35.00(2.62)	30.70(1.78)	-	21
4706.543		0	-0.880	-	97.10(2.75)	75.20(2.20)	30.60(1.83)	-	-	-	60.00(2.83)	66.10(2.12)	-	21
4797.153		0.559	-0.950	69.40(2.28)	-	-	-	-	-	-	35.20(2.67)	36.20(1.99)	55.50(2.18)	21
4811.342		0.064	-1.140	-	101.0(3.16)	77.00(2.56)	23.80(1.96)	36.5(2.44)	-	-	-	-	-	21
4825.478		0.182	-0.86	-	-	-	38.10(2.18)	-	-	-	-	-	-	21
4859.039		0.32	-0.83	-	-	-	34.30(2.19)	-	-	-	-	-	-	21
4947.02		0.559	-1.250	59.90(2.35)	-	35.10(2.18)	-	-	-	-	-	-	-	21
4961.387		0.631	-0.710	-	93.20(3.19)	-	-	-	-	24.40(1.73)	41.50(2.67)	35.40(1.80)	-	21
4989.95		0.63	-0.500	-	-	-	-	32.7(2.22)	-	-	-	-	-	21
5089.832		0.204	-1.16	71.42(2.05)	-	-	-	-	-	24.20(1.66)	-	-	-	21
5130.59		1.3	0.1	-	-	71.20(2.57)	28.10(2.07)	41.6(1.95)	-	-	-	-	-	23
5212.361		0.204	-0.870	-	-	-	-	23.3(1.97)	-	-	-	-	-	21
5255.506		0.204	-0.820	-	-	-	-	-	-	-	47.70(2.50)	-	-	21
5276.869		0.859	-0.440	73.60(2.16)	-	-	-	-	-	-	-	-	-	23
5287.133		0.744	-1.300	60.40(2.60)	49.50(2.69)	27.20(2.24)	-	-	-	-	-	24.20(2.22)	-	21
5293.163		0.822	-0.060	98.50(2.31)	-	80.90(2.39)	24.30(1.63)	53.8(2.38)	-	-	60.90(2.77)	29.10(1.88)	88.50(2.28)	23
5311.453		0.986	-0.420	-	79.60(3.03)	53.20(2.38)	-	-	-	-	33.80(2.63)	65.10(1.96)	-	23
5319.815		0.55	-0.210	103.0(2.22)	108.7(2.87)	83.40(2.27)	30.90(1.68)	52.3(2.23)	-	-	65.50(2.77)	23.50(1.74)	-	23
5356.967		1.264	-0.250	76.00(2.51)	-	42.10(2.13)	-	-	-	-	30.90(2.51)	-	42.40(1.97)	23
5361.51		0.68	-0.4	-	-	-	-	-	-	-	54.40(2.75)	-	-	23
5371.927		1.412	0.003	-	-	-	-	24.9(2.24)	-	-	43.60(2.76)	-	-	23
5442.264		0.68	-0.910	-	84.40(3.09)	-	-	-	-	-	31.30(2.59)	-	48.50(2.08)	23
5485.696		1.264	-0.120	-	79.20(2.91)	51.80(2.22)	-	-	-	-	43.90(2.74)	32.30(1.84)	55.60(2.09)	23

The abundance obtained from each line is given in parenthesis.

Table A2 : continues....

Wavelength(Å)	El	E_{low} (eV)	log gf	HD 24035	HD 32712	HD 36650	HD 94518	HD 147609	HD 154276	HD 179832	HD 207585	HD 211173	HD 219116	Ref
5548.448		0.55	-1.34	61.27(2.39)	-	-	-	-	-	-	43.80(2.57)	-	39.20(2.17)	21
5688.518		0.986	-0.25	81.09(2.24)	81.40(2.70)	-	-	-	-	-	-	49.50(2.06)	65.70(2.09)	23
5702.238		0.744	-0.770	-	-	-	-	-	-	-	-	-	-	23
5718.118		1.41	-0.340	57.30(2.34)	-	-	-	-	-	-	-	-	-	23
5744.777		0.986	-1.03	-	-	-	-	-	-	-	-	-	23.80(2.01)	21
5770.489		1.08	-1.030	-	-	-	-	-	-	-	-	-	-	23
5825.857		1.08	-0.760	68.00(2.58)	61.80(2.82)	30.00(2.13)	-	-	-	-	20.50(2.51)	20.60(1.93)	-	21
4318.927	Sm II	0.28	-0.270	-	-	-	-	-	-	-	-	-	-	21
4424.337		0.485	-0.26	-	-	-	41.70(1.75)	43.0(1.79)	-	-	67.00(2.71)	-	-	21
4434.318		0.378	-0.576	-	-	-	36.30(1.79)	42.2(1.99)	-	-	65.00(2.85)	-	-	21
4458.509		0.104	-1.11	95.36(2.39)	-	-	25.50(1.75)	-	-	-	50.20(2.59)	-	79.50(2.19)	21
4499.475		0.248	-1.413	78.90(2.40)	62.10(2.38)	41.40(1.91)	-	-	-	31.10(1.94)	27.30(2.32)	29.80(1.70)	47.40(1.88)	21
4519.63		0.543	-0.751	-	-	56.70(1.97)	-	22.7(1.86)	-	37.90(1.82)	52.80(2.75)	38.60(1.60)	78.90(2.30)	21
4566.21		0.33	-1.245	-	71.20(2.58)	48.00(1.98)	-	-	-	38.10(2.07)	-	35.10(1.75)	-	21
4577.69		0.25	-0.77	-	-	-	-	-	-	41.90(2.07)	-	-	-	21
4642.228		0.379	-0.951	-	80.70(2.62)	62.00(2.10)	-	-	-	-	51.30(2.71)	-	71.50(2.09)	21
4674.593		0.184	-1.055	107.1(2.67)	-	-	-	-	-	-	-	-	-	21
4676.902		0.04	-1.407	-	75.20(2.45)	49.00(1.82)	-	-	-	-	-	36.50(1.60)	61.60(1.92)	21
4704.4		0	-1.562	89.61(2.46)	-	-	20.10(1.91)	25.3(2.22)	-	-	40.40(2.58)	-	74.10(2.31)	21
4791.58		0.104	-1.846	-	53.10(2.32)	26.00(1.78)	-	-	-	23.10(1.95)	-	-	-	21
4844.209		0.277	-1.558	-	-	-	-	-	-	-	27.60(2.47)	-	-	21
4854.368		0.379	-1.873	-	31.40(2.16)	-	-	-	-	-	-	-	24.10(1.95)	21
4205.042	Eu II	0	0.117	-	-	-	-	-	-	-	-	-	-	24
6437.64		1.319	-0.276	28.70(0.77)	20.60(0.86)	-	-	-	-	-	-	-	-	24
6645.064		1.38	0.204	41.04(0.62)	33.70(0.79)	-	-	-	-	25.10(0.85)	-	-	23.30(0.34)	24

The abundance obtained from each line is given in parenthesis.

References: 1. Kurucz and Peytremann (1975), 2. Laughlin and Victor (1974), 3. Lincke and Ziegenbein (1971), 4. NBS in Kurucz database, 5. Garz (1973), 6. Schulz-Gulde (1969), 7. Kurucz (1988) 8. MFW in Kurucz database, 9. Smith and Kuehne (1978), 10. Fuhr *et al.* (1988), 11. Heise (1974), 12. Bielski (1975), 13. Warner (1968), 14. CB in Kurucz database, 15. Hannaford *et al.* (1982), 16. Cowley and Corliss (1983), 17. Biemont *et al.* (1981), 18. estimated from multiplet table intensity, 19. Andersen *et al.* (1975), 20. Arnesen *et al.* (1977), 21. Meggers *et al.* (1975), 22. Lage and Whaling (1976), 23. Ward *et al.* (1985), 24. Biemont *et al.* (1982)

Chapter 4

Analysis of CH and CEMP stars^{*}

4.1 Introduction

Being enriched with carbon (and neutron-capture elements), the atmospheres of the less-evolved, low-mass stars form a unique treasure trove of information for the astrophysicists seeking the chemical evolution history of the Galaxy. Thus, studies on the metal-poor stars such as CH stars (Keenan 1942), with their more metal-poor counterparts, Carbon Enhanced Metal-Poor (CEMP) stars offer the best means to constrain the neutron-capture nucleosynthesis processes, especially the nucleosynthesis occurring in the Asymptotic Giant Branch (AGB) stars. The spectra of these peculiar stars show strong CH and C₂ molecular bands and features due to enhanced neutron-capture elements compared to the normal stars. They are characterized by C/O > 1.

The CEMP stars are more metal-poor ([Fe/H] < -1) than the classical CH stars

*Main results from this chapter are published in Purandardas *et al.* (2019), Shejelammal *et al.* (2021), Shejelammal and Goswami (2021).

(Lucatello *et al.* 2005; Aoki *et al.* 2007; Abate *et al.* 2016; Hansen *et al.* 2016c,a) with $[\text{C}/\text{Fe}] > 1$ (Beers and Christlieb 2005; Abate *et al.* 2016). They were identified among the Very Metal-Poor stars discovered in the extensive spectroscopic survey to identify a large sample of most metal-poor stars, the HK survey (Beers *et al.* 1985, 1992, 2007; Beers 1999), and later in a number of successive surveys like the Hamburg/ESO Survey (HES; Christlieb *et al.* 2001a,b; Christlieb 2003; Christlieb *et al.* 2008), Sloan Digital Sky Survey (SDSS; York *et al.* 2000), Sloan Extension for Galactic Understanding and Exploration (SEGUE; Yanny *et al.* 2009) etc. A number of other large sky survey programs in the past were also dedicated to identify the Galactic carbon stars, for instance, the First Byurakan Spectral Sky Survey (Gigoyan *et al.* 1998), the Automatic Plate Measuring survey (Totten and Irwin 1998; Ibata *et al.* 2001), infrared objective-prism surveys (Alksnis *et al.* 2001), Large sky Area Multi-Object Fiber Spectroscopic Telescope (LAMOST) pilot survey (Cui *et al.* 2012; Deng *et al.* 2012; Zhao *et al.* 2012). It has been identified that the fraction of CEMP stars in the Galactic halo increases with decreasing metallicity; $\sim 20\%$ for $[\text{Fe}/\text{H}] < -2$ (Norris *et al.* 1997; Rossi *et al.* 1999, 2005; Christlieb 2003; Cohen *et al.* 2005; Marsteller *et al.* 2005; Frebel *et al.* 2006; Lucatello *et al.* 2006; Carollo *et al.* 2012; Lee *et al.* 2013), $\sim 40\%$ for $[\text{Fe}/\text{H}] < -3$ (Aoki *et al.* 2013; Lee *et al.* 2013; Yong *et al.* 2013), $\sim 75\%$ for $[\text{Fe}/\text{H}] < -4$ (Lee *et al.* 2013; Placco *et al.* 2014; Frebel and Norris 2015), and thus making them important tools for studies of the formation and evolution of early Galactic halo.

Beers and Christlieb (2005) put forward the first classification scheme for CEMP stars, and classified them into different sub-classes depending on the level of enrichment of neutron-capture elements Ba and Eu; CEMP-s (show enhanced abundances of s-process elements), CEMP-r (show strong enhancement of r-process elements), CEMP-r/s (show simultaneous enhancement of both s- and r-process elements), and CEMP-no (do not show any enhanced abundance of neutron-capture elements). A slight deviation from the original classification scheme has been

adopted by several authors (Aoki *et al.* 2007; Abate *et al.* 2016; Frebel 2018; Hansen *et al.* 2019). High-resolution spectroscopic analyses have shown that, at present, about 80% of the CEMP stars are CEMP-s stars (Aoki *et al.* 2007), and about half of the CEMP-s stars are CEMP-r/s stars (Sneden *et al.* 2008; Käppeler *et al.* 2011; Bisterzo *et al.* 2011).

The diverse abundance pattern observed in the CEMP stars points to different formation scenarios. CH, CEMP-s, and CEMP-r/s stars belong to the main sequence or giant phase of stellar evolution. Hence, the observed overabundances of the carbon and neutron-capture elements are attributed to an extrinsic origin. In the case of CH and CEMP-s stars, enriched in s-process elements, the most accepted scenario involves binary mass-transfer from an AGB companion. There exist a number of proposed scenarios for the simultaneous r- and s- process enrichment observed in CEMP-r/s stars (Jonsell *et al.* 2006 and references therein); however, none of them could successfully reproduce the observed frequency and high [hs/ls] ratio of CEMP-r/s stars (Abate *et al.* 2016). An intermediate neutron-capture process (i-process) that operates with neutron densities in between s- and r-process had been invoked to explain the observed abundances of CEMP-r/s stars. Hampel *et al.* (2016, 2019) could successfully reproduce the observed abundance trend of several CEMP-r/s stars considering this production scenario. The i-process was originally proposed by Cowan and Rose (1977). Among the proposed scenarios for the nucleosynthesis sites of the i-process are, massive ($5 - 10 M_{\odot}$) super-AGB stars (Doherty *et al.* 2015; Jones *et al.* 2016), evolved low-mass stars (Herwig *et al.* 2011; Hampel *et al.* 2019), low-mass, low-metallicity ($[\text{Fe}/\text{H}] \leq -3$) stars (Campbell and Lattanzio 2008; Campbell *et al.* 2010; Cruz *et al.* 2013; Cristallo *et al.* 2016) and Rapidly Accreting White Dwarfs (Herwig *et al.* 2014; Denissenkov *et al.* 2017). Clarkson *et al.* (2018) and Banerjee *et al.* (2018) have suggested that massive ($M \geq 20 M_{\odot}$), metal-poor stars could also play a role in the production of i-process elements. Despite several efforts, large uncertainties still exist regarding the i-process nucleosynthesis and the possible astrophysical sites of its

occurrence (Frebel 2018; Koch *et al.* 2019). It has been found from the long-term radial velocity monitoring studies that the vast majority of CH stars (McClure and Woodsworth 1990; Jorissen *et al.* 2016b) and CEMP-s and CEMP-r/s stars (Lucatello *et al.* 2005; Starkenburg *et al.* 2014; Jorissen *et al.* 2016b; Hansen *et al.* 2016c) are most likely binaries, thus strongly favoring the binary mass transfer scenario.

Just like CEMP-r/s stars, the origins of CEMP-no and CEMP-r stars are also not clearly understood. The suggested origin for CEMP-r stars is that they were formed from the ISM pre-enriched by core-collapse SNe, neutron star mergers, neutron star - black hole mergers (Surman *et al.* 2008; Arcones and Thielemann 2013; Rosswog *et al.* 2014; Drout *et al.* 2017; Lippuner *et al.* 2017). The suggested progenitors for the origin of carbon enhancement of CEMP-no stars, that polluted ISM, are faint SNe, spinstars, metal-free massive stars, binary mass-transfer from extremely metal-poor AGB stars (Heger and Woosley 2010; Nomoto *et al.* 2013; Chiappini 2013; Tominaga *et al.* 2014).

In this chapter, we have presented a detailed spectroscopic analysis of thirteen carbon stars selected from various sources in the literature, in order to understand their formation history from a detailed elemental abundance analysis. The structure of this chapter is as follows. Observations and data reduction are presented in Section 4.2. Radial velocity of the stars and stellar atmospheric parameters are presented in Section 4.3. The same Section also provides a brief discussion on the stellar mass. Section 4.4 provides a discussion on elemental abundance determination and abundance uncertainties. Classification of program stars is discussed in Section 4.5. In Section 4.6, binary status of the programs stars is discussed. Section 4.7 provides a discussion on the analysis of various abundance profiles of the program stars, and the interpretations. Origin(s) of the program stars are discussed in Section 4.8. The parametric model-based analysis is discussed in Section 4.9. Results of the kinematic analysis are provided in Section 4.10, followed by

the discussion on the individual stars in Section 4.11. Conclusion are drawn in Section 4.12.

4.2 Stellar sample: selection, observation/data acquisition and data reduction

Out of the total thirteen objects analyzed here, five objects, BD–19 132, BD–19 290, BD+19 3109, HD 30443, and HD 202851 are selected from the catalogue of CH star by Bartkevicius (1996). The objects, HE 0457–1805, HE 0920–0506, HE 1157–0518, HE 1304–2111, HE 1327–2116, and HE 1354–2257 are selected from the candidate metal-poor stars identified in the Hamburg/ESO survey (HES) (Christlieb 2003) and in the HK survey of Beers *et al.* (1992). The stars HE 0457–1805, HE 1157–0518, and HE 1354–2257 are also listed in the catalogue of carbon stars identified from the Hamburg/ESO survey (HES) by Christlieb *et al.* (2001a). The objects HE 0920–0506 and HE 1327–2116 are listed in the catalogue of bright metal-poor candidates from the HES by Frebel *et al.* (2006). The objects HE 1157–0518 and HE 1327–2116 are also listed in the catalogue of candidate metal-poor stars identified from the HES by Christlieb *et al.* (2008). The detailed object selection criteria is discussed in Section 2.2. The objects LAMOSTJ091608.81+230734.6 and LAMOSTJ151003.74+305407.3 are selected from the catalogue of carbon stars identified from the LAMOST DR2 by Ji *et al.* (2016). The spectra of the objects BD–19 132, BD–19 290, HD 30443, LAMOSTJ091608.81+230734.6, BD+19 3109, and HD 202851 at a resolution of $\lambda/\delta\lambda \sim 60,000$ and of the object LAMOSTJ151003.74+305407.3 at a resolution of $\lambda/\delta\lambda \sim 30,000$ are obtained using the HCT/HESP. For all these objects, we have taken three frames each with an exposure of 2700 sec (2400 sec for HD 30443) and then co-added to improve the quality (S/N ratio) of the resulting spectra. This S/N ratio enhanced spectra are then used for further analysis. The high resolution

($\lambda/\delta\lambda \sim 86,000$) spectra of the objects HE 0457–1805, HE 0920–0506, and HE 1327–2116 are obtained with the Mercator/HERMES. The reduced, wavelength calibrated spectra of the objects HE 1157–0518, HE 1304–2111, and HE 1354–2257 at a resolution of $\lambda/\delta\lambda \sim 50,000$ were taken from the SUBARU/HDS archive (<http://jvo.nao.ac.jp/portal/v2/>). The SUBARU spectra covers 4100 - 6850 Å in wavelength. The spectra have a gap between 5440 and 5520 Å because of the separation of the two CCDs used. The basic information of the program stars are given in Table 4.1, and sample spectra of a few program stars are shown in Figure 4.1.

TABLE 4.1: Primary information of the program stars.

Star	RA(2000)	Dec.(2000)	B	V	J	H	K	Exposure (seconds)	Date of obs.	Source of spectrum	S/N		
											4200 Å	5500 Å	7700 Å
BD-19 132	00 50 24.16	-19 04 40.19	13.25	10.73	8.083	7.354	7.070	2700(3)	07/11/2017	HESP	11.37	30.71	40.93
BD-19 290	01 40 34.11	-18 56 51.52	12.41	11.07	8.710	8.102	7.914	2700(3)	08/11/2017	HESP	6.41	23.59	47.07
HD 30443	04 49 16.02	+35 00 6.49	11.2	8.82	4.62	3.28	2.83	2400(3)	07/11/2017	HESP	22.38	53.30	62.96
HE 0457-1805	04 59 43.56	-18 01 11.99	12.372	11.014	8.937	8.421	8.186	1800(15)	04/01/2016	HERMES	15.82	55.48	89.05
LAMOSTJ091608.81+230734.6	09 16 8.82	+23 07 34.86	11.44	10.40	8.654	8.141	8.022	2700(3)	04/04/2018	HESP	21.38	37.15	42.38
HE 0920-0506	09 23 05.96	-05 19 32.75	11.80	10.95	10.317	9.971	9.900	780(10)	21/01/2019	HERMES	14.00	51.88	49.89
HE 1157-0518	12 00 08.06	-05 34 43.12	16.273	15.120	13.418	12.917	12.846	1800	25/05/2003	SUBARU	9.32	25.15	-
HE 1304-2111	13 07 27.26	-21 27 34.24	14.547	13.061	9.651	9.009	8.764	1200	25/05/2003	SUBARU	5.21	21.53	-
HE 1327-2116	13 30 19.36	-21 32 03.33	12.714	11.651	9.893	9.412	9.275	1200(3)	01/02/2019	HERMES	13.85	29.60	68.14
HE 1354-2257	13 57 43.30	-23 12 34.55	15.22	14.00	11.809	11.290	11.110	1800	26/05/2003	SUBARU	6.39	35.56	-
LAMOSTJ151003.74+305407.3	15 10 3.30	+30 54 7.36	13.50	11.38	9.33	8.737	8.539	2700(3)	23/05/2018	HESP	10.77	33.67	70.17
BD+19 3109	16 29 26.99	+19 30 34.46	11.88	10.29	8.051	7.40	7.253	2700(3)	23/05/2018	HESP	7.80	48.27	95.90
HD 202851	21 18 43.49	-01 32 03.34	10.89	9.67	7.711	7.174	7.029	2700(3)	07/11/2017	HESP	17.01	31.82	54.57

The number of frames taken are given with exposure time, in parenthesis.

4.3 Stellar atmospheric parameters and radial velocity

The radial velocities of the program stars are calculated from the Doppler equation using the measured wavelength shift of a set of clean spectral lines of several elements. While the objects BD–19 290, HE 1157–0518, HE 1327–2116, HE 1354–2257, LAMOSTJ151003.74+305407.3, and BD+19 3109 are found to be high radial-velocity ($|V_r| > 100 \text{ km s}^{-1}$) objects with V_r in the range -181.89 to $+289.46 \text{ km s}^{-1}$, BD–19 132, HD 30443, HE 0457–1805, LAMOSTJ091608.81+230734.6, HE 0920–0506, HE 1304–2111, and HD 202851 are low velocity ($|V_r| < 100 \text{ km s}^{-1}$) objects with V_r in the range $+2.14$ to $+66.61 \text{ km s}^{-1}$. The equivalent width measured from a set of clean Fe I and Fe II lines are used for the derivation of the stellar atmospheric parameters following the procedure in Section 2.6.4. The lines are selected such that they have equivalent width and excitation potential in the range 18 - 180 mÅ and 0 - 6 eV respectively. The abundances derived from Fe I and Fe II lines as functions of excitation potentials and equivalent widths are shown in Figure 4.2. The derived atmospheric parameters, along with the available literature values, as well as the radial velocities of the program stars, are given in Table 4.2.

The $\log g$ value is estimated employing the parallax method as well (Section 2.6.4.1). The stellar masses are found from their positions on the H-R diagram ($\log T_{\text{eff}}$ v/s $\log (L/L_\odot)$). The H-R diagram is generated using the stellar evolutionary tracks of Girardi *et al.* (2000). We have used $z = 0.0004$ tracks for the objects BD–19 132, BD–19 290, HD 30443, HE 0457–1805, HE 1157–0518, HE 1327–2116, LAMOSTJ151003.74+305407.3, and BD+19 3109 and $z=0.004$ tracks for LAMOSTJ091608.81+230734.6, HE 0920–0506, and HD 202851. These H-R diagrams are shown in Figure 4.3. We could not determine the masses of the objects HE 1304–2111 and HE 1354–2257, as the tracks corresponding to

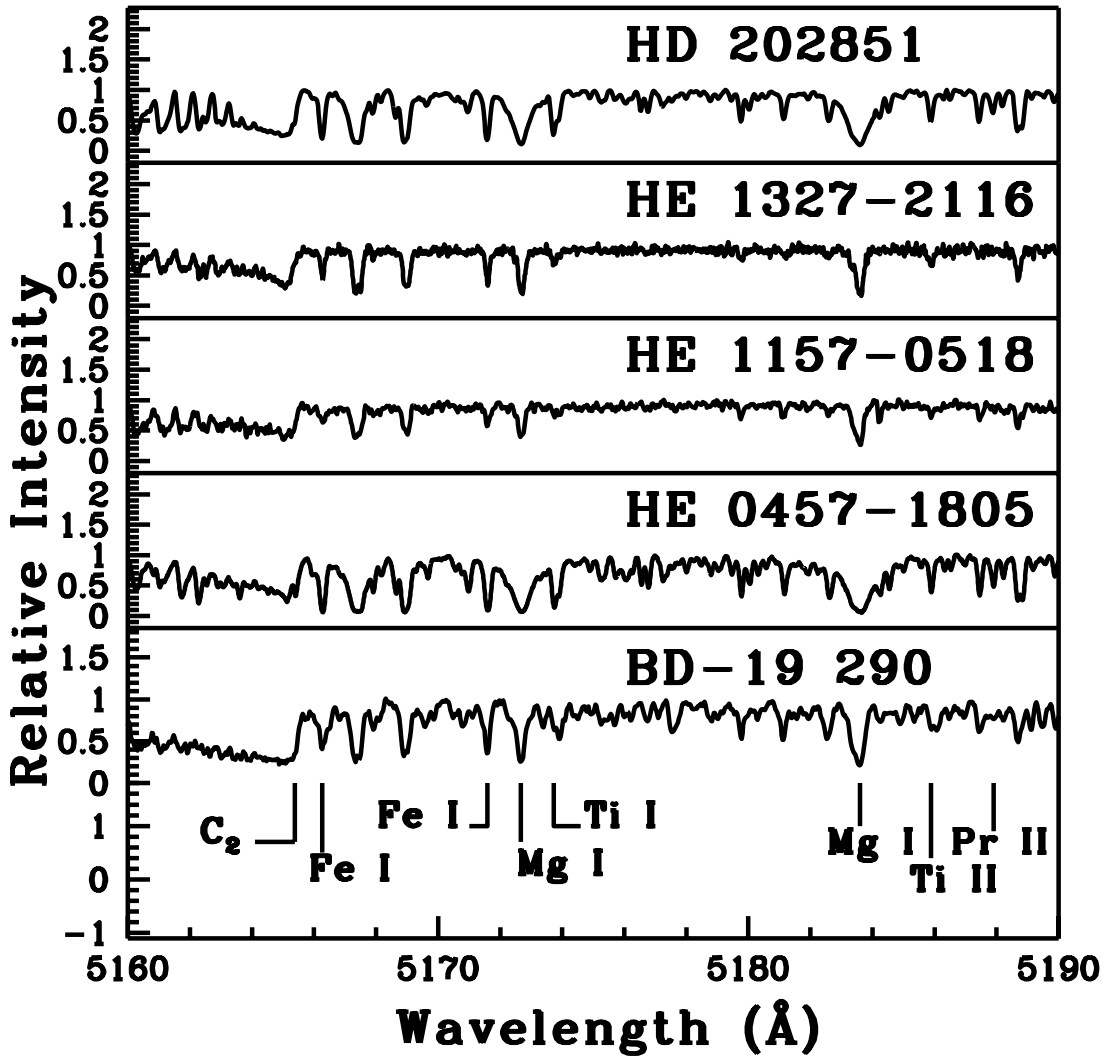


FIGURE 4.1: Sample spectra of the program stars in the wavelength region 5160 to 5190 Å.

their luminosity and temperatures are not available. We could find only an upper limit to the mass of the stars BD-19 132, HD 30443, HE 0457-1805, LAMOSTJ151003.74+305407.3, and BD+19 3109. The mass estimates and log g values estimated from the parallax method (Section 2.6.4.1) are given in Table 4.3. For the stars LAMOSTJ091608.81+230734.6 and HE 0920-0506, the spectroscopic log g is ~ 0.9 dex lower than that estimated from parallax method. In some carbon stars, such inconsistency between the spectroscopic atmospheric parameters and those derived from the evolutionary tracks could arise as their evolutionary

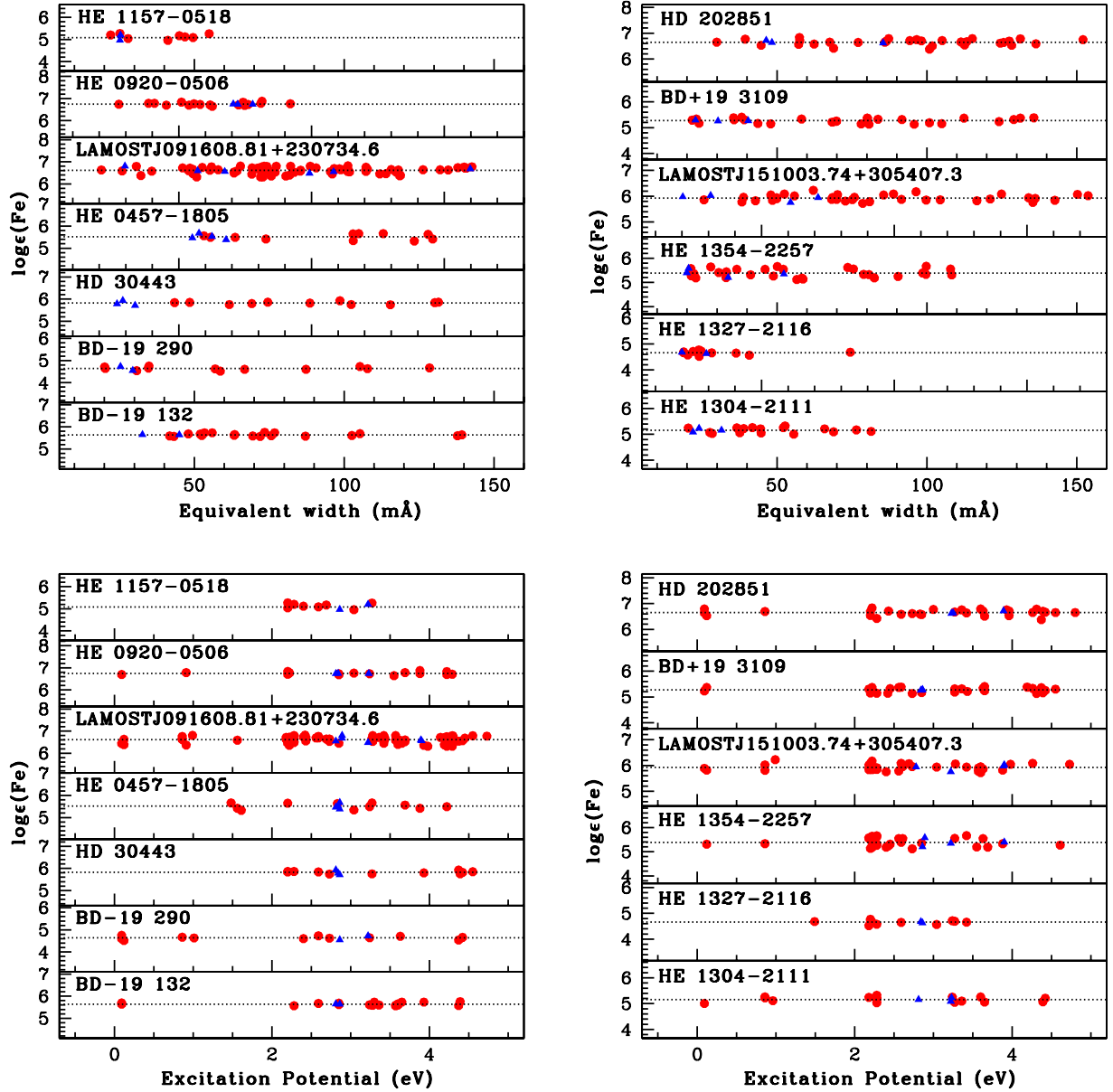


FIGURE 4.2: Iron abundances of the program stars derived from individual Fe I and Fe II lines as function of excitation potential (lower panel), and equivalent width (upper panel). The dotted lines correspond to the derived and adopted Fe abundance for each star. Solid circles correspond to Fe I, and solid triangles correspond to Fe II lines.

TABLE 4.2: Derived atmospheric parameters and radial velocity of the program stars.

Star	T_{eff} (K)	$\log g$ cgs	ζ (km s $^{-1}$)	[Fe I/H]	[Fe II/H]	V_r (km s $^{-1}$)	Reference
	± 100	± 0.2	± 0.2				
BD-19 132	4005	1.13	2.02	-1.86 \pm 0.06	-1.86 \pm 0.01	+3.94 \pm 0.81	1
BD-19 290	4315	0.61	3.10	-2.86 \pm 0.07	-2.86 \pm 0.13	+106.28 \pm 0.90	1
HD 30443	4040	2.05	2.70	-1.68 \pm 0.05	-1.69 \pm 0.11	66.61 \pm 0.20	1
HE 0457-1805	4435	0.70	1.97	-1.98 \pm 0.13	-1.98 \pm 0.12	+62.83 \pm 0.02	1
	4484	0.77	-	-1.46	-	-	2
LAMOSTJ091608.81+230734.6	4820	1.43	1.62	-0.89 \pm 0.14	-0.89 \pm 0.12	+16.13 \pm 4.30	1
HE 0920-0506	5380	2.65	0.69	-0.75 \pm 0.06	-0.75 \pm 0.01	+49.60 \pm 0.03	1
	5291	2.99	-	-1.39	-	-	3
	-	-	-	-1.01	-	-	4
HE 1157-0518	5050	2.52	2.15	-2.42 \pm 0.15	-2.42 \pm 0.16	+116.02 \pm 0.70	1
	4900	2.00	-	-2.40	-	-	5
HE 1304-2111	4325	1.06	0.63	-2.34 \pm 0.10	-2.34 \pm 0.07	+2.14 \pm 0.34	1
HE 1327-2116	4835	1.50	3.45	-2.84 \pm 0.07	-2.84 \pm 0.05	+176.77 \pm 0.06	1
	4868	0.55	-	-3.48	-	-	3
	-	-	-	-2.93	-	-	4
HE 1354-2257	4700	1.13	1.86	-2.11 \pm 0.17	-2.11 \pm 0.15	+289.46 \pm 1.80	1
LAMOSTJ151003.74+305407.3	4500	1.55	1.24	-1.57 \pm 0.12	-1.57 \pm 0.12	-141.58 \pm 3.57	1
	4358.31	0.956	1.667	-1.346	-	-	6
BD+19 3109	4035	0.75	2.05	-2.23 \pm 0.09	-2.23 \pm 0.02	-181.89 \pm 1.38	1
HD 202851	4900	2.20	1.54	-0.85 \pm 0.11	-0.85 \pm 0.05	+22.22 \pm 0.90	1
	4800	2.10	1.50	-0.70	-	-	7
	4733	1.60	-	-0.88	-	-	8

References: 1. Our work, 2. Kennedy *et al.* (2011), 3. Beers *et al.* (2017), 4. Frebel *et al.* (2006), 5. Aoki *et al.* (2007), 6. Hayes *et al.* (2018), 7. Sperauskas *et al.* (2016), 8. Arentsen *et al.* (2019b)

tracks shift towards lower temperatures (Marigo 2002; Jorissen *et al.* 2016a).

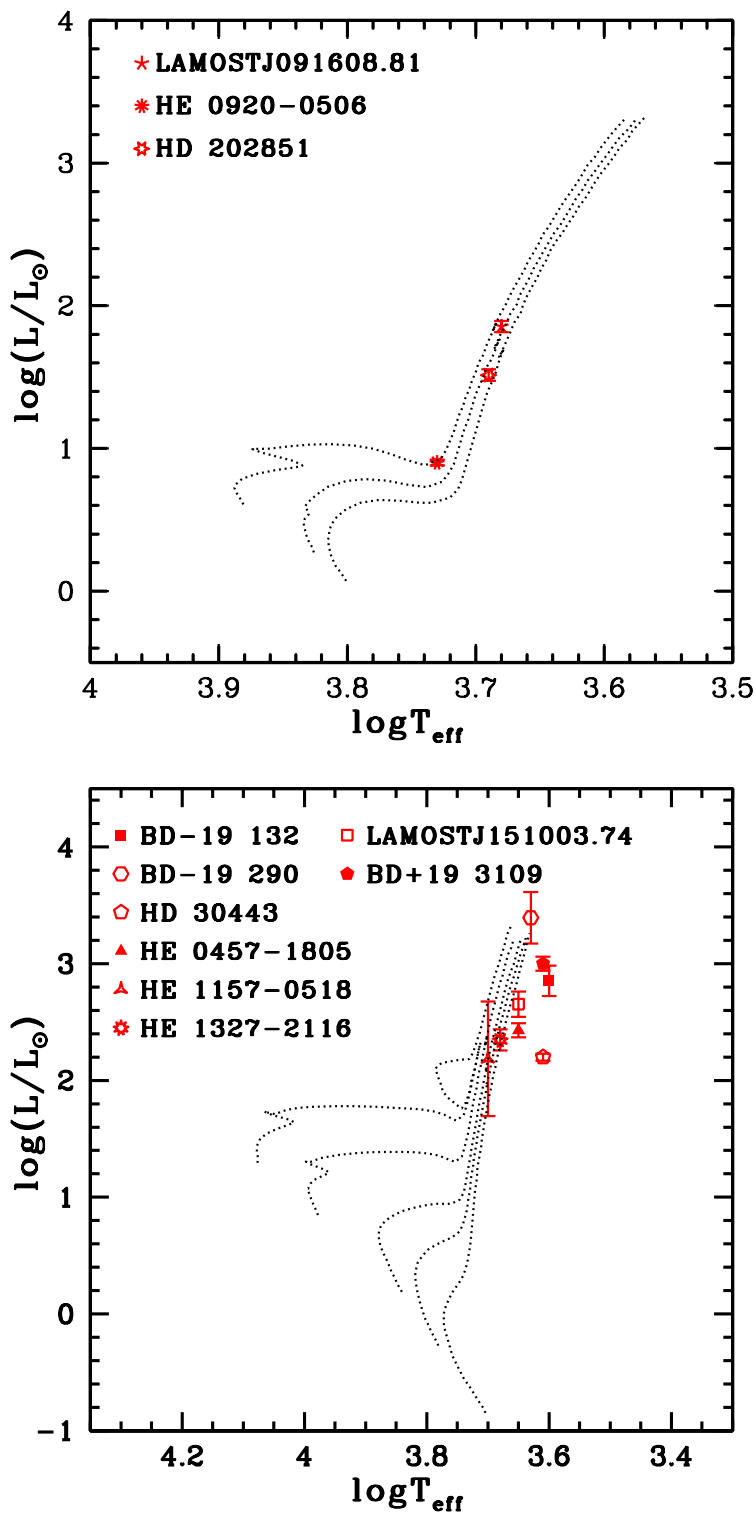


FIGURE 4.3: The evolutionary tracks (Girardi *et al.* 2000) for 1.0 , 1.1 , and 1.3 M $_\odot$ for $z = 0.004$ (upper panel), and for 0.6 , 0.8 , 1.0 , 1.4 , and 1.8 M $_\odot$ for $z = 0.0004$ (lower panel) are shown from bottom to top.

TABLE 4.3: Mass and log g estimated from the parallax method

Star name	Parallax (mas)	M_{bol}	$\log(L/L_\odot)$	Mass(M_\odot)	log g (cgs)	log g (spectroscopic) (cgs)
BD-19 132	0.3556 ± 0.0560	-2.395 ± 0.345	2.854 ± 0.138	< 0.60	—	1.13
BD-19 290	0.1449 ± 0.0417	-3.745 ± 0.334	3.390 ± 0.260	1.00 ± 0.40	0.54 ± 0.07	0.61
HD 30443	2.1612 ± 0.0460	0.76 ± 0.05	2.20 ± 0.03	< 0.60	—	2.05
HE 0457-1805	0.467 ± 0.0309	-1.341 ± 0.14	2.43 ± 0.05	< 0.60	—	0.70
LAMOSTJ091608.81+230734.6	1.0543 ± 0.0517	0.105 ± 0.107	1.854 ± 0.043	1.10 ± 0.05	2.33 ± 0.03	1.43
HE 0920-0506	2.3764 ± 0.0653	2.488 ± 0.06	0.90 ± 0.02	1.30 ± 0.005	3.50 ± 0.03	2.65
HE 1157-0518	0.0778 ± 0.0397	-0.725 ± 1.222	2.186 ± 0.490	1.00 ± 0.60	2.02 ± 0.25	2.52
HE 1304-2111	22.7558 ± 0.040	9.229 ± 0.004	-1.797 ± 0.002	—	—	1.06
HE 1327-2116	0.3428 ± 0.0358	-1.130 ± 0.228	2.35 ± 0.09	0.70 ± 0.10	1.63 ± 0.03	1.50
HE 1354-2257	0.0150 ± 0.0514	5.638 ± 3.231	4.151 ± 1.292	—	—	1.13
LAMOSTJ151003.74+305407.3	0.2778 ± 0.0346	1.891 ± 0.271	2.653 ± 0.109	< 0.60	—	1.55
BD+19 3109	0.3764 ± 0.0284	-2.765 ± 0.165	3.000 ± 0.060	< 0.60	—	0.75
HD 202851	2.2160 ± 0.0982	0.955 ± 0.999	1.514 ± 0.040	1.05 ± 0.05	2.66 ± 0.02	2.20

4.4 Abundance determination and discussion

The details of the abundance derivation of each element, along with the details of HFS and the NLTE corrections used are discussed in this Section.

4.4.1 Light elements: C, N, O, $^{12}\text{C}/^{13}\text{C}$, Na, α -, and Fe-peak elements

The abundance of oxygen is derived from the spectral synthesis calculation of forbidden [O I] 6300.304 Å line. This line is insensitive to NLTE effect. The other oxygen forbidden line at 6363.776 Å is not usable for the abundance determination in any of the program stars. A discussion on the blends that affect the [O I] lines is given in Section 3.4.1. Even though the [O I] forbidden line at 6300.304 Å is affected by Ni I blend, its effect decreases and becomes negligible in stars with metallicity < -1 (Allende Prieto *et al.* 2001). Due to the poor SNR, the O I triplet lines around 7770 Å are not usable for abundance analysis in any of the program stars. We could determine the oxygen abundance only in seven stars: BD–19 132, BD–19 290, HD 30443, LAMOSTJ091608.81+230734.6, HE 0920–0506, HE 1354–2257, and HD 202851, with HD 30443 showing the highest enhancement of $[\text{O}/\text{Fe}] \sim 1.41$. In other stars $[\text{O}/\text{Fe}]$ ranges from -0.14 to 1.34 .

Once the oxygen abundance is determined, the carbon abundance is derived from the C_2 molecular bands at 5165 and 5635 Å by spectral synthesis calculation. The spectral synthesis fits for these two regions for a few program stars are shown in Figure 4.4. The C_2 band at 5165 Å is noisy in the spectra of BD–19 132 and HE 1304–2111; so we could not use this region in these stars. In all other stars, we derived the carbon abundance from both the regions. The abundances

derived from these two bands are consistent within 0.3 dex. The average abundance from these two C_2 regions is taken as the final carbon abundance. All the stars except BD-19 132, LAMOSTJ091608.81+230734.6, HE 0920-0506, and HD 202851 show $[C/\text{Fe}] > 1$, with BD+19 3109 being the most carbon enhanced with $[C/\text{Fe}] \sim 2.47$.

We could determine nitrogen abundance in all the stars except HE 1304-2111. The nitrogen abundance is derived from ^{12}CN band at 4215 Å region in HD 30443, HE 1157-0518, and HE 1354-2257. In all other stars, the ^{12}CN lines at 8000 Å region are used to estimate the nitrogen abundance. Except HD 30443, LAMOSTJ091608.81+230734.6, HE 0920-0506, and HE 1354-2257, all other stars show $[\text{N}/\text{Fe}] > 1$. Once the carbon, nitrogen, and oxygen abundances were derived, we re-derived the oxygen abundance. Then, with this oxygen abundance, carbon and nitrogen abundances are re-estimated. This iterative process is repeated until a convergence is obtained.

The ^{12}CN lines at 8003.292, 8003.553, 8003.910 Å, and ^{13}CN lines at 8004.554, 8004.728, 8004.781 Å are used to derive the carbon isotopic ratio, $^{12}\text{C}/^{13}\text{C}$ in the HSEP and HERMES spectra of the stars that cover these regions. The SUBARU spectra used for three objects, however extend only till 6800 Å in the wavelength region. The values obtained for this ratio in BD-19 132, BD-19 290, HD 30443, HE 0457-1805, LAMOSTJ091608.81+230734.6, HE 1327-2116, LAMOSTJ151003.74+305407.3, BD+19 3109, and HD 202851 are 18, 4, 9.33, 23, 8.67, 7, 13.33, 9, and 42 respectively. For CEMP-s and CEMP-r/s stars, the values of $^{12}\text{C}/^{13}\text{C}$ ratio are found in the range 2.5 - 40 (Bisterzo *et al.* 2011). The spectrum synthesis fit for this region is shown in Figure 4.5.

The equivalent width measurements of several lines listed in Table B2 (Appendix B, Section 4.13) are used to derive the abundance of Na, Mg, Si, Ca, Ti, Cr, Ni, and Zn. We could not estimate sodium abundance in HE 1157-0518. The stars

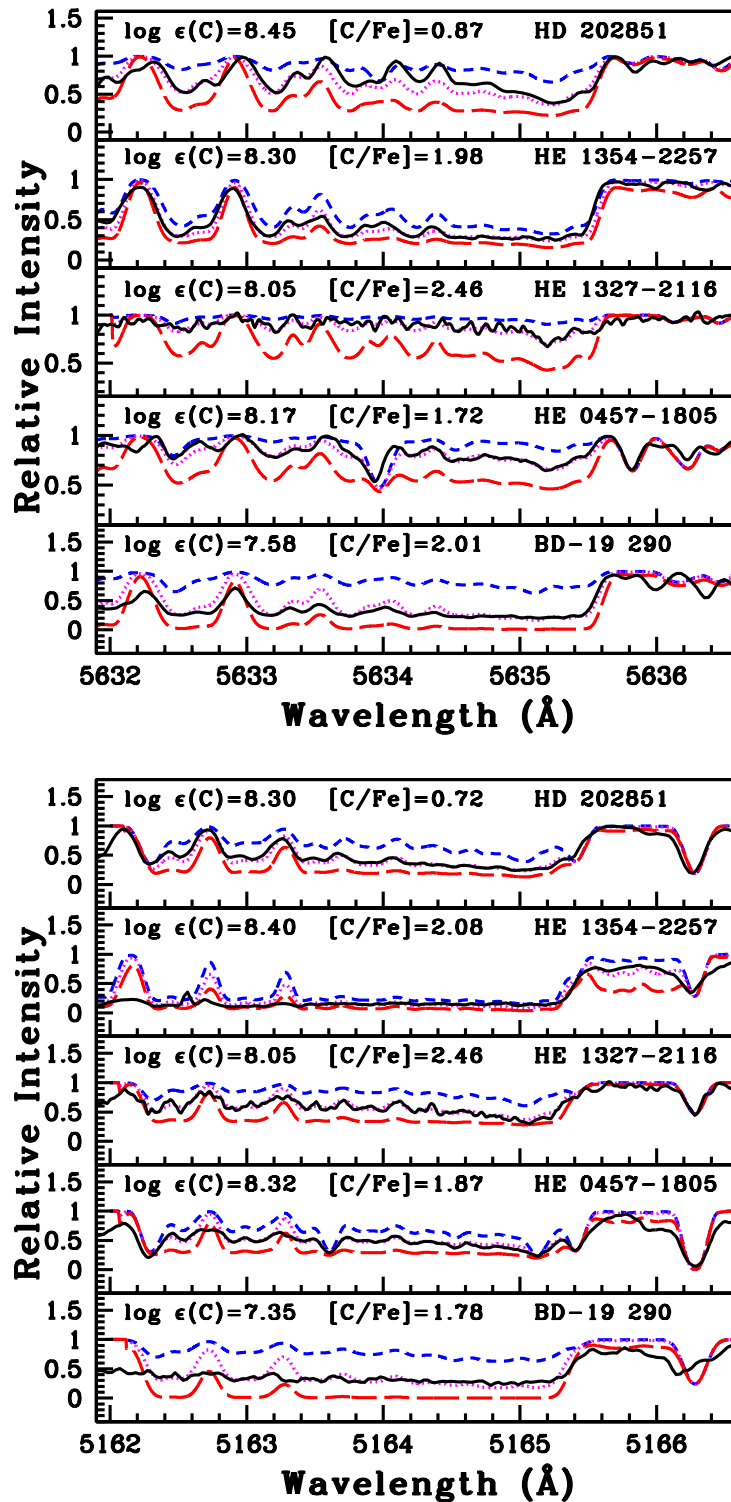


FIGURE 4.4: Synthesis of C₂ band around 5165 Å (lower panel) and 5635 Å (upper panel). Dotted and solid lines represent synthesized and observed spectra respectively. short-dashed and long-dashed lines represent the synthetic spectra for $\Delta [C/Fe] = -0.3$ and $+0.3$ respectively.

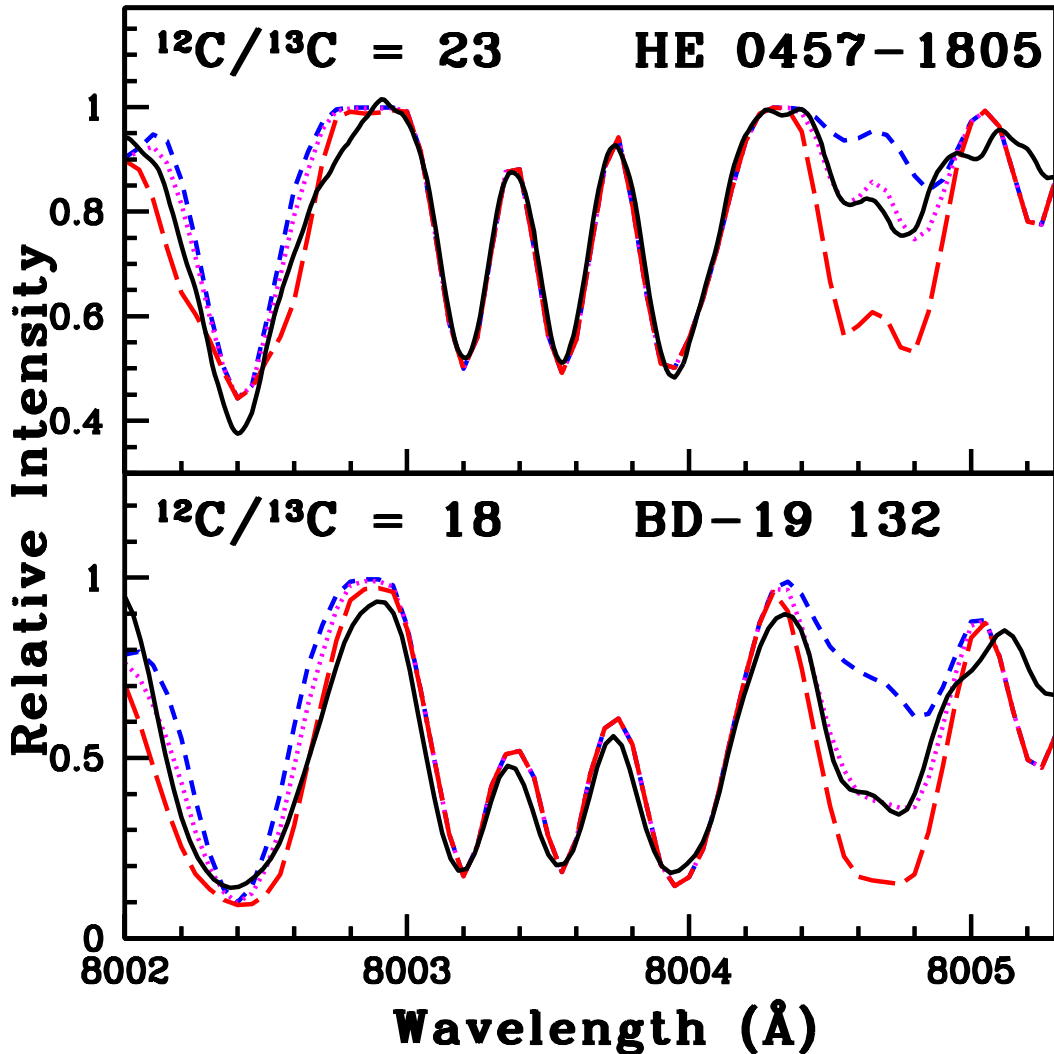


FIGURE 4.5: Spectral synthesis of CN band around 8005 Å. Dotted and solid lines represent synthesized and observed spectra respectively. short-dashed and long-dashed lines are the synthetic spectra for $^{12}\text{C}/^{13}\text{C} \simeq 90$ and 4 respectively.

HE 0457–1805 and HE 1304–2111 show $[\text{Na}/\text{Fe}] > 2$ with values of 2.20 and 2.83, respectively. In HE 1304–2111, the lines used to derive the Na abundance were very strong, so this abundance may not be reliable. The NLTE corrections for these lines were not available. The stars, BD–19 132, and BD–19 290 have $[\text{Na}/\text{Fe}] > 1$. In very metal-poor stars, Na suffers large uncertainties due to the NLTE corrections or 3D hydrodynamical model atmospheres (Bisterzo *et al.* 2011; Andrievsky *et al.* 2007). The NLTE effect may reduce the Na abundance by up to 0.7 dex (Andrievsky *et al.* 2007). However, the Na I 5682.633, 5688.205 Å

lines have negligible NLTE effect (Takeda *et al.* 2003). We have used these two weak lines to derive the Na abundance in most of the stars. The Mg abundance is derived mainly from Mg I 4702.991, 4730.029, 5528.405, 5711.088 Å lines. The Mg abundance of the program stars are in the range $-0.02 \leq [\text{Mg}/\text{Fe}] \leq 1.32$, with HE 0457–1805 being the most enriched in Mg.

The elements Sc, V, Mn, Co, and Cu show HFS. The abundances of these elements are derived using the spectral synthesis calculation, taking the hyperfine components into account. The hyperfine components of these elements are taken from Prochaska and McWilliam (2000) and Prochaska *et al.* (2000). Sc abundance is derived mainly from the Sc II lines at 6245.637, 6309.920, and 6604.601 Å. In the case of HE 1327–2116, Sc II 4374.457, 5031.021 Å lines were used. It shows near-solar value in HD 30443, LAMOSTJ091608.81+230734.6, and HE 1354–2257. While in HE 0920–0506 and HE 1327–2116, scandium is slightly under abundant with $[\text{Sc}/\text{Fe}] \sim -0.25$, in all other stars it ranges from 0.27 to 0.81. Spectral synthesis calculation of the V I lines at 4864.731, 5727.048, and 6251.827 Å are used to derive the vanadium abundance. We could not estimate vanadium abundance in HE 1327–2116 as there is no clean lines available. Three objects in our sample, BD–19 290, HE 1304–2111, and HE 1354–2257 show $[\text{V}/\text{Fe}] > 1$, whereas it ranges from –0.64 to 0.78 in other stars. The Mn abundance is estimated from the Mn I lines at 4451.586, 4470.140, 4761.530, 6013.513, and 6021.89 Å. We have derived the Co abundance from Co I lines at 5342.695 and 5483.344 Å, and Cu abundance from Cu I line at 5105.537 Å. In the case of BD+19 3109, cobalt abundance is derived from the lines Co I 4792.846, 4867.872, and 4792.846 Å. The Co I 4118.770, 4121.320 Å lines are used in the case of HE 1327–2116.

A comparison of the light element abundances observed in our program stars with their counterparts in normal stars and other classes of chemically peculiar stars is shown in Figures 4.6 and 4.7. While the estimated abundances of the elements Si, Ca, Sc, Ti, Co, and Zn in all the program stars follow the Galactic

trend (similar to that observed in normal stars), Na, Mg, V, Cr, Mn, and Ni are enhanced in a few program stars. Such enhancements of Na, Mg, and/or Fe-peak elements are observed in a few CEMP stars such as HE 1327–2326 (Aoki *et al.* 2006; Frebel 2008), and SMSS J031300.36–670839.3 (Bessell *et al.* 2015). The models of spinstar (Maeder *et al.* 2015; Maeder and Meynet 2015), faint SNe (Iwamoto *et al.* 2005; Tominaga *et al.* 2007; Bessell *et al.* 2015) have been used to reproduce their observed abundance pattern. According to Aoki *et al.* (2006), either faint SNe or AGB-binary mass transfer along with the accretion of metals from the ISM might explain the observed abundance pattern of HE 1327–2326. Chojalin *et al.* (2017) have suggested that spinstar could also have played a role in the formation of some CEMP-s stars, and the abundance patterns of CEMP-s stars may be resulting from several sources. From these facts, the observed enhanced abundances of Na, Mg, V, Cr, Mn, and Ni in the program stars may be attributed to the pre-enriched ISM from which they were formed. Also, some of the CEMP-s and CEMP-r/s stars show enhanced abundances of Na and/or Mg at low metallicities (Bisterzo *et al.* 2011 and references therein, Allen *et al.* 2012, Karinkuzhi *et al.* 2021, Goswami *et al.* 2021). A discussion on the Na and Mg abundances is provided in Section 4.7.3.

4.4.2 Heavy elements

4.4.2.1 The light s-process elements: Rb, Sr, Y, Zr

The spectral synthesis calculation of Rb I 7800.259 Å resonance line is used to derive the rubidium abundance in the program stars, by taking the hyperfine components from Lambert and Luck (1976). Rb I 7947.597 Å was very weak, and could not be used for the abundance determination. We could determine Rb abundance only in the stars whose spectra are obtained from the HESP and

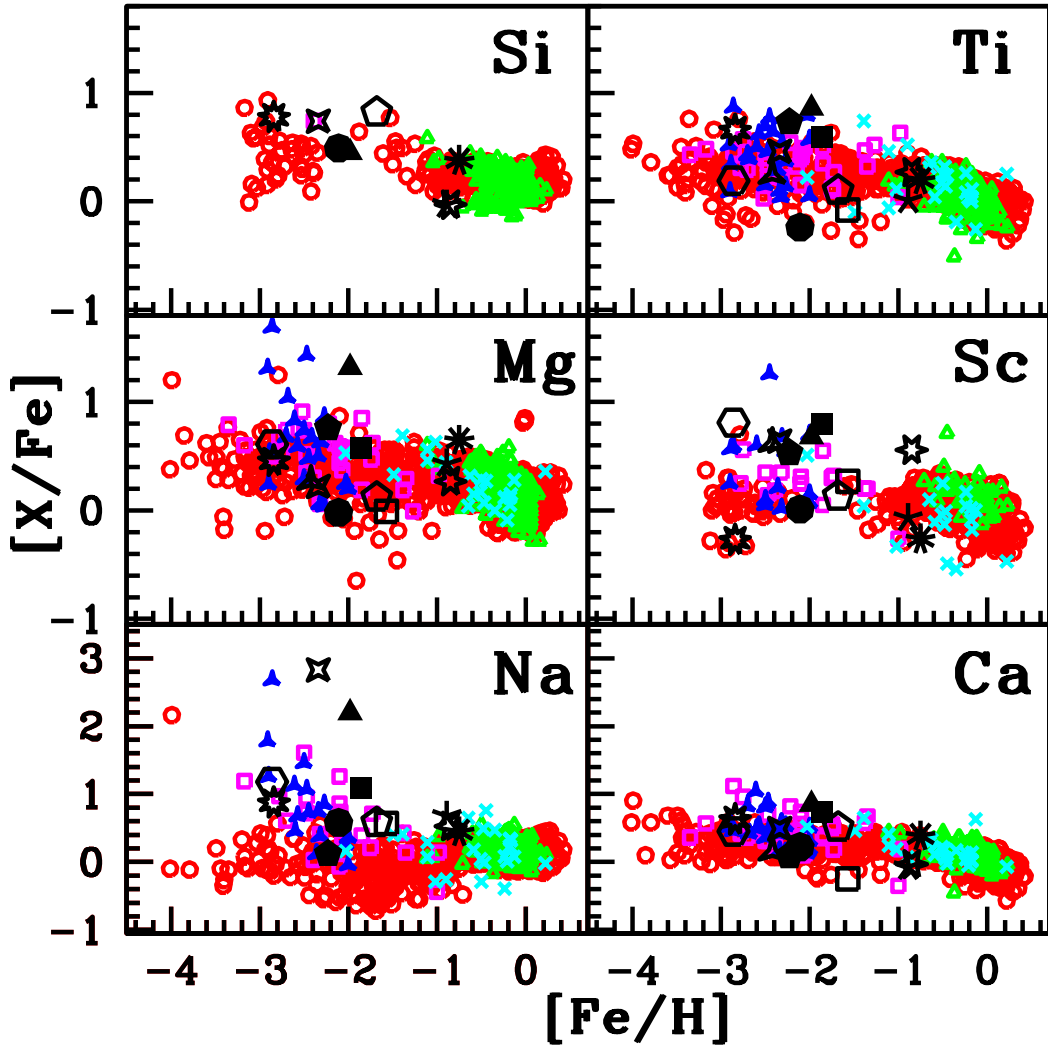


FIGURE 4.6: Observed $[X/\text{Fe}]$ ratios of the light elements in the program stars with respect to metallicity $[\text{Fe}/\text{H}]$. Red open circles represent normal giants from literature (Honda *et al.* 2004; Venn *et al.* 2004; Aoki *et al.* 2005, 2007; Reddy *et al.* 2006; Luck and Heiter 2007; Hansen *et al.* 2016a; Yoon *et al.* 2016). Magenta open squares and blue starred triangles are CEMP-s and CEMP-r/s stars respectively from literature (Masseron *et al.* 2010; Purandardas *et al.* 2019; Karinkuzhi *et al.* 2021; Purandardas and Goswami 2021). Cyan crosses and green open triangles are CH (Vanture 1992; Karinkuzhi and Goswami 2014, 2015; Goswami *et al.* 2016) and Ba stars (Allen and Barbuy 2006; de Castro *et al.* 2016; Yang *et al.* 2016; Karinkuzhi *et al.* 2018a; Shejee-lammal *et al.* 2020) respectively from literature. BD-19 132 (filled square), BD-19 290 (open hexagon), HD 30443 (open pentagon), HE 0457-1805 (filled triangle), LAMOSTJ091608.81+230734.6 (five-sided cross), HE 0920-0506 (nine-sided cross), HE 1157-0518 (starred triangle), HE 1304-2111 (four-sided star), HE 1327-2116 (nine-sided star), HE 1354-2257 (filled circle), LAMOSTJ151003.74+305407.3 (open square), BD+19 3109 (filled pentagon), and HD 202851 (six-sided star).

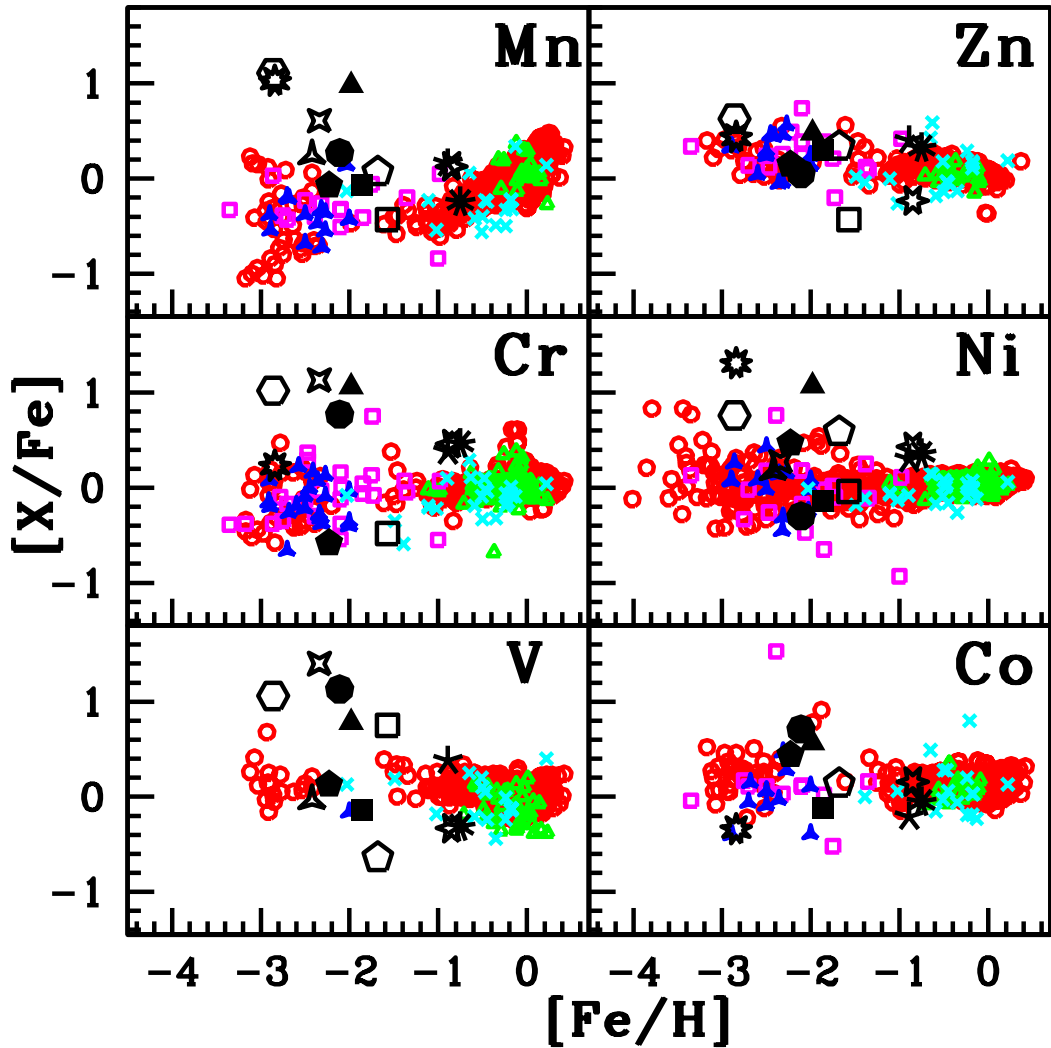


FIGURE 4.7: Observed $[X/\text{Fe}]$ ratios of the light elements in the program stars with respect to metallicity $[\text{Fe}/\text{H}]$. Symbols have the same meaning as in Figure 4.6.

HERMES. It is enhanced in BD–19 290 and HE 0457–1805 with $[\text{Rb}/\text{Fe}] > 1$, shows near-solar value in the stars: BD–19 132, HD 30443, HE 0920–0506, LAMOSTJ151003.74+305407.3, BD+19 3109, and HD 202851, whereas LAMOSTJ091608.81+230734.6 shows a mild enhancement with $[\text{Rb}/\text{Fe}] \sim 0.47$.

Strontium abundance is derived from the spectral synthesis calculation of Sr I 4607.327 Å line, with $\log g f$ value taken from Bergemann *et al.* (2012). We could estimate strontium abundance only in seven objects; BD–19 132, HD 30443,

HE 0457–1805, LAMOSTJ091608.81+230734.6, HE 0920–0506, HE 1354–2257, and HD 202851, and they show $[\text{Sr}/\text{Fe}] \geq 0.74$. It has been proven that the Sr I lines are affected by NLTE effects (Barklem and O’Mara 2000; Short and Hauschildt 2006). The NLTE corrections of Sr I 4607.327 Å line is adopted from Bergemann *et al.* (2012). They have calculated the NLTE corrections for different combinations of stellar atmospheric parameters for four different stars. For the star HD 122563, the NLTE correction is +0.47 dex, which has got similar atmospheric parameters ($T_{\text{eff}} = 4600$ K, $\log g = 1.60$, $\zeta = 1.80$ km s $^{-1}$, $[\text{Fe}/\text{H}] = -2.50$) as BD–19 132, HD 30443, HE 0457–1805, LAMOSTJ091608.81+230734.6, and HE 1354–2257. For these stars, we have applied this correction term to our estimated abundance of Sr. For the stars HE 0920–0506 and HD 202851, the NLTE correction ($\sim +0.17$ and $+0.32$ dex) has been taken from Table 3 of Bergemann *et al.* (2012), which corresponds to a similar combination of atmospheric parameters as them. The spectrum synthesis fits for Sr I 4607.327 Å line for the program stars are shown in Figure 4.8

The yttrium abundance is derived from Y I 6435.004 Å line using spectrum synthesis calculation, and also using the equivalent width measurements of the Y II lines listed in Table B2 (Appendix B, Section 4.13). We could not estimate Y I abundances in BD–19 290, HD 30443, HE 1157–0518, HE 1304–2111, and HE 1327–2116, and Y II abundance in HE 1354–2257 as no good lines are detected in their spectra due to these species. It is enhanced in all the program stars with $[\text{X}/\text{Fe}] \geq 0.69$. The zirconium abundance is estimated using the spectral synthesis calculation of Zr I 6134.585 Å and Zr II 5112.297 Å, and equivalent width measurement of several Zr I and Zr II lines whenever available. We could not estimate Zr I abundance in HE 1157–0518, and Zr II abundance in HD 30443 and HE 1354–2257. The abundance estimated from Zr I lines are in the range 0.63 - 2.43, and that from Zr II lines are in the range 0.55 - 2.06.

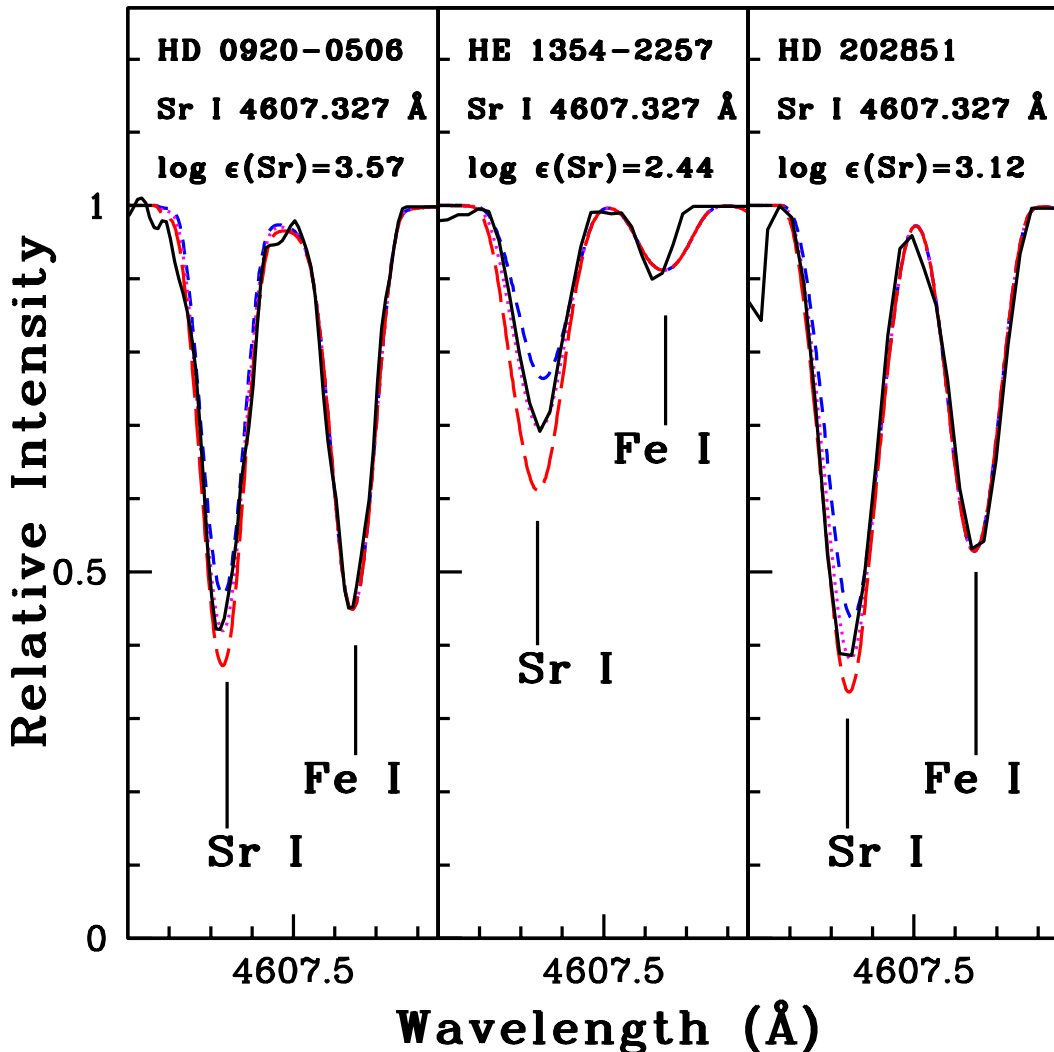


FIGURE 4.8: Synthesis of Sr I line at 4607.327 Å. Dotted and solid lines represent synthesized and observed spectra respectively. short-dashed and long-dashed lines represent the synthetic spectra for $\Delta[\text{Sr}/\text{Fe}] = -0.3$ and $+0.3$ respectively.

4.4.2.2 The heavy s-process elements: Ba, La, Ce, Pr, Nd

The barium abundance is derived from the spectral synthesis calculation of Ba II 5853.668 Å line in BD-19 132, HD 30443, HE 0457-1805, LAMOSTJ091608.81+230734.6, HE 0920-0506, HE 1157-0518, HE 1327-2116, and HD 202851. This line is blended in all other stars and could not be used for abundance determination. This line is known to be affected by NLTE effect. The NLTE corrections to the

abundance derived from this line are adopted from Andrievsky *et al.* (2009), which are +0.22, 0.00, 0.00, 0.00, 0.00, +0.41, +0.28, and +0.35 dex, respectively for the above objects. The Ba II 4934.076, 6141.713, and 6496.897 Å lines are also used for the estimation of Ba abundance. The line list for Ba II 6496.897 Å line is taken from linemake[†] atomic and molecular line database (Placco *et al.* 2021). The hyperfine components of other lines are taken from McWilliam (1998). Barium is enhanced in all the program stars with $[\text{Ba}/\text{Fe}] > 1$. The spectral synthesis fits for Ba II 5853.668 and 6141.713 Å lines are shown in Figure 4.9.

Spectral synthesis calculation of La II 4748.726, 4921.776, 5259.379, 5301.969, 5303.528 Å lines, whenever available, is used to derive the abundance of lanthanum in the program stars. The hyperfine components of La II 4921.776 Å line are taken from Jonsell *et al.* (2006), and 5301.969, 5303.528 Å lines from Lawler *et al.* (2001), whereas it is not available for 4748.726 and 5259.379 Å lines. We could not find any useful lines due to La in the star HE 1157–0518 for abundance determination. In all other stars, it is enhanced with $[\text{La}/\text{Fe}] \geq 1.25$ with BD–19 132 showing the highest enhancement of $[\text{La}/\text{Fe}] \sim 2.66$. Equivalent width measurements of several spectral lines were used to derive the abundances of Ce, Pr, and Nd. All these elements are enhanced in all our program stars with $[\text{X}/\text{Fe}] > 1.0$.

Finally, the $[\text{ls}/\text{Fe}]$, $[\text{hs}/\text{Fe}]$, and $[\text{hs}/\text{ls}]$ ratios of the program stars are estimated. We have also estimated the $[\text{s}/\text{Fe}]$ ratio, an indicator of total s-process content of the star (s refers to the s-process elements Sr, Y, Zr, Ba, La, Ce, and Nd). The neutron-density dependent $[\text{Rb}/\text{Zr}]$ ratio is also estimated. The values for these ratios are given in Table 4.4.

[†]linemake contains laboratory atomic data (transition probabilities, hyperfine and isotopic substructures) published by the Wisconsin Atomic Physics and the Old Dominion Molecular Physics groups. These lists and accompanying line list assembly software have been developed by C. Sneden and are curated by V. Placco at <https://github.com/vmplacco/linemake>.

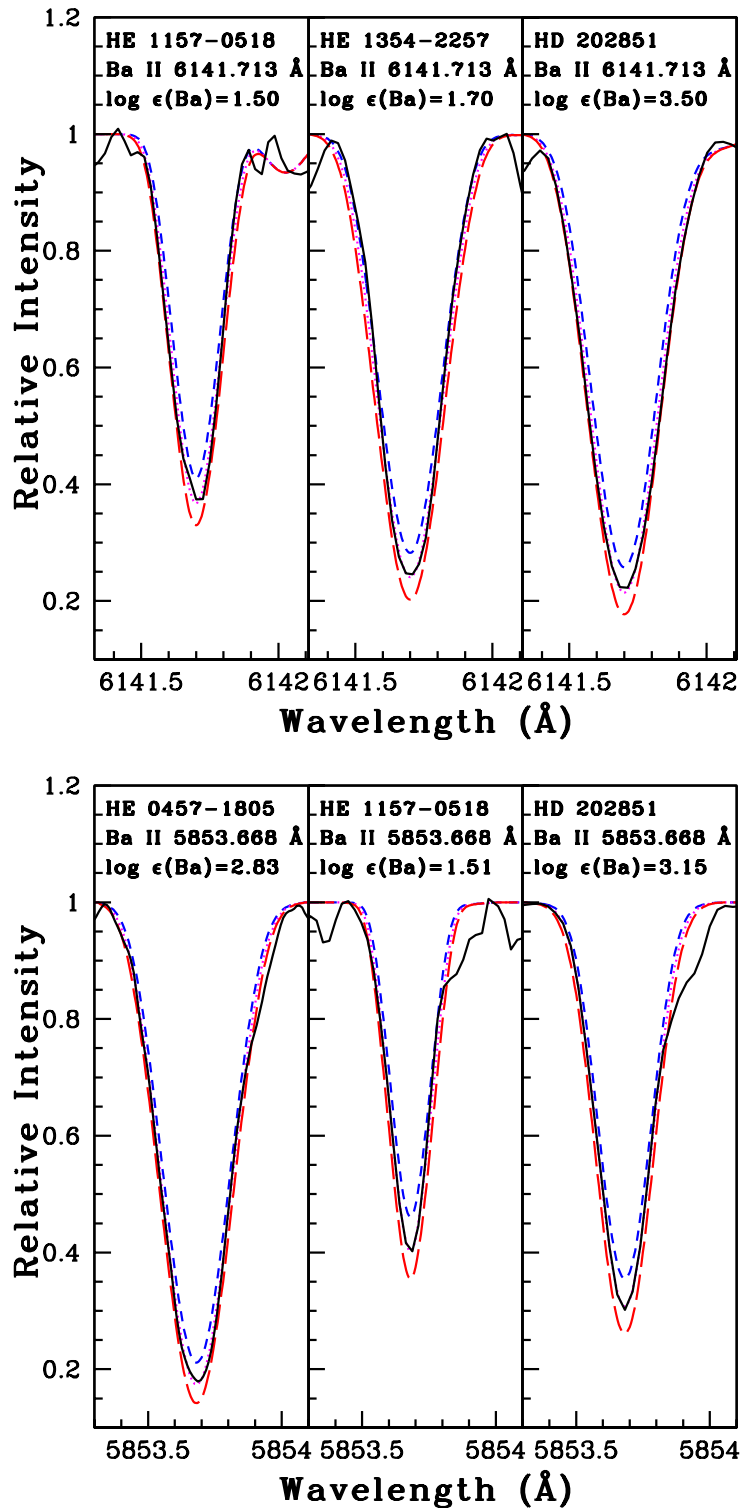


FIGURE 4.9: Synthesis of Ba II 5853.668 Å (lower panel) and 6141.713 Å (upper panel) lines. Dotted and solid lines represent synthesized and observed spectra respectively. short-dashed and long-dashed lines represent the synthetic spectra for Δ [Ba/Fe] = -0.3 and $+0.3$ respectively.

TABLE 4.4: Estimates of [ls/Fe], [hs/Fe], [s/Fe], [hs/ls], [Rb/Zr]

Star name	[Fe/H]	[ls/Fe]	[hs/Fe]	[s/Fe]	[hs/ls]	[Rb/Zr]
BD-19 132	-1.86	1.38	2.52	2.34	1.14	-2.07
BD-19 290	-2.86	1.05	1.89	1.61	0.84	-0.25
HD 30443	-1.68	1.24	2.24	1.81	1.00	-1.54
HE 0457-1805	-1.98	1.88	2.38	2.16	0.50	-1.02
LAMOSTJ091608.81+230734.6	-0.89	1.20	1.57	1.41	0.37	-0.92
HE 0920-0506	-0.75	1.29	1.22	1.15	-0.07	-1.29
HE 1157-0518	-2.42	1.27	1.86	1.37	0.59	-
HE 1304-2111	-2.34	0.98	1.56	1.37	0.58	-
HE 1327-2116	-2.84	0.92	1.75	1.48	0.83	-
HE 1354-2257	-2.11	1.85	1.61	1.71	-0.24	-
LAMOSTJ151003.74+305407.3	-1.57	1.30	1.44	1.40	0.14	-0.99
BD+19 3109	-2.23	0.91	1.64	1.40	0.73	-0.72
HD 202851	-0.85	1.31	1.83	1.61	0.52	-1.95

4.4.2.3 The r-process elements: Sm, Eu

The abundance of samarium is derived from the equivalent width measurements of Sm II lines listed in Table B2 (Appendix B, Section 4.13). The [Sm/Fe] values in our program stars are in the range 1.34 - 2.41. The europium abundance is derived from the spectral synthesis calculation of Eu II 6645.064 Å line in all our program stars. None of the stars has usable 6437.640 Å line for abundance determination. In the stars HE 0920-0506 and HE 1354-2257, we could use Eu II 4129.725 Å line also. This line is affected by NLTE effect, and the appropriate NLTE correction ($\sim +0.16$) is adopted from Mashonkina *et al.* (2008). The hyperfine components of Eu are taken from Worley *et al.* (2013). In HE 0920-0506, Eu is mildly under abundant with $[\text{Eu}/\text{Fe}] \sim -0.20$. All other the stars show enhancement of Eu with $[\text{Eu}/\text{Fe}] \geq 0.7$ except HE 1354-2257 where it is moderately enhanced with

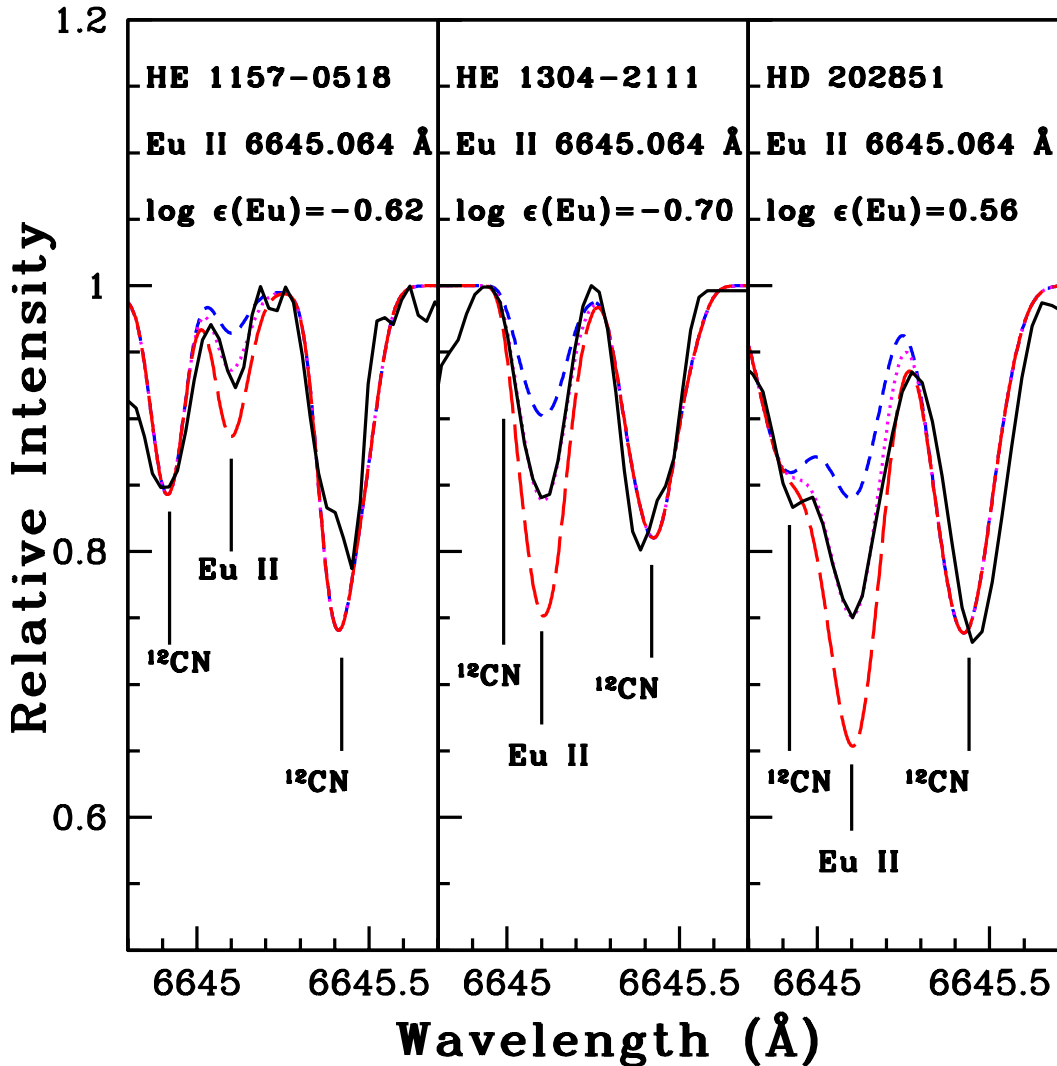


FIGURE 4.10: Synthesis of Eu II 6645.064 Å line. Dotted and solid lines represent synthesized and observed spectra respectively. short-dashed and long-dashed lines represent the synthetic spectra for $\Delta \text{[Eu/Fe]} = -0.3$ and $+0.3$ respectively.

$[\text{Eu}/\text{Fe}] \sim 0.47$. The spectral synthesis fits for Eu II 6645.064 Å line are shown in Figure 4.10.

In Tables 4.5 - 4.8, the abundances derived from the lines showing NLTE effect are given separately after the NLTE correction. Figure 4.11 shows a comparison of the observed abundances of heavy elements in our program stars with their counterparts in normal stars and other chemically peculiar stars. From the figure, it is clear that our program stars show clear over-abundance of heavy elements

TABLE 4.5: Elemental abundances in BD–19 132, BD–19 290, and HD 30443

	Z	BD–19 132			BD–19 290			HD 30443			
		solar log ϵ^*	log ϵ	[X/H]	[X/Fe]	log ϵ	[X/H]	[X/Fe]	log ϵ	[X/H]	
C (C ₂ band 5165 Å)	6	8.43	-	-	-	7.35(syn)	-1.08	1.78	8.43(syn)	0	1.68
C (C ₂ band 5635 Å)	6	8.43	7.27(syn)	-1.16	0.7	7.58(syn)	-0.85	2.01	8.43(syn)	0	1.68
¹² C/ ¹³ C	-	-	-	-	18	-	-	4	-	-	9.33
N	7	7.83	7.43(syn)(3)	-0.40	1.46	6.86(syn)(3)	-0.97	1.89	6.55(syn)	-1.28	0.4
O	8	8.69	7.06(syn)(1)	-1.63	0.23	7.17(syn)(1)	-1.52	1.34	8.42(syn)	-0.27	1.41
Na I	11	6.24	5.47±0.07(2)	-0.77	1.09	4.56±0.13(2)	-1.68	1.18	5.14±0.20(3)	-1.1	0.58
Mg I	12	7.6	6.32±0.02(2)	-1.28	0.58	5.35(1)	-2.25	0.61	6.04±0.13(2)	-1.56	0.12
Si I	14	7.51	-	-	-	-	-	-	6.65±0.05(2)	-0.86	0.82
Ca I	20	6.34	5.21±0.11(4)	-1.13	0.73	3.93±0.05(4)	-2.41	0.45	5.17±0.17(4)	-1.17	0.51
Sc II	21	3.15	2.09(syn)(1)	-1.06	0.8	1.10±0.07(syn)(2)	-2.05	0.81	1.60(syn)	-1.55	0.13
Ti I	22	4.95	3.68±0.14(7)	-1.27	0.59	2.28±0.0(2)	-2.67	0.19	3.37±0.16(9)	-1.58	0.1
Ti II	22	4.95	3.42±0.13(7)	-1.53	0.33	2.17±0.03(3)	-2.78	0.08	3.68±0.25(4)	-1.27	0.41
V I	23	3.93	1.93(syn)(1)	-2.00	-0.14	2.13(syn)(1)	-1.80	1.06	1.61(syn)	-2.32	-0.64
Cr II	24	5.64	-	-	-	3.80±0.10(2)	-1.84	1.02	-	-	-
Mn I	25	5.43	3.50(syn)(1)	-1.93	-0.07	3.68(syn)(1)	-1.75	1.11	3.88(syn)	-1.61	0.07
Fe I	26	7.5	5.64±0.06(19)	-1.86	-	4.64±0.07(12)	-2.86	-	5.82±0.05(11)	-1.68	-
Fe II	26	7.5	5.64±0.01(2)	-1.86	-	4.64±0.13(2)	-2.86	-	5.81±0.11(3)	-1.69	-
Co I	27	4.99	3.01(syn)(1)	-1.98	-0.12	-	-	-	3.45(syn)	-1.54	0.14
Ni I	28	6.22	4.22±0.18(4)	-2.00	-0.14	4.12±0.04(3)	-2.10	0.76	5.13±0.22(3)	-1.09	0.59
Cu I	29	4.19	-	-	-	-	-	-	-	-	-
Zn I	30	4.56	3.00(1)	-1.56	0.3	2.33(1)	-2.23	0.63	3.22(1)	-1.34	0.34
Rb I	37	2.52	0.75(syn)(1)	-1.77	0.09	0.72(syn)(1)	-1.80	1.06	0.90(syn)	-1.62	0.06
Sr I _{NLTE}	38	2.87	3.07(syn)(1)	0.2	2.06	-	-	-	1.93(syn)	-0.94	0.74
Y I	39	2.21	2.43(syn)(1)	0.22	2.08	-	-	-	-	-	-
Y II	39	2.21	2.71±0.13(3)	0.5	2.36	0.38±0.10(2)	-1.83	1.03	1.90±0.04(2)	-0.31	1.37
Zr I	40	2.58	2.88(syn)(1)	0.3	2.16	1.03±0.10(2)	-1.55	1.31	2.50(syn)	-0.08	1.6
Zr II	40	2.58	2.29±0.07(2)	-0.29	1.57	0.78(syn)(1)	-1.80	1.06	-	-	-
Ba II _{LTE}	56	2.18	2.66(syn)(1)	0.48	2.34	1.03(syn)(1)	-1.15	1.71	-	-	-
Ba II _{NLTE}	56	2.18	2.58(syn)(1)	0.4	2.26	-	-	-	2.72(syn)	0.54	2.22
La II	57	1.1	1.90(syn)(2)	0.8	2.66	0.22(syn)(1)	-0.88	1.98	1.40(syn)	0.3	1.98
Ce II	58	1.58	2.20±0.13(3)	0.62	2.48	0.63±0.13(4)	-0.95	1.91	2.18±0.15(4)	0.60	2.28
Pr II	59	0.72	1.43±0.11(3)	0.71	2.57	-0.14±0.12(2)	-0.86	2.00	1.71±0.07(4)	0.98	2.67
Nd II	60	1.42	2.20±0.14(6)	0.78	2.64	0.53±0.13(6)	-0.89	1.97	2.21±0.18(9)	0.79	2.47
Sm II	62	2.41	1.17±0.11(6)	0.21	2.07	0.19±0.02(3)	-0.77	2.09	1.52±0.17(5)	0.56	2.24
Eu II _{LTE}	63	0.52	-0.05(syn)(1)	-0.57	1.29	-1.02(syn)(1)	-1.54	1.32	0.65(syn)	0.13	1.81

* Asplund *et al.* (2009), The number of lines used to determine abundance is indicated in parentheses.

with respect to the normal stars. A comparison of the elemental abundances in the program stars with the literature value is given in Table 4.9.

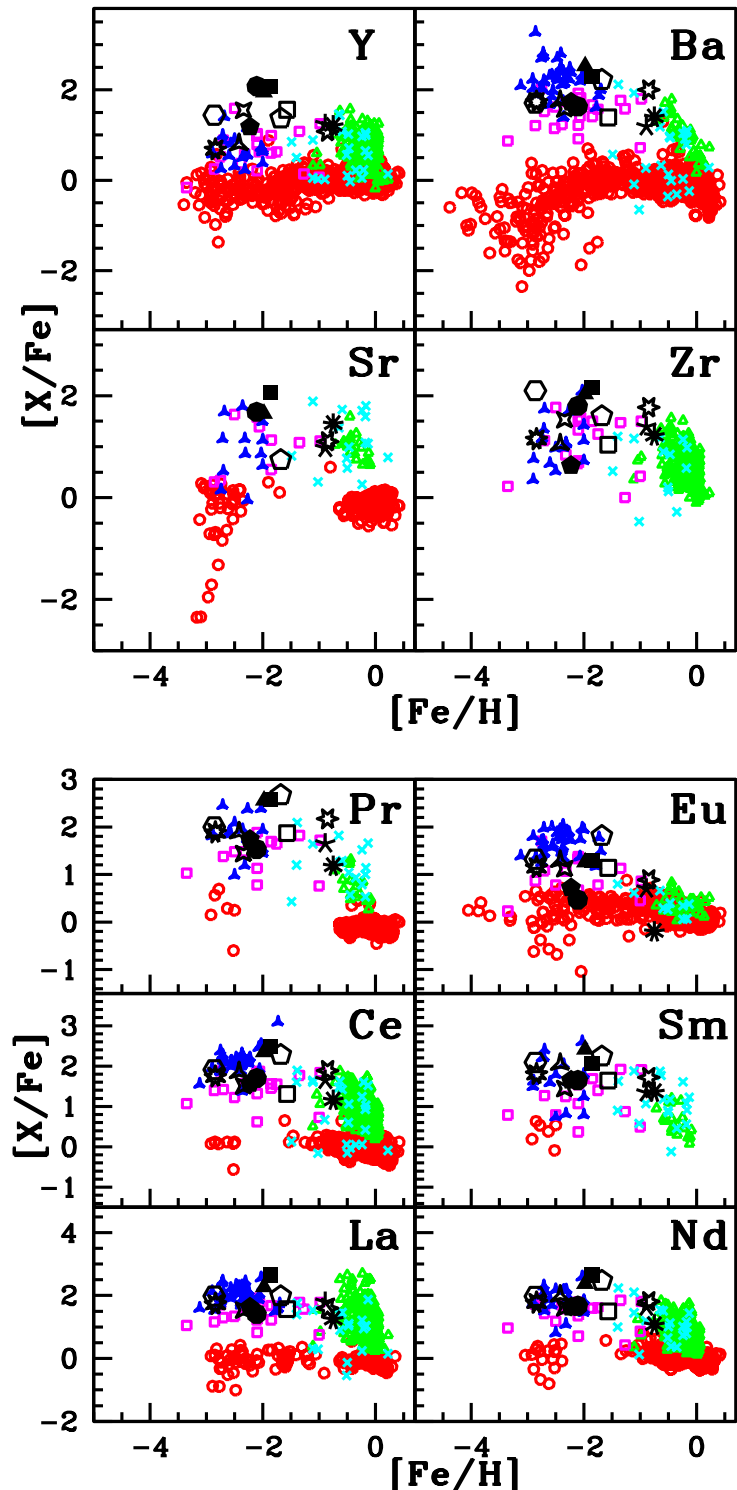


FIGURE 4.11: Observed $[X/\text{Fe}]$ ratios of the heavy elements in the program stars with respect to metallicity $[\text{Fe}/\text{H}]$. Symbols have same meaning as in Figure 4.6

TABLE 4.6: Elemental abundances in HE 0457–1805, LAMOSTJ091608.81+230734.6, and HE 0920–0506

Z	HE 0457–1805			LAMOSTJ091608.81+230734.6			HE 0920–0506				
	solar log ϵ^*	log ϵ	[X/H]	[X/Fe]	log ϵ	[X/H]	[X/Fe]	log ϵ	[X/H]	[X/Fe]	
C (C ₂ band 5165 Å)	6	8.43	8.32(syn)	-0.11	1.87	7.90(syn)	-0.53	0.36	8.20(syn)	-0.23	0.52
C (C ₂ band 5635 Å)	6	8.43	8.17(syn)	-0.26	1.72	7.90(syn)	-0.53	0.36	8.30(syn)	-0.13	0.62
¹² C/ ¹³ C	—	—	—	—	23	—	—	8.67	—	—	—
N	7	7.83	7.52±0.07(syn)(3)	-0.31	1.67	7.79(syn)(3)	-0.04	0.85	7.53±0.20(syn)(3)	-0.30	0.45
O	8	8.69	—	—	—	7.76(syn)	-0.93	-0.04	7.80(syn)(1)	-0.89	-0.14
Na I	11	6.24	6.46±0.06(3)	0.22	2.2	6.03±0.15(4)	-0.21	0.68	5.94±0.09(3)	-0.30	0.45
Mg I	12	7.6	6.94±0.14(2)	-0.66	1.32	7.12±0.15(2)	-0.46	0.43	7.50±0.03(3)	-0.10	0.65
Si I	14	7.51	5.98±0.17(2)	-1.53	0.45	6.59±0.18(3)	-0.92	-0.03	7.14±0.17(2)	-0.37	0.38
Ca I	20	6.34	5.21±0.12(7)	-1.13	0.85	5.38±0.15(10)	-0.96	-0.07	5.98±0.11(16)	-0.36	0.39
Se II	21	3.15	1.85(syn)(1)	-1.30	0.68	2.19(syn)	-0.96	-0.07	2.14(syn)(2)	-1.09	-0.26
Ti I	22	4.95	3.83±0.17(6)	-1.12	0.86	4.07±0.17(12)	-0.88	0.01	4.40±0.08(8)	-0.55	0.2
Ti II	22	4.95	3.40±0.14(5)	-1.55	0.43	3.77±0.17(4)	-1.18	-0.29	4.34±0.08(8)	-0.61	0.14
V I	23	3.93	2.73(syn)(2)	-1.20	0.78	3.42(syn)	-0.51	0.38	2.87(syn)(1)	-1.06	-0.31
Cr I	24	5.64	4.72±0.10(4)	-0.92	1.06	5.13±0.18(6)	-0.51	0.38	5.36±0.09(10)	-0.28	0.47
Cr II	24	5.64	4.58±0.04(2)	-1.06	0.92	—	—	—	5.37±0.07(3)	-0.27	0.48
Mn I	25	5.43	4.43(syn)(2)	-1.00	0.98	4.70(syn)	-0.73	0.16	4.44±0.01(syn)(2)	-0.99	-0.24
Fe I	26	7.5	5.52±0.13(11)	-1.98	—	6.61±0.14(73)	-0.89	—	6.75±0.06(17)	-0.75	—
Fe II	26	7.5	5.52±0.12(4)	-1.98	—	6.61±0.12(6)	-0.89	—	6.75±0.01(3)	-0.75	—
Co I	27	4.99	3.58(syn)(1)	-1.41	0.57	3.89(syn)	-1.10	-0.21	4.19(syn)(1)	-0.80	-0.05
Ni I	28	6.22	5.31±0.08(7)	-0.91	1.07	5.63±0.11(11)	-0.59	0.3	5.83±0.10(10)	-0.39	0.36
Cu I	29	4.19	2.21(syn)(1)	-1.98	0	—	—	—	3.19(syn)(1)	-1.00	-0.25
Zn I	30	4.56	3.10(1)	-1.50	0.48	4.11(1)	-0.49	0.4	4.34±0.12(2)	-0.22	0.53
Rb I	37	2.52	1.95(syn)(1)	-0.57	1.41	2.10(syn)	-0.42	0.47	1.70(syn)(1)	-0.82	-0.07
Sr I _{LTE}	38	2.87	2.54(syn)(1)	-0.33	1.65	2.95(syn)	0.08	0.97	3.57(syn)(1)	0.7	1.45
Y I	39	2.21	3.01(syn)(1)	0.8	2.78	2.56(syn)	0.35	1.24	2.32(syn)(1)	0.11	0.86
Y II	39	2.21	2.18±0.20(4)	-0.03	1.95	2.32±0.10(6)	0.11	1	2.67±0.11(6)	0.46	1.21
Zr I	40	2.58	3.03(syn)(1)	0.45	2.43	3.08(syn)	0.5	1.39	3.05(syn)(1)	0.47	1.22
Zr II	40	2.58	2.63(syn)(1)	0.05	2.03	2.73(syn)	0.15	1.04	2.38(syn)(1)	-0.20	0.55
Ba II _{LTE}	56	2.18	—	—	—	—	—	—	2.83(syn)(1)	0.65	1.4
Ba II _{NLTE}	56	2.18	2.73(syn)(1)	0.55	2.53	2.48(syn)	0.3	1.19	2.83(syn)(1)	0.65	1.4
La II	57	1.1	1.39±0.02(syn)(3)	0.29	2.27	2.00(syn)	0.9	1.79	1.60(syn)(2)	0.5	1.25
Ce II	58	1.58	1.95±0.15(6)	0.37	2.35	2.34±0.11(7)	0.76	1.65	1.99±0.14(6)	0.41	1.16
Pr II	59	0.72	1.30±0.11(6)	0.58	2.56	1.48±0.18(6)	0.76	1.65	1.15±0.03(2)	0.43	1.18
Nd II	60	1.42	1.81±0.11(9)	0.39	2.37	2.17±0.17(9)	0.75	1.64	1.74±0.14(4)	0.32	1.07
Sm II	62	2.41	1.39±0.11(7)	0.43	2.41	1.41±0.11(10)	0.45	1.34	1.57±0.18(4)	0.61	1.36
Eu II _{LTE}	63	0.52	-0.20(syn)(1)	-0.72	1.26	0.33(syn)	-0.19	0.7	-0.39(syn)(1)	-0.91	-0.16
Eu II _{NLTE}	63	0.52	—	—	—	—	—	—	-0.43(syn)(1)	-0.95	-0.20

* Asplund *et al.* (2009), The number of lines used to determine abundance is indicated in parentheses.

4.4.3 Abundance uncertainties

The uncertainty in each elemental abundance is calculated for a representative star HD 202851 using the procedure in Section 2.6.6. The differential abundances, $\Delta \log \epsilon$, for the variations in each stellar atmospheric parameters are given in Table 4.10.

TABLE 4.7: Elemental abundances in HE 1157–0518, HE 1304–2111, and HE 1327–2116

	Z	HE 1157–0518			HE 1304–2111			HE 1327–2116			
		solar log ϵ^*	log ϵ	[X/H]	[X/Fe]	log ϵ	[X/H]	[X/Fe]	log ϵ	[X/H]	[X/Fe]
C (C ₂ band 5165 Å)	6	8.43	8.18(syn)	-0.25	2.17	-	-	-	8.05(syn)	-0.38	2.46
C (C ₂ band 5635 Å)	6	8.43	8.45(syn)	0.02	2.44	8.33(syn)	-0.10	2.24	8.05(syn)	-0.38	2.46
¹² C/ ¹³ C	-	-	-	-	-	-	-	-	-	-	7
N	7	7.83	6.93(syn)	-0.90	1.52	-	-	-	7.50±0.10(syn)(3)	-0.33	2.51
Na I	11	6.24	-	-	-	6.73±0.12(2)	0.49	2.83	4.28(1)	-1.96	0.88
Mg I	12	7.6	5.45(1)	-2.15	0.27	5.46(1)	-2.12	0.22	5.22(1)	-2.38	0.46
Si I	14	7.51	-	-	-	5.91±0.01(2)	-1.60	0.74	5.45(1)	-2.06	0.78
Ca I	20	6.34	4.07±0.13(4)	-2.27	0.15	4.49±0.16(2)	-1.85	0.49	4.13±0.06(5)	-2.21	0.63
Sc II	21	3.15	1.35(syn)(1)	-1.80	0.62	1.45(syn)(1)	-1.70	0.64	0.03±0.01(2)	-3.12	-0.27
Ti I	22	4.95	2.36(1)	-2.59	-0.17	3.07±0.14(3)	-1.88	0.46	2.77±0.02(2)	-2.18	0.66
Ti II	22	4.95	2.59±0.17(3)	-2.36	0.06	2.54(1)	-2.41	-0.07	2.59±0.08(4)	-2.36	0.48
V I	23	3.93	1.75(syn)(1)	-2.18	0.24	2.99±0.23(syn)(2)	-0.94	1.4	-	-	-
Cr I	24	5.64	3.18±0.11(2)	-2.46	-0.04	4.43±0.11(4)	-1.21	1.13	3.03±0.01(2)	-2.61	0.23
Cr II	24	5.64	-	-	-	-	-	-	-	-	-
Mn I	25	5.43	3.25±0.08(syn)(2)	-2.18	0.24	3.70(syn)(1)	-1.73	0.61	3.61±0.03(syn)(2)	-1.81	1.03
Fe I	26	7.5	5.08±0.15(10)	-2.42	-	5.16±0.10(16)	-2.34	-	4.66±0.07(11)	-2.84	-
Fe II	26	7.5	5.08±0.16(2)	-2.42	-	5.16±0.07(3)	-2.34	-	4.66±0.04(2)	-2.84	-
Co I	27	4.99	-	-	-	4.29(syn)(1)	-0.70	1.64	1.81±0.07(2)	-3.18	-0.34
Ni I	28	6.22	3.97±0.10(3)	-2.25	0.17	4.15±0.15(4)	-2.07	0.27	4.69±0.06(3)	-1.53	1.31
Cu I	29	4.19	-	-	-	1.40(syn)(1)	-2.81	-0.47	-	-	-
Zn I	30	4.56	-	-	-	-	-	-	2.16(1)	-2.40	0.44
Y II	39	2.21	0.58±0.08(4)	-1.63	0.79	0.75±0.12(2)	-1.46	0.88	0.06±0.02(2)	-2.15	0.69
Zr I	40	2.58	-	-	-	1.77±0.03(2)	-0.81	1.53	1.81(syn)(1)	-0.77	2.07
Zr II	40	2.58	1.20(syn)(1)	-1.38	1.04	1.32(syn)(1)	-1.26	1.08	0.89(syn)(1)	-1.69	1.15
Ba II _{LTE}	56	2.18	1.50(syn)(2)	-0.68	1.74	1.42±0.05(syn)(2)	-0.76	1.58	-	-	-
Ba II _{NLTE}	56	2.18	1.51(syn)(1)	-0.67	1.75	-	-	-	1.08(syn)(1)	-1.10	1.74
La II	57	1.1	-	-	-	0.30(syn)(2)	-0.80	1.54	0(syn)(1)	-1.10	1.74
Ce II	58	1.58	1.00±0.14(4)	-0.58	1.84	0.75±0.26(2)	-0.83	1.51	0.49±0.10(5)	-1.09	1.75
Pr II	59	0.72	0.18±0.11(4)	-0.54	1.88	-0.06(1)	-0.78	1.56	-0.23(1)	-0.95	1.89
Nd II	60	1.42	0.99±0.14(13)	-0.43	1.99	0.69±0.03(2)	-0.73	1.61	0.36±0.08(8)	-1.06	1.78
Sm II	62	2.41	0.59±0.19(2)	-0.37	2.05	0.06±0.02(2)	-0.90	1.44	-0.07±0.15(4)	-1.03	1.81
Eu II _{LTE}	63	0.52	-0.62(syn)(1)	-1.14	1.28	-0.70(syn)(1)	-1.22	1.12	-1.16	-1.68	1.16

* Asplund *et al.* (2009), The number of lines used to determine abundance is indicated in parentheses.

4.5 Classification of the program stars

All the stars analyzed here are metal-poor objects with [Fe/H] < -1, except LAMOSTJ091608.81+230734.6, HE 0920–0506, and HD 202851 with metallicities [Fe/H]~ -0.89, -0.75, and -0.85. Six objects in the sample are very metal-poor with [Fe/H] < -2. Except LAMOSTJ091608.81+230734.6 and HE 0920–0506 where carbon is moderately enhanced with values 0.36 and 0.57 respectively, all other stars in our sample show enhanced abundance of carbon with [C/Fe] ≥ 0.70 . According to Beers and Christlieb (2005), the stars with [Fe/H] ≤ -2 and [C/Fe] > 1 are Carbon Enhanced Metal-Poor (CEMP) stars. However, a number of stars

TABLE 4.8: Elemental abundances in HE 1354–2257, LAMOSTJ151003.74+305407.3, BD+19 3109, and HD 202851

Z	HE 1354–2257			LAMOSTJ151003.74+305407.3			BD+19 3109			HD 202851			
	solar log ^a	log _e	[X/H]	[X/Fe]	log _e	[X/H]	[X/Fe]	log _e	[X/H]	[X/Fe]	log _e	[X/H]	[X/Fe]
C (C ₂ band 5165 Å)	6	8.43	8.40(syn)	-0.03	2.08	8.60(syn)	0.17	1.74	8.69	0.26	2.49	8.30(syn)	-0.13 0.72
C (C ₂ band 5635 Å)	6	8.43	8.30(syn)	-0.13	1.98	8.60(syn)	0.17	1.74	8.65	0.22	2.45	8.45(syn)	0.02 0.87
¹² C/ ¹³ C	—	—	—	—	—	—	13.33	—	—	9	—	—	42
N	7	7.83	6.23(syn)	-1.60	0.51	7.53(syn)(3)	-0.30	1.27	7.83(syn)(3)	0	2.23	8.40±0.02(syn)(3)	-0.57 1.42
O	8	8.69	7.09(syn)(1)	-1.60	0.51	—	—	—	—	—	8.19(syn)(1)	-0.50 0.35	
Na I	11	6.24	4.71±0.06(2)	-1.53	0.58	5.24±0.05(2)	-1.00	0.57	4.13±0.02(2)	-2.11	0.12	5.92±0.08(3)	-0.32 0.53
Mg I	12	7.6	5.47(1)	-2.13	-0.02	6.20±0.18(3)	-1.58	-0.01	6.13±0.14(3)	-1.47	0.76	7.02±0.10(2)	-0.58 0.27
Si I	14	7.51	5.89±0.16(2)	-1.62	0.49	—	—	—	—	—	6.63(1)	-0.88 -0.03	
Ca I	20	6.34	4.45±0.13(7)	-1.89	0.22	4.52±0.13(8)	-1.82	-0.25	4.20±0.11(7)	-2.14	0.09	5.46±0.14(8)	-0.88 -0.03
Sc II	21	3.15	1.05(syn)(1)	-2.10	0.01	1.85(syn)	-1.30	0.27	1.45(syn)(1)	-1.70	0.53	2.86(syn)(1)	-0.29 0.56
Ti I	22	4.95	2.60(1)	-2.35	-0.24	3.30±0.14(4)	-1.65	-0.08	3.45±0.10(6)	-1.50	0.73	4.37±0.15(13)	-0.58 0.27
Ti II	22	4.95	2.70±0.07(4)	-2.25	-0.14	3.21±0.19(5)	-1.74	-0.17	3.14±0.13(5)	-1.81	0.42	4.40±0.17(9)	-0.55 0.3
V I	23	3.93	2.95(syn)(2)	-0.98	1.13	3.11(syn)	-0.82	0.75	1.833(syn)(1)	-2.10	0.13	2.75(syn)(1)	-1.18 -0.33
Cr I	24	5.64	—	—	—	3.59±0.10(5)	-2.05	-0.48	2.83±0.09(7)	-2.81	-0.58	5.25±0.13(9)	-0.39 0.46
Cr II	24	5.64	4.30±0.08(2)	-1.34	0.77	—	—	—	—	—	—	5.20±0.19(3)	-0.44 0.41
Mn I	25	5.43	3.59(syn)(1)	-1.84	0.27	3.43(syn)	-2.00	-0.43	3.13(syn)(2)	-2.30	-0.07	4.71(syn)(1)	-0.72 0.13
Fe I	26	7.5	5.39±0.17(20)	-2.11	-	5.93±0.12(35)	-1.57	-	5.27±0.09(27)	-2.23	-	6.65±0.01(30)	-0.85 -
Fe II	26	7.5	5.39±0.15(4)	-2.11	-	5.93±0.12(4)	-1.57	-	5.27±0.02(3)	-2.23	-	6.65±0.07(3)	-0.85 -
Co I	27	4.99	3.59(syn)(1)	-1.40	0.71	—	—	—	3.20±0.07(3)	-1.79	0.44	4.30(syn)(1)	-0.69 0.16
Ni I	28	6.22	3.81±0.20(3)	-2.41	-0.30	4.61±0.17(6)	-1.61	-0.04	4.46±0.12(3)	-1.76	0.47	5.80±0.12(11)	-0.42 0.43
Cu I	29	4.19	—	—	—	—	—	—	—	—	—	2.85(syn)(1)	-1.34 -0.49
Zn I	30	4.56	2.50(1)	-2.06	0.05	2.56±0.14(2)	-2.00	-0.43	2.48(1)	-2.08	0.15	3.48(1)	-1.08 -0.23
Rb I	37	2.52	—	—	—	1.00(syn)	-1.52	0.05	0.20(syn)(1)	-2.32	-0.09	1.49(syn)(1)	-1.03 -0.18
Sr I _{NLTE}	38	2.87	2.44(syn)(1)	-0.43	1.68	—	—	—	—	—	—	3.12(syn)(1)	0.25 1.1
Y I	39	2.21	2.18(syn)(1)	-0.03	2.08	2.20(syn)	-0.01	1.56	1.16(syn)(1)	-1.05	1.18	2.44(syn)(1)	0.23 1.08
Y II	39	2.21	—	—	3.05±0.11(2)	0.84	2.4	1.42±0.16(3)	-0.79	1.44	3.05±0.08(4)	0.84 1.69	
Zr I	40	2.58	2.27(syn)(1)	-0.31	1.8	2.05(syn)	-0.53	1.04	0.98(syn)(1)	-1.60	0.63	3.50(syn)(1)	0.92 1.77
Zr II	40	2.58	—	—	—	2.09(syn)	-0.49	1.08	1.28(1)(1)	-1.30	0.93	3.79(syn)(1)	1.21 2.06
Ba II _{LTE}	56	2.18	1.70(syn)(2)	-0.48	1.63	2.00(syn)	-0.18	1.39	1.68(syn)(1)	-0.60	1.73	3.50(syn)(1)	1.32 2.17
Ba II _{NLTE}	56	2.18	—	—	—	—	—	—	—	—	—	3.15(syn)(1)	0.97 1.82
La II	57	1.1	0.40(syn)(1)	-0.70	1.41	1.10(syn)	0	1.57	0.50(syn)(1)	-0.60	1.63	1.85(syn)(2)	0.75 1.6
Ce II	58	1.58	1.17±0.07(4)	-0.41	1.7	1.32±0.13(7)	-0.26	1.31	0.92±0.11(7)	-0.66	1.57	2.62±0.14(8)	1.04 1.89
Pr II	59	0.72	0.14±0.09(3)	-0.58	1.53	1.02±0.11(5)	0.3	1.87	0.23±0.12(4)	-0.49	1.74	2.04±0.14(4)	1.32 2.17
Nd II	60	1.42	0.98±0.13(9)	-0.44	1.67	1.35±0.14(12)	-0.07	1.5	0.82±0.09(14)	-0.60	1.63	2.38±0.11(9)	0.96 1.81
Sm II	62	2.41	0.50±0.08(3)	-0.46	1.65	1.03±0.08(6)	0.07	1.64	0.38±0.11(8)	-0.58	1.65	1.83±0.09(6)	0.87 1.72
Eu II _{LTE}	63	0.52	-1.12(syn)(1)	-1.64	0.47	0.09(syn)	-0.43	1.14	-0.99(syn)(1)	-1.51	0.72	0.56(syn)(1)	0.04 0.89
Eu II _{NLTE}	63	0.52	-1.16(syn)(1)	-1.68	0.43	—	—	—	—	—	—	—	—

* Asplund *et al.* (2009), The number of lines used to determine abundance is indicated in parentheses.

with $[\text{Fe}/\text{H}] < -1$ are identified as CEMP stars in literature (Jonsell *et al.* 2006; Goswami *et al.* 2006; Aoki *et al.* 2007; Goswami and Aoki 2010; Masseron *et al.* 2010; Abate *et al.* 2016; Purandardas *et al.* 2019; Karinkuzhi *et al.* 2021; Goswami *et al.* 2021). Several authors have adopted different lower limits for $[\text{C}/\text{Fe}]$ ratio to define the CEMP stars, for instance, $[\text{C}/\text{Fe}] \geq 0.7$ (Carollo *et al.* 2012; Lee *et al.* 2013; Norris *et al.* 2013a; Skúladóttir *et al.* 2015), $[\text{C}/\text{Fe}] > 0.9$ (Jonsell *et al.* 2006; Masseron *et al.* 2010), $[\text{C}/\text{Fe}] > 1$ (Abate *et al.* 2016; Hansen *et al.* 2019). However, in the case of evolved metal-poor giants, the carbon abundance will be lower compared to their earlier evolutionary stages due to the internal mixing of the CNO processed material from the stellar interiors (Gratton *et al.* 2000; Spite *et al.* 2005, 2006; Aoki *et al.* 2007; Placco *et al.* 2014). This will be discussed in

TABLE 4.9: Comparison of the elemental abundances of our program stars with the literature values.

Star name	[Fe/H]	[C/Fe]	[N/Fe]	[Mg/Fe]	[Ca/Fe]	[Ti/Fe]	[Cr/Fe]	[Mn/Fe]	Ref.
HE 0457–1805	−1.98	1.80	1.67	1.32	0.85	0.86	1.06	0.98	1
	−1.46	0.99	—	—	—	—	—	—	2
HE 0920–0506	−0.75	0.57	0.45	0.65	0.39	0.20	0.47	−0.24	1
	−1.01	0.09	—	—	—	—	—	—	3
	−1.39	1.19	—	—	—	—	—	—	4
HE 1157–0518	−2.42	2.31	1.52	0.27	0.15	0.06	−0.04	0.24	1
	−2.40	2.15	1.56	0.50	0.16	0.09	−0.28	—	5
HE 1327–2116	−2.84	2.46	2.51	0.46	0.63	0.66	0.23	1.03	1
	−2.93	1.11	—	—	—	—	—	—	3
	−2.31	2.73	—	—	—	—	—	—	4
LAMOSTJ151003.74+305407.3	−1.57	1.74	1.27	−0.01	−0.25	−0.08	−0.48	−0.43	1
	−1.35	0.81	—	0.21	0.36	—	0.11	−0.15	6
HD 202851	−0.85	0.72	1.42	0.27	−0.03	0.30	0.46	0.13	1
	−0.70	—	—	—	—	0.00	−0.20	—	7
Star name	[Fe/H]	[Ni/Fe]	[Y/Fe]	[Ba/Fe]	[La/Fe]	[Ce/Fe]	[Nd/Fe]	Ref.	
HE 0457–1805	−1.98	1.06	1.95	2.53	2.27	2.35	2.37	1	
	−1.46	—	—	—	—	—	—	2	
HE 0920–0506	−0.75	0.36	1.21	1.40	1.25	1.16	1.07	1	
	−1.01	—	—	—	—	—	—	3	
	−1.39	—	—	—	—	—	—	4	
HE 1157–0518	−2.42	0.17	0.79	1.75	—	1.84	1.99	1	
	−2.40	—	—	2.14	—	—	—	5	
HE 1327–2116	−2.84	1.31	0.69	1.74	1.74	1.75	1.78	1	
	−2.93	—	—	—	—	—	—	3	
	−2.31	—	—	—	—	—	—	4	
LAMOSTJ151003.74+305407.3	−1.57	−0.04	1.56	1.39	1.57	1.31	1.50	1	
	−1.35	0.07	—	—	—	—	—	6	
HD 202851	−0.85	0.43	1.08	2.00	1.60	1.89	1.81	1	
	−0.70	—	1.30	1.60	1.40	1.30	1.60	7	

References: 1. Our work, 2. Kennedy *et al.* (2011), 3. Frebel *et al.* (2006), 4. Beers *et al.* (2017), 5. Aoki *et al.* (2007), 6. Hayes *et al.* (2018), 7. Sperauskas *et al.* (2016)

TABLE 4.10: Change in the abundances ($\Delta \log \epsilon$) of different elemental species with the variations in stellar atmospheric parameters for the representative star HD 202851 (columns 2 - 5). The rms uncertainty, computed from the random error (σ_{ran}) and the differential abundances given in second to fifth columns, is given in sixth column. Total uncertainty in [X/Fe] of each elemental species is given in seventh column.

Element	ΔT_{eff} (± 100 K)	$\Delta \log g$ (± 0.2 dex)	$\Delta \zeta$ (± 0.2 km s^{-1})	$\Delta [\text{Fe}/\text{H}]$ (± 0.1 dex)	$(\sum \sigma_i^2)^{1/2}$	$\sigma_{[X/\text{Fe}]}$
C	± 0.07	± 0.10	∓ 0.10	± 0.10	0.19	0.24
N	± 0.13	± 0.03	0.00	± 0.02	0.14	0.20
O	0.00	± 0.04	± 0.02	0.00	0.05	0.15
Na I	± 0.06	∓ 0.02	∓ 0.06	∓ 0.01	0.10	0.17
Mg I	± 0.07	∓ 0.06	∓ 0.07	± 0.01	0.10	0.17
Si I	± 0.01	∓ 0.01	∓ 0.07	± 0.01	0.07	0.16
Ca I	± 0.09	∓ 0.02	∓ 0.09	∓ 0.01	0.14	0.20
Sc II	∓ 0.03	± 0.08	∓ 0.10	± 0.03	0.14	0.21
Ti I	± 0.13	∓ 0.01	∓ 0.07	∓ 0.02	0.16	0.21
Ti II	∓ 0.01	± 0.07	∓ 0.11	± 0.03	0.15	0.21
V I	± 0.15	∓ 0.01	∓ 0.04	∓ 0.02	0.16	0.21
Cr I	± 0.12	∓ 0.01	∓ 0.09	∓ 0.01	0.16	0.21
Cr II	∓ 0.07	± 0.08	∓ 0.03	± 0.02	0.16	0.22
Mn I	± 0.10	∓ 0.03	∓ 0.13	∓ 0.01	0.17	0.22
Fe I	± 0.09	± 0.01	∓ 0.11	0.00	0.14	—
Fe II	∓ 0.09	± 0.09	∓ 0.07	± 0.05	0.16	—
Co I	± 0.09	± 0.01	∓ 0.03	0.00	0.10	0.17
Ni I	± 0.07	± 0.01	∓ 0.08	0.00	0.11	0.18
Cu I	± 0.14	∓ 0.01	∓ 0.18	∓ 0.01	0.23	0.27
Zn I	∓ 0.04	± 0.05	∓ 0.09	± 0.02	0.11	0.18
Rb I	± 0.10	0.00	∓ 0.03	0.00	0.11	0.18
Sr I	± 0.14	∓ 0.02	∓ 0.16	± 0.02	0.22	0.26
Y I	± 0.16	0.00	∓ 0.01	∓ 0.01	0.16	0.22
Y II	0.00	± 0.05	∓ 0.14	± 0.03	0.16	0.22
Zr I	± 0.11	∓ 0.01	∓ 0.10	∓ 0.02	0.15	0.21
Zr II	∓ 0.01	± 0.06	∓ 0.19	± 0.02	0.20	0.26
Ba II	± 0.03	± 0.02	∓ 0.07	± 0.05	0.10	0.19
La II	± 0.02	± 0.08	∓ 0.09	± 0.03	0.13	0.20
Ce II	± 0.01	± 0.07	∓ 0.13	± 0.03	0.16	0.22
Pr II	± 0.02	± 0.08	∓ 0.11	± 0.03	0.16	0.22
Nd II	± 0.02	± 0.07	∓ 0.14	± 0.03	0.16	0.23
Sm II	± 0.01	± 0.08	∓ 0.08	± 0.03	0.12	0.20
Eu II	∓ 0.02	± 0.08	∓ 0.02	± 0.03	0.09	0.18

detail in the next section. So, while setting the limit for the [C/Fe] ratio of CEMP stars, the evolutionary stage of the star should also be taken care of. Aoki *et al.* (2007) have taken into consideration the luminosity of the star, which represents the evolutionary stage, to account for the depletion of surface carbon, to set a threshold [C/Fe] that defines CEMP star population. The following empirical definition is given by Aoki *et al.* (2007) for the CEMP stars;

$$[\text{C}/\text{Fe}] \begin{cases} \geq +0.7; & \text{if } \log(L/L_{\odot}) \leq 2.3 \\ \geq +3.0 - \log(L/L_{\odot}); & \text{if } \log(L/L_{\odot}) > 2.3 \end{cases}$$

We have adopted this criteria to define the CEMP stars in our sample, which is demonstrated in Figure 4.12. It is clear from the figure that CEMP stars and non-carbon-enhanced metal-poor stars belong to two different regions of the diagram. Even though the star HD 202851 shows a [C/Fe] value that resembles CEMP stars according to this definition, because of its higher metallicity, $[\text{Fe}/\text{H}] \sim -0.85$, we classify it as a CH star. The stars LAMOSTJ091608.81+230734.6, HE 0920–0506, and HD 202851 are found to be CH stars, whereas all other ten stars in our sample are CEMP stars.

There exist a number of classification schemes in the literature for the sub-classification of CEMP stars (Abate *et al.* 2016; Frebel 2018; Hansen *et al.* 2019), the classification of Beers and Christlieb (2005) being the pioneering one. Beers and Christlieb (2005) and Abate *et al.* (2016) considered [Ba/Fe], [Eu/Fe], and [Ba/Eu] ratios to define CEMP sub-classes, Hansen *et al.* (2019) considered [Sr/Ba] ratio, and Frebel (2018) considered [Sr/Ba], [Sr/Eu], [Ba/Pb], and [La/Eu] ratios. Goswami *et al.* (2021) revisited all these classification schemes, and came up with a slightly modified criteria in terms of [Ba/Eu] and [La/Eu]. We adopted this scheme to sub-classify our CEMP stars which is as follows;

-CEMP-s; $[\text{Ba}/\text{Fe}] \geq 1$

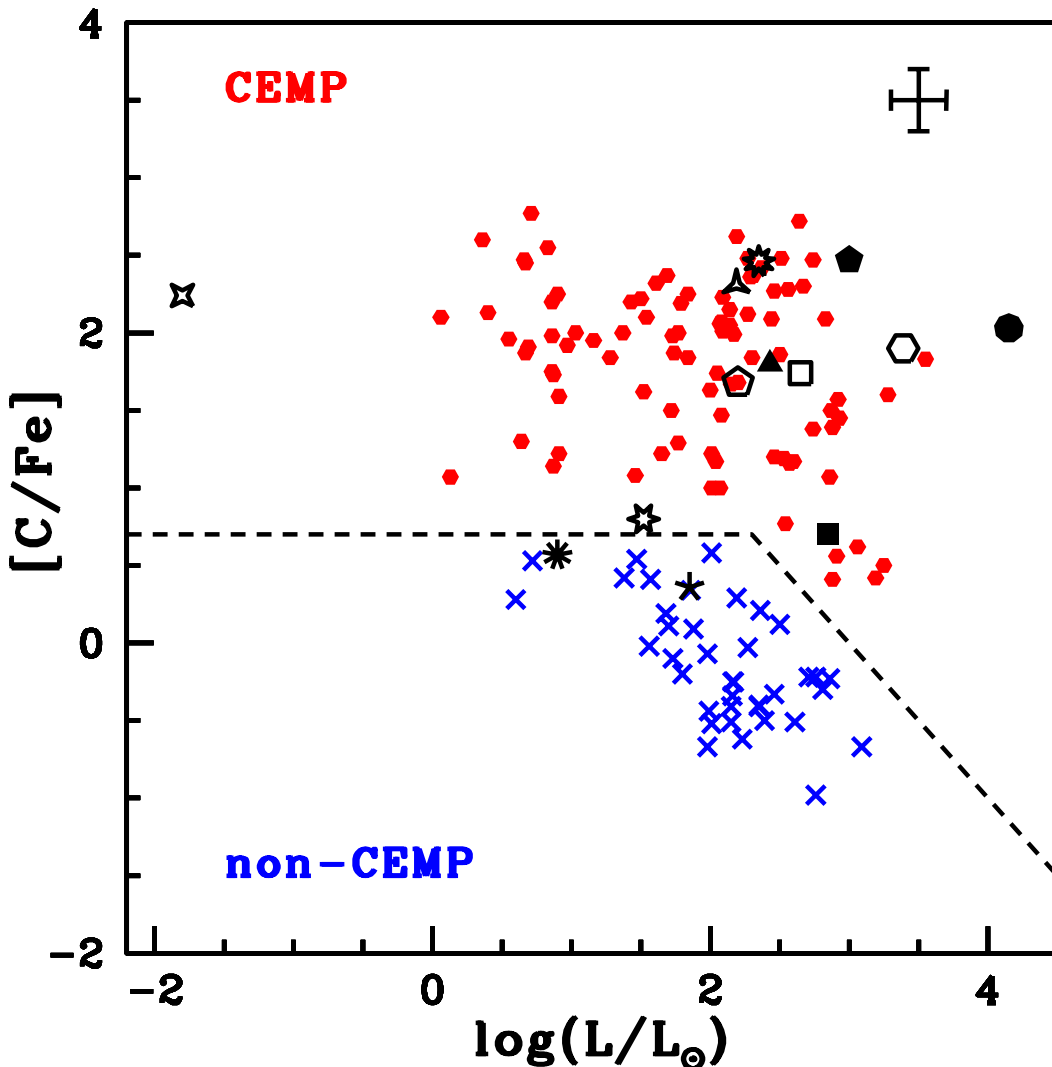


FIGURE 4.12: Observed $[C/Fe]$ ratios as a function of $\log(L/L_\odot)$. Red filled hexagons represent CEMP stars from literature (Aoki *et al.* 2007 and references therein, Goswami *et al.* 2016; Purandardas *et al.* 2019; Karinkuzhi *et al.* 2021; Goswami *et al.* 2021). Blue crosses represent carbon-normal metal-poor stars from literature (Aoki *et al.* 2005, 2007; Cayrel *et al.* 2004; Honda *et al.* 2004). BD-19 132 (filled square), BD-19 290 (open hexagon), HD 30443 (open pentagon), HE 0457-1805 (filled triangle), LAMOSTJ091608.81+230734.6 (five-sided cross), HE 0920-0506 (nine-sided cross), HE 1157-0518 (starred triangle), HE 1304-2111 (four-sided star), HE 1327-2116 (nine-sided star), HE 1354-2257 (filled circle), LAMOSTJ151003.74+305407.3 (open square), BD+19 3109 (filled pentagon), and HD 202851 (six-sided star). The threshold $[C/Fe]$ is shown by the dashed line. A representative error bar is shown at the top right corner.

- (i) $[\text{Eu}/\text{Fe}] < 1$, $[\text{Ba}/\text{Eu}] > 0$, and/or $[\text{La}/\text{Eu}] > 0.5$
- (ii) $[\text{Eu}/\text{Fe}] \geq 1$, $[\text{Ba}/\text{Eu}] > 1$, and/or $[\text{La}/\text{Eu}] > 0.7$

-CEMP-r/s; $[\text{Ba}/\text{Fe}] \geq 1$, $[\text{Eu}/\text{Fe}] \geq 1$

- (iii) $0 \leq [\text{Ba}/\text{Eu}] \leq 1$ and/or $0 \leq [\text{La}/\text{Eu}] \leq 0.7$

Figure 4.13 depicts this classification scheme. The regions marked as (i) and (ii) are two CEMP-s star regions corresponding to the above mentioned conditions (i) and (ii), respectively, and the region marked as (iii) corresponds to CEMP-r/s stars. In this figure, the stars BD-19 290, HD 30443, HE 1157-0518, HE 1304-2111, HE 1327-2116, and LAMOSTJ151003.74+305407.3 occupy the region (iii) and they are found to be CEMP-r/s stars. We could not locate the position of the star HE 1157-0518 in the $[\text{La}/\text{Fe}]$ - $[\text{Eu}/\text{Fe}]$ plot as La abundance could not be estimated in this star. In both the plots, the object HE 0457-1805 clearly lie in the region (ii), and the objects HE 1354-2257 and BD+19 3109 in the region (i), and they are identified to be CEMP-s stars. The star BD-19 132 lies marginally in the region (ii) in the $[\text{Ba}/\text{Fe}]$ - $[\text{Eu}/\text{Fe}]$ plot, but it clearly lies in the region (ii) in the $[\text{La}/\text{Fe}]$ - $[\text{Eu}/\text{Fe}]$ plot; hence, it is identified as a CEMP-s star. The estimated $[\text{C}/\text{Fe}]$, $[\text{Ba}/\text{Eu}]$, and $[\text{La}/\text{Eu}]$ ratios of the program stars are given in Table 4.11.

4.6 Binary status of the program stars

The precise radial velocity monitoring studies have shown that most of the CH stars (McClure and Woodsworth 1990; Jorissen *et al.* 2016b), and a high fraction of CEMP-s and CEMP-r/s stars (Lucatello *et al.* 2005; Starkenburg *et al.* 2014; Jorissen *et al.* 2016b) are in binary systems. The compilation of Duquennoy and Mayor (1991) and Starkenburg *et al.* (2014) have shown the binary fraction of

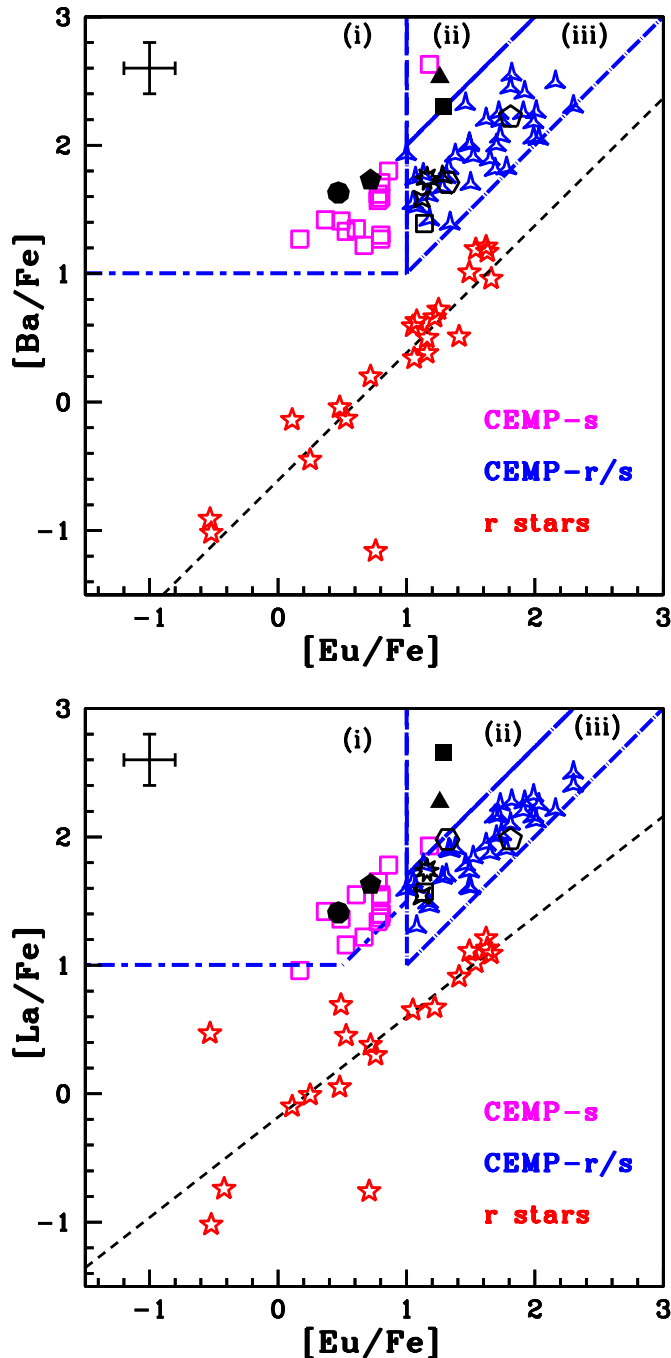


FIGURE 4.13: Observed $[\text{Ba}/\text{Fe}]$ (upper panel) and $[\text{La}/\text{Fe}]$ (lower panel) as functions of observed $[\text{Eu}/\text{Fe}]$ for CEMP and r stars. Magenta squares, blue starred triangles, and red five-sided stars represent CEMP-s, CEMP-r/s, and r (including both CEMP-r and rI/rII stars) stars, respectively from literature (Masseron *et al.* 2010; Karinkuzhi *et al.* 2021; Purandardas *et al.* 2019; Goswami *et al.* 2021). BD-19 132 (filled square), BD-19 290 (open hexagon), HD 30443 (open pentagon), HE 0457-1805 (filled triangle), LAMOSTJ091608.81+230734.6 (five-sided cross), HE 0920-0506 (nine-sided cross), HE 1157-0518 (starred triangle), HE 1304-2111 (four-sided star), HE 1327-2116 (nine-sided star), HE 1354-2257 (filled circle), LAMOSTJ151003.74+305407.3 (open square), BD+19 3109 (filled pentagon), and HD 202851 (six-sided star). Region (i) and (ii) are the CEMP-s, and (iii) is CEMP-r/s star region as given by Goswami *et al.* (2021). The dashed line is the least-square fit to the observed abundances in r-stars. A representative error bar is shown at the top left corner of each panel.

TABLE 4.11: The [C/Fe], [Ba/Eu] and [La/Eu] ratios in the program stars

Star name	[Fe/H]	[C/Fe]	[Ba/Fe]	[La/Fe]	[Eu/Fe]	[Ba/Eu]	[La/Eu]
BD–19 132	−1.86	0.70	2.30	2.66	1.29	1.01	1.37
BD–19 290	−2.86	1.90	1.71	1.98	1.32	0.39	0.60
HD 30443	−1.68	1.68	2.22	1.98	1.81	0.41	0.17
HE 0457–1805	−1.98	1.80	2.53	2.27	1.26	1.43	1.01
LAMOSTJ091608.81+230734.6	−0.89	0.36	1.19	1.79	0.70	0.49	1.09
HE 0920–0506	−0.75	0.57	1.40	1.25	−0.20	1.60	1.45
HE 1157–0518	−2.42	2.31	1.75	—	1.28	0.47	—
HE 1304–2111	−2.34	2.24	1.58	1.54	1.12	0.46	0.42
HE 1327–2116	−2.84	2.46	1.74	1.74	1.16	0.58	0.58
HE 1354–2257	−2.11	2.03	1.63	1.41	0.47	1.16	0.94
LAMOSTJ151003.74+305407.3	−1.57	1.74	1.39	1.57	1.14	0.25	0.43
BD+19 3109	−2.23	2.47	1.73	1.63	0.72	1.01	0.85
HD 202851	−0.85	0.80	2.00	1.60	0.89	1.11	0.71

CEMP-s and CEMP-r/s stars to be 100%. However, a few recent studies have reported a binary frequency of $82\pm10\%$ for CEMP-s and CEMP-r/s stars (Hansen *et al.* 2016c), and $17\pm9\%$ for CEMP-no stars (Hansen *et al.* 2016b).

Our radial velocity estimates, along with those from Gaia (Gaia Collaboration *et al.* 2018), are presented in Table 4.12. Radial velocity data are not available in literature for the stars HE 1157–0518 and HE 1354–2257. The objects HD 30443, HE 0457–1805, BD+19 3109, and HD 202851 are confirmed binaries with periods of 2954 ± 77 days (McClure and Woodsworth 1990), 2724 ± 23 days (Jorissen *et al.* 2016b), 2129 ± 13 , and 1295 ± 6 days respectively (Sperauskas *et al.* 2016). The estimated radial velocities of these objects differ by, ~5 km s $^{-1}$ for BD+19 3109 and HD 202851, ~3 km s $^{-1}$ for HD 30443, and ~2 km s $^{-1}$ for HE 0457–1805, from the literature values available in the Gaia archive. For the objects BD–19 132, BD–19 290, HE 0920–0506, HE 1304–2111, and LAMOSTJ151003.74+305407.3 our estimates show a difference of ~13 , 6, 3, 17, and 4 km s $^{-1}$ respectively from those listed in the Gaia archive. This may be an indication that these stars could possibly be binaries. However, we note that, in the case of LAMOSTJ151003.74+305407.3,

TABLE 4.12: Radial velocity data of the program stars

Star	V_r (km s $^{-1}$) (our estimate)	V_r (km s $^{-1}$) (Gaia)	period (days)
BD-19 132	+3.94±0.81	+16.97±0.79	RV variation
BD-19 290	+106.28±0.90	+111.99±0.73	RV variation
HD 30443	+66.61±0.20	+63.17±0.22	2954±77
HE 0457-1805	+62.83±0.02	+60.80±0.35	2724±23
LAMOSTJ091608.81+230734.6	+16.13±4.30	+17.33±0.40	-
HE 0920-0506	+49.60±0.03	+52.44±1.27	RV variation
HE 1157-0518	+116.02±0.70	-	-
HE 1304-2111	+2.14±0.34	+19.33±0.59	RV variation
HE 1327-2116	+176.77±0.06	+177.43±1.46	-
HE 1354-2257	+289.46±1.80	-	-
LAMOSTJ151003.74+305407.3	-141.58±3.57	-145.25±0.003	RV variation
BD+19 3109	-181.89±1.38	-187.09±1.55	2129±13
HD 202851	+22.22±0.90	+17.38±1.22	1295±6

with the uncertainty in the radial velocity, the lower-limit of our radial velocity estimate is almost consistent with the Gaia value.

Spite *et al.* (2013) have introduced for the first time the existence of low- and high-carbon bands (carbon bimodality) in CEMP stars, and later elaborated by Bonifacio *et al.* (2015) and Hansen *et al.* (2015). Investigation of Yoon *et al.* (2016) showed that majority of the stars with $A(C) > 7.1$ in the $A(C)$ - [Fe/H] diagram belong to binary systems. A detailed discussion on the classification scheme based on the $A(C)$ - [Fe/H] diagram is given in the Section 4.7.1. We have used $A(C)$ - [Fe/H] plot (described in Section 3.5) to understand the binary nature of our program stars. Before using this diagram for this purpose, the carbon abundance should be corrected to account for any internal mixing mentioned in the

previous section. Placco *et al.* (2014) have calculated the corrections to the carbon abundance for $0.0 \leq \log g \leq 5.0$, $-5.5 \leq [\text{Fe}/\text{H}] \leq 0.00$, and $-1.0 \leq [\text{C}/\text{Fe}] \leq 3.0$. We have obtained the corrections to the estimated carbon abundances of our program stars using the public online tool (<http://vplacco.pythonanywhere.com/>) developed by Placco *et al.* (2014). The necessary corrections have been applied to our estimates of carbon abundance and, then used in Figure 4.14. It is to be noted that all our program stars lie in the region of binary stars. This might be a robust indication that all the program stars are likely binaries.

4.7 Abundance profile analysis and interpretations

The detailed analysis of the abundance profiles of the program stars, and their interpretation are discussed here. We have extended the diagnostics to understand the nature of companion AGB stars, discussed in Section 3.6, to the lower metallicity regime.

4.7.1 Carbon, nitrogen, oxygen abundances

The analysis of Spite *et al.* (2013) for a sample of dwarf and main sequence turn-off CEMP stars (~ 50 objects) with $[\text{Fe}/\text{H}] < -1.80$ have shown that the CEMP stars show bimodality in the absolute carbon abundance, that is, they show two distinct absolute carbon abundance $A(\text{C})$ values. The stars with $[\text{Fe}/\text{H}] \geq -3.4$ (CEMP-s and CEMP-r/s) populate the high-carbon region at $A(\text{C}) \sim 8.25$, and the stars with $[\text{Fe}/\text{H}] < -3.4$ (CEMP-no) populate the low-carbon region at $A(\text{C}) \sim 6.80$. This analysis did not consider any giants so as to avoid any carbon dilution resulting from any mixing processes. Later, Bonifacio *et al.* (2015) confirmed the bimodality of CEMP stars from an extended sample of CEMP stars that included dwarfs and

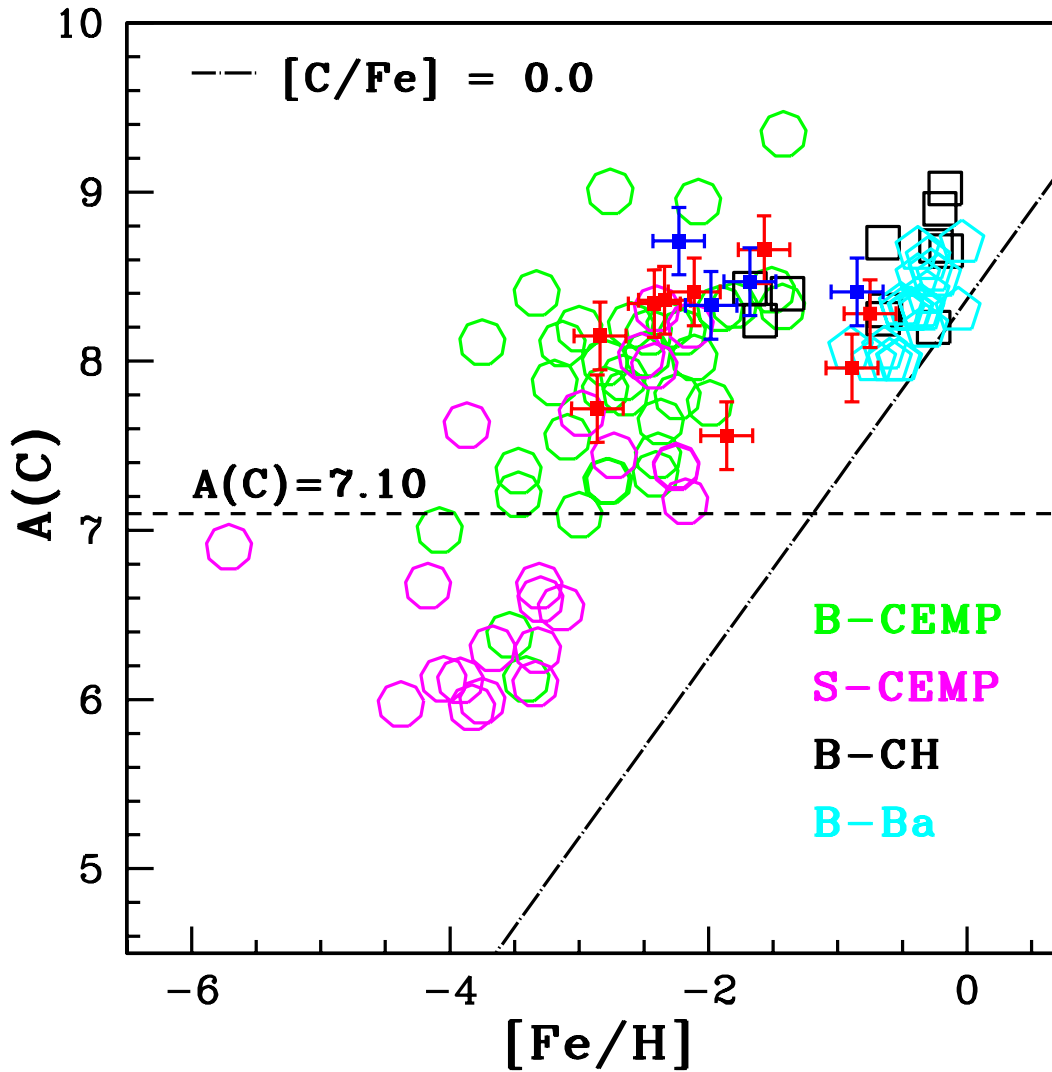


FIGURE 4.14: Distribution of $A(C)$ as a function of $[Fe/H]$ for known (and likely) binary and single stars. The binary and single stars are separated by the dashed line at $A(C) = 7.10$. The long-dash dot line corresponds to $[C/Fe] = 0$. Green and magenta open hexagons represent binary and single CEMP stars, respectively from literature (Yoon *et al.* 2016). Black open squares represent the binary CH stars from literature (Purandardas *et al.* 2019; Karinkuzhi and Goswami 2014, 2015; Luck 2017). Binary Ba stars from literature (Karinkuzhi *et al.* 2018a) are represented by cyan open pentagons. The prefixes B- and S- in the figure imply binary and single stars, respectively. The blue squares represent the confirmed binary program stars, and the red squares represent the program stars with unknown binary status.

main sequence turn-off stars, along with a few sub-giants and lower RGB giants. In both the studies, they noted a clear separation between the two carbon bands. Their interpretation of this bimodality is that the carbon in the stars of these two carbon bands have different astrophysical origin. The carbon in the high-carbon band stars are of extrinsic origin - resulting from the mass transfer from a low-mass AGB companion, and carbon in the low-carbon band stars owe to an intrinsic origin - C-enriched ISM from which they were formed, despite a few of them are binaries as noted by Starkenburg *et al.* (2014) and Bonifacio *et al.* (2015). Subsequently, Hansen *et al.* (2015) also noted the bimodal carbon distribution of CEMP stars for their sample of (\sim 64 objects) CEMP stars. However, they found a smooth transition between the two carbon bands, in contrast to the well separated bands reported by Spite *et al.* (2013) and Bonifacio *et al.* (2015), with three CEMP-no stars occupying the high-carbon band. This observation points to the importance of the knowledge of the binary status of the CEMP stars in order to better constrain the accurate origin of the observed abundances in the CEMP sub-classes.

In an attempt to address this question, Yoon *et al.* (2016) have compiled an extensive set of 305 CEMP stars from literature with $[\text{Fe}/\text{H}] < -1$ and $[\text{C}/\text{Fe}] \geq 0.70$. The sample comprised of 147 CEMP-s and CEMP-r/s stars (together they denoted as CEMP-s stars), and 127 CEMP-no stars, out of which, the binary status of 35 CEMP-s and 22 CEMP-no stars are known. They also noted the carbon bimodality, but at $A(\text{C})$ values lower than that noted by Spite *et al.* (2013); the low- and high-carbon bands peaking at $A(\text{C}) \sim 6.28$ and 7.96, respectively. Based on the behaviour of $A(\text{C})$ with respect to $[\text{Fe}/\text{H}]$, these stars were grouped into three groups; CEMP-s stars being the members of Group I, and CEMP-no stars being members of Group II and III. Their analysis have confirmed the interpretation put forward by Spite *et al.* (2013) and Bonifacio *et al.* (2015) for the origin of carbon. Also they presented the $A(\text{C})$ - $[\text{Fe}/\text{H}]$ diagram as a powerful tool to distinguish between the CEMP-no, CEMP-s, and CEMP-r/s sub-classes. According

to this study, the absolute carbon abundance $A(C) \sim 7.1$ separates the majority of binary stars, which lie above this carbon abundance, from single stars, despite a few outliers. Also, stars with $A(C) \leq 7.1$ are classified as CEMP-no stars, and those with $A(C) > 7.1$ are classified as CEMP-s and CEMP-r/s stars.

The distribution of the $A(C)$ as a function of $[Fe/H]$ for the program stars is shown in Figure 4.15. It is clear from the figure that, at higher metallicities, the carbon abundance show almost similar values (high-carbon band), while the bimodality becomes significant at lower metallicities ($\sim [Fe/H] < -2$). The stars LAMOSTJ091608.81+230734.6, HE 0920–0506, and HD 202851 lie among the CH stars, and other program stars lie among the CEMP-s and CEMP-r/s stars, with all the stars lying in the high-carbon band. It is also noted that all our program stars lie in the region ($A(C) > 7.1$) of binary stars that bear the signatures of binary mass transfer from the low-mass AGB companions according to Bonifacio *et al.* (2015).

As mentioned in the Section 4.5, the surface carbon abundance (as well as nitrogen and oxygen abundances) of a star is related to its evolutionary stage. When a star evolves into a red giant, the surface carbon abundance decreases due to the internal mixing that brings the CNO processed material from the stellar interiors to the surface, known as First Dredge-Up (FDU). Some extra mixing processes in addition to the internal mixing are also found to operate in more evolved giants. Here, the mixing between the surface and the hydrogen burning layer in the upper RGB stars converts C to N through the CNO cycle, and this tends to decrease the carbon abundance further (Charbonnel 1995). This has been observed in more evolved metal-poor field giants (Charbonnel *et al.* 1998; Gratton *et al.* 2000; Spite *et al.* 2005, 2006), and giants in globular and open clusters (Gilroy 1989; Grundahl *et al.* 2002; Shetrone 2003; Jacobson *et al.* 2005). This internal mixing processes result in an increase of nitrogen abundance at the expense of carbon and oxygen (the CN and ON cycles).

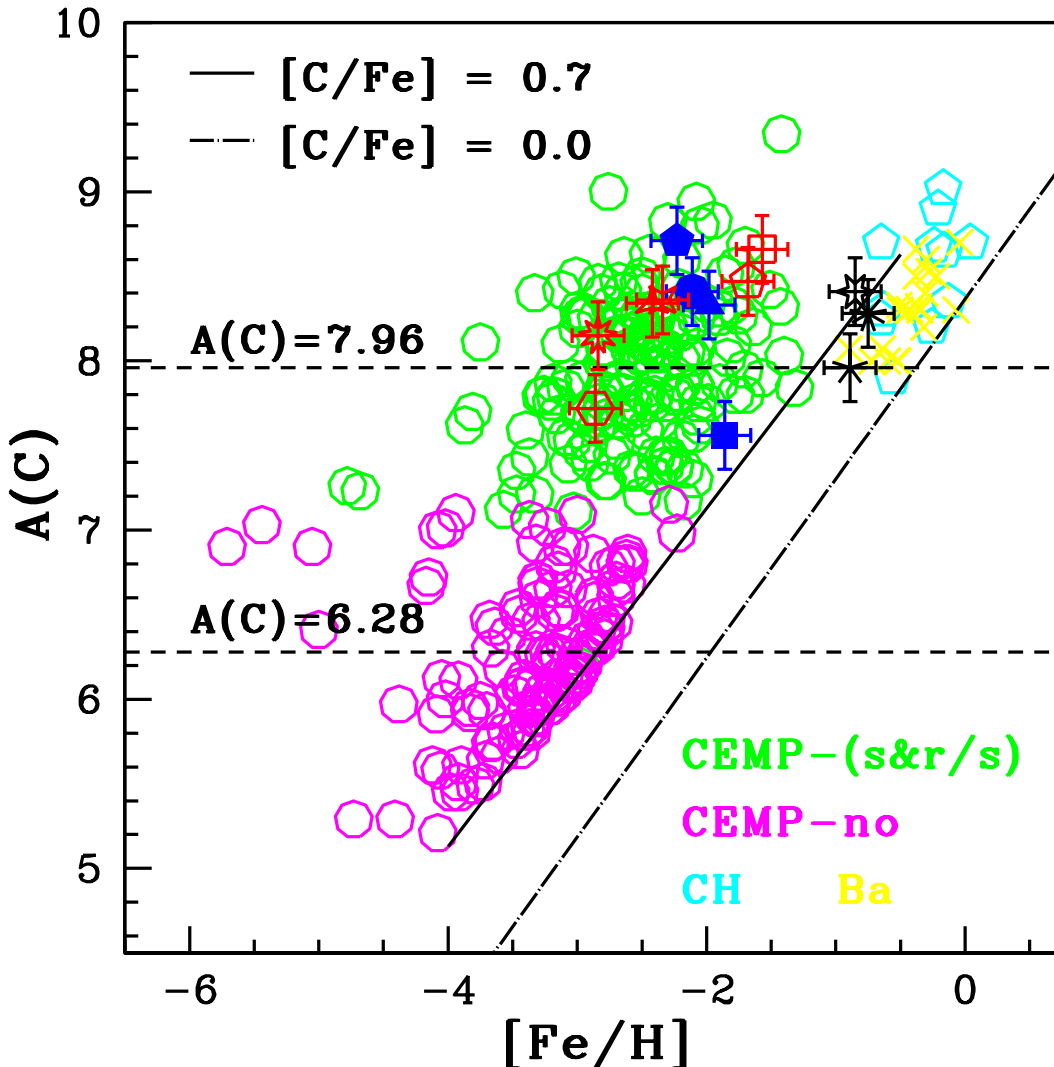


FIGURE 4.15: The $A(C)$ - $[\text{Fe}/\text{H}]$ diagram. Green open hexagons represent CEMP-s and CEMP-r/s stars, and magenta open hexagons represent CEMP-no stars from literature (Yoon *et al.* 2016). Cyan open pentagons are the CH stars from literature (Purandaras *et al.* 2019; Karinkuzhi and Goswami 2014, 2015; Luck 2017). Yellow crosses are the Ba stars from literature (Karinkuzhi *et al.* 2018a; Shejelammal *et al.* 2020). All red, blue, and black symbols, respectively represent CEMP-r/s, CEMP-s, and CH stars of our sample. BD-19 132 (filled square), BD-19 290 (open hexagon), HD 30443 (open pentagon), HE 0457-1805 (filled triangle), LAMOSTJ091608.81+230734.6 (five-sided cross), HE 0920-0506 (nine-sided cross), HE 1157-0518 (starred triangle), HE 1304-2111 (four-sided star), HE 1327-2116 (nine-sided star), HE 1354-2257 (filled circle), LAMOSTJ151003.74+305407.3 (open square), BD+19 3109 (filled pentagon), and HD 202851 (six-sided star). The low- and high-carbon bands at $A(C) = 6.28$ and 7.96 noted by Yoon *et al.* (2016) is shown as dashed lines. The solid line corresponds to $[\text{C}/\text{Fe}] = 0.70$, and long-dash dot line to $[\text{C}/\text{Fe}] = 0$.

From Figure 4.3, and from the estimated $\log g$ values, all our program stars are found to be on the Red Giant Branch (RGB). The observed [C/Fe], [N/Fe], and [O/Fe] ratios of the program stars are shown in Figure 4.16. Carbon abundance is available for all the program stars, nitrogen abundance for twelve stars, and oxygen abundance for seven stars. Nine out of the thirteen program stars show $[C/Fe] > 1$, eight stars show $[N/Fe] > 1$, and two stars show $[O/Fe] > 1$. While the nine objects in our sample show similar [C/Fe] ratio, four objects BD–19 132, LAMOSTJ091608.81+230734.6, HE 0920–0506, and HD 202851, show lowest [C/Fe]. From the Figure 4.16, it is clear that the stars BD–19 132, LAMOSTJ091608.81+230734.6, and HD 202851 are enhanced in nitrogen, and show lower [O/Fe], may be an indication of the CNO cycle and internal mixing. If that is the case, these stars are expected to show low [C/N] and high [N/O] ratio. According to Spite *et al.* (2005), the stars with $[C/N] < -0.6$ are mixed stars, and those with $[C/N] > -0.6$ are unmixed stars. The [C/N] and [N/O] ratios of the program stars are shown in Figure 4.17. The stars BD–19 132 and HD 202851 lie in the region of mixed stars, whereas the star LAMOSTJ091608.81+230734.6 lies marginally in this region, and they show higher [N/O] ratio. Figure 4.16 combined with Figure 4.17 suggest that both the CN and ON cycle might have operated in these stars which altered the surface CNO abundances through mixing. If the nitrogen abundance is altered only due to the CN processing, then the [C+N/Fe] ratios of the mixed and unmixed stars will be similar, with lower $^{12}\text{C}/^{13}\text{C}$ ratio for the mixed stars, and if the ON cycle also contributed to the N enhancement, such stars show [C+N/Fe] excess compared to the unmixed stars of similar metallicity (Spite *et al.* 2005, 2006). The observed [C+N/Fe] ratios of the program stars are shown in Figure 4.18 (left panel). The star BD–19 132, which is a CEMP-s star, lies below the bulk of other CEMP stars in the sample. This star shows lower [C+N/Fe] compared to other CEMP stars. Among the three CH stars (of similar metallicity), LAMOSTJ091608.81+230734.6 and HE 0920–0506 show similar [C+N/Fe] values, indicating that nitrogen enhancement resulted from the CN cycle. However, HD 202851 shows [C+N/Fe] excess

compared to the other two CH stars; this may indicate the occurrence of the ON cycle. To check whether the [C+N/Fe] excess of HD 202851 resulted from the ON cycle, we have estimated the [C+N+O/Fe] abundance of the program stars, and compared with the [C+N+O/Fe] estimate of HD 202851. In the case of the CN and NO cycles in operation, the value of [C+N+O/Fe] ratio of the star should be similar to those observed in other stars. The [C+N+O/Fe] ratios of the program stars are shown in Figure 4.18 (right panel). However, as seen from the figure, HD 202851 shows [C+N+O/Fe] excess compared to other CH stars, and BD-19 132 shows a lower value than the other CEMP stars. Both these stars show similar [C/Fe], [N/Fe], [C+N/Fe], and [C+N+O/Fe] values. BD-19 132 and HD 202851 exhibit relatively higher $^{12}\text{C}/^{13}\text{C}$ ratios (18 and 42 respectively) (Tables 4.5 and 4.8). This suggests that the nitrogen overabundance ($[\text{N}/\text{Fe}] > 1$) in these two stars may not have resulted from an in-situ enhancement. It may be either the signature of a massive AGB companion with Hot-Bottom Burning (HBB), or the nitrogen enhanced primordial matter from which these stars were formed. We will explore the possibility of HBB using different abundance ratios in the next few sections.

4.7.2 The [hs/ls] ratio

Here, we examine another diagnostic of companion AGB star's mass, and indicator of s-process efficiency, the [hs/ls] ratio, where hs stands for heavy s-process elements and ls stands for light s-process elements. At higher neutron exposures, the second peak (hs) s-process elements are produced over the first peak (ls), resulting in high [hs/ls] ratio. Since the neutron exposure increases with decreasing metallicity, the [hs/ls] ratio is anti-correlated with metallicity. Also, the neutron source $^{13}\text{C}(\alpha, n)^{16}\text{O}$ is found to be anti-correlated with metallicity (Clayton 1988; Wallerstein *et al.* 1997). Hence, positive values for [hs/ls] ratio could be seen in low-mass, low-metallicity AGB stars (Goriely and Mowlavi 2000; Busso *et al.*

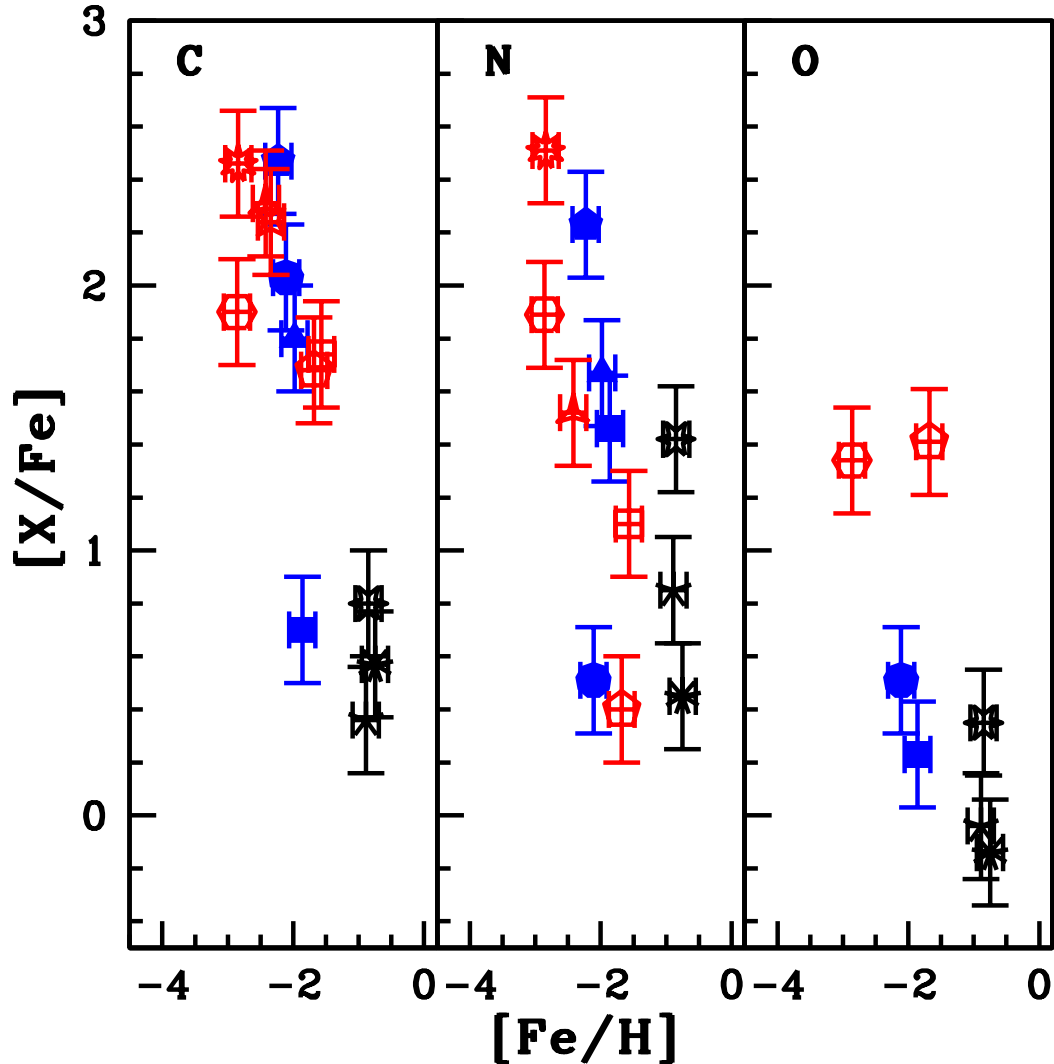


FIGURE 4.16: Observed $[\text{C}/\text{Fe}]$, $[\text{N}/\text{Fe}]$, and $[\text{O}/\text{Fe}]$ as functions of observed $[\text{Fe}/\text{H}]$ for the program stars. Red symbols are CEMP-r/s stars, blue symbols CEMP-s stars, and black symbols CH stars. BD-19 132 (filled square), BD-19 290 (open hexagon), HD 30443 (open pentagon), HE 0457-1805 (filled triangle), LAMOSTJ091608.81+230734.6 (five-sided cross), HE 0920-0506 (nine-sided cross), HE 1157-0518 (starred triangle), HE 1304-2111 (four-sided star), HE 1327-2116 (nine-sided star), HE 1354-2257 (filled circle), LAMOSTJ151003.74+305407.3 (open square), BD+19 3109 (filled pentagon), and HD 202851 (six-sided star).

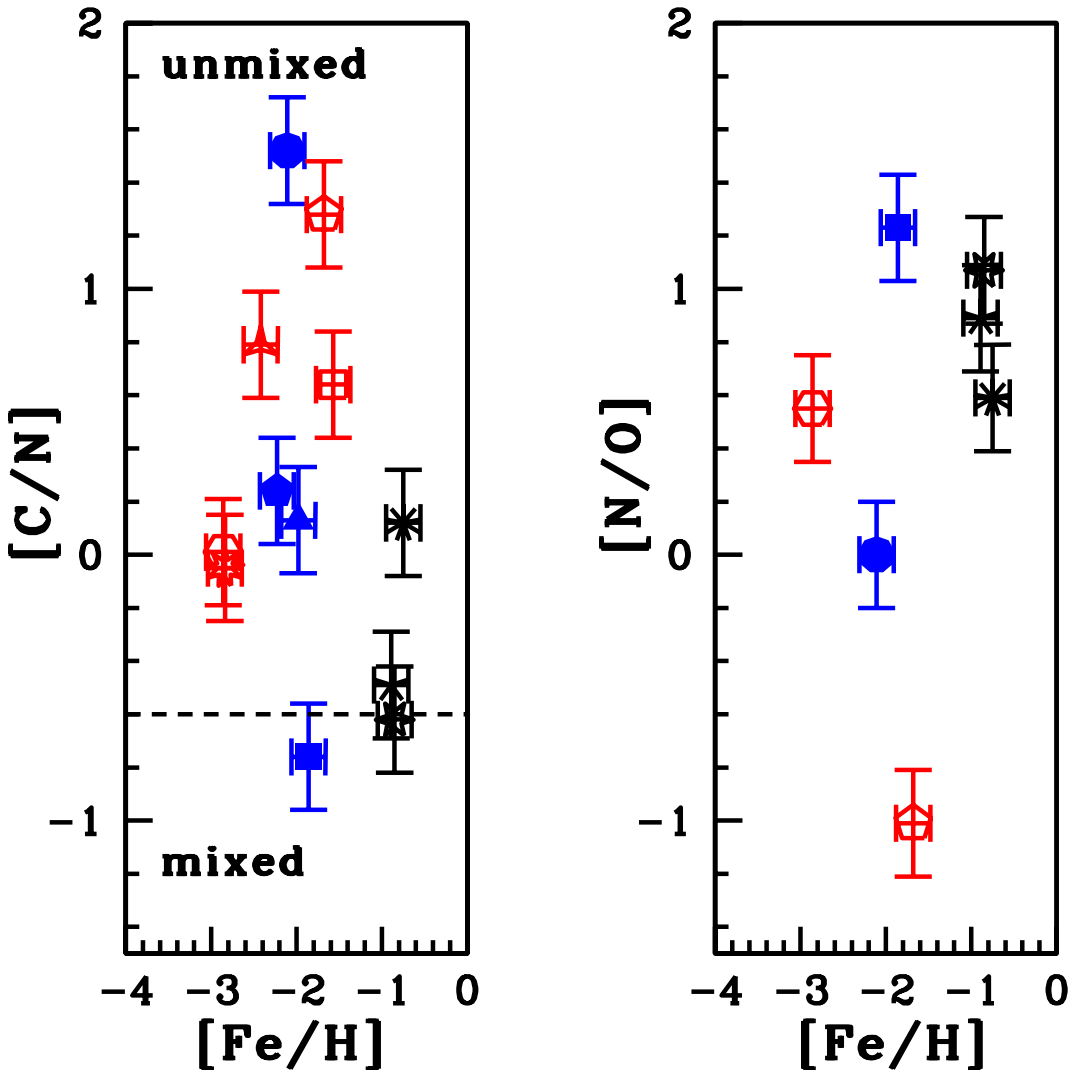


FIGURE 4.17: Observed $[C/N]$ (left panel) and $[N/O]$ (right panel) as functions of observed $[Fe/H]$ for the program stars. BD-19 132 (filled square), BD-19 290 (open hexagon), HD 30443 (open pentagon), HE 0457-1805 (filled triangle), LAMOSTJ091608.81+230734.6 (five-sided cross), HE 0920-0506 (nine-sided cross), HE 1157-0518 (starred triangle), HE 1304-2111 (four-sided star), HE 1327-2116 (nine-sided star), HE 1354-2257 (filled circle), LAMOSTJ151003.74+305407.3 (open square), BD+19 3109 (filled pentagon), and HD 202851 (six-sided star).

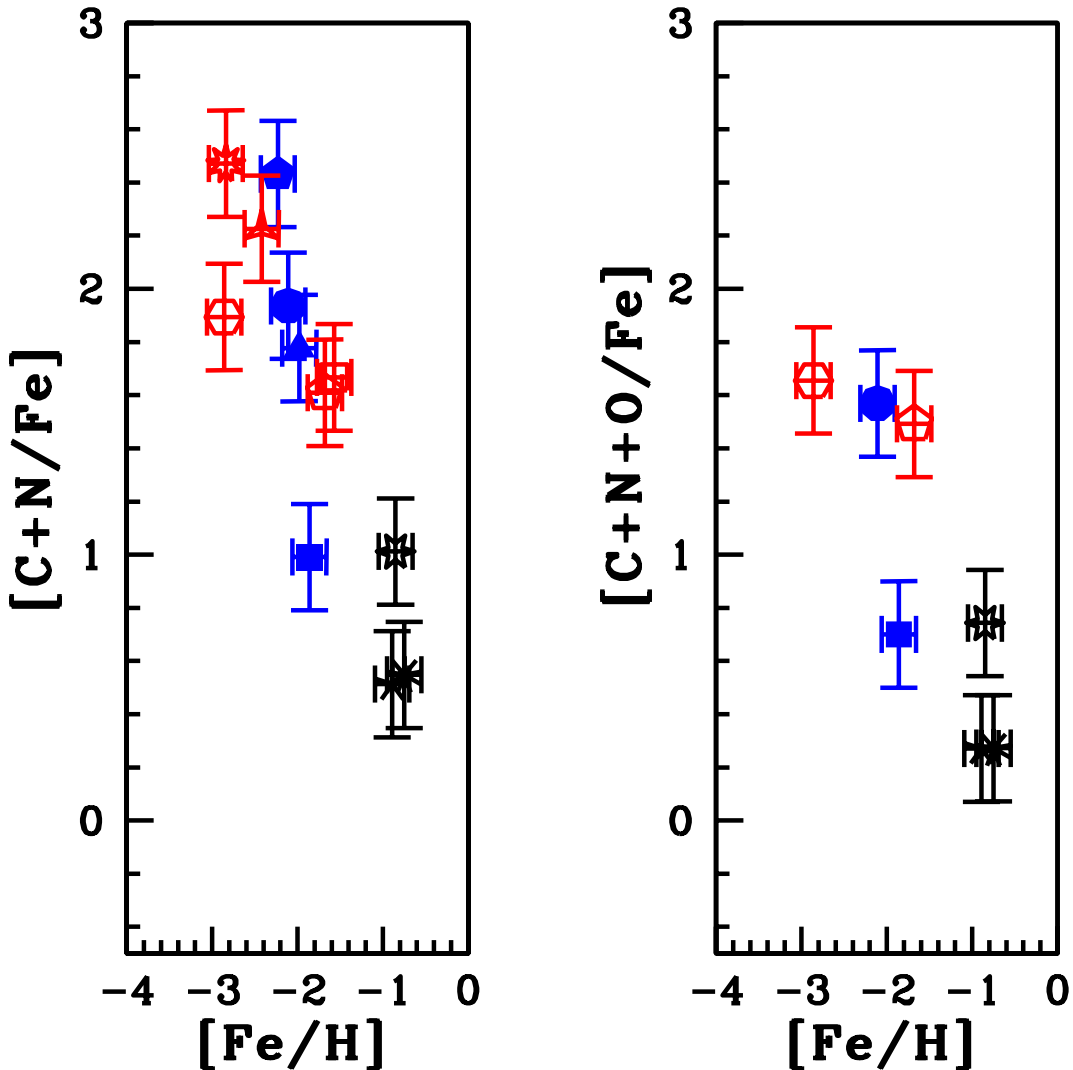


FIGURE 4.18: Observed $[C+N/Fe]$ ratio (left panel) and $[C+N+O/Fe]$ ratio (right panel) as functions of observed $[Fe/H]$ for the program stars. BD-19 132 (filled square), BD-19 290 (open hexagon), HD 30443 (open pentagon), HE 0457-1805 (filled triangle), LAMOSTJ091608.81+230734.6 (five-sided cross), HE 0920-0506 (nine-sided cross), HE 1157-0518 (starred triangle), HE 1304-2111 (four-sided star), HE 1327-2116 (nine-sided star), HE 1354-2257 (filled circle), LAMOSTJ151003.74+305407.3 (open square), BD+19 3109 (filled pentagon), and HD 202851 (six-sided star).

2001), whereas in the case of massive AGB stars ($5 - 8 M_{\odot}$), where the neutron source is $^{22}\text{Ne}(\alpha, n)^{25}\text{Mg}$, this ratio gives negative values (Goriely and Siess 2005; Karakas 2010; Karakas *et al.* 2012; van Raai *et al.* 2012; Karakas and Lattanzio 2014). A detailed discussion on this topic is given in Section 3.6.1.

The CEMP-r/s stars generally show higher [hs/ls] value compared to the CEMP-s stars (Abate *et al.* 2015a; Hollek *et al.* 2015). However, there is no clear distinction observed between the [hs/ls] ratios of the CEMP-r/s and CEMP-s stars. Analysis of Goswami *et al.* (2021) have shown that CEMP-s stars and CEMP-r/s stars peak at [hs/ls] values $\sim 0.65 \pm 0.35$ and 1.06 ± 0.32 , respectively, with an overlap between them in the range $0 < [\text{hs}/\text{ls}] < 1.5$. Karinkuzhi *et al.* (2021) also noted in their sample of CEMP stars the overlap of [hs/ls] ratio between CEMP-s and CEMP-r/s stars. The [hs/ls] ratios observed in our program stars are below 1.50 (Table 4.4), and we could not see any distinction between these two classes of stars in terms of the [hs/ls] ratio (Figure 4.19). All the six CEMP-r/s stars in our sample show positive values of [hs/ls] (Figure 4.19). All the other program stars except HE 0920–0506 and HE 1354–2257 show positive [hs/ls] ratio, indicating a low-mass AGB companion. These two stars have [hs/ls] values of -0.07 and -0.24 , respectively, indicating a clear over-production of ls elements over hs elements, a trend observed in massive AGB stars. In the literature, a few CEMP-s stars are known to show negative values for [hs/ls] ratio. For instance, Hansen *et al.* (2019) present a star HE 2158–5134 that shows $[\text{hs}/\text{ls}] \sim -0.15$, and Aoki *et al.* (2002) noted a value ~ -0.36 for the object CS 22942–019. Analysis of Bisterzo *et al.* (2011) have shown that the abundance pattern in CS 22942–019 could be reproduced by $2.0 M_{\odot}$ AGB model.

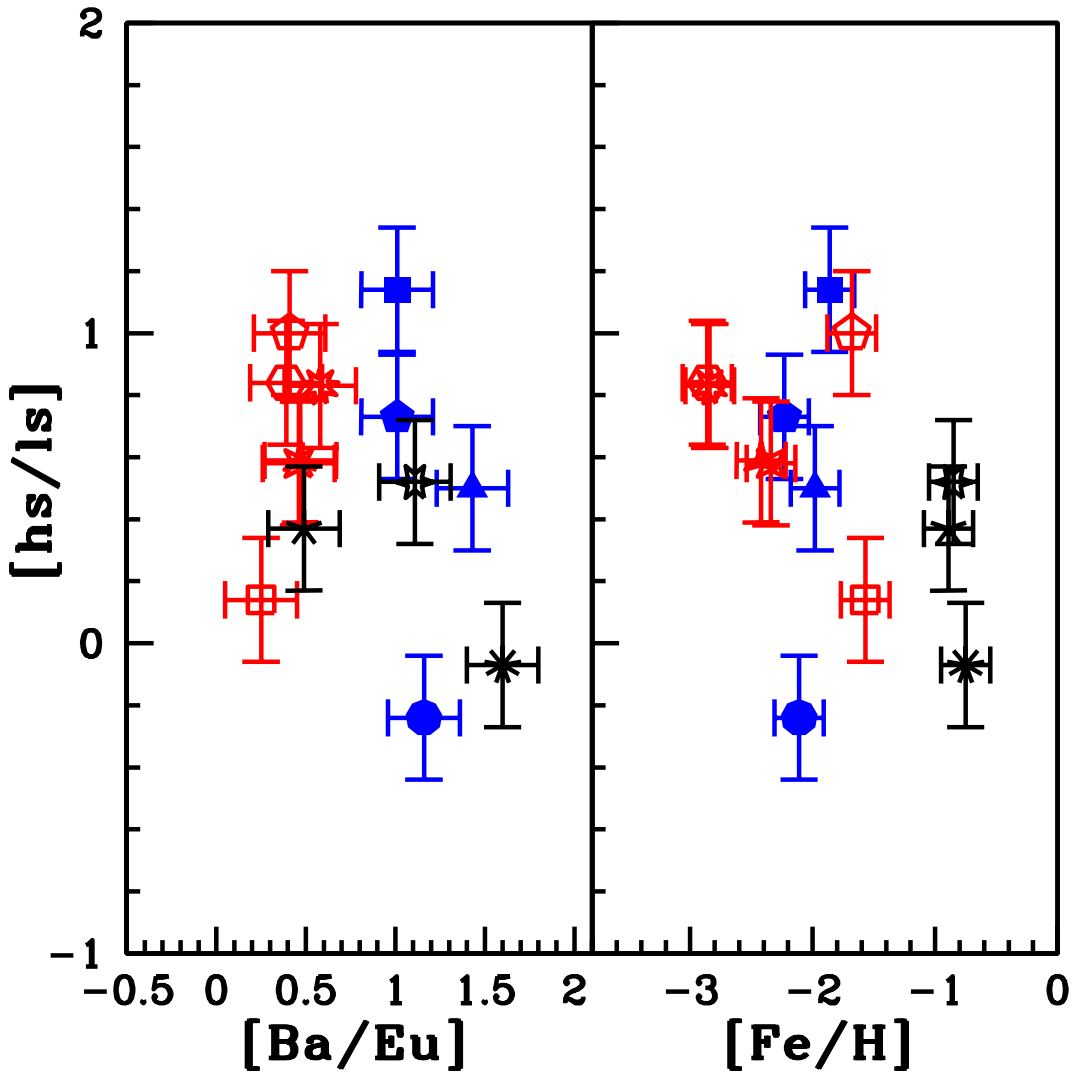


FIGURE 4.19: The [hs/ls] ratio as a function of [Ba/Eu] (left panel) and [Fe/H] (right panel) for the program stars . Red symbols are CEMP-r/s stars, blue symbols CEMP-s stars, and black symbols CH stars. BD–19 132 (filled square), BD–19 290 (open hexagon), HD 30443 (open pentagon), HE 0457–1805 (filled triangle), LAMOSTJ091608.81+230734.6 (five-sided cross), HE 0920–0506 (nine-sided cross), HE 1157–0518 (starred triangle), HE 1304–2111 (four-sided star), HE 1327–2116 (nine-sided star), HE 1354–2257 (filled circle), LAMOSTJ151003.74+305407.3 (open square), BD+19 3109 (filled pentagon), and HD 202851 (six-sided star).

4.7.3 Na, Mg and heavy elements

The detailed discussion on the production mechanisms of Na and Mg is provided in the Section 3.6.3. Four out of the twelve program stars for which we could estimate the Na abundance show enhancement of Na with $[\text{Na}/\text{Fe}] > 1$. The objects HE 0457–1805 and HE 1304–2111 show the largest enhancement with $[\text{Na}/\text{Fe}] \sim 2.20$ and 2.83 respectively. The star HE 0457–1805 is enhanced in magnesium as well with $[\text{Mg}/\text{Fe}] \sim 1.32$. Similar values of Na and Mg enhancement are observed by others in CEMP stars (Aoki *et al.* 2007, 2008), which are considered as extreme cases of Ba-enhanced CEMP stars. The Na enhancement through the Ne - Na cycle is expected in massive AGB stars where HBB operates (Mowlavi 1999b). HBB also results in an increased surface abundance of N through the CN cycle (Sugimoto 1971; Lattanzio *et al.* 1996; Goriely and Siess 2005; Karakas and Lattanzio 2003, 2014; Ventura and D’Antona 2005). Since the HBB is responsible for the over-production of N and Na in massive stars, they should be correlated if the abundance peculiarity is the result of massive AGB star nucleosynthesis. But, we could not see any such trend in our sample of program stars (Figure 4.20, upper panel, left column). The diffusive mixing and H-burning in the massive AGB stars can reduce the s-process efficiency, and it should be anti-correlated with the products of HBB (Goriely and Siess 2005). However, we have not noticed any such behaviour among our program stars (Figure 4.20, upper panel, right column). Enhanced Mg is also expected in the massive AGB stars, resulting from the α -capture reaction of ^{22}Ne . Hence, the same aspects of Na as explained above is expected in the case of Mg too. No such trend is noted for the program stars (Figure 4.20, lower panel). All the Na and Mg enhanced stars in our sample show positive values for the $[\text{hs}/\text{ls}]$ ratio as discussed in the previous section. These facts therefore rule out the possibility of the stars being influenced by the pollution from massive AGB stars with HBB.

The objects HE 0920–0506 and HE 1354–2257 with negative $[\text{hs}/\text{ls}]$, as discussed

in Section 4.7.2, do not show any N, Na, and Mg enhancement. So, this discards the possibility of massive AGB star companions for them. Similarly, for the objects BD–19 132 and HD 202851 (discussed in Section 4.7.1), the possibility of massive AGB star companions is discarded.

The AGB models of Bisterzo *et al.* (2010) predict higher Na and Mg abundances at lower metallicities. They have studied the nucleosynthesis in low-mass AGB stars ($M_{\text{AGB}}^{\text{ini}} \sim 1.3 - 2 M_{\odot}$) of metalliicity [Fe/H] in the range $-3.6 - -1$ and for different ^{13}C pocket efficiency. The major neutron source is the $^{13}\text{C}(\alpha, n)^{16}\text{O}$ reaction during the interpulse phase. The $^{22}\text{Ne}(\alpha, n)^{25}\text{Mg}$ source is also considered to be partially activated during the TP. These models include the production of primary Na through $^{22}\text{Ne}(n, \gamma)^{23}\text{Na}$, and subsequently primary Mg via $^{23}\text{Na}(n, \gamma)^{24}\text{Mg}$, $^{22}\text{Ne}(\alpha, n)^{25}\text{Mg}$, and $^{22}\text{Ne}(\alpha, \gamma)^{26}\text{Mg}$, as described in Section 3.6.3. The amount of the primary Na and Mg produced is shown to increase with decreasing metallicity and/or increasing $M_{\text{AGB}}^{\text{ini}}$ (Figure 15 of Bisterzo *et al.* 2010). Bisterzo *et al.* (2011) performed a comparison of abundance patterns of a sample of 100 CEMP-s stars collected from literature with the AGB nucleosynthesis models of Bisterzo *et al.* (2010). Among this sample, nine stars show $[\text{Na}/\text{Fe}] \geq 1$ with two stars showing $[\text{Na}/\text{Fe}] \sim 2.68$ (CS 29528–028, $[\text{Fe}/\text{H}] \sim -2.86$, Aoki *et al.* 2007) and $[\text{Na}/\text{Fe}] \sim 2.71$ (SDSS 1707+58, $[\text{Fe}/\text{H}] \sim -2.52$, Aoki *et al.* 2008). These two stars are also enhanced in Mg with $[\text{Mg}/\text{Fe}] \sim 1.69$ and 1.13, respectively. The analysis of Bisterzo *et al.* (2011) have shown that the higher Na abundances of CS 29528–028 and SDSS 1707+58 could be reproduced by the AGB models of $M_{\text{AGB}}^{\text{ini}} \sim 1.5 M_{\odot}$. Their higher $[\text{ls, hs}/\text{Fe}]$ values could be reproduced by the $M_{\text{AGB}}^{\text{ini}} \sim 2.0 M_{\odot}$ models. The entire observed abundance pattern could not be reproduced by the same AGB model.

In AGB models, considering the Partial Mixing (PM) of protons, ^{23}Na is produced efficiently, that is almost fifty times higher than that produced in the H-burning

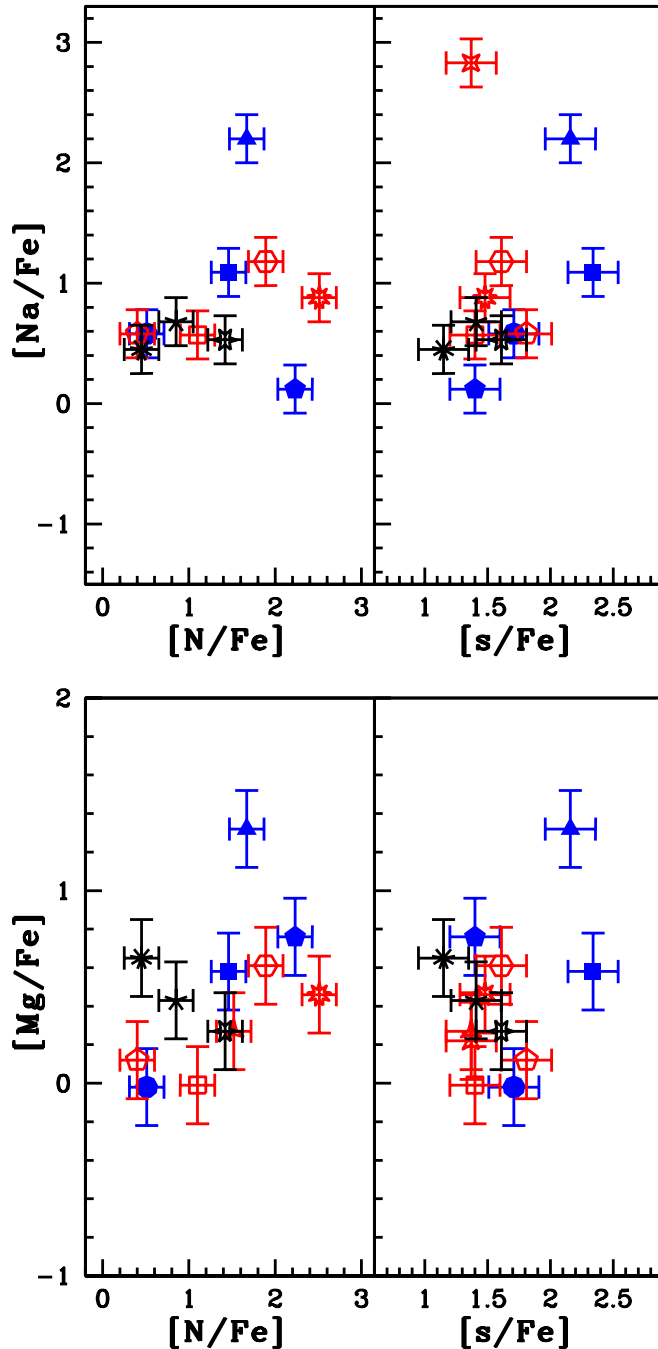


FIGURE 4.20: The observed $[Na/Fe]$ (upper panel) and $[Mg/Fe]$ (lower panel) ratios as a function of $[N/Fe]$ and $[s/Fe]$ for the program stars. Red symbols are CEMP-r/s stars, blue symbols CEMP-s stars, and black symbol CH star. BD-19 132 (filled square), BD-19 290 (open hexagon), HD 30443 (open pentagon), HE 0457-1805 (filled triangle), LAMOSTJ091608.81+230734.6 (five-sided cross), HE 0920-0506 (nine-sided cross), HE 1157-0518 (starred triangle), HE 1304-2111 (four-sided star), HE 1327-2116 (nine-sided star), HE 1354-2257 (filled circle), LAMOSTJ151003.74+305407.3 (open square), BD+19 3109 (filled pentagon), and HD 202851 (six-sided star).

shell (Goriely and Mowlavi 2000). In such a scenario, Na is produced in the inter-shell, in a region above the region of s-process, and a correlation between [Na/Fe] and [s/Fe] is expected. This will entirely depend on the extent of partial mixing zone. However, these models could not explain the least Na-enriched CEMP-s and most Na-enriched CEMP-r/s stars (Figure 19 of Karinkuzhi *et al.* 2021). Better models with improved simulations are needed to explain this.

4.7.4 The [Rb/Zr] ratio

Based on the CNO abundances, [hs/ls] ratio, Na and Mg abundances in the program stars, we have ruled out the possibility of massive AGB companions for our program stars. We have tried to establish an upper limit to the companion’s mass from the neutron-density dependent [Rb/Zr] ratio. Recalling the discussion in Section 3.6.2, massive AGB stars ($M \geq 4 M_{\odot}$) are characterized by positive values of [Rb/Zr] ratio, and low-mass AGB stars ($M \leq 3 M_{\odot}$) by negative values of [Rb/Zr] ratio. The estimated values of the [Rb/Zr] ratio for our program stars are given in Table 4.4. All the nine stars where we could estimate this ratio show a negative value, indicating a low-mass AGB companion. The observed range of [Rb/Fe] and [Zr/Fe] in our program stars, along with those observed in the intermediate-mass AGB stars, is shown in Figure 4.21. It is clear from the figure that the [Rb/Fe] and [Zr/Fe] ratios observed in the program stars do not match closely with their counterparts observed in the intermediate-mass AGB stars.

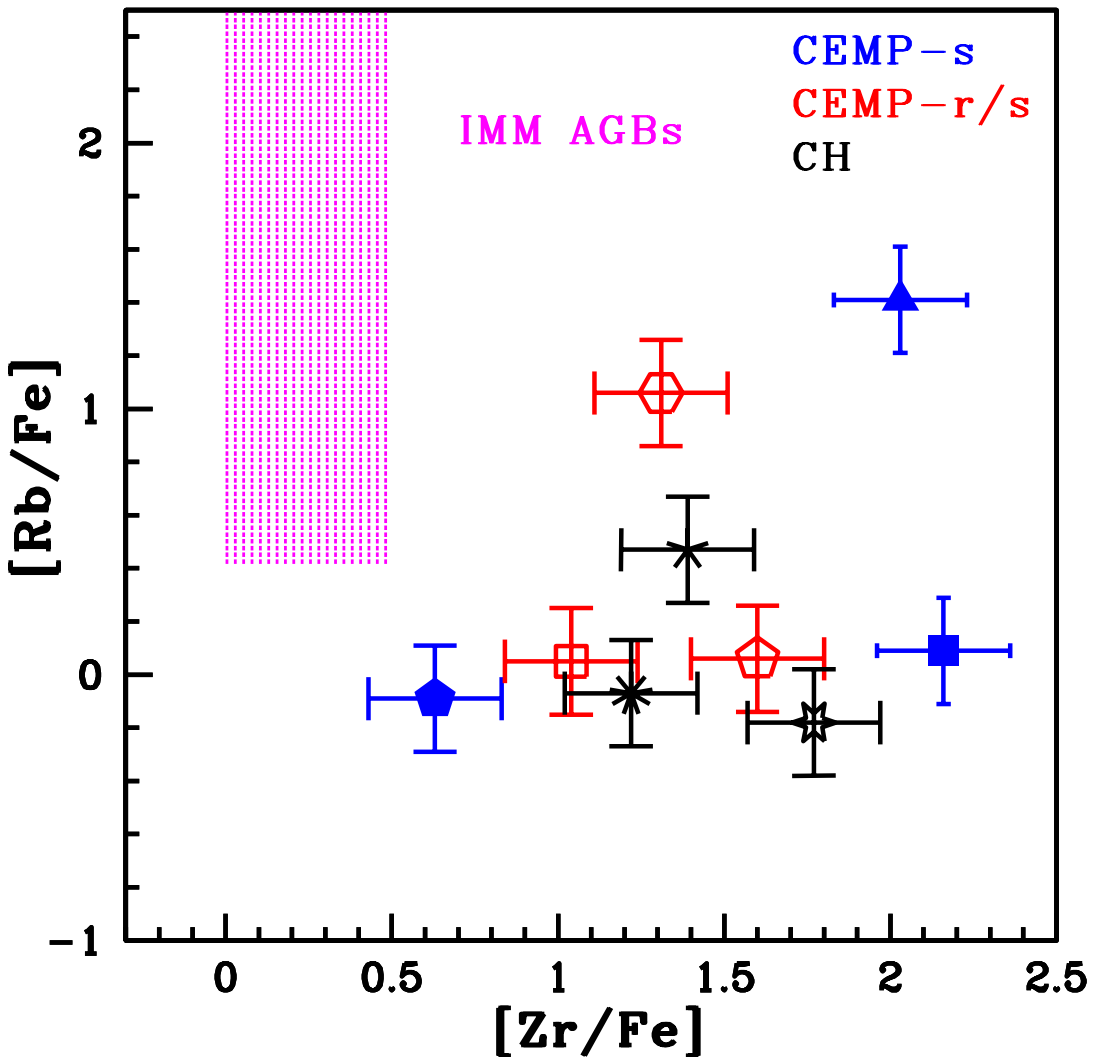


FIGURE 4.21: The observed $[\text{Rb}/\text{Fe}]$ and $[\text{Zr}/\text{Fe}]$ in the program stars. BD-19 132 (filled square), BD-19 290 (open hexagon), HD 30443 (open pentagon), HE 0457-1805 (filled triangle), LAMOSTJ091608.81+230734.6 (five-sided cross), HE 0920-0506 (nine-sided cross), LAMOSTJ151003.74+305407.3 (open square), BD+19 3109 (filled pentagon), and HD 202851 (six-sided star). The observed ranges of $[\text{Rb}/\text{Fe}]$ and $[\text{Zr}/\text{Fe}]$ in intermediate-mass AGB stars of the Galaxy and the Magellanic Clouds (van Raai *et al.* 2012) are shown as shaded region.

4.8 Origin of CEMP-r/s stars: clues from the abundance pattern

The CEMP-s stars are considered as the metal-poor analog of Ba and CH stars, and the binary mass transfer from an evolved low-mass AGB companion is the most accepted scenario for their abundance peculiarity (Herwig 2005). Comparison of observed abundances in the CEMP-s stars with theoretical model predictions also confirms the binary mass-transfer from low-mass AGB companions (Bisterzo *et al.* 2011; Placco *et al.* 2013; Hollek *et al.* 2015).

With the knowledge that r-process and s-process are ascribed to different astrophysical sites (Burbidge *et al.* 1957), several formation scenarios for CEMP-r/s stars have been proposed in the literature (Cohen *et al.* 2003; Qian and Wasserburg 2003; Zijlstra 2004; Barbuy *et al.* 2005; Wanajo *et al.* 2006; Jonsell *et al.* 2006; Bisterzo *et al.* 2011), most of them suggesting different independent processes for the r- and s- peculiarity. One scenario describes that the CEMP-r/s star could have been a secondary in a binary system formed out of r-process enriched ISM, and its s-elements and carbon enhancement is due to the later pollution from the AGB companion through mass-transfer mechanism(s) (Hill *et al.* 2000; Cohen *et al.* 2003; Ivans *et al.* 2005). But, this scenario could not successfully explain the observed frequency of CEMP-r/s stars. The study by Barklem *et al.* (2005) have revealed that an order of 1% of population II stars are CEMP-r/s stars. Cohen *et al.* (2003) have discussed another scenario that considers a triple system in which the star could have been the least massive tertiary, polluted first with the r-elements from a massive primary exploded as supernova, and later, polluted with s-elements by the secondary star that evolved into an AGB star. This hypothesis had been discarded, as such a dynamically stable triple system is unlikely to exists. Accretion Induced Collapse (AIC) in a binary system have

been suggested by Qian and Wasserburg (2003) and Cohen *et al.* (2003), but discarded since it is physically uncertain with the existing neutrino theories (Qian and Woosley 1996). Another scenario is a binary picture in which the primary star evolved through AGB, contributed the s-rich material to the secondary star, and later exploded as a Type 1.5 supernova (Zijlstra 2004; Wanajo *et al.* 2005), depositing r-material on the surface of the secondary. Abate *et al.* (2016) have calculated the frequency of CEMP-r/s stars among the CEMP-s stars for all these formation scenarios. The theoretical frequency predicted in most of the scenarios underestimates the observed frequency ($\sim 54\%$ in their sample) at least by a factor of five. The simulation based on the hypothesis of independent enrichment of s- and r- elements could predict a frequency ($\sim 22\%$) that approaches the observations. However, it fails to reproduce the observed correlation between the Ba and Eu abundances, and higher [hs/ls] ratios in CEMP-r/s stars. The simulations of Jonsell *et al.* (2006) for a high neutron density s-process in AGB star in a binary system also could not reproduce the observed abundance pattern in CEMP-r/s stars. From the analysis of a sample of CEMP stars (~ 18 objects), Allen *et al.* (2012) argued that CEMP-r/s stars have the same astrophysical origin as CEMP-s stars.

The analysis based on different abundance profile in Section 4.7 have shown that there is no distinction between the CEMP-s and CEMP-r/s stars. The overlap of [hs/ls] ratio between the CEMP-s and CEMP-r/s stars indicates that the origin of both the groups of stars owes a common astrophysical site and formation process, but under different conditions. The higher [hs/ls] ratio, more precisely, the higher [hs/Fe] ratio of the CEMP-r/s stars (Figure 4.22, upper panel) compared to the CEMP-s stars, indicates a higher neutron exposure for their formation than the classical s-process. The tight correlation between the observed [Eu/Fe] and [hs/Fe] ratios in CEMP-r/s stars (Figure 4.22, lower panel) points towards a single stellar site where both the s- and r- process elements could be produced simultaneously, which indicates a higher neutron density than the classical s-process

neutron density.

The intermediate neutron-capture process, i-process, originally proposed by Cowan and Rose (1977), has been explored recently by several authors to explain the CEMP-r/s phenomena (Dardelet *et al.* 2014; Hampel *et al.* 2016, 2019; Hansen *et al.* 2016c). Higher neutron densities than that required for the classical s-process, of the order of $10^{15} - 10^{17}$ cm $^{-3}$, intermediate between the s- and r-process neutron densities, could be achieved when a substantial amount of hydrogen rich-material is mixed into the intershell region of the evolved red giant stars (Proton Ingestion Episode, PIE) undergoing helium shell flash (Cowan and Rose 1977). Several sites have been proposed to host the PIEs in order for the i-process nucleosynthesis to take place. Simulations have shown that the neutron densities of the order of $10^{12} - 10^{15}$ cm $^{-3}$ can be achieved in very low-metallicity ($z \leq 10^{-4}$), low-mass ($M \leq 2M_{\odot}$) AGB stars (Fujimoto *et al.* 2000; Campbell and Lattanzio 2008; Lau *et al.* 2009; Cristallo *et al.* 2009; Campbell *et al.* 2010; Stancliffe *et al.* 2011). A similar neutron density is achieved during the dual core flash (H flash following the PIEs during the He flash) in low-mass, extremely low-metallicity ($z \leq 10^{-5}$) stars (Fujimoto *et al.* 1990; Hollowell *et al.* 1990; Lugaro *et al.* 2009), in the very-late thermal pulses of post-AGB stars (Herwig *et al.* 2011, 2014; Bertolli *et al.* 2013; Woodward *et al.* 2015), during the thermal pulses of low-metallicity super-AGB stars (Doherty *et al.* 2015; Jones *et al.* 2016), in Rapidly Accreting White Dwarfs (RAWD) (Denissenkov *et al.* 2019), and in massive ($M \geq 20 M_{\odot}$) metal-poor stars (Banerjee *et al.* 2018). A recent study by Karinkuzhi *et al.* (2021) has reported low-mass ($1 M_{\odot}$), low-metallicity ([Fe/H]~−2.5) AGB stars as sites of the i-process. Several other studies have also shown that the models of i-process in low-mass low-metallicity AGBs could successfully reproduce the observed abundances of CEMP-r/s stars (Hampel *et al.* 2016, 2019; Goswami *et al.* 2021).

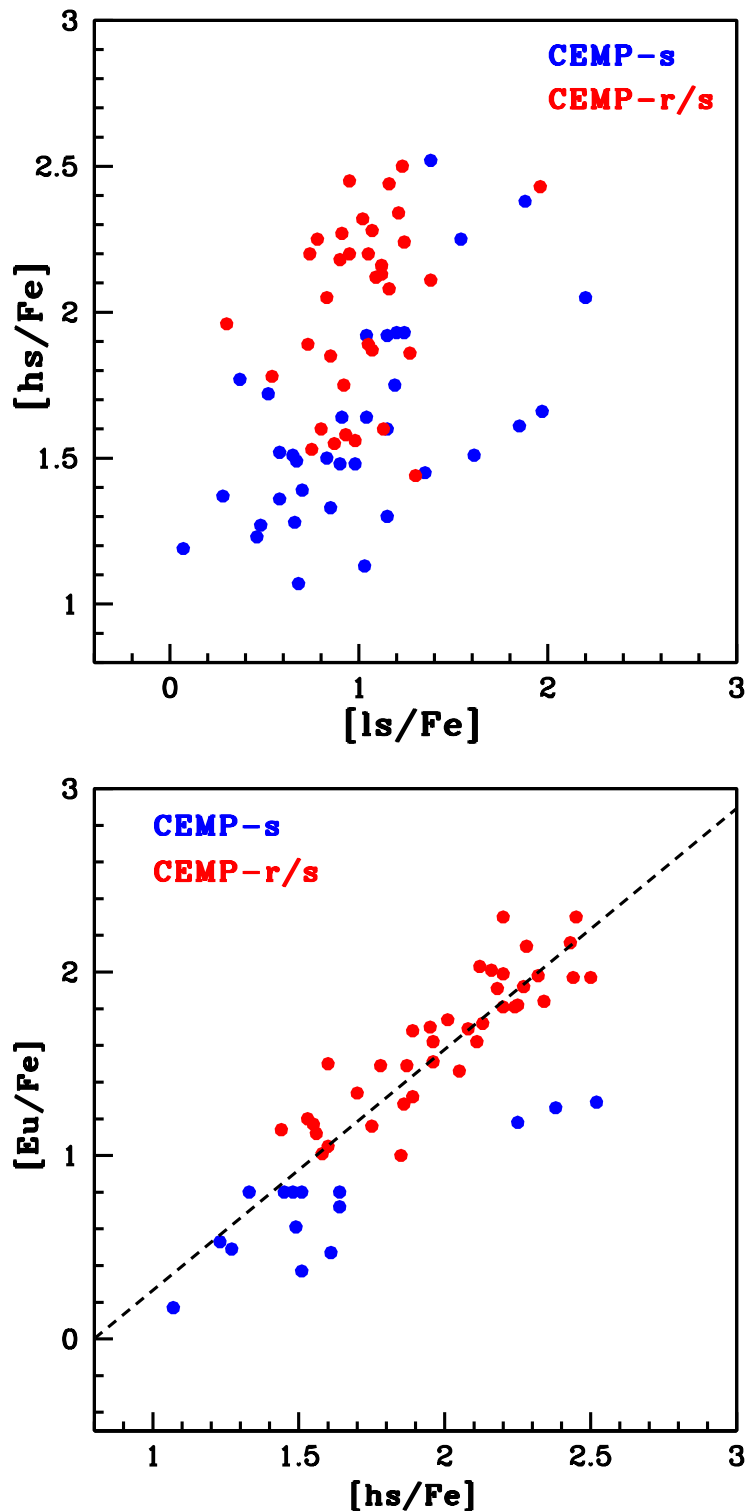


FIGURE 4.22: The observed $[hs/Fe]$ - $[ls/Fe]$ (upper panel) and $[Eu/Fe]$ - $[hs/Fe]$ (lower panel) in CEMP-s (blue circles) and CEMP-r/s (red circles) stars from literature (Goswami *et al.* 2021, references therein).

4.9 Parametric model-based analysis

The details and results of the parametric model-based analysis performed for our stellar sample is discussed in this section.

4.9.1 CEMP-r/s stars

From the analysis of our sample, a higher neutron density, along with a high [hs/Fe] ratio, suggest extreme conditions for the i-process, i.e., low-mass and low-metallicity AGB stars. Hampel *et al.* (2016) successfully used the simulations based on the i-process occurring in low-mass, low-metallicity ($1 M_{\odot}$, $z \sim 10^{-4}$) AGB stars to reproduce the observed abundance patterns of 20 CEMP-r/s stars. Later, this method has been extended successfully to a sample of seven low-Pb post-AGB stars in the Magellanic Cloud (Hampel *et al.* 2019). Hampel *et al.* (2016) used a single-zone nuclear network calculation to simulate the properties of the intershell region of low-mass ($1 M_{\odot}$), low-metallicity ($z \sim 10^{-4}$) AGB star, and studied the neutron-capture nucleosynthesis under the influence of different constant neutron densities ranging from 10^7 to 10^{15} cm^{-3} . The physical input conditions of intershell region are adapted from Stancliffe *et al.* (2011), and the composition from Abate *et al.* (2015b). The considered temperature and density of the intershell region are $1.5 \times 10^8 \text{ K}$ and 1600 g cm^{-3} , respectively. Compared to the classical s-process, at i-process neutron densities, this simulation resulted in an increased production of heavy s-, and r-process elements, and similar abundances of light s-process elements, as typically observed for CEMP-r/s stars (Abate *et al.* 2015a; Hollek *et al.* 2015). In these simulations, a range of temperatures (1.0×10^8 - $2.2 \times 10^8 \text{ K}$) and densities (800 - 3200 g cm^{-3}) have been considered. However, no significant changes have been noticed within the given range of temperature and density.

We have used the i-process model yields [X/Fe], from Hampel *et al.* (2016), and compared with the observed [X/Fe] (X stands for neutron capture elements) of the CEMP-r/s stars in our sample for the neutron densities ranging from 10^9 to 10^{15} cm $^{-3}$. A further dilution of the accreted material can occur on the surface of the CEMP-r/s stars as in the case of similarly formed CEMP-s stars (Stancliffe *et al.* 2007, 2013). The neutron-density responsible for the observed abundances in the star is derived by fitting the observed abundance with the dilution factor incorporated parametric model function:

$$X = X_i \cdot (1-d) + X_{\odot} \cdot d$$

where X represents the final abundance, X_i the i-process abundance, d is the dilution factor, and X_{\odot} is the solar-scaled abundance. Here, d is a free parameter that can be varied to find the best fit between the model and the observational data for each constant neutron density. The best fit model is found using χ^2_{\min} method, where χ^2 is defined as;

$$\chi^2 = \sum_Z \frac{([X_Z/\text{Fe}]_{\text{obs}} - [X_Z/\text{Fe}]_{\text{mod}})^2}{\sigma_{Z,\text{obs}}^2}$$

where $[X_Z/\text{Fe}]_{\text{obs}}$, $[X_Z/\text{Fe}]_{\text{mod}}$ are the observed and model abundances of the element with atomic number Z. $\sigma_{Z,\text{obs}}^2$ is the observed uncertainty for $[X_Z/\text{Fe}]_{\text{obs}}$. The best fit model is selected in such a way that it shows least deviation from the observation, that is by minimizing the χ^2 . The best fits obtained for the CEMP-r/s stars are shown in Figure 4.23. The neutron density responsible for the observed abundances in the stars BD-19 290, HD 30443, HE 1157-0518, HE 1304-2111, HE 1327-2116, and LAMOSTJ151003.74+305407.3 are found to be $n \sim 10^{11}$, 10^{14} , 10^{12} , 10^{13} , 10^{11} , and 10^{12} , respectively.

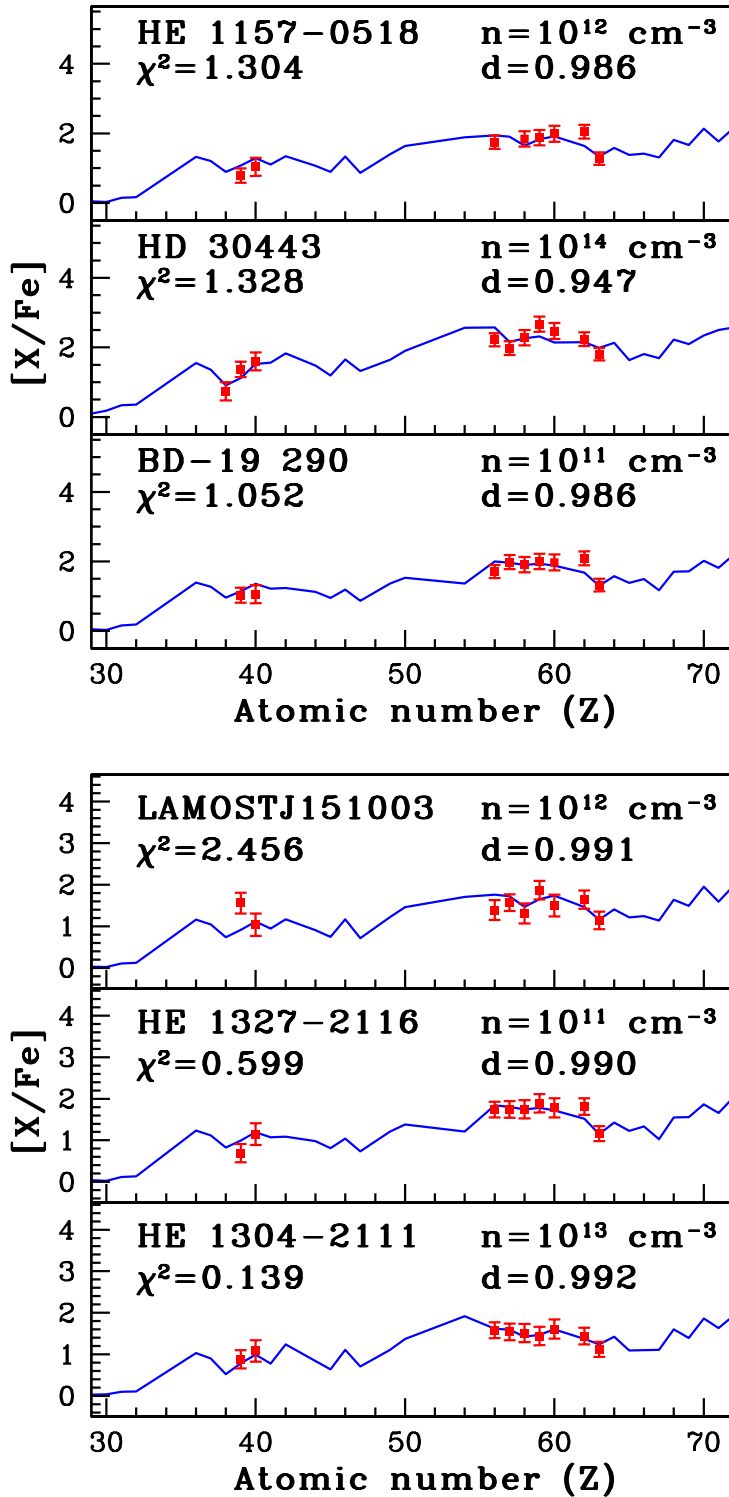


FIGURE 4.23: Parametric model fits for CEMP-r/s stars. The best fit for the parametric model function is represented by the solid curves. The observed abundances are indicated by the points with error bars.

4.9.2 CH and CEMP-s stars: parametric model-based analysis using FRUITY models

We have conducted a parametric model-based analysis for the CEMP-s and CH stars in our sample to find the mass of their AGB companion stars. The observed abundances in these stars are compared with the predicted abundances for AGB stars from FRUITY models (Cristallo *et al.* 2009, 2011, 2015). The best fit mass of the companion AGB star is derived by fitting the observed abundance with the parametric model function of Husti *et al.* (2009) by minimizing the χ^2 value. The procedure is same as that adopted for Ba stars as described in Section 3.7.2. The best fits obtained for these stars are given in Figure 4.24. The objects BD–19 132, HE 0457–1805, BD+19 3109, and HD 202851 are found to have companions of mass $M \sim 2.0 M_{\odot}$. The objects LAMOSTJ091608.81+230734.6, HE 0920–0506, and HE 1354–2257 have companions of mass $M \sim 2.5 M_{\odot}$.

4.10 Kinematic Analysis

The kinematic analysis of the stellar sample is performed as described in Section 2.7. The components of the spatial velocity, total space velocity, and the probability that a star belongs to a particular Galactic population are presented in Table 4.13.

While the stars BD–19 290, HE 1157–0518, HE 1327–2116, HE 1354–2257, LAMOSTJ151003.74+305407.3, and BD+19 3109 belong to the Galactic halo, the other seven objects BD–19 132, HD 30443, HE 0457–1805, LAMOSTJ091608.81+230734.6, HE 0920–0506, HE 1304–211,1 and HD 202851 are found to belong to the Galactic disk.

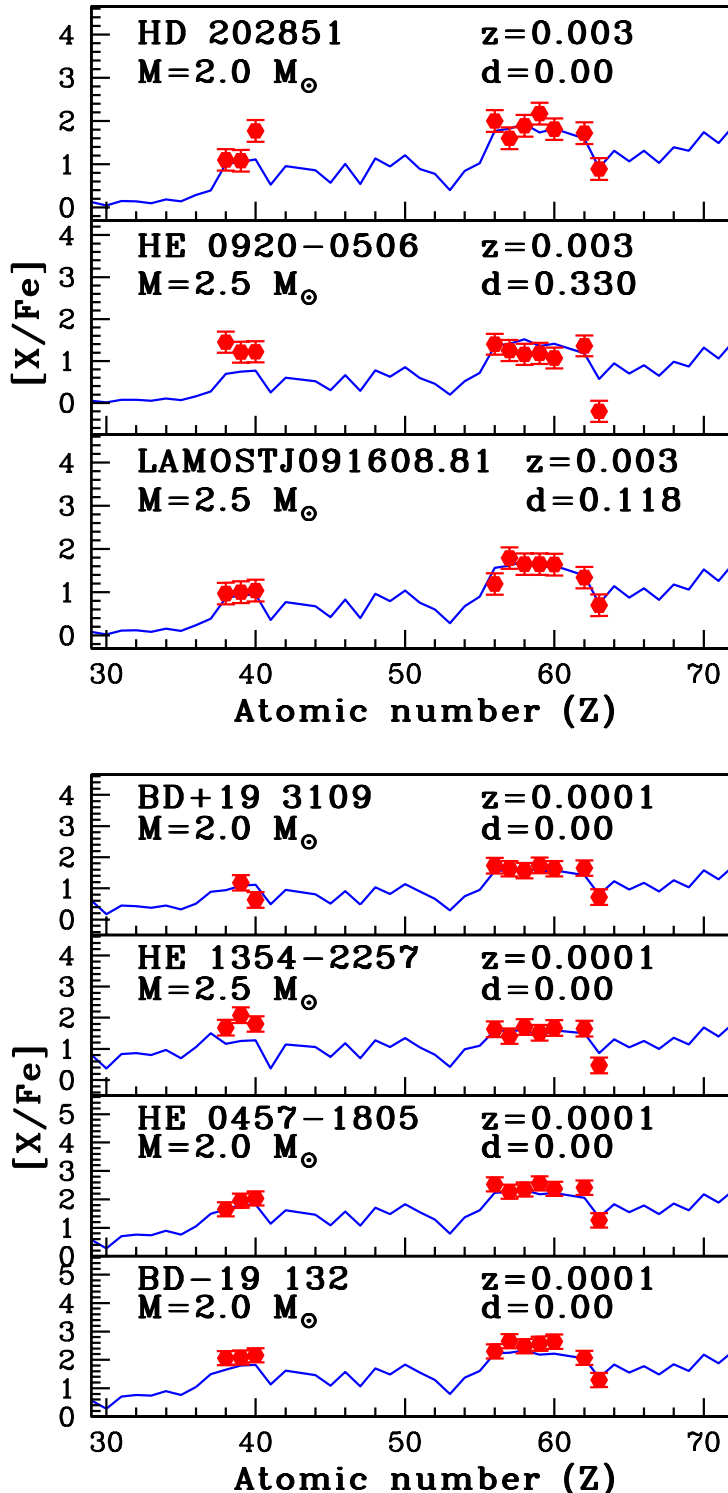


FIGURE 4.24: The parametric model fits for CH (upper panel) and CEMP-s stars (lower panel). The best fit for the parametric model function is represented by the solid curves. The observed abundances are indicated by the points with error bars.

TABLE 4.13: Estimates of spatial velocity and probabilities for the membership to the Galactic population of the program stars

Star name	U_{LSR} (km s^{-1})	V_{LSR} (km s^{-1})	W_{LSR} (km s^{-1})	V_{spa} (km s^{-1})	P_{thin}	P_{thick}	P_{halo}	Population
BD-19 132	13.66 ± 1.06	-69.13 ± 12.91	-6.75 ± 1.79	70.79 ± 12.56	0.90	0.10	0.00	Thin disk
BD-19 290	-252.60 ± 68.56	-573.19 ± 168.57	-38.00 ± 16.68	627.56 ± 182.56	0.00	0.00	1.00	Halo
HD 30443	-60.89 ± 0.25	-2.20 ± 0.62	11.72 ± 0.30	62.04 ± 0.21	0.02	0.95	0.03	Thick disk
HE 0457-1805	-33.97 ± 5.88	-31.96 ± 14.12	-9.62 ± 18.18	47.62 ± 16.30	0.98	0.02	0.00	Thin disk
LAMOSTJ091608.81+230734.6	-12.14 ± 2.99	1.57 ± 1.41	2.71 ± 2.95	12.53 ± 1.98	0.99	0.01	0.00	Thin disk
HE 0920-0506	-28.00 ± 0.48	-34.21 ± 0.34	-2.38 ± 0.84	44.27 ± 0.52	0.98	0.02	0.00	Thin disk
HE 1157-0518	-113.96 ± 69.93	-449.47 ± 202.19	-154.28 ± 130.96	488.68 ± 241.24	0.00	0.00	1.00	Halo
HE 1304-2111	2.68 ± 0.18	-41.47 ± 0.25	-32.03 ± 0.27	52.47 ± 0.35	0.92	0.08	0.00	Thin disk
HE 1327-2116	-192.58 ± 31.16	-529.30 ± 46.59	-3.95 ± 13.17	563.26 ± 54.50	0.00	0.00	1.00	Halo
HE 1354-2257	-695.99 ± 3045.67	-1855.03 ± 5913.33	-295.05 ± 1636.19	2003.14 ± 4853.64	0.00	0.00	1.00	Halo
LAMOSTJ151003.74+305407.3	-16.38 ± 2.84	-207.80 ± 20.74	-49.68 ± 8.67	214.25 ± 22.33	0.00	0.29	0.71	Halo
BD+19 3109	-122.65 ± 1.87	-253.64 ± 13.83	41.66 ± 11.43	284.80 ± 11.44	0.00	0.01	0.99	Halo
HD 202851	64.35 ± 1.90	-38.17 ± 2.92	-40.82 ± 1.68	85.23 ± 0.68	0.72	0.28	0.00	Thin disk

4.11 Discussion on individual stars

In this section, we provide a discussion of the individual stars, summarizing the results of the above analyses.

BD–19 132, BD–19 290, HD 30443, BD+19 3109: These object are listed in the CH star catalogue of Bartkevicius (1996). We present, the first-time abundance analysis results for these objects. Our analysis have shown that BD–19 132 and BD+19 3109 are CEMP-s stars, and BD–19 290 and HD 30443 are CEMP-r/s stars. HD 30443 and BD+19 3109 are confirmed binaries with periods of 2954 ± 77 (McClure and Woodsworth 1990) and 2129 ± 13 days (Sperauskas *et al.* 2016), respectively. We found that BD–19 290 and BD+19 3109 are high radial-velocity objects ($|V_r| > 100 \text{ km s}^{-1}$), HD 30443 and BD–19 132 are low radial velocity ($|V_r| < 70 \text{ km s}^{-1}$) objects. Yamashita (1975) classified HD 30443 as CH star, and BD+19 3109 as CH like star. Kinematic analysis have shown that HD 30443 belongs to the Galactic thick disk, BD–19 132 to the Galactic thin disk, and BD–19 290 and BD+19 3109 to the Galactic halo populations. From the neutron density dependent [Rb/Zr] ratio, these objects are found to have low-mass AGB companions.

LAMOSTJ091608.81+230734.6, LAMOSTJ151003.74+305407.3: From the multiple line indices measured from the stellar spectra from LAMOST DR2, Ji *et al.* (2016) have identified the objects LAMOSTJ091608.81+230734.6 and LAMOSTJ151003.74+305407.3 to be CH stars. We present the first-time abundance analysis for the object LAMOSTJ091608.81+230734.6. Our detailed abundance analysis confirms LAMOSTJ091608.81+230734.6 to be a CH star, and LAMOSTJ151003.74+305407.3 to be a CEMP-r/s star. Our kinematic analysis shows that LAMOSTJ091608.81+230734.6 belongs to the Galactic thin disk, and the latter to the Galactic halo. The spatial velocity estimate of LAMOSTJ151003.74+305407.3

is similar to the typical velocity of halo objects, $V_{spa} > 180 \text{ km s}^{-1}$ (Chen *et al.* 2004). Also it satisfies the criteria $[\text{Fe}/\text{H}] < -0.90$ and $V_{\text{LSR}} < -120 \text{ km s}^{-1}$ of Eggen (1997) to be a halo object.

HE 0920–0506, HE 1327–2116: These two objects belong to the sample of bright metal-poor candidates selected from the HES (Frebel *et al.* 2006) through medium-resolution ($R \sim 2000$) spectroscopic analysis. Frebel *et al.* (2006) have derived the metallicity of these objects from the Ca II K 3933 Å line using the calibration equation of Beers (1999). Within the error limits, these estimates agrees with our metallicity values. A more refined analysis of Beers *et al.* (2017) using the same medium-resolution spectra as Frebel *et al.* (2006) had reported the stellar atmospheric parameters (T_{eff} , $\log g$, $[\text{Fe}/\text{H}]$) $\sim(5291 \text{ K}, 2.99, -1.39)$ and $(4868 \text{ K}, 0.55, -3.48)$ respectively for HE 0920–0506 and HE 1327–2116. In the case of HE 0920–0506, while our estimate of temperature agrees with their temperature estimate, our estimates of surface gravity is ~ 0.34 dex lower and metallicity is ~ 0.64 dex higher. In the case of HE 1327–2116, the temperature estimates are in agreement, whereas our estimates of metallicity and surface gravity respectively are 0.64 and 0.95 dex higher than their estimates. These differences in the atmospheric parameters may be due to the difference in the method adopted for their determination and also due to the different resolution of the spectra used. While Frebel *et al.* (2006) reported the carbon abundances $[\text{C}/\text{Fe}] \sim 0.09$ and 1.11 respectively for HE 0920–0506 and HE 1327–2116, Beers *et al.* (2017) reported $[\text{C}/\text{Fe}] \sim 1.19$ and 2.64. Our estimates of carbon abundance for these two stars are $[\text{C}/\text{Fe}] \sim 0.57$ and 2.46 respectively. Our analysis shows that HE 0920–0506 is a CH star, and HE 1327–2116 is a CEMP-r/s star. While the former belongs to the Galactic thin disk, HE 1327–2116 belongs to the Galactic halo.

HE 0457–1805, HE 1157–0518: These two objects are listed among the

faint high latitude carbon stars identified from the HES (Christlieb *et al.* 2001a). Goswami (2005) identified HE 0457–1805 as a potential CH star candidate from low-resolution spectroscopic analysis. The object HE 0457–1805 is a confirmed binary with a period of 2724 ± 23 days (Jorissen *et al.* 2016b). The object HE 1157–0518 is a VMP star with $[\text{Fe}/\text{H}] \sim -2.42$, whereas HE 0457–1805 is a metal-poor star with $[\text{Fe}/\text{H}] \sim -1.98$. Our analysis shows that HE 0457–1805 is a CEMP-s star, and HE 1157–0518 is a CEMP-r/s star. Aoki *et al.* (2007) could not determine the Eu abundance for HE 1157–0518, however, they have classified it as a CEMP-s star. Our estimates of atmospheric parameters are in agreement with those of Aoki *et al.* (2007) except for the $\log g$ value, which is 0.5 dex lower than our estimate. The abundances of C, N, Mg, Ca, Ti, and Cr also match well within the error limits. However, our estimate $[\text{Ba}/\text{Fe}] \sim 1.75$ is ~ 0.40 dex lower than their estimate. For the object HE 0457–1805, the estimated atmospheric parameters are in agreement with Kennedy *et al.* (2011) except for $[\text{Fe}/\text{H}]$, which is 0.5 dex higher than our estimate. HE 0457–1805 is found to be a member of the Galactic thin disk, and it is a low spatial-velocity object. HE 1157–0518 is found to belong to the Galactic halo with a probability of 100%. It is a high spatial-velocity and high radial-velocity object.

HE 1304–2111, HE 1354–2257: Both these objects are found to be very metal-poor stars with $[\text{Fe}/\text{H}] \sim -2.34$ and -2.11 , respectively. Ours is the first-time abundance analysis for these objects. HE 1304–2111 is found to be a CEMP-r/s star, whereas the latter is a CEMP-s star. While HE 1304–2111 is a disk object, HE 1354–2257 is found to belong to the Galactic halo population.

HD 202851: This object is listed in the CH star catalogue of Bartkevicius (1996). Our analysis shows this star to be a CH giant with $[\text{Fe}/\text{H}] \sim -0.85$. Sperauskas *et al.* (2016) confirmed this object to be a binary with a period of 1295 ± 6 days

from radial velocity studies. HD 202851 is found to be a low velocity object, and belongs to the Galactic thin disk with 72% probability. The estimated atmospheric parameters of this star by Sperauskas *et al.* (2016) (T_{eff} , $\log g$, ζ , [Fe/H]) $\sim(4800$ K, 2.1, 1.5, -0.70) are in close agreement with our estimates (4900 K, 2.2, 1.54, -0.85). Arentsen *et al.* (2019b) determined the atmospheric parameters of this star from medium-resolution ($R\sim10,000$) spectra obtained with X-shooter spectrograph (Vernet *et al.* 2011) of Very Large Telescope (VLT). Their estimates for T_{eff} , $\log g$, and [Fe/H] are 4733 K, 1.6, and -0.88 . The negative value obtained for the [Rb/Zr] ratio in this star confirms low-mass AGB companion for HD 202851.

4.12 Conclusions

Detailed spectroscopic analyses of thirteen potential CH/CEMP stars are carried out based on high-quality, high-resolution spectra obtained with the HCT/HESP, Mercator/HERMES, and SUBARU/HDS. We have estimated the abundances of twenty eight elements including both light and neutron-capture process elements as well as carbon isotopic ratio. We present the first-time abundance analysis for the objects BD–19 132, BD–19 290, HD 30443, LAMOSTJ091608.81+230734.6, HE 1304–2111, HE 1354–2257, and BD+19 3109. Although a few light element abundances are available in the literature for the rest of the objects in our sample, we have presented for the first time a detailed abundance analyses for these objects.

The objects HD 30443, HE 0457–1805, BD+19 3109, and HD 202851 are confirmed binaries. The difference in the estimated radial velocities of the stars BD–19 132, BD–19 290, HE 0920–0506, HE 1304–2111, and LAMOSTJ151003.74+305407.3 from the Gaia values may be a robust indication that they are likely binaries. In the $A(C)$ - [Fe/H] diagram, all the program stars fall in the region occupied by the binary stars. The kinematic analysis shows that the seven low radial-velocity

($|V_r| < 100 \text{ km s}^{-1}$) objects in our sample, BD–19 132, HD 30443, HE 0457–1805, LAMOSTJ091608.81+230734.6, HE 0920–0506, HE 1304–2111 and HD 202851, are members of the Galactic disk population, and the rest six high radial-velocity ($|V_r| > 100 \text{ km s}^{-1}$) objects belong to the Galactic halo population. From their position on the H-R diagram, all the stars are found to be low-mass objects ($\sim 1 M_\odot$) except for HE 1304–2111 and HE 1354–2257. We note that the evolutionary tracks corresponding to the luminosity and temperature of HE 1304–2111 and HE 1354–2257 are not available.

The objects LAMOSTJ091608.81+230734.6, HE 0920–0506, and HD 202851 are found to be CH stars, while the remaining ten objects in our sample are bona fide CEMP stars. Four objects, BD–19 132, HE 0457–1805, HE 1354–2257, and BD+19 3109, are CEMP-s stars, whereas BD–19 290, HD 30443, HE 1157–0518, HE 1304–2111, HE 1327–2116, and LAMOSTJ151003.74+305407.3 are found to be CEMP-r/s stars. Our analysis based on various diagnostics confirms the pollution from low-mass AGB companions. There is no clear separation between the CEMP-s and CEMP-r/s stars as long as different abundance profiles are concerned. The parametric model considering the i-process in low-mass, low-metallicity AGB stars could successfully reproduce the observed abundances in the CEMP-r/s stars. The parametric model analysis, based on the predictions from the FRUITY models, performed for the CEMP-s and CH stars, confirms the former low-mass AGB companions with masses $M \leq 2.5 M_\odot$.

4.13 Appendix B

Atomic lines and line information used to derive the elemental abundances are listed in Tables B1 and B2.

Table B1 : Equivalent widths (in mÅ) of Fe lines used for deriving atmospheric parameters

Wavelength(Å)	El	E_{low} (eV)	log gf	BD-19132	BD-19290	HD30443	HE0457-1805	LAMOSTJ091608	HE0920-0506	HE1157-0518	HE1304-2111	HE1327-2116	HE1354-2257	LAMOSTJ151003	BD+193109	HD202851	References
4132.9	Fe I	2.85	-1.01	-	-	-	-	-	76.1(6.73)	-	-	-	-	-	-	-	1
4337.05		1.56	-1.7	-	-	-	145.6(5.42)	-	-	-	-	-	-	-	-	-	1
4422.568		2.845	-1.11	-	-	-	-	74.8(6.69)	-	-	-	-	-	-	-	-	1
4445.471		0.087	-5.38	105.3(5.69)	34.9(4.75)	-	-	77.50(6.44)	-	-	-	-	-	-	-	77.1(6.64)	1
4466.551		2.832	-0.590	-	-	-	-	-	-	-	-	-	-	-	-	136.4(6.59)	1
4484.22		3.603	-0.720	-	-	-	-	91.70(6.40)	-	-	41.8(5.26)	-	-	88.1(5.72)	-	-	1
4489.739		0.121	-3.966	-	-	-	-	133.5(6.39)	-	-	-	-	108.3(5.31)	-	-	128.3(6.53)	1
4531.626		3.211	-2.511	-	-	-	-	-	-	-	-	83.4(4.68)	-	-	-	-	1
4547.847		3.546	-0.780	-	-	-	-	-	62.6(6.65)	-	-	-	-	-	-	-	1
4595.358		3.301	-1.72	56.0(5.73)	-	-	-	-	-	-	-	-	-	-	-	-	1
4619.288		3.603	-1.120	63.5(5.65)	-	-	-	84.2(6.60)	-	-	-	-	-	76.7(5.95)	-	87.3(6.79)	1
4625.045		3.241	-1.34	-	20.3(4.64)	-	61.9(5.49)	-	58.0(6.73)	-	36.6(5.25)	-	-	-	-	-	1
4630.12		2.278	-2.600	-	-	-	-	-	-	28.4(5.03)	-	50.1(5.66)	-	-	-	-	1
4635.846		2.845	-2.42	48.0(5.68)	-	-	-	56.2(6.45)	-	-	-	-	-	-	24.0(5.17)	57.2(6.57)	1
4637.503		3.283	-1.39	69.5(5.59)	-	-	-	86.3(6.53)	-	-	-	-	-	-	-	-	1
4643.464		3.654	-1.29	53.4(5.73)	-	-	-	53.7(6.60)	-	-	-	-	-	-	38.2(5.40)	-	1
4690.138		3.686	-1.64	-	-	-	-	53.7(6.60)	-	-	-	-	-	-	-	-	1
4733.591		1.484	-2.71	-	-	127.0(5.66)	-	-	-	-	-	-	-	-	-	-	1
4787.827		2.998	-2.770	-	-	-	-	-	-	-	-	-	-	-	-	39.4(6.77)	1
4788.751		3.236	-1.810	52.5(5.61)	-	-	-	-	-	-	-	-	-	-	-	-	1
4789.651		3.546	-0.91	-	-	-	-	-	-	-	-	33.0(5.20)	-	-	-	-	2
4882.143		3.417	-1.64	-	-	-	-	82.1(6.80)	-	-	-	-	-	55.7(5.94)	-	-	1
4907.732		3.43	-1.84	-	-	-	-	61.7(6.62)	-	-	-	-	-	-	-	-	1
4908.031		4.217	-1.396	-	-	-	-	39.8(6.58)	-	-	-	-	-	-	-	-	2
4917.229		4.191	-1.18	-	-	-	-	35.7(6.38)	-	-	-	-	-	-	-	-	1
4924.77		2.278	-2.220	-	-	-	-	111(6.64)	-	22.1(5.20)	52.7(5.32)	-	48.8(5.26)	112(5.85)	-	-	1
4930.315		3.959	-1.350	-	-	-	-	-	-	-	-	-	-	-	-	44.7(6.53)	1
4939.687		0.859	-3.340	-	128.5(4.67)	-	-	142(6.64)	-	-	-	-	99.7(5.33)	173(6.02)	-	-	1
4967.89		4.191	-0.622	-	-	-	-	82.8(6.7)	-	-	-	-	-	-	35.5(5.38)	-	3
4969.917		4.216	-0.71	-	-	-	-	56.7(6.31)	45.3(6.70)	-	-	-	-	-	-	-	1
4985.253		3.93	-0.560	76.8(5.73)	-	77.5(5.80)	-	84.8(6.36)	-	-	-	-	-	-	-	96.6(6.75)	3
5001.863		3.882	0.01	-	-	-	-	-	-	32.8(4.84)	-	-	78.9(5.33)	-	-	-	1
5005.711		3.883	-0.18	-	-	-	-	82.8(5.42)	-	81.3(6.88)	-	-	-	-	-	-	3
5006.119		2.833	-0.61	-	-	-	-	143.9(5.63)	-	-	-	-	-	-	-	-	3
5022.236		3.984	-0.53	-	-	-	-	80.8(6.31)	-	-	-	-	-	96(6.05)	-	-	1

The abundance obtained from each line is given in parenthesis.

Table B1 : continues....

Wavelength(Å)	El	E_{low} (eV)	log gf	BD-19132	BD-19290	HD30443	HE0457-1805	LAMOSTJ091608	HE0920-0506	HE1157-0518	HE1304-2111	HE1327-2116	HE1354-2257	LAMOSTJ151003	BD+193109	HD202851	References
5028.126		3.573	-1.474	41.8(5.59)	-	-	-	71.9(6.59)	-	-	-	-	-	42.6(5.78)	-	-	3
5044.211		2.851	-2.15	63.3(5.62)	-	-	-	-	-	-	-	-	22.3(5.36)	-	-	-	1
5049.819		2.278	-1.420	-	-	-	-	160.4(6.77)	-	72.5(6.71)	27.9(5.04)	-	76.5(5.17)	-	-	-	1
5079.223		2.2	-2.067	-	-	147.8(5.86)	115.6(5.65)	-	-	-	-	27.3(4.72)	-	-	-	112.6(6.54)	1
5083.338		0.958	-2.958	-	-	-	-	-	-	-	81.4(5.11)	-	-	-	-	-	1
5109.652		4.302	-0.98	-	-	-	-	62.3(6.77)	-	-	-	-	-	-	-	-	1
5127.359		0.915	-3.307	-	-	-	-	133.2(6.37)	80.9(6.78)	32.8(4.89)	-	-	-	-	-	-	1
5141.739		2.424	-2.150	-	-	-	-	-	-	-	-	-	-	-	78.1(5.14)	-	1
5151.911		1.011	-3.32	-	107.8(4.63)	-	-	-	-	-	-	-	-	-	-	-	1
5159.058		4.283	-0.82	-	-	-	-	55.3(6.46)	-	-	-	-	-	-	-	-	1
5187.915		4.143	-1.26	-	-	-	-	54.2(6.71)	-	-	-	-	-	-	-	-	1
5195.468		4.22	-0.02	-	-	-	71.2(5.49)	-	74.2(6.83)	-	-	-	-	-	-	-	1
5198.711		2.222	-2.135	-	-	-	-	-	-	-	20.6(4.67)	58.3(5.18)	-	112.4(5.37)	-	-	1
5215.179		3.266	-0.933	102.6(5.61)	-	114.9(5.75)	-	121(6.67)	-	-	20.7(4.69)	-	-	91.7(5.31)	113.3(6.67)	1	
5226.862		3.038	-0.667	-	-	-	115.7(5.34)	-	92.0(6.76)	-	-	45.4(4.57)	-	-	-	-	1
5242.491		3.634	-0.840	-	20.1(4.71)	-	-	95.7(6.58)	-	-	-	46.0(5.54)	84.2(5.87)	58.2(5.33)	94.3(6.71)	1	
5247.05		0.087	-4.946	139.3(5.64)	66.8(4.60)	-	-	-	53.8(6.70)	-	55.6(5.01)	-	-	136.1(5.89)	124.1(5.23)	115.2(6.79)	1
5250.209		0.121	-4.938	-	58.7(4.52)	-	-	120.4(6.63)	-	-	-	-	-	131.1(5.82)	131.2(5.37)	-	1
5253.462		3.283	-1.67	-	-	-	-	92.1(6.8)	-	-	-	-	78.6(6.06)	-	-	-	1
5263.305		3.265	-0.970	-	-	-	-	-	-	44.7(5.05)	-	75.5(5.55)	-	-	-	-	1
5281.79		3.038	-1.020	-	-	-	-	-	41.2(4.96)	-	-	-	-	150.6(5.94)	-	-	1
5307.37		1.61	-2.192	-	-	-	138.7(5.32)	-	-	-	-	-	-	-	-	-	1
5322.04		2.28	-2.840	72.0(5.57)	-	83.5(5.86)	-	81.2(6.48)	-	-	-	-	-	76.4(5.88)	47.9(5.14)	68.9(6.42)	4
5339.93		3.27	-0.680	-	-	-	117.8(5.66)	132.7(6.63)	-	55.0(5.26)	-	-	-	-	100.9(5.19)	-	4
5364.858		4.445	0.22	-	-	-	-	110.5(6.68)	-	-	-	-	-	-	-	-	3
5365.399		3.573	-1.44	43.2(5.57)	-	-	-	86.7(6.8)	-	-	-	-	-	55.7(5.9)	-	-	3
5367.479		4.415	0.35	-	34.7(4.66)	99.4(5.82)	-	113.5(6.57)	-	-	44.5(5.21)	-	-	-	69.9(5.25)	111.4(6.66)	1
5369.961		4.37	0.35	87.1(5.58)	30.8(4.54)	110.7(5.92)	-	114.3(6.54)	-	-	-	-	-	-	80.2(5.36)	100.9(6.38)	1
5379.574		3.694	-1.480	-	-	-	-	-	40.8(6.78)	-	-	-	-	-	-	-	1
5383.369		4.312	0.5	-	-	-	-	130(6.65)	-	-	-	-	-	-	80.7(5.13)	131.2(6.78)	1
5393.17		3.24	-0.720	-	-	-	-	-	-	-	24.2(4.71)	-	-	-	-	-	4
5445.042		4.39	-0.020	73.5(5.75)	-	69.0(5.75)	-	-	-	27.6(5.07)	-	-	-	-	43.6(5.16)	98.2(6.70)	1
5543.936		4.217	-1.14	-	-	-	-	58.8(6.74)	-	-	-	-	-	-	-	-	1
5569.62		3.42	-0.490	-	-	-	-	125.7(6.45)	-	-	-	31.2(4.66)	99.8(5.67)	-	-	125.6(6.64)	4
5576.09		3.43	-0.851	-	-	-	-	113.5(6.69)	-	-	-	-	-	-	68.4(5.21)	-	1

The abundance obtained from each line is given in parenthesis.

Table B1 : continues....

Wavelength(Å)	El	E_{low} (eV)	log gf	BD-19132	BD-19290	HD30443	HE0457-1805	LAMOSTJ091608	HE0920-0506	HE1157-0518	HE1304-2111	HE1327-2116	HE1354-2257	LAMOSTJ151003	BD+193109	HD202851	References
5586.756		3.368	-0.210	137.8(5.60)	-	-	-	157.8(6.71)	-	-	68.9(5.10)	-	-	-	-	152.1(6.75)	1
5615.644		3.332	-0.140	-	-	-	-	-	-	-	-	-	-	-	129.0(5.31)	-	1
5618.631		4.209	-1.38	-	-	-	-	51.4(6.72)	-	-	-	-	-	-	-	-	1
5701.544		2.559	-2.216	-	-	-	-	108.5(6.69)	-	-	-	-	52.1(5.54)	90.7(5.79)	80.1(5.37)	-	1
5741.848		4.256	-1.73	-	-	-	-	20.8(6.63)	-	-	-	-	-	-	-	-	1
5753.12		4.26	-0.760	-	-	-	-	77.6(6.72)	-	-	-	-	-	58.6(6.08)	23.1(5.33)	67.6(6.65)	1
5809.22		3.88	-1.690	-	-	-	-	-	27.4(6.74)	-	-	-	-	-	-	-	4
5856.088		4.294	-1.64	-	-	-	-	34(6.79)	-	-	-	-	-	-	-	-	1
5859.586		4.549	-0.386	-	-	-	-	83.1(6.79)	-	-	-	-	-	-	-	-	2
5862.357		4.549	-0.051	-	-	-	-	81.7(6.31)	61.8(6.71)	-	-	-	-	-	-	-	3
5883.813		3.959	-1.360	-	-	-	-	-	-	-	-	-	-	-	-	57.6(6.71)	1
5956.692		0.859	-4.605	-	-	-	-	95.9(6.62)	-	-	38.9(5.22)	-	-	81.6(5.81)	-	86.5(6.69)	1
6003.01		3.881	-1.12	-	-	-	-	-	-	-	-	-	-	47.7(5.82)	-	-	1
6024.049		4.548	-0.120	-	-	54.1(5.85)	-	-	-	-	-	-	-	-	35.7(5.30)	86.0(6.65)	1
6082.71		2.222	-3.573	-	-	-	-	55.2(6.66)	-	-	-	-	-	28.3(5.86)	21.7(5.29)	57.5(6.83)	1
6136.994		2.198	-2.95	-	-	-	-	84.5(6.47)	51.0(6.84)	-	-	-	-	78.3(5.88)	-	-	1
6137.694		2.588	-1.403	-	105.3(4.73)	-	-	157.5(6.76)	-	-	40.4(4.65)	98.6(5.39)	-	135.7(5.38)	-	-	1
6151.62		2.18	-3.290	-	-	-	-	79.8(6.71)	-	-	20.4(5.24)	-	21.3(5.57)	62.4(6.01)	39.1(5.30)	-	4
6173.34		2.22	-2.880	-	-	-	-	101.7(6.72)	-	-	-	30.6(5.41)	108.2(6.17)	-	-	-	4
6180.204		2.727	-2.78	-	-	-	-	64.8(6.64)	-	-	-	-	43.2(5.96)	-	-	-	1
6200.314		2.608	-2.437	-	-	-	-	-	-	-	-	36.6(5.54)	85(5.96)	-	-	-	1
6213.429		2.222	-2.66	-	-	-	-	113(6.68)	-	-	-	-	102.7(5.88)	-	-	-	1
6219.279		2.198	-2.433	-	-	-	-	120.5(6.56)	-	25.2(5.27)	-	-	-	140.4(6.08)	-	-	1
6240.646		2.222	-3.380	-	-	-	-	70.8(6.49)	38.6(6.78)	-	-	-	27.9(5.64)	54.1(5.84)	-	-	1
6246.318		3.603	-0.960	75.7(5.60)	-	-	-	-	-	-	-	-	-	-	-	-	1
6252.554		2.404	-1.687	-	87.3(4.60)	-	-	155.1(6.73)	-	46.9(5.12)	-	-	82.5(5.19)	152.2(5.76)	-	-	1
6254.258		2.279	-2.48	-	-	-	-	-	-	-	-	-	73.6(5.62)	117.3(5.86)	-	-	1
6280.617		0.859	-4.39	-	-	-	-	120.5(6.75)	-	-	52.1(5.26)	-	-	-	-	-	1
6297.8		2.222	-2.74	-	-	-	-	90.3(6.36)	55.7(6.76)	-	-	-	-	-	-	-	1
6301.5		3.654	-0.672	-	-	-	-	107.8(6.45)	-	-	37.6(5.06)	-	-	-	69.6(5.24)	101.8(6.51)	3
6318.018		2.453	-2.33	-	-	-	-	-	-	-	-	-	41.2(5.31)	-	83.7(5.32)	-	3
6322.69		2.588	-2.426	-	-	-	-	-	-	-	-	-	33.1(5.44)	99.7(6.08)	-	-	3
6335.328		2.198	-2.230	-	-	146.4(5.84)	-	128(6.46)	-	-	26.4(4.77)	58.7(5.14)	-	105.0(5.15)	127.5(6.69)	1	
6336.823		3.686	-1.05	-	-	-	-	-	-	-	-	-	22.9(5.19)	-	-	-	1
6393.602		2.432	-1.620	-	-	-	-	158.3(6.71)	-	-	-	-	90.4(5.25)	-	-	-	1

The abundance obtained from each line is given in parenthesis.

Table B1 : continues....

Wavelength(Å)	El	E_{low} (eV)	log gf	BD-19132	BD-19290	HD30443	HE0457-1805	LAMOSTJ091608	HE0920-0506	HE1157-0518	HE1304-2111	HE1327-2116	HE1354-2257	LAMOSTJ151003	BD+193109	HD202851	References
6408.016		3.687	-1.048	-	-	-	59.4(5.56)	93.5(6.52)	-	-	-	-	-	-	-	-	1
6416.933		4.796	-0.885	-	-	-	-	-	-	-	-	-	-	-	-	29.9(6.65)	3
6419.95		4.73	-0.09	-	-	-	-	81.3(6.77)	-	-	-	-	-	53.5(6.05)	-	-	3
6421.349		2.278	-2.027	-	-	-	-	-	-	65.9(5.21)	22.2(4.58)	80.7(5.32)	153.1(5.91)	-	-	-	1
6430.85		2.18	-2.010	-	-	-	-	151.5(6.63)	-	-	26.5(4.52)	107.9(5.55)	160.5(5.84)	-	-	-	4
6481.87		2.278	-2.984	-	-	-	-	99.5(6.8)	-	-	-	-	-	-	-	-	1
6574.227		0.99	-5.04	-	-	-	-	73.2(6.81)	-	-	-	-	-	69.5(6.23)	-	-	1
6575.019		2.588	-2.820	52.0(5.67)	-	48.4(5.84)	-	79.4(6.69)	-	-	-	-	-	-	-	62.4(6.58)	1
6592.91		2.72	-1.470	-	57.0(4.62)	129.7(5.74)	-	131.8(6.53)	-	-	-	-	56.6(5.12)	-	95.8(5.13)	124.5(6.61)	4
6593.871		2.432	-2.422	-	-	-	-	107.1(6.55)	-	-	-	-	-	-	-	105.1(6.71)	1
6677.989		2.692	-1.470	-	-	-	-	148.4(6.64)	-	45.0(5.17)	-	-	-	169(6.07)	-	-	1
6739.521		1.557	-4.95	-	-	-	-	28.6(6.59)	-	-	-	-	-	-	-	-	1
6750.15		2.424	-2.621	-	-	-	-	113.7(6.82)	-	-	-	-	-	-	-	-	1
4416.83	Fe II	2.778	-2.6	-	-	-	-	-	-	-	-	-	-	71.3(5.95)	-	-	1
4491.405		2.855	-2.700	-	-	-	57.6(5.68)	-	-	-	-	-	33.7(5.21)	-	22.8(5.29)	-	1
4508.288		2.855	-2.210	45.0(5.64)	29.5(4.55)	33.5(5.71)	67.8(5.39)	-	-	25.2(4.97)	-	29.2(4.63)	-	-	40.4(5.27)	-	1
4515.339		2.84	-2.480	-	-	26.7(5.79)	62.5(5.53)	-	70.5(6.75)	-	-	20.0(4.68)	-	-	30.3(5.26)	-	1
4520.224		2.81	-2.600	32.7(5.65)	-	28.9(5.93)	55.1(5.47)	-	-	-	-	-	-	-	-	-	1
4629.339		2.807	-2.280	-	-	-	-	108.3(6.55)	77.8(6.74)	-	31.5(5.16)	-	-	-	-	-	1
4731.453		2.891	-3.360	-	-	-	-	-	-	-	-	-	20.5(5.58)	-	-	-	1
4923.927		2.891	-1.32	-	-	-	-	159.8(6.68)	-	-	-	-	-	-	-	-	1
5197.56		3.23	-2.250	-	-	-	-	-	72.2(6.74)	-	24.0(5.23)	-	-	-	-	85.4(6.62)	4
5234.62		3.22	-2.240	-	25.4(4.73)	-	-	99.2(6.48)	-	25.4(5.20)	22.0(5.09)	-	52.3(5.35)	60.9(5.76)	-	-	4
5534.83		3.25	-2.770	-	-	-	-	-	-	-	-	-	-	-	-	48.3(6.64)	4
6247.55		3.89	-2.340	-	-	-	-	57.1(6.6)	-	-	-	-	-	20.3(5.98)	-	46.4(6.72)	4
6369.462		2.891	-4.253	-	-	-	-	-	-	-	-	-	-	-	-	-	2
6456.383		3.903	-2.075	-	-	-	-	67.3(6.56)	-	-	-	-	19.9(5.40)	30.8(6.03)	-	-	1

The abundance obtained from each line is given in parenthesis.

References: 1. Fuhr *et al.* (1988), 2. Bridges and Kornblith (1974), 3. Kurucz (1988), 4. Lambert *et al.* (1996)

Table B2 : Equivalent widths (in mÅ) of lines used for deriving elemental abundances

Wavelength(Å)	El	E_{low} (eV)	log gf	BD-19132	BD-19290	HD30443	HE0457-1805	LAMOSTJ091608	HE0920-0506	HE1157-0518	HE1304-2111	HE1327-2116	HE1354-2257	LAMOSTJ151003	BD+193109	HD202851	References
5682.633	Na I	2.102	-0.700	120.0(5.52)	31.5(4.65)	99.20(4.96)	140.1(6.49)	109.4(6.15)	66.9(5.89)	-	129.8(6.65)	-	27.3(4.76)	-	21.5(4.14)	93.0(5.90)	1
5688.205		2.1	-0.450	130.5(5.42)	35.4(4.47)	135.5(5.11)	149.6(6.39)	106.8(5.86)	-	-	170.5(6.81)	17.1(4.28)	35.5(4.67)	-	31.8(4.11)	104.3(5.84)	1
6154.226		2.102	-1.560	-	-	-	-	59.90(6.16)	24.9(5.88)	-	-	-	-	23.10(5.27)	-	-	1
6160.747		2.104	-1.260	-	-	86.60(5.36)	112.3(6.51)	66.40(5.97)	46.1(6.04)	-	-	-	-	35.20(5.20)	-	66.4(6.00)	1
4702.991	Mg I	4.346	-0.666	-	-	-	144.4(6.85)	-	173.0(7.54)	-	-	-	-	116.9(5.85)	115.9(6.05)	151.9(6.95)	2
4730.029		4.346	-2.523	37.1(6.30)	-	-	-	-	-	-	-	-	-	28.4(6.29)	-	-	2
5528.405		4.346	-0.620	-	89.4(5.35)	173.00(5.95)	-	175.6(7.23)	165.6(7.47)	67.0(5.45)	68.5(5.46)	65.0(5.22)	-	138.9(6.00)	141.5(6.06)	171.8(7.09)	2
5711.088		4.346	-1.833	92.4(6.33)	-	84.00(6.13)	106.2(7.04)	92.80(7.01)	86.1(7.49)	-	-	-	12.4(5.47)	64.30(6.20)	-	-	2
5690.425	Si I	4.929	-1.870	-	-	29.80(6.69)	-	31.90(6.67)	32.5(7.02)	-	-	-	-	-	-	-	3
5948.541		5.083	-1.23	-	110.0(6.99)	-	-	61.40(6.72)	65.8(7.26)	-	24.8(5.91)	-	25.7(6.01)	-	-	90.8(6.63)	3
6131.852		5.616	-1.140	-	-	19.60(6.62)	-	-	-	-	-	-	-	-	-	-	3
6145.016		5.616	-0.820	-	-	-	24.6(6.10)	31.60(6.38)	-	-	-	-	-	-	-	-	4
6237.319		5.613	-0.530	-	98.7(6.80)	-	27.5(5.87)	-	-	-	27.0(5.92)	10.2(5.45)	20.2(5.78)	-	-	-	4
4283.011	Ca I	1.886	-0.224	-	-	-	114.3(5.09)	-	101.8(5.80)	-	-	-	-	-	-	-	5
4318.652		1.899	-0.208	-	-	-	128.8(5.35)	-	-	-	-	-	-	-	-	-	5
4425.437		1.879	-0.385	-	-	-	-	-	102.4(5.95)	66.0(4.60)	-	-	-	-	-	-	5
4435.679		1.89	-0.52	-	57.8(4.00)	-	-	-	91.5(5.86)	-	-	-	-	119.2(4.77)	-	-	5
4455.887		1.899	-0.510	-	-	-	-	-	-	38.8(4.03)	-	-	-	-	-	-	5
4456.616		1.899	-1.66	-	-	-	-	-	58.7(6.12)	-	-	-	-	-	-	-	5
4578.55		2.521	-0.56	-	-	-	73.9(5.22)	-	70.2(5.94)	-	-	17.2(4.17)	-	-	-	-	5
5260.387		2.521	-1.900	-	-	65.40(5.38)	-	-	-	-	-	-	-	-	-	-	5
5261.704		2.521	-0.730	-	-	147.70(5.21)	-	-	-	-	-	-	-	-	-	-	5
5265.56		2.52	-0.11	-	40.4(3.90)	-	-	-	-	-	50.3(4.38)	-	-	-	-	-	5
5349.465		2.709	-1.178	-	-	80.30(5.09)	-	38.20(5.42)	-	-	-	-	-	-	-	-	5
5512.98		2.932	-0.29	-	-	-	-	69.90(5.36)	-	-	-	-	-	-	-	-	5
5581.965		2.523	-1.833	116.9(5.13)	-	-	-	-	-	-	10.5(4.02)	-	39.60(4.41)	56.7(4.36)	-	-	5
5590.114		2.521	-0.710	-	-	-	-	89.50(5.67)	-	12.4(4.22)	-	13.04(4.12)	23.1(4.38)	35.30(4.33)	47.4(4.21)	74.6(5.43)	5
5594.462		2.523	-0.050	-	58.7(3.89)	-	113.9(5.04)	-	-	31.8(3.91)	-	-	-	-	-	-	5
5857.451		2.932	0.23	-	-	-	-	93.60(5.27)	93.8(6.01)	-	-	36.8(4.17)	44.9(4.35)	76.20(4.47)	59.7(4.01)	94.5(5.34)	5
6102.723		1.879	-0.890	-	-	-	-	102.0(5.26)	-	-	44.2(4.18)	53.4(4.35)	103.5(4.59)	98.2(4.12)	115.9(5.63)	5	
6162.173		1.899	0.1	-	137.6(3.92)	-	-	-	142.5(5.91)	-	-	-	105.7(4.34)	-	-	-	5
6166.439		2.521	-0.900	-	-	-	82.0(5.36)	64.10(5.33)	57.9(5.87)	-	-	-	-	-	37.5(4.16)	72.1(5.54)	5
6169.042		2.523	-0.55	-	-	-	-	79.50(5.26)	78.2(6.04)	-	-	-	36.2(4.47)	-	-	-	5
6169.563		2.523	-0.27	-	-	-	-	-	93.4(6.11)	-	-	-	-	83.30(4.53)	-	96.0(5.37)	5
6439.075		2.525	0.47	-	-	-	-	157.5(5.64)	136.8(6.03)	-	-	-	103.7(4.66)	-	137.5(4.24)	155.9(5.61)	5

The abundance obtained from each line is given in parenthesis.

Table B2 : continues....

Wavelength(Å)	El	E_{low} (eV)	log gf	BD-19132	BD-19290	HD30443	HE0457-1805	LAMOSTJ091608	HE0920-0506	HE1157-0518	HE1304-2111	HE1327-2116	HE1354-2257	LAMOSTJ151003	BD+193109	HD202851	References
6449.808		2.523	-0.550	138.0(5.12)	-	-	98.6(5.25)	86.90(5.37)	82.0(6.11)	-	-	-	-	70.30(4.61)	-	92.6(5.55)	5
6455.598		2.523	-1.350	-	-	-	-	-	47.9(6.05)	-	-	-	-	-	-	-	5
6471.662		2.525	-0.590	152.7(5.36)	-	-	-	-	80.6(6.12)	-	-	-	42.9(4.62)	56.80(4.48)	68.0(4.28)	-	5
6493.781		2.521	0.14	-	-	-	134.9(5.16)	117.9(5.27)	110.8(5.99)	69.1(4.12)	-	-	-	-	-	112.0(5.23)	5
6499.65		2.523	-0.590	-	-	-	-	-	68.7(5.81)	-	-	-	-	-	-	-	5
4453.312	Ti I	1.43	-0.051	-	-	-	-	-	35.2(4.48)	-	-	-	-	-	-	59.2(4.34)	6
4512.734		0.836	-0.480	-	-	160.80(3.25)	-	84.90(4.04)	55.7(4.44)	-	-	-	-	-	-	-	6
4533.239		0.848	0.476	-	-	-	142.2(3.71)	-	-	-	-	-	62.2(2.60)	-	-	-	6
4617.269		1.749	0.389	-	-	-	-	87.00(4.29)	51.1(4.38)	-	-	12.9(2.76)	-	-	-	81.0(4.25)	6
4656.468		0	-1.345	-	-	-	124.4(3.83)	-	-	-	-	-	-	-	-	-	6
4759.272		2.255	0.514	-	-	-	57.7(3.89)	40.30(3.82)	33.8(4.30)	-	-	-	-	-	-	-	6
4778.255		2.24	-0.220	-	-	68.50(3.74)	-	-	-	-	-	-	-	-	-	38.1(4.54)	6
4820.41		1.503	-0.441	-	-	-	-	-	-	25.4(3.17)	-	-	-	-	-	-	6
4840.874		0.899	-0.509	163.9(3.80)	-	175.30(3.45)	-	81.20(3.98)	52.4(4.39)	-	-	-	-	78.00(3.19)	-	89.1(4.27)	6
4926.147		0.818	-2.17	78.8(3.83)	-	-	-	-	-	-	-	-	-	-	-	-	6
4999.5		0.83	0.31	-	-	-	-	-	28.4(2.36)	82.8(3.13)	-	-	-	-	-	133.6(4.31)	6
5007.21		0.82	0.17	-	-	-	-	131.4(4.25)	-	-	-	68.5(2.79)	-	-	-	-	6
5009.646		0.021	-2.259	-	-	-	81.4(3.92)	-	-	-	-	-	-	-	-	-	6
5024.842		0.818	-0.602	-	-	176.50(3.36)	118.7(4.05)	82.10(3.95)	56.9(4.51)	-	-	-	-	90.20(3.30)	-	94.3(4.33)	6
5039.96		0.02	-1.13	-	68.4(2.32)	-	-	-	-	-	-	-	-	-	-	104.5(4.12)	6
5064.653		0.048	-0.991	-	-	-	139.7(3.56)	-	66.8(4.32)	-	-	-	-	-	-	-	6
5210.386		0.047	-0.884	-	84.8(2.24)	-	110.0(3.79)	71.2(4.37)	-	77.6(2.90)	-	-	143.9(3.23)	-	-	-	6
5460.499		0.05	-2.88	-	-	105.50(3.46)	-	27.30(4.26)	-	-	-	-	-	-	-	-	6
5471.197		1.443	-1.440	-	-	-	-	-	-	-	-	-	-	-	32.6(3.45)	-	6
5739.982		2.236	-0.67	-	-	-	-	-	-	-	-	-	-	-	-	23.6(4.62)	6
5918.535		1.07	-1.460	103.4(3.64)	-	78.70(3.27)	-	33.30(4.16)	-	-	-	-	-	25.70(3.50)	-	36.6(4.30)	6
5922.11		1.046	-1.466	95.3(3.50)	-	77.00(3.22)	-	35.10(4.17)	-	-	-	-	-	-	-	45.0(4.44)	6
5937.811		1.067	-1.89	-	-	-	-	-	-	-	-	-	-	-	38.6(3.36)	-	6
5941.751		1.05	-1.510	95.8(3.56)	-	77.80(3.28)	-	30.70(4.14)	-	-	-	-	-	-	-	31.7(4.24)	6
5965.828		1.879	-0.409	-	-	-	-	-	-	-	-	-	-	-	57.0(3.38)	-	6
5978.543		1.873	-0.496	-	-	-	-	-	-	-	-	-	-	-	52.6(3.39)	-	6
6064.629		1.046	-1.944	-	-	-	-	-	-	-	-	-	-	-	-	26.8(4.56)	6
6303.757		1.443	-1.566	-	-	-	-	25.00(4.03)	-	-	-	-	-	-	43.5(3.64)	-	6
6556.062		1.46	-1.074	89.1(3.59)	-	67.60(3.30)	-	-	-	-	-	-	-	-	-	42.5(4.45)	6
6599.133		0.9	-2.085	-	-	-	-	-	-	-	-	-	-	-	60.2(3.49)	-	6

The abundance obtained from each line is given in parenthesis.

Table B2 : continues....

Wavelength(Å)	El	E_{low} (eV)	log gf	BD-19132	BD-19290	HD30443	HE0457-1805	LAMOSTJ091608	HE0920-0506	HE1157-0518	HE1304-2111	HE1327-2116	HE1354-2257	LAMOSTJ151003	BD+193109	HD202851	References
4161.535	Ti II	1.084	-2.360	-	-	-	-	-	-	-	-	41.9(2.51)	-	-	-	92.8(4.35)	6
4417.719		1.165	-1.430	-	-	-	-	-	84.4(4.27)	-	-	-	-	-	-	-	6
4418.33		1.237	-2.460	-	-	-	-	-	68.9(4.41)	-	-	-	-	-	-	-	6
4443.794		1.08	-0.700	-	-	-	-	-	130.6(4.40)	-	-	-	-	-	-	157.1(4.15)	6
4468.52		1.13	-0.6	-	-	-	-	-	134.9(4.41)	-	-	-	-	-	-	-	6
4493.51		1.08	-2.73	60.0(3.34)	-	-	-	-	-	-	-	17.8(2.58)	-	-	-	-	6
4563.761		1.22	-0.960	139.8(3.33)	114.3(2.20)	154.20(3.31)	-	-	-	-	-	-	-	-	124.4(3.00)	-	6
4568.314		1.22	-2.650	61.1(3.47)	-	74.70(3.83)	59.4(3.30)	69.10(3.98)	-	-	-	-	-	30.20(3.02)	42.1(3.03)	-	6
4571.96		1.571	-0.53	123.1(4.73)	-	-	135.1(3.25)	-	-	-	-	-	-	140.4(3.16)	-	-	6
4636.32		1.164	-2.855	-	-	-	-	-	-	-	-	-	-	-	-	67.0(4.42)	6
4708.665		1.236	-2.210	-	-	-	-	-	-	-	-	-	-	-	-	86.9(4.29)	6
4764.526		1.236	-2.770	62.0(3.57)	-	62.40(3.79)	64.9(3.48)	-	40.0(4.26)	-	-	-	22.2(2.80)	49.90(3.47)	-	76.8(4.61)	6
4779.985		2.048	-1.37	-	20.9(2.16)	-	-	-	-	18.3(2.75)	-	37.0(2.70)	-	-	57.0(3.14)	97.5(4.64)	6
4798.521		1.08	-2.43	-	296(2.14)	-	-	72.10(3.62)	64.9(4.44)	-	-	-	42.2(2.68)	-	-	82.4(4.21)	6
4805.085		2.061	-1.100	87.9(3.56)	-	-	-	-	-	33.2(2.54)	-	-	-	-	-	-	6
4865.612		1.116	-2.61	73.7(3.43)	-	-	-	71.30(3.82)	-	-	-	-	31.8(2.70)	-	-	80.6(4.38)	6
5185.9		1.89	-1.35	-	-	-	94.4(3.37)	82.10(3.66)	65.8(4.23)	21.8(2.61)	99.50(5.36)	-	48.4(2.64)	86.30(3.34)	87.2(3.32)	-	6
5226.543		1.566	-1.300	-	-	-	-	-	81.0(4.30)	32.1(2.42)	-	-	-	-	-	-	6
5336.771		1.58	-1.700	81.4(3.23)	-	-	-	-	-	-	-	-	-	-	-	107.4(4.56)	6
5381.015		1.566	-2.08	-	-	-	94.1(3.61)	-	-	-	-	23.5(2.55)	-	46.00(3.07)	69.9(3.20)	-	6
5418.751		1.581	-1.999	-	50.8(4.42)	-	-	-	-	-	-	-	-	-	-	-	7
4351.05	Cr I	0.97	-1.45	-	-	-	-	-	67.0(5.21)	17.3(3.26)	-	-	-	-	-	-	6
4600.748		1.004	-1.260	-	-	-	-	-	-	87.0(4.52)	-	-	-	-	-	-	6
4616.12		0.982	-1.190	-	-	-	-	-	80.6(5.33)	-	-	-	-	-	-	-	6
4626.173		0.968	-1.320	-	-	-	-	-	-	-	-	-	-	-	73.7(2.71)	-	6
4652.157		1.004	-1.030	-	-	-	-	-	82.5(5.24)	-	-	-	-	-	-	-	6
4737.347		3.087	-0.099	-	-	-	-	-	50.9(5.46)	-	29.9(4.29)	-	-	-	-	73.5(5.31)	6
4829.372		2.544	-0.810	-	-	-	-	-	46.4(5.47)	-	-	-	-	-	-	58.8(5.08)	6
4870.801		3.079	0.05	-	-	-	-	-	-	-	42.0(4.51)	-	-	-	-	-	6
4942.49		0.941	-2.294	-	-	-	-	-	-	-	-	-	-	-	33.9(2.91)	99.5(5.55)	6
5247.565		0.961	-1.640	-	-	-	134.1(4.71)	-	68.8(5.28)	-	-	-	-	81.80(3.60)	77.3(2.86)	-	6
5296.691		0.982	-1.400	-	-	-	-	131.8(5.17)	-	-	-	21.6(3.03)	-	-	-	114.3(5.18)	6
5298.277		0.983	-1.15	-	-	-	-	-	-	-	100.0(4.39)	34.1(3.02)	-	-	-	125.6(5.19)	6
5300.744		0.982	-2.120	-	-	-	104.1(4.70)	-	-	-	-	-	-	49.00(3.68)	46.1(2.92)	-	6
5312.871		3.45	-0.562	-	-	-	21.8(4.87)	-	-	-	-	-	-	-	-	28.6(5.23)	6

The abundance obtained from each line is given in parenthesis.

Table B2 : continues....

Wavelength(Å)	El	E_{low} (eV)	log gf	BD-19132	BD-19290	HD30443	HE0457-1805	LAMOSTJ091608	HE0920-0506	HE1157-0518	HE1304-2111	HE1327-2116	HE1354-2257	LAMOSTJ151003	BD+193109	HD202851	References
5345.801		1.003	-0.980	-	-	-	-	150.1(5.12)	94.2(5.37)	-	-	-	-	128.7(3.64)	122.9(2.91)	145.7(5.16)	6
5348.312		1.003	-1.290	-	-	-	148.6(4.62)	121.6(4.86)	84.7(5.43)	18.8(3.10)	-	-	-	106.5(3.62)	95.6(2.81)	-	6
5409.772		1.03	-0.720	-	-	-	-	156.1(4.98)	107.8(5.42)	-	-	-	-	130.0(3.41)	125.4(2.70)	168.4(5.25)	6
5787.965		3.323	-0.083	-	-	-	-	-	41.4(5.37)	-	-	-	-	-	-	65.9(5.32)	6
6362.862		0.941	-3.623	-	-	-	-	33.00(5.33)	-	-	-	-	-	-	-	-	6
4588.19	Cr II	4.072	-0.63	-	-	-	81.1(4.55)	-	-	-	-	-	-	-	-	-	6
4634.07		4.072	-1.240	-	25.9(3.87)	-	-	-	58.0(5.41)	-	-	-	-	44.6(4.24)	-	-	6
4812.337		3.864	-1.800	-	39.4(3.73)	-	-	-	-	-	-	-	-	-	-	-	6
4848.25		3.864	-1.140	-	-	-	46.5(4.60)	-	-	-	-	-	-	35.9(4.36)	-	-	6
5305.853		3.827	-2.357	-	-	-	-	-	30.9(5.42)	-	-	-	-	-	-	36.1(5.40)	7
5308.404		4.072	-1.81	-	-	-	-	-	-	-	-	-	-	-	-	37.8(5.16)	6
5334.869		4.073	-1.562	-	-	-	-	-	45.4(5.29)	-	-	-	-	-	-	43.5(5.04)	7
4470.472	Ni I	3.399	-0.310	30.8(4.19)	-	-	-	-	-	-	-	-	-	-	-	-	7
4686.207		3.597	-0.64	-	-	-	62.8(5.19)	64.70(5.44)	-	-	-	-	-	-	44.7(4.59)	75.0(5.77)	7
4703.803		3.658	-0.735	-	-	-	-	-	45.1(5.87)	-	-	-	-	-	-	-	7
4714.408		3.38	0.23	-	-	-	-	-	-	-	-	-	-	30.5(3.59)	-	-	8
4731.793		3.833	-0.85	-	-	-	-	-	32.9(5.80)	-	-	-	-	-	-	61.0(5.92)	8
4732.46		4.106	-0.55	-	-	-	-	-	-	-	-	10.1(4.65)	-	-	-	-	8
4752.415		3.658	-0.7	-	-	-	-	-	46.8(5.88)	-	-	-	-	40.90(4.76)	-	76.4(5.91)	8
4756.51		3.48	-0.340	-	-	104.50(4.95)	94.1(5.39)	-	66.3(5.96)	-	-	-	-	-	-	90.8(5.69)	7
4821.13		4.153	-0.85	-	-	-	23.3(5.25)	37.40(5.73)	-	-	-	-	-	-	-	-	7
4852.56		3.542	-1.07	-	-	-	-	-	38.0(5.86)	-	-	16.7(4.76)	-	-	-	-	7
4953.2		3.74	-0.67	-	-	-	66.5(5.41)	59.80(5.51)	42.8(5.81)	-	-	-	-	22.00(4.45)	-	-	1
4980.166		3.606	-0.110	-	-	-	-	-	-	28.10(4.00)	-	-	-	72.90(4.55)	-	-	8
5035.357		3.635	0.29	78.9(4.21)	-	-	-	-	82.2(5.89)	-	-	-	-	-	-	-	8
5081.107		3.847	0.3	52.8(4.02)	-	-	-	-	-	38.7(4.23)	-	-	-	-	-	-	8
5082.35		3.657	-0.54	-	-	-	-	77.40(5.63)	-	-	32.2(4.06)	-	-	36.50(4.49)	-	-	8
5084.089		3.678	0.03	75.0(4.45)	-	-	-	-	-	15.6(3.92)	-	-	20.7(3.87)	-	-	-	1
5099.927		3.678	-0.100	-	-	-	-	-	-	-	-	-	-	-	-	97.4(5.78)	1
5102.96		1.676	-2.62	-	44.9(4.07)	-	-	-	-	-	-	-	-	93.90(4.87)	89.0(4.45)	-	8
5115.389		3.834	-0.11	-	-	-	-	-	-	11.7(4.09)	-	-	-	-	-	83.3(5.64)	8
5146.48		3.706	0.12	-	55.4(4.15)	-	-	-	64.9(5.46)	-	-	-	-	-	-	-	9
6086.28		4.266	-0.53	-	-	-	-	53.50(5.79)	-	-	-	-	-	-	-	-	8
6175.36		4.089	-0.530	-	-	64.10(5.38)	-	52.30(5.55)	-	-	-	-	-	-	-	52.0(5.64)	8
6176.807		4.088	-0.260	-	-	-	-	-	-	-	-	-	13.8(4.67)	-	-	70.5(6.01)	7

The abundance obtained from each line is given in parenthesis.

Table B2 : continues....

Wavelength(Å)	El	E_{low} (eV)	log gf	BD-19132	BD-19290	HD30443	HE0457-1805	LAMOSTJ091608	HE0920-0506	HE1157-0518	HE1304-2111	HE1327-2116	HE1354-2257	LAMOSTJ151003	BD+193109	HD202851	References
6177.236		1.826	-3.5	-	-	-	57.7(5.38)	38.40(5.56)	-	-	-	-	-	-	-	-	7
6186.71		4.106	-0.777	-	-	-	37.9(5.28)	41.80(5.62)	-	-	-	-	-	-	-	-	8
6204.6		4.088	-1.130	-	-	-	-	32.40(5.76)	-	-	-	-	-	-	-	31.3(5.82)	8
6327.593		1.676	-3.150	-	-	-	-	79.10(5.72)	29.4(5.65)	-	-	-	-	-	66.8(4.34)	75.7(5.84)	8
6378.247		4.154	-0.89	-	-	-	29.3(5.26)	31.40(5.57)	24.6(5.88)	-	-	-	-	-	-	37.8(5.79)	7
6643.629		1.676	-2.300	-	102.2(4.14)	177.80(5.06)	-	-	-	14.6(3.89)	61.3(4.31)	-	34.8(3.98)	106.6(4.53)	-	-	1
4722.15	Zn I	4.029	-0.370	-	27.4(2.33)	-	-	-	68.2(4.25)	-	-	-	29.9(2.50)	34.80(2.66)	-	-	10
4810.53		4.08	-0.170	48.3(3.00)	-	54.70(3.22)	69.9(3.10)	-	-	-	-	22.5(2.16)	-	33.80(2.46)	29.6(2.48)	64.1(3.48)	10
6362.34		5.8	0.15	-	-	-	-	29.60(4.11)	29.2(4.42)	-	-	-	-	-	-	-	10
4883.684	Y II	1.084	0.07	-	-	-	-	145.4(2.37)	103.9(2.81)	73.5(0.67)	-	79.7(0.08)	-	-	-	169.0(2.97)	11
5087.416		1.084	-0.170	-	-	-	-	-	90.8(2.76)	-	-	59.1(0.06)	-	-	-	164.9(3.12)	11
5119.112		0.992	-1.360	-	-	-	-	-	-	-	-	-	-	172.7(3.13)	89.2(1.55)	104.3(3.11)	11
5200.406		0.992	-1.360	-	-	158.80(1.94)	-	-	78.0(2.71)	35.5(0.55)	-	-	-	-	-	-	11
5205.724		1.033	-0.34	-	-	-	-	-	79.1(2.55)	41.8(0.48)	-	-	-	-	-	-	11
5289.815		1.033	-1.85	-	-	-	63.50(2.27)	-	-	-	-	-	-	-	44.4(1.23)	78.2(2.99)	11
5402.774		1.839	-0.51	-	25.9(0.46)	71.70(1.87)	-	77.50(2.20)	49.8(2.56)	-	-	-	-	-	-	-	11
5544.611		1.738	-1.090	101.0(2.64)	-	-	-	64.50(2.36)	38.3(2.62)	-	14.1(0.83)	-	-	-	-	-	11
5546.009		1.748	-1.11	-	-	-	-	-	-	-	-	-	-	124.9(2.97)	-	-	11
5662.925		1.944	0.16	156.8(2.64)	52.7(0.31)	-	-	105.3(2.26)	-	22.7(0.61)	-	17.7(0.04)	-	-	-	-	12
6613.733		1.748	-1.1	123.5(2.85)	-	-	-	74.20(2.49)	-	-	12.1(0.67)	-	-	-	54.5(1.47)	-	11
4739.48	Zr I	0.651	0.23	-	8.3(0.95)	-	-	84.30(3.30)	-	-	30.9(1.80)	-	-	47.30(1.89)	-	-	13
4772.323		0.623	0.04	-	8.3(1.10)	-	-	60.90(2.92)	-	-	-	-	-	63.90(2.27)	-	-	13
4805.889		0.687	-0.42	-	-	-	-	40.40(3.06)	-	-	-	-	-	-	-	-	13
6134.585		0	-1.280	-	-	-	-	54.10(3.18)	-	-	19.2(1.75)	-	-	32.50(2.15)	-	-	13
4317.321	Zr II	0.713	-1.38	98.3(2.24)	-	-	-	-	-	-	-	-	-	-	53.7(1.28)	-	13
5112.297		1.665	-0.59	88.0(2.34)	-	-	-	-	-	-	-	-	-	-	-	-	13
4257.12	Ce II	0.46	-1.116	-	-	-	-	-	-	-	-	-	-	36.80(1.15)	-	-	14
4336.244		0.704	-0.564	-	47.3(0.64)	-	-	82.70(2.32)	-	-	-	20.1(0.52)	-	-	-	-	14
4349.789		0.701	-0.107	-	-	-	-	-	44.3(2.11)	-	-	-	-	65.90(1.34)	-	-	14
4364.653		0.495	-0.201	-	-	-	-	-	41.9(1.86)	-	-	-	-	-	94.5(1.08)	-	14
4407.273		0.701	-0.741	-	-	74.10(1.59)	-	-	-	-	21.6(0.67)	-	-	53.70(1.32)	-	-	14
4418.78		0.863	0.177	-	-	-	-	-	41.1(1.88)	-	-	-	-	-	-	-	14
4427.916		0.535	-0.460	-	-	-	107.5(1.83)	-	-	-	-	32.8(0.46)	-	-	-	-	14
4460.207		0.477	0.171	-	-	-	-	-	-	-	-	98.0(0.54)	-	-	-	-	14
4483.893		0.864	0.01	-	-	-	124.4(2.16)	-	-	38.5(0.99)	-	-	-	-	-	14	

The abundance obtained from each line is given in parenthesis.

Table B2 : continues....

Wavelength(Å)	El	E_{low} (eV)	log gf	BD-19132	BD-19290	HD30443	HE0457-1805	LAMOSTJ091608	HE0920-0506	HE1157-0518	HE1304-2111	HE1327-2116	HE1354-2257	LAMOSTJ151003	BD+193109	HD202851	References	
4486.909		0.295	-0.474	-	-	-	-	-	48.3(2.19)	-	-	-	-	67.00(1.44)	-	-	14	
4497.846		0.958	-0.349	-	-	-	-	60.90(2.28)	-	-	-	-	48.2(1.11)	-	-	80.5(2.90)	14	
4508.079		0.621	-1.238	-	-	-	70.8(1.84)	-	-	-	-	-	-	-	36.1(1.04)	57.4(2.58)	14	
4560.28		0.91	0	-	-	-	-	-	34.4(0.96)	-	43.1(0.58)	-	-	-	-	-	-	14
4562.359		0.477	0.081	-	-	140.60(1.39)	-	-	62.9(0.87)	-	-	97.8(1.20)	-	-	-	103.5(2.30)	14	
4628.161		0.516	0.008	174.3(2.31)	-	145.40(1.57)	-	120.8(2.43)	-	-	62.2(0.33)	-	-	105.1(0.95)	115.7(2.69)	14		
4725.069		0.521	-1.204	-	32.1(0.65)	47.90(1.41)	-	-	-	-	-	-	-	40.6(0.87)	-	-	14	
4747.167		0.32	-1.246	-	-	86.90(1.65)	-	-	-	-	-	-	-	50.80(1.25)	53.7(0.86)	-	14	
4773.941		0.924	-0.498	-	-	-	-	-	-	-	-	-	-	-	42.3(0.77)	-	-	14
4873.999		1.107	-0.892	-	-	-	61.7(1.83)	49.60(2.22)	-	-	12.5(0.84)	-	-	-	-	53.6(2.67)	14	
5187.458		1.211	-0.104	-	60.9(0.78)	-	102.7(1.94)	86.20(2.35)	-	-	-	-	58.5(1.25)	-	-	82.9(2.68)	14	
5274.229		1.044	-0.323	-	89.2(0.46)	-	-	-	-	62.2(1.19)	-	-	-	96.10(1.21)	89.2(0.84)	-	7	
5330.556		0.869	-0.760	103.2(2.06)	-	-	-	72.30(2.23)	-	-	-	-	39.8(1.12)	59.40(1.53)	-	70.9(2.60)	14	
6034.205		1.458	-1.019	53.6(2.23)	-	-	55.5(2.10)	42.10(2.52)	-	-	-	-	-	-	-	35.2(2.74)	14	
5188.217	Pr II	0.922	-1.145	53.4(1.52)	-	54.70(1.82)	41.5(1.25)	26.00(1.59)	-	-	-	-	-	20.40(1.18)	-	36.0(2.17)	14	
5219.045		0.795	-0.24	112.1(1.47)	-	-	101.5(1.31)	-	-	11.9(0.31)	21.3(-0.06)	-	24.0(0.06)	77.20(1.02)	60.3(0.37)	-	15	
5259.728		0.633	-0.682	93.4(1.30)	-	116.40(1.70)	91.1(1.31)	65.90(1.60)	12.1(1.12)	-	-	-	-	61.90(1.04)	-	72.7(2.15)	15	
5292.619		0.648	-0.300	-	53.1(-0.06)	141.50(1.68)	104.6(1.21)	83.40(1.62)	22.8(1.17)	10.8(0.15)	-	-	33.3(0.13)	-	54.5(0.10)	77.3(1.90)	15	
5322.772		0.482	-0.315	-	55.9(-0.23)	-	131.8(1.51)	90.30(1.58)	-	12.4(0.04)	-	20.4(-0.23)	49.5(0.23)	98.00(0.98)	79.3(0.28)	86.9(1.94)	14	
6165.891		0.923	-0.205	-	-	125.60(1.64)	102.4(1.22)	59.20(1.24)	-	8.70(0.21)	-	-	-	63.00(0.87)	50.3(0.18)	-	14	
4446.384	Nd II	0.204	-0.590	-	-	-	139.7(1.99)	-	-	49.4(0.84)	-	-	-	110.9(1.27)	93.6(0.75)	-	16	
4451.563		0.38	-0.040	-	-	-	145.4(1.76)	115.1(2.04)	-	-	-	-	-	-	112.6(0.84)	119.8(2.52)	16	
4556.133		0.064	-1.610	123.1(2.14)	-	152.30(2.43)	-	76.60(2.13)	-	17.0(0.99)	-	-	-	-	58.1(0.76)	-	-	14
4703.572		0.38	-1.07	-	58.8(0.50)	-	-	-	-	-	-	-	-	-	-	-	-	14
4706.543		0	-0.880	-	-	-	-	-	-	-	-	-	-	-	-	-	-	14
4797.153		0.559	-0.950	-	-	-	-	-	-	29.1(0.67)	-	41.7(0.82)	-	-	-	-	-	14
4811.342		0.064	-1.140	148.9(2.05)	90.7(0.50)	177.70(2.24)	127.3(1.82)	92.80(2.00)	38.4(1.91)	-	-	47.7(0.52)	79.9(1.15)	-	85.3(0.68)	98.4(2.59)	14	
4825.478		0.182	-0.86	-	-	-	-	112.4(2.37)	34.9(1.62)	43.0(0.90)	-	44.0(0.33)	-	-	-	-	-	14
4859.039		0.32	-0.83	-	-	-	-	-	41.1(0.99)	-	38.8(0.39)	63.6(0.80)	-	-	-	87.5(2.29)	14	
4947.02		0.559	-1.250	109.0(2.08)	28.9(0.40)	107.80(2.02)	-	-	-	-	-	29.5(0.85)	58.00(1.42)	56.0(0.96)	62.3(2.35)	14		
4961.387		0.631	-0.710	-	58.7(0.40)	138.60(2.02)	-	96.00(2.32)	-	39.0(1.18)	-	-	63.0(1.04)	98.20(1.56)	-	-	-	14
5130.59		1.3	0.1	-	-	-	-	-	33.4(1.79)	37.0(1.09)	-	-	-	-	-	-	-	16
5212.361		0.204	-0.870	-	123.9(0.70)	-	137.4(1.76)	-	-	60.1(1.17)	-	-	87.5(1.13)	104.7(1.21)	103.3(0.80)	99.6(2.41)	14	
5255.506		0.204	-0.820	-	-	-	-	-	-	41.9(0.82)	-	51.2(0.36)	83.5(0.98)	-	105.9(0.78)	-	-	14
5276.869		0.859	-0.440	-	-	140.20(2.05)	-	-	-	22.4(0.82)	-	-	-	71.80(1.15)	65.8(0.67)	-	-	16

The abundance obtained from each line is given in parenthesis.

Table B2 : continues....

Wavelength(Å)	El	E_{low} (eV)	log gf	BD-19132	BD-19290	HD30443	HE0457-1805	LAMOSTJ091608	HE0920-0506	HE1157-0518	HE1304-2111	HE1327-2116	HE1354-2257	LAMOSTJ151003	BD+193109	HD202851	References
5287.133		0.744	-1.300	101.5(2.17)	-	111.90(2.34)	78.1(1.74)	-	-	-	-	-	-	39.30(1.39)	42.4(0.96)	49.5(2.31)	14
5293.163		0.822	-0.060	-	-	-	-	-	-	46.9(0.86)	-	51.2(0.34)	-	-	-	-	16
5311.453		0.986	-0.420	-	-	117.00(2.03)	93.8(1.63)	-	-	-	28.2(0.71)	-	49.8(1.04)	-	58.1(0.84)	66.8(2.23)	16
5319.815		0.55	-0.210	-	-	-	-	-	43.2(1.64)	63.0(0.94)	-	59.3(0.25)	-	-	-	-	16
5356.967		1.264	-0.250	126.0(2.34)	-	-	-	-	-	-	-	-	30.90(2.51)	68.20(1.42)	-	72.2(2.38)	16
5361.51		0.68	-0.4	-	106.9(0.65)	-	-	-	-	51.3(1.10)	-	36.0(0.30)	-	92.40(1.16)	94.2(0.85)	-	16
5371.927		1.412	0.003	-	-	-	-	-	-	-	-	-	-	-	-	-	16
5442.264		0.68	-0.910	143.8(2.39)	-	-	115.8(1.95)	84.40(2.19)	-	28.1(1.19)	-	-	-	86.00(1.56)	71.0(0.92)	-	16
5485.696		1.264	-0.120	-	-	-	107.2(1.79)	77.70(1.96)	-	-	-	-	-	68.70(1.28)	-	-	16
5688.518		0.986	-0.25	-	-	-	-	-	-	-	-	32.8(0.43)	-	-	-	-	16
5718.118		1.41	-0.340	-	-	120.10(2.41)	-	-	-	-	-	-	-	48.90(1.39)	37.4(0.78)	-	16
5825.857		1.08	-0.760	-	-	123.90(2.38)	95.2(1.85)	65.90(2.08)	-	-	-	-	-	50.00(1.40)	49.4(0.93)	59.3(2.33)	14
4318.927	Sm II	0.28	-0.270	-	-	176.80(1.69)	-	-	-	-	-	55.1(-0.19)	-	-	-	-	14
4424.337		0.485	-0.26	-	-	-	-	-	47.0(1.68)	-	34.7(0.08)	-	-	-	-	-	14
4434.318		0.378	-0.576	108.3(1.14)	52.8(-0.21)	127.50(1.29)	-	-	-	-	24.8(-0.24)	-	-	-	80.1(0.50)	-	14
4458.509		0.104	-1.11	-	44.3(-0.19)	-	-	76.30(1.45)	-	-	28.0(0.05)	-	56.1(0.51)	-	67.7(0.34)	71.8(1.74)	14
4499.475		0.248	-1.413	81.6(1.18)	-	94.10(1.41)	81.5(1.29)	52.10(1.34)	-	16.6(0.73)	-	-	28.3(0.42)	61.20(1.04)	51.2(0.52)	59.4(1.89)	14
4519.63		0.543	-0.751	-	-	-	-	-	-	-	-	-	-	81.70(1.07)	59.6(0.46)	-	14
4566.21		0.33	-1.245	-	-	-	88.7(1.36)	57.80(1.38)	22.5(1.46)	-	-	-	-	63.70(1.01)	-	-	14
4577.69		0.25	-0.77	-	-	-	-	-	-	-	33.0(-0.07)	-	-	-	-	-	14
4615.444		0.544	-1.262	-	-	-	-	50.60(1.49)	-	-	-	-	-	-	25.0(0.21)	53.9(1.94)	14
4642.228		0.379	-0.951	-	-	-	-	71.20(1.45)	27.4(1.39)	-	-	23.6(0.08)	-	88.90(1.15)	-	-	14
4674.593		0.184	-1.055	-	-	-	116.9(1.54)	68.10(1.23)	-	-	-	-	-	-	66.3(0.28)	-	14
4676.902		0.04	-1.407	94.2(1.04)	-	-	-	62.30(1.28)	-	16.3(0.46)	-	21.6(0.08)	-	-	-	-	14
4704.4		0	-1.562	99.7(1.23)	-	-	102.5(1.46)	73.10(1.62)	32.0(1.75)	-	-	-	-	65.00(0.89)	-	-	14
4726.026		0.333	-1.849	-	-	-	-	31.80(1.42)	-	-	-	-	-	27.70(1.02)	22.6(0.40)	-	14
4791.58		0.104	-1.846	84.7(1.35)	-	99.40(1.65)	81.6(1.41)	-	-	-	-	25.6(0.57)	-	-	42.5(1.73)	-	14
4815.805		0.185	-1.501	-	23.2(-0.17)	-	-	-	-	-	-	-	-	-	45.9(0.30)	-	14
4844.209		0.277	-1.558	-	-	96.60(1.57)	87.3(1.46)	-	-	-	-	-	-	-	-	53.2(1.87)	14
4854.368		0.379	-1.873	44.4(1.07)	-	-	53.0(1.23)	32.10(1.49)	-	-	-	-	-	-	-	29.1(1.79)	14

The abundance obtained from each line is given in parenthesis.

References: 1. Kurucz and Peytremann (1975), 2. Lincke and Ziegenbein (1971), 3. Garz (1973), 4. Schulz-Gulde (1969), 5. NBS in Kurucz database, 6. MFW in Kurucz database, 7. Kurucz (1988), 8. Fuhr *et al.* (1988), 9. Heise (1974), 10. Warner (1968), 11. Hannaford *et al.* (1982), 12. Cowley and Corliss (1983), 13. Biemont *et al.* (1981), 14. Meggers *et al.* (1975), 15. Lage and Whaling (1976), 16. Ward *et al.* (1985)

Chapter 5

Conclusions and future work

The thesis sought to comprehend the role of metal-poor stars in the Galactic chemical enrichment. In particular, we aimed to provide tighter observational constraints, in the form of observed abundances, to the low-mass ($0.8 - 3.0 M_{\odot}$) AGB nucleosynthesis in the Galaxy from a detailed chemical composition analysis of a sample of metal-poor stars at different metallicities.

The low- and intermediate-mass stars ($0.8 - 10 M_{\odot}$) are the predominant population of our Galaxy. These stars contribute significantly to the chemical evolution of the Universe as they evolve through different evolutionary stages. The majority of elements heavier than Fe are produced by these stars through slow- (s-) and rapid- (r-) neutron-capture processes. The origin and evolution of these heavy elements remains poorly understood. The atmospheres of low-mass, metal-poor stars in the Galaxy bear the fingerprints of the chemical evolution history of the Galaxy. The diverse abundance pattern observed in them points at different formation scenarios. Estimated abundances of these extrinsic stars provide insights into the poorly understood origin and evolution of elements in the early Galaxy. The last two decades have witnessed an increase in the high-resolution spectroscopic studies

of these stars, especially the CEMP stars. However, there are many questions associated with their origin and the evolution of heavy elements in the Galaxy. The abundance data available for metal-poor stars has been exploited extensively to constrain the Galactic chemical evolution. Many studies have highlighted the scope of enhancing such studies based on larger homogeneous abundance data, especially for the heavy elements in the low-metallicity regime.

In this thesis, we investigated the contribution of low-mass stars to the Galactic chemical enrichment from a detailed abundance analysis of a stellar sample of 23 objects ranging in metallicity $[Fe/H]$ from -2.86 to $+0.23$. The stellar sample is comprised of three subsets: i) a comparatively metal-rich Ba star sample; ii) a moderately metal-poor CH star sample; and iii) a very metal-poor CEMP-s and CEMP-r/s star sample. The analysis is based on high-quality, high-resolution spectra obtained with HCT/HESP ($R \sim 30,000$ and $60,000$), Mercator/HERMES ($R \sim 86,000$), VLT/UVES ($R \sim 48,000$), ESO-MPG/FEROS ($R \sim 48,000$), and SUBARU/HDS ($R \sim 50,000$). Some important results obtained from the program stars are briefly summarized in Table 5.1 for a quick review. We have derived necessary clues about the evolutionary nature of these objects from a careful analysis of their abundance patterns and a comparison of their observed abundance patterns with their counterparts available in the literature for different classes of metal-poor stars. Clues to the production of heavy-elements by the neutron-capture process operating at low-metallicity are also derived. For the first time, we investigated the possible origin(s) of these stars using various abundance profiles and abundance ratios. The physical properties as well as the initial mass of their companion AGB stars were investigated from their surface chemical composition analysis. We presented the first-ever mass estimate for the companion AGB stars of all the Ba, CH and CEMP-s stars in our sample except for HD 147609. We have used the least or little explored neutron-density dependent $[Rb/Zr]$ ratio for the first time for our stellar sample and derived an upper limit to the initial mass of their companions.

The main results obtained from this study are summarized below:

- Among the 23 objects in our sample, we present the first ever detailed high-resolution optical spectroscopic analysis for 12 objects: BD–19 132, BD–19 290, HD 30443, HE 0457–1805, LAMOSTJ091608.81+230734.6, HE 0920–0506, HE 1304–2111, HE 1327–2116, HE 1354–2257, LAMOSTJ151003.74+305407.3, BD+19 3109, and HD 179832. For the other 11 objects in the sample, although a few studies are available in the literature, they lack in various abundance details. For instance, i) abundance of Rb, a key s-process element for finding the neutron density at the s-process site that serves as an indicator of the mass of the companion AGB stars, ii) abundances of several key elements such as C, N, O, carbon isotopic ratio $^{12}\text{C}/^{13}\text{C}$, and several neutron-capture elements. For these objects, we have presented updated elemental abundances along with new results from a detailed spectroscopic analysis.
- **Stellar atmospheric parameters:** The stellar sample is found to cover ranges in metallicity $[\text{Fe}/\text{H}]$ from -2.86 to $+0.23$, surface temperature T_{eff} from 4005 to 6350 K, surface gravity $\log g$ from 0.61 to 4.28, and micro-turbulent velocity ζ from 0.63 to 3.45 km s^{-1} .
- **Stellar mass:** The mass of the Ba stars ranges from 0.70 to $2.50 M_{\odot}$. All the CEMP and CH stars for which mass could be estimated are found to be low-mass with mass $\leq 1.3 M_{\odot}$.
- **Elemental abundances and classification:** We have estimated the abundances of 28 elements, including light elements, α -process, Fe-peak and neutron-capture elements. We have also derived the carbon isotopic ratio $^{12}\text{C}/^{13}\text{C}$, an important indicator of mixing, whenever possible. All the program stars except HD 154276 show enhanced abundances of neutron-capture elements. Using the observed abundances and following the robust classification schemes, we found nine objects in our sample to be Ba stars, three

CH stars, four CEMP-s stars, six CEMP-r/s stars, and the star HD 154276 is found to be a normal metal-poor star.

- **Carbon:** We could determine the carbon abundance in all the program stars except for the Ba star HD 179832, and the normal metal-poor star HD 154276. The estimated carbon abundance $[C/Fe]$ in Ba stars ranges from -0.28 to 0.61 . For CH stars, this ratio ranges from 0.36 to 0.80 . The CEMP stars in our sample show an enhanced abundance of carbon with $[C/Fe] \geq 1.68$, except for BD-19 132 ($[C/Fe] \sim 0.70$).
- **Nitrogen:** Nitrogen abundance is estimated in all the program stars except the Ba stars HD 147609 and HD 179832, the normal metal-poor star HD 154276, and the CEMP star HE 1304-2111. The estimated nitrogen abundance $[N/Fe]$ is in the range of $0.47 - 1.41$ for the Ba stars, $0.45 - 1.42$ for the CH stars, and $0.40 - 2.51$ for the CEMP stars. The Ba stars HD 24035 and HD 94518, the CH star HD 202851, and all the CEMP stars except HD 30443 and HE 1354-2257, show an enhanced abundance of nitrogen with $[N/Fe] > 1$. The CEMP stars HE 1327-2116, and BD+19 3109 show the largest enhancement in our sample with $[N/Fe] \sim 2.51$ and 2.23 respectively.
- **Oxygen:** Oxygen abundance is estimated in all the Ba stars except for HD 24035. The observed oxygen abundance $[O/Fe]$ in them ranges from -0.47 to 0.97 . In the Ba stars HD 94518, HD 147609, and HD 207585, oxygen is enhanced with $[O/Fe] > 0.60$. The normal metal-poor star HD 154276 shows a mild enhancement with a value of $[O/Fe] \sim 0.32$. The abundance of oxygen is estimated for all the three CH stars and four CEMP stars BD-19 132, BD-19 290, HD 30443, and HE 1354-2257. The $[O/Fe]$ ranges from -0.14 to 0.35 for the CH stars and from 0.23 to 1.41 for the CEMP stars. The CEMP stars BD-19 290 and HD 30443 have the highest oxygen enhancement, with $[O/Fe]$ ratio 1.34 and 1.41 , respectively.

- **Carbon isotopic ratio $^{12}\text{C}/^{13}\text{C}$:** We have estimated the carbon isotopic ratio for 13 stars in our sample. The $^{12}\text{C}/^{13}\text{C}$ ratio ranges from 4.0 to 42.0. The low values of this ratio suggest that the observed abundance patterns of these stars are extrinsic in nature.
- **Odd-Z elements- Na, Al:** We could estimate the Na abundance in all the program stars except the CEMP star HE 1157–0518. The estimated Na abundance [Na/Fe] in the Ba stars is either near-solar or slightly enhanced with values ranging from 0.05 to 0.42. The CH stars show moderate enhancement with [Na/Fe] values ranging from 0.45 to 0.68. The CEMP stars show [Na/Fe] values in the range of 0.12 - 2.83. Among the four Na-enhanced CEMP stars, HE 0457–1805, and HE 1304–2111 show $[\text{Na}/\text{Fe}] > 2$, with HE 1304–2111 ($[\text{Na}/\text{Fe}] \sim 2.83$) showing the highest reported value of Na for CEMP stars. Such higher values, although not common, are not unusual in lower metallicity.
The Al abundance could be determined only in 2 stars: HD 154276, a normal star, and HD 211173, a Ba star. The estimated abundances of aluminium [Al/Fe] show near-solar values (~ -0.10) in these two objects.
- **α -elements:** The α -elements show near-solar values in all the Ba stars, in the normal star HD 154276, and in the CH stars. Except for HD 30443, and LAMOSTJ151003.74+305407.3, which show near-solar values, the CEMP stars show enhancement of α -elements with $[\alpha/\text{Fe}]$ in the range of 0.22 - 0.66.
- **Fe-peak elements:** In our sample, all the Ba stars, the normal star HD 154276, and all the CH stars except HD 202851 show near-solar abundance values for Fe-peak elements. While the CEMP stars BD–19 132, HE 1157–0518, LAMOSTJ151003.74+305407.3, and BD+19 3109 show a near-solar abundance of Fe-peak elements, the remaining CEMP stars show $[\text{X}/\text{Fe}]$ in the range of 0.27 - 0.96.

- **Neutron-capture elements:** Except for the normal star HD 154276, all of the other stars in our sample have been found to be enhanced in neutron-capture elements. The estimated [ls/Fe] and [hs/Fe] are in the range of (0.91 - 1.88 and 1.44 - 2.52) for the CEMP stars, in the range of (1.20 - 1.31 and 1.22 - 1.83) for the CH stars, and in the range of (0.37 - 1.41 and 0.66 - 1.66) for the Ba stars. The total s-process content [s/Fe] of the program stars is found to be in the range of 0.64 - 2.34 except for the normal star HD 154276 where it is \sim 0.11.
- **Evolutionary stage:** From the positions on the H-R diagram, all the program stars are found to belong either to the main-sequence or the giant branch. In our sample, we found 16 giants, three sub-giants, one main-sequence turn-off star, and one dwarf. Stellar nucleosynthesis theories do not support the observed enhanced abundance of heavy elements in the evolutionary stages to which these stars belong. This, when combined with the observed abundance, suggests that the enhanced abundance of these elements is not in-situ. This indicates pollution from external sources.
- **Radial velocity:** The estimated radial velocities of the program stars are in the range of -181.89 - $+289.46$ km s $^{-1}$. All the Ba stars, CH stars, and four CEMP stars - BD-19 132, HD 30443, HE 0457-1805, and HE 1304-2111 are found to be low radial-velocity ($|V_r| < 100$ km s $^{-1}$) objects. The remaining six CEMP stars, BD-19 290, HE 1157-0518, HE 1327-2116, HE 1354-2257, LAMOSTJ151003.74+305407.3, and BD+19 3109 are found to be high radial-velocity ($|V_r| > 100$ km s $^{-1}$) objects.

Seven stars in our sample HD 24035, HD 147609, HD 207585, HD 30443, HE 0457-1805, BD+19 3109, and HD 202851 are confirmed binaries. For eight stars HD 36650, HD 154276, HD 219116, BD-19 132, BD-19 290, HE 0920-0506, HE 1304-2111 and LAMOSTJ151003.74+305407.3, our radial velocity estimates show deviations from the radial velocity estimates

listed in the Gaia archive. This may be an indication that these stars are in binary systems.

- **Absolute carbon abundance as diagnostic of binarity:** The absolute carbon abundance $A(C)$ - metallicity $[Fe/H]$, diagram can be used to distinguish between majority of binary and single stars. In the absence of long-term radial velocity-monitoring studies, this diagram can be used to understand the binary status of the program stars. According to Yoon *et al.* (2016), the majority of the binary stars lie above the value of $A(C) \sim 7.1$. All the program stars are found to occupy the region in this diagram that are occupied by confirmed binary stars. Thus, from the locations of our program stars in this diagram, as well as from the the radial velocity estimates, we infer that the program stars are binaries and that the observed increase in the abundances of neutron-capture elements could be due to pollution from binary companions.

Furthermore, based on the $A(C)$ - $[Fe/H]$ diagram, all of our program stars are Group I objects by Yoon *et al.* (2016) that reside in the high-carbon band region at $A(C) \sim 7.96$. The stars of Group I are known to be the products of binary mass-transfer from an AGB companion. We may therefore infer that these stars owe their abundance pattern to a binary AGB companion.

- **Nature of companion AGB stars:** We have investigated the nature of the companion AGB stars of our program stars using several diagnostics such as C, N, O, Na, and Mg abundances, $[hs/ls]$ and $[Rb/Zr]$ ratios. From our analysis, we found that all these diagnostics are robust indicators of mass for companion AGB stars.

- **CNO abundances:** The positions of the stars on the $A(C)$ - $[Fe/H]$ diagram indicate that they are in the region of binary stars known to be polluted by low-mass AGB stars. Among our sample, the Ba stars HD 24035 and HD 94518, the CEMP star BD-19 132 and the CH star HD 202851 show enhanced abundance of nitrogen ($[N/Fe] > 1$)

compared to carbon, a behaviour that is characteristic of massive AGB stars with HBB. Our analysis based on [C/N] ratio has shown that all these stars have undergone internal mixing ($[C/N] < -0.6$) that altered the C and N abundance through the CN cycle. The $[C+N+O/Fe]$ values of the stars BD–19 132, and HD 202851, on the other hand, may indicate pollution from massive AGB companion. We have examined this possibility using abundances of other elements.

- **Na and Mg abundances:** In massive AGB stars, where the neutron source is $^{22}\text{Ne}(\alpha, n)^{25}\text{Mg}$ reaction, Na is found to be produced in abundance through the Ne - Na cycle. These stars also show an enhanced abundance of Mg produced from the α -capture reactions of ^{22}Ne . Besides Na and Mg, N is also produced in abundance in these stars through HBB. As a result, the abundance of Na and Mg are expected to be correlated with the abundance of N. Furthermore, the diffusive mixing and the H-burning in the massive AGB stars reduce the s-process efficiency, leading to an anti-correlation of s-process elements and nitrogen. We could not find any enhancement of Na and Mg in the Ba stars as compared to the disk dwarfs and field giants of the Galaxy. This discards the operation of $^{22}\text{Ne}(\alpha, n)^{25}\text{Mg}$ neutron source and rules out the possibility of a massive AGB companion for them. The four CEMP stars BD–19 132, BD–19 290, HE 0457–1805, and HE 1304–2111, on the other hand, are enhanced in Na with $[\text{Na}/\text{Fe}] > 1$. The star HE 0457–1805 is enhanced in Mg as well ($[\text{Mg}/\text{Fe}] > 1$). However, the absence of $[\text{Na}/\text{Fe}] - [\text{N}/\text{Fe}]$, $[\text{Mg}/\text{Fe}] - [\text{N}/\text{Fe}]$ correlations, and $[\text{Na}/\text{Fe}] - [\text{s}/\text{Fe}]$, $[\text{Mg}/\text{Fe}] - [\text{s}/\text{Fe}]$ anti-correlations for the sample of CH and CEMP stars rules out massive AGB star companions.
- **The $[\text{hs}/\text{ls}]$ ratio as an indicator of the neutron source:** The ratio of abundances of heavy s-process elements to the light s-process elements, the $[\text{hs}/\text{ls}]$ ratio, is an indicator of s-process efficiency in AGB

stars. The AGB models predict a positive value for this ratio in low-mass AGB stars ($M \leq 3 M_{\odot}$) and a negative value in the case of massive AGB stars ($M > 3 M_{\odot}$). All the stars in our sample show positive values for this ratio except for the CH star HE 0920–0506, and the CEMP star HE 1354–2257. However, these two stars do not show any enhancement of N, Na, and Mg that is expected in massive AGB stars. This, combined with the negative values of [hs/ls] ratio, discarded the possibility of massive AGB companions for these two objects. Furthermore, for the objects BD–19 132, and HD 202851 with enhanced nitrogen abundance, the positive [hs/ls] ratio values, as well as the conclusion drawn from the Na and Mg abundances, rule out pollution from massive AGB companions.

- **The [Rb/Zr] ratio as a probe of the neutron density at the s-process site:** Rb is a unique probe of the neutron density at the s-process site and hence a powerful diagnostic of the mass of the AGB star. AGB models and observations have shown that massive AGB stars ($M \geq 4 M_{\odot}$) are characterized by positive values of the [Rb/Zr] ratio and low-mass AGB stars ($M \leq 3 M_{\odot}$) by negative values of the [Rb/Zr]. However, this important neutron density dependent abundance ratio, [Rb/Zr], is not explored by many to determine the mass of the AGBs. We have examined the [Rb/Zr] ratio for our stellar sample, and investigated the characteristics of their companion AGB stars. We could estimate the values of the [Rb/Zr] ratio in 13 program stars, and all of them show a negative value for this ratio. We have made a comparison of the observed Rb and Zr abundances in the program stars with their counterparts observed in low- and intermediate-mass AGB stars of the Galaxy and the Magellanic Clouds. It has been shown that the observed ranges of Rb and Zr in the program stars are incompatible with those observed in the intermediate-mass AGB stars. This confirmed that all

the program stars are polluted by the low-mass AGB companions ($M \leq 3 M_{\odot}$).

- **i-process and the origin of CEMP-r/s stars:** The origin of CEMP-r/s stars is still a puzzling problem. We have conducted a comprehensive analysis of the observed abundance patterns of the CEMP-s and CEMP-r/s stars, including data from literature. The CEMP-s stars and CEMP-r/s stars could not be distinguished in terms of any of the abundance profiles considered. The continuity between the CEMP-s and CEMP-r/s stars in terms of various abundance profiles and abundance ratios confirms the same astrophysical site for both the classes of stars. The similar [ls/Fe] values, but higher [hs/Fe] values, and the tight correlation between [Eu/Fe] and [hs/Fe] of the CEMP-r/s stars compared to the CEMP-s stars indicate a higher neutron exposure and higher neutron density requirement than that for the classical s-process that produces the CEMP-s stars. We have confirmed from our analysis that a modified s-process in AGB stars, called the i-process, that requires a neutron density between s- and r-process neutron densities, is responsible for the observed abundances of the CEMP-r/s stars in our sample.
- **Parametric model-based analysis:** From the analysis based on different diagnostics, we have found that none of the program stars are polluted by massive AGB stars. Our analysis, based on different abundance ratios and abundance profiles, confirmed the low-mass AGB companions of the program stars. To strengthen our results, we have conducted a parametric-model based analysis for our sample. The observed abundances of neutron-capture elements in our program stars are compared with the predictions of stellar nucleosynthesis models appropriate for each class of the stars. The parametric model-based study for the program stars corroborated the results we have obtained from the abundance profile analysis.

- **Ba, CH, and CEMP-s stars:** A comparison of the observed abundances of these stars with the predictions from the FRUITY models of AGB stars that considers a dilution factor in the parametric model function confirmed that the AGB stars that polluted them are low-mass stars with masses $M \leq 3 M_{\odot}$.
 - **CEMP-r/s stars:** We have conducted the i-process parametric model-based analysis of the CEMP-r/s stars to confirm their origin. The observed abundance patterns in the CEMP-r/s stars of our sample are well reproduced by the i-process yields [X/Fe] of low-mass, low-metallicity AGB stars. The neutron densities responsible for the observed abundance patterns of the CEMP-r/s stars BD−19 290, HD 30443, HE 1157−0518, HE 1304−2111, HE 1327−2116 and LAMOSTJ151003.74+305407.3 are found to be $n \sim 10^{11}, 10^{14}, 10^{12}, 10^{13}, 10^{11}$, and 10^{12} respectively.
- **Kinematic analysis:** A kinematic analysis of the program stars has been performed to understand their spatial distributions. This information is just as important as elemental abundance information in constraining the evolution of the Galaxy. The Ba and CH stars are found to be members of the Galactic disk population, and the majority of the CEMP stars are found to belong to the Galactic halo.

Our analysis of stars at the given range of metallicity has shown that the stars are polluted by ejecta from the low-mass AGB companions. The studies on the Galactic chemical evolution would thus remain incomplete without considering the contribution of these low-mass stars. We also confirm that low-mass stars began contributing to the Galactic chemical evolution at metallicities as low as $[Fe/H] \sim -3$.

TABLE 5.1: Program stars with important results

Star name	[Fe/H]	[C/Fe]	$^{12}\text{C}/^{13}\text{C}$	[Ba/Eu]	[hs/ls]	[Rb/Zr]	Galactic population
Ba stars							
HD 24035	-0.51	0.41	—	1.22	0.20	—	Disk
HD 32712	-0.25	-0.05	20.00	1.05	1.15	-1.65	Disk
HD 36650	-0.02	-0.22	7.34	0.70	0.28	-1.33	Disk
HD 94518	-0.55	-0.28	—	0.75	0.19	—	Disk
HD 147609	-0.28	0.38	—	1.27	0.06	—	Disk
HD 179832	+0.23	—	—	0.41	0.19	-2.64	Disk
HD 207585	-0.38	0.61	—	1.32	0.64	—	Disk
HD 211173	-0.17	-0.23	20.00	0.44	0.26	-1.38	Disk
HD 219116	-0.45	0.02	7.34	0.79	0.62	—	Disk
Normal metal-poor star							
HD 154276	-0.10	—	—	—	0.33	—	Disk
CH stars							
LAMOSTJ091608.81+230734.6	-0.89	0.36	8.67	0.49	0.37	-0.92	Disk
HE 0920–0506	-0.75	0.57	—	1.60	-0.07	-1.29	Disk
HD 202851	-0.85	0.80	42.00	1.11	0.52	-1.95	Disk
CEMP-s stars							
BD–19 132	-1.86	0.70	18.00	1.01	1.14	-2.07	Disk
HE 0457–1805	-1.98	1.83	23.00	1.43	0.50	-1.02	Disk
HE 1354–2257	-2.11	2.03	—	1.16	-0.24	—	Halo
BD+19 3109	-2.23	2.47	9.00	1.01	0.73	-0.72	Halo
CEMP-r/s stars							
BD–19 290	-2.86	1.90	4.00	0.39	0.84	-0.25	Halo
HD 30443	-1.68	1.68	9.33	0.41	1.00	-1.54	Disk
HE 1157–0518	-2.42	2.31	—	0.47	0.59	—	Halo
HE 1304–2111	-2.34	2.24	—	0.46	0.58	—	Disk
HE 1327–2116	-2.84	2.46	7.00	0.58	0.83	—	Halo
LAMOSTJ151003.74+305407.3	-1.57	1.74	13.33	0.25	0.14	-0.99	Halo

Our abundance results, combined with the results from earlier studies, can be used to constrain the nucleosynthesis as well as the physical properties of low-mass AGB stars.

5.1 Future work

- In the thesis, we have considered the analysis of only CEMP-s and CEMP-r/s sub-classes. In the future, we would like to enhance this study by considering a larger sample of extremely metal-poor, low-mass stars. They are important

probes for studying the very early Galactic nucleosynthesis and the nature of the first stars (Pop III stars). The surface chemical composition of CEMP-no stars is thought to have an intrinsic origin, making them ideal candidates for such studies (Spite *et al.* 2013; Bonifacio *et al.* 2015; Hansen *et al.* 2015; Yoon *et al.* 2016). They are direct descendants of first generation stars and exhibit abundance patterns similar to Pop III stars (Frebel 2008; Nomoto *et al.* 2013; Spite *et al.* 2013; Choplin *et al.* 2017; Ezzeddine *et al.* 2019). A number of scenarios have been proposed for their origin (Hansen *et al.* 2015 and references therein). However, the exact origin of these stars is not yet confirmed. We propose to conduct analysis of a sample of CEMP-no stars with the aim of deriving clues to their origin. The high-resolution data required for such a study are obtained from HCT/HESP, Mercator/HERMES, and SUBARU/HDS.

- The present study focused mainly on the abundance of heavy elements. It would be interesting to study the behaviour of light elements such as C, N, O, Na, Mg, and Al with respect to the neutron source and neutron density. In particular, understanding the observed overabundance of Na in the low-metallicity regime is still a challenge.
- All the extrinsic stars analyzed in this study are found to have a low-mass AGB companion. It would be worthwhile to investigate if this result holds true for all extrinsic stars in the Galaxy. To conduct such a study, we require homogeneous abundance data for a still larger sample of extrinsic stars in AGB binary systems. This is expected to provide a better understanding of AGB stars' contributions to the Galactic chemical enrichment and shed light on the chemical evolution history of galaxies.

Successful observing proposals

Sl.No.	Title of the proposal	Proposal code**	Instrument	Allotted	Clear	Investigators*
				nights	nights	
1	Spectroscopy of potential CH star candidates	HCT-2016-C3-P10	HCT/HFOSC	4	4	AG (PI), SJ (Co-PI)
2	Spectroscopy of potential CH star candidates	HCT-2017-C1-P03	HCT/HFOSC	4	4	AG (PI), SJ (Co-PI)
3	Spectroscopy of potential CH star candidates	HCT-2017-C2-P02	HCT/HFOSC	3	2	AG (PI), SJ (Co-PI)
			HCT/HESP			
4	Spectroscopy of potential CH star candidates	HCT-2017-C3-P05	HCT/HESP	4	4	AG (PI), SJ (Co-PI)
5	Spectroscopy of potential CH star candidates	HCT-2018-C1-P01	HCT/HESP	3	3	AG (PI), SJ (Co-PI)
6	Spectroscopy of metal-poor stars	HCT-2018-C1-P07	HCT/HESP	3.5	3	SJ (PI), AG (Co-PI)
7	Spectroscopy of metal-poor stars	HCT-2018-C2-P03	HCT/HESP	2	0	SJ (PI), AG (Co-PI)
8	Spectroscopy of potential CH star candidates	HCT-2018-C2-P02	HCT/HESP	2	2	AG (PI), SJ (Co-PI)
9	Spectroscopy of metal-poor stars	HCT-2018-C3-P44	HCT/HESP	3	2.5	SJ (PI), AG (Co-PI)
10	Spectroscopy of potential CH star candidates	HCT-2018-C3-P52	HCT/HESP	3	2	AG (PI), SJ (Co-PI)
11	Spectroscopy of metal-poor stars	HCT-2019-C1-P63	HCT/HESP	4	1.5	SJ (PI), AG (Co-PI)
12	Spectroscopy of potential CH star candidates	HCT-2019-C1-P61	HCT/HESP	3	1.5	AG (PI), SJ (Co-PI)
13	Spectroscopy of metal-poor stars	HCT-2019-C2-P55	HCT/HESP	3	1	SJ (PI), AG (Co-PI)
14	Spectroscopy of potential CH star candidates	HCT-2019-C2-P06	HCT/HESP	3	1	AG (PI), SJ (Co-PI)
15	Spectroscopy of metal-poor stars	HCT-2019-C3-P18	HCT/HFOSC	4	1	SJ (PI), AG (Co-PI)
16	Spectroscopy of potential CH star candidates	HCT-2019-C3-P26	HCT/HFOSC	3	2	AG (PI), SJ (Co-PI)
17	Identification of most metal-poor stars based on low-resolution spectroscopy	HCT-2020-C1-P12	HCT/HFOSC	5	3	SJ (PI), AG (Co-PI)
18	Identification of most metal-poor stars based on low-resolution spectroscopy	HCT-2020-C2-P06	HCT/HFOSC	6	2.5	SJ (PI), AG (Co-PI)
19	Identification of most metal-poor stars based on low-resolution spectroscopy	HCT-2020-C3-P08	HCT/HFOSC	4.5	3.5	SJ (PI), AG (Co-PI)
20	Identification of most metal-poor stars based on low-resolution spectroscopy	HCT-2021-C1-P09	HCT/HFOSC	4	2.5	SJ (PI), AG (Co-PI)
		HCT-2021-C2-P16	HCT/HFOSC	3.5	0	SJ (PI), AG (Co-PI)
		HCT-2021-C3-P06	HCT/HFOSC	4	2	SJ (PI), AG (Co-PI)

*AG: Aruna Goswami, SJ: Shejeelammal J

**Cycles: C1: January - April, C2: May - August, C3: September - December

Bibliography

- Abate, C., Pols, O. R., Izzard, R. G. and Karakas, A. I., 2015a, “Carbon-enhanced metal-poor stars: a window on AGB nucleosynthesis and binary evolution. II. Statistical analysis of a sample of 67 CEMP-s stars”, *Astron. Astrophys.*, **581**, A22. [DOI], [ADS], [arXiv:1507.04662 [astro-ph.SR]]
- Abate, C., Pols, O. R., Karakas, A. I. and Izzard, R. G., 2015b, “Carbon-enhanced metal-poor stars: a window on AGB nucleosynthesis and binary evolution. I. Detailed analysis of 15 binary stars with known orbital periods”, *Astron. Astrophys.*, **576**, A118. [DOI], [ADS], [arXiv:1502.07759 [astro-ph.SR]]
- Abate, Carlo, Stancliffe, Richard J. and Liu, Zheng-Wei, 2016, “How plausible are the proposed formation scenarios of CEMP-r/s stars?”, *Astron. Astrophys.*, **587**, A50. [DOI], [ADS], [arXiv:1601.00976 [astro-ph.SR]]
- Abbondanno, U., Aerts, G., Alvarez-Velarde, F., Álvarez-Pol, H., Andriamonje, S., Andrzejewski, J., Badurek, G., Baumann, P., Bečvář, F., Benlliure, J., Berthoumieux, E., Calviño, F., Cano-Ott, D., Capote, R., Cennini, P., Chepel, V., Chiaveri, E., Colonna, N., Cortes, G., Cortina, D., Couture, A., Cox, J., Dababneh, S., Dahlfors, M., David, S., Dolfini, R., Domingo-Pardo, C., Duran, I., Embid-Segura, M., Ferrant, L., Ferrari, A., Ferreira-Marques, R., Frais-Koelbl, H., Furman, W., Goncalves, I., Gallino, R., Gonzalez-Romero, E., Goverdovski, A., Gramegna, F., Griesmayer, E., Gunsing, F., Haas, B., Haight, R., Heil, M., Herrera-Martinez, A., Isaev, S., Jericha, E., Käppeler, F., Kadi,

Y., Karadimos, D., Kerveno, M., Ketlerov, V., Koehler, P., Konovalov, V., Kratička, M., Lamboudis, C., Leeb, H., Lindote, A., Lopes, I., Lozano, M., Lukic, S., Marganiec, J., Marrone, S., Martinez-Val, J., Mastinu, P., Mengoni, A., Milazzo, P. M., Molina-Coballes, A., Moreau, C., Mosconi, M., Neves, F., Oberhummer, H., O'Brien, S., Pancin, J., Papaevangelou, T., Paradela, C., Pavlik, A., Pavlopoulos, P., Perlado, J. M., Perrot, L., Pignatari, M., Plag, R., Plompen, A., Plukis, A., Poch, A., Policarpo, A., Pretel, C., Quesada, J., Raman, S., Rapp, W., Rauscher, T., Reifarth, R., Rosetti, M., Rubbia, C., Rudolf, G., Rullhusen, P., Salgado, J., Soares, J. C., Stephan, C., Tagliente, G., Tain, J., Tassan-Got, L., Tavora, L., Terlizzi, R., Vannini, G., Vaz, P., Ventura, A., Vilamarín, D., Vincente, M. C., Vlachoudis, V., Voss, F., Wendler, H., Wiescher, M. and Wissak, K., 2004, "Neutron Capture Cross Section Measurement of ^{151}Sm at the CERN Neutron Time of Flight Facility (n_TOF)", *Phys. Rev. L.*, **93**(16), 161103. [DOI], [ADS]

Abbott, B. P., Abbott, R., Abbott, T. D., Acernese, F., Ackley, K., Adams, C., Adams, T., Addesso, P., Adhikari, R. X., Adya, V. B., Affeldt, C., Afrough, M., Agarwal, B., Agathos, M., Agatsuma, K., Aggarwal, N., Aguiar, O. D., Aiello, L., Ain, A., Ajith, P., Allen, B., Allen, G., Allocca, A., Aloy, M. A., Altin, P. A., Amato, A., Ananyeva, A., Anderson, S. B., Anderson, W. G., Angelova, S. V., Antier, S., Appert, S., Arai, K., Araya, M. C., Areeda, J. S., Arnaud, N., Arun, K. G., Ascenzi, S., Ashton, G., Ast, M., Aston, S. M., Astone, P., Atallah, D. V., Aufmuth, P., Aulbert, C., AultONeal, K., Austin, C., Avila-Alvarez, A., Babak, S., Bacon, P., Bader, M. K. M., Bae, S., Baker, P. T., Baldaccini, F., Ballardin, G., Ballmer, S. W., Banagiri, S., Barayoga, J. C., Barclay, S. E., Barish, B. C., Barker, D., Barkett, K., Barone, F., Barr, B., Barsotti, L., Barsuglia, M., Barta, D., Bartlett, J., Bartos, I., Bassiri, R., Basti, A., Batch, J. C., Bawaj, M., Bayley, J. C., Bazzan, M., Bécsy, B., Beer, C., Bejger, M., Belahcene, I., Bell, A. S., Berger, B. K., Bergmann, G., Bero, J. J., Berry, C. P. L., Bersanetti, D., Bertolini, A., Betzwieser, J., Bhagwat, S., Bhandare, R., Bilenko, I. A., Billingsley, G., Billman, C. R., Birch, J., Birney,

R., Birnholtz, O., Biscans, S., Biscoveanu, S., Bisht, A., Bitossi, M., Biwer, C., Bizouard, M. A., Blackburn, J. K., Blackman, J., Blair, C. D., Blair, D. G., Blair, R. M., Bloemen, S., Bock, O., Bode, N., Boer, M., Bogaert, G., Bohe, A., Bondu, F., Bonilla, E., Bonnand, R., Boom, B. A., Bork, R., Boschi, V., Bose, S., Bossie, K., Bouffanais, Y., Bozzi, A., Bradaschia, C., Brady, P. R., Branchesi, M., Brau, J. E., Briant, T., Brillet, A., Brinkmann, M., Brisson, V., Brockill, P., Broida, J. E., Brooks, A. F., Brown, D. A., Brown, D. D., Brunett, S., Buchanan, C. C., Buikema, A., Bulik, T., Bulten, H. J., Buonanno, A., Buskulic, D., Buy, C., Byer, R. L., Cabero, M., Cadonati, L., Cagnoli, G., Cahillane, C., Calderón Bustillo, J., Callister, T. A., Calloni, E., Camp, J. B., Canepa, M., Canizares, P., Cannon, K. C., Cao, H., Cao, J., Capano, C. D., Capocasa, E., Carbognani, F., Caride, S., Carney, M. F., Casanueva Diaz, J., Casentini, C., Caudill, S., Cavaglià, M., Cavalier, F., Cavalieri, R., Cella, G., Cepeda, C. B., Cerdá-Durán, P., Cerretani, G., Cesarini, E., Chamberlin, S. J., Chan, M., Chao, S., Charlton, P., Chase, E., Chassande-Mottin, E., Chatterjee, D., Chatzioannou, K., Cheeseboro, B. D., Chen, H. Y., Chen, X., Chen, Y., Cheng, H. P., Chia, H., Chincarini, A., Chiummo, A., Chmiel, T., Cho, H. S., Cho, M., Chow, J. H., Christensen, N., Chu, Q., Chua, A. J. K., Chua, S., Chung, A. K. W., Chung, S., Ciani, G., Ciolfi, R., Cirelli, C. E., Cirone, A., Clara, F., Clark, J. A., Clearwater, P., Cleva, F., Cocchieri, C., Coccia, E., Co-hadon, P. F., Cohen, D., Colla, A., Collette, C. G., Cominsky, L. R., Constancio, M., Jr., Conti, L., Cooper, S. J., Corban, P., Corbitt, T. R., Cordero-Carrión, I., Corley, K. R., Cornish, N., Corsi, A., Cortese, S., Costa, C. A., Coughlin, M. W., Coughlin, S. B., Coulon, J. P., Countryman, S. T., Couvares, P., Co-vas, P. B., Cowan, E. E., Coward, D. M., Cowart, M. J., Coyne, D. C., Coyne, R., Creighton, J. D. E., Creighton, T. D., Cripe, J., Crowder, S. G., Cullen, T. J., Cumming, A., Cunningham, L., Cuoco, E., Dal Canton, T., Dálya, G., Danilishin, S. L., D'Antonio, S., Danzmann, K., Dasgupta, A., Da Silva Costa, C. F., Dattilo, V., Dave, I., Davier, M., Davis, D., Daw, E. J., Day, B., De, S., DeBra, D., Degallaix, J., De Laurentis, M., Deléglise, S., Del Pozzo, W., Demos,

N., Denker, T., Dent, T., De Pietri, R., Dergachev, V., De Rosa, R., DeRosa, R. T., De Rossi, C., DeSalvo, R., de Varona, O., Devenson, J., Dhurandhar, S., Díaz, M. C., Di Fiore, L., Di Giovanni, M., Di Girolamo, T., Di Lieto, A., Di Pace, S., Di Palma, I., Di Renzo, F., Doctor, Z., Dolique, V., Donovan, F., Dooley, K. L., Doravari, S., Dorrington, I., Douglas, R., Dovale Álvarez, M., Downes, T. P., Drago, M., Dreissigacker, C., Driggers, J. C., Du, Z., Ducrot, M., Dupej, P., Dwyer, S. E., Edo, T. B., Edwards, M. C., Effler, A., Eggenstein, H. B., Ehrens, P., Eichholz, J., Eikenberry, S. S., Eisenstein, R. A., Essick, R. C., Estevez, D., Etienne, Z. B., Etzel, T., Evans, M., Evans, T. M., Factourovich, M., Fafone, V., Fair, H., Fairhurst, S., Fan, X., Farinon, S., Farr, B., Farr, W. M., Fauchon-Jones, E. J., Favata, M., Fays, M., Fee, C., Fehrmann, H., Feicht, J., Fejer, M. M., Fernandez-Galiana, A., Ferrante, I., Ferreira, E. C., Ferriini, F., Fidecaro, F., Finstad, D., Fiori, I., Fiorucci, D., Fishbach, M., Fisher, R. P., Fitz-Axen, M., Flaminio, R., Fletcher, M., Fong, H., Font, J. A., Forsyth, P. W. F., Forsyth, S. S., Fournier, J. D., Frasca, S., Frasconi, F., Frei, Z., Freise, A., Frey, R., Frey, V., Fries, E. M., Fritschel, P., Frolov, V. V., Fulda, P., Fyffe, M., Gabbard, H., Gadre, B. U., Gaebel, S. M., Gair, J. R., Gammaitoni, L., Ganija, M. R., Gaonkar, S. G., Garcia-Quiros, C., Garufi, F., Gateley, B., Gaudio, S., Gaur, G., Gayathri, V., Gehrels, N., Gemme, G., Genin, E., Gennai, A., George, D., George, J., Gergely, L., Germain, V., Ghonge, S., Ghosh, Abhirup, Ghosh, Archisman, Ghosh, S., Giaime, J. A., Giardina, K. D., Giazotto, A., Gill, K., Glover, L., Goetz, E., Goetz, R., Gomes, S., Goncharov, B., González, G., Gonzalez Castro, J. M., Gopakumar, A., Gorodetsky, M. L., Gossan, S. E., Gosselin, M., Gouaty, R., Grado, A., Graef, C., Granata, M., Grant, A., Gras, S., Gray, C., Greco, G., Green, A. C., Gretarsson, E. M., Groot, P., Grote, H., Grunewald, S., Gruning, P., Guidi, G. M., Guo, X., Gupta, A., Gupta, M. K., Gushwa, K. E., Gustafson, E. K., Gustafson, R., Halim, O., Hall, B. R., Hall, E. D., Hamilton, E. Z., Hammond, G., Haney, M., Hanke, M. M., Hanks, J., Hanna, C., Hannam, M. D., Hannuksela, O. A., Hanson, J., Hardwick, T., Harms, J., Harry, G. M., Harry, I. W., Hart, M. J., Haster, C. J., Haughian,

K., Healy, J., Heidmann, A., Heintze, M. C., Heitmann, H., Hello, P., Hemming, G., Hendry, M., Heng, I. S., Hennig, J., Heptonstall, A. W., Heurs, M., Hild, S., Hinderer, T., Hoak, D., Hofman, D., Holt, K., Holz, D. E., Hopkins, P., Horst, C., Hough, J., Houston, E. A., Howell, E. J., Hreibi, A., Hu, Y. M., Huerta, E. A., Huet, D., Hughey, B., Husa, S., Huttner, S. H., Huynh-Dinh, T., Indik, N., Inta, R., Intini, G., Isa, H. N., Isac, J. M., Isi, M., Iyer, B. R., Izumi, K., Jacqmin, T., Jani, K., Jaranowski, P., Jawahar, S., Jiménez-Forteza, F., Johnson, W. W., Johnson-McDaniel, N. K., Jones, D. I., Jones, R., Jonker, R. J. G., Ju, L., Junker, J., Kalaghatgi, C. V., Kalogera, V., Kamai, B., Kandasamy, S., Kang, G., Kanner, J. B., Kapadia, S. J., Karki, S., Karvinen, K. S., Kasprzack, M., Kastaun, W., Katolik, M., Katsavounidis, E., Katzman, W., Kaufer, S., Kawabe, K., Kéfélian, F., Keitel, D., Kemball, A. J., Kennedy, R., Kent, C., Key, J. S., Khalili, F. Y., Khan, I., Khan, S., Khan, Z., Khazanov, E. A., Kijbunchoo, N., Kim, Chunglee, Kim, J. C., Kim, K., Kim, W., Kim, W. S., Kim, Y. M., Kimbrell, S. J., King, E. J., King, P. J., Kinley-Hanlon, M., Kirchhoff, R., Kissel, J. S., Kleybolte, L., Klimenko, S., Knowles, T. D., Koch, P., Koehlenbeck, S. M., Koley, S., Kondrashov, V., Kontos, A., Korobko, M., Korth, W. Z., Kowalska, I., Kozak, D. B., Krämer, C., Kringle, V., Krishnan, B., Królak, A., Kuehn, G., Kumar, P., Kumar, R., Kumar, S., Kuo, L., Kutynia, A., Kwang, S., Lackey, B. D., Lai, K. H., Landry, M., Lang, R. N., Lange, J., Lantz, B., Lanza, R. K., Lartaux-Vollard, A., Lasky, P. D., Laxen, M., Lazzarini, A., Lazzaro, C., Leaci, P., Leavey, S., Lee, C. H., Lee, H. K., Lee, H. M., Lee, H. W., Lee, K., Lehmann, J., Lenon, A., Leonard, M., Leroy, N., Letendre, N., Levin, Y., Li, T. G. F., Linker, S. D., Littenberg, T. B., Liu, J., Lo, R. K. L., Lockerbie, N. A., London, L. T., Lord, J. E., Lorenzini, M., Loriette, V., Lormand, M., Losurdo, G., Lough, J. D., Lousto, C. O., Lovelace, G., Lück, H., Lumaca, D., Lundgren, A. P., Lynch, R., Ma, Y., Macas, R., Macfoy, S., Machenschalk, B., MacInnis, M., Macleod, D. M., Magaña Hernandez, I., Magaña-Sandoval, F., Magaña Zertuche, L., Magee, R. M., Majorana, E., Maksimovic, I., Man, N., Mandic, V., Mangano, V., Mansell, G. L., Manske, M.,

Mantovani, M., Marchesoni, F., Marion, F., Márka, S., Márka, Z., Markakis, C., Markosyan, A. S., Markowitz, A., Maros, E., Marquina, A., Martelli, F., Martellini, L., Martin, I. W., Martin, R. M., Martynov, D. V., Mason, K., Massera, E., Masserot, A., Massinger, T. J., Masso-Reid, M., Mastrogiovanni, S., Matas, A., Matichard, F., Matone, L., Mavalvala, N., Mazumder, N., McCarthy, R., McClelland, D. E., McCormick, S., McCuller, L., McGuire, S. C., McIntyre, G., McIver, J., McManus, D. J., McNeill, L., McRae, T., McWilliams, S. T., Meacher, D., Meadors, G. D., Mehmet, M., Meidam, J., Mejuto-Villa, E., Melatos, A., Mendell, G., Mercer, R. A., Merilh, E. L., Merzougui, M., Meshkov, S., Messenger, C., Messick, C., Metzdorff, R., Meyers, P. M., Miao, H., Michel, C., Middleton, H., Mikhailov, E. E., Milano, L., Miller, A. L., Miller, B. B., Miller, J., Millhouse, M., Milovich-Goff, M. C., Minazzoli, O., Minenkov, Y., Ming, J., Mishra, C., Mitra, S., Mitrofanov, V. P., Mitselmakher, G., Mittelman, R., Moffa, D., Moggi, A., Mogushi, K., Mohan, M., Mohapatra, S. R. P., Montani, M., Moore, C. J., Moraru, D., Moreno, G., Morriss, S. R., Mouris, B., Mow-Lowry, C. M., Mueller, G., Muir, A. W., Mukherjee, Arunava, Mukherjee, D., Mukherjee, S., Mukund, N., Mullavey, A., Munch, J., Muñiz, E. A., Muratore, M., Murray, P. G., Napier, K., Nardecchia, I., Naticchioni, L., Nayak, R. K., Neilson, J., Nelemans, G., Nelson, T. J. N., Nery, M., Neunzert, A., Nevin, L., Newport, J. M., Newton, G., Ng, K. K. Y., Nguyen, T. T., Nichols, D., Nielsen, A. B., Nissanke, S., Nitz, A., Noack, A., Nocera, F., Nolting, D., North, C., Nuttall, L. K., Oberling, J., O'Dea, G. D., Ogin, G. H., Oh, J. J., Oh, S. H., Ohme, F., Okada, M. A., Oliver, M., Oppermann, P., Oram, Richard J., O'Reilly, B., Ormiston, R., Ortega, L. F., O'Shaughnessy, R., Ossokine, S., Ottaway, D. J., Overmier, H., Owen, B. J., Pace, A. E., Page, J., Page, M. A., Pai, A., Pai, S. A., Palamos, J. R., Palashov, O., Palomba, C., Pal-Singh, A., Pan, Howard, Pan, Huang-Wei, Pang, B., Pang, P. T. H., Pankow, C., Pannarale, F., Pant, B. C., Paoletti, F., Paoli, A., Papa, M. A., Parida, A., Parker, W., Pasucci, D., Pasqualetti, A., Passaquieti, R., Passuello, D., Patil, M., Patricelli, B., Pearlstone, B. L., Pedraza, M., Pedurand, R., Pekowsky, L., Pele, A., Penn, S.,

Perez, C. J., Perreca, A., Perri, L. M., Pfeiffer, H. P., Phelps, M., Piccinni, O. J., Pichot, M., Piergiovanni, F., Pierro, V., Pillant, G., Pinard, L., Pinto, I. M., Pirello, M., Pitkin, M., Poe, M., Poggiani, R., Popolizio, P., Porter, E. K., Post, A., Powell, J., Prasad, J., Pratt, J. W. W., Pratten, G., Predoi, V., Prestegard, T., Prijatelj, M., Principe, M., Privitera, S., Prodi, G. A., Prokhorov, L. G., Puncken, O., Punturo, M., Puppo, P., Pürrer, M., Qi, H., Quetschke, V., Quintero, E. A., Quitzow-James, R., Raab, F. J., Rabeling, D. S., Radkins, H., Raffai, P., Raja, S., Rajan, C., Rajbhandari, B., Rakhmanov, M., Ramirez, K. E., Ramos-Buades, A., Rapagnani, P., Raymond, V., Razzano, M., Read, J., Regimbau, T., Rei, L., Reid, S., Reitze, D. H., Ren, W., Reyes, S. D., Ricci, F., Ricker, P. M., Rieger, S., Riles, K., Rizzo, M., Robertson, N. A., Robie, R., Robinet, F., Rocchi, A., Rolland, L., Rollins, J. G., Roma, V. J., Romano, R., Romel, C. L., Romie, J. H., Rosińska, D., Ross, M. P., Rowan, S., Rüdiger, A., Ruggi, P., Rutins, G., Ryan, K., Sachdev, S., Sadecki, T., Sadeghian, L., Sakellariadou, M., Salconi, L., Saleem, M., Salemi, F., Samajdar, A., Sammut, L., Sampson, L. M., Sanchez, E. J., Sanchez, L. E., Sanchis-Gual, N., Sandberg, V., Sanders, J. R., Sassolas, B., Sathyaprakash, B. S., Saulson, P. R., Sauter, O., Savage, R. L., Sawadsky, A., Schale, P., Scheel, M., Scheuer, J., Schmidt, J., Schmidt, P., Schnabel, R., Schofield, R. M. S., Schönbeck, A., Schreiber, E., Schuette, D., Schulte, B. W., Schutz, B. F., Schwalbe, S. G., Scott, J., Scott, S. M., Seidel, E., Sellers, D., Sengupta, A. S., Sentenac, D., Sequino, V., Sergeev, A., Shaddock, D. A., Shaffer, T. J., Shah, A. A., Shahriar, M. S., Shaner, M. B., Shao, L., Shapiro, B., Shawhan, P., Sheperd, A., Shoemaker, D. H., Shoemaker, D. M., Siellez, K., Siemens, X., Sieniawska, M., Sigg, D., Silva, A. D., Singer, L. P., Singh, A., Singhal, A., Sintes, A. M., Slagmolen, B. J. J., Smith, B., Smith, J. R., Smith, R. J. E., Somala, S., Son, E. J., Sonnenberg, J. A., Sorazu, B., Sorrentino, F., Souradeep, T., Spencer, A. P., Srivastava, A. K., Staats, K., Staley, A., Steinke, M., Steinlechner, J., Steinlechner, S., Steinmeyer, D., Stevenson, S. P., Stone, R., Stops, D. J., Strain, K. A., Stratta, G., Strigin, S. E., Strunk, A., Sturani, R., Stuver, A. L., Summerscales, T. Z., Sun, L.,

Sunil, S., Suresh, J., Sutton, P. J., Swinkels, B. L., Szczepańczyk, M. J., Tacca, M., Tait, S. C., Talbot, C., Talukder, D., Tanner, D. B., Tápai, M., Taracchini, A., Tasson, J. D., Taylor, J. A., Taylor, R., Tewari, S. V., Theeg, T., Thies, F., Thomas, E. G., Thomas, M., Thomas, P., Thorne, K. A., Thorne, K. S., Thrane, E., Tiwari, S., Tiwari, V., Tokmakov, K. V., Toland, K., Tonelli, M., Tornasi, Z., Torres-Forné, A., Torrie, C. I., Töyrä, D., Travasso, F., Traylor, G., Trinastic, J., Tringali, M. C., Trozzo, L., Tsang, K. W., Tse, M., Tso, R., Tsukada, L., Tsuna, D., Tuyenbayev, D., Ueno, K., Ugolini, D., Unnikrishnan, C. S., Urban, A. L., Usman, S. A., Vahlbruch, H., Vajente, G., Valdes, G., van Bakel, N., van Beuzekom, M., van den Brand, J. F. J., Van Den Broeck, C., Vander-Hyde, D. C., van der Schaaf, L., van Heijningen, J. V., van Veggel, A. A., Vardaro, M., Varma, V., Vass, S., Vasúth, M., Vecchio, A., Vedovato, G., Veitch, J., Veitch, P. J., Venkateswara, K., Venugopalan, G., Verkindt, D., Vetrano, F., Viceré, A., Viets, A. D., Vinciguerra, S., Vine, D. J., Vinet, J. Y., Vitale, S., Vo, T., Vocca, H., Vorvick, C., Vyatchanin, S. P., Wade, A. R., Wade, L. E., Wade, M., Walet, R., Walker, M., Wallace, L., Walsh, S., Wang, G., Wang, H., Wang, J. Z., Wang, W. H., Wang, Y. F., Ward, R. L., Warner, J., Was, M., Watchi, J., Weaver, B., Wei, L. W., Weinert, M., Weinstein, A. J., Weiss, R., Wen, L., Wessel, E. K., Weßels, P., Westerweck, J., Westphal, T., Wette, K., Whelan, J. T., Whitcomb, S. E., Whiting, B. F., Whittle, C., Wilken, D., Williams, D., Williams, R. D., Williamson, A. R., Willis, J. L., Willke, B., Wimmer, M. H., Winkler, W., Wipf, C. C., Wittel, H., Woan, G., Woehler, J., Wofford, J., Wong, K. W. K., Worden, J., Wright, J. L., Wu, D. S., Wysocki, D. M., Xiao, S., Yamamoto, H., Yancey, C. C., Yang, L., Yap, M. J., Yazback, M., Yu, Hang, Yu, Haocun, Yvert, M., Zadrożny, A., Zanolin, M., Zelenova, T., Zendri, J. P., Zevin, M., Zhang, L., Zhang, M., Zhang, T., Zhang, Y. H., Zhao, C., Zhou, M., Zhou, Z., Zhu, S. J., Zhu, X. J., Zimmerman, A. B., Zucker, M. E., Zweizig, J., (LIGO Scientific Collaboration, Virgo Collaboration, Burns, E., Veres, P., Kocevski, D., Racusin, J., Goldstein, A., Connaughton, V., Briggs, M. S., Blackburn, L.,

- Hamburg, R., Hui, C. M., von Kienlin, A., McEnery, J., Preece, R. D., Wilson-Hodge, C. A., Bissaldi, E., Cleveland, W. H., Gibby, M. H., Giles, M. M., Kippen, R. M., McBreen, S., Meegan, C. A., Paciesas, W. S., Poolakkil, S., Roberts, O. J., Stanbro, M., Gamma-ray Burst Monitor, (Fermi, Savchenko, V., Ferrigno, C., Kuulkers, E., Bazzano, A., Bozzo, E., Brandt, S., Chenevez, J., Courvoisier, T. J. L., Diehl, R., Domingo, A., Hanlon, L., Jourdain, E., Laurent, P., Lebrun, F., Lutovinov, A., Mereghetti, S., Natalucci, L., Rodi, J., Roques, J. P., Sunyaev, R., Ubertini, P. and (INTEGRAL, 2017, “Gravitational Waves and Gamma-Rays from a Binary Neutron Star Merger: GW170817 and GRB 170817A”, *Astrophys. J. Lett.*, **848**(2), L13. [DOI], [ADS], [arXiv:1710.05834 [astro-ph.HE]]
- Abia, C. and Wallerstein, G., 1998, “Heavy-element abundances in seven SC stars and several related stars”, *Mon. Not. Roy. Astron. Soc.*, **293**(1), 89–106. [DOI], [ADS]
- Abia, C., Busso, M., Gallino, R., Domínguez, I., Straniero, O. and Isern, J., 2001, “The ^{85}Kr s-Process Branching and the Mass of Carbon Stars”, *Astrophys. J.*, **559**(2), 1117–1134. [DOI], [ADS], [arXiv:astro-ph/0105486 [astro-ph]]
- Afşar, M., Sneden, C. and For, B. Q., 2012, “Chemical Compositions of Thin-disk, High-metallicity Red Horizontal-branch Field Stars”, *Astron. J.*, **144**(1), 20. [DOI], [ADS], [arXiv:1205.3659 [astro-ph.SR]]
- Alksnis, A., Balklavs, A., Dzervitis, U., Eglitis, I., Paupers, O. and Pundure, I., 2001, “General Catalog of Galactic Carbon Stars by C. B. Stephenson. Third Edition”, *Balt. Astron.*, **10**, 1–318. [DOI], [ADS]
- Allen, D. M. and Barbuy, B., 2006, “Analysis of 26 barium stars. I. Abundances”, *Astron. Astrophys.*, **454**(3), 895–915. [DOI], [ADS], [arXiv:astro-ph/0604036 [astro-ph]]

- Allen, D. M., Ryan, S. G., Rossi, S., Beers, T. C. and Tsangarides, S. A., 2012, “Elemental abundances and classification of carbon-enhanced metal-poor stars”, *Astron. Astrophys.*, **548**, A34. [DOI], [ADS], [arXiv:1210.5009 [astro-ph.SR]]
- Allende Prieto, Carlos, Lambert, David L. and Asplund, Martin, 2001, “The Forbidden Abundance of Oxygen in the Sun”, *Astrophys. J. Lett.*, **556**(1), L63–L66. [DOI], [ADS], [arXiv:astro-ph/0106360 [astro-ph]]
- Alonso, A., Arribas, S. and Martínez-Roger, C., 1994, “Broad band JHK infrared photometry of an extended sample of late type dwarfs and subdwarfs.”, *Astron. Astrophys. Suppl.*, **107**, 365–383. [ADS]
- Alonso, A., Arribas, S. and Martínez-Roger, C., 1995, “Determination of bolometric fluxes for F, G and K subdwarfs.”, *Astron. Astrophys.*, **297**, 197–215. [ADS]
- Alonso, A., Arribas, S. and Martínez-Roger, C., 1996, “The empirical scale of temperatures of the low main sequence (F0V-K5V).”, *Astron. Astrophys.*, **313**, 873–890. [ADS]
- Alonso, A., Arribas, S. and Martínez-Roger, C., 1999, “The effective temperature scale of giant stars (F0-K5). II. Empirical calibration of T_{eff} versus colours and [Fe/H]”, *Astron. Astrophys. Suppl.*, **140**, 261–277. [DOI], [ADS]
- Alonso, A., Arribas, S. and Martínez-Roger, C., 2001, “Erratum: The effective temperature scale of giant stars (F0-K5). II. Empirical calibration of T_{eff} versus colours and [Fe/H]”, *Astron. Astrophys.*, **376**, 1039. [DOI], [ADS]
- Alpher, R. A., Bethe, H. and Gamow, G., 1948, “The Origin of Chemical Elements”, *Physical Review*, **73**(7), 803–804. [DOI], [ADS]
- Amarsi, A. M., Asplund, M., Collet, R. and Leenaarts, J., 2016, “Non-LTE oxygen line formation in 3D hydrodynamic model stellar atmospheres”, *Mon. Not. Roy. Astron. Soc.*, **455**(4), 3735–3751. [DOI], [ADS], [arXiv:1511.01155 [astro-ph.SR]]

- Andersen, T., Poulsen, O., Ramanujam, P. S. and Petkov, A. P., 1975, “Lifetimes of some excited states in the rare earths: La ii, Ce ii, Pr ii, Nd ii, Sm ii, Yb i, Yb ii, and Lu ii”, *Solar Phys.*, **44**(2), 257–267. [DOI], [ADS]
- Andrievsky, S. M., Spite, M., Korotin, S. A., Spite, F., Bonifacio, P., Cayrel, R., Hill, V. and François, P., 2007, “NLTE determination of the sodium abundance in a homogeneous sample of extremely metal-poor stars”, *Astron. Astrophys.*, **464**(3), 1081–1087. [DOI], [ADS], [arXiv:astro-ph/0701199 [astro-ph]]
- Andrievsky, S. M., Spite, M., Korotin, S. A., Spite, F., François, P., Bonifacio, P., Cayrel, R. and Hill, V., 2009, “Evolution of the barium abundance in the early Galaxy from a NLTE analysis of the Ba lines in a homogeneous sample of EMP stars”, *Astron. Astrophys.*, **494**(3), 1083–1090. [DOI], [ADS], [arXiv:0902.0450 [astro-ph.GA]]
- Antipova, L. I., Boyarchuk, A. A., Pakhomov, Yu. V. and Panchuk, V. E., 2004, “Analysis of Atmospheric Abundances in Classical Barium Stars”, *Astronomy Reports*, **48**(7), 597–610. [DOI], [ADS]
- Aoki, W., Frebel, A., Christlieb, N., Norris, J. E., Beers, T. C., Minezaki, T., Barklem, P. S., Honda, S., Takada-Hidai, M., Asplund, M., Ryan, S. G., Tsangarides, S., Eriksson, K., Steinhauer, A., Deliyannis, C. P., Nomoto, K., Fujimoto, M. Y., Ando, H., Yoshii, Y. and Kajino, T., 2006, “HE 1327-2326, an Unevolved Star with $[Fe/H] < -5.0$. I. A Comprehensive Abundance Analysis”, *Astrophys. J.*, **639**(2), 897–917. [DOI], [ADS], [arXiv:astro-ph/0509206 [astro-ph]]
- Aoki, Wako, Ryan, Sean G., Norris, John E., Beers, Timothy C., Ando, Hiroyasu and Tsangarides, Stelios, 2002, “A Subaru/High Dispersion Spectrograph Study of Lead (Pb) Abundances in Eight s-Process Element-rich, Metal-poor Stars”, *Astrophys. J.*, **580**(2), 1149–1158. [DOI], [ADS], [arXiv:astro-ph/0208020 [astro-ph]]
- Aoki, Wako, Honda, Satoshi, Beers, Timothy C., Kajino, Toshitaka, Ando, Hiroyasu, Norris, John E., Ryan, Sean G., Izumiura, Hideyuki, Sadakane, Kozo and

- Takada-Hidai, Masahide, 2005, “Spectroscopic Studies of Very Metal-poor Stars with the Subaru High Dispersion Spectrograph. III. Light Neutron-Capture Elements”, *Astrophys. J.*, **632**(1), 611–637. [DOI], [ADS], [arXiv:astro-ph/0503032 [astro-ph]]
- Aoki, Wako, Beers, Timothy C., Christlieb, Norbert, Norris, John E., Ryan, Sean G. and Tsangarides, Stelios, 2007, “Carbon-enhanced Metal-poor Stars. I. Chemical Compositions of 26 Stars”, *Astrophys. J.*, **655**(1), 492–521. [DOI], [ADS], [arXiv:astro-ph/0609702 [astro-ph]]
- Aoki, Wako, Beers, Timothy C., Sivarani, Thirupathi, Marsteller, Brian, Lee, Young Sun, Honda, Satoshi, Norris, John E., Ryan, Sean G. and Carollo, Daniela, 2008, “Carbon-Enhanced Metal-Poor Stars. III. Main-Sequence Turnoff Stars from the SDSS SEGUE Sample”, *Astrophys. J.*, **678**(2), 1351–1371. [DOI], [ADS], [arXiv:0801.4187 [astro-ph]]
- Aoki, Wako, Beers, Timothy C., Lee, Young Sun, Honda, Satoshi, Ito, Hiroko, Takada-Hidai, Masahide, Frebel, Anna, Suda, Takuma, Fujimoto, Masayuki Y., Carollo, Daniela and Sivarani, Thirupathi, 2013, “High-resolution Spectroscopy of Extremely Metal-poor Stars from SDSS/SEGUE. I. Atmospheric Parameters and Chemical Compositions”, *Astron. J.*, **145**(1), 13. [DOI], [ADS], [arXiv:1210.1946 [astro-ph.SR]]
- Arcones, A. and Thielemann, F. K., 2013, “Neutrino-driven wind simulations and nucleosynthesis of heavy elements”, *Journal of Physics G Nuclear Physics*, **40**(1), 013201. [DOI], [ADS], [arXiv:1207.2527 [astro-ph.SR]]
- Arentsen, A., Starkenburg, E., Shetrone, M. D., Venn, K. A., Depagne, É. and McConnachie, A. W., 2019a, “Binarity among CEMP-no stars: an indication of multiple formation pathways?”, *Astron. Astrophys.*, **621**, A108. [DOI], [ADS], [arXiv:1811.01975 [astro-ph.SR]]
- Arentsen, Anke, Prugniel, Philippe, Gonneau, Anais, Lançon, Ariane, Trager, Scott, Peletier, Reynier, Lyubenova, Mariya, Chen, Yan-Ping, Falcón Barroso,

- Jesús, Sánchez Blázquez, Patricia and Vazdekis, Alejandro, 2019b, “Stellar atmospheric parameters for 754 spectra from the X-shooter Spectral Library”, *Astron. Astrophys.*, **627**, A138. [DOI], [ADS], [arXiv:1907.06391 [astro-ph.SR]]
- Argast, D., Samland, M., Gerhard, O. E. and Thielemann, F. K., 2000, “Metal-poor halo stars as tracers of ISM mixing processes during halo formation”, *Astron. Astrophys.*, **356**, 873–887. [ADS], [arXiv:astro-ph/9911178 [astro-ph]]
- Argast, D., Samland, M., Thielemann, F. K. and Qian, Y. Z., 2004, “Neutron star mergers versus core-collapse supernovae as dominant r-process sites in the early Galaxy”, *Astron. Astrophys.*, **416**, 997–1011. [DOI], [ADS], [arXiv:astro-ph/0309237 [astro-ph]]
- Arnesen, A., Bengtsson, A., Hallin, R., Lindskog, J., Nordling, C. and Noreland, T., 1977, “Lifetime Measurements in La II with the Beam-Laser Method”, *Physica Scripta*, **16**, 31–34. [DOI], [ADS]
- Arnould, M. and Mowlavi, N., 1995, “Non-Explosive Hydrogen Burning: Where Do We Stand ?”, in *Liege International Astrophysical Colloquia*, (Eds.) Noels, A., Fraipont-Caro, D., Gabriel, M., Grevesse, N., Demarque, P., Liege International Astrophysical Colloquia, 32, Academic Press. Academic Press. [ADS], [arXiv:astro-ph/9512027 [astro-ph]]
- Arnould, M., Goriely, S. and Jorissen, A., 1999, “Non-explosive hydrogen and helium burnings: abundance predictions from the NACRE reaction rate compilation”, *Astron. Astrophys.*, **347**, 572–582. [ADS], [arXiv:astro-ph/9904407 [astro-ph]]
- Asplund, Martin, Grevesse, Nicolas, Sauval, A. Jacques and Scott, Pat, 2009, “The Chemical Composition of the Sun”, *Ann. Rev. Astron. Astrophys.*, **47**(1), 481–522. [DOI], [ADS], [arXiv:0909.0948 [astro-ph.SR]]
- Axer, M., Fuhrmann, K. and Gehren, T., 1994, “Spectroscopic analyses of metal-poor stars. I. Basic data and stellar parameters.”, *Astron. Astrophys.*, **291**, 895–909. [ADS]

- Banerjee, Projjwal, Qian, Yong-Zhong and Heger, Alexander, 2018, “New Neutron-capture Site in Massive Pop III and Pop II Stars as a Source for Heavy Elements in the Early Galaxy”, *Astrophys. J.*, **865**(2), 120. [DOI], [ADS], [arXiv:1711.05964 [astro-ph.SR]]
- Barbuy, B., Jorissen, A., Rossi, S. C. F. and Arnould, M., 1992, “Light element abundances in barium stars.”, *Astron. Astrophys.*, **262**, 216. [ADS]
- Barbuy, B., Spite, M., Spite, F., Hill, V., Cayrel, R., Plez, B. and Petitjean, P., 2005, “New analysis of the two carbon-rich stars CS 22948-27 and CS 29497-34: Binarity and neutron capture elements”, *Astron. Astrophys.*, **429**, 1031–1042. [DOI], [ADS], [arXiv:astro-ph/0409213 [astro-ph]]
- Barklem, P. S. and O’Mara, B. J., 2000, “Broadening of lines of Beii, Srii and Baii by collisions with hydrogen atoms and the solar abundance of strontium”, *Mon. Not. Roy. Astron. Soc.*, **311**(3), 535–540. [DOI], [ADS]
- Barklem, P. S., Christlieb, N., Beers, T. C., Hill, V., Bessell, M. S., Holmberg, J., Marsteller, B., Rossi, S., Zickgraf, F. J. and Reimers, D., 2005, “The Hamburg/ESO R-process enhanced star survey (HERES). II. Spectroscopic analysis of the survey sample”, *Astron. Astrophys.*, **439**(1), 129–151. [DOI], [ADS], [arXiv:astro-ph/0505050 [astro-ph]]
- Bartkevicius, A., 1996, “A New Version of the Catalog of CH and Related Stars (CH95 Catalog)”, *Balt. Astron.*, **5**, 217–229. [DOI], [ADS]
- Baschek, B., Scholz, M. and Sedlmayr, E., 1977, “Non-LTE analysis of neutral oxygen lines in A-type stars.”, *Astron. Astrophys.*, **55**, 375–386. [ADS]
- Battistini, Chiara and Bensby, Thomas, 2015, “The origin and evolution of the odd-Z iron-peak elements Sc, V, Mn, and Co in the Milky Way stellar disk”, *Astron. Astrophys.*, **577**, A9. [DOI], [ADS], [arXiv:1502.01152 [astro-ph.GA]]
- Beer, H. and Macklin, R. L., 1989, “Measurement of the 85Rb and 87Rb Capture Cross Sections for s-Process Studies”, *Astrophys. J.*, **339**, 962. [DOI], [ADS]

- Beer, Hermann, 1991, “Capture Cross Section Measurements of Krypton and Xenon Isotopes and the Fundamental Parameters of the s-Process”, *Astrophys. J.*, **375**, 823. [DOI], [ADS]
- Beers, T. C., Preston, G. W. and Shectman, S. A., 1985, “A search for stars of very low metal abundance. I.”, *Astron. J.*, **90**, 2089–2102. [DOI], [ADS]
- Beers, Timothy C., 1999, “Low-Metallicity and Horizontal-Branch Stars in the Halo of the Galaxy”, in *The Third Stromlo Symposium: The Galactic Halo*, (Eds.) Gibson, Brad K., Axelrod, Rim S., Putman, Mary E., Astronomical Society of the Pacific Conference Series, 165, Academic Press. Academic Press. [ADS]
- Beers, Timothy C. and Christlieb, Norbert, 2005, “The Discovery and Analysis of Very Metal-Poor Stars in the Galaxy”, *Ann. Rev. Astron. Astrophys.*, **43**(1), 531–580. [DOI], [ADS]
- Beers, Timothy C., Preston, George W. and Shectman, Stephen A., 1992, “A Search for Stars of Very Low Metal Abundance. II”, *Astron. J.*, **103**, 1987. [DOI], [ADS]
- Beers, Timothy C., Flynn, Chris, Rossi, Silvia, Sommer-Larsen, Jesper, Wilhelm, Ronald, Marsteller, Brian, Lee, Young Sun, De Lee, Nathan, Krugler, Julie, Deliyannis, Constantine P., Simmons, Andrew T., Mills, Elisabeth, Zickgraf, Franz-Josef, Holmberg, Johan, Önehag, Anna, Eriksson, Anders, Terndrup, Donald M., Salim, Samir, Andersen, Johannes, Nordström, Birgitta, Christlieb, Norbert, Frebel, Anna and Rhee, Jaehyon, 2007, “Broadband UBVR_CI_C Photometry of Horizontal-Branch and Metal-poor Candidates from the HK and Hamburg/ESO Surveys. I.”, *Astrophys. J. Suppl.*, **168**(1), 128–139. [DOI], [ADS], [arXiv:astro-ph/0610018 [astro-ph]]
- Beers, Timothy C., Placco, Vinicius M., Carollo, Daniela, Rossi, Silvia, Lee, Young Sun, Frebel, Anna, Norris, John E., Dietz, Sarah and Masseron, Thomas,

- 2017, “Bright Metal-Poor Stars from the Hamburg/ESO Survey. II. A Chemo-dynamical Analysis”, *Astrophys. J.*, **835**(1), 81. [DOI], [ADS], [arXiv:1611.03762 [astro-ph.SR]]
- Bensby, T., Feltzing, S. and Lundström, I., 2003, “Elemental abundance trends in the Galactic thin and thick disks as traced by nearby F and G dwarf stars”, *Astron. Astrophys.*, **410**, 527–551. [DOI], [ADS]
- Bensby, T., Feltzing, S. and Lundström, I., 2004, “Oxygen trends in the Galactic thin and thick disks”, *Astron. Astrophys.*, **415**, 155–170. [DOI], [ADS], [arXiv:astro-ph/0310741 [astro-ph]]
- Bensby, T., Feltzing, S., Lundström, I. and Ilyin, I., 2005, “ α -, r-, and s-process element trends in the Galactic thin and thick disks”, *Astron. Astrophys.*, **433**(1), 185–203. [DOI], [ADS], [arXiv:astro-ph/0412132 [astro-ph]]
- Bensby, T., Feltzing, S. and Oey, M. S., 2014, “Exploring the Milky Way stellar disk. A detailed elemental abundance study of 714 F and G dwarf stars in the solar neighbourhood”, *Astron. Astrophys.*, **562**, A71. [DOI], [ADS], [arXiv:1309.2631 [astro-ph.GA]]
- Bergemann, M., Hansen, C. J., Bautista, M. and Ruchti, G., 2012, “NLTE analysis of Sr lines in spectra of late-type stars with new R-matrix atomic data”, *Astron. Astrophys.*, **546**, A90. [DOI], [ADS], [arXiv:1207.2451 [astro-ph.SR]]
- Bertolli, M. G., Herwig, F., Pignatari, M. and Kawano, T., 2013, “Systematic and correlated nuclear uncertainties in the i-process at the neutron shell closure N = 82”, *arXiv e-prints*, arXiv:1310.4578. [ADS], [arXiv:1310.4578 [astro-ph.SR]]
- Bessell, Michael S., Collet, Remo, Keller, Stefan C., Frebel, Anna, Heger, Alexander, Casey, Andrew R., Masseron, Thomas, Asplund, Martin, Jacobson, Heather R., Lind, Karin, Marino, Anna F., Norris, John E., Yong, David, Da Costa, Gary, Chan, Conrad, Magic, Zazralt, Schmidt, Brian and Tisserand, Patrick, 2015, “Nucleosynthesis in a Primordial Supernova: Carbon and Oxygen

- Abundances in SMSS J031300.36-670839.3”, *Astrophys. J. Lett.*, **806**(1), L16. [DOI], [ADS], [arXiv:1505.03756 [astro-ph.SR]]
- Bidelman, William P. and Keenan, Philip C., 1951, “The Ba II Stars.”, *Astrophys. J.*, **114**, 473. [DOI], [ADS]
- Bielski, A., 1975, “A critical survey of atomic transition probabilities for Cu I.”, *J. Quant. Spectr. Radi. Transfer.*, **15**(6), 463–472. [DOI], [ADS]
- Biemont, E., Grevesse, N., Hannaford, P. and Lowe, R. M., 1981, “Oscillator strengths for Zr I and Zr II and a new determination of the solar abundance of zirconium.”, *Astrophys. J.*, **248**, 867–873. [DOI], [ADS]
- Biemont, E., Karner, C., Meyer, G., Traeger, F. and Zu Putlitz, G., 1982, “Absolute transition probabilities in the spectra of Eu II. III. Astrophysical applications.”, *Astron. Astrophys.*, **107**, 166–171. [ADS]
- Bisterzo, S., Gallino, R., Straniero, O., Cristallo, S. and Käppeler, F., 2010, “s-Process in low-metallicity stars - I. Theoretical predictions”, *Mon. Not. Roy. Astron. Soc.*, **404**(3), 1529–1544. [DOI], [ADS], [arXiv:1001.5376 [astro-ph.SR]]
- Bisterzo, S., Gallino, R., Straniero, O., Cristallo, S. and Käppeler, F., 2011, “The s-process in low-metallicity stars - II. Interpretation of high-resolution spectroscopic observations with asymptotic giant branch models”, *Mon. Not. Roy. Astron. Soc.*, **418**(1), 284–319. [DOI], [ADS], [arXiv:1108.0500 [astro-ph.SR]]
- Bisterzo, S., Gallino, R., Käppeler, F., Wiescher, M., Imbriani, G., Straniero, O., Cristallo, S., Görres, J. and deBoer, R. J., 2015, “The branchings of the main s-process: their sensitivity to α -induced reactions on ^{13}C and ^{22}Ne and to the uncertainties of the nuclear network”, *Mon. Not. Roy. Astron. Soc.*, **449**(1), 506–527. [DOI], [ADS], [arXiv:1507.06798 [astro-ph.SR]]
- Bisterzo, S., Travaglio, C., Wiescher, M., Käppeler, F. and Gallino, R., 2017, “Galactic Chemical Evolution: The Impact of the ^{13}C -pocket Structure on the

- s-process Distribution”, *Astrophys. J.*, **835**(1), 97. [DOI], [ADS], [arXiv:1701.01056 [astro-ph.SR]]
- Boehm-Vitense, E., 1980, “The white dwarf companion of the barium star ZET Cap.”, *Astrophys. J. Lett.*, **239**, L79–L83. [DOI], [ADS]
- Böhm-Vitense, Erika, Carpenter, Kenneth, Robinson, Richard, Ake, Tom and Brown, Jeffery, 2000, “Do All BA II Stars Have White Dwarf Companions?”, *Astrophys. J.*, **533**(2), 969–983. [DOI], [ADS]
- Bond, H. E., 1974, “The subgiant CH stars.”, *Astrophys. J.*, **194**, 95–107. [DOI], [ADS]
- Bonifacio, P., Caffau, E., Spite, M., Limongi, M., Chieffi, A., Klessen, R. S., François, P., Molnar, P., Ludwig, H. G., Zaggia, S., Spite, F., Plez, B., Cayrel, R., Christlieb, N., Clark, P. C., Glover, S. C. O., Hammer, F., Koch, A., Monaco, L., Sbordone, L. and Steffen, M., 2015, “TOPoS . II. On the bimodality of carbon abundance in CEMP stars Implications on the early chemical evolution of galaxies”, *Astron. Astrophys.*, **579**, A28. [DOI], [ADS], [arXiv:1504.05963 [astro-ph.GA]]
- Boothroyd, Arnold I. and Sackmann, I. J., 1992, “Breakdown of the Core Mass–Luminosity Relation at High Luminosities on the Asymptotic Giant Branch”, *Astrophys. J. Lett.*, **393**, L21. [DOI], [ADS]
- Boyarchuk, A. A., Antipova, L. I., Boyarchuk, M. E. and Savanov, I. S., 2001, “A Comparative Analysis of Chemical Abundances in the Atmospheres of Red Giants of Different Age Groups”, *Astronomy Reports*, **45**(4), 301–308. [DOI], [ADS]
- Bridges, J. M. and Kornblith, R. L., 1974, “Arc Measurements of Fe I Oscillator Strengths”, *Astrophys. J.*, **192**, 793–818. [DOI], [ADS]
- Brooke, James S. A., Bernath, Peter F., Schmidt, Timothy W. and Bacsikay, George B., 2013, “Line strengths and updated molecular constants for the C₂

- Swan system”, *J. Quant. Spectr. Radi. Transfer.*, **124**, 11–20. [DOI], [ADS], [arXiv:1212.2102 [astro-ph.SR]]
- Buntain, J. F., Doherty, C. L., Lugaro, M., Lattanzio, J. C., Stancliffe, R. J. and Karakas, A. I., 2017, “Partial mixing and the formation of ^{13}C pockets in AGB stars: effects on the s-process elements”, *Mon. Not. Roy. Astron. Soc.*, **471**(1), 824–838. [DOI], [ADS], [arXiv:1706.05802 [astro-ph.SR]]
- Burbidge, E. Margaret, Burbidge, G. R., Fowler, William A. and Hoyle, F., 1957, “Synthesis of the Elements in Stars”, *Reviews of Modern Physics*, **29**(4), 547–650. [DOI], [ADS]
- Busso, M., Gallino, R. and Wasserburg, G. J., 1999, “Nucleosynthesis in Asymptotic Giant Branch Stars: Relevance for Galactic Enrichment and Solar System Formation”, *Ann. Rev. Astron. Astrophys.*, **37**, 239–309. [DOI], [ADS]
- Busso, Maurizio, Gallino, Roberto, Lambert, David L., Travaglio, Claudia and Smith, Verne V., 2001, “Nucleosynthesis and Mixing on the Asymptotic Giant Branch. III. Predicted and Observed s-Process Abundances”, *Astrophys. J.*, **557**(2), 802–821. [DOI], [ADS], [arXiv:astro-ph/0104424 [astro-ph]]
- Campbell, S. W. and Lattanzio, J. C., 2008, “Evolution and nucleosynthesis of extremely metal-poor and metal-free low- and intermediate-mass stars. I. Stellar yield tables and the CEMPs”, *Astron. Astrophys.*, **490**(2), 769–776. [DOI], [ADS], [arXiv:0901.0799 [astro-ph.SR]]
- Campbell, S. W., Lugaro, M. and Karakas, A. I., 2010, “Evolution and nucleosynthesis of extremely metal-poor and metal-free low- and intermediate-mass stars. II. s-process nucleosynthesis during the core He flash”, *Astron. Astrophys.*, **522**, L6. [DOI], [ADS], [arXiv:1010.1987 [astro-ph.SR]]
- Carollo, Daniela, Beers, Timothy C., Bovy, Jo, Sivarani, Thirupathi, Norris, John E., Freeman, Ken C., Aoki, Wako, Lee, Young Sun and Kennedy, Catherine R., 2012, “Carbon-enhanced Metal-poor Stars in the Inner and Outer Halo

- Components of the Milky Way”, *Astrophys. J.*, **744**(2), 195. [DOI], [ADS], [arXiv:1103.3067 [astro-ph.GA]]
- Cayrel, R., Depagne, E., Spite, M., Hill, V., Spite, F., François, P., Plez, B., Beers, T., Primas, F., Andersen, J., Barbuy, B., Bonifacio, P., Molaro, P. and Nordström, B., 2004, “First stars V - Abundance patterns from C to Zn and supernova yields in the early Galaxy”, *Astron. Astrophys.*, **416**, 1117–1138. [DOI], [ADS], [arXiv:astro-ph/0311082 [astro-ph]]
- Cenarro, A. J., Peletier, R. F., Sánchez-Blázquez, P., Selam, S. O., Toloba, E., Cardiel, N., Falcón-Barroso, J., Gorgas, J., Jiménez-Vicente, J. and Vazdekis, A., 2007, “Medium-resolution Isaac Newton Telescope library of empirical spectra - II. The stellar atmospheric parameters”, *Mon. Not. Roy. Astron. Soc.*, **374**(2), 664–690. [DOI], [ADS], [arXiv:astro-ph/0611618 [astro-ph]]
- Cescutti, G., Hirschi, R., Nishimura, N., Hartogh, J. W. den, Rauscher, T., Murphy, A. St J. and Cristallo, S., 2018, “Uncertainties in s-process nucleosynthesis in low-mass stars determined from Monte Carlo variations”, *Mon. Not. Roy. Astron. Soc.*, **478**(3), 4101–4127. [DOI], [ADS], [arXiv:1805.01250 [astro-ph.SR]]
- Chamberlain, Joseph W. and Aller, Lawrence H., 1951, “The Atmospheres of A-Type Subdwarfs and 95 Leonis.”, *Astrophys. J.*, **114**, 52. [DOI], [ADS]
- Charbonnel, C., 1995, “A Consistent Explanation for $^{12}\text{C}/\text{ }^{13}\text{C}$, ^{7}Li and ^{3}He Anomalies in Red Giant Stars”, *Astrophys. J. Lett.*, **453**, L41. [DOI], [ADS], [arXiv:astro-ph/9511080 [astro-ph]]
- Charbonnel, Corinne, Brown, Jeffery A. and Wallerstein, George, 1998, “Mixing processes during the evolution of red giants with moderate metal deficiencies: the role of molecular-weight barriers”, *Astron. Astrophys.*, **332**, 204–214. [ADS], [arXiv:astro-ph/9712207 [astro-ph]]
- Chen, B., Vergely, J. L., Valette, B. and Carraro, G., 1998, “Comparison of two different extinction laws with HIPPARCOS observations”, *Astron. Astrophys.*, **336**, 137–149. [ADS], [arXiv:astro-ph/9805018 [astro-ph]]

- Chen, Y. Q., Nissen, P. E. and Zhao, G., 2004, “The [Zn/Fe] - [Fe/H] trend for disk and halo stars”, *Astron. Astrophys.*, **425**, 697–705. [DOI], [ADS], [arXiv:astro-ph/0406612 [astro-ph]]
- Chiappini, C., 2013, “First stars and reionization: Spinstars”, *Astronomische Nachrichten*, **334**(6), 595–604. [DOI], [ADS]
- Choplin, Arthur, Hirschi, Raphael, Meynet, Georges and Ekström, Sylvia, 2017, “Are some CEMP-s stars the daughters of spinstars?”, *Astron. Astrophys.*, **607**, L3. [DOI], [ADS], [arXiv:1710.05564 [astro-ph.SR]]
- Choplin, Arthur, Hirschi, Raphael, Meynet, Georges, Ekström, Sylvia, Chiappini, Cristina and Laird, Alison, 2018, “Non-standard s-process in massive rotating stars. Yields of 10-150 M_⊙ models at Z = 10⁻³”, *Astron. Astrophys.*, **618**, A133. [DOI], [ADS], [arXiv:1807.06974 [astro-ph.SR]]
- Christlieb, N., Green, P. J., Wisotzki, L. and Reimers, D., 2001a, “The stellar content of the Hamburg/ESO survey II. A large, homogeneously-selected sample of high latitude carbon stars”, *Astron. Astrophys.*, **375**, 366–374. [DOI], [ADS], [arXiv:astro-ph/0106240 [astro-ph]]
- Christlieb, N., Wisotzki, L., Reimers, D., Homeier, D., Koester, D. and Heber, U., 2001b, “The stellar content of the Hamburg/ESO survey I. Automated selection of DA white dwarfs”, *Astron. Astrophys.*, **366**, 898–912. [DOI], [ADS], [arXiv:astro-ph/0011453 [astro-ph]]
- Christlieb, N., Beers, T. C., Thom, C., Wilhelm, R., Rossi, S., Flynn, C., Wisotzki, L. and Reimers, D., 2005, “The stellar content of the Hamburg/ESO survey. III. Field horizontal-branch stars in the Galaxy”, *Astron. Astrophys.*, **431**, 143–148. [DOI], [ADS], [arXiv:astro-ph/0411300 [astro-ph]]
- Christlieb, N., Schörck, T., Frebel, A., Beers, T. C., Wisotzki, L. and Reimers, D., 2008, “The stellar content of the Hamburg/ESO survey. IV. Selection of candidate metal-poor stars”, *Astron. Astrophys.*, **484**(3), 721–732. [DOI], [ADS], [arXiv:0804.1520 [astro-ph]]

Christlieb, Norbert, 2003, “Finding the Most Metal-poor Stars of the Galactic Halo with the Hamburg/ESO Objective-prism Survey (With 6 Figures)”, *Reviews in Modern Astronomy*, **16**, 191. [DOI], [ADS], [arXiv:astro-ph/0308016 [astro-ph]]

Clarkson, O., Herwig, F. and Pignatari, M., 2018, “Pop III i-process nucleosynthesis and the elemental abundances of SMSS J0313-6708 and the most iron-poor stars”, *Mon. Not. Roy. Astron. Soc.*, **474**(1), L37–L41. [DOI], [ADS], [arXiv:1710.01763 [astro-ph.SR]]

Clayton, Donald D., 1988, “Nuclear cosmochemistry within analytic models of the chemical evolution of the solar neighbourhood.”, *Mon. Not. Roy. Astron. Soc.*, **234**, 1–36. [DOI], [ADS]

Cohen, Judith G., Christlieb, Norbert, Qian, Y. Z. and Wasserburg, G. J., 2003, “Abundance Analysis of HE 2148-1247, A Star with Extremely Enhanced Neutron Capture Elements”, *Astrophys. J.*, **588**(2), 1082–1098. [DOI], [ADS], [arXiv:astro-ph/0301460 [astro-ph]]

Cohen, Judith G., Shectman, Stephen, Thompson, Ian, McWilliam, Andrew, Christlieb, Norbert, Melendez, Jorge, Zickgraf, Franz-Josef, Ramírez, Solange and Swenson, Amber, 2005, “The Frequency of Carbon Stars among Extremely Metal-poor Stars”, *Astrophys. J. Lett.*, **633**(2), L109–L112. [DOI], [ADS], [arXiv:astro-ph/0510105 [astro-ph]]

Cohen, Judith G., McWilliam, Andrew, Shectman, Stephen, Thompson, Ian, Christlieb, Norbert, Melendez, Jorge, Ramirez, Solange, Swensson, Amber and Zickgraf, Franz-Josef, 2006, “Carbon Stars in the Hamburg/ESO Survey: Abundances”, *Astron. J.*, **132**(1), 137–160. [DOI], [ADS], [arXiv:astro-ph/0603582 [astro-ph]]

Cooke, Ryan J. and Madau, Piero, 2014, “Carbon-enhanced Metal-poor Stars: Relics from the Dark Ages”, *Astrophys. J.*, **791**(2), 116. [DOI], [ADS], [arXiv:1405.7369 [astro-ph.GA]]

- Cowan, J. J. and Rose, W. K., 1977, “Production of ^{14}C and neutrons in red giants.”, *Astrophys. J.*, **212**, 149–158. [DOI], [ADS]
- Cowley, C. R. and Corliss, C. H., 1983, “Moderately accurate oscillator strengths from NBS intensities - II.”, *Mon. Not. Roy. Astron. Soc.*, **203**, 651–659. [DOI], [ADS]
- Cristallo, S., Straniero, O., Gallino, R., Piersanti, L., Domínguez, I. and Lederer, M. T., 2009, “Evolution, Nucleosynthesis, and Yields of Low-Mass Asymptotic Giant Branch Stars at Different Metallicities”, *Astrophys. J.*, **696**(1), 797–820. [DOI], [ADS], [arXiv:0902.0243 [astro-ph.SR]]
- Cristallo, S., Piersanti, L., Straniero, O., Gallino, R., Domínguez, I., Abia, C., Di Rico, G., Quintini, M. and Bisterzo, S., 2011, “Evolution, Nucleosynthesis, and Yields of Low-mass Asymptotic Giant Branch Stars at Different Metallicities. II. The FRUITY Database”, *Astrophys. J. Suppl.*, **197**(2), 17. [DOI], [ADS], [arXiv:1109.1176 [astro-ph.SR]]
- Cristallo, S., Straniero, O., Piersanti, L. and Gobrecht, D., 2015, “Evolution, Nucleosynthesis, and Yields of AGB Stars at Different Metallicities. III. Intermediate-mass Models, Revised Low-mass Models, and the ph-FRUITY Interface”, *Astrophys. J. Suppl.*, **219**(2), 40. [DOI], [ADS], [arXiv:1507.07338 [astro-ph.SR]]
- Cristallo, S., Karinkuzhi, D., Goswami, A., Piersanti, L. and Gobrecht, D., 2016, “Constraints of the Physics of Low-mass AGB Stars from CH and CEMP Stars”, *Astrophys. J.*, **833**(2), 181. [DOI], [ADS], [arXiv:1610.05475 [astro-ph.SR]]
- Cruz, M. A., Serenelli, A. and Weiss, A., 2013, “S-process in extremely metal-poor, low-mass stars”, *Astron. Astrophys.*, **559**, A4. [DOI], [ADS], [arXiv:1308.2224 [astro-ph.SR]]
- Cseh, B., Lugaro, M., D’Orazi, V., de Castro, D. B., Pereira, C. B., Karakas, A. I., Molnár, L., Plachy, E., Szabó, R., Pignatari, M. and Cristallo, S., 2018, “The s

process in AGB stars as constrained by a large sample of barium stars”, *Astron. Astrophys.*, **620**, A146. [DOI], [ADS], [arXiv:1810.01788 [astro-ph.SR]]

Cui, Xiang-Qun, Zhao, Yong-Heng, Chu, Yao-Quan, Li, Guo-Ping, Li, Qi, Zhang, Li-Ping, Su, Hong-Jun, Yao, Zheng-Qiu, Wang, Ya-Nan, Xing, Xiao-Zheng, Li, Xin-Nan, Zhu, Yong-Tian, Wang, Gang, Gu, Bo-Zhong, Luo, A. Li, Xu, Xin-Qi, Zhang, Zhen-Chao, Liu, Gen-Rong, Zhang, Hao-Tong, Yang, De-Hua, Cao, Shu-Yun, Chen, Hai-Yuan, Chen, Jian-Jun, Chen, Kun-Xin, Chen, Ying, Chu, Jia-Ru, Feng, Lei, Gong, Xue-Fei, Hou, Yong-Hui, Hu, Hong-Zhuan, Hu, Ning-Sheng, Hu, Zhong-Wen, Jia, Lei, Jiang, Fang-Hua, Jiang, Xiang, Jiang, Zi-Bo, Jin, Ge, Li, Ai-Hua, Li, Yan, Li, Ye-Ping, Liu, Guan-Qun, Liu, Zhi-Gang, Lu, Wen-Zhi, Mao, Yin-Dun, Men, Li, Qi, Yong-Jun, Qi, Zhao-Xiang, Shi, Huo-Ming, Tang, Zheng-Hong, Tao, Qing-Sheng, Wang, Da-Qi, Wang, Dan, Wang, Guo-Min, Wang, Hai, Wang, Jia-Ning, Wang, Jian, Wang, Jian-Ling, Wang, Jian-Ping, Wang, Lei, Wang, Shu-Qing, Wang, You, Wang, Yue-Fei, Xu, Ling-Zhe, Xu, Yan, Yang, Shi-Hai, Yu, Yong, Yuan, Hui, Yuan, Xiang-Yan, Zhai, Chao, Zhang, Jing, Zhang, Yan-Xia, Zhang, Yong, Zhao, Ming, Zhou, Fang, Zhou, Guo-Hua, Zhu, Jie and Zou, Si-Cheng, 2012, “The Large Sky Area Multi-Object Fiber Spectroscopic Telescope (LAMOST)”, *Research in Astronomy and Astrophysics*, **12**(9), 1197–1242. [DOI], [ADS]

Cutri, R. M., Skrutskie, M. F., van Dyk, S., Beichman, C. A., Carpenter, J. M., Chester, T.,Cambresy, L., Evans, T., Fowler, J., Gizis, J., Howard, E., Huchra, J., Jarrett, T., Kopan, E. L., Kirkpatrick, J. D., Light, R. M., Marsh, K. A., McCallon, H., Schneider, S., Stiening, R., Sykes, M., Weinberg, M., Wheaton, W. A., Wheelock, S. and Zacarias, N., 2003, “VizieR Online Data Catalog: 2MASS All-Sky Catalog of Point Sources (Cutri+ 2003)”, *VizieR Online Data Catalog*, II/246. [ADS]

Dardelet, L., Ritter, C., Prado, P., Heringer, E., Higgs, C., Sandalski, S., Jones, S., Denisenkov, P., Venn, K., Bertolli, M., Pignatari, M., Woodward, P. and Herwig, F., 2014, “i process and CEMP-s+r stars”, in *XIII Nuclei in the Cosmos (NIC*

- XIII), Sissa Medialab srl Partita IVA: 01097780322. Sissa Medialab srl Partita IVA: 01097780322. [ADS]
- de Castro, D. B., Pereira, C. B., Roig, F., Jilinski, E., Drake, N. A., Chavero, C. and Sales Silva, J. V., 2016, “Chemical abundances and kinematics of barium stars”, *Mon. Not. Roy. Astron. Soc.*, **459**(4), 4299–4324. [DOI], [ADS], [arXiv:1604.03031 [astro-ph.SR]]
- Deng, Li-Cai, Newberg, Heidi Jo, Liu, Chao, Carlin, Jeffrey L., Beers, Timothy C., Chen, Li, Chen, Yu-Qin, Christlieb, Norbert, Grillmair, Carl J., Guhathakurta, Puragra, Han, Zhan-Wen, Hou, Jin-Liang, Lee, Hsu-Tai, Lépine, Sébastien, Li, Jing, Liu, Xiao-Wei, Pan, Kai-Ke, Sellwood, J. A., Wang, Bo, Wang, Hong-Chi, Yang, Fan, Yanny, Brian, Zhang, Hao-Tong, Zhang, Yue-Yang, Zheng, Zheng and Zhu, Zi, 2012, “LAMOST Experiment for Galactic Understanding and Exploration (LEGUE) — The survey’s science plan”, *Research in Astronomy and Astrophysics*, **12**(7), 735–754. [DOI], [ADS], [arXiv:1206.3578 [astro-ph.GA]]
- Denisenkov, P. A. and Ivanov, V. V., 1987, “Sodium Synthesis in Hydrogen Burning Stars”, *Soviet Astronomy Letters*, **13**, 214. [ADS]
- Denissenkov, P. A. and Weiss, A., 1996, “Deep diffusive mixing in globular-cluster red giants.”, *Astron. Astrophys.*, **308**, 773–784. [ADS]
- Denissenkov, Pavel A. and Tout, Christopher A., 2003, “Partial mixing and formation of the ^{13}C pocket by internal gravity waves in asymptotic giant branch stars”, *Mon. Not. Roy. Astron. Soc.*, **340**(3), 722–732. [DOI], [ADS]
- Denissenkov, Pavel A., Herwig, Falk, Battino, Umberto, Ritter, Christian, Pignatari, Marco, Jones, Samuel and Paxton, Bill, 2017, “I-process Nucleosynthesis and Mass Retention Efficiency in He-shell Flash Evolution of Rapidly Accreting White Dwarfs”, *Astrophys. J. Lett.*, **834**(2), L10. [DOI], [ADS], [arXiv:1610.08541 [astro-ph.SR]]

- Denissenkov, Pavel A., Herwig, Falk, Woodward, Paul, Andrassy, Robert, Pignatari, Marco and Jones, Samuel, 2019, “The i-process yields of rapidly accreting white dwarfs from multicycle He-shell flash stellar evolution models with mixing parametrizations from 3D hydrodynamics simulations”, *Mon. Not. Roy. Astron. Soc.*, **488**(3), 4258–4270. [DOI], [ADS], [arXiv:1809.03666 [astro-ph.SR]]
- Dodelson, Scott and Schmidt, Fabian, 2021, “4 - The origin of species”, in *Modern Cosmology (Second Edition)*, (Eds.) Dodelson, Scott, Schmidt, Fabian, 2, p. 85–109, Academic Press, second edition edn. [DOI], [ADS]
- Doherty, Carolyn L., Gil-Pons, Pilar, Lau, Herbert H. B., Lattanzio, John C. and Siess, Lionel, 2014, “Super and massive AGB stars - II. Nucleosynthesis and yields - $Z = 0.02, 0.008$ and 0.004 ”, *Mon. Not. Roy. Astron. Soc.*, **437**(1), 195–214. [DOI], [ADS], [arXiv:1310.2614 [astro-ph.SR]]
- Doherty, Carolyn L., Gil-Pons, Pilar, Siess, Lionel, Lattanzio, John C. and Lau, Herbert H. B., 2015, “Super- and massive AGB stars - IV. Final fates - initial-to-final mass relation”, *Mon. Not. Roy. Astron. Soc.*, **446**(3), 2599–2612. [DOI], [ADS], [arXiv:1410.5431 [astro-ph.SR]]
- Dominy, J. F., 1984, “The chemical composition and evolutionary state of the early R stars.”, *Astrophys. J. Suppl.*, **55**, 27–43. [DOI], [ADS]
- Drake, N. A. and Pereira, C. B., 2008, “Light Element Abundances in Two Chemically Peculiar Stars: HD 104340 and HD 206983”, *Astron. J.*, **135**(3), 1070–1082. [DOI], [ADS]
- Dray, Lynnette M., Tout, Christopher A., Karakas, Amanda I. and Lattanzio, John C., 2003, “Chemical enrichment by Wolf-Rayet and asymptotic giant branch stars”, *Mon. Not. Roy. Astron. Soc.*, **338**(4), 973–989. [DOI], [ADS]
- Drout, M. R., Piro, A. L., Shappee, B. J., Kilpatrick, C. D., Simon, J. D., Contreras, C., Coulter, D. A., Foley, R. J., Siebert, M. R., Morrell, N., Boutsia, K., Di Mille, F., Holoiien, T. W. S., Kasen, D., Kollmeier, J. A., Madore,

- B. F., Monson, A. J., Murguia-Berthier, A., Pan, Y. C., Prochaska, J. X., Ramirez-Ruiz, E., Rest, A., Adams, C., Alatalo, K., Bañados, E., Baughman, J., Beers, T. C., Bernstein, R. A., Bitsakis, T., Campillay, A., Hansen, T. T., Higgs, C. R., Ji, A. P., Maravelias, G., Marshall, J. L., Moni Bidin, C., Prieto, J. L., Rasmussen, K. C., Rojas-Bravo, C., Strom, A. L., Ulloa, N., Vargas-González, J., Wan, Z. and Whitten, D. D., 2017, “Light curves of the neutron star merger GW170817/SSS17a: Implications for r-process nucleosynthesis”, *Science*, **358**(6370), 1570–1574. [DOI], [ADS], [arXiv:1710.05443 [astro-ph.HE]]
- Duquennoy, A. and Mayor, M., 1991, “Multiplicity among solar-type stars in the solar neighbourhood. II - Distribution of the orbital elements in an unbiased sample.”, *Astron. Astrophys.*, **500**, 337–376. [ADS]
- Edvardsson, B., Andersen, J., Gustafsson, B., Lambert, D. L., Nissen, P. E. and Tomkin, J., 1993, “The chemical evolution of the galactic disk. I. Analysis and results.”, *Astron. Astrophys.*, **500**, 391–442. [ADS]
- Eggen, Olin J., 1997, “The Abundance of CN. Calcium and Heavy Elements in High Velocity Stars.”, *Astron. J.*, **114**, 825. [DOI], [ADS]
- El Eid, Mounib F. and Champagne, Arthur E., 1995, “Sodium Enrichment in A–F Type Supergiants”, *Astrophys. J.*, **451**, 298. [DOI], [ADS]
- Eriksson, K. and Toft, S. C., 1979, “The O I triplet lambda 7773 Å in late-type giant stars.”, *Astron. Astrophys.*, **71**, 178–197. [ADS]
- Escorza, A., Karinkuzhi, D., Jorissen, A., Siess, L., Van Winckel, H., Pourbaix, D., Johnston, C., Miszalski, B., Oomen, G. M., Abdul-Masih, M., Boffin, H. M. J., North, P., Manick, R., Shetye, S. and Mikołajewska, J., 2019, “Barium and related stars, and their white-dwarf companions. II. Main-sequence and subgiant starss”, *Astron. Astrophys.*, **626**, A128. [DOI], [ADS], [arXiv:1904.04095 [astro-ph.SR]]
- Ezzeddine, Rana, Frebel, Anna, Roederer, Ian U., Tominaga, Nozomu, Tumlinson, Jason, Ishigaki, Miho, Nomoto, Ken’ichi, Placco, Vinicius M. and Aoki,

- Wako, 2019, “Evidence for an Aspherical Population III Supernova Explosion Inferred from the Hyper-metal-poor Star HE 1327-2326”, *Astrophys. J.*, **876**(2), 97. [DOI], [ADS], [arXiv:1904.03211 [astro-ph.SR]]
- Fenner, Y., Campbell, S., Karakas, A. I., Lattanzio, J. C. and Gibson, B. K., 2004, “Modelling self-pollution of globular clusters from asymptotic giant branch stars”, *Mon. Not. Roy. Astron. Soc.*, **353**(3), 789–795. [DOI], [ADS], [arXiv:astro-ph/0406360 [astro-ph]]
- Fields, Brian D., Molaro, Paolo and Sarkar, Subir, 2014, “Big-Bang Nucleosynthesis”, *arXiv e-prints*, arXiv:1412.1408. [ADS], [arXiv:1412.1408 [astro-ph.CO]]
- Frankowski, A. and Jorissen, A., 2006, “The puzzling case of 56 Pegasi: a fast rotator seen nearly pole-on”, *The Observatory*, **126**, 25–37. [ADS], [arXiv:astro-ph/0512036 [astro-ph]]
- Frebel, A., 2008, “Metal-poor Stars”, in *New Horizons in Astronomy*, (Eds.) Frebel, A., Maund, J. R., Shen, J., Siegel, M. H., Astronomical Society of the Pacific Conference Series, 393, Academic Press. Academic Press. [ADS], [arXiv:0802.1924 [astro-ph]]
- Frebel, Anna, 2018, “From Nuclei to the Cosmos: Tracing Heavy-Element Production with the Oldest Stars”, *Annual Review of Nuclear and Particle Science*, **68**(1), 237–269. [DOI], [ADS], [arXiv:1806.08955 [astro-ph.SR]]
- Frebel, Anna and Norris, John E., 2015, “Near-Field Cosmology with Extremely Metal-Poor Stars”, *Ann. Rev. Astron. Astrophys.*, **53**, 631–688. [DOI], [ADS], [arXiv:1501.06921 [astro-ph.SR]]
- Frebel, Anna, Christlieb, Norbert, Norris, John E., Beers, Timothy C., Bessell, Michael S., Rhee, Jaehon, Fechner, Cora, Marsteller, Brian, Rossi, Silvia, Thom, Christopher, Wisotzki, Lutz and Reimers, Dieter, 2006, “Bright Metal-poor Stars from the Hamburg/ESO Survey. I. Selection and Follow-up Observations from 329 Fields”, *Astrophys. J.*, **652**(2), 1585–1603. [DOI], [ADS], [arXiv:astro-ph/0608332 [astro-ph]]

- Frebel, Anna, Johnson, Jarrett L. and Bromm, Volker, 2009, “The minimum stellar metallicity observable in the Galaxy”, *Mon. Not. Roy. Astron. Soc.*, **392**(1), L50–L54. [DOI], [ADS], [arXiv:0811.0020 [astro-ph]]
- Frischknecht, Urs, Hirschi, Raphael, Pignatari, Marco, Maeder, André, Meynet, George, Chiappini, Cristina, Thielemann, Friedrich-Karl, Rauscher, Thomas, Georgy, Cyril and Ekström, Sylvia, 2016, “s-process production in rotating massive stars at solar and low metallicities”, *Mon. Not. Roy. Astron. Soc.*, **456**(2), 1803–1825. [DOI], [ADS], [arXiv:1511.05730 [astro-ph.SR]]
- Fryer, Christopher L., Herwig, Falk, Hungerford, Aimee and Timmes, F. X., 2006, “Supernova Fallback: A Possible Site for the r-Process”, *Astrophys. J. Lett.*, **646**(2), L131–L134. [DOI], [ADS], [arXiv:astro-ph/0606450 [astro-ph]]
- Fuhr, J. R., Martin, G. A. and Wiese, W. L., 1988, “Atomic transition probabilities. Iron through Nickel”, *Journal of Physical and Chemical Reference Data*, **17**. [ADS]
- Fujimoto, Masayuki Y., Iben, Icko, Jr. and Hollowell, David, 1990, “Helium Flashes and Hydrogen Mixing in Low-Mass Population III Stars”, *Astrophys. J.*, **349**, 580. [DOI], [ADS]
- Fujimoto, Masayuki Y., Ikeda, Yasufumi and Iben, Icko, Jr., 2000, “The Origin of Extremely Metal-poor Carbon Stars and the Search for Population III”, *Astrophys. J. Lett.*, **529**(1), L25–L28. [DOI], [ADS]
- Gaia Collaboration, Katz, D., Antoja, T., Romero-Gómez, M., Drimmel, R., Reylé, C., Seabroke, G. M., Soubiran, C., Babusiaux, C., Di Matteo, P., Figueras, F., Poggio, E., Robin, A. C., Evans, D. W., Brown, A. G. A., Vallenari, A., Prusti, T., de Bruijne, J. H. J., Bailer-Jones, C. A. L., Biermann, M., Eyer, L., Jansen, F., Jordi, C., Klioner, S. A., Lammers, U., Lindegren, L., Luri, X., Mignard, F., Panem, C., Pourbaix, D., Randich, S., Sartoretti, P., Siddiqui, H. I., van Leeuwen, F., Walton, N. A., Arenou, F., Bastian, U., Cropper, M., Lattanzi, M. G., Bakker, J., Cacciari, C., Casta n, J., Chaoul,

L., Cheek, N., De Angeli, F., Fabricius, C., Guerra, R., Holl, B., Masana, E., Messineo, R., Mowlavi, N., Nienartowicz, K., Panuzzo, P., Portell, J., Riello, M., Tanga, P., Thévenin, F., Gracia-Abril, G., Comoretto, G., Garcia-Reinaldos, M., Teyssier, D., Altmann, M., Andrae, R., Audard, M., Bellas-Velidis, I., Benson, K., Berthier, J., Blomme, R., Burgess, P., Busso, G., Carry, B., Cellino, A., Clementini, G., Clotet, M., Creevey, O., Davidson, M., De Ridder, J., Delchambre, L., Dell’Oro, A., Ducourant, C., Fernández-Hernández, J., Fouesneau, M., Frémat, Y., Galluccio, L., García-Torres, M., González-Núñez, J., González-Vidal, J. J., Gosset, E., Guy, L. P., Halbwachs, J. L., Hambly, N. C., Harrison, D. L., Hernández, J., Hestroffer, D., Hodgkin, S. T., Hutton, A., Jasniewicz, G., Jean-Antoine-Piccolo, A., Jordan, S., Korn, A. J., Krone-Martins, A., Lanazafame, A. C., Lebzelter, T., Löfller, W., Manteiga, M., Marrese, P. M., Martín-Fleitas, J. M., Moitinho, A., Mora, A., Muinonen, K., Osinde, J., Pancino, E., Pauwels, T., Petit, J. M., Recio-Blanco, A., Richards, P. J., Rimoldini, L., Sarro, L. M., Siopis, C., Smith, M., Sozzetti, A., Süveges, M., Torra, J., van Reeven, W., Abbas, U., Abreu Aramburu, A., Accart, S., Aerts, C., Altavilla, G., Álvarez, M. A., Alvarez, R., Alves, J., Anderson, R. I., Andrei, A. H., Anglada Varela, E., Antiche, E., Arcay, B., Astraatmadja, T. L., Bach, N., Baker, S. G., Balaguer-Núñez, L., Balm, P., Barache, C., Barata, C., Barbato, D., Barblan, F., Barklem, P. S., Barrado, D., Barros, M., Barstow, M. A., Bartholomé Muñoz, L., Bassilana, J. L., Becciani, U., Bellazzini, M., Berihuete, A., Bertone, S., Bianchi, L., Bienaymé, O., Blanco-Cuaresma, S., Boch, T., Boeche, C., Bombrun, A., Borrachero, R., Bossini, D., Bouquillon, S., Bourda, G., Bragaglia, A., Bramante, L., Breddels, M. A., Bressan, A., Brouillet, N., Brüsemeister, T., Brugaletta, E., Bucciarelli, B., Burlacu, A., Busonero, D., Butkevich, A. G., Buzzi, R., Caffau, E., Cancelliere, R., Cannizzaro, G., Cantat-Gaudin, T., Carballo, R., Carlucci, T., Carrasco, J. M., Casamiquela, L., Castellani, M., Castro-Ginard, A., Charlot, P., Chemin, L., Chiavassa, A., Cocozza, G., Costigan, G., Cowell, S., Crifo, F., Crosta, M., Crowley, C., Cuypers, J., Dafonte, C., Damerdji, Y., Dapergolas, A., David, P., David, M., de Laverny,

P., De Luise, F., De March, R., de Souza, R., de Torres, A., Debosscher, J., del Pozo, E., Delbo, M., Delgado, A., Delgado, H. E., Diakite, S., Diener, C., Distefano, E., Dolding, C., Drazinos, P., Durán, J., Edvardsson, B., Enke, H., Eriksson, K., Esquej, P., Eynard Bontemps, G., Fabre, C., Fabrizio, M., Faigler, S., Falc a, A. J., Farràs Casas, M., Federici, L., Fedorets, G., Fernique, P., Filippi, F., Findeisen, K., Fonti, A., Fraile, E., Fraser, M., Frézouls, B., Gai, M., Galleti, S., Garabato, D., García-Sedano, F., Garofalo, A., Garralda, N., Gavel, A., Gavras, P., Gerssen, J., Geyer, R., Giacobbe, P., Gilmore, G., Girona, S., Giuffrida, G., Glass, F., Gomes, M., Granvik, M., Gueguen, A., Guerrier, A., Guiraud, J., Gutié, R., Haigron, R., Hatzidimitriou, D., Hauser, M., Haywood, M., Heiter, U., Helmi, A., Heu, J., Hilger, T., Hobbs, D., Hofmann, W., Holland, G., Huckle, H. E., Hypki, A., Icardi, V., Janßen, K., Jevardat de Fombelle, G., Jonker, P. G., Juhász, Á. L., Julbe, F., Karampelas, A., Kewley, A., Klar, J., Kochoska, A., Kohley, R., Kolenberg, K., Kontizas, M., Kontizas, E., Koposov, S. E., Kordopatis, G., Kostrzewa-Rutkowska, Z., Koubsky, P., Lambert, S., Lanza, A. F., Lasne, Y., Lavigne, J. B., Le Fustec, Y., Le Poncin-Lafitte, C., Lebreton, Y., Leccia, S., Leclerc, N., Lecoeur-Taibi, I., Lenhardt, H., Leroux, F., Liao, S., Licata, E., Lindstrøm, H. E. P., Lister, T. A., Livanou, E., Lobel, A., López, M., Managau, S., Mann, R. G., Mantelet, G., Marchal, O., Marchant, J. M., Marconi, M., Marinoni, S., Marschalkó, G., Marshall, D. J., Martino, M., Marton, G., Mary, N., Massari, D., Matijević, G., Mazeh, T., McMillan, P. J., Messina, S., Michalik, D., Millar, N. R., Molina, D., Molinaro, R., Molnár, L., Montegriffo, P., Mor, R., Morbidelli, R., Morel, T., Morris, D., Mulone, A. F., Muraveva, T., Musella, I., Nelemans, G., Nicastro, L., Noval, L., O'Mullane, W., Ordénovic, C., Ordóñez-Blanco, D., Osborne, P., Pagani, C., Pagano, I., Pailler, F., Palacin, H., Palaversa, L., Panahi, A., Pawlak, M., Piersimoni, A. M., Pineau, F. X., Plachy, E., Plum, G., Poujoulet, E., Prša, A., Pulone, L., Racero, E., Ragaini, S., Rambaux, N., Ramos-Lerate, M., Regibo, S., Riclet, F., Ripepi, V., Riva, A., Rivard, A., Rixon, G., Roegiers, T.,

Roelens, M., Rowell, N., Royer, F., Ruiz-Dern, L., Sadowski, G., Sagristà Sel-lés, T., Sahlmann, J., Salgado, J., Salguero, E., Sanna, N., Santana-Ros, T., Sarasso, M., Savietto, H., Schultheis, M., Sciacca, E., Segol, M., Segovia, J. C., Ségransan, D., Shih, I. C., Siltala, L., Silva, A. F., Smart, R. L., Smith, K. W., Solano, E., Solitro, F., Sordo, R., Soria Nieto, S., Souchay, J., Spagna, A., Spoto, F., Stampa, U., Steele, I. A., Steidelmüller, H., Stephenson, C. A., Stoev, H., Suess, F. F., Surdej, J., Szabados, L., Szegedi-Elek, E., Tapiador, D., Taris, F., Tauran, G., Taylor, M. B., Teixeira, R., Terrett, D., Teyssandier, P., Thuillot, W., Titarenko, A., Torra Clotet, F., Turon, C., Ulla, A., Utrilla, E., Uzzi, S., Vaillant, M., Valentini, G., Valette, V., van Elteren, A., Van Hemelryck, E., van Leeuwen, M., Vaschetto, M., Vecchiato, A., Veljanoski, J., Viala, Y., Vicente, D., Vogt, S., von Essen, C., Voss, H., Votruba, V., Voutsinas, S., Walmsley, G., Weiler, M., Wertz, O., Wevers, T., Wyrzykowski, Ł., Yoldas, A., Žerjal, M., Ziaeepour, H., Zorec, J., Zschocke, S., Zucker, S., Zurbach, C. and Zwitter, T., 2018, “Gaia Data Release 2. Mapping the Milky Way disc kinematics”, *Astron. Astrophys.*, **616**, A11. [DOI], [ADS], [arXiv:1804.09380 [astro-ph.GA]]

Gallino, Roberto, Arlandini, Claudio, Busso, Maurizio, Lugaro, Maria, Travaglio, Claudia, Straniero, Oscar, Chieffi, Alessandro and Limongi, Marco, 1998, “Evolution and Nucleosynthesis in Low-Mass Asymptotic Giant Branch Stars. II. Neutron Capture and the S-Process”, *Astrophys. J.*, **497**(1), 388–403. [DOI], [ADS]

Gallino, Roberto, Bisterzo, S., Husti, L., Käppeler, F., Cristallo, S. and Straniero, O., 2006, “ ^{22}Ne a primary source of neutron for the s-process and a major neutron poison in CEMP AGB stars”, in *International Symposium on Nuclear Astrophysics - Nuclei in the Cosmos*, (Eds.) Mengoni, Alberto, Cederkall, Joakim, D’Auria, John, Fraile, Luis, Fynbo, Hans, Hass, Michael, Jeanne, Melanie Marie, Hjorth Jensen, Morten, Kaeppler, Franz, Kratz, Karl Ludwig, Lindroos, Mats, Menna, Mariano, Meynet, Georges, Riisager, Karsten, ASP Conference Series, Academic Press. Academic Press. [ADS]

- García-Hernández, D. A., García-Lario, P., Plez, B., D'Antona, F., Manchado, A. and Trigo-Rodríguez, J. M., 2006, “Rubidium-Rich Asymptotic Giant Branch Stars”, *Science*, **314**(5806), 1751. [DOI], [ADS], [arXiv:astro-ph/0611319 [astro-ph]]
- García-Hernández, D. A., García-Lario, P., Plez, B., Manchado, A., D'Antona, F., Lub, J. and Habing, H., 2007, “Lithium and zirconium abundances in massive Galactic O-rich AGB stars”, *Astron. Astrophys.*, **462**(2), 711–730. [DOI], [ADS], [arXiv:astro-ph/0609106 [astro-ph]]
- García-Hernández, D. A., Manchado, A., Lambert, D. L., Plez, B., García-Lario, P., D'Antona, F., Lugaro, M., Karakas, A. I. and van Raai, M. A., 2009, “Rb-Rich Asymptotic Giant Branch Stars in the Magellanic Clouds”, *Astrophys. J. Lett.*, **705**(1), L31–L35. [DOI], [ADS], [arXiv:0909.4391 [astro-ph.SR]]
- Garz, T., 1973, “Absolute Oscillator Strengths of SI I Lines between 2500 Å and 9000 Å”, *Astron. Astrophys.*, **26**, 471. [ADS]
- Gibson, B. K., 1997, “Galactic winds and the photochemical evolution of elliptical galaxies: the classic model revisited”, *Mon. Not. Roy. Astron. Soc.*, **290**(3), 471–489. [DOI], [ADS], [arXiv:astro-ph/9705104 [astro-ph]]
- Gigoyan, K. S., Hambaryan, V. V. and Azzopardi, M., 1998, “First Byurakan Spectral Sky Survey. Stars of late spectral types. $-11^\circ \leq \delta \leq -7^\circ$ belt”, *Astrophysics*, **41**(4), 356–366. [DOI], [ADS]
- Gilroy, Kalpana Krishnaswamy, 1989, “Carbon Isotope Ratios and Lithium Abundances in Open Cluster Giants”, *Astrophys. J.*, **347**, 835. [DOI], [ADS]
- Girardi, L., Bressan, A., Bertelli, G. and Chiosi, C., 2000, “Evolutionary tracks and isochrones for low- and intermediate-mass stars: From 0.15 to 7 M_{sun} , and from $Z=0.0004$ to 0.03 ”, *Astron. Astrophys. Suppl.*, **141**, 371–383. [DOI], [ADS], [arXiv:astro-ph/9910164 [astro-ph]]

- Giridhar, Sunetra, 2010, “Spectral Classification: Old and Contemporary”, in *Principles and Perspectives in Cosmochemistry*, Astrophysics and Space Science Proceedings, 16, Springer. Springer. [DOI], [ADS], [arXiv:1003.4002 [astro-ph.SR]]
- Goriely, S. and Mowlavi, N., 2000, “Neutron-capture nucleosynthesis in AGB stars”, *Astron. Astrophys.*, **362**, 599–614. [ADS]
- Goriely, S. and Siess, L., 2005, “The s-process Nucleosynthesis”, in *From Lithium to Uranium: Elemental Tracers of Early Cosmic Evolution*, (Eds.) Hill, Vanessa, Francois, Patrick, Primas, Francesca, Proceedings of the international Astronomical Union, 228, Cambridge University Press. Cambridge University Press. [DOI], [ADS]
- Görres, J., Arlandini, C., Giesen, U., Heil, M., Käppeler, F., Leiste, H., Stech, E. and Wiescher, M., 2000, “Low-energy resonances in $^{14}\text{N}(\alpha,\gamma)^{18}\text{F}$ and their astrophysical implications”, *Phys. Rev. C*, **62**(5), 055801. [DOI], [ADS]
- Goswami, A. and Prantzos, N., 2000, “Abundance evolution of intermediate mass elements (C to Zn) in the Milky Way halo and disk”, *Astron. Astrophys.*, **359**, 191–212. [ADS], [arXiv:astro-ph/0005179 [astro-ph]]
- Goswami, Aruna, 2005, “CH stars at high Galactic latitudes”, *Mon. Not. Roy. Astron. Soc.*, **359**(2), 531–544. [DOI], [ADS], [arXiv:astro-ph/0507202 [astro-ph]]
- Goswami, Aruna and Aoki, Wako, 2010, “HD 209621: abundances of neutron-capture elements*”, *Mon. Not. Roy. Astron. Soc.*, **404**(1), 253–264. [DOI], [ADS], [arXiv:1002.4477 [astro-ph.SR]]
- Goswami, Aruna, Aoki, Wako, Beers, Timothy C., Christlieb, Norbert, Norris, John E., Ryan, Sean G. and Tsangarides, Stelios, 2006, “A high-resolution spectral analysis of three carbon-enhanced metal-poor stars”, *Mon. Not. Roy. Astron. Soc.*, **372**(1), 343–356. [DOI], [ADS], [arXiv:astro-ph/0608106 [astro-ph]]

- Goswami, Aruna, Bama, P., Shantikumar, N. S. and Devassy, Deepthi, 2007, “Low-resolution spectroscopy of high Galactic latitude objects: A search for CH stars”, *Bulletin of the Astronomical Society of India*, **35**, 339. [ADS]
- Goswami, Aruna, Karinkuzhi, Drisya and Shantikumar, N. S., 2010, “The CH fraction of carbon stars at high Galactic latitudes”, *Mon. Not. Roy. Astron. Soc.*, **402**(2), 1111–1125. [DOI], [ADS], [arXiv:0912.4347 [astro-ph.SR]]
- Goswami, Aruna, Aoki, Wako and Karinkuzhi, Drisya, 2016, “Subaru/HDS study of CH stars: elemental abundances for stellar neutron-capture process studies”, *Mon. Not. Roy. Astron. Soc.*, **455**(1), 402–422. [DOI], [ADS], [arXiv:1510.07814 [astro-ph.SR]]
- Goswami, Partha Pratim, Rathour, Rajeev Singh and Goswami, Aruna, 2021, “Spectroscopic study of CEMP-(s & r/s) stars. Revisiting classification criteria and formation scenarios, highlighting i-process nucleosynthesis”, *Astron. Astrophys.*, **649**, A49. [DOI], [ADS], [arXiv:2101.09518 [astro-ph.SR]]
- Gratton, R., D’Orazi, V., Pacheco, T. A., Zurlo, A., Desidera, S., Meléndez, J., Mesa, D., Claudi, R., Janson, M., Langlois, M., Rickman, E., Samland, M., Moulin, T., Soenke, C., Cascone, E., Ramos, J., Rigal, F., Avenhaus, H., Beuzit, J. L., Biller, B., Boccaletti, A., Bonavita, M., Bonnefoy, M., Brandner, W., Chauvin, G., Cudel, M., Daemgen, S., Delorme, P., Desgrange, C., Engler, N., Feldt, M., Fontanive, C., Galicher, R., Garufi, A., Gasparri, D., Ginski, C., Girard, J., Hagelberg, J., Hunziker, S., Kasper, M., Keppler, M., Lagrange, A. M., Lannier, J., Lazzoni, C., Le Coroller, H., Ligi, R., Lombart, M., Maire, A. L., Mayer, M. R., Mazevert, S., Ménard, F., Mouillet, D., Perrot, C., Peretti, S., Petrus, S., Potier, A., Rouan, D., Schmid, H. M., Schmidt, T. O. B., Sissa, E., Stolker, T., Salter, G., Vigan, A. and Wildi, F., 2021, “Investigating three Sirius-like systems with SPHERE”, *Astron. Astrophys.*, **646**, A61. [DOI], [ADS], [arXiv:2012.05575 [astro-ph.SR]]

- Gratton, R. G., Sneden, C., Carretta, E. and Bragaglia, A., 2000, “Mixing along the red giant branch in metal-poor field stars”, *Astron. Astrophys.*, **354**, 169–187. [ADS]
- Grundahl, F., Briley, M., Nissen, P. E. and Feltzing, S., 2002, “Abundances of RGB stars in NGC 6752”, *Astron. Astrophys.*, **385**, L14–L17. [DOI], [ADS]
- Habing, Harm J. and Whitelock, Patricia A., 2004, “AGB Stars as Tracers of Stellar Populations”, in *Asymptotic Giant Branch Stars*, Springer. [DOI], [ADS]
- Hampel, Melanie, Stancliffe, Richard J., Lugaro, Maria and Meyer, Bradley S., 2016, “The Intermediate Neutron-capture Process and Carbon-enhanced Metal-poor Stars”, *Astrophys. J.*, **831**(2), 171. [DOI], [ADS], [arXiv:1608.08634 [astro-ph.SR]]
- Hampel, Melanie, Karakas, Amanda I., Stancliffe, Richard J., Meyer, Bradley S. and Lugaro, Maria, 2019, “Learning about the Intermediate Neutron-capture Process from Lead Abundances”, *Astrophys. J.*, **887**(1), 11. [DOI], [ADS], [arXiv:1910.11882 [astro-ph.SR]]
- Han, Zhanwen, Eggleton, Peter P., Podsiadlowski, Philipp and Tout, Christopher A., 1995, “The formation of barium and CH stars and related objects”, *Mon. Not. Roy. Astron. Soc.*, **277**(4), 1443–1462. [DOI], [ADS]
- Hannaford, P., Lowe, R. M., Grevesse, N., Biemont, E. and Whaling, W., 1982, “Oscillator strengths for Y I and Y II and the solar abundance of yttrium.”, *Astrophys. J.*, **261**, 736–746. [DOI], [ADS]
- Hansen, C. J., Nordström, B., Hansen, T. T., Kennedy, C. R., Placco, V. M., Beers, T. C., Andersen, J., Cescutti, G. and Chiappini, C., 2016a, “Abundances of carbon-enhanced metal-poor stars as constraints on their formation”, *Astron. Astrophys.*, **588**, A37. [DOI], [ADS], [arXiv:1511.07812 [astro-ph.SR]]
- Hansen, C. J., Hansen, T. T., Koch, A., Beers, T. C., Nordström, B., Placco, V. M. and Andersen, J., 2019, “Abundances and kinematics of carbon-enhanced

- metal-poor stars in the Galactic halo. A new classification scheme based on Sr and Ba”, *Astron. Astrophys.*, **623**, A128. [DOI], [ADS], [arXiv:1901.05968 [astro-ph.SR]]
- Hansen, T., Hansen, C. J., Christlieb, N., Beers, T. C., Yong, D., Bessell, M. S., Frebel, A., García Pérez, A. E., Placco, V. M., Norris, J. E. and Asplund, M., 2015, “An Elemental Assay of Very, Extremely, and Ultra-metal-poor Stars”, *Astrophys. J.*, **807**(2), 173. [DOI], [ADS], [arXiv:1506.00579 [astro-ph.SR]]
- Hansen, T. T., Andersen, J., Nordström, B., Beers, T. C., Placco, V. M., Yoon, J. and Buchhave, L. A., 2016b, “The role of binaries in the enrichment of the early Galactic halo. II. Carbon-enhanced metal-poor stars: CEMP-no stars”, *Astron. Astrophys.*, **586**, A160. [DOI], [ADS], [arXiv:1511.08197 [astro-ph.SR]]
- Hansen, T. T., Andersen, J., Nordström, B., Beers, T. C., Placco, V. M., Yoon, J. and Buchhave, L. A., 2016c, “The role of binaries in the enrichment of the early Galactic halo. III. Carbon-enhanced metal-poor stars - CEMP-s stars”, *Astron. Astrophys.*, **588**, A3. [DOI], [ADS], [arXiv:1601.03385 [astro-ph.SR]]
- Hansen, Terese, Andersen, Johannes, Nordström, Birgitta, Buchhave, Lars A. and Beers, Timothy C., 2011, “The Binary Frequency of r-Process-element-enhanced Metal-poor Stars and Its Implications: Chemical Tagging in the Primitive Halo of the Milky Way”, *Astrophys. J. Lett.*, **743**(1), L1. [DOI], [ADS], [arXiv:1110.4536 [astro-ph.GA]]
- Harris, M. J., Lambert, D. L. and Smith, V. V., 1985, “Oxygen isotopic abundances in evolved stars. I. Six barium stars.”, *Astrophys. J.*, **292**, 620–627. [DOI], [ADS]
- Hayes, Christian R., Majewski, Steven R., Shetrone, Matthew, Fernández-Alvar, Emma, Allende Prieto, Carlos, Schuster, William J., Carigi, Leticia, Cunha, Katia, Smith, Verne V., Sobeck, Jennifer, Almeida, Andres, Beers, Timothy C., Carrera, Ricardo, Fernández-Trincado, J. G., García-Hernández, D. A., Geisler, Doug, Lane, Richard R., Lucatello, Sara, Matthews, Allison M., Minniti, Dante, Nitschelm, Christian, Tang, Baitian, Tissera, Patricia B. and Zamora,

- Olga, 2018, “Disentangling the Galactic Halo with APOGEE. I. Chemical and Kinematical Investigation of Distinct Metal-poor Populations”, *Astrophys. J.*, **852**(1), 49. [DOI], [ADS], [arXiv:1711.05781 [astro-ph.GA]]
- Heger, Alexander and Woosley, S. E., 2010, “Nucleosynthesis and Evolution of Massive Metal-free Stars”, *Astrophys. J.*, **724**(1), 341–373. [DOI], [ADS], [arXiv:0803.3161 [astro-ph]]
- Heil, M., Käppeler, F., Uberseder, E., Gallino, R., Bisterzo, S. and Pignatari, M., 2008a, “Stellar (n,γ) cross sections for Br and Rb: Matching the weak and main s-process components”, *Phys. Rev. C*, **78**(2), 025802. [DOI], [ADS]
- Heil, M., Käppeler, F., Uberseder, E., Gallino, R. and Pignatari, M., 2008b, “Neutron capture cross sections for the weak s process in massive stars”, *Phys. Rev. C*, **77**(1), 015808. [DOI], [ADS]
- Heil, M., Winckler, N., Dababneh, S., Käppeler, F., Wissak, K., Bisterzo, S., Gallino, R., Davis, A. M. and Rauscher, T., 2008c, “ $^{176}\text{Lu}/^{176}\text{Hf}$: A Sensitive Test of s-Process Temperature and Neutron Density in AGB Stars”, *Astrophys. J.*, **673**(1), 434–444. [DOI], [ADS]
- Heise, H., 1974, “Experimental Oscillator Strengths for NI I and NI N Lines”, *Astron. Astrophys.*, **34**, 275. [ADS]
- Henry, R. B. C., Edmunds, M. G. and Köppen, J., 2000, “On the Cosmic Origins of Carbon and Nitrogen”, *Astrophys. J.*, **541**(2), 660–674. [DOI], [ADS], [arXiv:astro-ph/0004299 [astro-ph]]
- Herwig, F., 2000, “The evolution of AGB stars with convective overshoot”, *Astron. Astrophys.*, **360**, 952–968. [ADS], [arXiv:astro-ph/0007139 [astro-ph]]
- Herwig, Falk, 2005, “Evolution of Asymptotic Giant Branch Stars”, *Ann. Rev. Astron. Astrophys.*, **43**(1), 435–479. [DOI], [ADS]

- Herwig, Falk, Langer, Norbert and Lugaro, Maria, 2003, “The s-Process in Rotating Asymptotic Giant Branch Stars”, *Astrophys. J.*, **593**(2), 1056–1073. [DOI], [ADS], [arXiv:astro-ph/0305491 [astro-ph]]
- Herwig, Falk, Pignatari, Marco, Woodward, Paul R., Porter, David H., Rockefeller, Gabriel, Fryer, Chris L., Bennett, Michael and Hirschi, Raphael, 2011, “Convective-reactive Proton- ^{12}C Combustion in Sakurai’s Object (V4334 Sagittarii) and Implications for the Evolution and Yields from the First Generations of Stars”, *Astrophys. J.*, **727**(2), 89. [DOI], [ADS], [arXiv:1002.2241 [astro-ph.SR]]
- Herwig, Falk, Woodward, Paul R., Lin, Pei-Hung, Knox, Mike and Fryer, Chris, 2014, “Global Non-spherical Oscillations in Three-dimensional 4π Simulations of the H-ingestion Flash”, *Astrophys. J. Lett.*, **792**(1), L3. [DOI], [ADS], [arXiv:1310.4584 [astro-ph.SR]]
- Hill, V., Barbuy, B., Spite, M., Spite, F., Cayrel, R., Plez, B., Beers, T. C., Nordström, B. and Nissen, P. E., 2000, “Heavy-element abundances in the CH/CN-strong very metal-poor stars CS 22948-27 and CS 29497-34”, *Astron. Astrophys.*, **353**, 557–568. [ADS]
- Hollek, Julie K., Frebel, Anna, Placco, Vinicius M., Karakas, Amanda I., Shetrone, Matthew, Sneden, Christopher and Christlieb, Norbert, 2015, “The Chemical Abundances of Stars in the Halo (CASH) Project. III. A New Classification Scheme for Carbon-enhanced Metal-poor Stars with s-process Element Enhancement”, *Astrophys. J.*, **814**(2), 121. [DOI], [ADS], [arXiv:1510.06825 [astro-ph.SR]]
- Hollowell, David, Iben, Icko, Jr. and Fujimoto, Masayuki Y., 1990, “Hydrogen Burning and Dredge-up during the Major Core Helium Flash in a $Z = 0$ Model Star”, *Astrophys. J.*, **351**, 245. [DOI], [ADS]
- Honda, Satoshi, Aoki, Wako, Kajino, Toshitaka, Ando, Hiroyasu, Beers, Timothy C., Izumiura, Hideyuki, Sadakane, Kozo and Takada-Hidai, Masahide, 2004, “Spectroscopic Studies of Extremely Metal-Poor Stars with the Subaru

- High Dispersion Spectrograph. II. The r-Process Elements, Including Thorium”, *Astrophys. J.*, **607**(1), 474–498. [DOI], [ADS], [arXiv:astro-ph/0402298 [astro-ph]]
- Husti, Laura, Gallino, Roberto, Bisterzo, Sara, Straniero, Oscar and Cristallo, Sergio, 2009, “Barium Stars: Theoretical Interpretation”, *Pub. Astron. Soc. Aus.*, **26**(3), 176–183. [DOI], [ADS], [arXiv:0909.5560 [astro-ph.SR]]
- Ibata, Rodrigo, Lewis, Geraint F., Irwin, Michael, Totten, Edward and Quinn, Thomas, 2001, “Great Circle Tidal Streams: Evidence for a Nearly Spherical Massive Dark Halo around the Milky Way”, *Astrophys. J.*, **551**(1), 294–311. [DOI], [ADS], [arXiv:astro-ph/0004011 [astro-ph]]
- Iben, I., Jr., 1975, “Thermal pulses: p-capture, alpha -capture, s-process nucleosynthesis; and convective mixing in a star of intermediate mass.”, *Astrophys. J.*, **196**, 525–547. [DOI], [ADS]
- Iliadis, Christian, D’Auria, John M., Starrfield, Sumner, Thompson, William J. and Wiescher, Michael, 2001, “Proton-induced Thermonuclear Reaction Rates for A=20-40 Nuclei”, *Astrophys. J. Suppl.*, **134**(1), 151–171. [DOI], [ADS]
- Iocco, Fabio, Mangano, Gianpiero, Miele, Gennaro, Pisanti, Ofelia and Serpico, Pasquale D., 2009, “Primordial nucleosynthesis: From precision cosmology to fundamental physics”, *Physics Reports*, **472**(1-6), 1–76. [DOI], [ADS], [arXiv:0809.0631 [astro-ph]]
- Ivans, Inese I., Sneden, Christopher, Gallino, Roberto, Cowan, John J. and Preston, George W., 2005, “Near-Ultraviolet Observations of CS 29497-030: New Constraints on Neutron-Capture Nucleosynthesis Processes”, *Astrophys. J. Lett.*, **627**(2), L145–L148. [DOI], [ADS], [arXiv:astro-ph/0505002 [astro-ph]]
- Iwamoto, Nobuyuki, Umeda, Hideyuki, Tominaga, Nozomu, Nomoto, Ken’ichi and Maeda, Keiichi, 2005, “The First Chemical Enrichment in the Universe and the Formation of Hyper Metal-Poor Stars”, *Science*, **309**(5733), 451–453. [DOI], [ADS], [arXiv:astro-ph/0505524 [astro-ph]]

- Izzard, R. G., Lugaro, M., Karakas, A. I., Iliadis, C. and van Raai, M., 2007, “Reaction rate uncertainties and the operation of the NeNa and MgAl chains during HBB in intermediate-mass AGB stars”, *Astron. Astrophys.*, **466**(2), 641–648. [DOI], [ADS], [arXiv:astro-ph/0703078 [astro-ph]]
- Jacobson, H. R., Pilachowski, C. A. and Friel, E. D., 2005, “Na and Al Abundances of Open Clusters IC 4756, NGC 6939, and NGC 7142”, in *American Astronomical Society Meeting Abstracts*, American Astronomical Society Meeting Abstracts, 207, Academic Press. Academic Press. [ADS]
- Jaeger, M., Kunz, R., Mayer, A., Hammer, J. W., Staudt, G., Kratz, K. L. and Pfeiffer, B., 2001, “ $^{22}\text{Ne}(\alpha, n)^{25}\text{Mg}$: The Key Neutron Source in Massive Stars”, *Phys. Rev. L.*, **87**(20), 202501. [DOI], [ADS]
- Jeffery, C. Simon, 2010, “Stellar Structure and Evolution: An Introduction”, in *Principles and Perspectives in Cosmochemistry*, Astrophysics and Space Science Proceedings, 16, Springer. Springer. [DOI], [ADS]
- Ji, Wei, Cui, Wenyuan, Liu, Chao, Luo, Ali, Zhao, Gang and Zhang, Bo, 2016, “Carbon Stars from LAMOST DR2 Data”, *Astrophys. J. Suppl.*, **226**(1), 1. [DOI], [ADS], [arXiv:1606.08932 [astro-ph.SR]]
- Johnson, Dean R. H. and Soderblom, David R., 1987, “Calculating Galactic Space Velocities and Their Uncertainties, with an Application to the Ursa Major Group”, *Astron. J.*, **93**, 864. [DOI], [ADS]
- Johnson, H. R., Milkey, R. W. and Ramsey, L. W., 1974, “Formation of the Luminosity-Sensitive 0 I Multiplet at 7774 Å”, *Astrophys. J.*, **187**, 147–150. [DOI], [ADS]
- Jones, S., Ritter, C., Herwig, F., Fryer, C., Pignatari, M., Bertolli, M. G. and Paxton, B., 2016, “H ingestion into He-burning convection zones in super-AGB stellar models as a potential site for intermediate neutron-density nucleosynthesis”, *Mon. Not. Roy. Astron. Soc.*, **455**(4), 3848–3863. [DOI], [ADS], [arXiv:1510.07417 [astro-ph.SR]]

- Jonsell, K., Barklem, P. S., Gustafsson, B., Christlieb, N., Hill, V., Beers, T. C. and Holmberg, J., 2006, “The Hamburg/ESO R-process enhanced star survey (HERES). III. HE 0338-3945 and the formation of the r + s stars”, *Astron. Astrophys.*, **451**(2), 651–670. [DOI], [ADS], [arXiv:astro-ph/0601476 [astro-ph]]
- Jorissen, A. and Mayor, M., 1988, “Radial velocity monitoring of a sample of barium and S stars using CORAVEL : towards an evolutionary link between barium and S stars ?”, *Astron. Astrophys.*, **198**, 187–199. [ADS]
- Jorissen, A., Frayer, D. T., Johnson, H. R., Mayor, M. and Smith, V. V., 1993, “S stars : infrared colors, technetium and binarity.”, *Astron. Astrophys.*, **271**, 463–481. [ADS]
- Jorissen, A., Schmitt, J. H. M. M., Carquillat, J. M., Ginestet, N. and Bickert, K. F., 1996, “New X-ray sources detected among mild barium and S stars.”, *Astron. Astrophys.*, **306**, 467. [ADS]
- Jorissen, A., Van Eck, S., Mayor, M. and Udry, S., 1998, “Insights into the formation of barium and Tc-poor S stars from an extended sample of orbital elements”, *Astron. Astrophys.*, **332**, 877–903. [ADS], [arXiv:astro-ph/9801272 [astro-ph]]
- Jorissen, A., Hansen, T., Van Eck, S., Andersen, J., Nordström, B., Siess, L., Torres, G., Masseron, T. and Van Winckel, H., 2016a, “HE 0017+0055: A probable pulsating CEMP-rs star and long-period binary”, *Astron. Astrophys.*, **586**, A159. [DOI], [ADS], [arXiv:1510.06045 [astro-ph.SR]]
- Jorissen, A., Van Eck, S., Van Winckel, H., Merle, T., Boffin, H. M. J., Andersen, J., Nordström, B., Udry, S., Masseron, T., Lenaerts, L. and Waelkens, C., 2016b, “Binary properties of CH and carbon-enhanced metal-poor stars”, *Astron. Astrophys.*, **586**, A158. [DOI], [ADS], [arXiv:1510.05840 [astro-ph.SR]]
- Kaeppler, F., Wiescher, M., Giesen, U., Goerres, J., Baraffe, I., El Eid, M., Raiteri, C. M., Busso, M., Gallino, R., Limongi, M. and Chieffi, A., 1994, “Reaction Rates for ^{18}O (alpha , gamma) ^{22}Ne , ^{22}Ne (alpha , gamma) ^{26}Mg , and ^{22}Ne (

- alpha , n) 25Mg in Stellar Helium Burning and s-Process Nucleosynthesis in Massive Stars”, *Astrophys. J.*, **437**, 396. [DOI], [ADS]
- Käppeler, F., Gallino, R., Bisterzo, S. and Aoki, Wako, 2011, “The s process: Nuclear physics, stellar models, and observations”, *Reviews of Modern Physics*, **83**(1), 157–194. [DOI], [ADS], [arXiv:1012.5218 [astro-ph.SR]]
- Karakas, A. I., 2010, “Updated stellar yields from asymptotic giant branch models”, *Mon. Not. Roy. Astron. Soc.*, **403**(3), 1413–1425. [DOI], [ADS], [arXiv:0912.2142 [astro-ph.SR]]
- Karakas, A. I. and Lattanzio, J. C., 2003, “Production of Aluminium and the Heavy Magnesium Isotopes in Asymptotic Giant Branch Stars”, *Pub. Astron. Soc. Aus.*, **20**(3), 279–293. [DOI], [ADS]
- Karakas, A. I., Lugaro, M. A., Wiescher, M., Görres, J. and Ugalde, C., 2006, “The Uncertainties in the $^{22}\text{Ne}+\alpha$ -Capture Reaction Rates and the Production of the Heavy Magnesium Isotopes in Asymptotic Giant Branch Stars of Intermediate Mass”, *Astrophys. J.*, **643**(1), 471–483. [DOI], [ADS], [arXiv:astro-ph/0601645 [astro-ph]]
- Karakas, Amanda I. and Lattanzio, John C., 2014, “The Dawes Review 2: Nucleosynthesis and Stellar Yields of Low- and Intermediate-Mass Single Stars”, *Pub. Astron. Soc. Aus.*, **31**, e030. [DOI], [ADS], [arXiv:1405.0062 [astro-ph.SR]]
- Karakas, Amanda I. and Lugaro, Maria, 2016, “Stellar Yields from Metal-rich Asymptotic Giant Branch Models”, *Astrophys. J.*, **825**(1), 26. [DOI], [ADS], [arXiv:1604.02178 [astro-ph.SR]]
- Karakas, Amanda I., García-Hernández, D. A. and Lugaro, Maria, 2012, “Heavy Element Nucleosynthesis in the Brightest Galactic Asymptotic Giant Branch Stars”, *Astrophys. J.*, **751**(1), 8. [DOI], [ADS], [arXiv:1203.2931 [astro-ph.SR]]
- Karinkuzhi, D., Van Eck, S., Jorissen, A., Goriely, S., Siess, L., Merle, T., Escorza, A., Van der Swaelmen, M., Boffin, H. M. J., Masseron, T., Shetye, S. and Plez,

- B., 2018a, “When binaries keep track of recent nucleosynthesis. The Zr-Nb pair in extrinsic stars as an s-process diagnostic”, *Astron. Astrophys.*, **618**, A32. [DOI], [ADS], [arXiv:1807.06332 [astro-ph.SR]]
- Karinkuzhi, D., Van Eck, S., Goriely, S., Siess, L., Jorissen, A., Merle, T., Escorza, A. and Masseron, T., 2021, “Low-mass low-metallicity AGB stars as an efficient i-process site explaining CEMP-rs stars”, *Astron. Astrophys.*, **645**, A61. [DOI], [ADS], [arXiv:2010.13620 [astro-ph.SR]]
- Karinkuzhi, Drisya and Goswami, Aruna, 2014, “Chemical analysis of CH stars - I. Atmospheric parameters and elemental abundances”, *Mon. Not. Roy. Astron. Soc.*, **440**(2), 1095–1113. [DOI], [ADS], [arXiv:1410.0111 [astro-ph.SR]]
- Karinkuzhi, Drisya and Goswami, Aruna, 2015, “Chemical analysis of CH stars - II. Atmospheric parameters and elemental abundances”, *Mon. Not. Roy. Astron. Soc.*, **446**(3), 2348–2362. [DOI], [ADS], [arXiv:1412.3548 [astro-ph.SR]]
- Karinkuzhi, Drisya, Goswami, Aruna, Sridhar, Navin, Masseron, Thomas and Purandardas, Meenakshi, 2018b, “Chemical analysis of three barium stars: HD 51959, HD 88035, and HD 121447”, *Mon. Not. Roy. Astron. Soc.*, **476**(3), 3086–3096. [DOI], [ADS], [arXiv:1802.01343 [astro-ph.SR]]
- Keenan, Philip C., 1942, “The Spectra of CH Stars”, *Astrophys. J.*, **96**, 101. [DOI], [ADS]
- Keenan, Philip C., 1954, “Classification of the S-Type Stars.”, *Astrophys. J.*, **120**, 484. [DOI], [ADS]
- Keller, S. C., Bessell, M. S., Frebel, A., Casey, A. R., Asplund, M., Jacobson, H. R., Lind, K., Norris, J. E., Yong, D., Heger, A., Magic, Z., da Costa, G. S., Schmidt, B. P. and Tisserand, P., 2014, “A single low-energy, iron-poor supernova as the source of metals in the star SMSS J031300.36-670839.3”, *Nature*, **506**(7489), 463–466. [DOI], [ADS], [arXiv:1402.1517 [astro-ph.SR]]

- Kennedy, Catherine R., Sivarani, Thirupathi, Beers, Timothy C., Lee, Young Sun, Placco, Vinicius M., Rossi, Silvia, Christlieb, Norbert, Herwig, Falk and Plez, Bertrand, 2011, “[O/Fe] Estimates for Carbon-enhanced Metal-poor Stars from Near-infrared Spectroscopy”, *Astron. J.*, **141**(3), 102. [DOI], [ADS], [arXiv:1101.2260 [astro-ph.SR]]
- Kiselman, D., 1993, “The 777 NM oxygen triplet in the Sun and solar-type stars, and its use for abundance analysis”, *Astron. Astrophys.*, **275**, 269. [ADS]
- Kobayashi, Chiaki, Umeda, Hideyuki, Nomoto, Ken’ichi, Tominaga, Nozomu and Ohkubo, Takuya, 2006, “Galactic Chemical Evolution: Carbon through Zinc”, *Astrophys. J.*, **653**(2), 1145–1171. [DOI], [ADS], [arXiv:astro-ph/0608688 [astro-ph]]
- Kobayashi, Chiaki, Karakas, Amanda I. and Umeda, Hideyuki, 2011, “The evolution of isotope ratios in the Milky Way Galaxy”, *Mon. Not. Roy. Astron. Soc.*, **414**(4), 3231–3250. [DOI], [ADS], [arXiv:1102.5312 [astro-ph.GA]]
- Kobayashi, Chiaki, Karakas, Amanda I. and Lugaro, Maria, 2020, “The Origin of Elements from Carbon to Uranium”, *Astrophys. J.*, **900**(2), 179. [DOI], [ADS], [arXiv:2008.04660 [astro-ph.GA]]
- Koch, Andreas, Reichert, Moritz, Hansen, Camilla Juul, Hampel, Melanie, Stancliffe, Richard J., Karakas, Amanda and Arcones, Almudena, 2019, “Unusual neutron-capture nucleosynthesis in a carbon-rich Galactic bulge star”, *Astron. Astrophys.*, **622**, A159. [DOI], [ADS], [arXiv:1812.07574 [astro-ph.GA]]
- Kurucz, R. L., 1988, “Semiempirical Determination of FeII Oscillator Strengths”, in *IAU Colloq. 94: Physics of Formation of FE II Lines Outside LTE*, (Eds.) Viotti, Roberto, Vittone, Alberto, Friedjung, Michael, Proceedings of the international Astronomical Union, 138, Dordrecht: D. Reidel Publishing Co. Dordrecht: D. Reidel Publishing Co. [DOI], [ADS]
- Kurucz, R. L., 1993, “VizieR Online Data Catalog: Model Atmospheres (Kurucz, 1979)”, *VizieR Online Data Catalog*, VI/39. [ADS]

- Kurucz, R. L. and Peytremann, E., 1975, “A table of semiempirical gf values. Pt 1: Wavelengths: 5.2682 NM to 272.3380 nm; Pt 2: Wavelengths: 272.3395 NM to 599.3892 nm; Pt 3: Wavelengths: 599.4004 NM to 9997.2746 NM”, *SAO Special Report*. [ADS]
- Lage, C. S. and Whaling, W., 1976, “Transition probabilities in Pr(II) and the solar praseodymium abundance.”, *J. Quant. Spectr. Radi. Transfer.*, **16**(6), 537–542. [DOI], [ADS]
- Lambert, D. L., 1978, “The abundances of the elements in the solar photosphere - VIII. Revised abundances of carbon, nitrogen and oxygen.”, *Mon. Not. Roy. Astron. Soc.*, **182**, 249–272. [DOI], [ADS]
- Lambert, D. L. and Luck, R. E., 1976, “Profiles of the RB I resonance lines in the Arcturus spectrum”, *The Observatory*, **96**, 100–104. [ADS]
- Lambert, David L., Smith, Verne V., Busso, Maurizio, Gallino, Roberto and Straniero, Oscar, 1995, “The Chemical Composition of Red Giants. IV. The Neutron Density at the s-Process Site”, *Astrophys. J.*, **450**, 302. [DOI], [ADS]
- Lambert, David L., Heath, James E., Lemke, Michael and Drake, Jeremy, 1996, “The Chemical Composition of Field RR Lyrae Stars. I. Iron and Calcium”, *Astrophys. J. Suppl.*, **103**, 183. [DOI], [ADS]
- Langer, N., Heger, A., Wellstein, S. and Herwig, F., 1999, “Mixing and nucleosynthesis in rotating TP-AGB stars”, *Astron. Astrophys.*, **346**, L37–L40. [ADS], [arXiv:astro-ph/9904257 [astro-ph]]
- Lattanzio, J., Frost, C., Cannon, R. and Wood, P. R., 1996, “Hot bottom burning in intermediate mass stars”, *Memorie della Societa Astronomica Italiana*, **67**, 729. [ADS]
- Lau, Herbert H. B., Stencliffe, Richard J. and Tout, Christopher A., 2009, “The evolution of low-metallicity asymptotic giant branch stars and the formation

- of carbon-enhanced metal-poor stars”, *Mon. Not. Roy. Astron. Soc.*, **396**(2), 1046–1057. [DOI], [ADS], [arXiv:0903.2324 [astro-ph.SR]]
- Laughlin, C. and Victor, G. A., 1974, “Multiplet Splittings and IS,3p, Intercombination-Line Oscillator Strengths in be i and MG I”, *Astrophys. J.*, **192**, 551–556. [DOI], [ADS]
- Lawler, J. E., Bonvallet, G. and Sneden, Christopher, 2001, “Experimental Radiative Lifetimes, Branching Fractions, and Oscillator Strengths for La II and a New Determination of the Solar Lanthanum Abundance”, *Astrophys. J.*, **556**(1), 452–460. [DOI], [ADS]
- Lee, Young Sun, Beers, Timothy C., Masseron, Thomas, Plez, Bertrand, Rockosi, Constance M., Sobeck, Jennifer, Yanny, Brian, Lucatello, Sara, Sivarani, Thirupathi, Placco, Vinicius M. and Carollo, Daniela, 2013, “Carbon-enhanced Metal-poor Stars in SDSS/SEGUE. I. Carbon Abundance Estimation and Frequency of CEMP Stars”, *Astron. J.*, **146**(5), 132. [DOI], [ADS], [arXiv:1310.3276 [astro-ph.SR]]
- Li, Haining, Tan, Kefeng and Zhao, Gang, 2018a, “A Catalog of 10,000 Very Metal-poor Stars from LAMOST DR3”, *Astrophys. J. Suppl.*, **238**(2), 16. [DOI], [ADS], [arXiv:1809.03881 [hep-ph]]
- Li, Yin-Bi, Luo, A. Li, Du, Chang-De, Zuo, Fang, Wang, Meng-Xin, Zhao, Gang, Jiang, Bi-Wei, Zhang, Hua-Wei, Liu, Chao, Qin, Li, Wang, Rui, Du, Bing, Guo, Yan-Xin, Wang, Bo, Han, Zhan-Wen, Xiang, Mao-Sheng, Huang, Yang, Chen, Bing-Qiu, Chen, Jian-Jun, Kong, Xiao, Hou, Wen, Song, Yi-Han, Wang, You-Fen, Wu, Ke-Fei, Zhang, Jian-Nan, Zhang, Yong, Wang, Yue-Fei, Cao, Zi-Huang, Hou, Yong-Hui and Zhao, Yong-Heng, 2018b, “Carbon Stars Identified from LAMOST DR4 Using Machine Learning”, *Astrophys. J. Suppl.*, **234**(2), 31. [DOI], [ADS], [arXiv:1712.07784 [astro-ph.SR]]

- Liang, Y. C., Zhao, G., Chen, Y. Q., Qiu, H. M. and Zhang, B., 2003, “Chemical compositions of four barium stars”, *Astron. Astrophys.*, **397**, 257–265. [DOI], [ADS], [arXiv:astro-ph/0312372 [astro-ph]]
- Limongi, Marco and Chieffi, Alessandro, 2018, “Presupernova Evolution and Explosive Nucleosynthesis of Rotating Massive Stars in the Metallicity Range $-3 \leq [\text{Fe}/\text{H}] \leq 0$ ”, *Astrophys. J. Suppl.*, **237**(1), 13. [DOI], [ADS], [arXiv:1805.09640 [astro-ph.SR]]
- Lincke, R. and Ziegenbein, B., 1971, “Messung von Oszillatorenstärken im Singulettssystem des neutralen Magnesiums”, *Zeitschrift fur Physik*, **241**(4), 369–379. [DOI], [ADS]
- Lippuner, Jonas, Fernández, Rodrigo, Roberts, Luke F., Foucart, Francois, Kasen, Daniel, Metzger, Brian D. and Ott, Christian D., 2017, “Signatures of hypermassive neutron star lifetimes on r-process nucleosynthesis in the disc ejecta from neutron star mergers”, *Mon. Not. Roy. Astron. Soc.*, **472**(1), 904–918. [DOI], [ADS], [arXiv:1703.06216 [astro-ph.HE]]
- Liu, Chao, Cui, Wen-Yuan, Zhang, Bo, Wan, Jun-Chen, Deng, Li-Cai, Hou, Yong-Hui, Wang, Yue-Fei, Yang, Ming and Zhang, Yong, 2015, “Spectral classification of stars based on LAMOST spectra”, *Research in Astronomy and Astrophysics*, **15**(8), 1137. [DOI], [ADS], [arXiv:1505.05940 [astro-ph.SR]]
- Lü, Phillip K., 1991, “Taxonomy of Barium Stars”, *Astron. J.*, **101**, 2229. [DOI], [ADS]
- Lucatello, Sara, Tsangarides, Stelios, Beers, Timothy C., Carretta, Eugenio, Gratton, Raffaele G. and Ryan, Sean G., 2005, “The Binary Frequency Among Carbon-enhanced, s-Process-rich, Metal-poor Stars”, *Astrophys. J.*, **625**(2), 825–832. [DOI], [ADS], [arXiv:astro-ph/0412422 [astro-ph]]
- Lucatello, Sara, Beers, Timothy C., Christlieb, Norbert, Barklem, Paul S., Rossi, Silvia, Marsteller, Brian, Sivarani, Thirupathi and Lee, Young Sun,

- 2006, “The Frequency of Carbon-enhanced Metal-poor Stars in the Galaxy from the HERES Sample”, *Astrophys. J. Lett.*, **652**(1), L37–L40. [DOI], [ADS], [arXiv:astro-ph/0609730 [astro-ph]]
- Luck, R. E. and Bond, Howard E., 1991, “Subgiant CH Stars. II. Chemical Compositions and the Evolutionary Connection with Barium Stars”, *Astrophys. J. Suppl.*, **77**, 515. [DOI], [ADS]
- Luck, R. E. and Lambert, D. L., 1985, “Carbon, nitrogen and oxygen in intermediate-mass supergiants : is oxygen underabundant ?”, *Astrophys. J.*, **298**, 782–802. [DOI], [ADS]
- Luck, R. Earle, 2017, “Abundances in the Local Region II: F, G, and K Dwarfs and Subgiants”, *Astron. J.*, **153**(1), 21. [DOI], [ADS], [arXiv:1611.02897 [astro-ph.SR]]
- Luck, R. Earle and Heiter, Ulrike, 2007, “Giants in the Local Region”, *Astron. J.*, **133**(6), 2464–2486. [DOI], [ADS]
- Lugaro, M. and Chieffi, A., 2011, “Radioactivities in Low- and Intermediate-Mass Stars”, in *Lecture Notes in Physics, Berlin Springer Verlag*, (Eds.) Diehl, Roland, Hartmann, Dieter H., Prantzos, Nikos, 812, Springer. [ADS]
- Lugardo, M., Campbell, S. W. and de Mink, S. E., 2009, “The Mystery of CEMPs+r Stars and the Dual Core-Flash Neutron Superburst”, *Pub. Astron. Soc. Aus.*, **26**(3), 322–326. [DOI], [ADS]
- Luo, A. Li, Zhang, Hao-Tong, Zhao, Yong-Heng, Zhao, Gang, Cui, Xiang-Qun, Li, Guo-Ping, Chu, Yao-Quan, Shi, Jian-Rong, Wang, Gang, Zhang, Jian-Nan, Bai, Zhong-Rui, Chen, Xiao-Yan, Wang, Feng-Fei, Guo, Yan-Xin, Chen, Jian-Jun, Du, Bing, Kong, Xiao, Lei, Ya-Juan, Li, Yin-Bi, Song, Yi-Han, Wu, Yue, Zhang, Yan-Xia, Zhou, Xin-Lin, Zuo, Fang, Du, Peng, He, Lin, Hou, Wen, Dong, Yi-Qiao, Li, Jian, Li, Guang-Wei, Li, Shuang, Song, Jing, Tian, Yuan, Wang, Meng-Xin, Wu, Ke-Fei, Yang, Hui-Qin, Yuan, Hai-Long, Cao, Shu-Yun, Chen, Hai-Yuan, Chen, Kun-Xin, Chen, Ying, Chu, Jia-Ru, Feng, Lei, Gong,

Xue-Fei, Gu, Bo-Zhong, Hou, Yong-Hui, Huo, Zhi-Ying, Hu, Hong-Zhuan, Hu, Ning-Sheng, Hu, Zhong-Wen, Jia, Lei, Jiang, Fang-Hua, Jiang, Xiang, Jiang, Zi-Bo, Jin, Ge, Li, Ai-Hua, Li, Qi, Li, Xin-Nan, Li, Yan, Li, Ye-Ping, Liu, Gen-Rong, Liu, Guan-Qun, Liu, Zhi-Gang, Lu, Qi-Shuai, Lu, Wen-Zhi, Luo, Yu, Mao, Yin-Dun, Men, Li, Ni, Ji-Jun, Qi, Yong-Jun, Qi, Zhao-Xiang, Shi, Huo-Ming, Su, Ding-Qiang, Sun, Shi-Wei, Su, Hong-Jun, Tang, Zheng-Hong, Tao, Qing-Sheng, Tu, Liang-Ping, Wang, Da-Qing, Wang, Dan, Wang, Guo-Min, Wang, Hai, Wang, Jia-Ning, Wang, Jian, Wang, Jian-Ling, Wang, Jian-Ping, Wang, Lei, Wang, Shou-Guan, Wang, Shu-Qing, Wang, Ya-Nan, Wang, You, Wang, Yue-Fei, Wei, Ming-Zhi, Xue, Xiang-Xiang, Xing, Xiao-Zheng, Xu, Ling-Zhe, Xu, Xin-Qi, Xu, Yan, Yang, De-Hua, Yang, Shi-Hai, Yao, Zheng-Qiu, Yu, Yong, Yuan, Hui, Zhai, Chao, Zhang, En-Peng, Zhang, Jing, Zhang, Li-Ping, Zhang, Wei, Zhang, Yong, Zhang, Zhen-Chao, Zhao, Ming, Zhou, Fang, Zhu, Yong-Tian, Zhu, Jie and Zou, Si-Cheng, 2012, “Data release of the LAMOST pilot survey”, *Research in Astronomy and Astrophysics*, **12**(9), 1243–1246. [DOI], [ADS]

MacConnell, D. J., Frye, R. L. and Upgren, A. R., 1972, “The absolute magnitude of the barium stars.”, *Astron. J.*, **77**, 384–391. [DOI], [ADS]

Maeder, André and Meynet, Georges, 2015, “The first stars: a classification of CEMP-no stars”, *Astron. Astrophys.*, **580**, A32. [DOI], [ADS], [arXiv:1506.04508 [astro-ph.SR]]

Maeder, André, Meynet, Georges and Chiappini, Cristina, 2015, “The first stars: CEMP-no stars and signatures of spinstars”, *Astron. Astrophys.*, **576**, A56. [DOI], [ADS], [arXiv:1412.5754 [astro-ph.SR]]

Maoz, Dan, 2016, *Astrophysics in a Nutshell*, Princeton University Press. [ADS]

Marigo, P., 2002, “Asymptotic Giant Branch evolution at varying surface C/O ratio: effects of changes in molecular opacities”, *Astron. Astrophys.*, **387**, 507–519. [DOI], [ADS], [arXiv:astro-ph/0203036 [astro-ph]]

- Marigo, P. and Aringer, B., 2009, “Low-temperature gas opacity. $\text{\textit{AESOPUS}}$: a versatile and quick computational tool”, *Astron. Astrophys.*, **508**(3), 1539–1569. [DOI], [ADS], [arXiv:0907.3248 [astro-ph.SR]]
- Marsteller, B., Beers, T. C., Rossi, S., Christlieb, N., Bessell, M. and Rhee, J., 2005, “Carbon-Enhanced Metal-Poor Stars in the Early Galaxy”, *Nucl. Phys. A*, **758**, 312–315. [DOI], [ADS], [arXiv:astro-ph/0408380 [astro-ph]]
- Mashonkina, L., Zhao, G., Gehren, T., Aoki, W., Bergemann, M., Noguchi, K., Shi, J. R., Takada-Hidai, M. and Zhang, H. W., 2008, “Non-LTE line formation for heavy elements in four very metal-poor stars”, *Astron. Astrophys.*, **478**(2), 529–541. [DOI], [ADS], [arXiv:0711.4454 [astro-ph]]
- Masseron, T., Johnson, J. A., Plez, B., van Eck, S., Primas, F., Goriely, S. and Jorissen, A., 2010, “A holistic approach to carbon-enhanced metal-poor stars”, *Astron. Astrophys.*, **509**, A93. [DOI], [ADS], [arXiv:0901.4737 [astro-ph.SR]]
- Matteucci, Francesca, 2016, “Introduction to Galactic Chemical Evolution”, in *Journal of Physics Conference Series*, Journal of Physics Conference Series, 703, Academic Press. Academic Press. [DOI], [ADS], [arXiv:1602.01004 [astro-ph.GA]]
- McClure, R. D., 1983, “The binary nature of the barium stars. II. Velocities, binary frequency, and preliminary orbits.”, *Astrophys. J.*, **268**, 264–273. [DOI], [ADS]
- McClure, R. D., 1984, “The binary nature of the CH stars.”, *Astrophys. J. Lett.*, **280**, L31–L34. [DOI], [ADS]
- McClure, R. D., Fletcher, J. M. and Nemec, J. M., 1980, “The binary nature of the barium stars.”, *Astrophys. J. Lett.*, **238**, L35–L38. [DOI], [ADS]
- McClure, Robert D. and Woodsworth, A. W., 1990, “The Binary Nature of the Barium and CH Stars. III. Orbital Parameters”, *Astrophys. J.*, **352**, 709. [DOI], [ADS]
- McWilliam, Andrew, 1998, “Barium Abundances in Extremely Metal-poor Stars”, *Astron. J.*, **115**(4), 1640–1647. [DOI], [ADS]

- McWilliam, Andrew, Preston, George W., Sneden, Christopher and Searle, Leonard, 1995a, “Spectroscopic Analysis of 33 of the Most Metal Poor Stars. II.”, *Astron. J.*, **109**, 2757. [DOI], [ADS]
- McWilliam, Andrew, Preston, George W., Sneden, Christopher and Shectman, Stephen, 1995b, “A Spectroscopic Analysis of 33 of the Most Metal-Poor Stars.I.”, *Astron. J.*, **109**, 2736. [DOI], [ADS]
- Meggers, W. F., Corliss, C. H. and Scribner, B. F., 1975, *Tables of spectral-line intensities. Part I, II - arranged by elements.*, NBS Monograph. [ADS]
- Meneguzzi, M., Audouze, J. and Reeves, H., 1971, “The production of the elements Li, Be, B by galactic cosmic rays in space and its relation with stellar observations.”, *Astron. Astrophys.*, **15**, 337. [ADS]
- Mennessier, M. O., Luri, X., Figueras, F., Gomez, A. E., Grenier, S., Torra, J. and North, P., 1997, “Barium stars, galactic populations and evolution.”, *Astron. Astrophys.*, **326**, 722–730. [ADS]
- Merle, T., Jorissen, A., Van Eck, S., Masseron, T. and Van Winckel, H., 2016, “To Ba or not to Ba: Enrichment in s-process elements in binary systems with WD companions of various masses”, *Astron. Astrophys.*, **586**, A151. [DOI], [ADS], [arXiv:1510.05908 [astro-ph.SR]]
- Merrill, P. W., 1922, “Stellar spectra of class S.”, *Astrophys. J.*, **56**, 457–482. [DOI], [ADS]
- Merrill, Paul W., 1952, “Spectroscopic Observations of Stars of Class S”, *Astrophys. J.*, **116**, 21. [DOI], [ADS]
- Meynet, G., Hirschi, R., Ekstrom, S., Maeder, A., Georgy, C., Eggenberger, P. and Chiappini, C., 2010, “Are C-rich ultra iron-poor stars also He-rich?”, *Astron. Astrophys.*, **521**, A30. [DOI], [ADS], [arXiv:1004.5024 [astro-ph.SR]]
- Mishenina, T. V., Soubiran, C., Kovtyukh, V. V. and Korotin, S. A., 2004, “On the correlation of elemental abundances with kinematics among galactic disk

- stars”, *Astron. Astrophys.*, **418**, 551–562. [DOI], [ADS], [arXiv:astro-ph/0401234 [astro-ph]]
- Mishenina, T. V., Bienaymé, O., Gorbaneva, T. I., Charbonnel, C., Soubiran, C., Korotin, S. A. and Kovtyukh, V. V., 2006, “Elemental abundances in the atmosphere of clump giants”, *Astron. Astrophys.*, **456**(3), 1109–1120. [DOI], [ADS], [arXiv:astro-ph/0605615 [astro-ph]]
- Mitchell, Walter E., Jr. and Mohler, Orren C., 1965, “CA i Lines in Auto-Ionization in the Solar Spectrum.”, *Astrophys. J.*, **141**, 1126. [DOI], [ADS]
- Mowlavi, N., 1999a, “On the third dredge-up phenomenon in asymptotic giant branch stars”, *Astron. Astrophys.*, **344**, 617–631. [ADS], [arXiv:astro-ph/9903473 [astro-ph]]
- Mowlavi, Nami, 1999b, “Sodium production in asymptotic giant branch stars”, *Astron. Astrophys.*, **350**, 73–88. [ADS], [arXiv:astro-ph/9910542 [astro-ph]]
- Mucciarelli, A., 2011, “Microturbulent velocity from stellar spectra: a comparison between different approaches”, *Astron. Astrophys.*, **528**, A44. [DOI], [ADS], [arXiv:1101.3426 [astro-ph.SR]]
- Ness, M. and Freeman, K., 2016, “The Metallicity Distribution of the Milky Way Bulge”, *Pub. Astron. Soc. Aus.*, **33**, e022. [DOI], [ADS], [arXiv:1511.07438 [astro-ph.GA]]
- Noguchi, Kunio, Aoki, Wako, Kawanomoto, Satoshi, Ando, Hiroyasu, Honda, Satoshi, Izumiura, Hideyuki, Kambe, Eiji, Okita, Kiichi, Sadakane, Kozo, Sato, Bun’ei, Tajitsu, Akito, Takada-Hidai, Tasahide, Tanaka, Wataru, Watanabe, Etsuji and Yoshida, Michitoshi, 2002, “High Dispersion Spectrograph (HDS) for the Subaru Telescope”, *Pub. Astron. Soc. Japan*, **54**, 855–864. [DOI], [ADS]
- Nomoto, Ken’ichi, Kobayashi, Chiaki and Tominaga, Nozomu, 2013, “Nucleosynthesis in Stars and the Chemical Enrichment of Galaxies”, *Ann. Rev. Astron. Astrophys.*, **51**(1), 457–509. [DOI], [ADS]

- Norris, John E., Ryan, Sean G. and Beers, Timothy C., 1997, “Extremely Metal-poor Stars. IV. The Carbon-rich Objects”, *Astrophys. J.*, **488**(1), 350–363. [DOI], [ADS]
- Norris, John E., Bessell, M. S., Yong, David, Christlieb, N., Barklem, P. S., Asplund, M., Murphy, Simon J., Beers, Timothy C., Frebel, Anna and Ryan, S. G., 2013a, “The Most Metal-poor Stars. I. Discovery, Data, and Atmospheric Parameters”, *Astrophys. J.*, **762**(1), 25. [DOI], [ADS], [arXiv:1208.2999 [astro-ph.GA]]
- Norris, John E., Yong, David, Bessell, M. S., Christlieb, N., Asplund, M., Gilmore, Gerard, Wyse, Rosemary F. G., Beers, Timothy C., Barklem, P. S., Frebel, Anna and Ryan, S. G., 2013b, “The Most Metal-poor Stars. IV. The Two Populations with $[Fe/H] < \sim -3.0$ ”, *Astrophys. J.*, **762**(1), 28. [DOI], [ADS], [arXiv:1211.3157 [astro-ph.GA]]
- North, P., Berthet, S. and Lanz, T., 1994, “The nature of the F STR lambda 4077 stars. III. Spectroscopy of the barium dwarfs and other CP stars.”, *Astron. Astrophys.*, **281**, 775–796. [ADS]
- Patronis, N., Dababneh, S., Assimakopoulos, P. A., Gallino, R., Heil, M., Käppler, F., Karamanis, D., Koehler, P. E., Mengoni, A. and Plag, R., 2004, “Neutron capture studies on unstable ^{135}Cs for nucleosynthesis and transmutation”, *Phys. Rev. C*, **69**(2), 025803. [DOI], [ADS]
- Pereira, C. B. and Drake, N. A., 2009, “High-resolution spectroscopic observations of two chemically peculiar metal-poor stars: HD 10613 and BD+04°2466”, *Astron. Astrophys.*, **496**(3), 791–804. [DOI], [ADS]
- Piersanti, L., Straniero, O. and Cristallo, S., 2007, “A method to derive the absolute composition of the Sun, the solar system, and the stars”, *Astron. Astrophys.*, **462**(3), 1051–1062. [DOI], [ADS], [arXiv:astro-ph/0611229 [astro-ph]]
- Piersanti, L., Cristallo, S. and Straniero, O., 2013, “The Effects of Rotation on s-process Nucleosynthesis in Asymptotic Giant Branch Stars”, *Astrophys. J.*, **774**(2), 98. [DOI], [ADS], [arXiv:1307.2017 [astro-ph.SR]]

- Pignatari, M., Gallino, R., Heil, M., Wiescher, M., Käppeler, F., Herwig, F. and Bisterzo, S., 2010, “The Weak s-Process in Massive Stars and its Dependence on the Neutron Capture Cross Sections”, *Astrophys. J.*, **710**(2), 1557–1577. [DOI], [ADS]
- Pilachowski, C. A., 1977, “The chemical compositions of the mild barium stars.”, *Astron. Astrophys.*, **54**, 465–474. [ADS]
- Placco, Vinicius M., Frebel, Anna, Beers, Timothy C., Karakas, Amanda I., Kennedy, Catherine R., Rossi, Silvia, Christlieb, Norbert and Stancliffe, Richard J., 2013, “Metal-poor Stars Observed with the Magellan Telescope. I. Constraints on Progenitor Mass and Metallicity of AGB Stars Undergoing s-process Nucleosynthesis”, *Astrophys. J.*, **770**(2), 104. [DOI], [ADS], [arXiv:1304.7869 [astro-ph.GA]]
- Placco, Vinicius M., Frebel, Anna, Beers, Timothy C. and Stancliffe, Richard J., 2014, “Carbon-enhanced Metal-poor Star Frequencies in the Galaxy: Corrections for the Effect of Evolutionary Status on Carbon Abundances”, *Astrophys. J.*, **797**(1), 21. [DOI], [ADS], [arXiv:1410.2223 [astro-ph.SR]]
- Placco, Vinicius M., Sneden, Christopher, Roederer, Ian U., Lawler, James E., Den Hartog, Elizabeth A., Hejazi, Neda, Maas, Zachary and Bernath, Peter, 2021, “Linemake: An Atomic and Molecular Line List Generator”, *Research Notes of the American Astronomical Society*, **5**(4), 92. [DOI], [ADS], [arXiv:2104.08286 [astro-ph.IM]]
- Plez, Bertrand, Smith, Verne V. and Lambert, David L., 1993, “Lithium Abundances and Other Clues to Envelope Burning in Small Magellanic Cloud Asymptotic Giant Branch Stars”, *Astrophys. J.*, **418**, 812. [DOI], [ADS]
- Pospelov, Maxim and Pradler, Josef, 2010, “Big Bang Nucleosynthesis as a Probe of New Physics”, *Annual Review of Nuclear and Particle Science*, **60**, 539–568. [DOI], [ADS], [arXiv:1011.1054 [hep-ph]]

- Prochaska, Jason X. and McWilliam, Andrew, 2000, “On the Perils of Hyperfine Splitting: A Reanalysis of MN and SC Abundance Trends”, *Astrophys. J. Lett.*, **537**(1), L57–L60. [DOI], [ADS], [arXiv:astro-ph/0005471 [astro-ph]]
- Prochaska, Jason X., Naumov, Sergei O., Carney, Bruce W., McWilliam, Andrew and Wolfe, Arthur M., 2000, “The Galactic Thick Disk Stellar Abundances”, *Astron. J.*, **120**(5), 2513–2549. [DOI], [ADS], [arXiv:astro-ph/0008075 [astro-ph]]
- Purandardas, Meenakshi and Goswami, Aruna, 2021, “Observational evidence points at AGB stars as possible progenitors of CEMP-s & r/s stars”, *arXiv e-prints*, arXiv:2108.06075. [ADS], [arXiv:2108.06075 [astro-ph.SR]]
- Purandardas, Meenakshi, Goswami, Aruna, Goswami, Partha Pratim, Shejelamal, J. and Masseron, Thomas, 2019, “Chemical analysis of CH stars - III. Atmospheric parameters and elemental abundances”, *Mon. Not. Roy. Astron. Soc.*, **486**(3), 3266–3289. [DOI], [ADS], [arXiv:1904.03904 [astro-ph.SR]]
- Qian, Y. Z., 2000, “Supernovae versus Neutron Star Mergers as the Major R-Process Sources”, *Astrophys. J. Lett.*, **534**(1), L67–L70. [DOI], [ADS], [arXiv:astro-ph/0003242 [astro-ph]]
- Qian, Y. Z. and Wasserburg, G. J., 2003, “Stellar Sources for Heavy r-Process Nuclei”, *Astrophys. J.*, **588**(2), 1099–1109. [DOI], [ADS], [arXiv:astro-ph/0301461 [astro-ph]]
- Qian, Y. Z. and Woosley, S. E., 1996, “Nucleosynthesis in Neutrino-driven Winds. I. The Physical Conditions”, *Astrophys. J.*, **471**, 331. [DOI], [ADS], [arXiv:astro-ph/9611094 [astro-ph]]
- Ram, Ram S., Brooke, James S. A., Bernath, Peter F., Sneden, Christopher and Lucatello, Sara, 2014, “Improved Line Data for the Swan System $^{12}\text{C}^{13}\text{C}$ Iso-topologue”, *Astrophys. J. Suppl.*, **211**(1), 5. [DOI], [ADS]

- Ramírez, I., Allende Prieto, C. and Lambert, D. L., 2013, “Oxygen Abundances in Nearby FGK Stars and the Galactic Chemical Evolution of the Local Disk and Halo”, *Astrophys. J.*, **764**(1), 78. [DOI], [ADS], [arXiv:1301.1582 [astro-ph.SR]]
- Raskin, G., van Winckel, H., Hensberge, H., Jorissen, A., Lehmann, H., Waelkens, C., Avila, G., de Cuyper, J. P., Degroote, P., Dubosson, R., Dumortier, L., Frémat, Y., Laux, U., Michaud, B., Morren, J., Perez Padilla, J., Pessemier, W., Prins, S., Smolders, K., van Eck, S. and Winkler, J., 2011, “HERMES: a high-resolution fibre-fed spectrograph for the Mercator telescope”, *Astron. Astrophys.*, **526**, A69. [DOI], [ADS], [arXiv:1011.0258 [astro-ph.IM]]
- Reddy, Bacham E., Tomkin, Jocelyn, Lambert, David L. and Allende Prieto, Carlos, 2003, “The chemical compositions of Galactic disc F and G dwarfs”, *Mon. Not. Roy. Astron. Soc.*, **340**(1), 304–340. [DOI], [ADS], [arXiv:astro-ph/0211551 [astro-ph]]
- Reddy, Bacham E., Lambert, David L. and Allende Prieto, Carlos, 2006, “Elemental abundance survey of the Galactic thick disc”, *Mon. Not. Roy. Astron. Soc.*, **367**(4), 1329–1366. [DOI], [ADS], [arXiv:astro-ph/0512505 [astro-ph]]
- Reimers, D., Koehler, T. and Wisotzki, L., 1996, “The Hamburg/ESO survey for bright QSOs. II. Follow-up spectroscopy of 160 quasars and Seyferts.”, *Astron. Astrophys. Suppl.*, **115**, 235. [ADS]
- Renda, Agostino, Fenner, Yeshe, Gibson, Brad K., Karakas, Amanda I., Lattanzio, John C., Campbell, Simon, Chieffi, Alessandro, Cunha, Katia and Smith, Verne V., 2004, “On the origin of fluorine in the Milky Way”, *Mon. Not. Roy. Astron. Soc.*, **354**(2), 575–580. [DOI], [ADS], [arXiv:astro-ph/0410580 [astro-ph]]
- Rojas, M., Drake, N. A., Pereira, C. B. and Kholtygin, A. F., 2013, “Physical Parameters and Chemical Composition of a Group of Mild Barium Stars”, *Astrophysics*, **56**(1), 57–67. [DOI], [ADS]

Romano, D., Karakas, A. I., Tosi, M. and Matteucci, F., 2010, “Quantifying the uncertainties of chemical evolution studies. II. Stellar yields”, *Astron. Astrophys.*, **522**, A32. [DOI], [ADS], [arXiv:1006.5863 [astro-ph.GA]]

Rossi, Silvia, Beers, Timothy C. and Sneden, Chris, 1999, “Carbon Abundances for Metal-Poor Stars Based on Medium-Resolution Spectra”, in *The Third Stromlo Symposium: The Galactic Halo*, (Eds.) Gibson, Brad K., Axelrod, Rim S., Putman, Mary E., Astronomical Society of the Pacific Conference Series, 165, Academic Press. Academic Press. [ADS]

Rossi, Silvia, Beers, Timothy C., Sneden, Chris, Sevastyanenko, Tatiana, Rhee, Jaehyon and Marsteller, Brian, 2005, “Estimation of Carbon Abundances in Metal-Poor Stars. I. Application to the Strong G-Band Stars of Beers, Preston, and Shectman”, *Astron. J.*, **130**(6), 2804–2823. [DOI], [ADS], [arXiv:astro-ph/0508202 [astro-ph]]

Rosswog, S., Korobkin, O., Arcones, A., Thielemann, F. K. and Piran, T., 2014, “The long-term evolution of neutron star merger remnants - I. The impact of r-process nucleosynthesis”, *Mon. Not. Roy. Astron. Soc.*, **439**(1), 744–756. [DOI], [ADS], [arXiv:1307.2939 [astro-ph.HE]]

Ryan, Sean G., Norris, John E. and Bessell, M. S., 1991, “Subdwarf Studies. IV. Element Abundance Ratios in Extremely Metal-deficient Stars”, *Astron. J.*, **102**, 303. [DOI], [ADS]

Schindler, M., Stencel, R. E., Linsky, J. L., Basri, G. S. and Helfand, D. J., 1982, “Ultraviolet and X-ray detection of the 56 Peg system (K0 II p+WD) : evidence for accretion of a cool stellar wind onto a white dwarf.”, *Astrophys. J.*, **263**, 269–276. [DOI], [ADS]

Schönrich, Ralph, Binney, James and Dehnen, Walter, 2010, “Local kinematics and the local standard of rest”, *Mon. Not. Roy. Astron. Soc.*, **403**(4), 1829–1833. [DOI], [ADS], [arXiv:0912.3693 [astro-ph.GA]]

- Schulz-Gulde, E., 1969, “Oscillator strengths of spectral lines of neutral and singly ionized silicon.”, *J. Quant. Spectr. Radi. Transfer.*, **9**(1), 13–29. [DOI], [ADS]
- Shappee, B. J., Simon, J. D., Drout, M. R., Piro, A. L., Morrell, N., Prieto, J. L., Kasen, D., Holoién, T. W. S., Kollmeier, J. A., Kelson, D. D., Coulter, D. A., Foley, R. J., Kilpatrick, C. D., Siebert, M. R., Madore, B. F., Murguia-Berthier, A., Pan, Y. C., Prochaska, J. X., Ramirez-Ruiz, E., Rest, A., Adams, C., Alatalo, K., Bañados, E., Baughman, J., Bernstein, R. A., Bitsakis, T., Boutsia, K., Bravo, J. R., Di Mille, F., Higgs, C. R., Ji, A. P., Maravelias, G., Marshall, J. L., Placco, V. M., Prieto, G. and Wan, Z., 2017, “Early spectra of the gravitational wave source GW170817: Evolution of a neutron star merger”, *Science*, **358**(6370), 1574–1578. [DOI], [ADS], [arXiv:1710.05432 [astro-ph.HE]]
- Shejeelammal, J. and Goswami, Aruna, 2019, “Probing the Galactic s-process nucleosynthesis using barium stars”, *BSRSL*, **88**, 215 – 223. [ADS]
- Shejeelammal, J. and Goswami, Aruna, 2020, “[Rb/Zr] ratio in Ba stars as a diagnostic of the companion AGB stellar mass”, *Journal of Astrophysics and Astronomy*, **41**(1), 37. [DOI], [ADS], [arXiv:2010.08131 [astro-ph.SR]]
- Shejeelammal, J. and Goswami, Aruna, 2021, “Probing the Nucleosynthetic Contribution of Low-metallicity, Low-mass Star Companions of CEMP Stars”, *Astrophys. J.*, **921**(1), 77. [DOI], [ADS], [arXiv:2108.01855 [astro-ph.SR]]
- Shejeelammal, J., Goswami, Aruna, Goswami, Partha Pratim, Rathour, Rajeev Singh and Masseron, Thomas, 2020, “Characterizing the companion AGBs using surface chemical composition of barium stars”, *Mon. Not. Roy. Astron. Soc.*, **492**(3), 3708–3727. [DOI], [ADS], [arXiv:2010.06949 [astro-ph.SR]]
- Shejeelammal, J., Goswami, Aruna and Shi, Jianrong, 2021, “HCT/HESP study of two carbon stars from the LAMOST survey”, *Mon. Not. Roy. Astron. Soc.*, **502**(1), 1008–1025. [DOI], [ADS], [arXiv:2101.11822 [astro-ph.SR]]

Shetrone, Matthew D., 2003, “Carbon Isotopes in Globular Clusters Down to the Bump in the Luminosity Function”, *Astrophys. J. Lett.*, **585**(1), L45–L48. [DOI], [ADS]

Short, C. I. and Hauschildt, P. H., 2006, “NLTE Strontium and Barium in Metal-poor Red Giant Stars”, *Astrophys. J.*, **641**(1), 494–503. [DOI], [ADS], [arXiv:astro-ph/0601210 [astro-ph]]

Si, Jian-Min, Li, Yin-Bi, Luo, A. Li, Tu, Liang-Ping, Shi, Zhi-Xin, Zhang, Jian-Nan, Wei, Peng, Zhao, Gang, Wu, Yi-Hong, Wu, Fu-Chao and Zhao, Yong-Heng, 2015, “Identifying Carbon stars from the LAMOST pilot survey with the efficient manifold ranking algorithm”, *Research in Astronomy and Astrophysics*, **15**(10), 1671. [DOI], [ADS]

Skúladóttir, Á., Tolstoy, E., Salvadori, S., Hill, V., Pettini, M., Shetrone, M. D. and Starkenburg, E., 2015, “The first carbon-enhanced metal-poor star found in the Sculptor dwarf spheroidal”, *Astron. Astrophys.*, **574**, A129. [DOI], [ADS], [arXiv:1411.7956 [astro-ph.GA]]

Sloan, G. C., Kraemer, K. E., Wood, P. R., Zijlstra, A. A., Bernard-Salas, J., Devost, D. and Houck, J. R., 2008, “The Magellanic Zoo: Mid-Infrared Spitzer Spectroscopy of Evolved Stars and Circumstellar Dust in the Magellanic Clouds”, *Astrophys. J.*, **686**(2), 1056–1081. [DOI], [ADS], [arXiv:0807.2998 [astro-ph]]

Smiljanic, R., Barbuy, B., de Medeiros, J. R. and Maeder, A., 2006, “Evidence for rotation-induced mixing in evolved intermediate mass stars”, in *Revista Mexicana de Astronomia y Astrofisica Conference Series*, Revista Mexicana de Astronomia y Astrofisica Conference Series, 26, Academic Press. Academic Press. [ADS], [arXiv:astro-ph/0603128 [astro-ph]]

Smiljanic, R., Porto de Mello, G. F. and da Silva, L., 2007, “Abundance analysis of barium and mild barium stars”, *Astron. Astrophys.*, **468**(2), 679–693. [DOI], [ADS], [arXiv:astro-ph/0702421 [astro-ph]]

- Smith, P. L. and Kuehne, M., 1978, "Oscillator Strengths of Neutral Titanium from Hook Method Measurements in a Furnace. I. Lines from the a^3F_2 , 3 and 4 Levels at 0, 0.021, and 0.048 eV", *Proceedings of the Royal Society of London Series A*, **362**(1709), 263–279. [DOI], [ADS]
- Smith, V. V., 1984, "An abundance analysis of the cool barium stars.", *Astron. Astrophys.*, **132**, 326–338. [ADS]
- Smith, V. V. and Lambert, D. L., 1985, "The chemical composition of red giants. I. Dredge-up in the M and MS stars.", *Astrophys. J.*, **294**, 326–338. [DOI], [ADS]
- Smith, V. V. and Lambert, D. L., 1986a, "Lithium in Late-Type Giants. IV. The Subgiant CH Stars", *Astrophys. J.*, **303**, 226. [DOI], [ADS]
- Smith, Verne V. and Lambert, David L., 1986b, "The Chemical Composition of Red Giants. II. Helium Burning and the s-Process in the MS and S Stars", *Astrophys. J.*, **311**, 843. [DOI], [ADS]
- Smith, Verne V. and Lambert, David L., 1988, "S-Process-Enriched Cool Stars with and without Technetium: Clues to Asymptotic Giant Branch and Binary Star Evolution", *Astrophys. J.*, **333**, 219. [DOI], [ADS]
- Smith, Verne V. and Lambert, David L., 1990, "The Chemical Composition of Red Giants. III. Further CNO Isotopic and s-Process Abundances in Thermally Pulsing Asymptotic Giant Branch Stars", *Astrophys. J. Suppl.*, **72**, 387. [DOI], [ADS]
- Smith, Verne V., Coleman, Howard and Lambert, David L., 1993, "Abundances in CH Subgiants: Evidence of Mass Transfer onto Main-Sequence Companions", *Astrophys. J.*, **417**, 287. [DOI], [ADS]
- Sneden, C., Lambert, D. L. and Pilachowski, C. A., 1981, "A study of CNO elements in barium stars.", *Astrophys. J.*, **247**, 1052–1062. [DOI], [ADS]
- Sneden, C., Cowan, J. J. and Gallino, R., 2008, "Neutron-capture elements in the early galaxy.", *Ann. Rev. Astron. Astrophys.*, **46**, 241–288. [DOI], [ADS]

- Sneden, Christopher, Lucatello, Sara, Ram, Ram S., Brooke, James S. A. and Bernath, Peter, 2014, “Line Lists for the A $^2\Pi$ -X $^2\Sigma^+$ (Red) and B $^2\Sigma^+$ -X $^2\Sigma^+$ (Violet) Systems of CN, $^{13}\text{C}^{14}\text{N}$, and $^{12}\text{C}^{15}\text{N}$, and Application to Astronomical Spectra”, *Astrophys. J. Suppl.*, **214**(2), 26. [DOI], [ADS], [arXiv:1408.3828 [astro-ph.SR]]
- Sneden, Christopher Alan, 1973, *Carbon and Nitrogen Abundances in Metal-Poor Stars.*, Ph.D. thesis, THE UNIVERSITY OF TEXAS AT AUSTIN. [ADS]
- Sperauskas, J., Začs, L., Schuster, W. J. and Deveikis, V., 2016, “The Binary Nature of CH-Like Stars”, *Astrophys. J.*, **826**(1), 85. [DOI], [ADS]
- Spite, M., Cayrel, R., Plez, B., Hill, V., Spite, F., Depagne, E., François, P., Bonifacio, P., Barbuy, B., Beers, T., Andersen, J., Molaro, P., Nordström, B. and Primas, F., 2005, “First stars VI - Abundances of C, N, O, Li, and mixing in extremely metal-poor giants. Galactic evolution of the light elements”, *Astron. Astrophys.*, **430**, 655–668. [DOI], [ADS], [arXiv:astro-ph/0409536 [astro-ph]]
- Spite, M., Cayrel, R., Hill, V., Spite, F., François, P., Plez, B., Bonifacio, P., Molaro, P., Depagne, E., Andersen, J., Barbuy, B., Beers, T. C., Nordström, B. and Primas, F., 2006, “First stars IX - Mixing in extremely metal-poor giants. Variation of the $^{12}\text{C}/^{13}\text{C}$, [Na/Mg] and [Al/Mg] ratios”, *Astron. Astrophys.*, **455**(1), 291–301. [DOI], [ADS], [arXiv:astro-ph/0605056 [astro-ph]]
- Spite, M., Caffau, E., Bonifacio, P., Spite, F., Ludwig, H. G., Plez, B. and Christlieb, N., 2013, “Carbon-enhanced metal-poor stars: the most pristine objects?”, *Astron. Astrophys.*, **552**, A107. [DOI], [ADS], [arXiv:1303.1791 [astro-ph.GA]]
- Stancliffe, R. J., Glebbeek, E., Izzard, R. G. and Pols, O. R., 2007, “Carbon-enhanced metal-poor stars and thermohaline mixing”, *Astron. Astrophys.*, **464**(3), L57–L60. [DOI], [ADS]

- Stancliffe, Richard J., Dearborn, David S. P., Lattanzio, John C., Heap, Stuart A. and Campbell, Simon W., 2011, “Three-dimensional Hydrodynamical Simulations of a Proton Ingestion Episode in a Low-metallicity Asymptotic Giant Branch Star”, *Astrophys. J.*, **742**(2), 121. [DOI], [ADS], [arXiv:1109.1289 [astro-ph.SR]]
- Stancliffe, Richard J., Kennedy, Catherine R., Lau, Herbert H. B. and Beers, Timothy C., 2013, “Modelling the nucleosynthetic properties of carbon-enhanced metal-poor RR Lyrae stars”, *Mon. Not. Roy. Astron. Soc.*, **435**(1), 698–706. [DOI], [ADS], [arXiv:1307.4762 [astro-ph.SR]]
- Starkenburg, Else, Shetrone, Matthew D., McConnachie, Alan W. and Venn, Kim A., 2014, “Binarity in carbon-enhanced metal-poor stars”, *Mon. Not. Roy. Astron. Soc.*, **441**(2), 1217–1229. [DOI], [ADS], [arXiv:1404.0385 [astro-ph.SR]]
- Steigman, Gary, 2007, “Primordial Nucleosynthesis in the Precision Cosmology Era”, *Annual Review of Nuclear and Particle Science*, **57**(1), 463–491. [DOI], [ADS], [arXiv:0712.1100 [astro-ph]]
- Straniero, O., Gallino, R., Busso, M., Chiefei, A., Raiteri, C. M., Limongi, M. and Salaris, M., 1995, “Radiative ^{13}C Burning in Asymptotic Giant Branch Stars and s-Processing”, *Astrophys. J. Lett.*, **440**, L85. [DOI], [ADS]
- Straniero, Oscar, Gallino, Roberto and Cristallo, Sergio, 2006, “s process in low-mass asymptotic giant branch stars”, *Nucl. Phys. A*, **777**, 311–339. [DOI], [ADS], [arXiv:astro-ph/0501405 [astro-ph]]
- Sugimoto, D., 1971, “Mixing between Stellar Envelope and Core in Advanced Phases of Evolution. III —Stellar Core of Initial Mass 1.5M_\odot —”, *Progress of Theoretical Physics*, **45**(3), 761–775. [DOI], [ADS]
- Surman, R., McLaughlin, G. C., Ruffert, M., Janka, H. Th. and Hix, W. R., 2008, “r-Process Nucleosynthesis in Hot Accretion Disk Flows from Black Hole-Neutron Star Mergers”, *Astrophys. J. Lett.*, **679**(2), L117. [DOI], [ADS], [arXiv:0803.1785 [astro-ph]]

- Takeda, Yoichi, 2021, “Rubidium abundances of galactic disk stars”, *Astronomische Nachrichten*, **342**(3), 515–530. [DOI], [ADS], [arXiv:2102.00245 [astro-ph.SR]]
- Takeda, Yoichi, Zhao, Gang, Takada-Hidai, Masahide, Chen, Yu-Qin, Saito, Yu-Ji and Zhang, Hua-Wei, 2003, “Non-LTE Analysis of the Sodium Abundance of Metal-Poor Stars in the Galactic Disk and Halo”, *Chin. J. Astron. Astrophys.*, **3**, 316–340. [DOI], [ADS], [arXiv:astro-ph/0304337 [astro-ph]]
- Tanvir, N. R., Levan, A. J., Fruchter, A. S., Hjorth, J., Hounsell, R. A., Wiersema, K. and Tunnicliffe, R. L., 2013, “A ‘kilonova’ associated with the short-duration γ -ray burst GRB 130603B”, *Nature*, **500**(7464), 547–549. [DOI], [ADS], [arXiv:1306.4971 [astro-ph.HE]]
- Thévenin, F. and Idiart, T. P., 1999, “Stellar Iron Abundances: Non-LTE Effects”, *Astrophys. J.*, **521**(2), 753–763. [DOI], [ADS], [arXiv:astro-ph/9906433 [astro-ph]]
- Timmes, F. X., Woosley, S. E. and Weaver, Thomas A., 1995, “Galactic Chemical Evolution: Hydrogen through Zinc”, *Astrophys. J. Suppl.*, **98**, 617. [DOI], [ADS], [arXiv:astro-ph/9411003 [astro-ph]]
- Tominaga, Nozomu, Umeda, Hideyuki and Nomoto, Ken’ichi, 2007, “Supernova Nucleosynthesis in Population III 13-50 M_{solar} Stars and Abundance Patterns of Extremely Metal-poor Stars”, *Astrophys. J.*, **660**(1), 516–540. [DOI], [ADS], [arXiv:astro-ph/0701381 [astro-ph]]
- Tominaga, Nozomu, Iwamoto, Nobuyuki and Nomoto, Ken’ichi, 2014, “Abundance Profiling of Extremely Metal-poor Stars and Supernova Properties in the Early Universe”, *Astrophys. J.*, **785**(2), 98. [DOI], [ADS], [arXiv:1309.6734 [astro-ph.SR]]
- Tomkin, J. and Lambert, D. L., 1979, “Magnesium isotopes and s-process elements in the barium star HR 774.”, *Astrophys. J.*, **227**, 209–219. [DOI], [ADS]
- Tomkin, J. and Lambert, D. L., 1983, “Heavy-element abundances in the classical barium star HR 774.”, *Astrophys. J.*, **273**, 722–741. [DOI], [ADS]

- Totten, E. J. and Irwin, M. J., 1998, “The APM survey for cool carbon stars in the Galactic halo - I”, *Mon. Not. Roy. Astron. Soc.*, **294**(1), 1–27. [DOI], [ADS]
- Travaglio, Claudia, Gallino, Roberto, Busso, Maurizio and Gratton, Raffaele, 2001, “Lead: Asymptotic Giant Branch Production and Galactic Chemical Evolution”, *Astrophys. J.*, **549**(1), 346–352. [DOI], [ADS], [arXiv:astro-ph/0011050 [astro-ph]]
- Travaglio, Claudia, Gallino, Roberto, Arnone, Enrico, Cowan, John, Jordan, Faith and Sneden, Christopher, 2004, “Galactic Evolution of Sr, Y, And Zr: A Multiplicity of Nucleosynthetic Processes”, *Astrophys. J.*, **601**(2), 864–884. [DOI], [ADS], [arXiv:astro-ph/0310189 [astro-ph]]
- Udry, S., Jorissen, A., Mayor, M. and Van Eck, S., 1998a, “A CORAVEL radial-velocity monitoring of giant BA and S stars: Spectroscopic orbits and intrinsic variations. I.”, *Astron. Astrophys. Suppl.*, **131**, 25–41. [DOI], [ADS], [arXiv:astro-ph/9801273 [astro-ph]]
- Udry, S., Mayor, M., Van Eck, S., Jorissen, A., Prevot, L., Grenier, S. and Lindgren, H., 1998b, “New CORAVEL spectroscopic-binary orbits of giant barium stars. II”, *Astron. Astrophys. Suppl.*, **131**, 43–47. [DOI], [ADS]
- Umeda, Hideyuki and Nomoto, Ken’ichi, 2005, “Variations in the Abundance Pattern of Extremely Metal-Poor Stars and Nucleosynthesis in Population III Supernovae”, *Astrophys. J.*, **619**(1), 427–445. [DOI], [ADS], [arXiv:astro-ph/0308029 [astro-ph]]
- Van Eck, S. and Jorissen, A., 1999, “The Henize sample of S stars. I. The technetium dichotomy”, *Astron. Astrophys.*, **345**, 127–136. [ADS], [arXiv:astro-ph/9903241 [astro-ph]]
- Van Eck, S. and Jorissen, A., 2000, “The Henize sample of S stars — III. Uncovering the binary intruders”, *Astron. Astrophys.*, **360**, 196–212. [ADS]

- Van Eck, S., Jorissen, A., Udry, S., Mayor, M., Burki, G., Burnet, M. and Catchpole, R., 2000, “The Henize sample of S stars. II. Data”, *Astron. Astrophys. Suppl.*, **145**, 51–65. [DOI], [ADS]
- Van Eck, Sophie, Neyskens, Pieter, Jorissen, Alain, Plez, Bertrand, Edvardsson, Bengt, Eriksson, Kjell, Gustafsson, Bengt, Jørgensen, Uffe Gråe and Nordlund, Åke, 2017, “A grid of MARCS model atmospheres for late-type stars. II. S stars and their properties”, *Astron. Astrophys.*, **601**, A10. [DOI], [ADS]
- van Raai, M. A., Lugaro, M., Karakas, A. I., García-Hernández, D. A. and Yong, D., 2012, “Rubidium, zirconium, and lithium production in intermediate-mass asymptotic giant branch stars”, *Astron. Astrophys.*, **540**, A44. [DOI], [ADS], [arXiv:1202.2620 [astro-ph.SR]]
- Vangioni-Flam, Elisabeth and Cassé, Michel, 1999, “Cosmic Lithium-Beryllium-Boron Story”, *Astrophys. Space Sci.*, **265**, 77–86. [DOI], [ADS], [arXiv:astro-ph/9902073 [astro-ph]]
- Vanture, Andrew D., 1992, “The CH Stars. III. Heavy Element Abundances”, *Astron. J.*, **104**, 1997–2004. [DOI], [ADS]
- Venn, Kim A., Irwin, Mike, Shetrone, Matthew D., Tout, Christopher A., Hill, Vanessa and Tolstoy, Eline, 2004, “Stellar Chemical Signatures and Hierarchical Galaxy Formation”, *Astron. J.*, **128**(3), 1177–1195. [DOI], [ADS], [arXiv:astro-ph/0406120 [astro-ph]]
- Ventura, P. and D’Antona, F., 2005, “Full computation of massive AGB evolution. I. The large impact of convection on nucleosynthesis”, *Astron. Astrophys.*, **431**, 279–288. [DOI], [ADS], [arXiv:astro-ph/0411191 [astro-ph]]
- Vernet, J., Dekker, H., D’Odorico, S., Kaper, L., Kjaergaard, P., Hammer, F., Randich, S., Zerbi, F., Groot, P. J., Hjorth, J., Guinouard, I., Navarro, R., Adolfse, T., Albers, P. W., Amans, J. P., Andersen, J. J., Andersen, M. I., Binetruy, P., Bristow, P., Castillo, R., Chemla, F., Christensen, L., Conconi,

- P., Conzelmann, R., Dam, J., de Caprio, V., de Ugarte Postigo, A., Delabre, B., di Marcantonio, P., Downing, M., Elswijk, E., Finger, G., Fischer, G., Flores, H., Fran ois, P., Goldoni, P., Guglielmi, L., Haigron, R., Hanenburg, H., Hendriks, I., Horrobin, M., Horville, D., Jessen, N. C., Kerber, F., Kern, L., Kiekebusch, M., Klescz, P., Klougart, J., Kragt, J., Larsen, H. H., Lizon, J. L., Lucuix, C., Mainieri, V., Manuputy, R., Martayan, C., Mason, E., Mazzoleni, R., Michaelsen, N., Modigliani, A., Moehler, S., M ller, P., Norup S rensen, A., N rregaard, P., P roux, C., Patat, F., Pena, E., Pragt, J., Reinero, C., Rigal, F., Riva, M., Roelfsema, R., Royer, F., Sacco, G., Santin, P., Schoenmaker, T., Spano, P., Sweers, E., Ter Horst, R., Tintori, M., Tromp, N., van Dael, P., van der Vliet, H., Venema, L., Vidali, M., Vinther, J., Vola, P., Winters, R., Wistisen, D., Wulterkens, G. and Zacchei, A., 2011, “X-shooter, the new wide band intermediate resolution spectrograph at the ESO Very Large Telescope”, *Astron. Astrophys.*, **536**, A105. [DOI], [ADS], [arXiv:1110.1944 [astro-ph.IM]]
- Wallerstein, George, Iben, Icko, Jr., Parker, Peter, Boesgaard, Ann Merchant, Hale, Gerald M., Champagne, Arthur E., Barnes, Charles A., K ppeler, Franz, Smith, Verne V., Hoffman, Robert D., Timmes, Frank X., Sneden, Chris, Boyd, Richard N., Meyer, Bradley S. and Lambert, David L., 1997, “Synthesis of the elements in stars: forty years of progress”, *Reviews of Modern Physics*, **69**(4), 995–1084. [DOI], [ADS]
- Wanajo, Shinya, Itoh, Naoki, Goriely, Stephane, Samyn, Mathieu and Ishimaru, Yuhri, 2005, “The r-process in supernovae with new microscopic mass formulae”, *Nucl. Phys. A*, **758**, 671–674. [DOI], [ADS]
- Wanajo, Shinya, Nomoto, Ken’ichi, Iwamoto, Nobuyuki, Ishimaru, Yuhri and Beers, Timothy C., 2006, “Enrichment of Very Metal Poor Stars with Both r-Process and s-Process Elements from 8-10 M_{solar} Stars”, *Astrophys. J.*, **636**(2), 842–847. [DOI], [ADS], [arXiv:astro-ph/0509788 [astro-ph]]

- Ward, L., Vogel, O., Arnesen, A., Hallin, R. and Wännström, A., 1985, “Accurate experimental lifetimes of excited levels in Nd II.”, *Physica Scripta*, **31**(3), 161–165. [DOI], [ADS]
- Warner, Brian, 1968, “Atomic oscillator strengths-IV. Transitions of the type s²-sp and ss-sp”, *Mon. Not. Roy. Astron. Soc.*, **140**, 53. [DOI], [ADS]
- Wisotzki, L., Koehler, T., Groote, D. and Reimers, D., 1996, “The Hamburg/ESO survey for bright QSOs. I. Survey design and candidate selection procedure.”, *Astron. Astrophys. Suppl.*, **115**, 227. [ADS]
- Wisotzki, L., Christlieb, N., Bade, N., Beckmann, V., Köhler, T., Vanelle, C. and Reimers, D., 2000, “The Hamburg/ESO survey for bright QSOs. III. A large flux-limited sample of QSOs”, *Astron. Astrophys.*, **358**, 77–87. [ADS], [arXiv:astro-ph/0004162 [astro-ph]]
- Woodward, Paul R., Herwig, Falk and Lin, Pei-Hung, 2015, “Hydrodynamic Simulations of H Entrainment at the Top of He-shell Flash Convection”, *Astrophys. J.*, **798**(1), 49. [DOI], [ADS]
- Woosley, S. E. and Weaver, Thomas A., 1995, “The Evolution and Explosion of Massive Stars. II. Explosive Hydrodynamics and Nucleosynthesis”, *Astrophys. J. Suppl.*, **101**, 181. [DOI], [ADS]
- Worley, C. C., Hill, V., Sobeck, J. and Carretta, E., 2013, “Ba and Eu abundances in M 15 giant stars”, *Astron. Astrophys.*, **553**, A47. [DOI], [ADS], [arXiv:1302.6122 [astro-ph.SR]]
- Xiang, M. S., Liu, X. W., Shi, J. R., Yuan, H. B., Huang, Y., Luo, A. L., Zhang, H. W., Zhao, Y. H., Zhang, J. N., Ren, J. J., Chen, B. Q., Wang, C., Li, J., Huo, Z. Y., Zhang, W., Wang, J. L., Zhang, Y., Hou, Y. H. and Wang, Y. F., 2017, “Estimating stellar atmospheric parameters, absolute magnitudes and elemental abundances from the LAMOST spectra with Kernel-based principal component analysis”, *Mon. Not. Roy. Astron. Soc.*, **464**(3), 3657–3678. [DOI], [ADS], [arXiv:1610.00083 [astro-ph.SR]]

Yamashita, Y., 1975, “CH-like stars.”, *Pub. Astron. Soc. Japan*, **27**, 325–331. [ADS]

Yan, Hongliang, Li, Haining, Wang, Song, Zong, Weikai, Yuan, Haibo, Xiang, Maosheng, Huang, Yang, Xie, Jiwei, Dong, Subo, Yuan, Hailong, Bi, Shaolan, Chu, Yaoquan, Cui, Xiangqun, Deng, Licai, Fu, Jianning, Han, Zhanwen, Hou, Jinliang, Li, Guoping, Liu, Chao, Liu, Jifeng, Liu, Xiaowei, Luo, Ali, Shi, Jianrong, Wu, Xuebing, Zhang, Haotong, Zhao, Gang and Zhao, Yongheng, 2022, “Overview of the LAMOST survey in the first decade”, *The Innovation*, **3**, 100224. [DOI], [ADS], [arXiv:2203.14300 [astro-ph.GA]]

Yang, Guo-Chao, Liang, Yan-Chun, Spite, Monique, Chen, Yu-Qin, Zhao, Gang, Zhang, Bo, Liu, Guo-Qing, Liu, Yu-Juan, Liu, Nian, Deng, Li-Cai, Spite, Francois, Hill, Vanessa and Zhang, Cai-Xia, 2016, “Chemical abundance analysis of 19 barium stars”, *Research in Astronomy and Astrophysics*, **16**(1), 19. [DOI], [ADS], [arXiv:1602.08704 [astro-ph.SR]]

Yanny, Brian, Rockosi, Constance, Newberg, Heidi Jo, Knapp, Gillian R., Adelman-McCarthy, Jennifer K., Alcorn, Bonnie, Allam, Sahar, Allende Prieto, Carlos, An, Deokkeun, Anderson, Kurt S. J., Anderson, Scott, Bailer-Jones, Coryn A. L., Bastian, Steve, Beers, Timothy C., Bell, Eric, Belokurov, Vasily, Bizyaev, Dmitry, Blythe, Norm, Bochanski, John J., Boroski, William N., Brinchmann, Jarle, Brinkmann, J., Brewington, Howard, Carey, Larry, Cudworth, Kyle M., Evans, Michael, Evans, N. W., Gates, Evalyn, Gänsicke, B. T., Gillespie, Bruce, Gilmore, Gerald, Nebot Gomez-Moran, Ada, Grebel, Eva K., Greenwell, Jim, Gunn, James E., Jordan, Cathy, Jordan, Wendell, Harding, Paul, Harris, Hugh, Hendry, John S., Holder, Diana, Ivans, Inese I., Ivezić, Željko, Jester, Sebastian, Johnson, Jennifer A., Kent, Stephen M., Kleinman, Scot, Kniazev, Alexei, Krzesinski, Jurek, Kron, Richard, Kuropatkin, Nikolay, Lebedeva, Svetlana, Lee, Young Sun, French Leger, R., Lépine, Sébastien, Levine, Steve, Lin, Huan, Long, Daniel C., Loomis, Craig, Lupton, Robert, Malanushenko, Olena, Malanushenko, Viktor, Margon, Bruce, Martinez-Delgado, David, McGehee, Peregrine, Monet, Dave,

Morrison, Heather L., Munn, Jeffrey A., Neilsen, Eric H., Jr., Nitta, Atsuko, Norris, John E., Oravetz, Dan, Owen, Russell, Padmanabhan, Nikhil, Pan, Kaike, Peterson, R. S., Pier, Jeffrey R., Platson, Jared, Re Fiorentin, Paola, Richards, Gordon T., Rix, Hans-Walter, Schlegel, David J., Schneider, Donald P., Schreiber, Matthias R., Schwabe, Axel, Sibley, Valena, Simmons, Audrey, Snedden, Stephanie A., Allyn Smith, J., Stark, Larry, Stauffer, Fritz, Steinmetz, M., Stoughton, C., SubbaRao, Mark, Szalay, Alex, Szkody, Paula, Thakar, Aniruddha R., Sivarani, Thirupathi, Tucker, Douglas, Uomoto, Alan, Vanden Berk, Dan, Vidrih, Simon, Wadadekar, Yogesh, Watters, Shannon, Wilhelm, Ron, Wyse, Rosemary F. G., Yarger, Jean and Zucker, Dan, 2009, “SEGUE: A Spectroscopic Survey of 240,000 Stars with $g = 14\text{--}20$ ”, *Astron. J.*, **137**(5), 4377–4399. [DOI], [ADS], [arXiv:0902.1781 [astro-ph.GA]]

Yong, David, Norris, John E., Bessell, M. S., Christlieb, N., Asplund, M., Beers, Timothy C., Barklem, P. S., Frebel, Anna and Ryan, S. G., 2013, “The Most Metal-poor Stars. III. The Metallicity Distribution Function and Carbon-enhanced Metal-poor Fraction”, *Astrophys. J.*, **762**(1), 27. [DOI], [ADS], [arXiv:1208.3016 [astro-ph.GA]]

Yoon, Jinmi, Beers, Timothy C., Placco, Vinicius M., Rasmussen, Kaitlin C., Carollo, Daniela, He, Siyu, Hansen, Terese T., Roederer, Ian U. and Zeanah, Jeff, 2016, “Observational Constraints on First-star Nucleosynthesis. I. Evidence for Multiple Progenitors of CEMP-No Stars”, *Astrophys. J.*, **833**(1), 20. [DOI], [ADS], [arXiv:1607.06336 [astro-ph.SR]]

York, Donald G., Adelman, J., Anderson, John E., Jr., Anderson, Scott F., Annis, James, Bahcall, Neta A., Bakken, J. A., Barkhouse, Robert, Bastian, Steven, Berman, Eileen, Boroski, William N., Bracker, Steve, Briegel, Charlie, Briggs, John W., Brinkmann, J., Brunner, Robert, Burles, Scott, Carey, Larry, Carr, Michael A., Castander, Francisco J., Chen, Bing, Colestock, Patrick L., Connolly, A. J., Crocker, J. H., Csabai, István, Czarapata, Paul C., Davis, John Eric, Doi, Mamoru, Dombeck, Tom, Eisenstein, Daniel, Ellman, Nancy,

Elms, Brian R., Evans, Michael L., Fan, Xiaohui, Federwitz, Glenn R., Fis-
celli, Larry, Friedman, Scott, Frieman, Joshua A., Fukugita, Masataka, Gille-
spie, Bruce, Gunn, James E., Gurbani, Vijay K., de Haas, Ernst, Haldeman,
Merle, Harris, Frederick H., Hayes, J., Heckman, Timothy M., Hennessy, G. S.,
Hindsley, Robert B., Holm, Scott, Holmgren, Donald J., Huang, Chi-hao, Hull,
Charles, Husby, Don, Ichikawa, Shin-Ichi, Ichikawa, Takashi, Ivezić, Željko,
Kent, Stephen, Kim, Rita S. J., Kinney, E., Klaene, Mark, Kleinman, A. N.,
Kleinman, S., Knapp, G. R., Korienek, John, Kron, Richard G., Kunszt, Pe-
ter Z., Lamb, D. Q., Lee, B., Leger, R. French, Limmongkol, Siriluk, Linden-
meyer, Carl, Long, Daniel C., Loomis, Craig, Loveday, Jon, Lucinio, Rich, Lup-
ton, Robert H., MacKinnon, Bryan, Mannery, Edward J., Mantsch, P. M.,
Margon, Bruce, McGehee, Peregrine, McKay, Timothy A., Meiksin, Avery,
Merelli, Aronne, Monet, David G., Munn, Jeffrey A., Narayanan, Vijay K.,
Nash, Thomas, Neilsen, Eric, Neswold, Rich, Newberg, Heidi Jo, Nichol, R. C.,
Nicinski, Tom, Nonino, Mario, Okada, Norio, Okamura, Sadanori, Ostriker,
Jeremiah P., Owen, Russell, Pauls, A. George, Peoples, John, Peterson, R. L.,
Petravick, Donald, Pier, Jeffrey R., Pope, Adrian, Pordes, Ruth, Prosapio, An-
gela, Rechenmacher, Ron, Quinn, Thomas R., Richards, Gordon T., Richmond,
Michael W., Rivetta, Claudio H., Rockosi, Constance M., Ruthmansdorfer,
Kurt, Sandford, Dale, Schlegel, David J., Schneider, Donald P., Sekiguchi, Maki,
Sergey, Gary, Shimasaku, Kazuhiro, Siegmund, Walter A., Smee, Stephen,
Smith, J. Allyn, Snedden, S., Stone, R., Stoughton, Chris, Strauss, Michael A.,
Stubbs, Christopher, SubbaRao, Mark, Szalay, Alexander S., Szapudi, Istvan,
Szokoly, Gyula P., Thakar, Anirudda R., Tremonti, Christy, Tucker, Douglas L.,
Uomoto, Alan, Vanden Berk, Dan, Vogeley, Michael S., Waddell, Patrick,
Wang, Shu-i., Watanabe, Masaru, Weinberg, David H., Yanny, Brian, Yasuda,
Naoki and SDSS Collaboration, 2000, “The Sloan Digital Sky Survey: Technical
Summary”, *Astron. J.*, **120**(3), 1579–1587. [DOI], [ADS], [arXiv:astro-ph/0006396
[astro-ph]]

Zhao, Gang, Zhao, Yong-Heng, Chu, Yao-Quan, Jing, Yi-Peng and Deng, Li-Cai,

- 2012, “LAMOST spectral survey — An overview”, *Research in Astronomy and Astrophysics*, **12**(7), 723–734. [DOI], [ADS]
- Zijlstra, Albert A., 2004, “Low-mass supernovae in the early Galactic halo: source of the double r/s-process enriched halo stars?”, *Mon. Not. Roy. Astron. Soc.*, **348**(2), L23–L27. [DOI], [ADS], [arXiv:astro-ph/0312481 [astro-ph]]